UNIVERSITY OF SOUTHAMPTON

FACULTY OF MEDICINE

Cancer Sciences Unit

THE MOLECULAR REGULATION OF APOPTOSIS IN B-CELL NEOPLASMS

Matthew John Carter Bsc (Hons) MRes.

Thesis for the degree of Doctor of Philosophy

September 2012

UNIVERSITY OF SOUTHAMPTON

ABSTRACT

FACULTY OF MEDICINE

CANCER SCIENCES UNIT

Doctor of Philosophy

The Molecular Regulation of Apoptosis in B-cell Neoplasms

Matthew John Carter BSc. (Hons) MRes.

Leukaemia and lymphoma represent the ninth and tenth most-common malignancies in the UK. Currently, therapeutic strategies utilise both chemotherapy and radiotherapy alongside the anti-CD20 monoclonal antibody Rituximab. Whilst such treatment regimes can yield impressive results, resistance and disease relapses are common. Therefore, additional therapies are required to improve patient survival and quality of life. Eliciting specific death of tumour cells and understanding the molecular mechanisms responsible provides a rational approach for developing these new therapies. One form of cell death induced in response to physiological or exogenous stress stimuli, oncogenic changes, or an absence of survival factors is termed apoptosis and is primarily regulated by the BH3-only subgroup of the Bcl-2 family.

Here, the regulation of this family of proteins was examined in a selection of murine lymphoma and leukaemia models after a selection of different apoptosis-inducing stimuli. Utilising a panel of primary murine lymphomas deficient in specific BH3-only genes, this investigation dissected the apoptotic cellular response to B cell receptor (BCR) and also TGF-β signalling. BCR signalling invoked a temporally biphasic cell death response, exhibiting both the hallmarks of apoptotic and non-apoptotic cell death. The BH3-only proteins Bim, Noxa, and Bik played key roles in BCR-induced apoptosis,

whilst only Bik appeared important in the non-apoptotic phase of cell death. Such upregulation of Bim and Bik appeared dependent upon the function of ERK and Syk kinases, respectively. Thereby, identifying a link between BCR signalling and specific death effector mechanisms. TGF-β signalling, however, was linked to the induction of the BH3-only protein Puma, which played a vital role in the rapid induction of apoptosis. Finally, two new models of B cell malignancy (Tcl-1, IgHTEμ) were established and characterised in the laboratory with the aim of addressing the general suitability of the BCR as a therapeutic target and the key role of Bim in the death response.

Together, these studies further our knowledge of how BCR and TGF-β signalling evoke apoptosis in lymphoma cells, highlight the diversity of BH3-only proteins involved, and provide a series of models in which to undertake rational combination therapies.

We anticipate that the knowledge gained will help to develop future therapeutic strategies, allowing targeting of specific aspects of tumour biology, in order to improve overall patient survival.

Table of Contents

Index of Figures

Index of Tables

Declaration of Authorship

I Matthew John Carter declare that the thesis entitled “The molecular regulation of Apoptosis in B-cell neoplasms” and the work presented in the thesis are both my own, and have been generated by me as the result of my own original research. I confirm that:

- this work was done wholly or mainly while in candidature for a research degree at this university;
- where any part of this thesis has been previously submitted for a degree of any other qualification at this university or any other institution, this has been clearly stated;
- where I have consulted the published work of others, this is always clearly attributed;
- where I have quoted from the work of others, the source is always given. With the exception of such quotations, this thesis is entirely my own work;
- I have acknowledged all main sources of help;
- Where the thesis is based on work done by myself jointly with others, I have made clear exactly what was done by others and what I have contributed myself;
- Part of this work has been/ is being published before submission in the following publications

Spender L.C, Carter M.J, O’Brien D.I, Clark L.J, Yu J, Michalak E, Happo L, Cragg M.S, and Inman G.J. Transforming Growth Factor-β directly induces PUMA during the rapid induction of apoptosis in Myc-driven B-cell lymphomas. Journal of Biological Chemistry, Manuscript submitted July 2012.

Signed: ……..

Date: ……..

Acknowledgements

I would firstly like to thank my supervisors Professor Mark Cragg and Professor Graham Packham. Both have provided invaluable advice in curbing my enthusiasm for ideas that had no hope of working or were technically impossible. I am particularly thankful for their ideas and the support they have offered throughout the course of my studies, without which this investigation would not have been possible. Particular thanks are owed to Professor Mark Cragg, who has undertaken as much, if not more, work than I in the preparation of this manuscript. His particular brand of pedantry has, although become infuriating at times, without doubt resulted in the production of this manuscript to an acceptable standard, which if left to my own devices would not have been achieved. There were 8 pages of the 300 plus in this manuscript that required no further corrections, an achievement which, to this day, remains one of my finest.

Thanks are also extended to Dr. E.L. Williams and K.L. Cox who performed the majority of the work characterising the Eμ-Myc lymphoma model, which I have made extensive use of in this investigation. Furthermore, I would like to thank everyone at the Tenovus Research Laboratory for providing a fun, friendly, and enthusiastic environment in which to complete my studies. Great thanks are also extended to all the BRF staff, who were incredibly helpful in the completion of the Eμ-Tcl1 and IgH.TEμ studies.

Thanks are also extended to the members of lad 2012, Chapman the elder, Chapman the younger, Sliding doors “flaccid” Young, Aussie Dave, Army boy Jim, and Douchebag “ghost-man” Blakemore. Things haven’t been particularly easy in 2012, however, our Friday night antics have softened the blow somewhat. Lad 2012 will forever remembered by the extensive liver damage that I’m sure will come back to haunt us in the future. Also a special thanks to Cabbage and Beau for listening so intently and giving me something to mop up.

Abbreviations

$[Ca^{2+}]I$	Intracellular Calcium Concentration
2-ME	2-Mercaptoethanol
A1	Bcl-2 associated protein A1
AID	Activation-induced deaminase
AIF	Apoptosis Inducing Factor
ALK	Activin Receptor-like Kinase
AM	Acetoxymethyl
AP-1	Activator Protein-1
APAF-1	Apoptotic Protease Activator Protein-1
ARF	Alternate Reading Frame
ARTS	Type 1 TNF shedding aminopeptidase regulator
ATF-2	Activating transcription factor-2
Atm	Ataxia telengiectasia-mutated
B-CLL	CLL B-lymphocytes
Bad	Bcl-2-associated death protein
BAF53	Brg1-associated factor 53
Bak	Bcl-2 associated killer
BANK	B-cell scaffold-protein with ankyrin repeats
Bax	Bcl-2 associated X-protein
Bcl-2	B-Cell Lymphoma-2
Bcl-w	Apoptosis regulator Bcl-w
Bcl-xL	B-cell lymphoma extra long
Bcl10	B-cell lymphoma 10
BCR	B-cell receptor
BH	Bcl-2 Homology Domain
bHLH	Basic helix-loop-helix
bHLH-Zip	Basic helix-loop-helix leucine zipper transcription factor

Bid	Bcl-2-interacting death protein
BiFC	Bi-fluorescence complementation
Bik	Bcl-2-interacting killer
Bim	Bcl-2-interacting mediator of cell death
BL	Burkitt's Lymphoma
Blk	B-lymphocyte Kinase
BLNK	B-cell linker protein
BM	Bone marrow
Bmf	Bcl-2 modifying factor
Bok	Bcl-2-related ovarian killer
BRCA	Breast cancer susceptibility protein
Btk	Bruton's tyrosine kinase
CARD	Caspase-activation and recruitment domain
CARMA1	CARD-containing membrane associated guanylate kinase-1
Caspase	Cysteine-aspartyl protease
CCL	Chemokine (C-C motif) ligand
CCR	C-C motif Chemokine receptor
CD	Cluster of differentiation
CD40L	CD40 ligand
cDNA	Complementary DNA
CHOP	CCAAT-enhancer binding protein homologous protein
CK2	Casein kinase-2
CLL	Chronic lymphocytic leukaemia
CLP	Common lymphoid progenitor
CMTM7	CKLF-like-MARVEL-TM domain-containing protein
CRAC	Calcium release activated Calcium channel
CREBP	cAMP response element binding protein
Csk	C-terminal Src kinase

CxCL	Chemokine (CXC motif) ligand
DAG	Diacylglycerol
DAXX	FAS-binding protein death domain associated protein
D_H	Heavy chain diversity region
$DiOC_6$	3,3'-dihexyloxacarbocyanine iodide
dKO	Double knockout
DLBCL	Diffuse large B-cell lymphoma
DLC-1	Dynein light chain 1
DMEM	Dublecco's modified eagles medium
Dnmt	DNA methyltransferase
Elk-1	E-twenty six-like transcription factor-1
EMT	Epithelial to mesenchymal transition
ER	Endoplasmic Reticullum
ERK	Extracellular signal-regulated kinase
FAM	5'6-carboxylfluoroscein
FCS	Foetal calf serum
FDCs	Follicular dendritic cells
FITC	Fluoroscein isothiocyanate
FKBP-12	FK506 binding protein-12
FLT3-L	Fms-related tyrosine kinase 3-ligand
Fmk	Fluoromethylketone
Foxc1	Forkhead C1
Foxo3a	Forkhead 03A
FRET	Fluorescence resonance energy transfer
Fyn	p59 Fyn
GADD	Growth arrest and DNA damage
GCN2	General control non-repressed 2
GCs	Germinal centres

GDP	Guanosine diphosphate
GEF	Guanine nucleotide exchange factor
GFP	Green fluorescent protein
GIT	Guanidinium isothiocyanate
Grb2	Growth factor receptor-bound protein 2
GSK-3	Glycogen synthase kinase-3
GSP	Gene-specific primer
GTP	Guanosine triphosphate
HAT	Histone acetyl transferase
HC	Heavy chain
HDAC	Histone de-acetylase
HEL	Hen egg lysozyme
Hrk	Harakiri
HRP	Horseradish peroxidase
HSCs	Haematopoietic stem cells
IAP	Inhibitor of apoptosis protein
Id	Idiotype
IFN	Interferon
Ig	Immunoglobulin
IgV_H	Immunoglobulin heavy chain variable region
IKK	IκB Kinase
IL	Interleukin
IL-7R	Interleukin-7 receptor
IP	Immunoprecipitate
IP_3	Inositol-1, 4, 5- trisphosphate
IP_3-R	Inositol-1, 4, 5- trisphosphate receptor
ITAM	Immunoreceptor tyrosine-based activation motif
IVC	Individually ventilated cage

IκB	Nuclear factor kappa-light-polypeptide gene inhibitor
J_H	immunoglobulin heavy chain joining region
J_L	immunoglobulin light chain joining region
JNK	c-Jun N-terminal kinase
LB	Lysogeny broth
LC	Immunoglobulin light chain
Lck	Lymphocyte specific kinase
Lin	Lineage marker
Lyn	Lck-yes-related novel kinase
M-CLL	IgVH mutated CLL
MAC	Mitochondrial apoptosis-induced channel
Mad	Max dimerisation protein
MALT1	Mucosa-associate lymphoid tissue lymphoma translocation protein-1
MAPK	Mitogen-activated protein kinase
Max	Myc-associated factor X
Mcl-1	Myeloid cell leukaemia 1
Mdm2	Mouse double minute 2
MEKK	MAPK-kinase kinases
MGB	Dihydrocyclopyrroloindole tripeptide minor groove binder
MH	Myc homology domain
MHC	Major histocompatibility complex
mIg	Membrane-spanning immunoglobulin
Miz-1	Myc-interacting Zinc finger protein-1
MKK	MAPK kinases
MOMP	Mitochondrial outer membrane permeablisation
MOPS	3-(N-morpholino)-propanesulfonic acid
mPTP	Mitochondrial permeability transition pore
mSin3a	Mammalian transcriptional co-repressor sin3a

mTOR	Mammalian target of Rapamycin
mTORC	Mammalian target of Rapamycin complex
Myc	Myelocytomatosis viral oncogene
N	Non-template nucleotides
Nck	Non-catalytic region of the tyrosine kinase adaptor protein
NEMO	NF-κB essential modulator
NES	Nuclear exclusion sequence
NF-κB	Nuclear factor kappa-light-chain enhancer of activated B-cells
NFAT	Nuclear factor of activated T-cells
NHL	Non-Hodgkin's lymphoma
NIK	NF-κB inducing kinase
NLS	Nuclear localisation sequence
Oligo-dT	Oligo-deoxyribothymidine
ORAI	Calcium release-activated calcium modulator
P	Palindromic nucleotides
P300	300 kDa HAT
P38	38 kDa MAPK
P90RSK	90 kDa ribosomal S6 kinase
PAK	P21-activated kinase
PARP	Poly-ADP-ribose polymerase
PBMC	Peripheral blood mononuclear cell
PBS	Phosphate-buffered saline
PDK-1	Phosphoinositide-dependent kinase-1
PH	Plekstrin homology domain
PI	Propidium Iodide
PI3K	Phosphatidylinositol-3-kinase
PI4K	Phosphatidylinositol-4-kinase
PI5K	Phosphatidylinositol-5-kinase

PIP_2	Phosphatidylinositol-4, 5-bisphosphate
PIP_3	Phosphatidyl-3, 4, 5-trisphosphate
PKA	Protein Kinase A
PKC	Protein Kinase C
PLC	Phospholipase C
PMA	Phorbyl-myristate acetate
PS	Phosphatidylserine
PTEN	Phosphatase and Tensin homologue
PTKs	Protein tyrosine kinases
Puma	P53-upregulated mediator of apoptosis
qPCR	Quantitative polymerase chain reaction
Rac-1	Ras-related C3-Botulinum toxin target 1
RAG	Recombination activating gene
Ras	Rat Sarcoma
RasGRP	Ras-guanylyl releasing protein
RE	Restriction endonuclease
RH	Rel homology domain
RhoA	Ras-homologue family member A
RIN	RNA integrity number
RIP	Receptor interacting Ser/Thr protein kinase
RIPA	Radioimmunoprecipitation assay buffer
RNAi	RNA interference
RNase	Ribonuclease
Ros	Reactive Oxygen species
rRNA	Ribosomal RNA
RT	Reverse transcriptase
RTKs	Receptor tyrosine kinases
SARA	SMAD anchor for receptor activation

SBE	SMAD binding element
Sca-1	Stem-cell antigen-1
SCs	Stromal cells
SDS	Sodium dodecylsulphate
SERCA	Sarcoplasmic/ Endoplasmic Reticullum ATPase
SFPTKs	Src-family protein tyrosine kinases
SH2	Src-homology 2 domain
Shc	SH2-containing adapter
SHIP	SH2-containing inositol phosphatase
SHM	Somatic hypermutation
SHP-1	SH2-domain-containing phosphatase-1
SiRNA	Short-interfering RNA
SLC	Surrogate light chain
SMAC	Second-mitochondrial activator of cell death
SMAD	Sma and Mad related family
SoS	Son of Sevenless
SPF	Specific-pathogen free
STIM	Stromal-interaction molecule 1
SV40	Simian vacuolating virus-40
Syk	Spleen tyrosine kinase
T1	Transitional 1
T2	Transitional 2
TAK	TGF-β activated kinase
tBid	truncated Bid
TBS	Tris-buffered saline
TBS-T	Tris-buffered saline Tween 20
Tcl1	T-cell leukaemia-1
TCR	T-cell receptor

TdT	Terminal deoxynucleotidyl transferase
TF	Transcription factor
Tg	Transgene/ transgenic
TGF-β	Transforming growth factor β
TIP48	TATA-box interacting protein of 48 kDa
TIP49	TATA-box interacting protein of 49 kDa
TNF	Tumour necrosis factor
TNF-R	Tumour necrosis factor-receptor
TRAF	TNF-R associated factor
TRRAP	Transformation/ transcription domain-associated protein
Tyr	Tyrosine
TβR	TGF- β receptor
U-CLL	IgVH unmutated CLL
Ub	Ubiquitin
UPR	Unfolded protein response
VCAM-1	Vascular cell adhesion molecule-1
V_L	Immunoglobulin light chain variable region
VLA-4	Very late antigen 4
WBC	White blood cell
WT	Wild-type
XID	X-linked immunodeficiency
XLA	X-linked agammaglobulinaemia
Zap70	Zeta-chain associated protein of 70 kDa
Zip	Leucine zipper domain

Chapter 1 Introduction

1.1 Cancer, Lymphoma & Leukaemia

Cancer is the fourth most common cause of mortality worldwide. According to Cancer research UK, 408,381 new cases were diagnosed in 2009 whilst 156,090 patients succumbed to the disease in the UK alone (1). Such figures portend that more than one in every three UK citizens will be diagnosed with cancer during their lifetime (2). Whilst conventional chemotherapy and radiotherapy regimens can yield extension of life, cures are rare. Therefore, further development of new therapeutic strategies and pharmaceutical agents is required in an attempt to improve overall patient survival.

Cancers arise from the emergence and expansion of autonomous clones exhibiting relentless cellular proliferation alongside a resistance towards the body's innate tumour-suppressive mechanisms. Such deleterious characteristics are acquired during tumourigenesis, via the accumulation of genetic abnormalities. Such abnormalities may be inherited or may be linked to environmental factors and/ or viral infection. Alternatively, many may arise due to spontaneous errors during DNA replication. Consequently, tissues that exhibit a rapid rate of renewal, such as the immune system, are particularly susceptible to the acquisition of spontaneous pathology-causing genetic abnormalities (3).

Although, as detailed above, cancer is a common disease, the emergence of a malignant, pathology-causing clone is seemingly an exceedingly rare event. At its inception the malignant clone represents only a single cell in the trillion cells of the human body. In addition, since only one in three individuals experience cancer, malignant transformation can be regarded as a one in three trillion cell event. Such protection from tumourigenesis is afforded by suppression of the spontaneous mutation rate to 1 per $1x10^{10}$ base pairs/ division alongside cell-intrinsic defence mechanisms and immune surveillance that counteract and delete clones exhibiting pre-neoplastic lesions (3, 4). Therefore, during tumourigenesis pre-malignant clones must acquire additional subversive mutations allowing evasion of intrinsic tumour suppression and immune surveillance in order to cause pathology (5, 6). Consequently,

malignant transformation should be considered a process of acquiring perpetual cellular proliferation alongside evasion of cell death and immune surveillance (5, 6).

Leukaemia and lymphoma represent the ninth and tenth most-common malignancies in the UK, accounting for 5.2% of new cases and 5.9% of cancer related deaths in 2009 (1, 2). As the subjects of intensive research, it is now known that leukaemia and lymphoma encompass a highly diverse multitude of diseases arising from myeloid or lymphoid cell lineages. This investigation shall focus upon one example of each in the form of chronic lymphocytic leukaemia (CLL) and Burkitt's lymphoma (BL) respectively.

Lymphoma is defined as a malignancy of the lymphatic system, primarily of the lymph nodes, and is comprised of both Hodgkin's and non-Hodgkin's lymphoma (NHL) subtypes which differ in pathological appearance and treatment regimes (7). NHL represents a collection of malignant diseases related only in their difference from Hodgkin's lymphoma; here we will consider Burkitt's lymphoma (BL) in more detail. First described by Dennis Burkitt in 1958, BL presents as a highly aggressive NHL with lymphadenopathy, recruitment of extranodal sites and less frequently an acute leukaemia (8-11). Due to its high rate of proliferation and cell death, BL appears histologically as a "starry sky" of lymphoblasts interspersed with tingible body macrophages (8, 10, 11). Characteristically, BL demonstrates overexpression and dysregulation of the c-Myc oncogene, with 80% of patients exhibiting the t (8:14) translocation, placing c-Myc adjacent to the Immunoglobulin (Ig) heavy chain (IgH) enhancer (8, 10, 11). The remaining 20% commonly display translocations placing the c-Myc oncogene adjacent to either λ or κ chain loci (8). At present, BL is categorised into three subgroups endemic, sporadic and immunodeficiency-associated BL. Endemic BL is geographically distributed to regions of endemic malaria in equatorial Africa and presents with jaw and kidney tumours in children of 4-7 years (8, 10, 11). In contrast, sporadic and immunodeficiency-associated BL have no specific geographical distribution and are more commonly associated with abdominal tumours (8, 10, 11). BL exhibits characteristic chemo-sensitivity resulting in 65-100% of treated patients entering remission with 47-86% maintaining remission one year post-therapy (8, 12). However, acquisition of innate resistance to frontline chemotherapy is common and

therefore, continuing study of BL and development of novel therapies remains a vital mainstay of cancer biology (12).

In contrast, leukaemia represents a multiple-subtype malignancy of blood cell forming tissues characterised by dramatic increases in circulating white blood cell numbers (7). Since CLL represents the most common adult leukaemia in the western world, we shall consider it in more detail. In 2009 CLL was responsible for the deaths of 1,090 patients and 2,798 new cases in the UK alone (1). Characteristically, CLL exhibits a blood lymphocyte count in excess of $5x10^{9}$ L^{-1} and an accumulation of homogenous, mature, cluster of differentiation (CD) 5^{+} B-lymphocytes in the peripheral blood, bone marrow and secondary lymphoid organs (13, 14). Morphological analysis reveals small, fragile lymphocytes prone to rupture upon preparation of blood smears, termed smudge cells. Unlike BL, CLL patients rarely exhibit characteristic genomic translocations. However, other genomic dysregulations such as deletions at 13q14, 11q22-23, 17p13 and trisomy 12 are common (14). Although CLL is a relatively indolent malignancy, there is significant heterogeneity in clinical course (15, 16). Such heterogeneity results from the existence of two distinct subtypes, determined by the presence of somatic mutations within the IgH variable (IgVH) region of the malignant clone. Patients exhibiting mutated IgVH (M-CLL) can expect a much better prognosis than those with unmutated IgVH (U-CLL), with a median survival of 293 months and 117 months, respectively (15, 16). Therefore, although M-CLL patients have a relatively good prognosis and require only minimal clinical intervention, significant advances in the treatment of U-CLL are required to improve overall patient survival.

Since both BL and CLL represent malignancies of B-cell origin, the B-cell receptor (BCR) plays a fundamental role in the aetiology, progression, and biology of both diseases and, therefore, shall be considered in further detail.

1.2 The B cell receptor in B-lymphocyte development

The BCR is the single-most influential determinant of B-cell development, survival and function. Receptor activation triggers diverse cellular responses ranging from activation, proliferation and differentiation to anergy, receptor editing and programmed cell death (17, 18). Such duplicity in cellular outcome provides vital

selective pressures during B-cell development, allowing both positive selection of B-cell progenitors possessing a functional BCR and negative selection of autoreactive B-lymphocytes (17, 19). The exact molecular basis for such disparate cellular outcomes is still largely unknown.

1.2.1 B-lymphopoiesis

Development of a mature, diverse and self-tolerant B-cell repertoire proceeds via progression through a well-defined series of developmental stages. In conjunction with micro-environmental cues, the Pre-B/B-cell receptor plays a fundamental role in shaping the B-cell repertoire, ensuring only signal competent, self-tolerant B-cells enter the periphery (4, 19-28).

1.2.1.1 Antigen-independent B-lymphopoiesis

The initial phases of B-lineage development occur within the foetal liver and adult bone marrow and occur in the absence of antigenic stimuli. As depicted in figure 1.1, the bone-marrow (BM) microenvironment provides distinct cellular niches that support the fledgling B-progenitor population through provision of vascular cell adhesion molecule 1 (VCAM-1): very late antigen-4 (VLA-4) dependent cell-cell contacts and a myriad of cytokines (20, 21, 29-33).

In particular, interleukin (IL) -7 and chemokine CXC motif ligand (CXCL) -12 appear to play prominent roles in B-lymphopoiesis, with additional roles played by Fms-related Tyrosine kinase 3-ligand (FLT3-L), Tumour necrosis factor-α (TNF-α), Transforming growth factor-β (TGF-β) and Interferon-γ (IFNγ) (20, 21, 29, 30, 32, 34). Furthermore, direct B-progenitor: BM stromal cell interactions provide key survival signals via c-Kit-mediated activation of the phosphatidylinositol 3-kinase (PI3K)/ Akt pathway and subsequent inhibition of apoptotic pathways (discussed later) (4, 20-22, 33, 35, 36).

Lymphoid lineage commitment occurs at an early stage via differentiation of pluripotent haematopoietic stem cells (HSCs) ($CD90^{low}$, Lineage marker $(Lin)^{-/low}$, stem cell antigen-1 ($Sca\text{-}1^{+}$)) to the common lymphoid progenitor (CLP) (4, 20-22, 37).

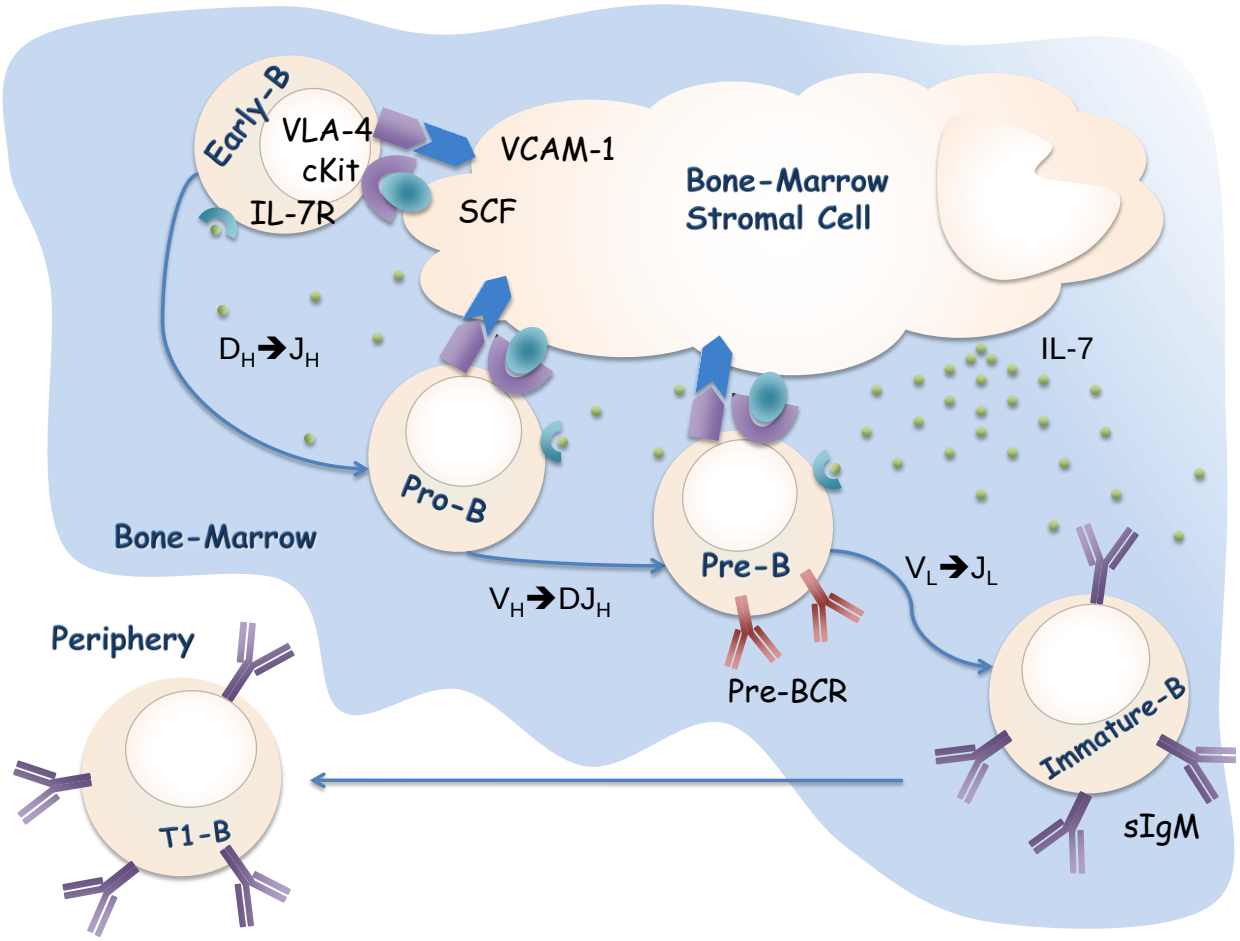

Figure 1.1 Schematic of antigen independent B-lymphopoiesis

B-cell progenitors demonstrate differing dependency upon the microenvironment throughout development. IL-7 is represented by green circles

CLP is phenotypically characterised as possessing none of the lineage markers of B, T and myeloid cells but is both c-Kit^{+} and IL-7 receptor (IL-7Rα)$^{+}$. It is further CD19^{-}, CD45R$^{+/-}$, CD10^{+}, CD34^{+}, CD38^{+}, terminal deoxynucleotidyl transferase (TdT)$^{+}$, recombination activating gene (RAG) 1/2^{+}, Lin^{-}, CD90^{-}, Sca-1^{low,} IL-7R$\alpha^{+,}$ cKit^{low} and has the ability to differentiate to B, T and Natural Killer (NK) cells but not to cells of the myeloid lineage (20, 21, 37).

B-lineage restriction occurs at the CLP-Early B-cell transition, characterised by expression of the B-cell-restricted genes CD79a and VpreB (20, 21). At this stage, RAG1 and RAG2-dependent recombination of the Ig heavy chain (Ig_H) locus is initiated, by joining of heavy chain diversity (D_H) and joining (J_H) regions (4, 20-22, 38). It is these joining regions which later help form the hyper-variable regions of the BCR responsible for antigen binding (4, 22). Since joining is clone-specific and imperfect, each cell exhibits a unique antigen binding profile and a huge diversity of antigen recognition is

generated in the B-cell repertoire as a whole (4, 22). Diversity is further enhanced by the addition of non-template (N) and palindromic (P) nucleotides to the joining region, the former being catalysed by TdT (4).

1.2.1.2 Pro-Pre B cell transition

Subsequent progression to the Pro-B cell stage is characterised by expression of the pan B-cell marker CD19, initiation of IgVH region DJ_H recombination, and subsequent joining to the μ constant region (4, 20-22, 38). However, despite completion of IgH recombination the pro-B-cell stage characteristically lacks strong expression of cytoplasmic μ heavy chains (μHC) (20, 21).

Progression to the Pre-B cell developmental stage is characterised primarily via subsequent surface expression of the μHC in association with the VpreB (Variable region-like) and λ5 (Constant region-like) complex known as the surrogate light chain (SLC), forming the Pre-BCR (4, 20-22, 38). Since the Pre-BCR provides a tonic maintenance signal (see below), cKit-mediated survival signals become redundant and detachment from stromal cells (SCs) ensues (20, 21). However, Pre B-cells continue to receive survival support in the form of soluble cytokines, such as IL-7 (4, 20-22, 39). Subsequent RAG1/2-mediated recombination of light-chain variable (V_L) and joining (J_L) regions allows expression of light chain (LC): μHC complexes, known as the mature BCR, and marks progression to the immature B-cell stage (20, 21).

1.2.1.3 Progression to the immature B-cell stage

Successful VJ_L recombination allows formation of the mature BCR and, in addition to loss of CD25 expression, marks attainment of immature B-cell developmental status (4, 20-22, 38, 39). Stromal factor independence allows immature B-cells to enter the periphery, via the blood stream, becoming transitional B-cells (4, 20-22, 39-41). Via passive transport, transitional B-cells translocate to secondary lymphoid organs, primarily the spleen in mice, where maturation to mature B-cells occurs (4, 20-22, 38, 40, 41).

Transitional B-cells sequentially proceed through two distinct developmental stages, termed transitional 1 (T1) and transitional 2 (T2), which differ in immunophenotype and occupancy of distinct sites within secondary lymphoid organs (40, 41). The

immunophenotype of T1 B cells closely resembles that of an immature B cell (IgM^+, $CD21^-$, IgD^-, $CD23^-$) whereas in contrast, T2 B cells possess an immunophenotype more closely resembling that of a mature B-cell (IgM^+, $CD21^+$, IgD^+ and $CD23^+$) (40, 41). Furthermore, T1 and T2 cells also demonstrate contrasting cellular outcomes upon BCR stimulation and dependence upon microenvironment signals (40, 42). Whilst T2 cells exhibit cellular proliferation and differentiation upon BCR signalling, T1 cells undergo significant clonal deletion via negative selection, discussed below (40, 43) (40, 43). This difference likely reflects a maturational checkpoint between T1 and T2 stages that allows functional BCR-signalling.

1.2.1.4 Progression to the mature B-cell stage

Reaching the mature B-cell developmental stage is associated with an IgM^{low}, IgD^{High}, $CD24^{low}$, $CD23^{High}$ immunophenotype and recirculation between secondary lymphoid organs via the bloodstream (40). Within the primary follicles of secondary lymphoid organs mature B-cells encounter antigen and begin the antigen dependent maturational process leading to effector function (40).

1.2.2 B-cell receptor-mediated clonal selection

1.2.2.1 Positive selection

The BCR and Pre-BCR should not simply be regarded as surface markers associated with various developmental stages of B-lymphopoiesis. They should in fact be viewed as central to the process, since they not only maintain the fledgling B-progenitor population but also drive development and effectively ensure the principle of self-tolerance.

Although imprecise VDJ_H recombination vastly enhances the diversity of antigen recognition, many resulting rearrangements fail to generate a signal competent BCR. In order to allow generation of a functional B-cell repertoire, only clones that have undertaken a productive rearrangement are permitted to progress through B-lymphopoiesis. Such so-called positive selection of signal competent clones is achieved via the provision of tonic survival signals by the resting BCR and Pre-BCR. These ensure progression of B-progenitors through the cellular developmental programme and maintenance of mature B-cells in the periphery (23-28, 40, 41, 43-45).

Evidence for such a role was provided by studies utilising Pre-BCR or BCR signalling deficient mice that displayed early stage B-cell developmental arrest, typically at the pro to pre B-cell transition (20, 21, 23, 26, 44). The observed developmental blockade could be overcome by re-introduction of fully functional BCR signalling components in the absence of antigen (19, 23, 26, 44, 46, 47). Furthermore, a complementary study performed by Tze et al demonstrated that resting BCR signals actively maintain the developmental status of immature B-cells (28). Tze et al demonstrated that inducible IgH ablation after the development of mature B-cells (via the Cre-Lox system) initiated re-expression of genes vital for Ig locus recombination, including Rag 1, Rag 2, and TdT, and therefore triggered reversion to a genetic programme of an earlier developmental stage (28). Such studies highlight that construction of a signal competent Pre-BCR/BCR represents a key checkpoint in B-lymphopoiesis which is a pre-requisite for maintaining developmental status and further differentiation along the developmental pathway.

Further to these findings, it has been demonstrated that the resting BCR provides key survival signals to mature and transitional B-cells (24, 25, 27). Inducible IgH or CD79a ablation in $CD21^{+}$ mature B-cells resulted in their apoptotic clonal deletion (24, 25, 27). Therefore, the maintenance and survival of mature and transitional B-cells demonstrate a strict dependency not only upon the presence of the BCR but also upon its ability to signal. These observations collectively point toward a signalling role for the BCR in its resting state, termed a tonic signal (see appendix A1 for further details). The tonic signalling mode of the Pre-BCR and BCR has been demonstrated to occur in an antigen-independent manner, resulting from basal signals emanating upon assembly of the BCR (19, 23). However, the role of antigen signalling in triggering the differentiation of T2 B-cells to mature B cells remains unclear (19, 40).

1.2.2.2 Negative selection

Although the Pre-BCR and BCR play a key maintenance role during B-lymphopoiesis, they also participate in the clonal deletion of autoreactive clones, and in doing-so impart self-tolerance. In humans B-lymphopoiesis culminates in the daily deposition of around $2x10^{7}$ immature B cells into the periphery (20, 21, 40, 41). Of these, only around 10% ($2x10^{6}$) will reach secondary lymphoid organs, and only a further 1% of which will subsequently enter the recirculating mature B cell pool ($1x10^{4}$) (20, 21, 40,

41, 43). Such losses are attributable to powerful negative selection mechanisms inducing the clonal deletion of immature B cells (20, 21, 40, 41). In fact negative selection occurs throughout B-cell development, as depicted in figure 1.2, and is responsible for imparting self-tolerance upon the humoral response (20, 21, 40, 41, 44).

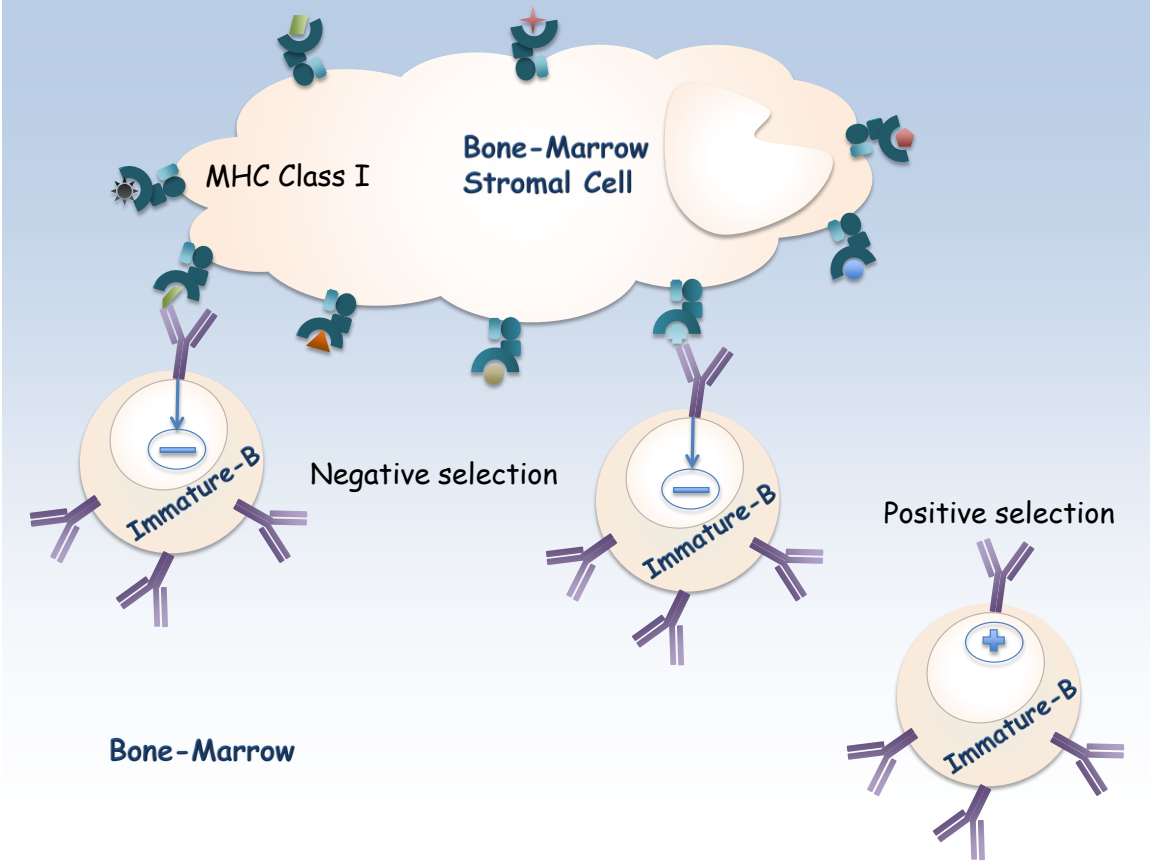

Figure 1.2 Schematic depicting positive and negative selection of immature B-lymphocytes

Engagement of BCRs via self-antigen expressed on the surface of bone marrow stromal cells invokes BCR signalling in the absence of co-stimulation in an inappropriate location and, therefore, drives negative selection. In contrast, non-autoreactive immature B-lymphocytes receive key tonic signals emanating from the BCR resulting in their positive selection.

Initial observations of negative selection were made by Hartley et al who crossed transgenic (tg) mice expressing anti-Hen egg Lysozyme (HEL) specific BCRs and HEL expressing mice (48). Subsequent phenotypic observation of their progeny revealed a complete lack of mature B-cells. Therefore, it was determined that powerful, central tolerance mechanisms prevented autoreactive clones reaching the periphery, via clonal deletion at an early developmental stage (48).

Such negative selection occurs in response to BCR activation in an inappropriate cellular context, for example, in the absence of co-stimulatory signals or at an inappropriate developmental stage (20, 21, 39-41, 43, 44). Such inappropriate signals are indicative of autoreactivity and therefore, steps are taken to remove the clone (40, 41, 43).

At least three distinct mechanisms exist for the removal of autoreactive clones: clonal deletion via an apoptotic demise, cellular anergy and receptor editing (4, 20-22, 39-41, 43, 44). The molecular mechanisms governing BCR-induced apoptosis are described in detail in section 2.8. It is proposed that the nature of the inappropriate antigen, and the affinity with which it is bound, dictates which of the three methods of clonal deletion is selected (39). A high-affinity interaction with membrane-bound antigen ultimately results in the apoptotic deletion of the clone (4, 20-22, 39-41, 43, 44). In contrast, low-affinity interaction with soluble antigen preferentially engages anergy (a prolonged period of cellular inactivity) or receptor editing (secondary light chain rearrangement) (39).

1.2.3 Antigen-dependent B-lymphopoiesis

Antigen-driven BCR activation stimulates further maturation of mature B-cells to effectors capable of immunoglobulin secretion and immunological memory (4, 22). Therefore, attainment of mature B-cell status marks the beginning of the antigen dependent phase of B-cell development. At rest, splenic mature naïve B-cells segregate into T-cell deficient B cell rich areas, such as the primary follicles, owing in part to CXCL-13 -mediated chemotaxis (41, 49, 50) (4, 41, 50, 51). Such segregation is maintained until antigen-dependent BCR signalling permits migration to the B/ T-zone boundaries (4, 22, 49, 50, 52, 53). Although B-lymphocyte activation may proceed in the absence of T-cell help (Thymus-independent antigens) (4, 22) here we will focus upon activation mediated solely by thymus-dependent antigens.

1.2.3.1 B-cell activation via B: T cell collaboration

In addition to its role in antigen-independent lymphopoiesis, the BCR is fundamental in driving further B-cell maturation in an antigen-dependent context.

Antigen-driven BCR signalling engages a programme of enhanced survival, proliferation, antigen presentation and upregulation of factors responsible for CD4+ T-cell activation (50, 52, 53). Upregulation of CC chemokine receptor (CCR)-7, the T-cell zone chemokine receptor, drives migration of B-cells to the B/ T-zone boundary via Chemokine (c-c motif) ligand (CCL)-21-mediated chemotaxis (4, 22, 49, 50, 52, 53). Migrating B-cells are met at the boundary by antigen experienced $CD4^+$ T-helper cells (T_H), which migrate to the B/T zone boundary via CXCL13-mediated chemotaxis in response to antigen (50, 54). Co-localisation of antigen-specific T_H and mature B-cells drives the formation of monogamous conjugates, allowing reciprocal cellular activation, as demonstrated in figure 1.3 (4, 22, 50, 52).

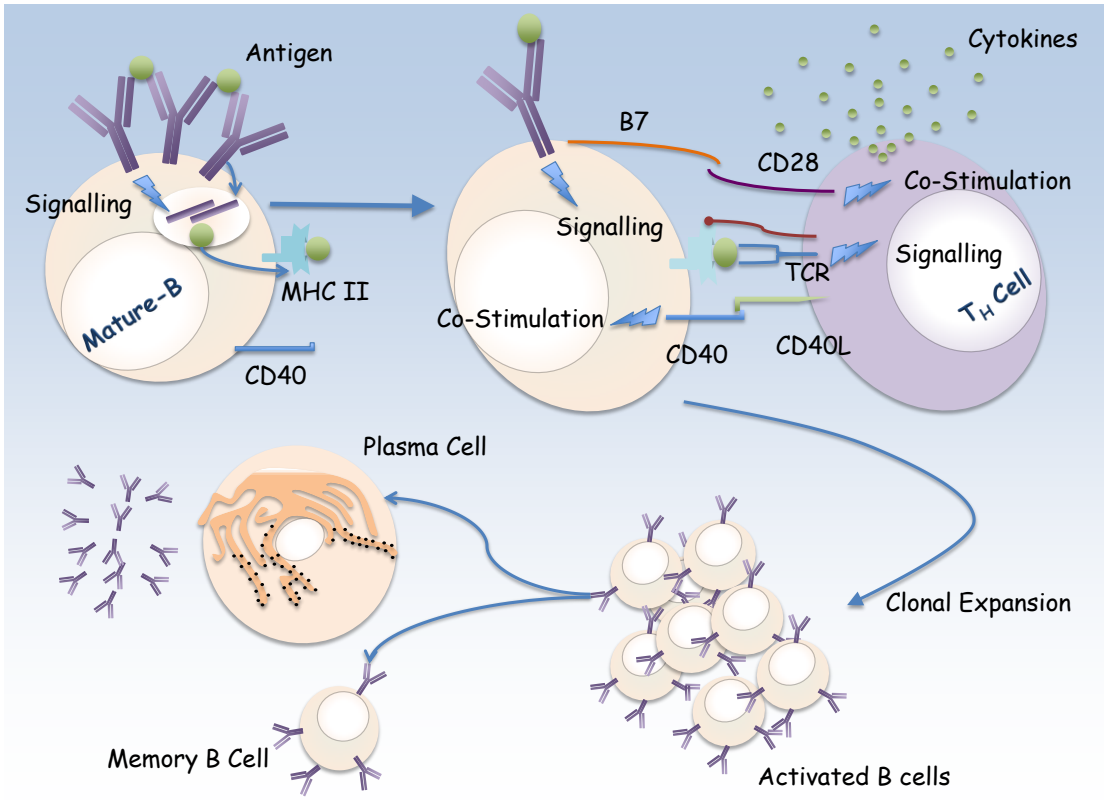

Figure 1.3 Schematic depiction of antigen dependent B-lymphopoiesis

Antigenic engagement of the BCR results in presentation of internalised antigen to T_H lymphocytes. Subsequent formation of monogamous conjugates with activated T_H lymphocytes provides co-stimulation, predominantly via CD40L: CD40, CD28: B7 interactions, and drives clonal expansion and differentiation of the B-cell to plasma or memory B-cells.

Such reciprocal activation is largely dependent upon the ability of the BCR to endocytose antigen and enter the endosomal antigen-processing pathway. Such processes culminate in major histocompatibility complex (MHC) class II-mediated

antigen presentation to $CD4^+$ T-cells, and T-cell receptor (TCR) activation (signal one) (4, 22, 50, 55, 56). Concomitantly B-cell activation triggers up regulation of the co-stimulatory factor B7, thus providing signal two to the $CD4^+$ T-cell, via interaction with CD28, and in collaboration with TCR signalling permits T-cell activation (50). Subsequent up regulation of $CD4^+$ T-cell CD40 ligand (CD40L) and IL-4 release provides B-cell co-stimulation, via interactions with CD40 and cytokine receptors respectively, allowing cellular proliferation and differentiation (4, 22, 50). Activated B-cells subsequently proliferate, forming foci, and differentiate to IgM-secreting plasma cells and memory B-cells (4, 22, 50, 57).

1.2.3.2 Affinity maturation and the germinal centre reaction

Characteristically, the humoral response exhibits an increase in immunoglobulin avidity as the response progresses (4). Termed affinity maturation, this process is facilitated by mutation and selection of clones encoding high affinity antibody within structures known as germinal centres (GCs) (57, 58).

Several days after activation, B and T_H cells migrate to primary follicles and rapidly proliferate forming a GC (57, 59). GCs provide an appropriate microenvironment for B-lymphocyte proliferation, activation and survival alongside production of high affinity, class-switched antibody (57-59).During the period of rapid proliferation GC B-lymphocytes down regulate surface BCR and progress through the centroblast and centrocyte stages whilst experiencing somatic hyper mutation (SHM), a sustained period of mutation centred upon the antigen-binding Ig hyper variable regions, undertaken by the enzyme activation-induced deaminase (AID) (4). SHM leads to an enhanced diversity of antigen binding sequences producing clones with both higher and lower affinity than the original (57-59). Subsequent selection of high affinity clones is thought to occur upon interaction with follicular dendritic cells (FDCs) (4, 22, 57-59). It is proposed that FDCs express high levels of the inhibitory Fc receptor (CD32b) and therefore, retain immune-complexes (Ab: Antigen complexes) on their cell surface (4, 22, 57). Antigen specific B-cells subsequently experience competition for immune complex binding allowing only clones of the highest affinity to experience subsequent antigen-mediated activation (4, 22, 57). However, a recent study conducted by Victora

et al highlight that high affinity clone selection may in fact be regulated by competition for T-cell help rather than antigen binding (60).

Furthermore, clones also experience class-switch recombination, where variable regions are spliced onto alternate constant regions allowing production of alternate Ig isotypes (4, 22). Subsequently, differentiation of high affinity clones to IgM and IgG secreting plasma cells or memory B-cells ensure production of high affinity Ig and immunological memory (4, 22, 57-59). Intriguingly, all such processes outlined above are largely determined by the molecular repercussions of BCR signalling, which we shall now consider.

1.3 B-cell receptor signalling

The BCR comprises a membrane-spanning immunoglobulin molecule (mIg) non-covalently associated in a 1:1 ratio with the CD79a/b heterodimer (61). Since the mIg cytoplasmic tail contains only three residues (of the sequence KVK), it is proposed that it is the CD79a/b heterodimer that is responsible for transducing antigen binding at the cell surface into intracellular signals and changes in cellular behaviour (62-64). Whilst the biochemical pathway initiated downstream of antigen binding has been extensively studied, the exact mechanism by which antigen-binding influences the BCR to initiate signalling remains highly debated.

1.3.1 Signal initiation

1.3.1.1 Antigen binding

Recent advances in the field can be consolidated to support one of two conflicting models regarding the mechanism by which antigen influences the BCR. Namely the conformation induced oligomerisation and dissociation activation models (61, 62, 65-67).

The conformation-induced activation model is supported by fluorescence resonance energy transfer (FRET) studies, which propose that antigen drives oligomerisation of the BCR forming microclusters from its monomeric resting state (61, 65, 67). However, microcluster-residing BCRs subsequently show a slight reduction in FRET, between acceptor and donor labelled mIg and CD79a, indicating that a substantial

conformational change of the cytoplasmic portion of the BCR is induced upon entry into microclusters (61). It is suggested that oligomerisation of the BCR is associated with antigen-induced exposure of homotypic aggregation motifs found within the Cμ4 domain of IgM, and that subsequent conformational changes are instigated leaving the BCR in a more "open" configuration. It is proposed that this "open" configuration facilitates activation of downstream kinases (61, 65, 67). However, since FRET is relatively insensitive to low affinity transient interactions it is unclear from these studies whether the BCR exists in a monomeric form at rest or as a transient low-affinity oligomer (62).

In direct contradiction however, Yang and Reth propose an alternative hypothesis in the form of the dissociation activation model. Recent bi-fluorescence complementation (BiFC) and native-polyacrylamide gel electrophoresis (PAGE) studies suggest that in the absence of antigen the BCR actually exists in an homo-oligomeric form (66). Such an observation has been described previously and is the source of much debate within the field (68). Interestingly, disruption of the formation of resting-state oligomers, by site-directed mutagenesis, resulted in the production of hyperactive BCR in comparison to its oligomeric form (66). Therefore, Yang and Reth propose that an antigen-influenced equilibrium exists between two BCR states, comprising both an autoinhibitted oligomeric state and a signalling competent monomeric state (66). In the absence of antigen the equilibrium largely favours the autoinhibitted oligomeric state, resulting in the presence of only a small population of signalling competent open monomers. It is predicted that these transient signalling competent monomers are responsible for providing resting-state tonic signals (66). Subsequent antigen binding is proposed to force oligomers apart, remove oligomeric auto-inhibition and permit receptor signalling (66). Such a model explains the observation that antigens rarely exhibit multiple epitopes per molecule, which would be required for efficient activation according to the cross-linking model. Therefore, such an occurrence would permit the same cellular outcome regardless of the nature of epitope spacing and/ or frequency. However, the work of Reth and Yang was undertaken using artificially expressed BCRs in both mouse and *Drosophila* cell lines. Therefore, whether these predictions hold true for endogenous BCR in human cells

remains to be determined. Furthermore, since dimerisation-induced association between the N and C-terminal halves of CFP and YFP results in covalent bonding, the BiFC assay itself may favour formation of resting state-oligomers. Therefore, further studies are required to definitively characterise the exact antigen-induced mechanisms that trigger BCR signalling.

1.3.1.2 Membrane proximal events

Regardless of the method of antigen-induced activation, signalling has been proposed to ensue upon antigen-driven translocation of the BCR to sphingolipid and cholesterol-rich lipid Rafts within the plasma membrane (69, 70). Contained within lipid Rafts are concentrates of the Sarcoma (Src)-family protein tyrosine (Tyr) kinases (SFPTKs) Lck-yes related novel kinase (Lyn), p59 Fyn (Fyn), B-lymphocyte kinase (Blk) and, lymphocyte-specific kinase (Lck) which anchor to the plasma membrane via acylation (70). Upon antigen-driven BCR and SFPTK co-localisation, SFPTKs gain access to and phosphorylate Tyrosine (tyr)-containing motifs within the cytoplasmic domains of CD79a and CD79b (71). Such motifs, known as Immunoreceptor tyrosine-based activation motifs (ITAMs), possess two precisely spaced tyrosine residues within the D/E X_7 D/E X_2 Y X_2 L/I X_7 Y X_2 L/I consensus sequence (64, 72). Phosphorylated ITAM tyrosines subsequently provide binding sites for src-homology-2 (SH2)-domain containing effectors, as depicted in figure 1.4, allowing formation of the BCR signalosome and recruitment of downstream kinases (64).

Mechanistically, ITAM phosphorylation appears to occur with a degree of asymmetry since preferential phosphorylation of N-terminal ITAM tyr residues is evident (73). However, ITAM phosphorylation also appears to demonstrate co-operativity as point mutation of the C-terminal ITAM tyr led to a reduction in N-terminal ITAM tyr phosphorylation (64).

Despite this apparent co-operativity, around 80% of CD79a / CD79b ITAMs demonstrate phosphorylation only at the N-terminal tyr following anti-IgM treatment, therefore, suggesting that only a minor proportion become dually phosphorylated (73).

However, It is apparent that CD79a and CD79b are not functionally equivalent.

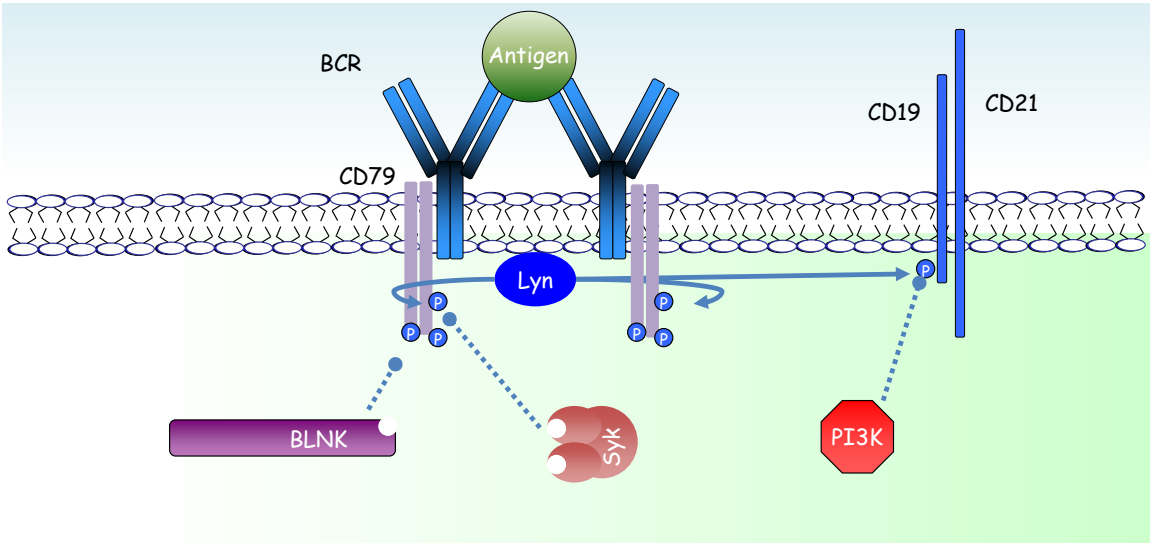

Figure 1.4 Membrane proximal BCR signalling
Upon antigenic engagement of the BCR, SFPTK activity is directed toward Tyr residues found within the ITAM motifs of CD79a/b heterodimers and CD19. The resultant phosphotyrosine residues form key binding sites for SH2 domain-containing effectors and adapters, including PI3K and Syk, facilitating their activation. Such steps permit the formation of a key BCR signalosome, a prerequisite for downstream signalling. Arrows denote direct phosphorylation, dashed lines represent recruitment.

Mutation studies examining the role of the C-terminal ITAM tyr residues of CD79a and CD79b reveal that only loss of the CD79b C-terminal tyr imparts a significant signalling deficiency (73). The reason for this discrepancy remains unknown. (Although, it is likely that CD79a and CD79b exhibit differential recruitment of downstream effectors.)

1.3.1.3 Setting the threshold for SFPTK activation

Simplistically, the threshold for B-cell activation reflects the strength of antigenic stimulus required to trigger the BCR-signalling programme. The threshold is defined at the molecular level by the relative extent of basal SFPTK activity. Such regulation is achieved by phosphorylation of the SFPTK C-terminal regulatory tyr (Y508 in Lyn), which resides within an SH2-domain binding motif (74, 75). The phosphorylated C-terminal tyr is subsequently engaged intramolecularly by the SH2 domain, occluding the domain and preventing further substrate binding (74). The activities of C-terminal Src kinase (CsK) effectively raise the B-cell activation threshold since SFPTK activity is reduced. Subsequent removal of the inactivating phosphorylation by the CD45 phosphatase, de-represses kinase activity and thus reduces the cellular activation threshold (75).

1.3.1.4 Linking CD79a/b to kinases

Although relatively infrequent, it is the dually phosphorylated CD79a/b ITAMs that subsequently propagate the initial membrane proximal signal via recruitment of the dual SH2-domain containing kinase spleen tyrosine kinase (Syk) (73, 76). Syk activation represents a crucial step in BCR signal transduction since loss of Syk severely impairs downstream effector activation (46, 47). Upon recruitment, Syk is phosphorylated at six distinct sites namely tyr 130, tyr 317, tyr 342, tyr 346, tyr 519, and tyr 520 leading to a ten-fold increase in kinase activity (76, 77). Phosphopeptide mapping studies, utilising Lyn-deficient and kinase dead Syk mutant DT40 lymphoma cells, demonstrate Lyn-dependent phosphorylation of linker region tyrs 317, 342, and 346 (76, 77). In contrast, the remaining tyr phosphorylation sites experience Syk-mediated autophosphorylation (76, 77). Interestingly however, tyr 317 appears to function as a negative regulator of Syk activity since Y317F mutant Syk demonstrates hyperactivation in response to BCR engagement (77).

Syk activation appears to occur congruently with activation of the tec-family kinase Bruton's Tyrosine Kinase (Btk) (78). Similar to Syk, functional Btk is required for normal BCR signalling, B-cell development and production of an effective hummoral immune response (79, 80). Furthermore, severe immunodeficiencies in both x-linked immunodeficiency (XID) mice and x-linked agammaglobulinaemia (XLA) patients have been attributable to point mutations of Btk (81) (82). XID mice commonly exhibit point mutations of the Btk Plekstrin homology (PH) domain, resulting in blockade of early B-cell development (82). Such observations imply that Btk activation proceeds in a PH domain-dependent manner. Therefore, phospholipid binding and recruitment to the plasma membrane likely represent key regulatory steps in Btk activation.

Btk activation and translocation to the plasma membrane is almost entirely dependent upon the activity of PI3K and the Btk PH domain (83-86). Typically, PI3K itself becomes activated upon BCR engagement via SFPTK-mediated phosphorylation of an ITAM motif centred upon tyrs 484 and 515 of the BCR co-receptor CD19 (83). Subsequent recruitment of the p85 regulatory subunit of PI3K, via its SH2 domain, permits kinase activation via co-localising enzyme with substrate (83). PI3K-mediated conversion of Phosphatidylinositol-4,5-bisphosphate (PIP_2) to Phosphatidylinositol-3,4,5-

trisphosphate (PIP_3) leads to PH domain-mediated Btk plasma membrane translocation (83-86). Subsequently the kinase activity of Btk is upregulated by SFPTK-mediated phosphorylation and autophosphorylation (83, 85, 86). Interestingly it appears as though the CD19 co-receptor ITAM plays a more fundamental role in PI3K activation than that of the BCR. Such an observation may explain the phenotype of $CD19^{-/-}$ mice which display reduced levels of mature B-cells, reduced proliferation in response to anti-IgM stimulation and an enhanced basal level of B-cell death (87).

CD19 phosphorylation-mediated PI3K activation represents a key step in BCR signalling since it not only mediates activation of Btk but also that of Protein Kinase B (PKB)/Akt (88). Like Btk, Akt is targeted to the plasma membrane via interactions made between its PH-domain and PIP_3 (89). Upon membrane-translocation Akt activation is ensured via two distinct activatory phosphorylation events at ser 473 and thr 308 (88-91). It has long been known that thr 308 phosphorylation is undertaken by 3-phosphoinisitide-dependent protein kinase-1 (PDK-1) which itself is activated upon PI3K-mediated PIP_3 production (91). However, the nature of the ser 473 kinase remained elusive for many years. Surprisingly mammalian target of Rapamycin (mTOR) was found to be the ser 473 kinase in *in vitro* kinase assays and *in vivo* (90). Best characterised in its complex with raptor, known as mTOR complex 1 (mTORC1), mTOR is responsible for the initiation of cap-dependent mRNA translation and resides downstream of Akt (92, 93). However, mTOR has also been described in a poorly understood complex with rictor known as mTORC2 (94). In fact, Sarbsaov et al demonstrated that the latter complex, mTORC2, is responsible for ser 473 phosphorylation and not mTORC1 (90). Akt is a key pro-survival kinase that influences the activity of numerous targets. Consequences of Akt activation of note include down regulation of glycogen synthase kinase-3 (GSK3) activity, sequestration of the pro-apoptotic BH3-only protein B-cell lymphoma 2 (Bcl-2) associated death promoter (Bad), inhibition of Forkhead transcription factor (TF) activity and up regulation of mTOR: raptor complex activity (17, 88, 93, 95-98).

1.3.2 Signal propagation

1.3.2.1 BLNK signalosome

The activation of Syk and Btk are pivotal events in BCR-signalling since they are responsible for signal propagation and recruitment of Ca^{2+} and mitogen activated

protein kinase (MAPK) signalling pathways (17, 99-102). Such propagation is achieved via assembly of a B-cell linker protein (BLNK)-centred signalosome, which functions as a scaffold, permitting further protein: protein interactions between phosphotyrosine binding adaptors and downstream effectors (17, 99-103).

The exact mechanism by which BLNK is recruited to a membrane proximal location is currently unclear. Kayak et al propose that BLNK is recruited directly to CD79a via an interaction between its SH2-domain and the non-ITAM Tyr 204 of CD79a, which is presumably phosphorylated by SFPTKs (103). However, it has been demonstrated that loss of the BLNK SH2 domain does not markedly impair its BCR-induced-phosphorylation (104). Therefore, an additional layer of complexity linking BLNK to CD79a/b heterodimers is likely. It has recently been demonstrated that the membrane spanning CKLF-like MARVEL transmembrane domain-containing protein-7 (CMTM7) may function as a link between CD79a/b heterodimers and BLNK (105). Such studies relied upon the observation of co-immunoprecipitation of CMTM7 alongside BLNK, Syk and IgH chains. However, the authors use 1% NP-40 containing lysis buffers for immunoprecipitation (IP), a concentration known to influence protein: protein interactions (106). Therefore, further detergent-free IP studies are required to confirm such a link. Furthermore, such observations were made under conditions of forced CMTM7 expression. Therefore, it remains unclear whether endogenous CMTM7 plays such a role in BCR signalling.

Regardless of the exact nature of recruitment, upon BCR engagement BLNK translocates to a membrane proximal location and in doing-so comes into close proximity with CD79-associated active Syk, as demonstrated in figure 1.5 (76, 103).

As a result BLNK undergoes at-least 5 distinct Syk-dependent tyr-phosphorylation events, forming multiple SH2-domain binding sites (100-102). Subsequent recruitment of phosphor-tyrosine (ptyr)-binding adaptor and effector proteins forms a BLNK-centred multi-pathway signalling complex including Phospholipase Cγ2 (PLCγ2), Vav, Btk, growth factor receptor-bound protein-2 (Grb2) and non-catalytic region of the

tyrosine kinase adaptor protein (Nck) (99-102).

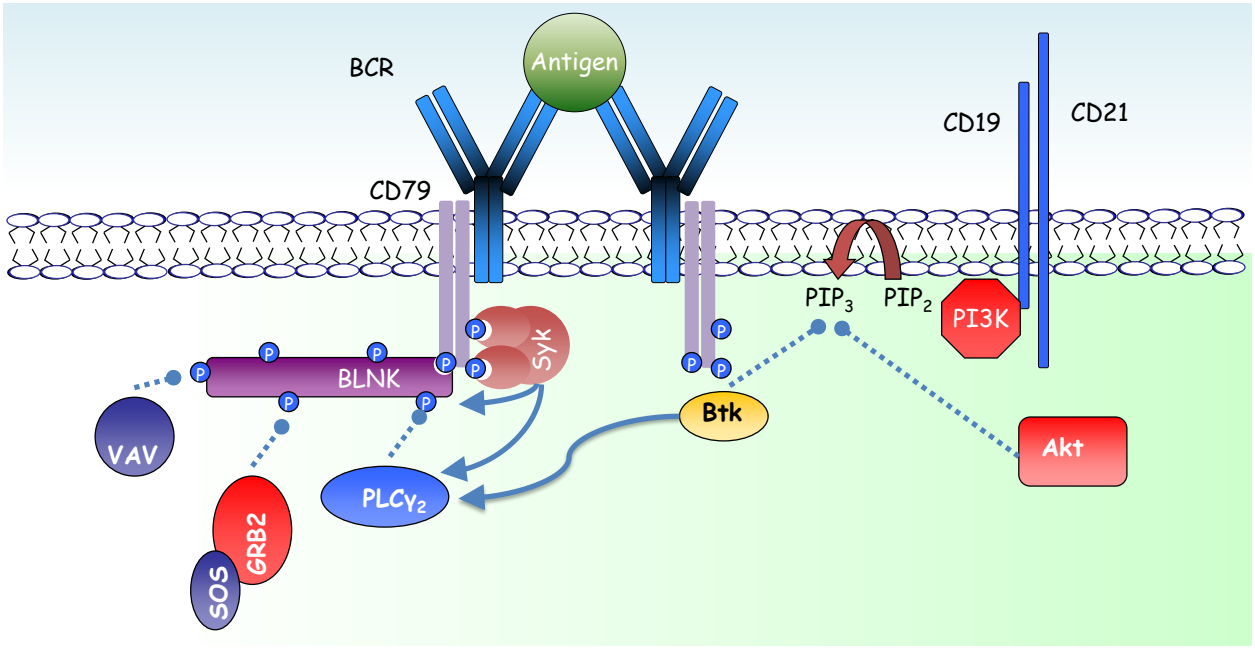

Figure 1.5 Formation of the BLNK signalosome
SFPTK-mediated CD79a/b heterodimers ITAM phosphorylation drives formation of a BLNK centred signalling complex. Syk mediated-BLNK phosphorylation provides specific docking sites for SH2-domain containing adapters and effectors. Furthermore, PI3K-mediated PIP3 production recruits both Btk and Akt to membrane proximal locations, facilitating their activation. Arrows denote direct phosphorylation, dashed lines represent recruitment.

The formation of such a complex links BCR signals to multiple downstream pathways resulting in effector activation and modification of cellular fate. The process of BLNK-signalosome construction also experiences negative regulation mediated by SH2-domain containing phosphatase-1 (SHP-1). SHP-1 mediated phosphotyrosine dephosphorylation of multiple substrates, including BLNK and ITAMs, leads to the damping down of BCR-signalling thereby promoting BLNK signalosome disassembly (107).

1.3.2.2 Phospholipase Cγ2 signalling

Following initiation, the BCR signal is potentiated and linked to downstream effectors via an increase in intracellular Ca^{2+} concentration ($[Ca^{2+}]_i$) achieved upon mobilisation of intracellular Ca^{2+} stores (17, 108-110). Initiation of Ca^{2+} signalling is enabled by the phospho-tyrosine dependent activation of the predominant Phospholipase C (PLC) isoform expressed in B-cells PLCγ2 (100, 111-113).

As a member of the phospho-inositide-specific family of phospholipases, PLCγ2 produces the second messengers inositol-1,4,5-trisphosphate (IP_3) and 1,2-diacylglycerol (DAG) from the plasma membrane component PIP_2 (114, 115). Subsequently, both IP_3 and DAG drive calcium mobilisation from intracellular stores, primarily the endoplasmic reticullum (ER), by interaction with IP_3 receptors and triggering activation of protein kinase C (PKC), respectively (114, 115). Similar to Btk and Akt, PLCγ2 activation requires plasma membrane translocation, allowing contact with its substrate, and tyr phosphorylation to achieve maximal activity (112, 116).

Recruitment of PLCγ2 to the BLNK signalosome drives translocation to the plasma membrane and leads to the co-localisation of PLCγ2 and active protein tyr kinases (PTKs) (47, 100, 102, 117). Subsequent PLCγ2 activation is driven via phosphorylation at tyr 753 and tyr 759 via an ill-defined mechanism resulting in enhanced PLCγ2 activity (113, 118). To date evidence points toward a role for Syk and Btk in PLCγ2 activation (47, 80, 113, 118). Both $Btk^{-/-}$ and $Syk^{-/-}$ DT40 lymphoma cell lines demonstrate a loss of PLCγ2 phosphorylation and Ca^{2+} mobilisation following BCR engagement which can be restored via reconstitution of WT Btk and Syk, respectively (47, 80). However, the role of Syk is unclear and challenging to dissect. Although $Syk^{-/-}$ cells demonstrate impaired PLCγ2 activation, Syk itself may not directly undertake activatory PLCγ2 phosphorylation. Instead the inability to activate PLCγ2 may be as a consequence of inefficient Syk-mediated BLNK phosphorylation and recruitment of PLCγ2 to a membrane proximal location.

The role of Btk in direct PLCγ2 activation however, is supported more clearly. The ability of Btk to phosphorylate, and therefore activate, PLCγ2 at tyr 753 and tyr 759 has been demonstrated both *in vitro* and downstream of BCR signalling *in vivo* (113, 118). However, additional PTKs may contribute to PLCγ2 activation since Btk siRNA knockdown and inhibition failed to completely block tyr 753 and tyr 759 phosphorylation (118). The findings of *in vitro* kinase assays highlight Syk, Src, Lck and Fyn PTKs as potential additional activators of PLCγ2 (113). A further intriguing concept is raised by Jumaa et al who demonstrate that Ca^{2+} mobilisation and PLCγ2 Tyr phosphorylation is not completely ablated in $BLNK^{-/-}$ mice (119). Therefore, PLCγ2

activation may not be strictly BLNK dependent and thus may undergo activation at an additional activation platform of unknown identity. Upon activatory Tyr phosphorylation, both the PLCγ2 PH and C2 domains target PLCγ2 to the plasma membrane allowing access to its substrate, and driving its enzymatic activity (114-116, 120).

1.3.2.3 Ca^{2+} mobilisation

BCR signalling generates a biphasic increase in $[Ca^{2+}]i$, the magnitude of which is directly proportional to the extent of receptor engagement and affinity of interaction (121). Initially a rapid transient spike in $[Ca^{2+}]i$ is observed followed by a prolonged low-level phase of raised $[Ca^{2+}]i$ termed the plateau (109, 121). Each individual phase reflects an increase in $[Ca^{2+}]i$ generated by two distinct mechanisms which differentially regulate Ca^{2+} sensitive pathways (108, 109).

The initial BCR-driven Ca^{2+} release is entirely dependent upon the activity of PLCγ2, via IP_3-mediated mobilisation of ER Ca^{2+} stores (122). Such Ca^{2+} stores are established and maintained via the activities of the sarcoplasmic/ endoplasmic reticulum ATPase (SERCA) via active transport of Ca^{2+} to the ER lumen, thus generating a significant electrochemical gradient (17, 92, 110, 120). Ca^{2+} store mobilisation is mediated via binding of IP_3 to the N-terminal region of the three conserved IP_3 receptors (IP_3R 1-3) (110, 122). Subsequent opening of a non-selective cation pore at the IP_3R C-terminus allows the release of ER Ca^{2+} into the cytosol (110, 122). Interestingly, SFPTKs potentiate IP3-mediated Ca^{2+} release via tyr phosphorylation-mediated upregulation of IP_3-R activity, in an interaction facilitated by B-cell scaffold-protein with ankyrin repeats (BANK) (123, 124). Additionally, regulation of the Ca^{2+} mobilisation machinery receives signal integration from the MAPK activation pathway, as outlined below. It has been demonstrated that BCR-mediated activation of Ras homologue family-member A (RhoA) positively regulates PIP_2 production via stimulation of phosphatidylinositol-4 kinase (PI4K) and phosphatidylinositol-5 kinase activities (PI5K) (125). Therefore RhoA may replenish PIP_2 levels at a BCR-proximal location thus, providing BCR-associated PLCγ2 with additional substrate and to maximise IP_3 production (125).

Ca^{2+} mobilisation via the above mechanism is solely responsible for generation of the transient spike in [Ca^{2+}]i and primarily results in activation of the nuclear factor kappa-light-chain-enhancer of activated B-cells (NF-κB) pathway, described below (108, 109).

The secondary plateau is achieved via influx of extracellular Ca^{2+} upon activation of the Ca^{2+} release activated Ca^{2+} channel (CRAC). Whilst studies directly assessing the impact of BCR signalling upon CRAC channels have yet to be performed, the specific molecular mechanisms linking ER Ca^{2+} depletion, mediated by other stimuli, to CRAC channel opening is becoming clearer. RNA interference (RNAi) studies highlight two key regulators of so-called capacitive Ca^{2+} entry in the form of stromal interaction molecule-1 (STIM1) and Ca^{2+} release-activated calcium modulator (ORAI), and recently their molecular functions have been elucidated (110, 126-128).

STIM1 is an ER-resident membrane spanning protein, which functions as a sensor of ER lumenal [Ca^{2+}] via its EF-hand domain (Ca^{2+} binding domain) (128, 129). It is proposed that resting ER localisation is ensured via specific Ca^{2+}: EF hand domain interactions, which upon lumenal Ca^{2+} depletion become disrupted (128, 129). Subsequently, STIM1 translocates to the plasma membrane forming aggregates known as puncta (128, 129). It is proposed that at this subcellular location STIM1 drives the tetramerisation of ORAI, which is found as a dimer at rest (130). In its tetrameric form ORAI is proposed to form a Ca^{2+} specific divalent cation channel and permit capacitive Ca^{2+} entry, although a role for other pore-forming proteins cannot be ruled out at this stage (130, 131). This distinct Ca^{2+} signal largely influences activity of the nuclear factor of activated T–cells (NFAT) pathway, outlined below (108, 109).

1.3.3 BCR-induced activation of molecular effectors

1.3.3.1 NFAT activation

BCR-signalling is capable of generating wholesale changes in B-cell behaviour, resulting from its ability to influence gene expression via activation of numerous transcription factor families. In order to convert membrane proximal BCR-signalling events to changes in gene expression, the BCR utilises raised [Ca^{2+}]i to activate the distinct but related transcription factor families NFAT and NF-κB (17, 108-110, 132). Although Ca^{2+} mediated activation is common to both pathways the nature of the Ca^{2+} signals

required for activation are significantly different (108, 109). Whilst NFAT activation requires extracellular calcium entry and prolonged increases in $[Ca^{2+}]i$, NF-κB activation requires only the intracellular Ca^{2+} store release provided by the initial ER-dependent transient Ca^{2+} spike (108, 109).

The NFAT-family of transcription factors encompasses five members (NFAT1-5) which bind target elements in DNA as homo or heterodimers (133). Transactivation of NFAT target genes is regulated primarily via nuclear exclusion. At rest NFAT is held in the cytoplasm due to phosphorylation of ser/ thr residues within four defined motifs comprising: two Ser-rich repeats (SRR1/2), a Ser-Pro repeat (SP repeat) and Lys-Thr-Ser (KTS) motifs (133-135). It is thought that nuclear exclusion is achieved by the phosphoserine-dependent masking of two NFAT nuclear localisation signal sequences (NLS) within the SP repeat motif (133, 134). NFAT dephosphorylation and subsequent nuclear translocation is achieved via Ca^{2+}/ calmodulin mediated activation of the phosphatase calcineurin (92).

Inactive calcineurin is found in close association with phosphorylated NFAT via interactions made between a region of its catalytic domain and the SPRIET docking sequence of NFAT (133, 136). However, calcineurin activity is inhibited due to occlusion of the active site by the intramolecular association of an α helical auto-inhibitory domain with the catalytic cleft (133, 136). Prolonged increases in $[Ca^{2+}]i$, such as that produced upon BCR signalling, result in the activation of calcineurin via the co-operative binding of four Ca^{2+} ions to the adapter protein calmodulin (92). Subsequent association with calcineurin triggers widespread conformational changes within the phosphatase, resulting in the displacement of the auto inhibitory domain and increases in calcineurin activity (133, 136) (92). Subsequently, NFAT phosphoserine and phosphothreonine residues are free to engage the calcineurin active site and become dephosphorylated (133, 136).

Upon translocation into the nucleus, NFAT influences transcription of numerous target genes via binding NFAT response elements alone or in concert with the unrelated transcription factor activator protein-1 (AP-1) (110, 133, 137). Such association with the c-jun n-terminal kinase (JNK) pathway-regulated AP-1 transcription factor reveals a

common theme in NFAT signalling, integration with MAPK signalling. Further integration is potentially provided via NFAT acting as a direct phosphorylation target of extracellular signal regulated kinase (ERK), 38 kDa MAPK (p38), JNK, casein Kinase 2 (CK2), GSK-3 and protein Kinase A (PKA) (133, 135, 138). Such phosphorylation events are believed to retain NFAT in the cytoplasm and therefore inhibit target transactivation (133, 135, 138). Further complexity is added by the fact that Akt down regulates GSK-3 activity and therefore, the PI3K pathway represents a positive regulator of NFAT signalling (17, 88). In summary, NFAT not only links BCR-induced Ca^{2+} signalling to changes in gene expression, but also represents a node of signal integration linking MAPKs with Ca^{2+} signals.

1.3.3.2 NF-κB activation

In addition to the NFAT family of transcription factors, BCR-signalling is linked to changes in gene expression undertaken by the NF-κB family, in a mechanism driven by the IP_3-mediated Ca^{2+} spike and DAG production (108, 109). BCR-induced Ca^{2+} transients appear to drive NF-κB activation upon substantial DAG production and subsequent activation of the ser/thr kinase PKC (139-142). Of the eleven reported PKC isoforms only a few, termed classical PKC, experience Ca^{2+} directed regulation that play the major role linking BCR-ligation to NF-κB activation (110, 140, 142, 143).

The regulation of PKC is elegant in its simplicity and is impacted by sequential interactions of various domains with components of the plasma membrane allowing translocation and interaction with its ligand DAG (120). At rest, PKC is inactivated by the intramolecular association of a non-phosphorylatable pseudo substrate sequence with the active site (120). Such inhibition is removed only upon Ca^{2+} driven translocation to the plasma membrane and interaction with anionic phospholipids via the C2 domain (120). Subsequent DAG binding, via the C1a/C1b domains, instigates global domain orientation changes resulting in the removal of the pseudo substrate sequence from the active site, thereby activating the kinase (120).

The NF-κB family of transcription factors comprises five members (p50, p52, Rel A, Rel B and cRel) that form dimers via Rel homology (RH) domain interactions (144). Although all are capable of binding target gene κB elements only Rel A, Rel B and cRel

are capable of recruiting co-activators and co-repressors via their transcription activating domain (143, 144).

NF-κB activation can be achieved via two distinct signalling pathways, outlined in figure 1.6, termed the canonical and non-canonical pathways. Each individual NF-κB activation pathway activates specific NF-κB dimers and therefore, leads to induction of a distinct group of target genes. However, BCR-ligation solely activates the canonical NF-κB pathway regulated by nuclear factor kappa-light-polypeptide gene in B-cells inhibitor (IκB) (110, 143, 145).

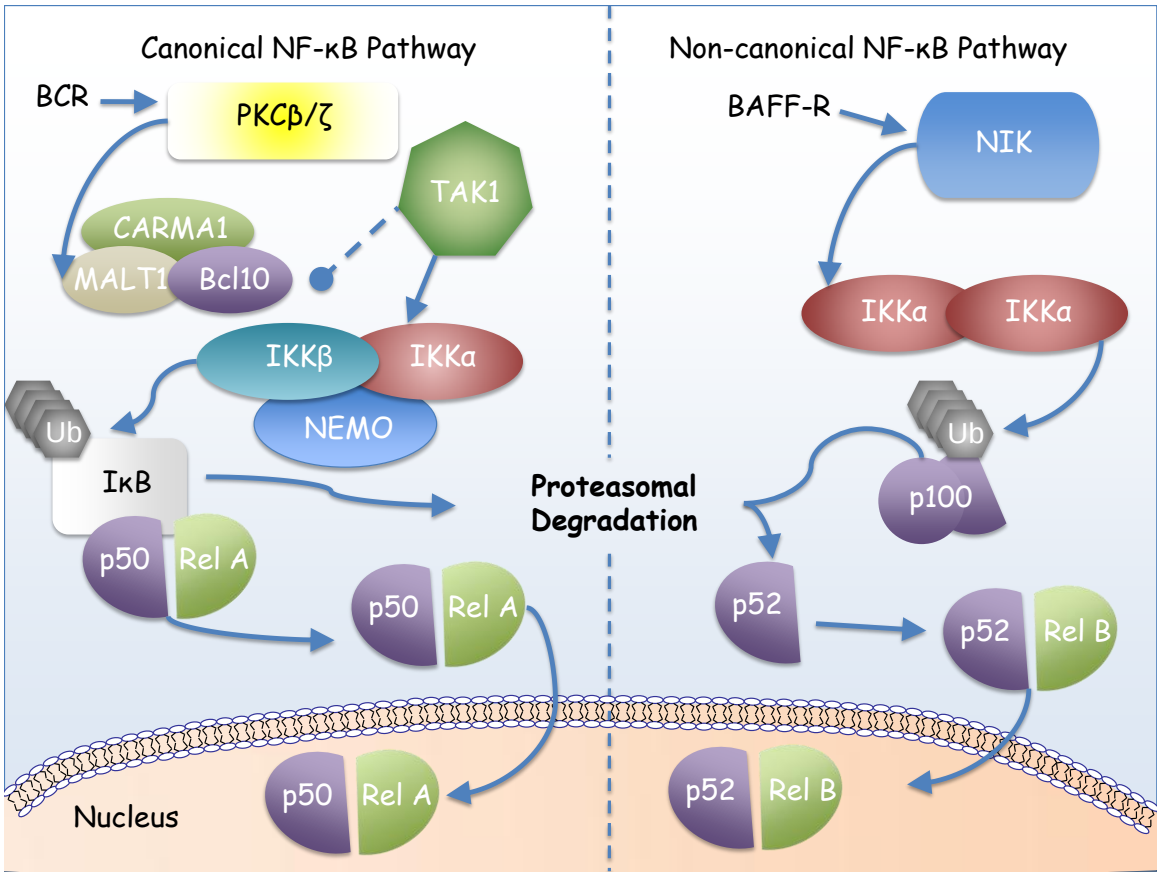

Figure 1.6 Schematic of the canonical and non-canonical NF-κB pathways

NF-κB activation is driven via two distinct pathways, termed the canonical and non-canonical pathways. Typically, the canonical NF-κB pathway activates p50: Rel A dimer whereas, the non-canonical pathway preferentially activates p52: Rel B. BCR signalling selectively activates the canonical NF-κB pathway whilst BAFF-R signalling leads to activation of NIK and the non-canonical pathway. Therefore, microenvironment signals co-operate with the BCR to provide activation of both arms of NF-κB signalling. Arrows denote direct phosphorylation, dashed lines represent recruitment. Ub = Ubiquitin.

Canonical pathway activation largely activates dimers of p50 and Rel A, which at rest associate with one of three negative regulators IκBα, IκBβ and IκBε (144). Crystal structures of IκBα p50: Rel A complexes demonstrate that IκBα masks the NLS of Rel

A, but not that of p50, whilst the nuclear export sequence (NES) of IκBα remains exposed (146). Therefore, in their inactive state NF-κB: IκB complexes shuttle between the cytoplasm and nucleus resulting in an inability to transactivate target genes (146). De-repression of NF-κB occurs via phosphorylation-mediated poly-ubiquitination and proteasomal degradation of IκB resulting in the release and nuclear translocation of NF-κB (143, 144). IκB phosphorylation is undertaken by IκB Kinase (IKK), a heterotrimeric complex of IKKα and IKKβ catalytic domains and their regulator NF-κB essential modulator (NEMO)/IκKγ (143, 144). Phosphorylation of IκB at conserved Ser residues results in polyubiquitination at Lys 48, proteasomal targeting and subsequent degradation (143, 144). Although usually heterotrimeric, IKK complexes formed from only IκKβ catalytic domains are sufficient to drive canonical NF-κB activation whereas, IκKα dimers are involved solely in non-canonical pathway activation (144). The non-canonical pathway utilises NF-κB inducing kinase (NIK) activated IκKα dimers that phosphorylate the p52 pre-cursor p100 targeting it for proteasomal processing resulting in production of active p52 that dimerises typically with Rel B (143, 144). Canonical NF-κB pathway activation transactivates numerous target genes associated with cellular survival such as B-cell Lymphoma-extra long (Bcl-xL) and Bcl-2-related protein A1 (A1) (17).

BCR engagement activates the classical PKC PKC-β which is responsible for linking BCR signals to the common NF-κB activation machinery (140). The exact molecular mechanism by which antigen receptor signalling activates NF-κB in B-cells remains poorly understood. However, the identity of the key molecular regulators is known namely: caspase-activation and recruitment domain (CARD) containing membrane associated guanylate kinase-1 (CARMA1), TGF-β-activated kinase-1 (TAK1), B-cell lymphoma 10 (Bcl10) and Mucosa-associated lymphoid tissue lymphoma translocation protein-1 (MALT1) (108, 139, 140, 142, 143, 147, 148). It is known that in BCR-stimulated cells PKCβ undertakes phosphorylation of CARMA1, which indirectly links CARMA1 to TAK1 (140, 142). By analogy to the TCR, it is suggested that CARMA1 phosphorylation drives formation of the so-called CBM complex, a molecular complex involving CARMA1, Bcl-10 and MALT-1 (142, 149). Indeed, mice deficient in any one of the CBM complex constituents demonstrate a significant impairment of mature B-cell

development, survival and responses toward antigen-receptor stimulation (139, 147, 148). It is suggested that the CBM complex recruits the E3-ubiquitin (Ub) ligase TNF receptor associated factor (TRAF) 6 and the E2 Ub enzyme Ubc13-Uev1A which leads to the ubiquitination of TRAF6 itself and NEMO (149). In turn, TRAF6 ubiquitination is proposed to directly activate TAK1, by a poorly defined mechanism, which subsequently phosphorylates, and activates, IKKβ within the activation loop, leading to IκB phosphorylation, ubiquitination and proteasomal degradation releasing NF-κB subunits (149).

1.3.3.3 MAPK activation

BCR engagement is further linked to transcriptional regulation and wholesale cellular changes by the activation of the mitogen activated protein kinases (MAPKs) ERK, JNK and p38 as demonstrated in figure 1.7 (150).

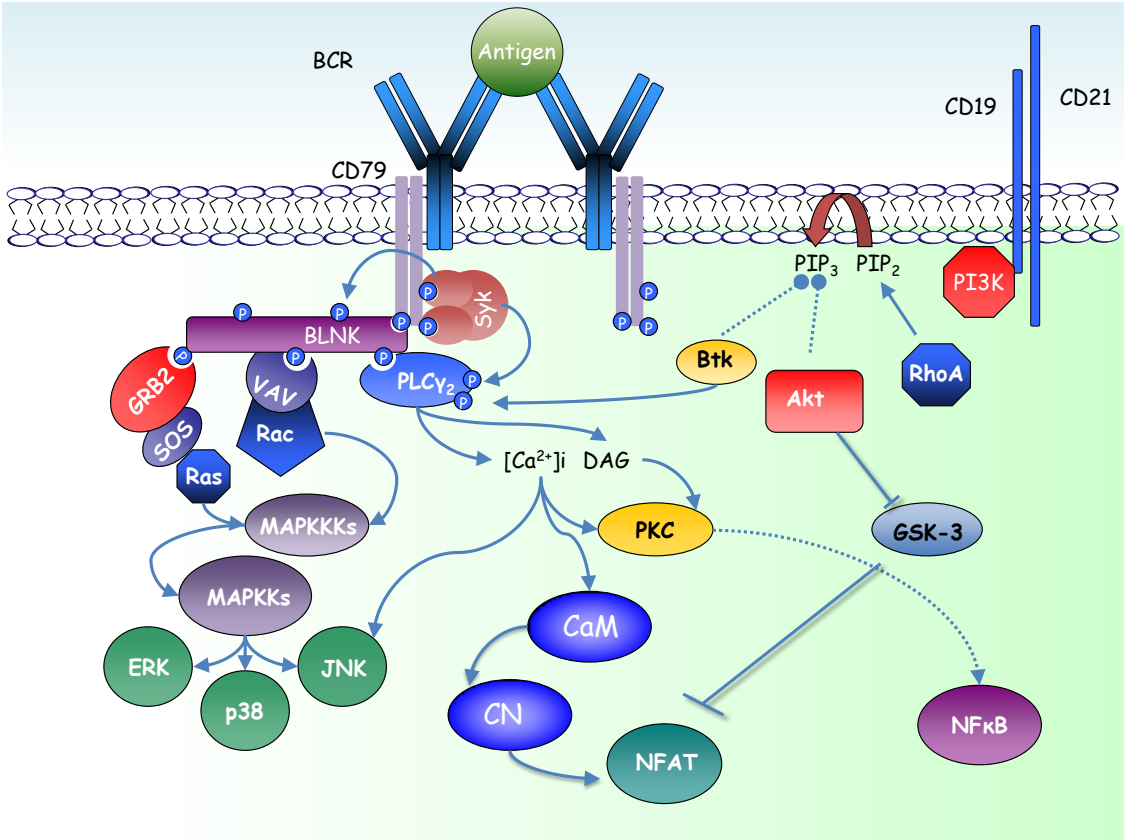

Figure 1.7 Linking the BLNK signalosome to downstream effectors

BCR ligation induces activation of numerous effector mechanisms including ERK, JNK, p38, NFAT, and NF-κB. Such events convert the membrane proximal signals into activation of transcription factors, thus influencing target gene transcription.

MAPK activation follows a general activatory phosphorelay system involving sequential phosphorylation of MAPK kinase kinases (MEKKs), MAPK kinases (MKKs) and ultimately MAPKs themselves (92, 150). Once active, MAPKs direct their activity toward a vast array of targets including transcription factors (TFs) and the apoptotic machinery (151-153). For instance, ERK regulates E-twenty six-like TF (Elk-1) and cellular myelocytomatosis viral oncogene (c-Myc), JNK influences c-Jun and activating transcription factor-2 (ATF-2) and p38 regulates ATF-2 and Myc-associated factor X (max) (17, 92, 150).

The ERK family, composed of the 44 KDa ERK1 and the 42 KDa ERK2, is classically activated downstream of growth-factor receptor tyrosine kinases (RTKs) via a phosphorelay system involving Son of sevenless (SOS), Rat Sarcoma GTPase (Ras), Raf (a MEKK) and MEK (an MKK) (92, 150). However, BCR signalling appears to display greater complexity, since ERK activation seems to be undertaken by at least two distinct pathways (the BLNK dependent and BLNK-independent pathways) (100-102, 117).

BLNK-independent ERK activation centres upon the Syk-dependent phosphorylation and recruitment of the SH2-domain containing (Shc) adapter to the phosphorylated ITAM of CD79a (154, 155). Membrane proximal Shc subsequently permits formation of an SH2-domain-dependent complex via sequential binding of GRB2 and SOS, the classical activators of the ERK pathway (154, 155). However, $Shc^{-/-}$ DT40 lymphomas display normal BCR-mediated ERK activation, thus Shc appears to be dispensable for ERK activation (101). Such experimental observations led to the development of the BLNK-dependent model, which demonstrates formation of the GRB2/SOS complex via recruitment to BLNK phospho-tyrosines (100-102).

Subsequent co-localisation of Ras and the guanine nucleotide exchange factor (GEF) SOS invokes widespread activatory conformational changes in Ras via SOS-mediated exchange of guanosine diphosphate (GDP) for guanosine triphosphate (GTP) (156). SOS appears to extend an α-helical domain into the nucleotide binding pocket of Ras disrupting binding sites for GDP α and β phosphates, thus driving dissociation (92, 156). Since GTP is approximately ten-fold more abundant in the cell/ cytoplasm, GTP

enters the active site via diffusion and initiates γ phosphate-dependent activatory conformational changes (92, 156). Since Ras is a membrane tethered GTPase, subsequent Raf interaction drives Raf plasma membrane translocation. Upon translocation, N-terminal regulatory domain de-phosphorylation occurs alongside p21 activated kinase (PAK) and Src-dependent ser 338 and tyr 341 phosphorylation respectively, resulting in activation (157). Sequential activation of MEK and ERK follow via dual phosphorylation of the kinase activation loops (157). However, Ras dominant negative mutant (Ras N17) expression in $GRB2^{-/-}$ DT40 lymphomas failed to completely ablate BCR-induced ERK phosphorylation (101). Such residual ERK activation displayed dependence upon PLCγ2-mediated DAG production, thereby implicating a possible role for PKC (101). PKC has been further implicated in ERK activation since the PKC activator phorbyl myristate acetate (PMA) triggers Shc and GRB2-independent activation of Ras and Raf (154, 158). Therefore in addition to BLNK-dependent/independent activation, ERK appears to display an alternate PKC-dependent activation pathway downstream of the BCR. Additional studies have also suggested a possible role for the Ras GEF Ras guanylyl releasing protein (RasGRP), which displays DAG-dependent plasma-membrane translocation upon BCR ligation resulting in co-localisation with Ras and enhanced activity (158).

Significantly less well-defined mechanisms link membrane proximal BCR signalling events to activation of JNK and p38 MAPKs. Reportedly, both JNK and p38 activation is facilitated by the Rho-family GTPase Ras-related C3 Botulinum toxin target 1 (rac-1) in complex with its GEF Vav located upon the phosphorylated BLNK scaffold (101, 117). Presumably Rac-1 induces activation of numerous MEKKKs which in-turn lead to phospho-relay-mediated JNK and p38 activation. Interestingly, JNK activation demonstrates a dependency upon increases in $[Ca^{2+}]i$, whilst p38 exhibits a direct requirement for DAG generation (101, 159). The molecular mechanisms for such a dependency remain unknown. However, a role for PKC may provide the most-likely explanation (101). Although the mechanism remains largely unknown, Rac-dependent JNK and p38 activation is vital for the B-cell development and maintenance in the periphery since Rac1/ Rac2 dual knockout leads to developmental arrest at the immature B cell stage (160).

Although it is generally thought that MAPK activation takes place at a membrane proximal location, an intriguing recent study identifies endocytosed BCRs as key signalling platforms linking the BCR to downstream effectors (55). Whilst MAPKs appear to co-localise alongside endocytosed BCR, upon inhibition of endocytosis active MAPKs revert to a membrane proximal localisation (55). Such membrane proximal MAPKS however, demonstrate hyperactivation whilst PI3K exhibits hypoactivation downstream of BCR signalling (55). Therefore, endocytosed BCRs appear not only to provide a platform for MAPK activation, but also to directly influence the nature of kinase activation.

1.4 Apoptosis and Apoptotic signalling

Whilst it has been demonstrated that the BCR provides key survival signals at rest and upon antigenic challenge, the BCR is also capable of triggering an apoptotic cell death in response to inappropriate engagement (48).

The term apoptosis, originally coined by Kerr, Wylie and Currie in 1972, describes a morphologically defined form of cell death. Apoptosis is characteristically accompanied by cytoplasmic shrinkage, nuclear condensation and the production of small, intact, organelle-containing vesicles termed apoptotic-bodies or “blebs” (161). A lack of cellular rupture gives rise to a predominantly non-inflammatory cell death event, which is aided by rapid phagocytosis of apoptotic bodies (161). Although originally a morphologically defined process, it is now clear that apoptosis also exhibits conserved biochemical characteristics including: caspase activation and cleavage, loss of plasma membrane asymmetry, internucleosomal DNA fragmentation and mitochondrial outer membrane permeablisation (MOMP).

Since these early observations, it has become apparent that apoptotic signalling can occur by one of two distinct pathways (162-164). The intrinsic pathway is responsive to a wide-range of cell intrinsic death stimuli, such as DNA damage and oncogenic stress, and centres upon mitochondria as the key regulatory site, as depicted in figure 1.8 (162-164).

In contrast, the extrinsic pathway responds largely to cell extrinsic death stimuli, such as engagement of TNF-receptor family (TNF-R) death receptors, allowing immune

effector-mediated cellular deletion (162-164). Largely, activation of the extrinsic apoptotic pathway occurs independently of mitochondria and centres upon direct recruitment of pro-caspases to specific activation platforms. At such platforms, pro-caspase dimerisation results in formation of a functional active site allowing subsequent autocleavage and full activity followed by instigation of the caspase-dependent cell death program (162-165).

The intrinsic apoptotic pathway is subject to strict regulation by members of the Bcl-2 family. The Bcl-2 family comprises two functional groups, either pro-apoptotic or pro-survival, which can be further sub-divided according to the number of Bcl-2 homology (BH) domains possessed, of which four in total exist (BH 1-4) (162-165). The pro-survival subgroup each possess four BH domains and comprises Bcl-2, B-Cell lymphoma extra long (Bcl-xL), apoptosis regulator Bcl-w (Bcl-w), induced myeloid cell leukaemia (Mcl-1) and A1 (162, 163).

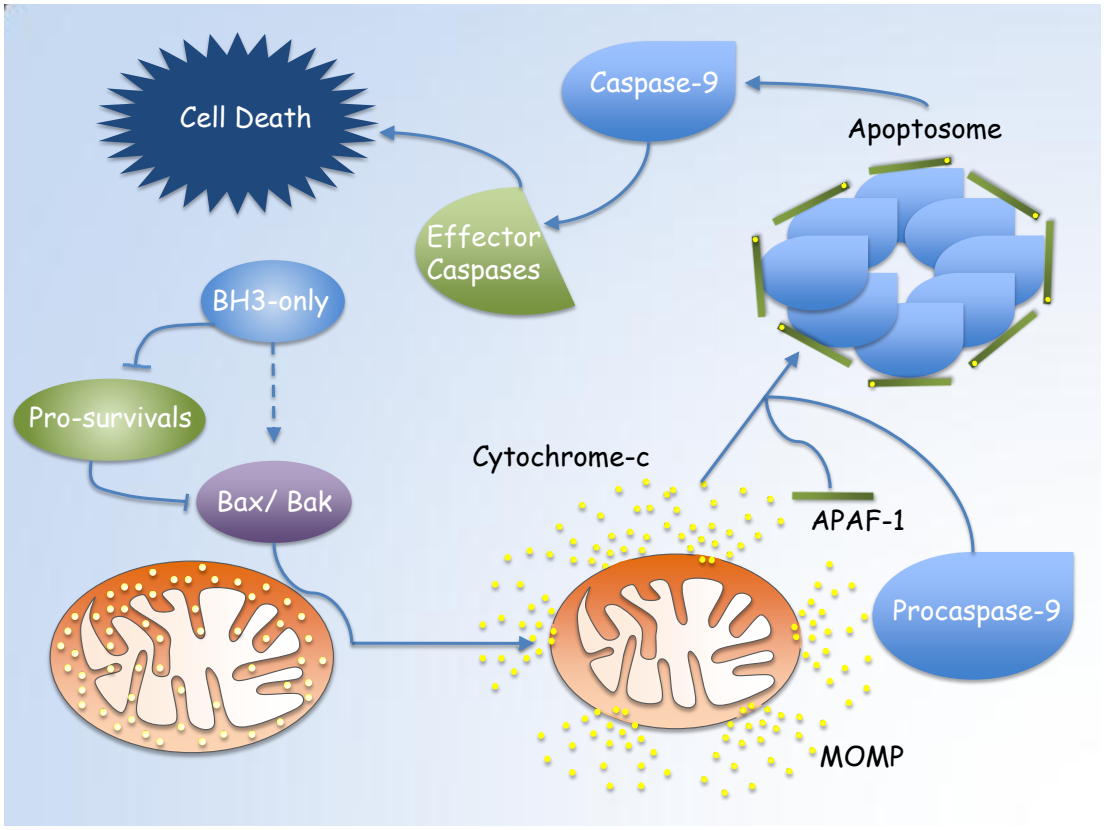

Figure 1.8 Schematic of the major events during intrinsic apoptosis
The pore-forming activities of Bax/ Bak facilitate permeablisation of the mitochondrial outer membrane allowing the release of Cytochrome-c into the cytoplasm. Cytochrome-c subsequently associates with APAF-1 and procaspase-9 in a heptameric structure, known as the apoptosome. Apoptosome formation drives procaspase-9 autocleavage and activation, resulting in initiation of the caspase activation cascade and ultimately cellular death. Bcl-2 family-members represent the central regulators of intrinsic

apoptosis via undertaking the molecular regulation of MOMP.

The pro-apoptotic subgroup can be subdivided into two further groups according to their BH domain content (162-164). Family members comprising at least 3 (BH1-3 and possibly BH4) BH domains form the Bax-like sub-group, containing Bcl-2-associated X-protein (Bax), Bcl-2 –associated killer protein (Bak) and Bcl-2 related ovarian killer (Bok). Although related structurally, no convincing data has been described alluding to a pro-apoptotic function for Bok and therefore, its function remains obscure (162-164). The BH3-only subgroup in contrast, solely contain the BH3 domain and comprises Bad, Bcl-2 interacting-death protein (Bid), Bcl-2-interacting killer (Bik), Bcl-2 interacting mediator of cell death (Bim), Bcl-2 modifying factor (Bmf), harakiri (Hrk), Noxa (Latin for damage), and p53 up-regulated mediator of apoptosis (Puma) (162-164).

1.4.1 Molecular regulation of Intrinsic Apoptosis

1.4.1.1 The role of Bax/ Bak in mitochondrial permeablisation

The nature of the mechanistic processes regulating Bax/ Bak homo-oligomerisation and MOMP remain controversial owing to the presence of conflicting models. However, all models agree that the remaining Bcl-2 family members play a central role (162-164).

In healthy cells, Bax is a cytosolic protein that, upon apoptotic stimuli, translocates and inserts into the outer mitochondrial membrane alongside an additional mitochondrion-resident Bax-like protein Bak (106, 162, 163, 166, 167). Resting Bax is maintained in the cytosol via sequestration of the outer mitochondrial membrane-targeting α9 helix, within a pocket formed by the BH1 and BH3 domains (168). Cellular stress triggers substantial Bax-conformational changes resulting in the exposure of the α9 helix, driving mitochondrial membrane insertion and homo-oligomerisation (168). Since Bax Bak double knockout (dKO) cells demonstrate complete resistance to intrinsic apoptotic stimuli, Bax/ Bak homo-oligomerisation represents the rate-limiting step for MOMP and the induction of intrinsic apoptosis (169, 170). However, the process by which Bax/ Bak homo-oligomerisation is linked to MOMP remains poorly defined (171-173).

Initial studies appeared to support one of two mutually exclusive models. It was proposed that either Bax/ Bak homo-oligomers directly facillitate mitochondrial permeablisation via pore forming activities, or alternatively, indirectly via recruitment of a non-selective inner mitochondiral membrane channel, the mitochondrial permeability transition pore (mPTP) (171, 173-176). Thought to consist of the adenine nucleotide translocator, a voltage-dependent anion channel and cyclophilin D, mPTP opening was proposed to initiate efflux of mitochodrial matrix contents into the inter-mitochodrial membrane space, triggering mitochondrial swelling and ultimately outer membrane rupture (176). Such rupture would subsequently allow release of apoptogenic factors from the inter-mitochondrial membrane space and trigger downstream effectors. However, mice lacking vital components of mPTP respond normally to apoptotic stimuli, but intriguingly demonstrate significant resistance toward necrotic and ischaemia-reperfusion injury-induced cell death (177, 178). Furthermore, during apoptosis it has been demonstrated that release of apoptogenic factors occurs in a selective process not associated with complete rupture of the outer membrane (174). Collectively, these results point toward a role for mPTP in necrotic cell death (and possibly late apoptosis). In contrast, it appears as though apoptotic MOMP occurs via a more selective process, suggesting recruitment and opening of an outer mitochondrial membrane pore.

Using cell-free systems, it has been demonstrated that Bax/ Bak homo-oligomers are capable of forming pores, potentially as a subunit of a mitochondrial apoptosis-induced channel (MAC), through which apoptogenic factors may pass (174, 175, 179). Indeed, MAC appear to form during early apoptosis, demonstrates dependency upon Bax/ Bak expression and possess identical electrophysical charactersitics to Bax homo-oligomers (174, 179). However, a direct requirement for MAC in apoptogenic factor release *in vivo* has yet to be determined and therefore, its role remains ambiguous.

Interestingly, the pore-forming activites of Bax/ Bak-like proteins may not be solely attributable to the formation of a macromolecular protein channels (171, 180-182). Indeed, several studies attribute the process of MOMP to interactions made between Bax/ Bak-like proteins and phospholipids (171, 180-182). Such studies propose that Bax/ Bak homo-oligomers drive recruitment of phospholipids with positive intrinsic

curvature (i.e. their molecular structure results in the enhancement of membrane curvature) resulting in the formation of lipid pores (180, 181).

1.4.1.2 The molecular events downstream of MOMP

Regardless of the exact molecular mechanism, MOMP initiates a programme of cellular destruction, via both cysteine-aspartyl protease (caspase) dependent and independent events. Such cellular destruction is initiated upon release of apoptogenic factors including cytochrome-c, endonuclease G, apoptosis-inducing factor (AIF), and second mitochondrial-derived activator of caspases/ diablo homologue (SMAC/Diablo) from the inter-mitochondrial membrane space into the cytosol (162, 163, 183-186).

Caspases represent an evolutionarily conserved family of cysteine-aspartyl proteases responsible for proteolytic cleavage of vital intracellular components during apoptosis. Family members are produced as inactive zymogens and are subdivided into two structurally and functionally related sub-types, known as initiator and effector caspases. Whilst all caspases exhibit a common domain organisation, consisting of pro, large, and small domains (which are proteolytically separated during activation), initiators and effectors differ in the length of the pro-domain (162-164, 187).

Initiator caspases (comprising caspases 1, 2, 8, 9, 10, 11, 12) possess a long pro-domain and are responsible for instigation of a caspase activation cascade via proteolytic activation of effector caspases. Activation of initiator caspases generally proceeds via multimerisation, therefore, promoting auto-cleavage at aspartate residues within the pro: large and large: small domain boundaries (162-164, 187). The active protease demonstrates a tetrameric organisation, comprising 2 small and 2 large domains, with each domain contributing to the function of the protease. Whilst the long domain donates a cysteine residue to form the active site, the short domain is responsible for interactions with substrates and, therefore, imparts substrate specificity (162-164, 187).

In contrast, effector caspases (caspases 3, 6, and 7) possess a short pro-domain (consisting of only a few amino acids in some cases) and cleave vital cellular components upon activation, ultimately giving rise to the apoptotic morphology. At present, over 200 effector caspase substrates have been identified, including: PARP,

IκBα, ATM, PKC, Sp-1, Actin, Lamin A, Lamin B, Bcl-2, Bcl-xL, Raf, Akt, β-Catenin, and inhibitor of caspase-activated DNase (ICAD). Cleavage of which, irreversibly commits cells to a cellular death outcome (162-164, 187).

Primarily, intrinsic apoptosis unleashes the activity of caspases via formation of the caspase activation platform, known as the apoptosome (162-164). Comprised of a heptamer of cytochrome-c, apoptotic protease activating factor 1 (APAF-1) and procaspase-9 complexes, the apoptosome promotes dimerisation and activation of caspase-9, resulting in autoprocessing to the 39/ 37 kDa active fragment (162-164, 188). Caspase-9 subsequently proceeds to proteolytically activate executioner caspases, caspases-3, 6 and 7, which undertake the cellular destruction programme by cleavage of vital cellular components (162-164). Furthermore, SMAC/ diablo release potentiates caspase activation via removal of inhibitor of apoptosis protein (IAP)-mediated suppression of caspase activity (45, 162, 164, 186). However, additional apoptogenic factors released from the inter mitochondrial membrane space also facilitate apoptotic deletion of cells via caspase-independent means. For instance, endonuclease G and AIF release driveinternucleosomal DNA cleavage and nuclear condensation independently of caspase activity (183-186). Furthermore, the very act of mitochondrial permeablisation may lead to ATP depletion, which itself is cytotoxic if prolonged.

1.4.1.3 The Bcl-2 family: a rheostat?

Upon observation of a direct association between Bcl-2 and Bax that quelled Bax activity, it was proposed that prosurvival members of the Bcl-2 family effectively restrain the pro-apoptotic activity of Bax-like proteins by direct association (189, 190). It was, therefore, suggested that the relative Bax: prosurvival ratio was an important determinant of cell fate (189, 190). However, an additional regulatory element in the form of BH3-only proteins were shown to act as de-repressors of Bax therefore, the Bcl-2 family acted as a variable resistor to cell death, hence the model was termed the rheostat model (189, 190). However, the rheostat model fell from favour since it could not reconcile the experimental observation that in healthy cells Bax resides within the cytosol whereas Bcl-2 is localised to the mitochondrial and ER membranes (106, 162, 163, 166, 167). Furthermore, the resting Bax: Bcl-2 co-immunoprecipitation studies

that underlined the rheostat model were demonstrated to be as a result of detergent-induced conformational changes and not physiologically relevant (106, 166). How the Bcl-2 family regulates Bax in healthy cells remains relatively ambiguous to this sub-compartmentalisation anomaly. However, further development of apoptotic models have begun to shed light on this intriguing mechanism.

One such model, the indirect activation model, proposes that pro-survival Bcl-2 family members bind only mitochondrially localised Bax/ Bak and prevent subsequent homo-oligomerisation and MOMP (169, 191). Upon induction of an apoptotic stimulus it is proposed that activation of BH3-only proteins drives heterodimerisation with pro-survival Bcl-2 family members, with a resulting displacement of Bax/ Bak releasing them to drive MOMP, as depicted in figure 1.9 (162-164, 169, 191).

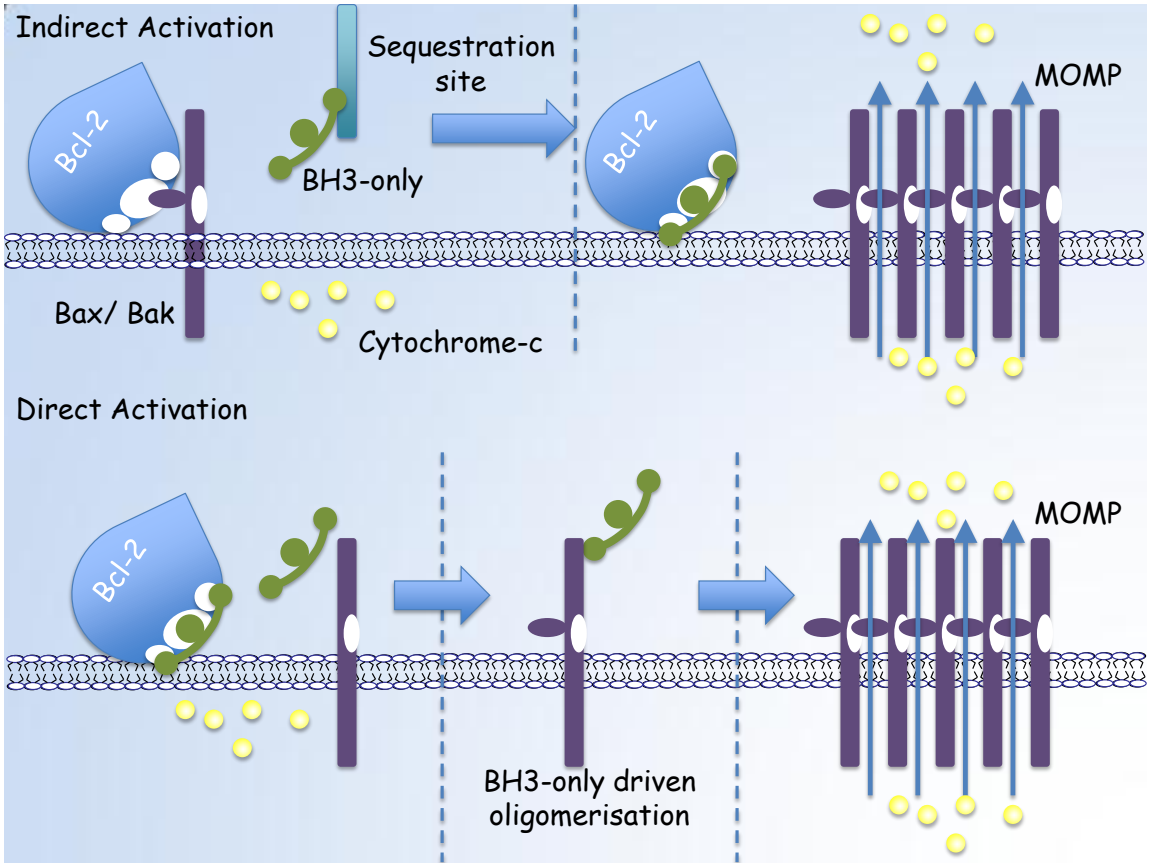

. Figure 1.9 The Direct and Indirect activation models

Schematic representing the roles for BH3-only proteins and prosurvival family members according to the indirect and direct activation models. The indirect activation model predicts that prosurvival family members repress Bax/ Bak oligomerisation, which upon stress signalling is reversed via BH3-only: prosurvival interaction. The direct activation model predicts that BH3-only proteins directly drive Bax/ Bak homo-oligomerisation, whilst prosurvival family members inhibit such a function by binding BH3-only proteins.

Subsequent studies demonstrated that BH3-only proteins display differential MOMP-inducing potency with Bim, Bid and Puma the most potent (192). The indirect activation model accounts for such differential potency by the relative affinity of each BH3-only protein for pro-survival Bcl-2 family members

Chen et al demonstrated that the relative potency of Bim, Bid and Puma is attributable to high affinity engagement of all five pro-survival proteins, thus maximally de-repressing Bax/ Bak and generating substantial MOMP (191, 192). In contrast, less potent BH3-only proteins only engage a discrete subset of pro-survival members therefore, imparting a reduced level of MOMP and apoptosis, as shown in table 1.1 (192).

BH3-only	Bcl-2	Bcl-Xl	Bcl-w	Mcl-1	A1
Bid	✓	✓	✓	✓	✓
Bim	✓	✓	✓	✓	✓
Puma	✓	✓	✓	✓	✓
Bad	✓	✓	✓	×	×
Bik	×	✓	✓	×	✓
Bmf	✓	✓	✓	×	×
Hrk	×	✓	✓	×	✓
Noxa	×	×	×	✓	✓

Table 1.1 Representation of the ability of BH3-only proteins to associate with prosurvival Bcl-2 family members

Adapted from Chen et al 2005. Binding calculated via peptide competition experiments utilising a Biacore detection system.

BH3-only protein: pro-survival interactions are thought to be exclusively dictated by the BH3 domain (193, 194). Structural studies have identified the presence of four vital hydrophobic pockets, within the hydrophobic binding groove of Bcl-xL, formed by aspects of the BH1, BH2 and BH3 domains, which contact key BH3 domain residues of BH3-only proteins (194). Consequently BH3-only protein pro-survival binding selectivity is thought to be achieved via variation in hydrophobic pocket contacting

residues of the BH3-domain (194). Indeed, some form of low affinity interaction between Bax/ Bak and pro-survivals does seem to be vital in the regulation of MOMP (195). However, the indirect activation model fails to account for the resting cytosolic localisation of Bax or provide an explanation as to how the Bcl-2 family can induce activation of Bax at this location.

In an attempt to address this issue the direct activation model, summarised in figure 1.9, states that Bid-like activator BH3-only proteins (Bid, Bim and possibly Puma) directly bind Bax inducing mitochondrial translocation and subsequent oligomerisation, thus accounting for their relative potency (168, 196-200). The remaining Bad-like BH3-only proteins (Bad, Bmf, Bik, Noxa, Hrk), which are unable to directly bind Bax/ Bak, are proposed to act as sensitisers by displacing activator BH3-only proteins from pro-survivals (172, 197, 198, 201). Within this model pro-survival Bcl-2 family members sequester BH3-only proteins, thus preventing Bax/ Bak activation, and also activated, mitochondrially localised Bax/ Bak thus preventing their effector function (45, 164, 172, 173, 197-199, 201).

Using BH3-domain peptides, evidence suggests that direct activators engage Bax via interaction with regions of the α1-α6 helices, destabilising α1-α9 interactions leading to α9 exposure and mitochondrial translocation (168, 200). Subsequently, it is proposed that upon Bax translocation, direct activators disengage and occupy an additional site upon Bax and drive homo-oligomerisation (168). Studies utilising Bak demonstrate dependence upon Bak BH1 and BH3 domains for oligomerisation, likely attributable to the BH3 domain of one Bak molecule binding to the BH1 domain of another (168).

The studies of Willis et al challenge this model as the physiologically relevant forms of Bim (Bim extra long (Bim_{EL}) and Bim long (Bim_L)) and Bid both fail to detectably bind Bax in non-denaturing conditions (191). Although, an interaction was indeed seen in the presence of the detergent triton X-100, known to alter Bax conformation, it is possible that Bax binding is an experimental artefact (191). Furthermore, the production of a Bim BH3 mutant (G94A) which ablates Bax binding in triton x-100 containing buffer had no effect upon the ability of Bim to induce cellular death (191).

And finally, cells deficient in Bid, Bim, and Puma were still able to undergo apoptosis despite not expressing any activator BH3-only proteins (191). Furthermore, the direct activation model relies upon experimental observations utilising BH3-peptides derived from activator BH3-proteins. Whilst these peptides appear to bind Bax, the interaction between full-length activators in cells has been difficult to assess.

1.4.1.4 A compromise?

Recent advances invoke the prospect of an intriguing model amalgamating aspects of both direct and indirect activation models. Studies of Bim BH3-mutants, where the Bim BH3 domain was exchanged for that of other BH3-only proteins, proposed that Bim indeed acts as a direct activator of Bax, yet also functions as a negative regulator of pro-survivals (196). Therefore, it is implied that the majority of BH3-only proteins act according to the indirect activation model; yet Bim, and presumably tBid, possess the additional ability to directly activate Bax/ Bak (196). The function of Puma as a direct Bax/ Bak activator remains ambiguous owing to conflicting reports (196, 199). However, recently Llambi and Green propose a unified model for the induction of MOMP amalgamating aspects of both direct and indirect activation models(202). Such studies utilised tBid BH3-mutants, whereby BH3 domains from a variety of Bcl-2 family members were utilised to replace the endogenous tBid BH3-domain. Such studies identified that prosurvival Bcl-2 family members were capable of inhibiting MOMP by both sequestering activated Bax/ Bak-like proteins and by sequestering activator BH3-only proteins (202). Therefore, it appears as though MOMP is regulated by a mechanism governed by the properties of both the indirect and direct activation models.

1.4.2 The retrotranslocation model

Although the studies of Merino et al appear to combine aspects of both indirect and direct activation models, both of these models fail to address how Bax is retained in its cytosolic location. However, a recent study by Edlich et al sheds light on how this process may be regulated. In an elegant study, Edlich et al demonstrated a direct Bax BH3-domain-dependent interaction between Bcl-xL and Bax in healthy cells. In fact, in healthy cells Bax appears to constantly traffic between the cytosol and mitochondria alongside Bcl-xL (203). Edlich et al further demonstrate that ablation of the Bax: Bcl-xL

interaction, by mutation of the Bax BH3 domain, resulted in accumulation of Bax at the mitochondria (203). Therefore, it is proposed that Bcl-xL functions to retrotranslocate Bax from the mitochondria to the cytosol thus, minimising the mitochondrial Bax pool available for activation. Whilst this study appears to explain the cytosolic localisation of Bax in healthy cells, it fails to address the way in which Bax activation at the mitochondrion occurs. It is likely that upon accumulation of Bax at the mitochondria, direct BH3-only protein-mediated activation induces conformational changes ultimately leading to homo-oligomerisation. Such a process is likely inhibited further by prosurvivals via binding activator BH3-only proteins and activated Bax/ Bak monomers thus sequestering their function. Furthermore, it remains unclear whether all prosurvivals function by retrotranslocation or that this function is specific to Bcl-xL.

1.4.3 BH3-only protein regulation

Irrespective of the model, it is clear that BH3-only proteins provide an apoptotic sensing function the apoptotic pathway.

BH3-only proteins experience complex and strict regulation at both transcriptional and post-translational levels. This complexity is most apparent in the multi-level regulation of Bim. At present the field of Bim regulation reveals a complex picture where regulatory mechanisms appear both stimulus and cell-type specific. Such complex regulation likely reflects convergence of a vast array of signalling pathways in order to determine the appropriateness of a Bim-induced apoptotic cellular outcome.

Growth factor signalling effectively represses Bim expression and function in both a PI3K and ERK dependent fashion. ERK signalling appears to reduce Bim protein levels via ERK-dependent phosphorylation at ser 69 resulting in proteasomal targeting and degradation (151, 204). Furthermore, PI3K-mediated Akt activation is implicated in the regulation of Bim via both transcriptional and post-translational mechanisms (96, 205, 206). Akt-driven phosphorylation of the Bim-regulating TF forkhead box 03a (FOXO3a) is thought to drive association between FOXO3a and 14-3-3, retaining it in the cytosol and preventing transactivation of Bim (96, 205). Additionally, Bim itself is reportedly sequestered to 14-3-3 via Akt-driven phosphorylation at ser 87 (206). Sequestration appears a common theme in Bim regulation since in healthy cells Bim is reportedly also

found in association with Dynein light chain-1 (DLC-1), via its conserved K/RXTQT motif, targeting Bim to microtubules and preventing mitochondrial translocation (207, 208).

The induction of Bim-dependent apoptosis is associated with the reversal of many of these regulatory strategies. Mobilisation from sequestration sites appears to ensue upon JNK-mediated phosphorylation of thr 56, which resides within the DLC-binding region, de-stabilising the Bim-DLC interaction (153, 209). Furthermore, it has been suggested that, upon neuronal growth factor withdrawal, JNK-mediated ser 65 phosphorylation of Bim_{EL} correlates with an enhancement of apoptotic potency, however, the mechanism for such enhancement remains unknown (210). Additionally Bim transcriptional regulation is evident upon CCAAT-enhancer binding protein homologous protein (CHOP) and AP-1-mediated transactivation following induction of the unfolded protein response (UPR) and neuronal growth factor withdrawal, respectively (211, 212).

Like Bim, Bad regulation is highly complex and proceeds predominantly via sequestration to 14-3-3, driven by phosphorylation of ser 112, 136 and 155 (213). Such phosphorylation events occur in a sequential fashion where 90 kDa ribosomal S6 kinase (p90RSK) mediated ser-112 phosphorylation and Akt-mediated ser 136 phosphorylation precede and augment phosphorylation of ser 155 (95, 213, 214). Since ser 155 resides within the Bad BH3 domain, PKA-mediated phosphorylation is proposed to neutralise Bad via de-stabilisation of interactions with pro-survivals (213, 215). Furthermore, Bad is purportedly regulated via JNK-mediated phosphorylation of ser 128 leading to enhancement of apoptotic potency (152).

In contrast, both Puma and Noxa regulation appears primarily directed to the transcript level. Both Puma and Noxa are direct transactivation targets of p53, with Puma one of the major contributors to p53-mediated apoptosis, although it also contributes to p53-independent glucocorticoid induced death (162, 216-219).

The BH3-only protein Bmf is heavily expressed in the haematopoietic lineage but is found in vanishingly small amounts elsewhere (220). Like Bim, Bmf is targeted to DLCs via the conserved K/RXTQT motif (207). However in contrast to Bim, Bmf associates

with DLC-2 and consequently associates with the myosin V actin motor complex thereby driving association with the actin cytoskeleton (207). Bmf activation ensues upon detachment of adherent cells, in a process termed anoikis, via mobilisation from the actin cytoskeleton (207).

Like Bmf, the BH3-only protein Bik is highly expressed in the haematopoietic lineage and becomes upregulated in response to numerous stimuli. However, its pro-apoptotic role appears largely redundant since $Bik^{-/-}$ mice demonstrate similar sensitivity to numerous apoptotic stimuli compared to their WT counterparts (221-223). Interestingly, Bim, Bik dKO mice demonstrate arrested spermatogenesis, a phenotype not seen in Bik or Bim KO mice alone (221). Therefore, indicating that BH3-only proteins co-operate to provide a cellular outcome, which is only disturbed upon loss of multiple genes.

An additional BH3-only regulatory mechanism centres upon caspase-mediated regulation, exemplified by activation of Bid. Uniquely, Bid is produced as a zymogen owing to masking of the BH3 domain by a canonical N-terminal BH3-like domain. Cleavage to its active form, truncated Bid (tBid), is evident downstream of TNFR-signalling and ER stress via caspases-8 and 2, respectively (165, 224). Additionally, Bad experiences caspase-mediated processing via caspases 2, 3, 7, 8 and 10 producing N-terminally truncated Bad, which is incapable of 14-3-3 interaction, thus aiding caspase-mediated positive feedback resulting in further MOMP (213).

1.4.4 BCR-induced Apoptosis

As discussed previously, inappropriate engagement the BCR rapidly induces clonal deletion via cell death, anergy or receptor editing (39). BCR-induced cell death exhibits apoptotic characteristics such as: loss of plasma membrane asymmetry, caspase-independent MOMP and poly-ADP ribose polymerase (PARP) cleavage (225-228). Such an apoptotic response occurs via the intrinsic apoptotic pathway, since over-expression of a Bcl-2 transgene completely blocks BCR-induced MOMP and BCR-induced death in normal B-cells (225-228). These observations indicate a prevailing role for BH3-only proteins in BCR-induced cell death (226).

Initial investigations revealed that a prominent role in BCR-induced apoptosis is played by Bim, as $Bim^{-/-}$ mice display significant resistance toward BCR-induced apoptosis compared to wild type (WT) mice (229). Subsequent studies revealed that BCR engagement induces a JNK-dependent skewing of Bim isoform expression from Bim_{EL} to the more pro-apoptotic Bim_L (230, 231). Such a skew is achieved via both ERK-mediated ser 69 phosphorylation-dependent proteasomal degradation of Bim_{EL} and a reciprocal increase in Bim_L expression (230). However, increased Bim_L expression cannot simply be attributed to enhanced transcription of Bim_L encoding mRNAs, since the Bim_{EL}: Bim_L mRNA ratio remains un-changed (231, 232). Instead, BCR engagement induces splicing of Bim_{EL} mRNA to the shorter Bim_L isoform (232). Therefore, these studies highlight Bim_{EL} mRNA as an intron retention form of Bim_L which can be spliced to unleash the more highly pro-apoptotic Bim_L (232). Although genetic loss of Bim significantly protects B-cells from BCR-induced apoptosis the level of protection is not as great as that observed in mice over-expressing a Bcl-2 transgene in B-lymphoid lineages (229, 233). Such studies therefore predict the existence of additional apoptotic mechanisms linking the BCR to cell death.

Subsequent studies have failed to reliably identify an involvement of additional BH3-only proteins. Jiang et al demonstrated that BCR-induced apoptosis requires synthesis of a new mRNA transcript within 3 hours of engagement (223). It was proposed subsequently that calcineurin and PI3K-dependent up regulation of Bik fulfils this requirement in the human B-cell lymphoma line B104 (223). However, the study failed to demonstrate impairment of BCR-induced apoptosis upon Bik knockout or small interfering RNA (siRNA) knockdown and therefore, the relevance of Bik up-regulation is currently unknown. Splenic B-cells from $Bik^{-/-}$ mice however, show no resistance toward BCR-induced apoptosis (222). It was initially postulated that the effect of Bik was masked by the far-greater contribution made by Bim in this model system. However, Bim and Bik dKO mice showed no greater resistance in comparison to $Bim^{-/-}$ mice alone (221). Therefore, at least in mouse splenic B-cells, Bik appears not to play a major role in BCR-induced apoptosis. However, the studies of Jiang et al utilised a human lymphoma cell-line therefore, it is possible that Bik plays a lymphoma-specific role not evident in normal splenic B-cells. Since malignant and non-malignant tumour

infiltrating B-lymphocytes demonstrate differential BCR signalling, it is plausible to suggest that the involvement of BH3-only proteins may also differ (234). Therefore, in order to address the role of Bik in BCR-induced apoptosis the sensitivity of Bik deficient lymphomas must be assessed.

An additional role for Bmf in BCR-induced apoptosis may be implied from the fact that $Bmf^{-/-}$ mice demonstrate a kinetic delay in the onset of BCR-induced apoptosis (235). Although the difference was not statistically significant, It is possible that the detrimental deletion of Bmf may be masked by the over-riding redundant function of Bim (235). In order to address such a question, dual knockouts of Bmf and Bim should be studied to determine whether genetic loss of both genes generates a resistance toward BCR-induced apoptosis equal to Bcl-2 over-expression.

The BH3-only protein Bad has also been implicated in BCR-induced apoptosis since BCR-ligation has been shown to induce dissociation of Bad from 14-3-3 allowing mitochondrial translocation and MOMP (236). Furthermore, differential regulation of Bad may represent an aspect of (immature vs. mature B-cell) differential BCR signalling since sequestration of Bad to lipid Rafts prevents its pro-apoptotic function in mature B-cells (236). However, the role of Bad in BCR-induced apoptosis remains ambiguous as studies utilising gene knockout and knockdown approaches have yet to be performed.

1.4.4.1 Caspases are the BCR-signalling induced executioners

Caspases represent the major executioners of BCR-induced apoptosis (193, 225). Activation of executioner caspases 3 and 7 appears to represent the final commitment to death, since the caspase-3-like caspase inhibitor DEVD-fluoromethylketone (fmk) ablates the response (193, 225, 237-239). The identity of key BCR-induced initiator caspases however, remains significantly less well defined.

Since caspase-independent MOMP represents a key step in the BCR-induced apoptotic programme, apoptosome-mediated activation of caspase-9 performs a key initiating role (193, 225, 237-239). Furthermore, it is proposed that caspase-9 participates in positive feedback MOMP, thus potentiating cytochrome c release from mitochondria (238).

However, a solely caspase-9-dependent initiation event does not satisfactorily explain the experimental observations. Although dominant negative caspase-9 expression does indeed severely reduce the extent of cell death the reduction is not complete (193). Therefore, additional initiator caspases may be involved. Such a role may be undertaken by caspase-2 since activatory caspase-2 processing is evident early during BCR-induced apoptosis (193).

Caspase-2 represents somewhat of an enigma, as it possesses characteristics of both initiator and executioner caspases. Possession of a long pro-domain and CARD domain alongside its propensity to undertake auto-activation at an activation platform resembles properties of initiator caspases (240, 241). However, substrate specificity and caspase-3 mediated activation points toward a function as an executioner caspase (240, 241).

Caspase-2 activation has been suggested to play a key initiation role in ER stress-induced apoptosis by proteolytic processing of Bid to tBid (224). Since ER stress has been implicated in the apoptotic response to BCR cross linking (See appendix A2 for further details), and dominant negative caspase-2 mutant expression significantly inhibits BCR-induced cell death, caspase-2 may in fact play a key role in the response (193, 242).

Interestingly, caspases have also been directly implicated in eliciting MOMP downstream of the BCR. It is reported that caspase-7-like activity is detectable prior to loss of mitochondrial membrane integrity in some models (243). Such caspase-7-like activity appears dependent upon calpain and therefore, highlights a potential Ca^{2+}-dependent mechanism linking the BCR to MOMP (243). However, it is generally accepted that caspase-9 represents the key initiation event, since blockade of MOMP by Bcl-2/ Bcl-xL/ A1 over-expression completely abrogates the apoptotic response in most models (193, 225, 237-239).

In addition, the extent of receptor cross-linking may influence the nature of the caspase-activation profile (244). It is proposed that an alternative caspase-8 dependent apoptotic pathway may be engaged upon extensive receptor cross linking (245).

However, such observations have yet to be repeated in additional models and therefore, caspase-9 appears to play the key initiating role in most situations.

1.4.4.2 Differential signalling modalities: Tolerance Vs. Activation

Although pathways linking the BCR to apoptosis are becoming clearer, the specific differences in BCR signals that dictate clonal deletion in immature B-cells and proliferation in mature B-cells remains completely unknown (4, 17, 20-22, 40, 41, 43, 227, 246-249). However, it appears as though the context of antigenic recognition may play an important role. For instance, even stimulation of mature B-cells in the absence of co-stimulatory signals results in the induction of cellular anergy rather than proliferation (247).

Furthermore, differential-signalling outcomes may be attributable to subtle variation in BCR-signalling programmes between different B-cell developmental subsets. Such variation is exemplified via the relative sensitivity of immature B-cells to BCR-induced Ca^{2+} signalling in comparison to mature B-cells, possibly attributable to elevated expression of Lyn, PLCγ2, Btk, BLNK and calcineurin (250-254). Furthermore, immature B-cells demonstrate reduced Syk expression and therefore, may demonstrate a deficiency in activating distinct downstream signalling pathways (253, 254). Such deficiency may be evident in the differential activation of NF-κB in cells undergoing clonal deletion and activation (247, 254). Clonal deletion is associated with not only impaired NF-κB activation, but also a genetic programme in which positive regulators of NF-κB are downregulated (247, 254). Therefore, it is tempting to speculate that an activatory response to BCR-cross linking is permitted via NF-κB–mediated up regulation of pro-survival Bcl-xL and A1 (17, 255). Conversely, loss of such signals may predispose the cell to clonal deletion.

In contrast to this notion Andrews & Rawlings demonstrate a remarkable similarity in the nature of downstream BCR signalling events in mouse T1 and mature follicular B-cells (256). In fact, identical activation of NF-κB, NFAT, Akt, p38, ERK and Ca^{2+} flux were detected upon receptor engagement (256). Despite sufficient BCR-induced NF-κB activation, it was demonstrated that T1 B-cells demonstrate impaired transcriptional up regulation of NF-κB targets Bcl-xL, A1 and c-Myc in comparison to BCR-stimulated

mature B-cells (256). Therefore, T1 B-cells appear to possess a pre-programmed nuclear non-responsiveness toward BCR signals. However, the exact molecular mechanisms of such a defect remain unknown.

Furthermore, differential regulation of the PI3K/ Akt pathway may also be responsible for instigation of different cellular outcomes downstream of BCR signalling (257). It has been demonstrated that immature B-cells exhibit heightened expression and activity of the negative regulator of PI3K phosphatase and tensin homologue (PTEN), in comparison to their mature counterparts (257). Although immature B-cells retain BCR-induced Akt activation, the extent of PIP_3 production is significantly reduced in comparison to mature B-cells (257). Therefore the heightened PTEN expression and activity may damp down PI3K signalling in immature B-cells (257). Further to this concept, a complete rescue of immature B-cells from BCR-induced apoptosis in PTEN knockout mice has been demonstrated (257). Therefore, it is possible that failure to generate prolonged activation of PI3K prevents induction of key survival signals and instigates an apoptotic response (257). Taken together with studies demonstrating that PI3K and not NF-κB is responsible for cellular survival downstream of tonic receptor signals (27), the role of the PI3K pathway warrants further investigation.

Whilst the search continues for specific molecular distinctions between BCR signals in immature and mature B cells, suggestions that the difference may be more straightforward have been made. Sproul et al demonstrate that receptor cross linking of immature B-cells fails to instigate BCR translocation to lipid Rafts and receptor mediated endocytosis, key features of mature B-cell cross linking (258). These observations suggest that the BCR of immature B-cells may not efficiently co-localise with SFPTKs and therefore, may exhibit reduced signalling efficiency in comparison to mature B-cells (258). Furthermore, differences in signalling outcome may be attributed to the fact that mature B-cells demonstrate a genetic programme more suited to ensuring cell survival than their immature counterparts exemplified by enhanced Bcl-2 and A1 expression (254).

In summary, numerous BCR signalling distinctions have been made between mature and immature B-cells however, the molecular mechanisms for alternate signalling

outcomes remains largely unknown. It is likely that alternate cellular outcomes reflect instigation of development-specific genetic programmes enabling cellular activation or clonal deletion and that no single factor is responsible.

1.5 Alternative cell death pathways

Although, apoptosis represents the most widespread form of cell death in mammalian systems, alternative modes also exist which invoke cell death in a fashion distinct from classical-apoptosis, as demonstrated in table 1.2.

1.5.1 Non-classical apoptosis

Although apoptosis is commonly regarded as a caspase-dependent phenomenon, significant redundancy in the apoptotic machinery permits cellular execution via numerous means. For instance, upon physiological or biochemical caspase-inhibition apoptosis may still proceed via caspase-independent mechanisms via mitochondrial release of apoptogenic factors (259-261). Various modes of non-classical apoptotic cell death exist, differing in their dependency upon the apoptotic machinery and biochemical features, as demonstrated in table 1.2 (259-261).

1.5.2 Necrosis and necroptosis

Historically, necrosis is regarded as cell death lacking any discernable morphological features and regulatory mechanisms resulting from physical injury or overload of cellular stresses (262). However, this view has been disputed in recent years. It now appears as though certain types of necrosis, termed necroptosis, represent biochemically-regulated processes that utilise components of the apoptotic machinery (262-265).

Cell death mode	Main biochemical features	Caspase dependence	Inhibitory interventions
Anoikis	Downregulation of EGFR Inhibition of ERK1 signalling Lack of β1 integrin engagement Overexpression of Bim Caspase-3, 6, 7 activation	++	Bcl-2 overexpression Z-VAD-fmk administration
Autophagic cell death	LC3 Lipidation Irreversible $\Delta\psi_m$	--	Vps34 inhibitors AMBRA1, ATG5, ATG7, ATG12 or BCN1 genetic inhibition
Caspase-dependent intrinsic apoptosis	MOMP Irreversible $\Delta\psi_m$	++	Bcl-2 overexpression Z-VAD-fmk administration
Caspase-independent intrinsic apoptosis	Release of IMS proteins Respiratory chain inhibition	--	Bcl-2 overexpression
Cornification	Activation of transglutaminases Caspase-14 activation	+	Genetic inhibition of TG1, TG3 or TG5 Genetic inhibition of caspase-14
Entosis	RHO activation ROCK1 activation	--	Genetic inhibition of metallothionein 2A Lysosomal inhibitors
Extrinsic apoptosis by death receptors	Death receptor signalling Caspase-8 (-10) activation Bid cleavage and MOMP Caspase-3, 6, 7 activation	++	CrmA expression Genetic inhibition of caspases 8 and 3 Z-VAD-fmk administration
Extrinsic apoptosis by dependence receptors	Dependence receptor signalling PP2A activation DAPK1 activation Caspase-9 activation Caspase-3, 6, 7 activation	++	Genetic inhibition of caspases 9 and 3 Genetic inhibition of PP2A Z-VAD-fmk administration
Mitotic catastrophe	Caspase-2 activation (in some instances) TP53 or TP73 activation (in some instances) Mitotic arrest	--	Genetic inhibition of TP53 (in some instances) Pharmacological of genetic inhibition of Caspase-2 (in some instances)
Necroptosis	Death receptor signalling Caspase-inhibition RIP1 and/or RIP3 activation	--	Administration of necrostatins Genetic inhibition of RIP1/ RIP3
Netosis	Caspase-inhibition NADPH oxidase activation NET release (in some instances)	--	Autophagy inhibition NADPH oxidase inhibition Genetic inhibition of PAD4
Parthanatosis	PARP1-mediated PAR accumulation Irreversible $\Delta\psi_m$ ATP and NADH depletion PAR binding to AIF and AIF nuclear translocation	--	Genetic inhibition of AIF Pharamacological or genetic inhibition of PARP1
Pyroptosis	Caspase-1 activation Caspase-7 activation Secretion of IL-1β and IL-18	++	Administation of Z-YVAD-fmk Genetic inhibition of Caspase-1

Table 1.2 Summary of the currently recognised forms of programmed cell death and their specific biochemical features

Adapted from Galluzzi et al 2011. Abbreviations: ATG, autophagy; BCN1, beclin 1; CrmA, cytokine response modifier A; DAPK1, death-associated protein kinase 1; EGFR, epidermal growth factor receptor; MAP1LC3, microtubule-associated protein 1 light chain 3; MOMP, mitochondrial outer membrane permeablisation; NET, neutrophil extracellular trap; PAD4, peptidylarginine deaminase 4; PAR, poly(ADP-ribose); PARP1, poly(ADP-ribose) polymerase 1; PP2A, protein phosphatase 2A; ROCK1, RHO-associated, coiled-coil containing protein kinase 1; SQSTM1, sequestosome 1; TG, transglutaminase; Z-VAD-fmk, N-benzyloxycarbonyl-Val-Ala-Asp-fluoromethylketone; Z-YVAD-fmk, N-benzyloxycarbonyl-Tyr-Val-Ala-DLAsp-fluoromethylketone.

For instance, death receptor signalling in apoptosis-deficient cells invokes a necrotic-like cell death that is blocked by pharmacological inhibitors of receptor-interacting ser/thr-protein kinase (RIP)-1 (263, 264). Furthermore, it has been revealed that mitochondrial dysfunction is highly associated with necrosis. Such an observation was

made in cyclophilin D over-expressing mice that demonstrate a heightened sensitivity to necrotic stimuli (177, 178). Therefore, it appears as though mPTP-dependent mitochondrial permeablisation plays a key role in some necrotic stimuli (177, 178). Interestingly, it now appears that necrosis and apoptosis may in fact be heavily intertwined. Hitomi et al utilised a genome-wide siRNA screen to reveal a highly complex necroptotic regulatory pathway, invoked upon caspase-inhibitor treatment, which involves regulators of apoptosis: PARP-2, AIF and Bmf (265). Taken together these results not only demonstrate that necrosis can be instigated by distinct molecular pathways, but also that there is significant overlap between apoptosis and necrosis (262). It is now proposed that under certain circumstances necrosis and apoptosis co-operate in cellular deletion, and that blockade of apoptosis allows the phenotype of programmed necrosis to be revealed.

1.5.3 Autophagy

Originally described in yeast, autophagy represents a stress-induced catabolic process, which replenishes cellular ATP levels and removes damaged or aged organelles during periods of nutrient or growth factor withdrawal in mammalian cells. Such catabolism is achieved via incorporation of cytoplasmic macromolecules and intact organelles into autophagosomes, which upon lysosomal fusion are targeted for bulk hydrolysis by lysosomal enzymes (266-268). Whilst regarded as a predominantly destructive process, autophagy is largely associated with a pro-survival response aimed at restoring bio-energetic homeostasis during periods of stress (269).

However, extensive autophagy also appears to be associated with the onset of programmed cell death by an as of yet poorly defined process (267, 268). Whilst morphologically distinct from apoptosis and associated with autophagosome formation, the exact role played by autophagy in the induction of non-apoptotic cell death remains unclear. It remains to be determined whether autophagy directly contributes towards cell death or is invoked as a survival pathway alongside cell death and has been termed as pro-death via guilt by association. However, some evidence from studies performed in Drosophila melanogaster suggest the autophagy may directly drive cell death. For instance, salivary gland degradation appeared impaired upon mutation of specific atg genes (270). Furthermore, Ras-mediated oncogene-

induced cell death has been demonstrated as reliant upon autophagy, via induction of Beclin-1 (271).In addition, evidence suggests that in apoptosis deficient cells autophagic regulators play a key role in the induction of non-apoptotic cellular death in response to etoposide and staurosporine (272). However, it is unclear as to whether this process occurs in apoptosis-sufficient cells.

Whilst the exact role of autophagy remains poorly defined, its regulatory machinery has been extensively elucidated in recent years. Key regulatory roles appear to be played by class iii PI3Ks, mTOR, the eukaryotic initiation factor 2α (eif2α) kinase general control non-repressed 2 (GCN2) and a vast array of autophagy-related (atg) genes, most prominently atg 6/ Beclin-1 (267, 268). Beclin-1 was the first human protein shown to participate in autophagy, and appears to function as a direct allosteric activator of the class iii PI3K vps34, which itself performs a role in autophagosome formation via PIP_3 production (273). Interestingly, Beclin-1 contains a putative BH3-domain and therefore, experiences direct regulation by pro-survival Bcl-2 family members. It is proposed that pro-survivals play an inhibitory role during autophagy, since liberation from Bcl-2 association seems to coincide with autophagosome formation (267, 268, 274).

Interestingly, autophagosome formation has been observed following BCR-engagement of the murine lymphoma cell-line WEHI-231 (275). However, studies upon the direct involvement of autophagy regulating genes upon the extent of BCR-induced cell death have yet to be performed. Therefore, whilst there is a tenuous link between autophagy and the BCR its role is currently far from clear.

It is apparent that the three major forms of cell death; discussed above, all display significant overlap in regulation, centring on the Bcl-2 family. Therefore, the Bcl-2 family appears to represent a pleiotropic regulator of cell death, and that subtle variation in its regulation may influence the mode of cell death generated.

1.6 TGF-β in tissue homeostasis

The concept of pleiotropism is commonplace throughout biology and perhaps none more intriguingly than in the case of TGF-β, a pleiotropic cytokine capable of both suppressing and facilitating tumourigenesis (276, 277).

Although TGF-β was initially identified via its ability to transform and enhance proliferation of mesenchymal cells, cells of epithelial, endothelial, and haematopoietic lineages generally exhibit growth arrest or apoptosis in response to TGF-β. Whilst the biology of TGF-β is complex and difficult to dissect, transgenic animal studies have provided useful insights into the biological activity of TGF-β. TGF-β-deficient mice exhibit widespread loss of immune homeostasis, and develop chronic inflammatory disease, attributable to enhanced white blood cell counts and tissue infiltration (278, 279). In contrast, hepatocyte-restricted ectopic TGF-β expression imparts an enhanced rate of hepatocyte apoptosis on the animals, resulting in hepatic fibrosis (280). Furthermore, TGF-β plays a vital role in deletion of low affinity post-SHM centroblasts during the germinal centre reaction and in gastric cell turnover (277, 281). Such observations identify a key role for TGF-β in ensuring normal cellular homeostasis via direct cell-death and growth arrest programmes.

Such growth arrest largely proceeds via induction of the cyclin-dependent kinase inhibitors $p15^{INK4a}$, $P21^{CIP1}$, and $p27^{KIP1}$ alongside concomitant suppression of c-Myc (277). It is proposed that such growth inhibitory, tumour suppressive functions of TGF-β are also harnessed by macrophages, which secrete TGF-β directly into neoplastic sites leading to tumour senescence (282). Such observations led to the prediction that TGF-β functions as a key tumour suppressor. Indeed, genetic abnormalities in the TGF-β pathway are common in tumours, most notably in epithelial-derived neoplasms. For instance > 50% of pancreatic cancers exhibit bi-allelic loss of Sma and mad related family (SMAD) 4, whilst SMAD2 is inactivated in a small proportion of colorectal cancers (276, 277). Furthermore, mono-allelic loss of SMAD4 or bi-allelic SMAD3 deletion correlates with the occurrence of gastric polyps and progression to colorectal adenocarcinoma (277, 283, 284). Therefore, there is a substantial body of evidence under-pinning the role of the TGF-β pathway as a key tumour suppressive mechanism.

However, TGF-β also appears capable of facilitating the process of tumourigenesis upon mutagenic loss of its growth suppression activity. It has been demonstrated that tumours exhibiting TGF-β pathway mutations demonstrate enhanced proliferation, migration and invasive behaviour in response to TGF-β, as evident in virtually all

epithelial-derived tumours (276, 277, 285). Such increases in cellular motility and invasion appear attributable to TGF-β-mediated epithelial to mesenchymal cell transition (EMT), a reversion of epithelial behaviour to that of a mesenchymal cell (285). EMT drives disassembly of cell: cell contacts, enhanced expression of factors required for cell motility, i.e. integrins, thus permitting cellular migration and tissue invasion thereby facilitating metastasis (285). Concomitantly, TGF-β-enhances cellular survival via suppression of Bim transcription and may also dampen tumour surveillance mechanisms of the immune system, preventing tumour recognition (276, 286).

Therefore depending upon the integrity of the TGF-β signalling cascade, TGF-β is capable of facilitating normal cell turnover alongside tumourigenesis. Such pleiotropism is utilised by multiple cancers to facilitate their survival and, therefore, represents a key area of study in cancer biology.

1.6.1 TGF-β and SMAD signalling

The human genome encodes three independent TGF-β isoforms (TGF-β1-3) that demonstrate tissue-specific and developmentally regulated expression, with TGF-β1 the most abundant (276). TGF-β family cytokines are secreted as part of a latent protein complex, which is thought to be subsequently activated by proteolytic processing in a poorly defined process (276). In their active configuration TGF-β family cytokines form disulphide-stabilised dimers, which signal via heterodimerisation of plasma membrane spanning type I and type II receptor ser/ thr kinases (TβRI and TβRII, respectively) (287). Subsequently, TGF-β receptor engagement is directly linked to transcriptional regulation of target genes via recruitment and phosphorylation of the SMAD family of proteins (287, 288). The SMAD family encompasses three functional groups: the receptor-regulated SMADs (R-SMADs) comprising SMAD1, 2, 3, 5 and 8, the co-mediator SMAD (Co-SMAD) SMAD4 and the inhibitory SMADs (I-SMADs) SMAD6 and 7 (287). In conjunction with SMAD4, R-SMADs directly link TGF-β to the transcriptional machinery in a process negatively regulated by I-SMADs (287).

As summarised in figure 1.10, TGF-β appears to initially bind TβRII and induces heterodimerisation via subsequent recruitment of the TβRI receptor activin receptor-like kinase (ALK)5 (289). Since type II receptors display constitutive kinase activity,

receptor co-localisation drives the TβRII-dependent phosphorylation of ALK5 within a specific region of the cytoplasmic tail, termed the GS region (289). In non-TGF-β stimulated cells, GS regions of TβIRs are blocked by binding of the FK506 binding protein-12 (FKBP12) competitor. However, TβRII-mediated phosphorylation of ALK5 drives FKBP12 dissociation and enhances the affinity of ALK5 for the R-SMAD SMAD2 (287, 290). Subsequent recruitment of SMAD2/3, via an interaction between phosphorylated GS motifs and a basic patch within the MH2 domain of SMAD2, enables ALK5-mediated phosphorylation of a key c-terminal ser-rich motif, known as the SSxS motif (290), as demonstrated in figure 1.10.

At rest SMAD2 is found in association with its binding partner SMAD anchor for receptor activation (SARA), which targets SMAD2 to endosomal compartments and the plasma membrane, via PIP_3 binding, where it facilitates an interaction with TGF-β receptors (291). Furthermore, SARA directly maintains SMAD2 in the cytoplasm via sequestration of its MH2-domain nuclear targeting sequence (292). TGF-β-induced SSXS motif phosphorylation subsequently de-stabilises interactions with SARA triggering dissociation and leading to the exposure of the nuclear targeting sequence (291, 292). Furthermore, phosphorylation drives SMAD2/3 homotrimerisation and enhances the affinity of SMAD2/3 for the co-SMAD SMAD4, leading to heteromerisation and nuclear translocation (287, 288). In association with multiple TFs, nuclear SMAD complexes subsequently engage targets containing the 5'-AGAC-3' SMAD binding element (SBE) and modulate transcription, as evident in figure 1.10 (287). However, SMAD: SBE interactions require the binding of additional factors for stabilisation due to their low affinity (277). Therefore, SMADs act as TFs in conjunction with two SMAD interacting proteins: DNA-binding co-factors and co-activators/co-repressors. Since DNA binding co-factors also possess their own binding sequence specificity they are able to influence the SMAD-target genes that are bound. In addition, since alternate cell types exhibit different levels of co-factor expression, SMAD-dependent transcriptional outcomes are highly context dependent and cell-type specific (277).

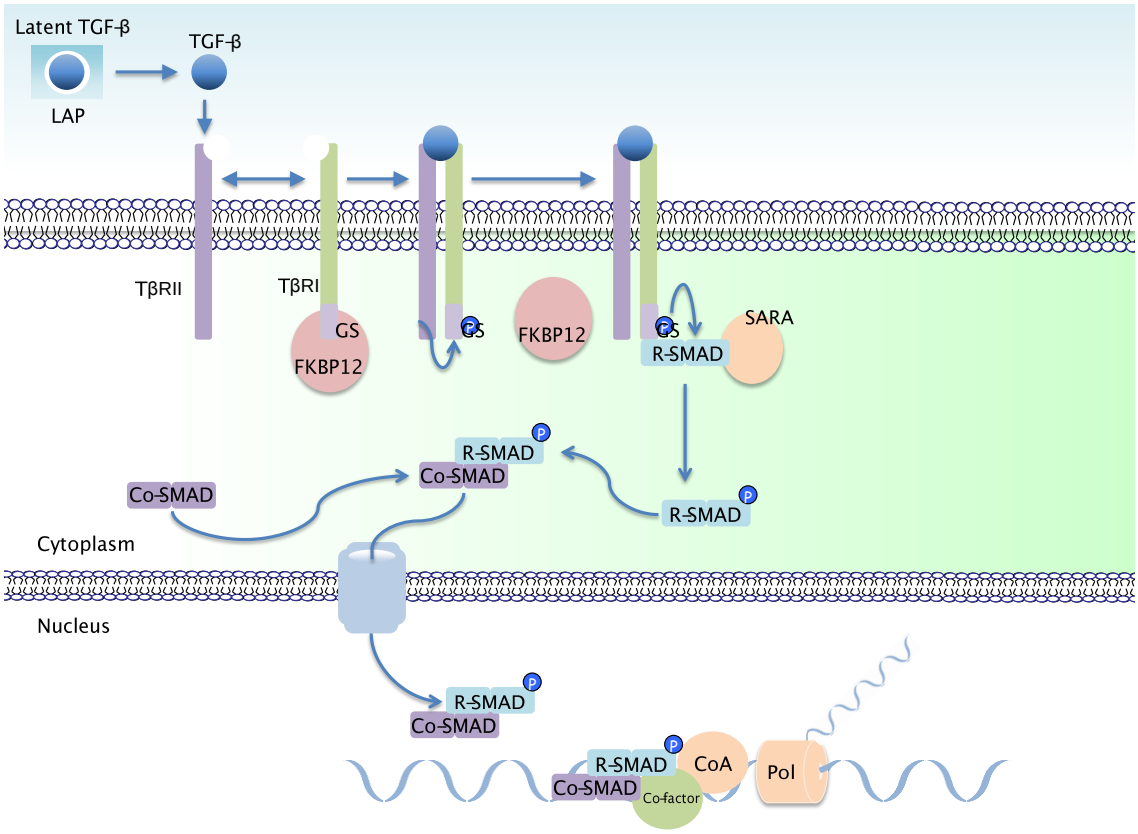

Figure 1.10 Schematic of TGF-β-induced SMAD signalling

TGF-β is secreted in an inactive latent form and is activate by proteolysis. TGF-β is initially bound by TβRII, resulting in the recruitment of TβRI and receptor heterodimerisation. The constitutively active TβRII then directly phosphorylates the GS region of TβRI and allows R-SMAD recruitment and subsequent phosphorylation. Phosphorylated R-SMADs subsequently heterodimerise with the Co-SMAD SMAD4, and enter the nucleus where target DNA sequences are bound in collaboration with additional DNA binding co-factors.

SMAD4, however, appears largely dispensable for SMAD complex nuclear translocation. Instead, SMAD4 appears vital for R-SMAD target recognition and contact with co-repressors or co-activators (293). Furthermore, TGF-β signalling has been demonstrated to activate PI3K, p38 and JNK in both a SMAD-dependent and -independent manner, potentially via growth arrest and DNA damage (GADD) 45β and TAK1 (294, 295).

1.6.2 TGF-β-induced apoptosis

TGF-β-induced apoptosis is evident in a vast array of cell types, most notably gastric cells, lymphocytes, and hepatocytes, and largely exhibits SMAD3/4-dependent engagement of intrinsic apoptosis and caspase activation (281, 296-301). Consequently, both pro-survival and pro-apoptotic members of the Bcl-2 family have

been implicated in the process, in particular the BH3-only protein Bim (298-302). Whilst TGF-β-mediated up-regulation of Bim appears largely cell-type specific, most models identify TGF-β-dependent transcriptional upregulation as a key initiating step (296, 298-301). Such transactivation appears to show dependency upon forkhead c1 (Foxc1), SMAD3/4, p38 and JNK depending upon the cell type in question (286, 294, 299-301). However, TGF-β signalling has also been linked to post-translational enhancement of Bim levels via SMAD-dependent upregulation of MAPK-regulating phosphatase 2 (MKP2). MKP2 is proposed to suppress basal levels of ERK phosphorylation, resulting in reduced Bim phosphorylation (presumably at ser 69), reduced proteasomal degradation, and subsequent enhancement of protein levels (302).

Furthermore, concomitant upregulation of the sensitiser BH3-only proteins Bik and Bmf at both mRNA and protein levels have been observed in lymphocytes and gastric cells (281, 298, 299). Whilst knockdown of Bik in lymphocytes successfully reduced the extent of TGF-β induced death, the role of Bmf appears context-dependent (281, 298, 299). It is evident that Bim and Bmf both mediate death signals downstream of TGF-β in lymphocytes; however, Bmf appears largely dispensable in gastric carcinoma cells (298, 299). Whilst active SMAD3/4 complexes are directly recruited to a putative SBE in the human Bik promoter, the molecular mechanisms governing TGF-β-induced Bmf upregulation remain largely unknown (281). Furthermore, additional studies provide a tentative link between TGF-β signalling and proteolytic processing of two additional BH3-only proteins, Bid and Bad, to more pro-apoptotic forms (297, 303). Although proteolytic activation of Bid is well documented, activation of Bad via this mechanism remains controversial (224). However, since experiments correlating genetic loss of Bid and Bad to an innate resistance toward TGF-β have yet to be performed, their role remains ambiguous.

Such studies conclusively determine that TGF-β signalling drives apoptosis by upregulation of pro-apoptotic genes; however, limited evidence is also available linking TGF-β to regulation of pro-survival Bcl-2 family members. Two studies have highlighted SMAD-dependent downregulation of Bcl-xL and Mcl-1, via indirect transcriptional repression and proteolysis, respectively, downstream of TGF-β signalling (281, 296).

Therefore, TGF-β appears to regulate cell survival via reciprocal regulation of both pro-apoptotic and pro-survival Bcl-2 family members.

Whilst the majority of studies demonstrate that TGF-β-induced apoptosis displays dependency upon the intrinsic apoptotic pathway, numerous studies have also observed features of extrinsic apoptosis. Such features include identification of caspase-8 as the key initiator caspase downstream of TGF-β and dependency upon the FAS-binding protein death domain-associated protein (DAXX) (294, 303). However, induction of intrinsic apoptosis represents the consensus view. Whilst the upstream regulatory role of SMADs 2,3, and 4 are well documented, additional factors have also been implicated including: SH2-containing inositol phosphatase (SHIP), SMAD7, death associated protein (DAP) and type 1 tumour necrosis factor shedding aminopeptidase regulator (ARTS) (294, 304-306). However, these additional mechanisms appear largely cell-type specific.

1.7 Myc driven tumourigenesis

The considerable pleiotropism in biological activity evident downstream of TGF-β signalling, however, does not reflect an unusual event in biology. In fact, such pleiotropic activity is commonplace, and is largely responsible for the concept of intrinsic tumour suppression, introduced previously. An additional example is found in the master transcriptional regulator c-Myc, which is able to drive both cellular proliferation and survival alongside apoptosis.

1.7.1 Myc structure and function

Myc family members, N-Myc, L-Myc and C-Myc, represent master transcriptional regulators of the basic-helix-loop-helix (bHLH) leucine zipper (Zip) domain containing TF superfamily (bHLH-Zip) (307). A recent estimate proposes that Myc directly binds approximately 4,000 genomic loci, culminating in transactivation of some 668 target genes, including 48 TFs, in human B-lymphocytes (308). Myc target genes often play distinct regulatory roles in proliferation, apoptosis, and growth arrest including: Bax, Puma, Bcl-2, Bcl-xL, caspases-1, 3, 8, and 9, E2F, Mcl-1, breast cancer susceptibility protein 2 (BRCA2), TGF-β, and $P21^{CIP1}$ (307, 309). As a consequence, Myc dysregulation is apparent in around 70% of all human cancers (307). Perhaps the best characterised

example is t(8:14) translocation of c-Myc proximal to the IgH locus enhancer, demonstrable in around 80% of BL patients (7, 307). Although tumours exhibit multiple modes of Myc dysregulation, over-expression of Myc family members represents a common outcome resulting in mitogen-independent proliferation, S-phase entry and angiogenesis (7, 307).

Myc family proteins bind E-box motif (5'-CAYGTG-3') containing genes, via their bHLH domains, as a Zip domain-mediated heterodimer with the bHLH-Zip TF Myc-associated factor x (max) (307, 310-312). Binding of Myc: max dimers permit direct transactivation of targets via recruitment of the transformation/transcription domain-associated protein (TRRAP) and brg1-associated factor 53 (BAF53) co-activators and associated histone acetyltransferases (HATs), i.e. general control of amino acid synthesis protein 5 (hGCN5), and helicases such as 48 kDa TATA-box interaction protein (TIP48) and 49 kDa TATA-box interaction protein (TIP49) (313-316). The interaction of Myc with its co-activators appears dependent upon two specific N-terminal Myc-homology domains (MHI-II), with MHII demonstrating particular functional importance (313-316). The function of Myc: max dimers, however, are actively antagonised by dimers of max dimerisation protein (mad) and max, which also bind the Myc: max recognition sequence 5'-CAYGTG-3' (317, 318). Mad-driven recruitment of mammalian transcriptional co-repressor sin3a (mSin3a), and associated histone de-acetylases (HDACs), subsequently culminates in the transcriptional repression of targets (317, 318).

Whilst Myc was initially identified as a key transactivator of target genes, an additional layer of complexity became apparent upon the demonstration of direct Myc-mediated target gene repression. Such repression is achieved via the ability of Myc to associate with the Zn-finger TF Myc-interacting Zn finger protein-1 (miz-1), via its bHLH domain (319). Myc: miz-1 association de-stabilises miz-1: target sequence interactions preventing HAT recruitment, thus removing the transactivatory function of miz-1 from its targets (309, 319). Therefore, Myc represents a key member of max centred transcriptional regulation, capable of both transactivation and repression of target genes. Furthermore, although the transforming potential of the Myc proto-oncogene was widely accepted, it was subsequently demonstrated that Myc displayed significant

pleiotropism since inducible over-expression of c-Myc leads to the rapid induction of apoptosis (320). Since this discovery, it is now widely accepted that evasion of Myc-induced apoptosis represents a key step in Myc-driven tumourigenesis. Such pleiotropism can be traced back to the concept of intrinsic tumour suppression, introduced in section 1.1, whereby oncogenic changes induce an in-built safety mechanism resulting in the removal of deleterious clones.

1.7.2 Modelling Myc driven tumours: The Eμ-Myc lymphoma model

Delineation of the mechanisms responsible for the evasion of Myc-induced apoptosis has been greatly aided by development of the murine Eμ-Myc spontaneous lymphoma model. The Eμ-Myc model aimed to recapitulate human BL by recreation of the t(8:14) translocation using the Eμ enhancer, thus generating B-lymphocyte-restricted Myc over-expression (42, 321). Myc transgene expressing, Eμ-Myc B-lymphocytes display a modest increase in Myc protein levels, despite a 10-fold increase in transcripts, and complete repression of endogenous c-Myc by negative feedback (322, 323). Such over-expression culminates in the spontaneous development of heterogeneous Pre-B/ immature B-cell lymphoblastic lymphoma and leukaemia at a median onset of 11 weeks (321).

Pre-malignant Eμ-Myc mice demonstrate an initial expansion of the pre-B cell compartment followed by a Myc-driven apoptotic population contraction (324-326). Such Myc-driven intrinsic tumour suppression imparts selective pressures upon pre-malignant clones, driving acquisition of genomic changes that subvert Myc-induced apoptosis (324, 327).

Myc-driven apoptosis appears dependent upon the BH3-only proteins Puma, Bim, Bmf, and Bad since targeted inactivation of each of these genes enhances the rate of Eμ-Myc lymphomagenesis (233, 328-330). Furthermore, Myc dysregulation has been linked to activation of an oncogene-induced DNA damage response and reactive oxygen species (Ros) production via Ataxia telengiectasia-mutated (ATM)-dependent activation of the p14 alternate reading frame (ARF)/Mouse double minute 2 (Mdm2)/p53 pathway (282). In light of this evidence it is perhaps unsurprising that pre-malignant clones of Eμ-Myc mice typically acquire genomic alterations resulting in

over-expression of Bcl-2 or, more commonly, inactivation of the ARF/Mdm2/p53 axis, immediately prior to malignant clone emergence (324, 327, 331, 332).

Although indispensable in the modelling of Myc-induced tumourigenesis, lymphomas emerging from Eμ-Myc mice do not entirely recapitulate human BL. Despite possession of the genetic lesion evident in 80% of BL cases, Eμ-Myc mice succumb to lymphoblastic lymphoma, whereas, BL is associated with a more mature GC-like immunophenotype (333, 334). It has been suggested that such a discrepancy is likely attributable to occurrence of t(8:14) translocation at a more developmentally mature stage in BL, in contrast to germ line translocation in Eμ-Myc mice.

Irrespective of these observations, micro-array analysis of oncogenic pathway signatures demonstrates that early Eμ-Myc tumours largely recapitulate the signalling abnormalities evident in BL (333). Therefore, it is possible that additional factors may facilitate the emergence of a GC-like malignant clone other than Myc translocation in BL (333, 335). Recent studies identify that alternative BCR signalling modes (i.e. tonic vs. antigen-dependent signals) may drive tumourigenesis at differential developmental stages. Such studies identified that chronic antigen exposure drives the emergence of a GC-like Eμ-Myc lymphoma (335). In conjunction with evidence suggesting BCR involvement in diffuse large B-cell lymphoma (DLBCL) and CLL, the role of BCR signals in tumourigenesis and tumour maintenance represents an essential avenue for further study (15, 51, 336).

1.8 Chronic Lymphocytic Leukaemia and the BCR

The concepts of BCR-driven survival and Myc signalling are amalgamated in the aetiology and maintenance of CLL and may, therefore, represent fruitful targets for therapeutic intervention.

1.8.1 CLL and antigenic drive

A vast array of largely circumstantial evidence has implicated antigen-driven BCR signalling in the selection, proliferation, and survival of malignant CLL B-lymphocytes (B-CLL) (13, 14, 336). Such a hypothesis was formulated upon observations of restricted IgVH gene usage (preferentially VH 1-69, VH 4-34 and VH 3-07) and

stereotyped BCRs amongst subsets of CLL patients (337, 338). Indeed, B-CLL exhibit a surface immunophenotype and gene expression profile indicative of a mature, antigen experienced B-lymphocyte (339, 340). Such a proposal seemed to be supported by the observation that *in vivo* B-CLL surface BCR levels appear suppressed, as if continually encountering antigen, and gradually recover when cultured *in vitro* (15, 336, 341). Furthermore as previously mentioned, BCR mutational status has also been determined as a major prognostic marker in CLL (15).

Collectively, such observations imply that antigen driven-BCR signals may play a role in CLL since use of structurally similar BCRs predicts a similar specificity in antigen binding amongst patients. Taken together with the observation that the immunophenotype of B-CLL most closely resembles that of a marginal zone B-cell (which commonly exhibit polyreactive, autoreactive BCRs), it is possible that antigenic drive may be provided by an auto-antigen (13, 14, 336).

The molecular characteristics of the B-CLL response to BCR signalling are becoming clearer thanks to studies utilising immobilised anti-BCR antibodies to mimic the affect of membrane-embedded antigen. Such studies identify BCR-driven engagement of the PI3K/Akt pathway and subsequent upregulation of Mcl-1 and c-Myc as key survival signals in B-CLL (342-344). Such dependency upon BCR-mediated upregulation of survival factors represents an attractive and potentially beneficial target for therapeutic intervention. Indeed, *in vitro* inhibition of BCR-mediated survival signalling, utilising the Syk-inhibitor R406, appears to instigate the apoptotic cell death of B-CLL via downregulation of PI3K/Akt signalling and Mcl-1 levels (345). Indeed, many new therapeutics for the treatment of CLL are targeted at aspects of the BCR signalling machinery. For instance inhibitors of Syk, PI3Kα/δ, and Btk (R788, Cal-101, and Ibrutinib, respectively) are currently the subjects of ongoing clinical trials (346, 347). However, since B-CLL fail to proliferate in vitro, owing to the absence of microenvironment support, assessment of the biology with which such agents provide a therapeutic effect required the development of a pre-clinical *in vivo* model of CLL (348). Such a requirement was met upon development of the Eμ-T-cell leukaemia protein 1 (Tcl1) mouse model of chronic lymphocytic leukaemia.

1.8.2 Modelling CLL

1.8.2.1 The Tcl1 oncogene

The Tcl1 proto-oncogene demonstrates significant expression in both normal and malignant lymphocytes up to the immature stage in the B-lineage (349). Dysregulation of Tcl1 expression is common in T-prolymphocytic leukaemia patients (via translocation to the TCR locus), whilst its expression has also been linked to the pathogenesis of CLL (350, 351). Tcl1 expression in CLL has been demonstrated to correlate with adverse clinical outcome and expression of the poor prognosis markers 70 kDa zeta-chain-associated protein (zap70), IgM^{high} and unmutated IgV_H (350, 351).

1.8.3.2 Tcl1 transgenic mice: models of human disease

Targeted dysregulation of Tcl1 expression has proved a useful tool in modelling human leukaemia in mice. Ectopic T-cell-restricted expression has been demonstrated to give rise to a mature T-cell leukaemia, whereas dysregulation in the B-lineages appears to give rise to a CLL like disease (352, 353). Observation of the latter was made in mice exhibiting a Tcl1 transgene proximal to the IgH enhancer, termed Eμ-Tcl1 mice (353). Such mice demonstrate overt B-cell leukaemia and splenomegaly, with median onset of approximately 15 months, exhibiting many of the molecular features of human CLL (353, 354). The malignant clone exhibits a low proliferative rate and a $B220^+$, IgM^+, $CD5^+$, $CD21^{low}$, $CD116^+$ immunophenotype alongside stereotyped and autoreactive BCRs, directed against phosphatidylcholine in some instances (353-355). In addition to a highly similar expression pattern of surface markers, Eμ-Tcl1 leukaemias appear to behave comparably to the highly aggressive U-CLL subset, and demonstrate an analogous response to fludarabine treatment (354, 355).

As such, the Eμ-Tcl1 mouse model appears to recapitulate many aspects of human CLL and thus represents an attractive pre-clinical model in which prospective therapeutic interventions can be trialled. Studies focusing upon pharmacological intervention in the BCR pathway have recently begun utilising the Eμ-Tcl1 model and have produced some promising results. Syngeneic Eμ-Tcl1 transfer experiments utilising the Syk inhibitor R788 (the pro-form of R406) demonstrate potent R788-mediated growth arrest and prolonged survival ranging from a median of 46 days in untreated mice to 172 days in treated mice (356). Therefore, Eμ-Tcl1 leukaemias appear sensitive to

perturbation of BCR signalling pathways and consequently, represent an appropriate model of CLL to assess the therapeutic potential of such agents.

1.8.3.3 The oncogenic activity of Tcl1

Whilst Tcl1 appears to directly influence CLL pathogenesis, the specific molecular mechanisms by which Tcl1 acts as an oncogene remain unclear. Studies suggest that Tcl1 co-immunoprecipitates with Akt and functions to enhance its kinase activity (357). However, Akt activation alone is insufficient to drive B-cell neoplasia and therefore, oncogenic Tcl1 may demonstrate additional Akt-independent effects (357). Since this initial study, the oncogenic activity of Tcl1 has been described to directly regulate DNA methyltransferase (Dnmt) activity (via interaction with Dnmt3A and Dnmt3B), to drive cAMP response element binding protein (CREBP)/ 300 kDa HAT (p300)-mediated NF-κB transactivation, and inhibit AP-1 mediated transactivation of targets (358, 359). However, such studies utilise a highly artificial system of forced over-expression in 293 cells and therefore, many of these interactions may be as a consequence of unnaturally high Tcl1 levels. Therefore, additional studies into the oncogenic properties of Tcl1 are required in more physiological settings.

1.8.3.4 The IgH.TEμ model of CLL

An additional murine model of human CLL has been developed recently, termed the IgH.TEμ model. Such mice demonstrate a Simian vacuolating virus 40 (SV40) virus large T antigen (T) coding region proximal to the Ig_H enhancer and therefore, exhibit B-cell restricted ectopic expression of the T antigen (360). The T antigen is proposed to function as an oncogene via inactivation of p53 and retinoblastoma (Rb) proteins, alongside instigation of genomic instability (360). Consequently, IgH.TEμ mice exhibit lymphadenopathy, splenomegaly and overt leukaemia alongside a $CD19^+$, $B220^+$, $CD5^+$, IgM^+, IgD^{low}, $CD21^-$, $CD23^-$ immunophenotype and germ line Ig_VH coding regions (360). Much like the Eμ-Tcl1 mouse the IgH.TEμ mouse model appears to recapitulate the immunophenotype and molecular characteristics of U-CLL. However, these data arise from a single study and further examination of the validity of this model is required prior to use as a pre-clinical model for CLL.

1.9 Aims and objectives

It is the aim of this investigation to characterise and harness the cellular response to pleiotropic, biological stimuli in the treatment of murine models of human B-cell neoplasms. Since BCR cross-linking results in the specific apoptotic demise of many B-cell neoplasms, therapeutic activation of BCR-signalling represents an attractive target. To date, studies aiming to specifically target the unique BCR of the malignant clone, and prevent depletion of the patients normal B-cells, have utilised malignant clone-specific anti-BCR mAbs, termed anti-idiotype (anti-Id) therapy. Proof of this concept was shown by the work of Vuist et al in 1994 who demonstrated that anti-Id mAb treatment of NHL patients induced a partial response in 63% of patients (244, 361). Such therapeutic responses occurred independently of patient Bcl-2 expression status and therefore, proved an attractive therapeutic strategy for highly chemo-resistant patients possessing high Bcl-2 expression levels (244, 361). However, due to its patient-specific nature, anti-Id treatment remains impractical for mass-use. Therefore, in order to exploit this weakness in malignant B-cells alternative strategies for pathway targeting or antibody production are required.

Alternative targeting may be provided by the development of small molecule inhibitors targeting aspects of the apoptotic pathways downstream of the BCR. Specific therapies may be harnessed to permit BH3-only protein reactivation, since dysregulation of their expression and function is associated with the onset of Lymphoma (12, 362, 363). Validation of this concept is provided by the studies of Nakagawa et al, who demonstrate that epigenetic silencing of Bim is associated with the development of chemo resistant BL (12). Subsequent reversal of silencing, via HDAC inhibitor treatment, unleashed the tumour suppressive qualities of Bim leading to the induction of cell death (12). Furthermore, BCR cross linking appears to engage differential signalling kinetics in malignant B-cells in comparison to wild-type tumour infiltrating B lymphocytes (234). Therefore, it is not implausible to suggest that differences in BCR signalling may be exploited in order to engender tumour-specificity.

To date few studies have focused upon BCR-induced apoptosis in primary lymphoma samples. Instead studies have focused upon the use of long-term well-established cell-lines, which are likely to signal differently to primary tumours.

Therefore, this investigation aims to

- Characterise the apoptotic response to BCR crosslinking in low passage number Eμ-Myc lymphoma cell lines
- Observe the impact of genetic loss of individual BH3-only proteins upon BCR-induced cell death in Eμ-Myc lymphoma cells
- Dissect the role of BCR-induced kinase signalling pathways in BCR-induced cell death
- Observe potential links between BCR-induced kinases and BH3-only protein regulation

Furthermore, since antigenic drive potentially contributes toward the maintenance and leukaemiagenesis of CLL (13, 14, 336), this investigation aims to assess the potential therapeutic benefit of BCR signal inhibition in a murine model of CLL. Specifically, this investigation aims to

- Characterise the Eμ-Tcl1 and IgH.TEμ mouse models of CLL
- Determine the fidelity with which such models recapitulate human CLL
- Observe the relative tumour suppressive roles of BH3-only proteins during leukaemiagenesis
- Undertake syngeneic transfer studies utilising Eμ-Tcl1 tumours and assess the impact of kinase inhibitors and mAb therapeutics upon survival.

Finally, since TGF-β and loss of BCR signals appear to co-operate in the death by neglect process of centroblast selection, we aim to assess the relative contribution of BH3-only proteins during TGF-β-induced apoptosis. This investigation, therefore, shall

- Utilise Eμ-Myc lymphoma cells as a model of GC centroblasts
- Identify the effect of TGF-β signalling upon BH3-only protein expression
- Assess the impact of genetic loss of BH3-only proteins upon the extent of TGF-β-induced cell death

Chapter 2 Materials and Methods

2.1 Cell culture materials

Cells were initially maintained in 15% Eμ-Myc medium (Dublecco's modified eagles medium (DMEM) (Life technologies, UK) supplemented with 15% foetal calf serum (FCS) (Lonza, CH), 2mM glutamine (Life technologies, UK), 1mM pyruvate (Life technologies, UK), 45 units/ml penicillin (Life technologies, UK), 45 μg/ml streptomycin (Life technologies, UK), 200 μM asparagine (Sigma, UK) and 50 μM 2-mercaptoethanol (Sigma, UK)) at 37˚C, 10% CO_2 in 6-well plates. Once cultures had become accustomed to tissue culture, cells were subsequently maintained in Eμ-Myc medium supplemented with 10% FCS (Lonza, CH) instead of 15% at 37˚C, 10% CO_2 in 6-well plates. In the case of Eμ-Myc lymphoma cells, cell-lines were maintained *in vitro* until passage number 25, after which they were subsequently discarded. Eμ-Myc tumour cell-lines were not used for study until after at least passage number 5. In addition to Eμ-Myc lymphoma cells, Myc tg and normal C57BL/6 B-lymphocytes were utilised, and maintained in vitro at 37°C, 10% CO_2 in 10% Eμ-Myc medium.

2.2 Antibodies and inhibitors

In-house monoclonal antibodies (mAbs), produced from antibody-secreting hybridoma supernatants, were purified on Protein A columns (Amersham Biosciences, UK) according to the manufacturer's instructions. mAb purity was ascertained via routine protein electrophoresis, and HPLC. mAb concentration was determined by use of the Nano-drop® spectrophotometer (Thermo scientific, UK) measuring absorbance at 280nm, using an extinction co-efficient of 1.45 for mouse IgG. To stimulate the BCR, cells were treated with Fc5μ chain specific Goat anti-Mouse IgM $F(Ab)_2$ (Jackson Immunotech, USA) or Rat Anti-Mouse IgM IgG2a (Mc39.12) (In-house).

Un-conjugated antibodies against caspase-3 (#9661), caspase-6 (#9762), caspase-7 (#9492), caspase-9 (#9504), PARP (#9542), pAkt (#4060), Akt (#9272), pERK (#9101), ERK (#4695), pp38 (#4631), p38 (#9212), pSMAD2 (#3101L) and Tubulin (#2144) were obtained from Cell signalling technologies, USA. Antibodies against elk-1 (I-20) and lamin-B (C-20) were purchased from Santa Cruz Biotechnology, USA. Anti-pJNK

(Ab4821), JNK (Ab10664), Mcl-1 (Y37) and c-Myc (Y69) antibodies were obtained from Abcam, UK. Anti foxo3a (07-702), myb (Clone 1-1), and SP-1 (07-645) antibodies were obtained from Millipore, USA. The polyclonal rabbit anti-Bim, Bad, and Puma (N-terminal) antibodies were obtained from Enzo Lifesciences, USA. The anti Bid antibody was obtained from R&D systems, USA. Rat anti-mouse mAbs against A1 (AC7), caspase-1 (18H2), caspase-2 (11B4), caspase-8 (1G12), caspase-11 (4711), caspase-12 (12G6), Bim (3C5), Bcl-xL (1C2), Bcl-w (13F9), CHOP (9C8) and Bmf (17A9) were the kind gift of Drs Andreas Strasser, David Huang, Claire Scott, and Lorraine O'Reilly (WEHI, Melbourne, Australia). Anti-Bcl-2 clones 3F11 and 610539, biotinylated anti-IgM^b (AF6-78) and anti-λ (R26-46) were obtained from BD Biosciences, USA. Fluorophore conjugated anti-CD5 (57-7.3), CD79b (555303), IgM^a (DS-1), B220 (RA3-6BS), and Streptavidin (5554060) were also obtained from BD Biosciences, USA. Fluoroscein isothiocyanate (FITC) conjugated anti-Human Bcl-2 (Clone 124) was obtained from DAKO, UK. Rat anti-mouse CD19 (1D3), CD38 (1A5E8), κ (HB58) and rat IgG2a isotype control (Mc.39.16) were produced, and fluorophore conjugated, in-house.

E64d, Necrostatin-1, 3-methyladenine, 2′,7′-Dichlorofluorescin diacetate, LY294002 and dihydroethidium were purchased from Sigma-aldrich, UK. LEHD-fluoromethylketone, the calpain inhibitor Cx295, Mg132, Latrunculin B, CA-074, SP600125, Bafilomycin A1, and Concanamycin A were obtained from Calbiochem, USA. R406, R788, and PD0325901 were obtained from Selleck chemicals, USA. DiOC6, Sytox-green, and Fluo-4-AM were purchased from Life technologies, UK. qVD-OPH was obtained from MP Biochemicals, USA. Annexin V was produced in-house by Dr. Patrick Duriez (Protein production service, Cancer sciences unit, Southampton).

2.3 Antibody dialysis

Dialysis was performed on in-house purified mAb using Slide-A-lyzer dialysis cassettes (Thermo Scientific, UK) according to manufacturer's instruction. Cassettes were placed in 2L phosphate-buffered saline (PBS) and the buffer changed every 2 hours with at least 3 changes.

2.4 Animals

Eμ-Tcl1, IgH.TEμ, and Eμ-Myc mice were initially backcrossed with C57BL/6 mice for at least 6 generations, once obtained, to give at least 10 back-crossings since their inception. Mice were maintained in local facilities and were cleared through the local ethical committee under Home Office licenses PPL30/2450 and 30/2451. Mice were assessed for possession of a Tcl1, SV40 large T antigen, or Myc transgene by PCR, as outlined in section 2.6.1-3. Subsequently, transgenic animals were maintained as heterozygotes alongside non-transgenic littermate controls and crossed with $Bim^{-/-}$ C57BL/6 mice, and the genotype of their offspring assessed by PCR, as outlined in section 2.6.4. Subsequent crossing yielded $Bim^{+/-}$ and $Bim^{-/-}$ mice carrying the relevant tumour driving oncogene. In order to track tumourigenesis, monthly tail blood samples were taken from Eμ-Tcl1 and IgH.TEμ mice and monitored for the occurrence of leukaemia, as outlined in section 2.5. Furthermore, all tg Eμ-Myc and IgH.TEμ mice presented with symptoms including hunching with laboured breath, withdrawal from littermates, agitated behaviour, and a generally unkempt appearance. However, Eμ-Tcl1 mice failed to exhibit such symptoms and unexpected mortality was common when tumours reached 80% of peripheral lymphocytes, see section 2.5. Therefore, an earlier humane end-point was established where mice were culled when tumours represented 80% of peripheral lymphocytes and was adhered to throughout remaining studies utilising Eμ-Tcl1 animals.

Once animals displayed symptoms of ill-health (or 80% $CD5^{+}$, $B220^{+}$ peripheral lymphocytes in the case of the Eμ-Tcl1 model) animals were culled via application of CO_2. Subsequently, mid-line dissection and autopsy was undertaken, during which the spleen, lymph nodes, thymus and bone marrow, were taken and placed in 10 ml ice-cold Eμ-Myc medium for further analysis. The weight, size and/ or number of cells were recorded for each organ following production of single cell suspensions, as outlined in section 2.7. Samples were then frozen at -80°C for one week before subsequent transfer to -180°C freezers for long-term storage. In addition sections of the lung, spleen, thymus, heart, liver, kidney, bone-marrow, lymph node and sternum were harvested and placed in formalin (Sigma-Aldrich, USA), and stored at 4°C for at least 24 hours followed by histological analysis. Haematoxylin and Eosin staining was

performed upon paraffin embedded sections by the Histochemistry research unit (Southampton, UK), and were observed under x10 magnification using a CKX41 light microscope (Olympus, UK).

2.5 Eμ-Tcl1 and IgH.TEμ tumour monitoring

Monthly, 50 μl tail blood samples were taken from Eμ-Tcl1 and IgH.TEμ mice and mixed with 10 μl Heparin Sulphate (Wockhardt, UK) to prevent clotting. 20 μl of blood, diluted 1/5 in PBS, was taken and diluted in 10 ml Coulter Isoton III diluent (Beckman Coulter, UK) prior to addition of 3-5 drops of zapoglobin red blood cell lytic reagent (Beckman Coulter, UK) and mixing. White blood cell (WBC) counts were subsequently undertaken using a Coulter Industrial D Cell counter (Beckman Coulter, UK), according to the manufacturer's instructions.

For immunostaining of IgH.TEμ mice, 10 μl un-diluted blood was also taken and stained with 1.25 μg/ ml anti-IgMa^{PE}, 6.25 μg/ ml anti-IgMb^{Biotin} and 5 μl anti-CD19^{APC} made up to a final volume of 100 μl with wash buffer (PBS, 1% BSA, 0.1% Sodium Azide) for 30 minutes on ice. Cells were subsequently washed by addition of 3 ml wash buffer, centrifuged at 1500 rpm/ 180x g, buffer discarded and re-suspended in approximately 100 μl. FITC-conjugated Streptavidin was subsequently applied at 5 μg/ ml for 30 minutes on ice. For immunostaining of Eμ-Tcl1 mice 10 μl un-diluted tail blood was stained with 5 μg/ ml anti-CD5^{FITC} alongside 5 μg/ ml B220PercP made up to a final volume of 100 μl with wash buffer for 30 minutes on ice. Cells of both IgH.TEμ and Eμ-Tcl1 mice were then washed and the buffer discarded. Subsequently, red blood cell lysis was performed by addition of 1 ml erythrolyse (AbD Serotec, UK) to cell pellets. Finally, cells were washed and re-suspended in 100 μl wash buffer and analysed by flow cytometry.

2.6 Mouse genotyping

In each case, to screen for the presence of the gene of interest, ear tips were obtained from prospective transgenic animals and digested in 50 mM Tris pH 8.9, 12.5 mM $MgCl_2$, 0.5% Tween-20, and 0.4 mg/ ml proteinase K for 18 hours at 55°C. Digests were diluted 1/5 with sterile H_2O and 1 μl of digested material containing DNA was assessed by genomic PCR

2.6.1 Eμ-Tcl1 tg detection

PCR analysis for Tcl1 transgene possession was performed using the following primers: Tcl1 univ. 5'-GCCGAGTGCCCGACACTC-3', Tcl1 Rev 5'-CATCTGGCAGCAGCTCGA-3' producing a product of approximately 250 bp in transgenic animal whereas. A typical result is outlined in appendix A3.Animals possessing the Tcl1 tg were marked and kept with non-transgenic littermate controls.

2.6.2 SV40 Large T Antigen detection

PCR analysis for possession of the SV40 large T antigen transgene was performed using the following primers: SV40 T antigen forward 5'-GGAAAGTCCTTGGGGTCTTC-3' AND SV40 T antigen reverse 5'-CACTTGTGTGGGTTGATTGC-3', producing a product of approximately 300 bp in transgenic animals. A typical result is outlined in appendix A4.

2.6.3 Myc tg detection

Possession of a Myc transgene was assessed by genomic PCR utilising the following primers: Myc-1 5'-CAGCTGGCGTAATAGCGAAGAG -3' and Myc-2 5'-CTCTGACTGGTGAGTACTCAACC -3', producing a product of approximately 900 bp. A typical result is outlined in appendix A5.

2.6.4 Bim status

Analysis of wild-type or targeted Bim allele possession, as described by Egle et al (233) was undertaken by genomic PCR. Briefly, three primers were utilised: common primer PB20 (5'-CATTCTCGTAAGTCCGAGTCT-3'), wild type allele primer PB335 (5'-GTGCTAACTGAAACCAGATTAG-3') and the targeted allele primer PB65 (5'-CTCAGTCCATTCATCAACAG-3'). WT alleles gave a band of approximately 300 bp owing to amplification using the PB20 and PB335 primers. In contrast, insertionally inactivated/ targeted alleles give a band of approximately 500 bp owing to amplification using the PB20 and PB65 primers. PCR products from heterozygotes possessed both WT and targeted allele bands whereas, homozygous WT or Bim-/- animals exhibited only the WT or targeted allele bands, respectively. A typical result is outlined in appendix A6.

2.7 Cell line derivation from Eμ-Myc, Eμ-Tcl1, and IgH.TEμ tumours

Spleens taken from terminal Eμ-Myc, Eμ-Tcl1, or IgH.TEμ mice were passed through a fine nylon mesh (Becton Dickinson, USA) to achieve a homogeneous cell suspension in 10 ml 15% Eμ-Myc medium. Cell suspensions were subsequently centrifuged at 15,000 rpm/ 180 xg for 5 minutes at 4°C and the medium discarded. Cell pellets were then resuspended in fresh 15% Eμ-Myc medium and maintained at 37˚C, 10% CO_2 in 6-well plates. In the case of Eμ-Myc lymphoma cells, cells were maintained until red blood cells and other cell types had disappeared, cell suspensions appeared morphologically homogeneous, and were dividing rapidly. Subsequently, cells were transferred into 10% Eμ-Myc medium and maintained at 10% CO_2 in 6-well plates until passage number 25, after which they were subsequently discarded. Eμ-Myc tumour cell-lines were not used for mechanistic studies until after at least passage number 5. In contrast to Eμ-Myc lymphoma cells, cells obtained from the spleens of terminal Eμ-Tcl1 and IgH.TEμ mice failed to proliferate in vitro and rapidly died.

In order to confirm the malignant nature of Eμ-Myc lymphomas and Eμ-Tcl1 and IgH.TEμ leukaemias, cells were centrifuged at 1500 rpm/ 180 xg for 5 minutes at room temperature and resuspended at $5x10^6$ cell/ml in sterile PBS. $1x10^6$ cells were subsequently re-passaged into C57 Black 6 (C57BL/6) mice by intravenous injection (except for Eμ-Tcl1 tumours, $1x10^7$ cells were given by intraperitoneal injection). Mice were subsequently monitored for signs of disease, as previously described and tumours were designated as malignant upon onset of symptoms of tumours in passaged mice.

2.8 Syngeneic transfer experiments of Eμ-Tcl1 cell lines

The well-studied Eμ-Tcl1 tumour cell line Eμ-Tcl1-002 was the generous gift of Prof D. Efremov (Rome, Italy), which represents a tumour derived from the initial study into Eμ-Tcl1 mice performed in C3H-C57BL/6 F1 mice. Therefore, subsequent syngeneic transfer experiments were carried out in C3H-C57BL/6 F1 mice (356) to prevent rejection. On day 0, $1x10^7$ Tcl1-002 cells were introduced by intraperitoneal injection, into 5 mice per group (2 males, 3 females), and the occurrence of leukaemic cells was

assessed as outlined in section 2.5. After 14 days, leukaemic cell populations had reached around 10% of peripheral lymphocytes and treatments were commenced as required. The effect of therapies upon blood counts and the leukaemic cell population was subsequently observed by flow cytometry and WBC counts every 2-3 days. Experimental end points were set to leukaemias reaching 80% of total PBMCs since mortality was unpredictable at higher proportions. Upon end-point attainment mice were sacrificed and processed, as before.

2.9 B-cell purification

Spleens were isolated from C57BL/6 or Myc tg mice and passed through a nylon mesh to achieve a single cell suspension, as in section 2.7. Splenic B-lymphocytes were subsequently isolated via use of a MACS B-cell isolation kit (Miltenyi Biotech, Deu) according to the manufacturer's instructions. Briefly, cell suspensions were incubated with an antibody cocktail containing biotin-conjugated anti-CD43, CD4, and Ter119 mAbs for 30 minutes on ice. Such antibodies label T-cells, natural killer (NK) cells, DCs, macrophages, granulocytes and erythrocytes, but not B-cells. Subsequently, cells were incubated alongside streptavidin-conjugated microbeads for 30 minutes on ice, and applied to a MACS column subjected to a magnetic field. Non-B-lymphocytes are retained within the column whereas pure B-lymphocytes exit the column and are collected. The purity of purified B-cells was subsequently assessed via flow cytometry using CD19 as a B-cell marker and CD3 as a marker of T-cells. Routinely, cell suspensions were >95% CD19 positive.

2.10 Extracellular flow cytometry

$2x10^5$ cells were centrifuged at 1500 rpm/ 180x g to pellet and re-suspended in a final volume of 100µl wash buffer alongside a final concentration of 10 µg/ ml FITC/PE conjugated antibody for 30 minutes on ice. Cells were then washed by application of 3 ml wash buffer and centrifuged at 1500 rpm/ 180x g. The supernatant was subsequently discarded and pellets were re-suspended in approximately 100 µl and analysed on a FACScan or FACScalibur flow cytometer (Becton Dickinson). Dot plots of live cell events, determined according to the FSC/SSC profile, were subsequently analysed using cellquest pro software (BD Biosciences, UK). For mouse blood samples,

10 μl tail blood was incubated with antibody and washed as described above. Where required, 1 μl conjugated streptavidin was incubated with cell pellets in a final volume of 100 μl wash buffer for 30 minutes on ice. Cells were then washed as before and red blood cells lysed using erythrolyse (AbD Serotec, UK) according to the manufacturer's instruction, followed by an additional wash step in was buffer and resuspended in 100 μl wash buffer.

2.11 Intracellular flow cytometry

$1x10^6$ cells were fixed in 0.05% w/v formaldehyde in PBS for 15 minutes at room temperature. Cells were then washed with wash buffer and resuspended in 100 μl 0.5% w/v saponin in PBS alongside a final concentration of 10 μg/ml fluorophore conjugated antibody for 30 minutes at room temperature in the dark. Cells were then washed twice with 0.05% w/v saponin in PBS and analysed by flow cytometry using a FACScalibur flow cytometer and cellquest pro software (BD Biosciences, UK).

2.12 Calcium flux assay

Changes in intracellular calcium levels were observed using the fluorescent Ca^{2+} probe Fluo-4 (Life technologies, UK), developed by Gee et al (364). Fluo-4 essentially represents a modified form of the well-characterised Ca^{2+} indicator Fluo-3, where two Fluorine atoms were substituted for Chlorine in order to enhance the magnitude of the emission maximum. The structure of Fluo-4 resembles that of a modified fluoroscein moiety and consequently exhibits absorption at 488 nm, and is excitable via argon-laser equipped flow cytometers at 488 nm. Upon Ca^{2+} binding Fluo-4 undergoes a 100-fold enhancement in fluorescence intensity, detectable in the FL-1 channel. However, no spectral shift is generated, as with Indo-1 and Fura-2 dyes, therefore Fluo-4 cannot be used to directly measure $[Ca^{2+}]I$, rather it indicates relative Ca^{2+} levels. Fluo-4 is applied in an acetoxymethyl (AM) pro-form, aiding crossing of the plasma membrane. Once in an intracellular environment cytoplasmic esterases cleave the ester-linked AM group, thus trapping the Fluo-4 probe in the cell.

$1x10^7$ cells were harvested and centrifuged at 1500 rpm/ 180x g for 5 minutes at room temperature. Cell pellets were resuspended at $1x10^7$/ ml using the residual growth medium and incubated with 0.004% w/v pluronic F-127 (Sigma-aldrich, UK) and 10 μM

Fluo-4 AM (Life technologies, UK) for 30 minutes at 37°C, 10% CO_2. Post-incubation, cells were centrifuged at 1500 rpm/ 180x g for 5 minutes, the supernatant discarded and resuspended in 2 ml 10% Eμ-Myc medium. Prior to analysis by flow cytometry, cells were rested by incubation at 37°C, 10% CO_2 for 30 minutes. A baseline value for resting cells was obtained and cells were subsequently treated as required. Results were analysed using Flowjo software (Treestar, USA) and plotted as change in Fluo-4 intensity over time. In order to calculate the percentage of cells that exhibited Ca^{2+} flux responses upon anti-IgM addition, a background fluorescence threshold of the 90% enhanced fluorescence with respect to un-stimulated cells was established. The peak percentage of cells exhibiting increased fluo-4 fluorescence was then calculated over time, and plotted as a kinetic trace.

2.13 In vitro cell death assays

2.13.1 Annexin V/ Propidium Iodide

The annexin V/ propidium Iodide (PI) death assay utilises both a vital stain, in the form of PI, and a stain that permits the detection of phosphatidylserine (PS) externalisation (annexin V FITC), a caspase-dependent process undertaken during apoptosis commitment. PI functions as a DNA interchelater and produces fluorescence detectable in the FL-2 channel upon excitation at 488 nm. Discrimination between dead and viable cells is ensured by the exclusion of PI from viable cells. Such exclusion is attributed to the polar nature of PI; ensuring translocation across intact plasma membranes is highly thermodynamically unfavourable. Conversely dead cells demonstrate a loss of plasma membrane integrity, allowing PI access to the nucleus and interchelation into DNA. PI determines whether cells are viable or dead however, provides no information on the specific mode of death. Detection of an apoptotic death is possible via the detection of PS externalisation prior to the loss of plasma membrane integrity. Detection of such events is enabled by the use of annexin V FITC, which binds PS in a Ca^{2+}-dependent manner. Only annexin V^+/ PI^- cells can be inferred as undergoing apoptosis since loss of plasma membrane integrity allows annexin V access to internal membrane leaflet PS and therefore does not reflect loss of plasma membrane asymmetry.

Annexin V/ PI death assays were performed as determined by Vermes et al (365). Cells were re-suspended at $1.6x10^6$ cells/ ml and 125 µl ($2x10^5$ cells) were loaded, per well, into a 96-well plate and 125 µl of medium containing an appropriate concentration of treatment applied as required. At allotted time-points cells were harvested by pipetting and stained with annexin V FITC at a final concentration of 160 ng/ ml or annexin V APC (BD Biosciences, UK)(0.4 µl/tube) and 3.6 µg/ml PI (Sigma, UK) in annexin V binding buffer (10 mM HEPES pH 7.4, 140 mM NaCl, 2.5mM $CaCl_2$) for 15-30 minutes at room temperature in the dark, and analysed on a FACScan flow cytometer (BD Biosciences, UK) using Cellquest pro software (BD Biosciences, UK).Cells were considered dead/ dying upon the attainment of Annexin V positivity. When considering the impact of various treatments upon viability, values obtained were subsequently corrected for background cell death levels recorded in a vehicle alone treated sample, using the equations:

Corrected % Viable = (% Viable in treated cells/ % Viable vehicle treated cells)*100

Corrected % Cell death = 100 – Corrected % Viable

Where viable cells were characterised as Annexin V^-/PI^- and dead cells either Annexin V^+/PI^- or Annexin V^+/PI^+.

2.13.2 $DiOC_6$/ PI

The 3,3'-dihexyloxacarbocyanine iodide ($DiOC_6$) / PI death assay allows analysis of the integrity of mitochondria during cell death processes. The assay relies upon $DiOC_6$-mediated staining of only mitochondria with an intact outer membrane. Mitochondria possessing an intact outer membrane demonstrate a significant mitochondrial membrane potential via the actions of oxidative phosphorylation. This membrane potential drives accumulation of $DiOC_6$ within the intermembranous space, therefore, producing a signal detectable in the FL-1 channel. Upon MOMP, loss of the mitochondrial membrane potential is detectable by a reduction in FL-1 detectable fluorescence.

$DiOC_6$ (Life Technologies, UK) was added to cell culture at a final concentration of 10 nM 30 minutes prior to harvesting, following the protocol suggested by Rottenberg et

al (366) . Cells were harvested by pipetting and centrifuged at 1500 rpm/ 480x g for 5 minutes to pellet. Pellets were washed with ice-cold PBS and re-suspended in 250 µL PBS containing 3.6 µg/ml PI and analysed on a FACScan flow cytometer (BD Biosciences, UK) using Cellquest pro software (BD Biosciences, UK).

2.13.3 Hypotonic PI

Analysis of cellular DNA content was performed as determined by Nicoletti et al (367). Hypotonic PI staining permits analysis of cellular DNA content via membrane permeablisation, permitting PI entry into the cell and access to the nucleus. PI interchelates into DNA with a stoichiometry of 1 PI molecule for every 4-5 bp. Therefore, the extent of PI fluorescence is proportional to the DNA content of the cell. Consequently, the hypotonic PI assay can be used for cell cycle analysis alongside detection of internucleosomal DNA degradation during apoptosis.

$2x10^5$ cells were taken and treated as required. Subsequently, cells were centrifuged at 1500 rpm/ 480x g at room temperature for 5 minutes and the growth medium discarded. Cell pellets were re-suspended in a hypotonic PI solution (50 µg/ml PI, 0.1% w/v Sodium citrate, 0.1% w/v triton x-100) and incubated in the dark at 4°C for 30 minutes. Events were subsequently analysed by flow cytometry using a FACScan flow cytometer (BD Biosciences, UK) and cellquest pro software (BD Biosciences, UK).

2.14 SDS-PAGE and Western blotting

2.14.1 Production of whole cell lysates

12 hours prior to commencement of the experiment $5x10^6$ cells per sample were plated out in a 6-well plate in a final volume of 3 ml. Cells were treated as required, without the addition of fresh medium, and harvested by pipetting at the appropriate time point. Cells were centrifuged at 1500 rpm/ 180x g for 5 minutes to pellet, and washed with 1 ml ice cold PBS and re-pelleted. Cell pellets were re-suspended in 25 µl ice-cold radioimmunoprecipitation assay (RIPA) buffer (1/500 protease inhibitor cocktail (Sigma-Aldrich, UK), 50 mM NaF, 2 mM Na_3VO_4, 50 mM Tris-HCl pH 8, 150 mM NaCl, 0.5% v/v Triton X-100, 0.5% w/v Sodium deoxycholate, and 0.1% w/v sodium dodecyl sulphate (SDS)) by pipetting and left on ice for 30 minutes with regular

agitation by vortexing. Lysates were centrifuged at 16,000x g for 15 minutes at 4˚C to pellet insoluble material. Lysates were subsequently stored at -20˚C.

2.14.2 Production of nuclear and cytoplasmic extracts

Subcellular fractionation was undertaken via a modified version of the protocol devised by Andrews and Faller (368). $3x10^7$ cells per sample were plated at $1x10^6$/ ml and allowed to rest for 12 hours. Cells were then treated as required. Cells were pelleted by centrifugation at 180x g for 10 minutes at 4°C and the supernatants discarded. Cell pellets were then re-suspended in ice cold PBS, re-pelleted by centrifugation, and the supernatants discarded. Cell pellets were then re-suspended in 400 µl ice cold hypotonic nuclear extraction buffer A (10 mM HEPES-KOH pH 7.9, 1.5 mM $MgCl_2$, 10 mM KCl, 0.5 mM dithiothreitol (DTT)). Cells were allowed to swell on ice for 10 minutes and then lysed by vortexing. In most cases, vortexing was insufficient to completely lyse cell pellets. Therefore, 0.1% NP40 was added to samples prior to vortexing to ensure efficient lysis. Lysates were then centrifuged at 180x g for 10 minutes at 4°C and the supernatant, containing the cytoplasmic extract, was stored for further use. The resulting nuclear pellets were then re-suspended in 35 µl ice cold high salt nuclear extraction buffer C (20 mM HEPES-KOH pH7.9, 25% Glycerol, 420 mM NaCl, 1.5 mM $MgCl_2$, 0.2 mM EDTA, 0.5 mM DTT) and incubated on ice for 20 minutes to precipitate DNA binding proteins. Insoluble material was then pelleted via centrifugation at 3,000x g for 30 minutes at 4°C. The supernatant (nuclear extract) was subsequently removed and stored at -80°C. The previously described cytoplasmic fraction was now subjected to trichloroacetic acid (TCA) precipitation to reduce the 400 µl volume. Briefly, 100 µl TCA was added to 400 µl of cytoplasmic extract and incubated for 10 minutes at 4°C, to precipitate proteins. Tubes were then centrifuged at 3,000x g for 5 minutes at 4°C to isolate precipitated proteins and the remaining supernatants discarded. Protein pellets were subsequently washed twice with ice-cold acetone, followed by centrifugation to pellet. Protein pellets were subsequently dried via placing tubes in a 95°C heat block for 5 minutes. Protein pellets were then re-dissolved in 35 µl RIPA buffer and stored at -80°C.

2.14.3 Protein quantification and SDS-PAGE

Protein content was quantified colourimetrically via application of 200 µl of the Bradford protein reagent (Bio-Rad, USA) to 5 µl 1/5 diluted lysate. Absorbance was measured using a plate-reader at 595 nm and compared to a bovine serum albumin (BSA) standard curve of known concentration. The Bradford assay relies upon the spectrophotometric shift of coomassie brilliant blue upon protein binding which produces a λ_{max} of 595 nm. 25 µg lysate was subsequently mixed with 8.8 µl 4x reducing-Laemlli loading buffer (900µl (80 mg/ml SDS, 0.1% bromophenol blue, 0.25 M Tris-HCl, 4 ml glycerol made up to 10 ml Milli-Q H_2O) +100 µl 2-mercaptoethanol (2-ME) (to give a final concentration of 1.3 mM)) and dH_2O to 35 µl. Samples were centrifuged at 16,000 x g for 2 minutes and incubated at 95˚C for 5 minutes, followed by centrifugation at 16,000 x g for 2 minutes. Samples were loaded in 10%, 12%, or 15% bis-tris NuPage polyacrylamide gels (Life technologies, UK) and run at 100V using 3-(N-morpholino)-propanesulfonic acid (MOPS) electrode buffer (5mM MOPS, 70mM SDS, 5mM Tris, 1mM EDTA).

2.14.4 Western blotting

For western blotting, lysates were transferred to an Opitran 0.2 µm nitrocellulose membrane (Whatman, USA) using the Xcell II TM blot module (Life technologies, UK) and NuPage transfer buffer (Life technologies, UK) containing 10% methanol at 30 V for 60-90 minutes. Membranes were subsequently washed for 2 minutes in Tris-buffered Saline (TBS) (10mM Tris, 150mM NaCl pH 7.6) 0.05% Tween) (TBS-T) with agitation. Membranes were blocked via application of 5% non-fat milk TBS-T for 1 hour at room temperature with agitation and subsequently rinsed thrice with TBS-T. Primary antibodies were applied at a 1/500 dilution in TBS-T, 5% BSA, 0.05% Sodium azide at 4˚C with agitation overnight. Membranes were then washed thrice with TBS-T for 5 minutes each at room temperature. Membranes were incubated with species-specific horseradish peroxidase (HRP)-conjugated $F(Ab)_2$ fragment (GE Bioscience, UK) in 5% non-fat milk TBS-T for 1 hour at room temperature. Bands were visualised using Immobilon western Chemiluminescent HRP substrate (Millipore, USA) and the UVP bio imager using vision works software (UVP, UK). Quantitation of western blots was performed using the densitometry function of vision works software (UVP, UK). Briefly,

bands were highlighted and the density measured and background corrected for by utilising the rolling disc background compensation tool set at 200 nm. Band density was then corrected for levels of protein loading by normalisation against a Tubulin control. Normalised values for treated samples were then divided by values obtained from un-treated cells at the same time point to give fold-change.

2.15 Immunoprecipitation

Protein complexes were immunoprecipitated (IPd) according to the methodology proposed by Hsu and Youle (106, 166). Cells were seeded at $1x10^6$/ ml, with a total cell number of $1x10^8$ cells per sample, 12 hours prior to the beginning of the experiment and treated as required.

Subsequently, cells were harvested by pipetting and centrifuged at 15,00rpm/ 180x g for 5 minutes to pellet. The supernatants were then discarded and cell pellets washed in ice-cold PBS. Cell suspensions were then centrifuged at 15,00rpm/ 180x g for 5 minutes and the supernatants discarded. Cell pellets were then solubilised in 1 ml of chaps lysis buffer (20 mM Tris pH 7.4, 142.5 mM KCl, 2 mM $CaCl_2$, 1% chaps) or IP lysis buffer (50 mM HEPES, 150 mM NaCl, 10 mM EGTA, 10% glycerol, 1% triton x-100). Lysates were then passed through a 21 gauge needle until homogeneous and left on ice for 30 minutes. Lysates were then centrifuged at 16,000x g at 4°C to pellet insoluble material.

Bradford assay-mediated protein quantification was then undertaken, as in section 2.9, and 500 μg cell lysate was utilised and made up to 500 μl with the appropriate lysis buffer. 30 μl was then removed and used as an input material sample. Protein-g sepharose beads (Amersham Biosciences, UK) were washed with the appropriate lysis buffer followed by centrifugation at 3,000x g to pellet five times and re-suspended to give a 50% v/v solution. In order to pre-clear the lysate, 50 μl of protein g-sepharose was added and incubated with end on end agitation for two hours at 4°C. Simultaneously; the remaining protein-g sepharose beads were blocked by incubation with normal mouse serum (5 μl/ 100 μl beads) at 4°C with end on end agitation for 2 hours. The pre-cleared lysates were then centrifuged at 3,000x g at 4°C for 15 minutes and the beads discarded. Blocked protein-g sepharose beads were also centrifuged

and washed in the appropriate lysis buffer three times before re-suspension to a 50% v/v solution.

Pre-cleared lysates were then subjected to a background reduction step, whereby 5 μl normal mouse serum and 50 μl blocked beads were added for 2 hours at 4°C with end on end rotation. After which, lysates were centrifuged at 3,000x g for 15 minutes at 4°C and the beads discarded. Simultaneously, 50 μl blocked beads were incubated with 2 μg/ml of the appropriate antibody for 2 hours at 4°C with end on end rotation. Subsequently, lysates were applied to the antibody: bead mixture and incubated overnight at 4°C with end on end agitation.

The following morning, lysates were centrifuged at 3,000x g at 4°C to pellet and the supernatant discarded. Pellets were washed 5 times in the appropriate lysis buffer and resuspended in 35 μl 2X Laemmli buffer, followed by heating to 95°C for 5 minutes. SDS-PAGE and western blot analysis were then undertaken as described in section 2.14, with the exception that anti-mouse/ rabbit True blot HRP conjugated secondary antibodies (eBioscience, UK) were used. True blot antibodies recognise only native IgG and were therefore utilised in order to reduce the detection of the antibody used for IP.

2.16 Quantitative PCR

2.16.1 RNA Purification

$1x10^6$ cells were plated in a 12-well plate, without adding fresh medium, in a final volume of 1ml and treated as required. Cells were harvested by pipetting and pelleted via centrifugation at 180x g for 5 minutes at 4°C. Total cellular RNA was purified via use of the Purelink RNA mini-Kit (Life technologies, UK). Briefly, the Purelink RNA mini-kit lyses and homogenises cells in the presence of guanidinium isothiocyanate (GIT), a chaotropic salt utilised to de-stabilise Hydrogen bonds and hydrophobic interactions, preventing ribonuclease (RNase) access to its substrates. Subsequently ethanol is added to precipitate RNA, which is subsequently applied to a membrane by centrifugation at 3,000x g for 30 seconds. Subsequently, numerous washing steps are performed to reduce GIT carryover. Purified RNA is subsequently eluted in RNase free

water. Isolated RNA was assessed for quantity and purity via use of the Nano-drop® RNA-80 programme (Thermo Scientific, UK). The absorbance ratio 260/ 280 nm was used to determine RNA purity, a value of 2 was interpreted as pure RNA, and 260/ 230 nm ratio used to determine isothiocyanate and protein contamination (a value of 2 was interpreted as pure RNA).

2.16.2 RNA stability assay

In order to determine the quality of purified RNA, the RNA assay of the Agilent 2100 Bio-analyzer (Agilent Technologies, USA) was utilised according to the manufacturer's instructions. The Agilent 2100 Bio-analyzer utilises micro-fluidics and a fluorescence detector to provide an on-chip electrophoresis system. Prior to sample loading a gel: fluorescent RNA-binding dye mixture is used to prime the chip; the mixture is forced into capillaries via the application of pressure. Subsequently, 1 µl of RNA molecular weight marker or sample is added to the appropriate wells and vortexed. Subsequently, the loaded chip is placed into the Agilent 2100 Bio-analyzer and the programme started.

Classically RNA integrity is determined by measuring the relative abundance of 28s/ 18s Ribosomal RNA (rRNA), which is present at a ratio of 2:1 in samples where RNA remains intact. Typically a 1% agarose, 18% formaldehyde gel is used for separation followed by quantification of 28s/ 18s rRNA bands. However, such a method requires large amounts of sample (approx. 2µg RNA) and is largely insensitive. In contrast to traditional techniques, the RNA integrity function of the Bio-analyzer utilises the RNA integrity number (RIN) as a measure of RNA integrity. The RIN algorithm takes account of the 28s/ 18s rRNA ratio in addition to the overall appearance of the fluidics trace producing a more accurate assessment of sample integrity. Usage of the RNA integrity function of the Agilent Bio-analyzer is preferential to conventional Agarose gel electrophoresis since only 1 pg of sample is required to provide highly sensitive and accurate results. Typically a RIN of 10 is required for micro-array analysis whereas a value of 5 is acceptable for Reverse-transcriptase polymerase chain reaction (RT-PCR). Only samples with a RIN of 5 or above were selected for further use.

2.16.3 cDNA synthesis

Complementary DNA (cDNA) synthesis was undertaken utilising the Superscript first-strand synthesis system (Life technologies, UK). All surfaces and equipment were wiped with 1% Virkon prior to commencement, to minimise the risk of nuclease contamination. 500 ng RNA was converted to cDNA: RNA heteroduplexes. Briefly, oligo-deoxyribothymidine (oligo-dT) was utilised to specifically prime 3' poly adenine tail possessing mRNAs, which were subsequently converted to RNA: DNA heteroduplexes via application of reverse transcriptase (RT). Subsequent RNase H treatment was undertaken to liberate single stranded cDNAs, which were subsequently stored at -20°C for further use.

2.16.4 Quantitative PCR (qPCR)

cDNA produced in section 2.11.3 was then diluted 1:3 in nuclease-free water. 0.5 μl (approximately 3 ng) cDNA was then mixed with 4 μl RNase-free H_2O, 5 μl Platinum quantitative polymerase chain reaction (qPCR) supermix-UND (Life technologies, UK) and 0.5 μl gene-specific Taqman FAM-TAMRA probe (Life technologies, UK) and analysed using a CFX96 Real time PCR detection system (Bio Rad, USA) using CFX manager software (Bio Rad, USA). Taqman master mixes contain both forward and reverse gene-specific primers (GSPs) alongside a gene-specific probe labelled with both a 5' 6-carboxylfluoroscein (FAM) fluorophore and a 3"-dihydrocyclopyrroloindole tripeptide minor groove binding quencher (MGB). In the absence of Taq polymerase FAM-MGB probes bind downstream of GSPs upon the target sequence and display no fluorescence due to the close-proximity of FAM with the MGB quencher. Taq 5'-3' exonuclease activity ensures degradation of the FAM-MGB probe ensues upon strand elongation, thus releasing the FAM fluorophore producing a fluorescent signal proportional to the amount of un-quenched probe and, therefore, the amount of target. The principles of qPCR dictate that the threshold cycle (c(T)), the number of cycles required for the fluorescent signal to reach a pre-determined value (the threshold), is directly proportional to the amount of starting material. c(T) values were calculated automatically by CFX manager software (Bio Rad, USA) which utilised an identical threshold for all qPCR reactions undertaken.

2.17 Generation of ShRNA expressing Eμ-Myc cell lines

2.17.1 Molecular Biology

In order to transform bacteria 1 μl of stock plasmid was placed in a transformation tube (Thermo Scientific, UK) and 20 μl commercially available chemically competent E.Coli DH5α (life technologies, UK) added and incubated on ice for 30 minutes. Tubes were transferred to a water bath at 42°C for 45 seconds and placed on ice for 5 minutes. 500 μl S.O.C. medium (2% Tryptone, 10 mM NaCl, 2.5 mM KCl, 10 mM $MgCl_2$, 10 mM $MgSO_4$, 20 mM glucose) (Life technologies, UK) was added and incubated at 37°C for 1 hour, without shaking. After 1 hour samples were streaked on an agar plate containing an appropriate antibiotic for positive selection. Plates were incubated overnight at 37°C to obtain colonies.

In order to determine whether colonies possessed the desired plasmid; typically, 10 colonies were selected and grown in 10 ml lysogeny broth (LB) containing an appropriate antibiotic for 8 hours at 37°C. Mini-prep purification of plasmid DNA was then undertaken utilising the Qiaprep spin mini-prep kit (Qiagen, USA). Essentially, the kit employs an alkaline lysis of bacterial cells followed by neutralisation and the addition of high salt concentrations to allow DNA precipitation. The lysates are then cleared by centrifugation and the supernatant applied to a silica-based membrane column, which allows preferential binding of plasmid DNA in high salt conditions. Subsequent wash steps remove endonucleases and reduce salt concentrations, followed by an elution step.

DNA was verified by the characteristic banding-pattern produced upon digestion with restriction endonucleases (RE). Typically, 1 μl of plasmid DNA was incubated with 2 μl of the appropriate restriction buffer (Promega, UK), 0.2 μl bovine serum albumin (Promega, UK), 1 μl RE (Promega, UK) and H_20 to 20 μl. Digests were incubated at 37°C for approximately 3 hours. Restriction digest products were subsequently analysed by 1% agarose gel electrophoresis. Positive colonies were then grown overnight in 10 ml LB supplemented with an appropriate antibiotic at 37°C with shaking to produce starter cultures. Starter cultures were then added 1:1000 to 150 ml LB supplemented with an appropriate antibiotic and grown overnight at 37°C with shaking.

Subsequently, plasmid DNA was isolated via use of the Hispeed Maxi prep kit (Qiagen, USA) using similar principles to those described above for mini-prep kits.

2.17.2 Transient transfection of ϕnix cells

24 hours prior to transfection, virus-producing amphotropic ϕnix cells were plated in a 6-well plate at around 30% confluency in complete medium (DMEM, 10% FCS, 2mM Glutamine, 1mM Pyruvate, 45 units/ml Penicillin, 45 μg/ml Streptomycin) and maintained at 37°C, 10% CO_2. Purified plasmids were then used to transfect ϕnix cells via Ca^{2+}: phosphate precipitation.

5 minutes prior to transfection ϕnix cells were subjected to 5 μM chloroquine treatment. Chloroquine is a well known inhibitor of endosomal acidification and, therefore, enhances the efficiency of DNA uptake via facilitating escape from endosomes. 10 μg of vector and 4 μg of the helper vector pCL.eco were mixed with 300 μl 2x HEPES buffered saline (280 mM NaCl, 50 mM HEPES, 28 mM Na_2HPO_4), 72 μl 1M $CaCl_2$ and made up to 600 μl with sterile H_2O. Subsequently, interactions between the negatively charged phosphate backbone of DNA and the excess Ca^{2+} cause DNA to precipitate out of solution. Subsequently, mixtures were immediately applied to ϕnix cells and incubated at 37°C, 5% CO_2. After 8 hours the medium was replaced. Transient expression of green-fluorescent protein (GFP) containing vectors was checked 24 hours later by fluorescence microscopy as a control for transfection efficiency. At this point the medium was replaced for 10% Eμ-Myc medium. After 48 hours, virus particles containing the construct of interest were harvested by removing the growth medium and filtered through a 0.2 μm filter (Corning, USA) to prevent carryover of ϕnix cells.

2.17.3 Spin infection of Eμ-Myc lymphomas

Once viral supernatants were harvested polybrene was added at 4 μg/ ml in order to enhance the efficiency of viral infection. Polybrene is a cationic polymer which appears to enhance the extent of virion entry via neutralisation of the charge repulsion that occurs between virions and sialic acid moieties. For infection, Eμ-Myc lymphoma cells were plated out in 12-well plates at $6x10^5$ cells/ well and 1.5 ml of virus-containing medium was applied. Plates were then centrifuged at 180x g at 37°C for 45 minutes to spin down viral particles on to cells. Plates were then returned to a 37°C, 10% CO_2

incubator. After 24 hours, the medium was replaced. In the case of GFP expressing vectors, Eμ-Myc lymphomas were assessed for GFP expression by fluorescence microscopy. Selection was subsequently applied to clones for one week in the form of 1 μg/ ml puromycin or 250 μg/ ml hygromycin, depending upon the construct utilised. The 5% highest GFP expressing clones were subsequently isolated by cell sorting using a FACSaria flow cytometer and sorting module (BD Biosciences, UK). In the case of Bcl-2 over-expressing constructs human Bcl-2 expression levels were assessed by intracellular flow cytometry, as outlined in section 2.11, and the highest expressing clones were collected and pooled.

2.18 Statistical analysis

Statistical analysis of *in vivo* survival data between mice of different genotypes was performed utilising Mantel-Cox statistical analysis. Data collected *in vitro* from tissues derived from mice of differing genotypes was analysed via utilisation of Student's un-paired T-Test, as has been utilised previously (324). In contrast, data comparing the effect of treatments upon the same cell line was analysed via use of a Student's paired T-test. In all cases, p values of less than 0.05 were considered significant. All statistical analyses were performed utilising Graphpad Prism 5 software (GraphPad Software Inc, USA).

Chapter 3 *In vitro* characterisation of Eμ-Myc lymphomas and their response toward BCR-stimulation

3.1 Chapter Introduction

Dysregulation of the Myc proto-oncogene is evident in approximately 70% of human cancers, culminating in the mitogen-independent induction of proliferation, cell cycle progression, and angiogenesis (7, 307) . In the case of Burkitt's lymphoma, dysregulation is attributable to translocation of Myc coding regions proximal to the IgH locus transcriptional enhacer region in around 80% of patients. In fact, all BL patients appear to exhibit Myc dysregulation to some degree since the remaining 20% commonly display alternative Myc translocations (8). BL represents a highly aggressive non-Hodgkin's lymphoma, associated with lymphadenopathy, a high proliferative rate and profound levels of cell death (8, 10, 11). Consequently upon histological examination, BL resembles a "starry sky" of lymphoblasts interspersed with macrophages actively engulfing apoptotic cells, known as tingible body macrophages (8, 10, 11).

Our understanding of Myc-driven tumourigenesis has been greatly enhanced by studies utilising Myc transgenic animals to model human disease, perhaps none-more so than the Eμ-Myc mouse developed by Harris et al (321). Harris et al engineered mice to re-create the t(8: 14) genetic lesion of BL via injection of (C57BL/6 x SJL/J) mouse embryos with a fusion construct containing human c-Myc and a murine plasmacytoma-derived IgH enhancer element (42, 321). The resulting Eμ-Myc mice were born at the predicted Mendelian frequencies and exhibited modest B-lymphocyte-restricted Myc over-expression and spontaneous development of pre-B/ immature B lymphoblastic lymphomas at a median onset of 11 weeks (42, 321-323). The onset of lymphoma was preceded by pre-malignant expansion of the pre-B cell compartment, followed by Myc-driven apoptotic contraction (324-326). As a consequence, such a selective pressure drives accumulation of mutations that subvert Myc-induced apoptosis, most commonly Bcl-2 over-expression and inactivation of the ARF/Mdm2/p53 axis (42, 321-324, 327, 331, 332). Therefore, Eμ-Myc mice provide a

genetically tractable model of human disease within which the stochastic accumulation of secondary genetic lesions may be studied. However, whilst Eμ-Myc lymphomas mimic the genetic lesion, biology and type of disease found in BL patients, they fail to satisfactorily recapitulate all aspects of human BL (333). For instance, BL is associated with a GC-like B-cell phenotype whereas, Eμ-Myc lymphomas resemble a much earlier developmental stage (333, 334).

The Eμ-Myc model was determined as an appropriate model in which to study the mechanisms of BCR-induced cell death, since it provides low-passage lymphoma cell lines that can be manipulated *in vitro*. It is anticipated that such lymphomas should more closely resemble the biology of primary tumours than the high-passage immortalised cell lines commonly used. It is largely accepted that BCR-induced cell death proceeds via an apoptotic caspase-dependent mechanism via the intrinsic apoptotic pathway (225-228, 243, 245). However, whilst this view represents the consensus it is not universally the case (245). Therefore, this investigation aimed to characterise Eμ-Myc lymphomas and determine the nature of the cellular response to BCR-stimulation in order to address the hypothesis that BCR-driven cell death proceeds via the intrinsic apoptotic pathway in Eμ-Myc lymphomas. Furthermore, whilst the roles of effector caspases are well defined, the exact roles of initiator caspases downstream of the BCR are significantly less well known. It is accepted that both Caspase-9 and Caspase-2 seem to play key roles, however the exact nature of the key initiating event remains ambiguous (193). Since genetic disruption of Caspase-2 appears to influence the rate of Myc-induced lymphomagenesis (369), such techniques are not appropriate for the study of BCR-induced cell death in this model.Therefore, this investigation aimed to identify which initiator caspases play key roles downstream of the BCR in Eμ-Myc lymphomas via a pharmacological route.

3.2 Eμ-Myc tumour presentation

3.2.1 Kaplan-Meier survival

Cohorts of Eμ-Myc transgenic mice on the C57BL/6 background were monitored for symptoms of tumours from birth. Tumours presented with a variety of symptoms

including: hunching with laboured breath, withdrawal from littermates, agitated behaviour, unkempt appearance, and occasionally visible lumps in the location of cervical, axillary, brachial, and inguinal lymph nodes. Upon detection of such symptoms, mice were culled and tissues processed as outlined in materials and methods section 2.4. The presence of tumour was confirmed upon autopsy, by examination of Haematoxylin and Eosin (H&E) stained tissues by microscopy, and malignancy confirmed by successful tumour re-passage into congenic C57BL/6 animals. As demonstrated in figure 3.1, at this facility Eμ-Myc mice display a greatly reduced rate of survival than that of congenic C57BL/6 mice ($p < 0.001$ by Mantel-Cox statistical testing). Such reduced survival correlated with the onset of spontaneous lymphomas, between 6 weeks and 6 months of age, affecting the spleen, thymus, and most-notably the inguinal and axillary lymph nodes of afflicted animals, as demonstrated in figure 3.1. Inguinal lymph nodes of tumour bearing mice were particularly affected, reaching a diameter of 10 mm in some cases whereas; C57BL/6 mice typically exhibit a diameter of less than 1 mm (315). The nature of tumour presentation and tumourigenicity rates are consistent with previous investigations, including those of our Australian collaborators (330).

3.2.2 Comparative histological examination of C57BL/6 and tumour bearing Eμ-Myc tissues

In order to ascertain the impact of spontaneous Eμ-Myc lymphomas upon the cellular architecture of secondary lymphoid organs, comparative histological examination of H&E stained tissues from afflicted Eμ-Myc and C57BL/6 congenic animals was undertaken. As demonstrated in figure 3.2, terminal Eμ-Myc mice (right panel) demonstrate vast enlargement of the thymus, spleen and inguinal lymph node alongside total breakdown of normal cellular architecture, in comparison to congenic animals (left panel). Such a phenotype was perhaps most notable in the spleen.

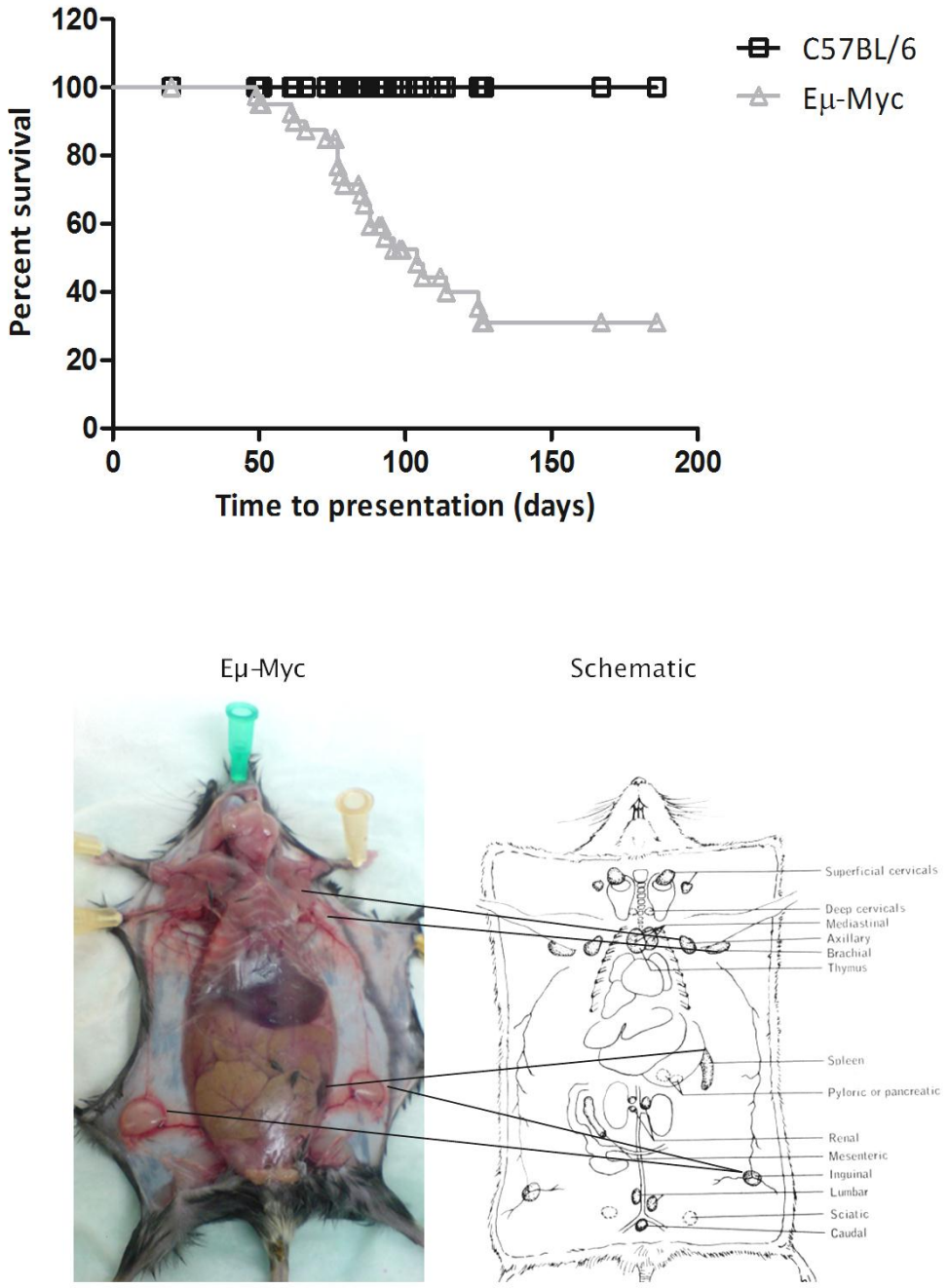

Figure 3.1 Kaplan Meier survival curve of Eμ-Myc and congenic C57BL/6 mice

A Cohorts of heterozygous Eμ-Myc (Δ) or congenic WT (□) mice on the C57BL/6 background were monitored, from birth, for the incidence of tumours. Upon the onset of tumour symptoms, mice were culled as outlined in materials and methods section 2.4. Eμ-Myc mice demonstrate an enhanced incidence of spontaneous tumours and diminished overall survival in comparison to congenic WT animals ($p < 0.0001$ by Mantel-Cox statistical testing). B Afflicted Eμ-Myc mice were subsequently observed for symptoms of tumours by mid-line dissection and autopsy. Typically, Eμ-Myc mice presented with lymphadenopathy, particularly of the inguinal and axillary lymph nodes, and mild splenomegaly. Data kindly provided by Dr. E.L. Williams.

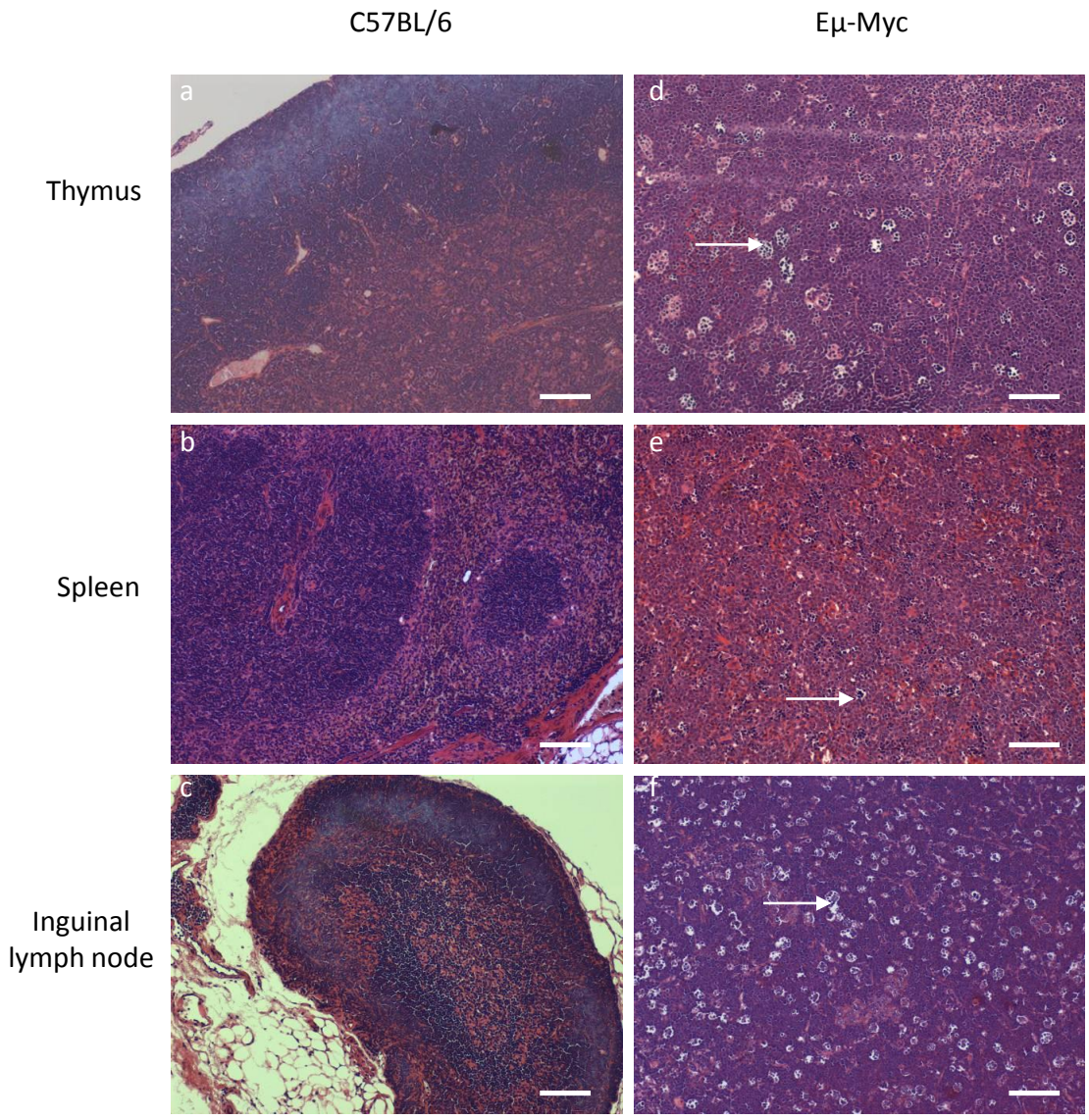

Figure 3.2 Histological examination of secondary lymphoid organ architecture in C57BL/6 and Eμ-Myc mice

Upon occurrence of tumour symptoms, mice were culled and dissected according to materials and methods section 2.4. Tissue sections were taken, fixed in formalin and paraffin embedded prior to staining with haematoxylin and eosin (H&E). Subsequently, the tissue architecture and the presence of tumour infiltrates was assessed in tumour bearing mice by light microscopy in comparison to congenic C57BL/6 mice. All slides were examined at 10 x magnification, scale bars are equivalent to 100 μm. Tissues from Eμ-Myc mice (right panels) demonstrate an increased size and complete loss of normal cellular architecture in comparison to congenic C57BL/6 mice (left panels). Furthermore, Eμ-Myc mice exhibit the "starry sky" appearance with tingible body macrophages (arrows) evident. Data kindly provided by Dr. E.L. Williams.

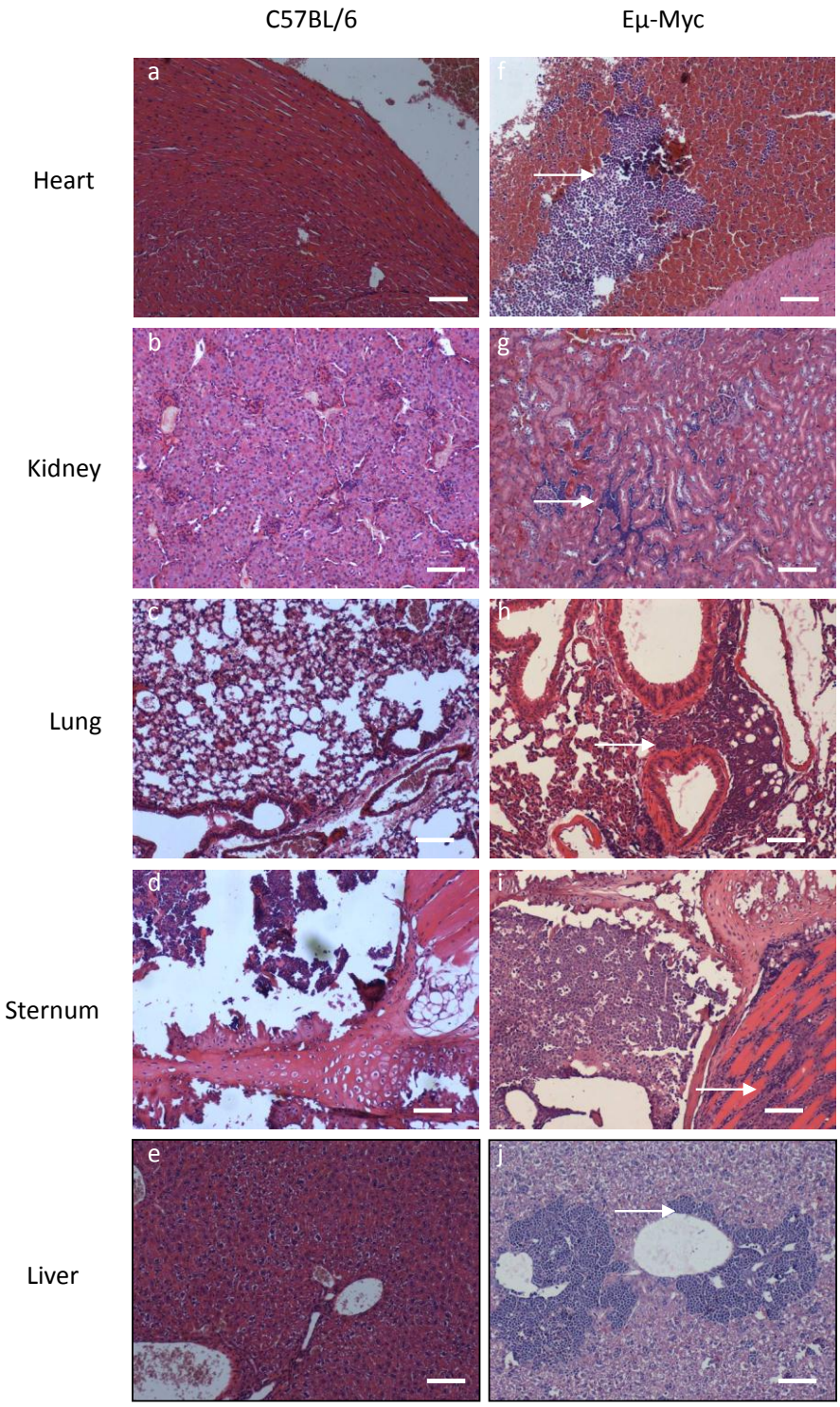

Figure 3.3 Histological examination of tumour infiltration in Eμ-Myc and congenic C57BL/6 mice

As in figure 3.2, mice were culled and tissues fixed in formalin prior to paraffin embedding and H&E staining. Areas of tumour infiltration are evident via the accumulation of darkened regions, indicated by arrows, in Eμ-Myc mice (right panels) in comparison to C57BL/6 congenic animals (left panels). Tumour infiltrates were evident in all tissues examined. Scale bars are equivalent to 100 μm. Data kindly provided by Dr. E.L. Williams.

Normal splenic architecture was evident in C57BL/6 animals with dense staining around central arterioles defining the white pulp, whereas the red pulp demonstrates a much reduced density of nuclei. Such architecture is completely destroyed in the spleens of Eμ-Myc mice, owing to tumour infiltration and proliferation. Notably, however, the tissues of Eμ-Myc mice exhibit the "starry sky" pattern of tingible body macrophages evident in BL, indicated by the white arrows. Therefore, at least histologically, spontaneous Eμ-Myc tumours appear to closely resemble human BL. Whilst it was clear that Eμ-Myc mice develop spontaneous lymphomas affecting secondary lymphoid organs, tumour metastasis and infiltration of non-lymphoid tissues remained to be determined. Therefore, comparative histological examination of H&E stained Eμ-Myc and C57BL/6 heart, kidney, lung, sternum and liver tissue samples was performed.

As demonstrated in figure 3.3, tumour infiltration was evident in all tissues analysed (denoted by the white arrows). The most profound tumour infiltration was evident in highly vascularised tissue such as the liver and kidneys whereas, infiltration into the heart and lung was less common. In stark contrast to secondary lymphoid organs, normal cellular architecture was largely intact in peripheral tissues of Eμ-Myc mice confirming Eμ-Myc lymphomas as predominantly tumours of lymphoid tissues.

3.3 Identification of the Eμ-Myc lymphoma immunophenotype

At autopsy, the spleen, thymus and lymph nodes of tumour bearing animals were harvested into Eμ-Myc medium and maintained *in vitro* at 37°C, 10% CO_2 with serial passaging until Eμ-Myc lymphoma cells exhibited extensive proliferation. Subsequently, the immunophenotype of the malignant clone was assessed by flow cytometry. Tumour cells were incubated with PE conjugated anti-CD19 (Clone 1D3) alongside IgM (Clone Mc39.12), IgD (Clone 1.19), pAb anti-IgG (Stratech, UK), or CD3 (Clone KT3) specific FITC conjugated antibodies. The resulting flow cytometry data is outlined in figure 3.4 and tables 3.1 and 3.2. As can be seen in tables 3.1 and 3.2, virtually all Eμ-Myc lymphomas analysed demonstrate a $CD19^+$ surface immunophenotype, with the exception of Eμ# 2, indicating a malignancy of B-cell origin. Furthermore, of the Eμ-Myc lymphomas derived at this institution, 55% were

positive for sIgM expression with 7 highly expressing clones, 2 mixed IgMHigh/ IgMlow tumours and a single weakly IgM expressing tumour, as observed by Harris et al (315). IgM expressing tumours were often negative/weak for IgD, with the exception of Eμ# 8 and 16.

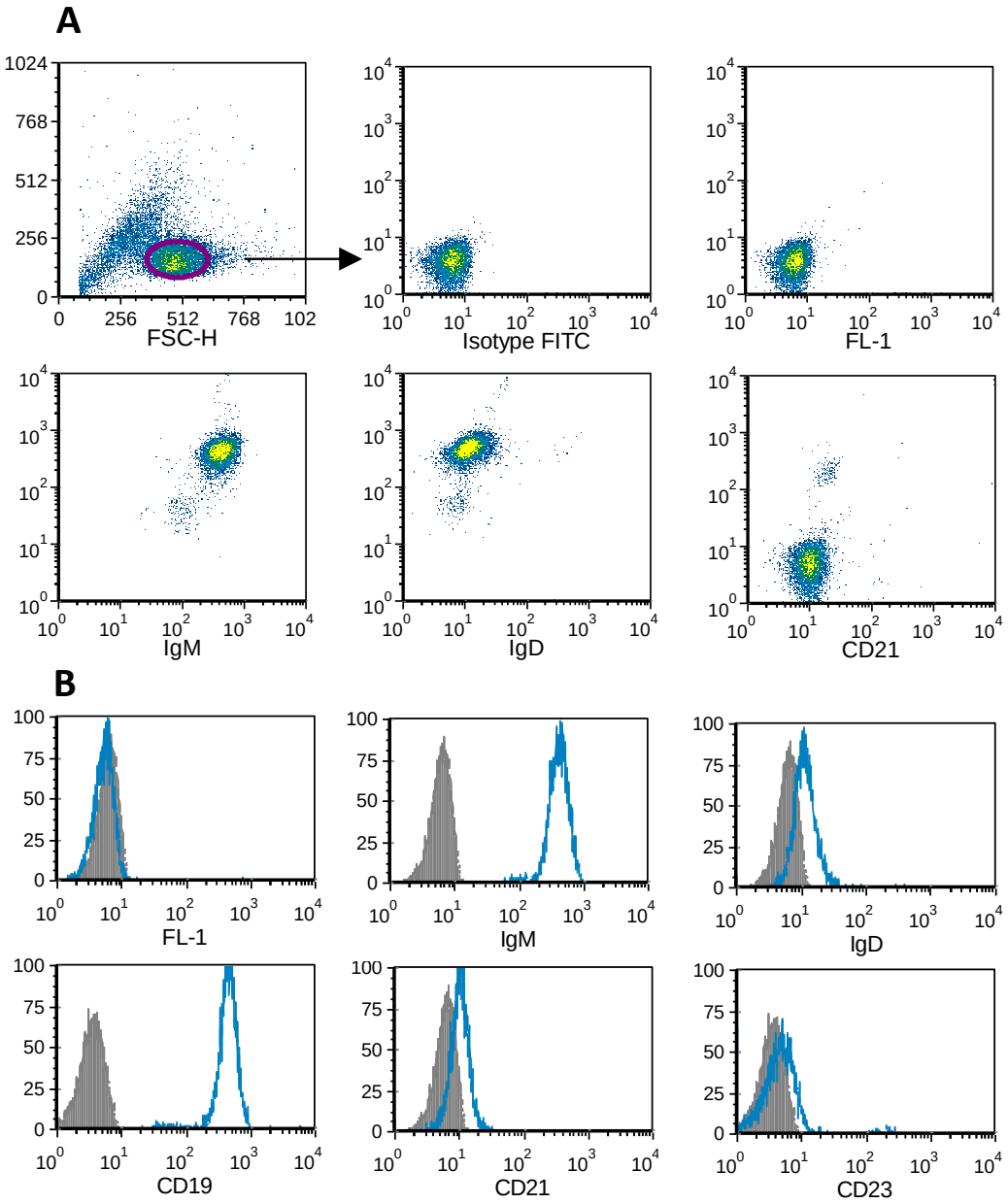

Figure 3.4 Immunophenotype analysis of Eμ-Myc tumours

Tumour cell lines derived from the spleens of Eμ-Myc mice were incubated with 5 μg/ ml anti-CD19^{PE} (Clone 1D3) or 10 μg/ml anti-CD23^{PE} in the presence of 10 μg/ ml anti-IgM^{FITC} (Clone Mc39.12), anti-IgD^{FITC} (Clone 1.19), anti-CD21^{FITC} (Clone 7G6), anti-CD3^{FITC} (Clone KT3) or an appropriate isotype control for 30 minutes at 4°C, washed, and analysed by flow cytometry. 10,000 viable cells, as determined by the FSC/ SSC profile, were gated and analysed for fluorescence in the FL-1 and FL-2 channels. A) Representative dot plots demonstrating fluorescence of both FITC and PE-conjugated antibodies and relevant isotype controls. B) The same data in A) is represented as histograms as an overlay of the appropriate isotype control (filled plot) and the indicated antibody (blue plot). Data demonstrates the

phenotype of D3 a CD19^{+}, IgM^{+}, IgD^{low}, CD21^{low}, CD23^{-}, Bim$^{-/-}$ Eμ-Myc lymphoma (D3). This an observation identifies that IgM positive Eμ-Myc tumours appear to represent a malignancy of immature B-cells. Of the remaining 9 tumours, 6 tumour cell lines showed negative expression for IgM, IgD, and IgG indicating a malignancy of an earlier developmental stage (Pre-B-cells). However, since this investigation is focused upon the use of IgM^{+} tumours, further immunophenotypic analysis was not performed on IgM^{-} tumours.

Lymphoma Cell line	CD3	CD19	IgM	IgD	IgG
Eμ# 1	N.D.	N.D.	N.D.	N.D.	N.D.
Eμ# 2	-	-	Wk	Wk	Wk
Eμ# 3	-	+	-	-	+
Eμ# 4	-	+	+	-	Wk
Eμ# 5	-	+	-	-	+
Eμ# 6	-	+	++	-	+
Eμ# 7	-	+	Mixed	-	-
Eμ# 8	-	+	++	Wk	-
Eμ# 9	-	+	-	-	-
Eμ# 10	-	+	-	-	Mixed
Eμ# 11	-	+	+	Wk	-
Eμ# 12	-	+	Mixed	-	-
Eμ# 13	-	+	-	-	-
Eμ# 14	-	+	-	-	-
Eμ# 15	-	+	+	-	-
Eμ# 16	-	+	+	+	-
Eμ# 17	-	+	-	-	-
Eμ# 18	-	+	-	-	-
Eμ# 19	-	+	-	-	-
Eμ# 20	-	+	+	+	-

Table 3.1 Summary of primary Eμ-Myc lymphoma immunophenotypes

Cells from the spleen, lymph node and thymus of primary Eμ-Myc lymphomas, derived at this institution, were stained as in figure 3.4 and analysed by flow cytometry. N.D. not determined, - negative for antigen expression, + positive for antigen expression, wk weak expression of antigen, mixed presence of both positive and negative populations. Data kindly provided by Dr. E.L. Williams.

Genotype	Lymphoma Cell line	CD19	IgM	IgD	CD21	CD23	Relative IgM
WT	Eμ# 16	+	+	-	low	-	40.825
	Eμ# 15	+	+	n.d	low	-	31.57
	Eμ# 8	+	+	-	low	-	29.87
	Eμ# 6	+	Mixed	-	low	-	6.652
	Eμ# 4	+	+	-	low	-	55.730
	AF47	+	+	low	+	-	59.40

Table 3.2 Summary of the immunophenotypes of primary WT Eμ-Myc lymphoma cell lines

Cells from the spleen, lymph node and thymus of primary Eμ-Myc lymphomas derived at this institution were stained as in figure 3.4 and analysed by flow cytometry. A geometric mean of less than 100 was determined as low expression of surface antigen and over 100 as high. Relative IgM expression levels were determined by dividing the geometric mean of IgM profiles by that of the relevant isotype control. N.D. not determined, - negative for antigen expression, + positive for antigen expression, wk weak expression of antigen, mixed presence of both positive and negative populations.

In order to further characterise the developmental status of IgM^+ Eμ-Myc lymphomas developed at this institution, additional immunophenotype analysis was performed by flow cytometry. Tumour cells were incubated with PE conjugated antibodies directed against CD19 (Clone 1D3) or CD23 (Clone B3B4) alongside IgM (Clone Mc39.12), IgD (Clone 1.19), and CD21 (Clone 7G6) specific FITC conjugated antibodies. As demonstrated in table 3.2, all IgM^+ tumours were $CD19^+$, 57% were IgD^{low}, 58% were $CD21^+$ and all were $CD23^-$. Therefore, the IgM^+ Eμ-Myc tumours developed at this institution, all display a highly similar $CD19^+$, IgM^+, IgD^{low}, $CD21l^{ow}$, $CD23^-$ immunophenotype. Such a phenotype is indicative of a T1 transitional B-cell, since the T2 status is associated with CD23 positivity. Therefore, in total a panel of 9 IgM^+ WT Eμ-Myc lymphomas was available for further use in characterisation of responses to BCR stimulation.

3.4 Characterisation of Eμ-Myc responses to BCR stimulation

It was next deemed necessary to determine the signalling competency of IgM^+ Eμ-Myc lymphoma BCRs and identify whether downstream signalling events were similar to those observed in normal B-cells. Activation of BCRs almost universally results in increases in $[Ca^{2+}]i$ via IP_3-mediated ER Ca^{2+} efflux and extracellular capacitance entry of Ca^{2+}, leading to two distinctive phases in the response termed the transient spike and the plateau, as outlined in section 1.3.2-3. In addition, BCR activation

characteristically imparts activation of the PI3K/ Akt and MAPK pathways (150). Therefore, it was deemed prudent to observe the functionality of these molecular signalling events in Eμ-Myc lymphomas.

3.4.1 BCR-induced Calcium flux analysis of Eμ-Myc lymphomas and normal B-cells

In order to observe BCR induced Ca^{2+} flux in purified normal C57BL/6 B-lymphocytes and Eμ-Myc lymphomas, cells were incubated with Fluo-4 AM and analysed by flow cytometry. Baseline Ca^{2+} readings were taken by analysis of un-treated samples for 35s. Subsequently, 60 μg/ml pAb ā IgM or an equivalent volume of PBS was added and the impact upon intracellular Ca^{2+} levels was observed. As demonstrated in figure 3.5A, addition of pAb ā IgM to both Eμ-Myc (middle panel) and normal B-cells (right panel) induced rapid increases in Fluo 4 fluorescence over time. Whereas, addition of PBS alone (left panel) failed to influence Fluo 4 fluorescence therefore indicating that vehicle alone did not substantially influence $[Ca^{2+}]i$. Consequently, such traces indicate that the BCRs of Eμ-Myc lymphomas are effectively linked to PLCγ2 and are capable of imparting a Ca^{2+} response following stimulation. As evident in 3.5B, Eμ-Myc lymphoma cells exhibited a substantially reduced extent of Ca^{2+} flux in comparison to normal C57BL/6 B-lymphocytes.

Kinetic analysis of pAb ā IgM-induced Ca2+ flux identifies the occurrence of a distinct transient Ca^{2+} spike persisting approximately 70s post-treatment in Eμ-Myc lymphomas, which subsequently appears to fall to a lower but sustained level, corresponding to the capacitive Ca^{2+} plateau, post 100 seconds. However, contrastingly, such distinct phases appear entirely absent from the traces of normal splenic B-cells, as outlined in figure 3.5B. The observed transient spikes appear similar in magnitude between Eμ-Myc lymphoma cells and normal C57BL/6 B-lymphocytes.

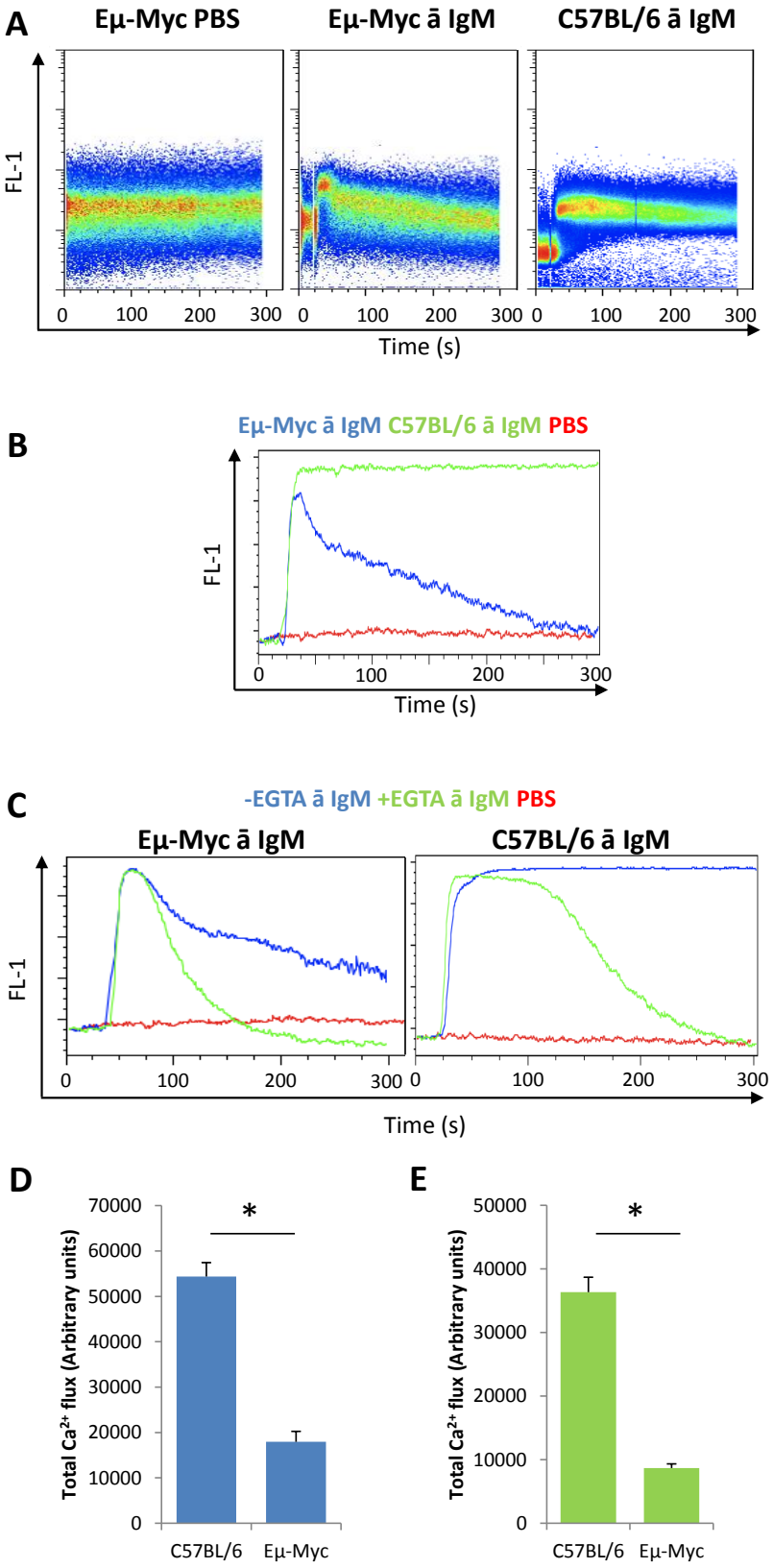

Figure 3.5 Analysis of Ca2+ flux response of Eμ-Myc lymphoma cells and normal B-cells to anti-IgM stimulation

Eμ-Myc lymphomas and purified C57BL/6 splenic B-cells were stained with Fluo-4 AM for 30 minutes at

37°C. Subsequently, cells were washed, rested, and incubated in the presence or absence of 5 mM EGTA for 5 minutes at 37°C and analysed by flow cytometry. Events from viable cells, assessed by FSC/ SSC, were collected for 35 seconds to give a baseline followed by treatment with PBS or 60 μg/ ml polyclonal anti-IgM $F(ab)_2$ (pAb ā IgM) for a further 5 minutes. A) Example dot-plots demonstrating changes in FL-1 over time upon addition of PBS (left panel) or pAb ā IgM to Eμ-Myc lymphomas (middle panel) and normal B-cells (right panel). B) PBS (red) or pAb ā IgM-induced Ca^{2+} flux in Eμ-Myc lymphomas (blue), or normal B-cells (green). C) Kinetic traces of PBS (red) or pAb ā IgM -induced Ca^{2+} flux in the presence (Green) or absence (Blue) of 70 mM EGTA in Eμ-Myc lymphomas (left panel) and normal B-cells (right panel). D-E) Total pAb ā IgM -induced Ca^{2+} flux quantification in D) the absence (blue bars) or E) presence (green bars) of EGTA. Values were obtained via calculation of the area under the curve (AUC), using Flowjo software (Treestar, USA). Bars represent the average of three C57BL/6 mice per group and values obtained from Eμ# 16, 15, and 4, performed in triplicate. Asterisks denote a statistically significant difference as adjudged by Student's un-paired T test analysis ($p< 0.05$).

However, the latter fail to exhibit a subsequent decline into an obvious plateau. As a result, normal B-cells exhibit significantly enhanced levels of total Ca^{2+} flux following BCR-stimulation in comparison to Eμ-Myc lymphoma cells, as shown in figure 3.5D. However, such reduced Ca^{2+} flux responses of Eμ-Myc lymphomas were not due to low-level BCR expression, since the Eμ-Myc lymphoma cells utilised (Eμ# 16, 15, and 8) all demonstrate a moderate levels of IgM expression, as outlined in table 3.2.

Since EGTA chelates extracellular Ca^{2+}, it can be utilised to effectively block capacitive Ca^{2+} entry and, therefore, allows specific observation of the transient phase. Therefore, 5 mM EGTA was applied to cells 5 minutes prior to pAb ā IgM treatment and Ca^{2+} flux analysis by flow cytometry.

As demonstrated in figure 3.5C (green traces), pre-treatment with EGTA effectively ablated the plateau phase in both Eμ-Myc lymphoma cells (left panel) and normal B-cells (right panel). However, normal B-cells appeared to exhibit an extended transient Ca^{2+} spike enduring for approximately 100s post-treatment in comparison to Eμ-Myc lymphoma cells. As a consequence, normal splenic B-cells exhibit an approximately 3-fold greater rise in $[Ca^{2+}]i$ mediated by the transient spike than Eμ-Myc lymphoma cells, as quantified in figure 3.5E. Therefore, collectively these results imply that whilst the BCRs of Eμ-Myc lymphomas appear to be linked effectively to the Ca^{2+} flux machinery, a much smaller magnitude response is initiated following stimulation in comparison to normal splenic B-cells. Interestingly, such observations are consistent when contrasting primary human cells and cell lines (M.S. Cragg verbal communication). Therefore, it is possible that specific microenvironment cues are

responsible for the enhanced Ca^{2+} flux evident in *ex vivo* lymphocytes in comparison to cell lines.

3.4.2 Analysis of BCR-induced PI3K/ Akt and MAPK activation in Eμ-Myc lymphomas

In order to confirm effective coupling of Eμ-Myc lymphoma cell BCRs to additional aspects of the BCR signalling machinery, analysis of BCR-induced PI3K/ Akt and MAPK activation was undertaken. Cells were re-suspended at $1x10^6$/ ml and treated with 2 μg/ ml pAb ā IgM for various time intervals. Subsequently, RIPA lysates were prepared and the extent of PI3K/ Akt and MAPK pathway activation was assessed by western blotting for phosphorylated kinases. Levels of phosphorylated kinases were ascertained by densitometry and normalised against total kinase levels and corrected for protein content via use of a Tubulin loading control.

As can be seen in figure 3.6, Eμ-Myc lymphoma cells demonstrate rapid phosphorylation of ERK, Akt, and JNK following BCR stimulation, indicating an effective link between the BCR and these pathways in Eμ-Myc lymphoma cells. On average, BCR-stimulation enhanced Akt phosphorylation to a maximum of 12-fold after 30 minutes, JNK 8-fold after 180 minutes, and ERK to a maximum of 3-fold after 5 minutes. Activation of Akt appeared to return to basal levels after 360 minutes post-stimulation whereas in contrast, phosphorylated ERK and JNK largely persisted above base-line levels throughout the treatment period (with the exception of ERK phosphorylation in Eμ# 16).

Enhanced phosphorylation of p38, however, was not evident downstream of BCR stimulation. In fact, p38 appeared hypo-phosphorylated in the majority of Eμ-Myc lymphomas in response to BCR activation, as demonstrated in figure 3.6F. In lymphomas, such as Eμ# 4, which failed to demonstrate de-phosphorylation of p38 upon BCR signalling, an unusual cyclical pattern of phosphorylation and de-phosphorylation was observed. As can be determined in figure 3.6A, p38 phosphorylation levels appear constant immediately following BCR stimulation.

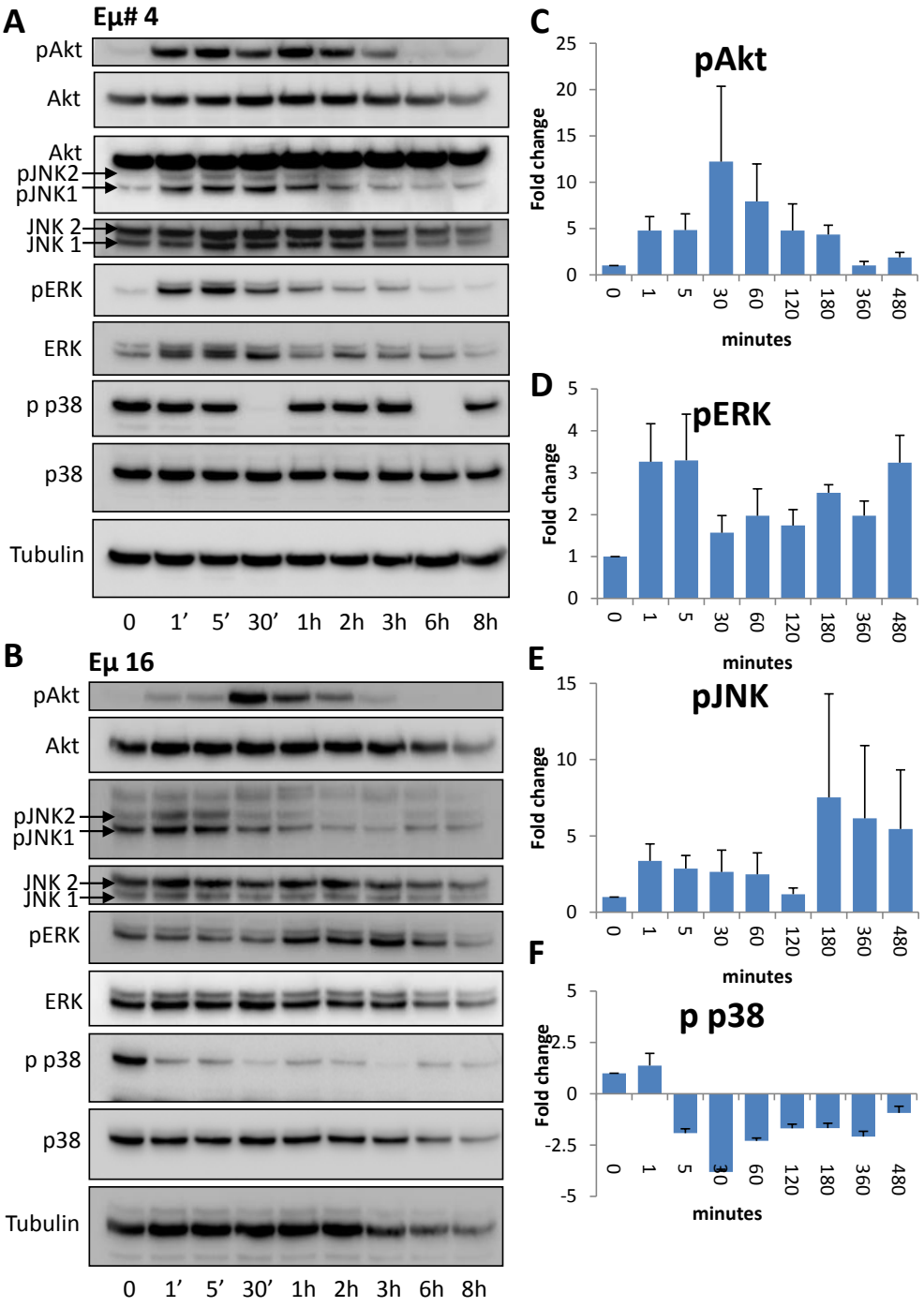

Figure 3.6 Analysis of pAb ā IgM-induced Akt/ MAPK activation in Eμ-Myc lymphoma cells

Eμ-Myc lymphomas were plated at 1x10^6/ ml, incubated with PBS or 2 μg/ ml pAb ā IgM for the indicated period of time. Cells were subsequently harvested, washed, lysed using RIPA buffer and allowed to lyse on ice for 30 minutes. Subsequently 35 μg of protein was loaded into an SDS-PAGE gel and the presence of phosphorylated Akt/ MAPKs was assessed by western blotting. A-B) Example western blots obtained from Eμ-Myc# 4 (A) and Eμ-Myc# 16 (B). C-F) Akt/ MAPK phosphorylation was quantified by densitometry and normalised to un-phosphorylated Akt/ MAPK and Tubulin values using UVP vision works software. Bars represent an average of data obtained from Eμ# 16, 15, 8, and 4, bars denote standard deviation.

However, after 30 minutes a complete lack of p38 phosphorylation was visible, which returned after an additional 30 minutes. Such a phenomenon was also evident

between the 6 and 8-hour time points. Whilst activatory p38 phosphorylation was not initiated downstream of the BCR in Eμ-Myc lymphomas, modulation of the phosphorylation status certainly was influenced by BCR signalling. Therefore, it can be concluded that the BCRs of Eμ-Myc lymphomas are effectively linked to aspects of the PI3K/ Akt and MAPK pathways.

3.5 Characterisation of the cell death response triggered downstream of BCR signalling

Since the BCRs of Eμ-Myc lymphomas appear functionally linked to downstream signalling machinery, further examination into the cellular outcome of BCR-engagement was undertaken. Eμ-Myc lymphomas were first screened for cell death in response to receptor activation via the use of anti-IgM antibodies.

3.5.1 Analysis of anti-IgM induced cell death by Annexin V/ PI flow cytometry

In order to determine whether BCR-stimulation influenced the viability of Eμ-Myc lymphomas or purified C57BL/6 splenic B-cells, Annexin V/ PI death assays were performed over a 6, 12 and 24 hour time course. Cells were plated out in a 96 well plate, to give $2x10^5$ cells/ well and subjected to treatment with an appropriate concentration of pAb ā IgM or Etoposide (as a positive control, known to induce apoptosis). Cells were then incubated at 37°C for the appropriate time period prior to harvesting by pipetting and analysis by Annexin V/ PI flow cytometry.

As demonstrated by the example dot plots demonstrated in figure 3.7A, cells were considered dead or undergoing cell death when significant FL-1 positivity was recorded using Etoposide treatment as a positive control. Identical analysis gates were then used for each subsequent sample analysed. pAb ā IgM treatment of Eμ-Myc lymphoma cells appeared to invoke accumulation of Annexin V^+/PI^- and Annexin V^+/PI^+ populations in a time and dose-dependent manner.

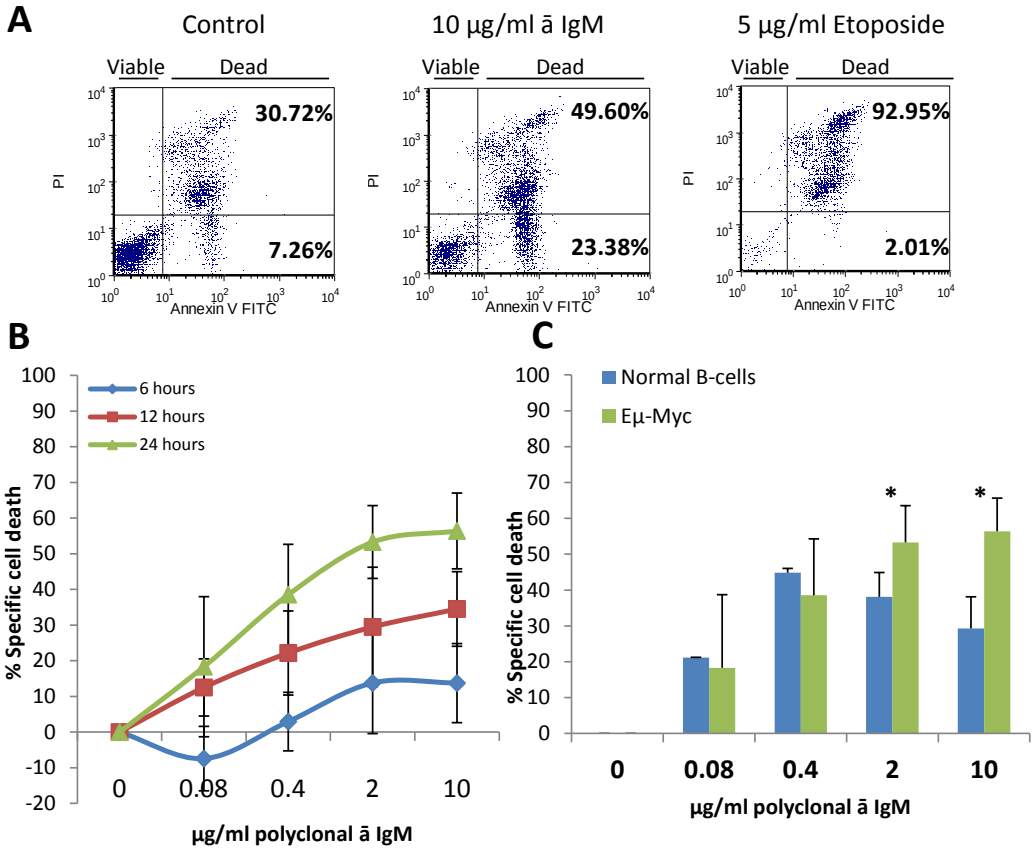

Figure 3.7 Analysis of pAb ā IgM-induced cell death in Eµ-Myc lymphoma cells

Eµ-Myc lymphomas or purified C57BL/6 splenic B-cells were plated at $1.6x10^6$/ ml and treated with pAb ā IgM, at the indicated final concentration, or an equivalent volume of PBS for 6, 12 and 24 hours. Subsequently, cells were harvested by pipetting and subjected to Annexin V^{FITC}/ PI staining for 15 minutes at room temperature and analysed by flow cytometry. Levels of specific cell death above background were calculated as in materials and methods section 2.13.1. A) Example Annexin V/ PI dot plots, cells to the right of the quadrant midline were adjudged to be dead. B) Levels of pAb ā IgM induced cell death in Eµ-Myc lymphomas at 6 (blue), 12 (red) and 24 (green) hours. C) Comparison between levels of pAb ā IgM-induced cell death in Eµ-Myc lymphomas (green) and normal splenic B-cells (blue) after 24 hours. Data represents the average of 4 independent experiments, each performed in triplicate. Error bars represent standard deviation. Asterisks denote a statistically significant difference ($p < 0.05$) by Student's un-paired T-test statistical testing.

Such accumulation appeared maximal 24 hours post- 10 and 2 µg /ml pAb ā IgM treatment, as demonstrated in figures 3.7A and 3.7B. Accumulation of such cellular populations is indicative of a loss of phospholipid asymmetry and plasma membrane integrity and therefore, is associated with induction of cell death. Similar cell death responses were also evident in response to monoclonal ā IgM (IgG2a) (see appendix A7) and Etoposide treatment. Therefore, two independent BCR cross-linking stimuli both lead to the induction of a cellular death programme in Eµ-Myc lymphoma cells.

However interestingly, mAb ā IgM treatment appeared to impart a significantly reduced cell death response in Eμ-Myc lymphoma cells than that of pAb anti-IgM. We reasoned that this could potentially be attributable to enhanced receptor cross-linking provided by the pAb. In order to test such a prediction, Eμ-Myc lymphoma cells were incubated with mAb anti-IgM in the presence or absence of anti-Fc antibodies to provide enhanced BCR cross-linking and the level of cell death compared to mAb treatment alone. As demonstrated in appendix A8, co-treatment of Eμ-Myc lymphomas with anti-Fc mAbs enhanced mAb ā IgM cell death. Therefore, such experiments demonstrate that the magnitude of ā IgM-induced cell death is proportional to the extent of receptor cross-linking.

Subsequently, we wished to compare the cell death response of Eμ-Myc lymphoma cells to that undertaken by purified C57BL/6 normal splenic B-cells. Splenic B-cells were isolated by MACS purification, as detailed in materials and methods section 2.13, typically to 98-99% purity (as assessed by CD19 expression by flow cytometry, see appendix A9 and subjected to pAb ā IgM for 24 hours, as before. As demonstrated in figure 3.7C, normal splenic B-cells also exhibit a cell death response toward pAb ā IgM treatment. However, the response demonstrates an atypical dose response curve with maximal death achieved at 0.4 μg/ml. At low doses, the response to pAb ā IgM appears comparable to that of Eμ-Myc lymphoma cells however, statistically significant differences are observed at 2 and 10 μg/ml doses. Therefore, Eμ-Myc lymphoma cells appear to demonstrate a slightly more extensive cell death in response to pAb ā IgM in comparison to normal splenic B-cells.

3.5.2 Adaptation to cell culture and effect upon BCR-induced cell death

Next we wished to determine whether clonal selection, in response to myriad *in vitro* pressures, during cell culture adaptation, alters the cellular response to BCR-engagement. Therefore, pAb ā IgM-induced cell death assays were performed, as before, utilising Eμ# 16, 15, 8 and 4 at different passage numbers. As can be seen in appendix A10, a sharp decline in the extent of BCR-induced cell death is evident after approximately passage number 22. Initial gradual increases in resistance toward pAb ā IgM culminate in near complete resistance after passage 30. Therefore, in order to

allow experiments utilising Eμ-Myc lymphomas to be directly comparable, lymphomas were only utilised for further experimentation up to passage number 20.

3.5.3 Apoptosis and BCR-induced cell death

Although figure 3.7 demonstrates that Eμ-Myc lymphoma cells undertake a cell death response toward BCR-engagement, it offers no information as to the identity of the cell death programme. Therefore, in order to determine whether BCR-engagement results in the induction of an apoptotic cell death, characteristic apoptotic molecular signatures were examined downstream of the BCR.

3.5.3.1 BCR-induced cell death and Phosphatidylserine externalisation

As previously described, loss of phospholipid asymmetry (detectable via PS externalisation), in the absence of widespread loss of plasma membrane integrity, represents a characteristic of an apoptotic cell death. In order to determine whether such a death programme was invoked downstream of the BCR, the levels of Annexin V^+/ PI^- (apoptotic) cells in vehicle treated (PBS) and pAb ā IgM treated Eμ-Myc lymphoma cells were assessed. As evident in figure 3.8, both Etoposide and pAb ā IgM treatment induce the accumulation of Annexin V^+/ PI^- cells in a time-dependent fashion. BCR-stimulation appears to yield reduced levels of apoptosis in comparison to that produced by Etoposide in the majority of cell lines. However, on average 10 μg/ml pAb ā IgM treatment appears to generate an approximately two-fold increase in the incidence of apoptotic cells after 12 hours. Therefore, BCR-induced cell death appears to possess at least one characteristic of an apoptotic cell death.

3.5.3.2 BCR-induced cell death and Caspase processing

Current convention requires that multiple molecular characteristics of apoptosis must be observed prior to determining its causal role in cellular death.

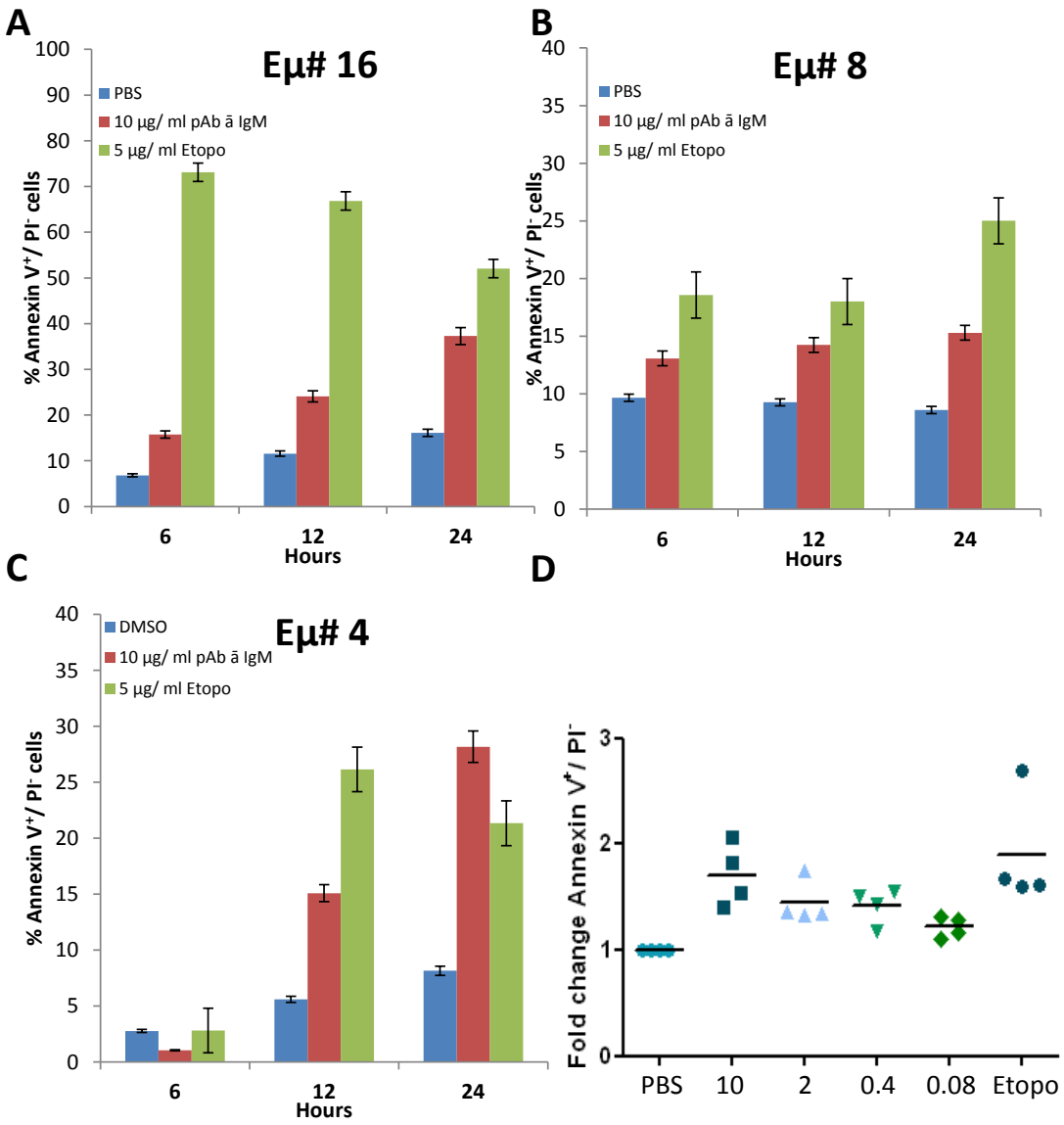

Figure 3.8 Observing the pAb ā IgM-induced accumulation of Annexin+/ PI- cells in Eμ-Myc lymphoma cells

Eμ-Myc lymphomas were treated and assessed for the presence of Annexin V^+/PI^- cells by flow cytometry as in figure 3.9. A-C) Percentage of Annexin V^+/ PI^- cells evident upon treatment with PBS (blue), 10 μg/ ml pAb ā IgM (red) or 5 μg/ ml Etoposide (green) with A) Eμ# 16, B) Eμ# 8 and C) Eμ# 4 cells. Data represents an average of a single experiment performed in triplicate. Error bars reflect standard error D) Plot of fold change in the percentage of Annexin V^+/ PI^- cells in four WT Eμ-Myc lymphomas in response to the indicated concentration (μg/ ml) of pAb ā IgM, PBS or Etoposide at 5 μg/ ml.

Therefore, an additional molecular characteristic of apoptosis, caspase processing, was examined following BCR-engagement. Cells were plated at $1x10^6$/ml and treated with 2 μg/ml pAb or mAb ā IgM for 12 or 18 hours and compared to cells treated with PBS alone. Cells were then harvested by pipetting, lysates prepared and analysed for caspase processing by western blotting. As evident in figure 3.9A and 3.9E, extensive

cleavage of the effector caspase substrate PARP was evident after 12 hours in both pAb and mAb ā IgM treated cells, demonstrating that significant caspase activity was evident at this time point. Such caspase activity was associated with proteolytic processing of initiator caspases 2 and 9 and effector caspases 3, 6 and 7, as shown in figure 3.9. BCR-induced processing of caspases 1 and 8 was also assessed. However, little or no processing was evident following BCR-engagement (see appendix A11). Of the initiator caspases activated downstream of the BCR, cleaved caspase-2 displayed the greatest induction reaching approximately five-fold, as shown in figure 3.9F. Caspase-3 represented the most highly activated effector caspase, reaching ten-fold accumulation of its active fragment following pAb ā IgM treatment for 18 hours. Therefore, BCR engagement of Eμ-Myc lymphoma cells appears to enhance processing and activity of initiator and effector caspases, reflecting an additional apoptotic characteristic.

3.5.3.3 BCR-induced cell death and Caspase-dependency

Whilst caspase activation and PARP cleavage appears correlated with BCR-induced cell death in Eμ-Myc lymphoma cells, the definite association with the cell death programme remains to be determined. In order to determine whether BCR-induced cell death exhibits caspase-dependency, the effect of the pan-caspase inhibitor qVD-OPH upon the process was assessed. As can be seen in figure 3.10B, pre-treatment with qVD-OPH significantly inhibits both pAb ā IgM and Etoposide-induced cell death after 24 hours. Such significant reduction demonstrates the reliance of BCR-induced cell death upon the activity of caspases. Taken together with the observations of Annexin V^+/ PI^- accumulation and caspase processing, it can be concluded that BCR engagement imparts an apoptotic cell death in Eμ-Myc lymphoma cell lines.

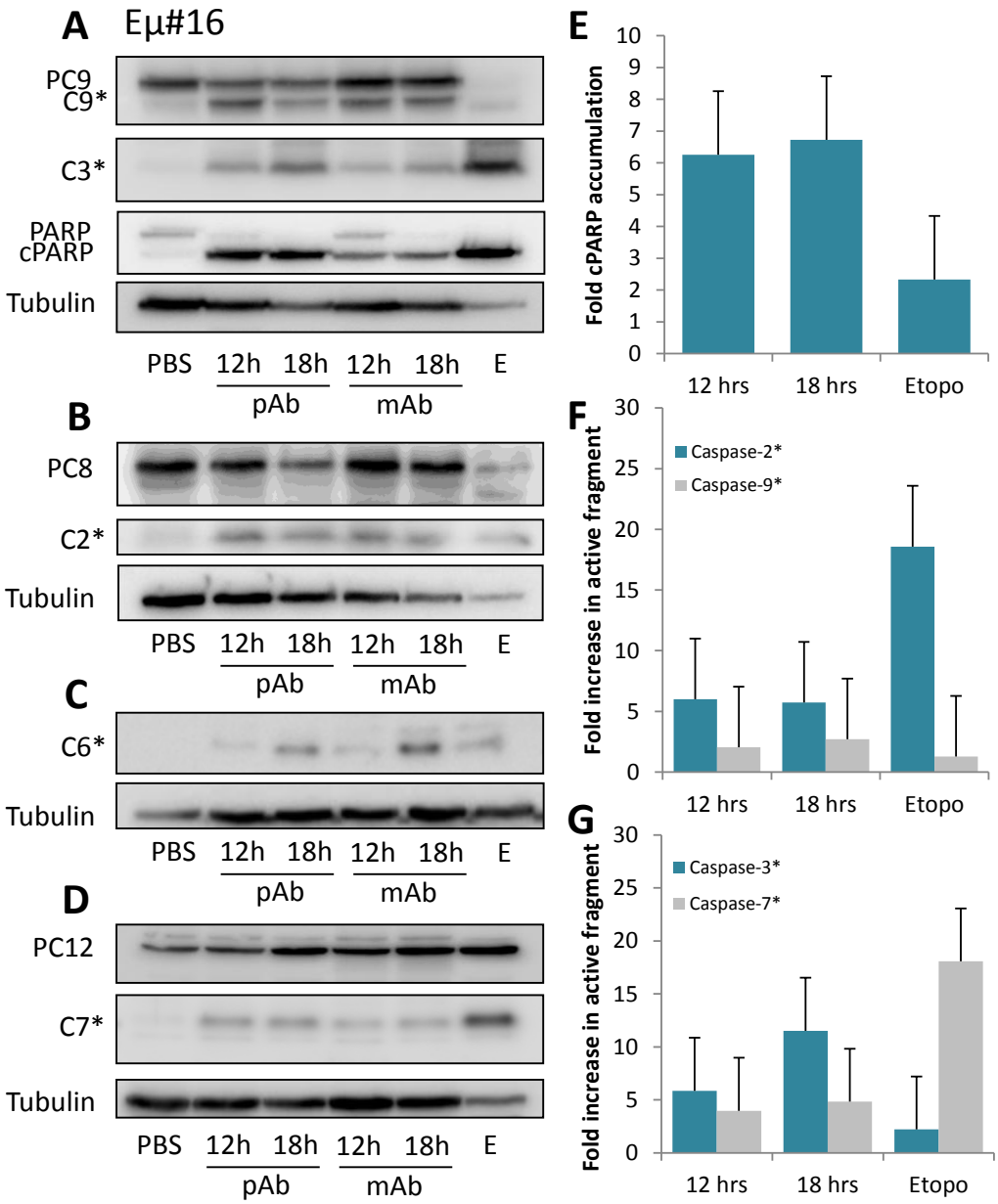

Figure 3.9 Assessment of pAb/mAb ā IgM-induced caspase activation in Eμ-Myc lymphoma cells

Eμ-Myc lymphomas were plated at 1x10^6/ ml, incubated with 2 μg/ ml pAb or mAb ā IgM or an equivalent volume of PBS for 12 or 18 hours and lysates prepared. Lysates were then analysed by western blotting for the effect of BCR stimulation upon the levels of both procaspases (PC) and active caspase fragments (denoted by *). A-D) Example western blots obtained from Eμ-Myc# 16 observing levels of caspases 2, 3, 6, 7 and 9 alongside PARP cleavage downstream of the BCR. E-G) Quantitation of E) PARP cleavage, F) initiator Caspase processing and G) effector caspase processing was performed by densitometry utilising UVP vision works software as outlined in materials and methods. Levels of active caspase fragments were assessed where available. Data represents the average of three independent experiments utilising Eμ# 16, 8 and 4. Error bars represent standard deviation.

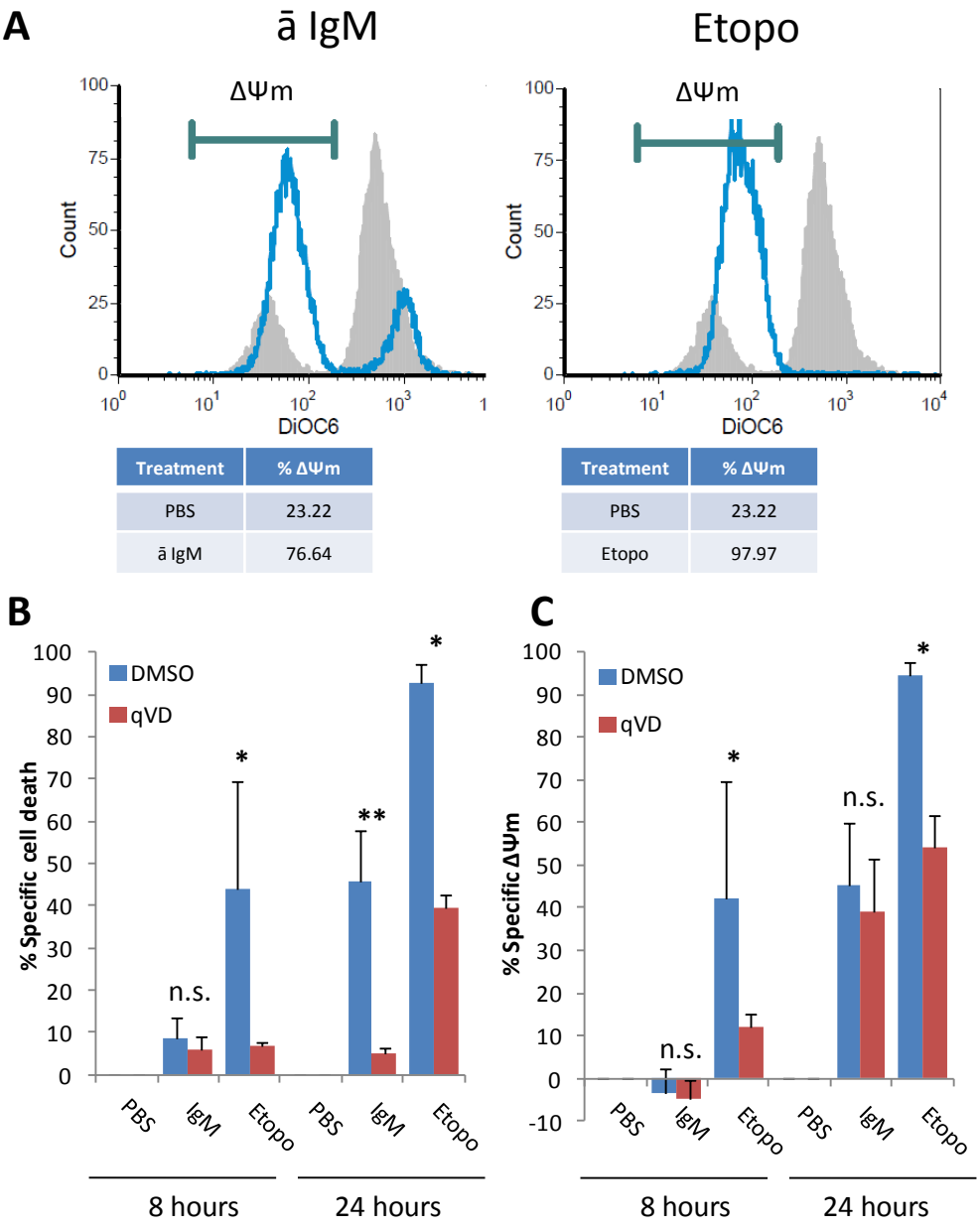

Figure 3.10 Analysis of the impact of BCR-stimulation upon mitochondrial membrane potential in Eμ-Myc lymphoma cells

Eμ-Myc lymphomas were plated at 1.6x10^6/ ml and pre-treated with the pan-caspase inhibitor qVD-OPH (25 μM) or an equivalent amount of DMSO for 30 minutes at 37°C. Cells were subsequently treated with 10 μg/ ml pAb ā IgM, 5 μg/ ml Etoposide or an equivalent volume of PBS for 8 and 24 hours. Cells were then harvested by pipetting and split into two tubes, one stained with 10 nM DiOC6/ PI and the other with Annexin V/ PI and analysed be flow cytometry, as before. A) Example histogram obtained upon DiOC6 staining demonstrating untreated cells (filled plot) and a blue shifted plot representing cells treated with 10 μg/ ml pAb ā IgM (left panel) or 5 μg/ ml Etoposide (right panel). B) The effect of caspase-inhibition upon pAb ā IgM or Etoposide-induced cell death. C) The effect of pAb ā IgM upon mitochondrial outer membrane integrity and Caspase dependency. Data represents an average of three independent experiments; each performed in triplicate utilising Eμ# 16, 8 and 4. Bars represent standard deviation. Asterisks represent statistically significant differences ($p < 0.05$) as adjudged by paired Student's T-test analysis n.s. denotes a non-significant difference.

3.5.4 BCR-induced cell death and MOMP via the extrinsic or intrinsic pathway

Since the intrinsic and extrinsic apoptotic pathways differ in their dependency upon caspase activity for MOMP, the occurrence of MOMP and the effect of qVD-OPH was examined downstream of the BCR. Eμ-Myc lymphoma cells were pre-incubated with 25 μM qVD-OPH or an equivalent volume of DMSO for 30 minutes at 37°C. Subsequently, cells were subjected to pAb ā IgM or Etoposide treatment for 8 and 24 hours. Samples were then split and analysed concurrently by $DiOC_6$ flow cytometry and Annexin V/ PI flow cytometry. Since $DiOC_6$ accumulates in the intermembranous space of mitochondria with a significant membrane potential (Ψ_m), fluorescence, detectable by flow cytometry, is produced. However, upon MOMP Ψ_m is lost, corresponding to a reduction in $DiOC_6$ fluorescence. As can be seen in figure 3.10A and C, both pAb ā IgM and Etoposide treatments are associated with a loss of $DiOC_6$ fluorescence intensity indicative of MOMP. However, in contrast to its effect on cell death, measured by annexin V/ PI in figure 3.10B, the pan-caspase inhibitor qVD-OPH failed to influence the extent of MOMP downstream of BCR engagement. Such an observation is indicative of activation of the intrinsic apoptotic pathway, which activates MOMP via upregulation of BH3-only proteins rather than via the activity of caspases (as is the case in the extrinsic pathway). Interestingly however, qVD-OPH appeared to significantly reduce the extent of MOMP induced by Etoposide at both 8 and 24 hours. Therefore, it appears as though the BCR and Etoposide induce differing model of apoptosis, with Etoposide mediating MOMP via direct caspase-activation in Eμ-Myc lymphoma cells. In contrast, the above studies demonstrate that BCR-induced apoptosis is associated with the onset of caspase-independent MOMP in Eμ-Myc lymphoma cells, a characteristic of intrinsic apoptosis.

In order to confirm that BCR engagement of Eμ-Myc lymphoma cells triggers apoptosis via the intrinsic pathway, cell lines were engineered to over-express a Bcl-2 transgene in order to block intrinsic apoptosis. Ecotropic phoenix cells were transiently transfected with the murine stem cell virus (MscV)-based pMscV-internal ribosome entry sequence (IRES)- Hygromycin resistance (HygroR) (pMIH) vector alone or encoding a human Bcl-2 transgene (pMIH Bcl-2).

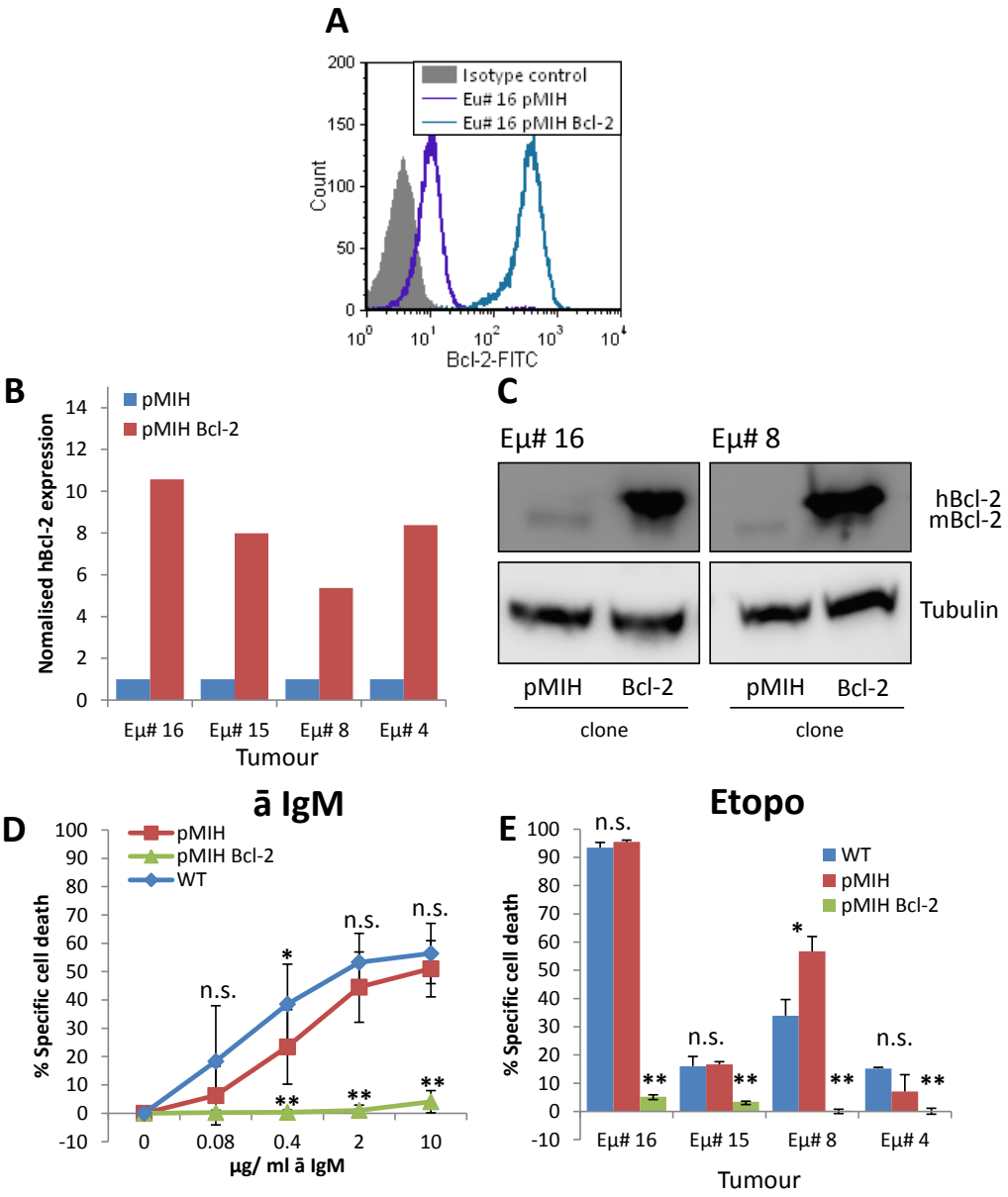

Figure 3.11 Examining the impact of forced human Bcl-2 transgene expression upon the extent of pAb ā IgM-induced cell death in Eμ-Myc lymphoma cells

Eμ-Myc lymphomas were engineered to over-express a human Bcl-2 (hBcl-2) transgene by transduction with pMIH Bcl-2 or an empty vector pMIH as a control, as outlined in materials and methods section 2.17 A) Cells were assessed for human Bcl-2 expression by intracellular flow cytometry using FITC conjugated anti-hBcl-2 (clone 124). B) Quantitation of hBcl-2 transgene over-expression. Geometric means for hBcl-2 were divided by those of isotype controls and normalised against empty vector expressing controls. C) Western blot analysis of human and mouse Bcl-2 levels in Eμ-Myc pMIH and Eμ-Myc pMIH Bcl-2. D-E) Eμ-Myc pMIH and pMIH Bcl-2 were assessed for sensitivity toward pAb ā IgM (24 hours) and 5 μg/ ml Etoposide (6 hours) induced cell death by Annexin V/PI flow cytometry as in figure 3.7. Data represents an average of values obtained from four different Eμ-Myc cell lines, each of which was the average of three independent experiments, each performed in triplicate. Asterisks represent a statistically significant difference ($p < 0.05$) as adjudged by paired Student's T-test statistical testing. Expression of a Bcl-2 transgene completely blocks both pAb ā IgM and Etoposide-induced cell death.

Such vectors induce secretion of recombinant virus particles from phoenix cells, which were subsequently utilised to stably transduce Eμ-Myc cells. Transduced Eμ-Myc cell lines were then selected by Hygromycin treatment and screened for expression of the Bcl-2 transgene by intracellular flow cytometry and western blot. As can be seen in figure 3.11A-B, Eμ-Myc cells transduced with pMIH Bcl-2 show a 6-10 fold increase in human Bcl-2 intensity by flow cytometry. Unusually, the human-specific anti-Bcl-2 FITC conjugated mAb (Clone 124) showed enhanced fluorescence in pMIH transfected Eμ-Myc in comparison to the isotype control. It is possible that a degree of cross reactivity with mouse Bcl-2 exists and is responsible for the small shift. In order to directly compare total levels of cellular Bcl-2 western blot analysis of pMIH and pMIH Bcl-2 transduced Eμ-Myc lymphomas was undertaken using anti-Bcl-2 antibodies that detect both human and murine Bcl-2.

As shown in figure 3.11C, transduction with pMIH Bcl-2 massively enhanced cellular levels of Bcl-2 in comparison to pMIH-transduced cells. Therefore, the pMIH Bcl-2 transduced Eμ-Myc lymphomas were taken forward for analysis upon the impact upon BCR-induced apoptosis. As demonstrated in figure 3.11D, transduction of Eμ-Myc lymphoma cells with the pMIH vector slightly, but not statistically significantly (except at the 0.4 μg/ml dose), reduced the level of cell death recorded following pAb ā IgM treatment for 24 hours. In contrast however, pMIH Bcl-2 transduced Eμ-Myc lymphoma cells demonstrated a near complete ablation of pAb ā IgM-induced cell death. Such an inhibition was not limited to pAb ā IgM, since pMIH Bcl-2 expression also correlated with complete resistance to Etoposide treatment after 6 hours. Since Bcl-2 negatively regulates the activities of BH3-only proteins, and therefore intrinsic apoptosis, such data confirm that BCR-induced apoptosis is dependent upon engagement of MOMP via the intrinsic apoptotic pathway in Eμ-Myc lymphomas.

3.6 Delineation of the identity of the key BCR-induced initiator Caspase

3.6.1 Examining the kinetics of BCR-mediated Caspase activation

Whilst figure 3.9 identified that Caspase 2 and Caspase-9 represented the sole initiator caspases activated downstream of the BCR in Eμ-Myc lymphoma cells, it remains unclear as to which plays the more prominent role. In an attempt to determine whether temporal spacing of initiator Caspase activation was evident following BCR engagement, kinetic analysis of caspase processing was undertaken by western blotting. As evident in figure 3.12, gradual accumulation of cleaved PARP was evident 10 hours post- pAb ā IgM treatment. Such processing was accompanied by a statistically significant increase in caspase-2, caspase-9, and caspase-3 active fragments (denoted by *) 9 hours post-treatment. Therefore, on average, at least, it appears as though processing of both effector and initiator Caspases are near simultaneous and not temporally distinct. However, within a single cell line, i.e. Eμ# 16, significant processing of caspase-9 could be observed prior to that of caspase-2.

Such an observation implies that caspase-9 may be the key initiator caspase downstream of the BCR, implying that BCR-induced apoptosis proceeds almost exclusively via the intrinsic apoptotic pathway, although is far from conclusive.

3.6.2 Use of Caspase-specific inhibitors to dissect initiator Caspase function

As demonstrated in figure 3.12, BCR-induced activation of caspases 2 and 9 were temporally indistinguishable. Therefore, in an attempt to dissect their function the reportedly caspase-specific inhibitors VDVAD-FMK and LEHD-FMK were examined for an effect upon the extent of caspase processing and BCR-induced cell death. Eμ-Myc lymphoma cells were plated out at 1x106/ ml and pre-treated with the indicated concentration of caspase-inhibitor or an equivalent volume of DMSO for 30 minutes at 37°C. Subsequently, cells were treated with 2 μg/ ml pAb ā IgM or an equivalent volume of PBS for 12 hours, lysed and examined for the extent of caspase processing by western blotting.

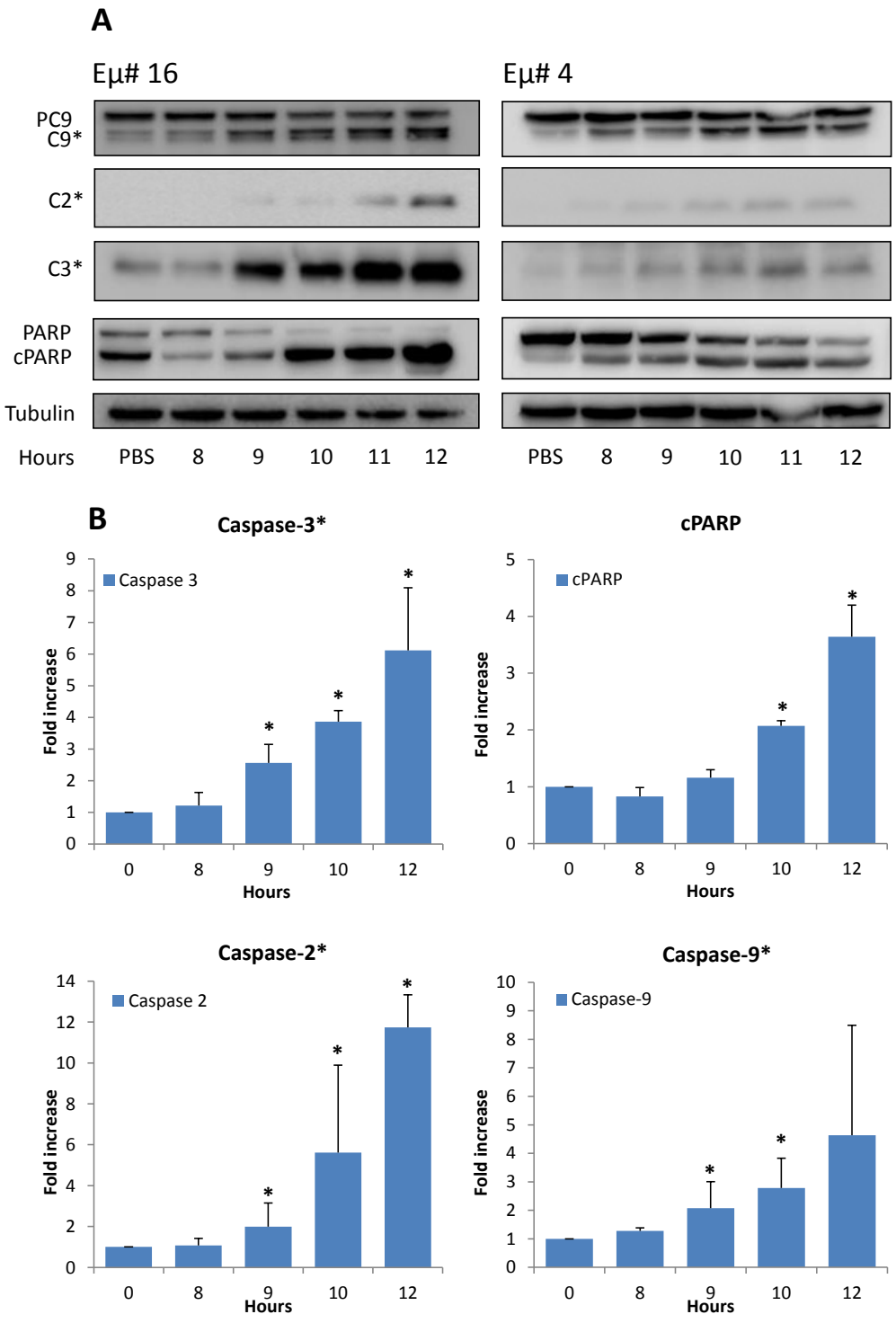

Figure 3.12 Kinetic analysis of pAb ā IgM-induced caspase activation in Eμ-Myc lymphoma cells

Eμ-Myc lymphomas were plated at 1x10^6/ ml, incubated with 2 μg/ ml pAb ā IgM or an equivalent volume of PBS for 8, 9, 10, 11 or 12 hours, harvested by pipetting and lysates prepared. Subsequently, pAb ā IgM-induced accumulation of caspase-2, 3, and 9 active fragments and PARP cleavage was assessed by western blotting. A) Example western blots from Eμ# 16 (left panel) and Eμ# 4 (right panel) demonstrating induction of caspase processing and PARP cleavage. B) The levels of active caspase fragments and cleaved PARP was assessed by densitometry using UVP vision works software (UVP, UK) and normalised against levels in the untreated sample. Data represents the average of three independent experiments utilising Eμ#16, 8 and 4 each performed once. Error bars represent standard deviation. Asterisks denote statistically significant differences ($p < 0.05$) as assessed by paired Student's T-test analysis.

As evident in figure 3.13B and C, 100 μM of the caspase-2 inhibitor VDVAD-FMK effectively blocked caspase-2 processing downstream of BCR engagement. However, it appeared to have little impact upon the levels of active caspase-9 or caspase-3 produced after BCR stimulation. Interestingly though, VDVAD-FMK appeared to reduce the levels of cell death generated upon pAb ā IgM treatment by roughly 50%. Such evidence may implicate caspase-2 as key in efficient activation of cell death. However, in the presence of VDVAD-FMK, BCR engagement appeared to lead to an enhancement of active caspase-3 levels in comparison to BCR-stimulation alone. Since PARP represents the major caspase-3 substrate, such an occurrence would be expected to lead to enhanced PARP cleavage. However, paradoxically enhanced caspase-3 activation in the presence of VDVAD-FMK correlated with a reduction in the level of PARP cleavage. Therefore, one explanation may be that VDVAD-FMK also inhibits the activity, but not processing, of caspase-3. Indeed, a small shift from the active p17 caspase-3 fragment to a p19 fragment is evident upon treatment with VDVAD-FMK. Therefore, it appears as though VDVAD-FMK also influences the activity of Caspase-3 and therefore, is not suitable to assess the impact of caspase-2 inhibition on cell death in the Eμ-Myc model. The caspase-9 specific inhibitor LEHD-FMK was also utilised to assess the impact of caspase-9 inhibition upon caspase processing and cell death downstream of the BCR. Cells were treated, as with VDVAD-FMK, and levels of active caspases were assessed by western blotting. As evident in Figure 3.14B, LEHD-FMK failed to completely block activation of caspase-9 and its downstream target caspase-3 post BCR-engagement. However, an approximate four-fold reduction in caspase-9 activation was achieved by a dose of 100 μM. Such inhibition appeared to have no impact upon caspase-3 activation or the extent of cell death, yet seemed to effectively inhibit the activity activation of caspase-2.

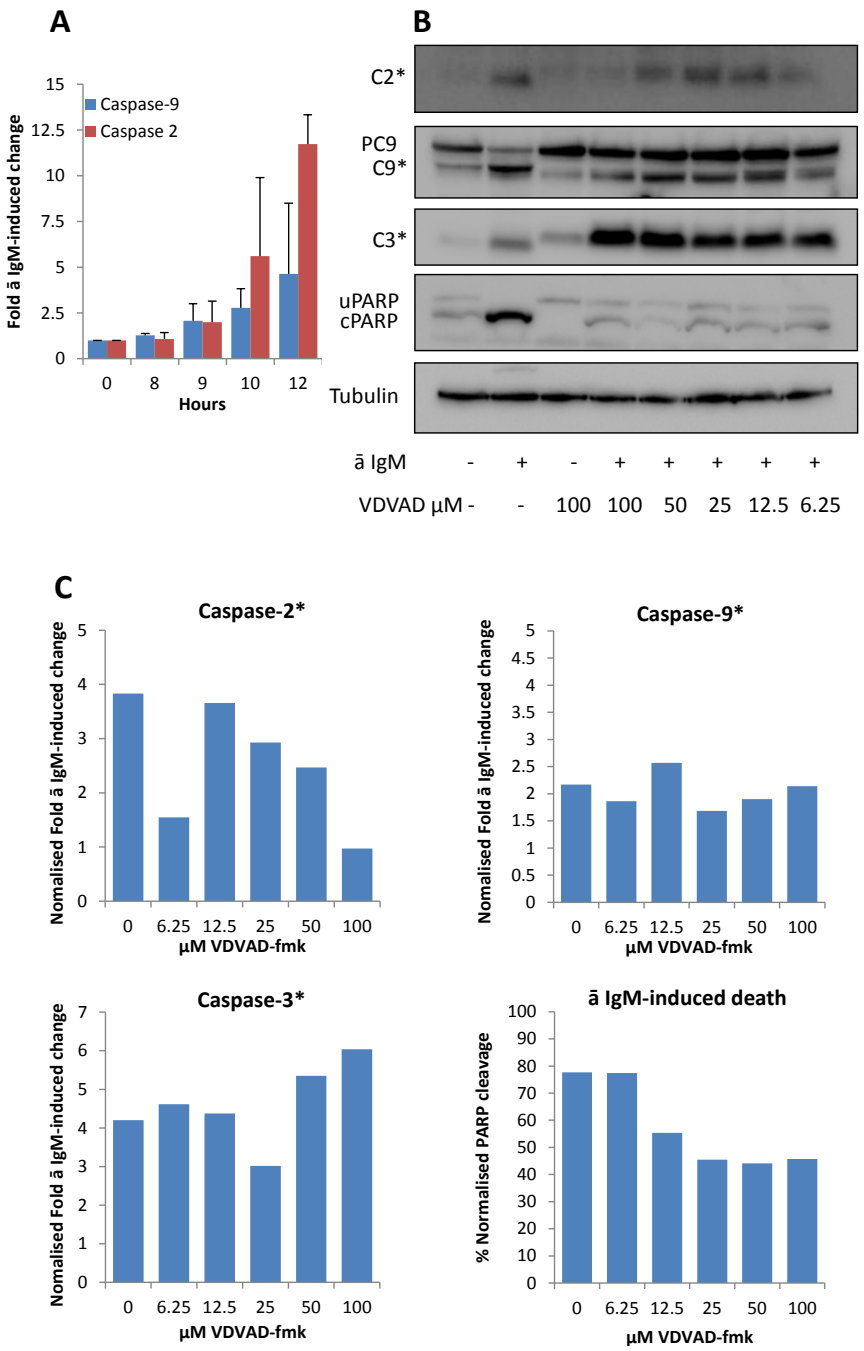

Figure 3.13 Examining the impact of caspase-2 inhibition upon Caspase-activation profiles and cell death downstream of the BCR

Eμ-Myc lymphoma cells were plated at 1x10^6/ ml and pre-treated with the caspase-2 specific inhibitor VDVAD-FMK at the indicated doses for 30 minutes at 37°C. Cells were subsequently incubated with 2 µg/ ml pAb ā IgM or an equivalent volume of PBS for 24 hours, harvested by pipetting and lysates prepared. Subsequently, the level of pAb ā IgM-induced cell death (as adjudged by PARP cleavage) and active caspase fragment generation was assessed by western blotting. A) Comparison of initiator caspase 2 and 9 activation kinetics. B) Western blotting analysis of the impact of VDVAD-FMK upon the extent of pAb ā IgM-induced caspase-activation and PARP cleavage. C) Quantification of active caspase fragments and PARP cleavage detected in 3.13B by densitometry using UVP vision works software (UVP, UK). Data represents a typical experiment.

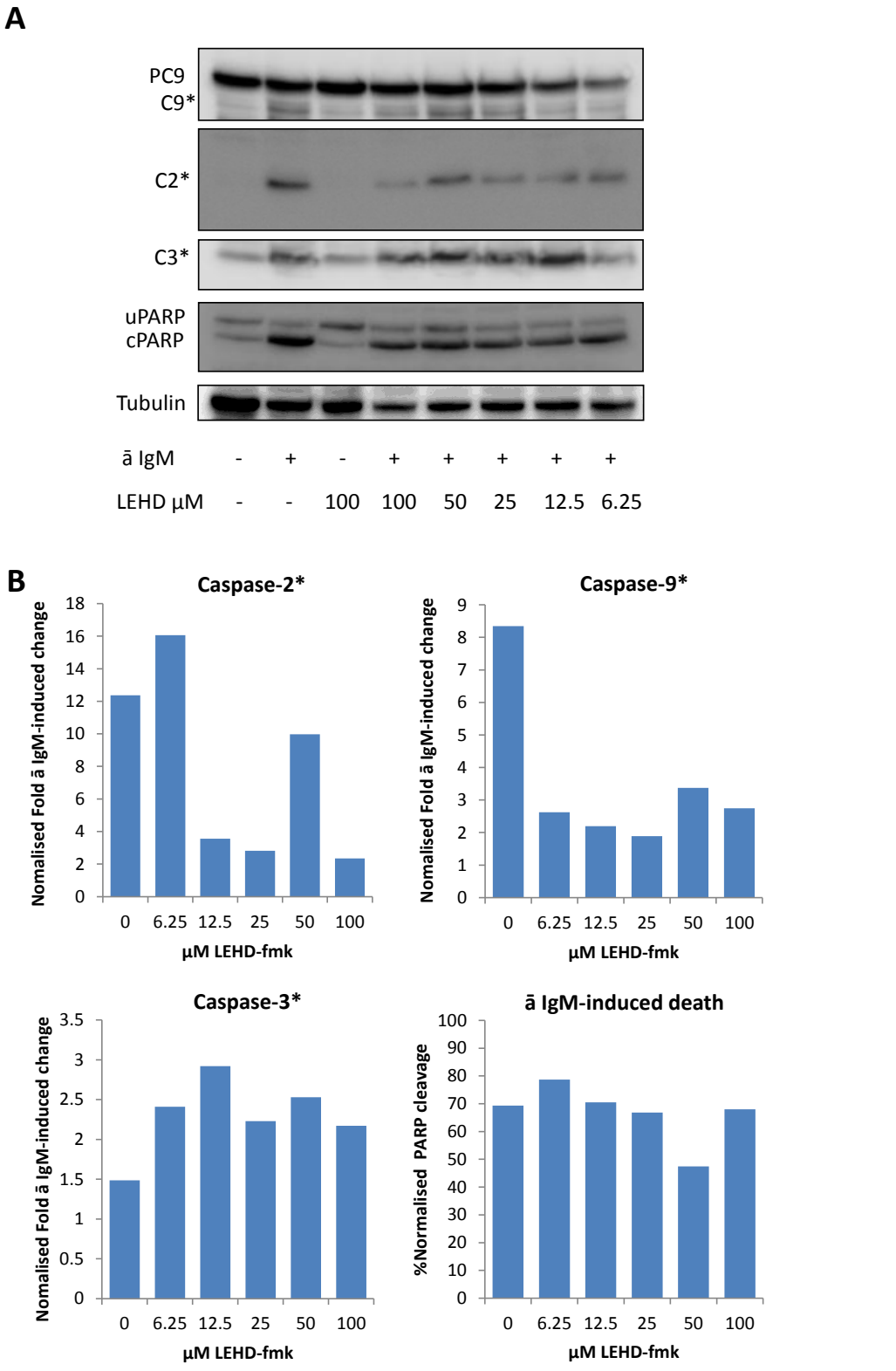

Figure 3.14 Examining the impact of caspase-9 inhibition upon Caspase-activation profiles and cell death downstream of the BCR

Eμ-Myc lymphoma cells were plated at 1x10^6/ ml and pre-treated with the caspase-9 specific inhibitor LEHD-FMK at the indicated doses for 30 minutes at 37°C. Cells were subsequently incubated with 2 μg/ ml pAb ā IgM or an equivalent volume of PBS for 24 hours, harvested by pipetting and lysates prepared. Subsequently, the level of cell death (as adjudged by PARP cleavage) and active caspase fragment generation induced by pAb ā IgM was assessed by western blotting. A) Western blotting analysis of the

impact of LEHD-FMK upon the extent of pAb ā IgM-induced cell death and caspase-activation. B) Quantification of active caspase fragments and PARP cleavage detected in 3.14A by densitometry using UVP vision works software. Data represents a typical experiment.

However, since LEHD-FMK effectively blocked caspase-2 activation (figure 3.14), yet VDVAD-FMK had no influence upon caspase-9 processing (figure 3.13), it appears as though caspase-9 is upstream of caspase-2 in Eμ-Myc lymphoma cells following BCR engagement. Such an observation is in agreement with the temporal separation of Caspase-9 and Caspase-2 processing evident in Eμ# 16 in figure 3.12.

3.7 Chapter Discussion

Here, the incidence and immunophenotype of spontaneous lymphomas arising in Eμ-Myc mice has been examined. The generation of such tumours allowed development of IgM^+ cell lines, providing an *in vitro* model in which the cellular responses to various stimuli could be examined and manipulated. Subsequently, characterisation of the cellular responses made by lymphoma cell lines to *in vitro* BCR stimulation was undertaken and dissection of the key molecular mechanims was begun.

In our hands, Eμ-Myc mice developed spontaneous B-cell lymphomas of B and Pre-B-cell origin afflicting the spleen, lymph node and thymus at an onset of between 6 weeks and 6 months. Such results are comparable to those obtained by other groups, who generally demonstrate median disease onset of 12 weeks ranging from 6 to 14 weeks in the individual, afflicting the spleen, lymph nodes and thymus (42, 233, 321-324, 327, 331, 332). Furthermore, Harris et al demonstrate that 100% of Eμ-Myc lymphomas were of B-cell origin and 48.4% stained positive for sIg, similar to our results. Furthermore, we demonstrate that IgM^+ Eμ-Myc lymphomas routinely display an immunophenotype indicative of a T1 transitional B-cell, as previously reported (233, 324).

We also demonstrate that BCR-engagement is effectively linked to downstream signalling machinery in Eμ-Myc lymphoma cells in the form of MAPKs and the Ca^{2+} mobilisation apparatus. However, our results demonstrate that Eμ-Myc lymphoma cells exhibit a BCR-induced Ca^{2+} flux response of reduced magnitude and duration, in

comparison to normal splenic B-cells. Such a reduction appears attributable to a reduction in magnitude of both IP_3-mediated ER Ca^{2+} efflux and capacitive Ca^{2+} entry.

Such differences may be attributable to the isolation of mixed populations of B-cell developmental stages by MACS purification. Consequently, anti-IgM treatment may engage antigen receptors of T1, T2 and non-class switched mature B-cells, which differ in the nature of response toward BCR-engagement (4, 17, 20-22, 40, 41, 43, 227, 246-254, 258).

T1 B-cells, such as Eμ-Myc lymphoma cells, appear to exhibit profoundly reduced IP_3 and DAG production, indicative of PLC activity, in response to BCR-engagement than their T2 or mature B-cell counterparts (370). Such reduced PLC-activation may be attributable to reduced Syk expression in immature B-cells and a reduced rate of receptor endocytosis, which is known to influence the strength of downstream pathway activation (55, 253, 254, 258). However, such a deficiency appears to be compensated for by an enhanced reliance upon capacitive Ca^{2+} entry and CRAC channel function, giving rise to an overall similar Ca^{2+} flux response (370). Therefore, whilst developmental stage differences may account for differential Ca^{2+} spike responses, it does not provide a satisfactory explanation for overall differences in total Ca^{2+} flux.

An additional explanation may be found in the differential cellular contexts in which *in vitro* and *ex vivo* lymphocytes are subjected to BCR stimulation. It is likely that *in vivo* normal splenic B-cells are subjected to microenvironment derived signals influencing Ca^{2+} flux responses to BCR engagement, such as BAFF or CD40 signalling (4, 22, 50, 145). Such signals however, may be absent from the long-term *in vitro* maintained Eμ-Myc lymphoma cells. Therefore, it is possible that microenvironment cues continue to influence the Ca^{2+} flux response of *ex vivo* lymphocytes, maintaining a more "excitable" cellular context and may account for the observed differences. However, it is also possible that such differences may be attributable to cell-line adaptation. For instance, such a phenomenon is commonly observed between primary human cells and *in vitro* maintained cell lines. Therefore, it appears as though culturing in vitro somehow maintains cells in a less excitable state.

It is also plausible that differences in BCR-induced Ca^{2+} flux may be attributable to biological differences between malignant and non-malignant cells. Indeed, normal human B-lymphocytes exhibit altered kinetics in kinase activation following BCR engagement in comparison to follicular lymphoma cells (234) Therefore, it is also possible that differential Ca^{2+} flux responses may also be evident. Furthermore, on average Eμ-Myc lymphoma cells appear to exhibit enhanced levels of Bcl-2 expression in comparison to normal B-cells, which may influence IP3-mediated ER Ca^{2+} release via an interaction made between its BH4 domain and IP3-Rs (327, 370).

In addition, we demonstrate that BCR engagement is linked to a negative cellular outcome in Eμ-Myc lymphomas, in the form of a Caspase-dependent cell death response driven by the intrinsic apoptotic pathway, as has been previously reported (193, 225-228, 237-239). We identify that forced over-expression of a Bcl-2 transgene blocks the apoptotic response to BCR engagement, as observed in (193, 225-228, 237-239), implicating BH3-only proteins in the response (assessed in chapter 4) as is reflected in the majority of studies (221, 223, 226, 229-233, 235, 236). Our findings contrast with observations that caspases directly contribute toward MOMP downstream of BCR engagement, as evident in the BL41, Ramos, and WEHI-231 long-term cell lines (243, 245). However, these observations are made in only a minority of cases, and most likely reflect stimulus or cell line-specific occurrences. In contrast, our finding that BCR-induced cellular death proceeds via intrinsic pathway-mediated MOMP is in agreement with the consensus view (193, 225-228, 237-239).

Our investigation, however, fails to reliably determine the identity of the key initiator caspase activated by BCR stimulation. On average, we observe simultaneous activation of caspase-2 and caspase-9 approximately 9 hours post-BCR engagement, an observation reflected in multiple studies (193, 225, 237-239). Intriguingly however, on an individual cell-line basis caspase-9 activation appeared to temporally precede that of caspase-2 in some lymphomas. However, such an event was not reproducible amongst multiple cell lines and therefore, cannot be guaranteed. We then utilised caspase-specific inhibitors and observed that caspase-2 may possibly reside downstream of caspase-9, thus highlighting caspase-9 as the key initiator caspase, as

suggested previously (193, 225, 237-239). However, caspase-specific inhibitors are notoriously cross-reactive (371, 372) and therefore, this investigation cannot reliably determine the nature of the key BCR-induced initiator caspase. Due to the highly redundant nature of caspases and their functions it seems unlikely that a single initiator caspase is responsible for activation of all downstream effector caspases. A much more likely scenario is that both caspase-9 and caspase-2 participate in apoptotic initiation, cleaving different targets associated with the response. Such a scenario seems to be supported by studies utilising dominant negative caspase-9 mutants to hinder BCR-induced effector caspase activation. Such studies identify that complete blockade of caspase-9 activity is insufficient to completely block the downstream response therefore, highlighting a possible role for caspase-2 (193). Such dual roles of caspases 9 and 2 could be assessed downstream of the BCR via generation of B-cell lines genetically deficient in both caspases, or expressing dominant negative mutant forms of both enzymes.

Interestingly, Eμ-Myc lymphoma cells appear to exhibit a gradual loss of sensitivity toward BCR-induced cell death over time, evident after around 23 *in vitro* passages. Such an observation likely reflects selection of clones exhibiting mutations in BCR-induced pathways that provide a significant survival advantage, for example constitutive ERK phosphorylation. However, whilst such an observation prevented use of Eμ-Myc lymphoma cells past passage 20, it does appear to give weight to the idea that long term *in vitro* maintenance may alter the response to BCR-ligation. Such an observation appears to validate our approach, using low-passage number lymphoma cell lines to more accurately reflect *in vivo* biology than long term *in vitro* cultures.

Therefore, in summary our findings demonstrate that Eμ-Myc lymphomas exhibit significant activation of PI3K/ Akt and MAPK pathways alongside a Ca^{2+} flux response to BCR engagement culminating in clonal deletion via the intrinsic apoptotic pathway. In the next chapter we shall aim to identify key components within the intrinsic pathway that facilitate the apoptotic deletion of Eμ-Myc lymphomas upon chronic BCR engagement.

Chapter 4 The impact of BCR engagement upon BH3-only and prosurvival Bcl-2 family members

4.1 Chapter Introduction

In the previous chapter it was demonstrated that BCR engagement drives caspase-dependent deletion of Eμ-Myc lymphomas via the intrinsic apoptotic pathway. Such observations predict that BCR-signalling directly influences the regulation of the Bcl-2 family, since its members are fundamental in controlling MOMP (162-164). Indeed, we and others demonstrate complete ablation of BCR-induced cell death following Bcl-2 overexpression, therefore implicating BH3-only proteins in the response (225-228).

A prominent role appears to be played by Bim, as its genetic loss significantly reduces the apoptotic response to BCR engagement in normal B-cells (229). JNK- and ERK-dependent skewing of Bim isoforms, preferentially to the more pro-apoptotic Bim_L isoform may help drive the apoptotic response (230, 231). However, protection afforded upon loss of Bim is not equivalent to that exhibited upon Bcl-2 over-expression (229, 233). Consequently, it is hypothesised that additional BH3-only proteins may facilitate the onset of cell death downstream of the BCR.

To date, studies highlight the possible involvement of Bik, Bad and Bmf as additional mediators of BCR-induced cell death (223, 235, 236). However, such studies fail to reliably assess their relative contribution to the response. Whilst Bik appears not to play a prominent role in normal B-cells, significant differences in malignant vs. non-malignant BCR signals may specifically activate Bik in malignant cells (221, 222, 234). Therefore, the relative importance of Bik to the response in malignant B-cells remains poorly understood and requires further characterisation.

Therefore, in this chapter it is aimed to address the hypothesis that: Multiple BH3-only proteins co-operate to drive a maximal apoptotic response downstream of BCR engagement. It is aimed to identify key players via analysis of Bcl-2 family transcript and protein levels following BCR engagement and assess their relative contribution to the response by gene knockout studies. Finally, we aim to assess whether loss of

multiple BH3-only proteins imparts a greater resistance to BCR-engagement than loss of Bim alone.

4.2 Analysing the impact of BCR signalling upon Bcl-2 family member transcript levels in Eμ-Myc lymphomas

Prior to analysis of BCR-induced Bcl-2 family transcriptional regulation, it was deemed necessary to perform several validatory steps to establish the quality of the isolated RNA, alongside the specificity and appropriateness of the chosen housekeeping genes. Furthermore, steps were taken to determine the relative gene expression levels of each target in an attempt to put any future BCR-induced transcriptional enhancements into context.

$1x10^6$ Eμ-Myc lymphoma cells (Eμ# 16, 15, 8, and AF47), per well, were plated in a 12-well plate in a final volume of 1 ml, using the residual culture medium. Subsequently, cells were treated with 2 μg/ ml pAb ā IgM or an equivalent volume of PBS for 2, 4, 6, and 8 hours. After which, cells were harvested and RNA isolated.

4.2.1 Analysis of the integrity of extracted RNA from Eμ-Myc lymphomas

In order to detect potential degradation and RNase contamination of purified samples, RNA extracts from Eμ-Myc lymphoma cells were analysed for the relative abundance of 28s/ 18s rRNA. Classically, 28s and 18s rRNA exist in a 2:1 ratio with any significant deviation likely attributable to sample degradation by RNases. The Agilent Bio-analyzer 2100 RNA stability program was utilised to measure 28s: 18s rRNA and to provide a value from which the quality of RNA could be assessed, known as the RIN value. Typically, a RIN value of 5 and above is suitable for RT-PCR and qPCR analysis of gene expression. As demonstrated in figure 4.1 A-B, RNA extracts from Eμ-Myc lymphomas gave clear 28s: 18s rRNA bands and produced RIN values over 5. As demonstrated in Figure 4.1C-D, partial RNA degradation was evident in the Eμ# 4 6-hour control (PBS-treated) sample. Since a value close to 5 was achieved, the series was discarded and the purification repeated until samples were obtained with reduced degradation. Since RNA extracts from Eμ-Myc lymphomas were deemed suitable, samples were utilised for further validation and analysis of Bcl-2 family member transcript levels.

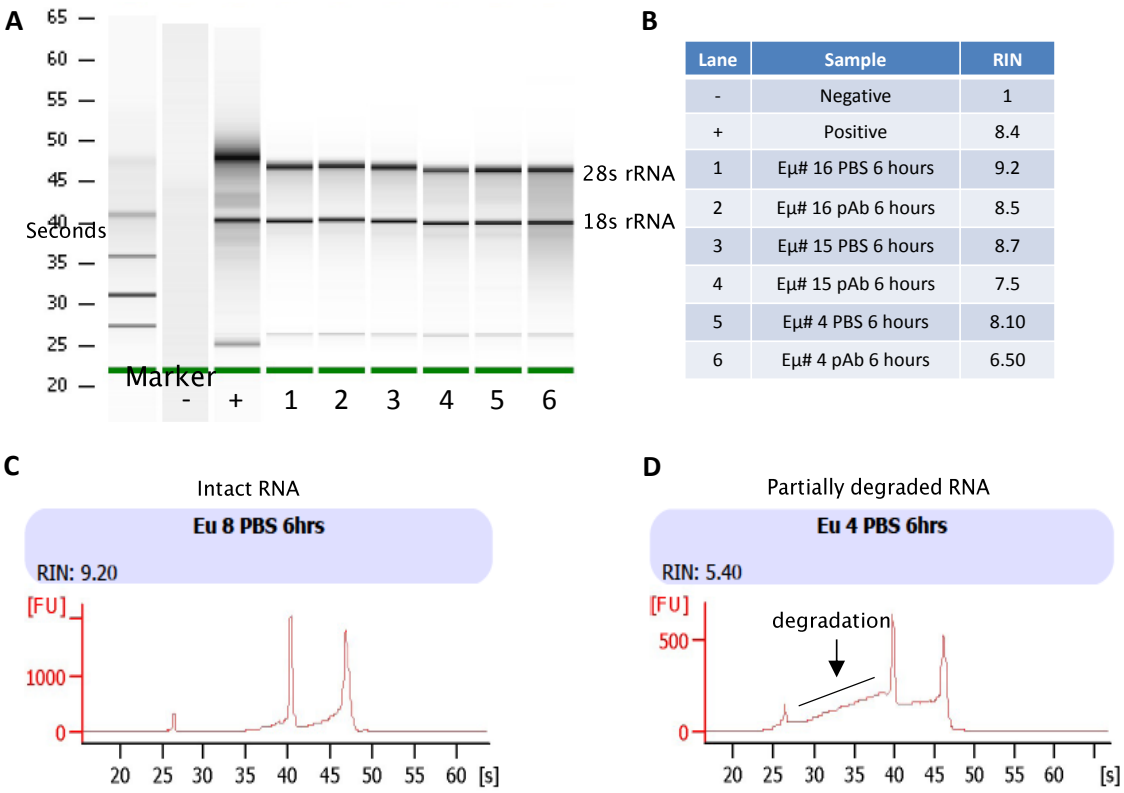

Lane	Sample	RIN
-	Negative	1
+	Positive	8.4
1	Eμ# 16 PBS 6 hours	9.2
2	Eμ# 16 pAb 6 hours	8.5
3	Eμ# 15 PBS 6 hours	8.7
4	Eμ# 15 pAb 6 hours	7.5
5	Eμ# 4 PBS 6 hours	8.10
6	Eμ# 4 pAb 6 hours	6.50

Figure 4.1 Assessment of purified Eμ-Myc RNA integrity

$1x10^6$ Eμ-Myc lymphoma cells were treated for the indicated time period with 2 μg/ ml pAb ā IgM or an equivalent volume of PBS. Cells were harvested by pipetting and RNA isolated via the use of the Purelink RNA mini-kit (Life technologies, UK). Subsequently, the integrity of purified RNA was assessed via use of the RNA stability program of the Agilent 2100 Bio-analyser, as outlined in materials and methods. **A)** Example gel image obtained from Agilent 2100 Bio-analyser, dark bands represent 28s and 18s rRNA. **B)** Typical RIN values obtained from the RNA stability assay of the Agilent 2100 Bio-analyser. **C-D)** Typical traces obtained from RNA stability assays depicting both intact and partially degraded RNA, respectively. A RIN value of 5 or above was deemed of sufficient quality for subsequent cDNA synthesis and analysis by qPCR. RIN values and traces are representative of all samples analysed. Substantial RNA degradation was not observed in any sample.

4.2.2 Validation of BH3-only and prosurvival Bcl-2 family member primer sets

In order to allow an accurate depiction of BH3-only and prosurvival Bcl-2 family member transcript levels, we first wished to validate a panel of qPCR primer sets for further use. Due to reduced expression levels and the requirement for precision, Taqman probes were utilised to amplify BH3-only cDNA, whereas conventional primers and the Sybr green method were deemed appropriate for prosurvival transcripts.

Initially, cDNA isolated from untreated Eμ-Myc lymphomas was titrated and amplified to determine whether the predicted inverse proportional relationship between c(T) and cDNA content was evident across the primer panel. As demonstrated in figures

4.2B and 4.3B, all primer sets gave progressively larger c(T) values with decreasing cDNA concentration, therefore, indicating that target c(T) was indeed proportional to the relative abundance of target sequence. Furthermore, all reactions produced sigmoidal amplification curves, as demonstrated in figures 4.2A and 4.3A, indicative of efficient amplification of each target across the primer panel.

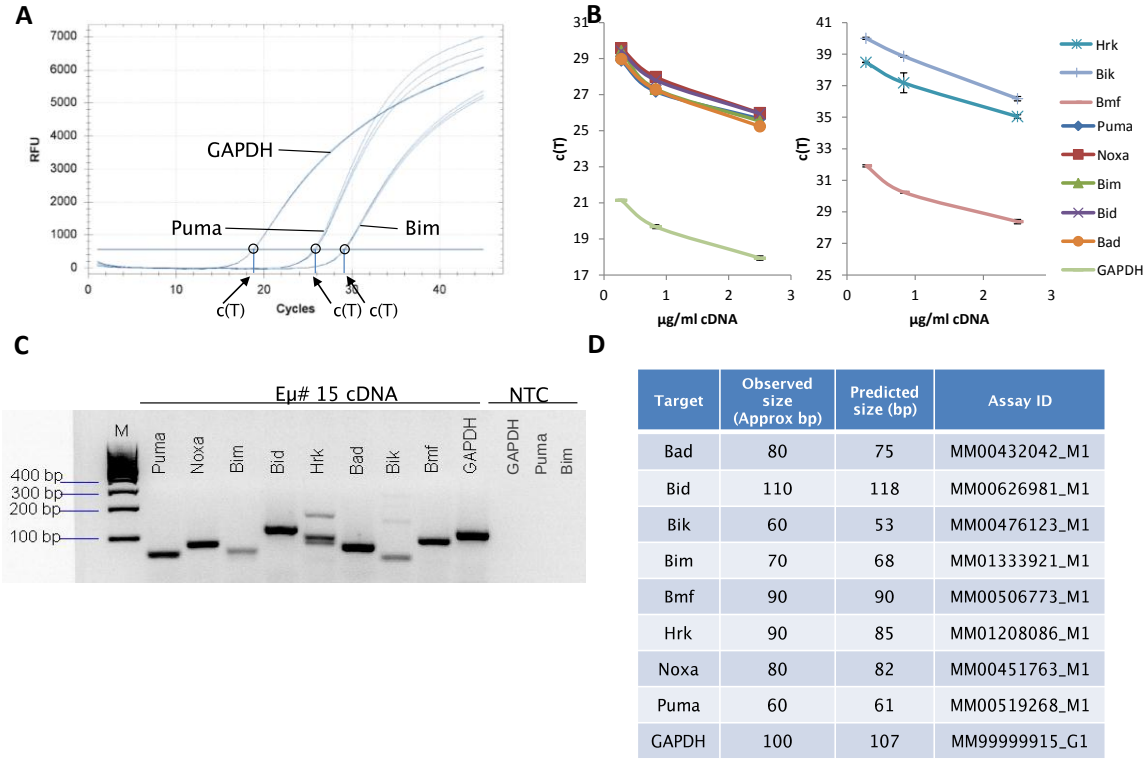

D

Target	Observed size (Approx bp)	Predicted size (bp)	Assay ID
Bad	80	75	MM00432042_M1
Bid	110	118	MM00626981_M1
Bik	60	53	MM00476123_M1
Bim	70	68	MM01333921_M1
Bmf	90	90	MM00506773_M1
Hrk	90	85	MM01208086_M1
Noxa	80	82	MM00451763_M1
Puma	60	61	MM00519268_M1
GAPDH	100	107	MM99999915_G1

Figure 4.2 Taqman qPCR primer validation

500 ng of non-degraded RNA was converted to cDNA and the indicated concentration was incorporated into qPCR reactions in a final reaction volume of 10 µl. **A)** Example traces obtained for Puma, Bim and GAPDH reactions produced using qPCR supermix-UDG (life technologies, UK). Reactions were analysed over 45 cycles using a C1000 thermal cycler fitted with the CFX96 fluorescence detector (Bio-Rad, UK) using CFX-manager software (Bio-Rad, UK). c(T) values were calculated utilising CFX-manager software (Bio-Rad, UK) and are indicated by the black arrows. Curves are representative of all targets **B)** cDNA was added to reactions at the indicated concentration and the impact upon c(T) was observed. Points represent the average values from Eμ# 16, 15, 8 and AF47 Eμ-Myc lymphoma cells, bars represent standard deviation **C)** The products of qPCR reactions were subjected to 2% agarose electrophoresis and the size, and specificity of products analysed by UV imaging. **D)** Table comparing the observed size and predicted size of products, as outlined by the manufacturer and the assay ID.

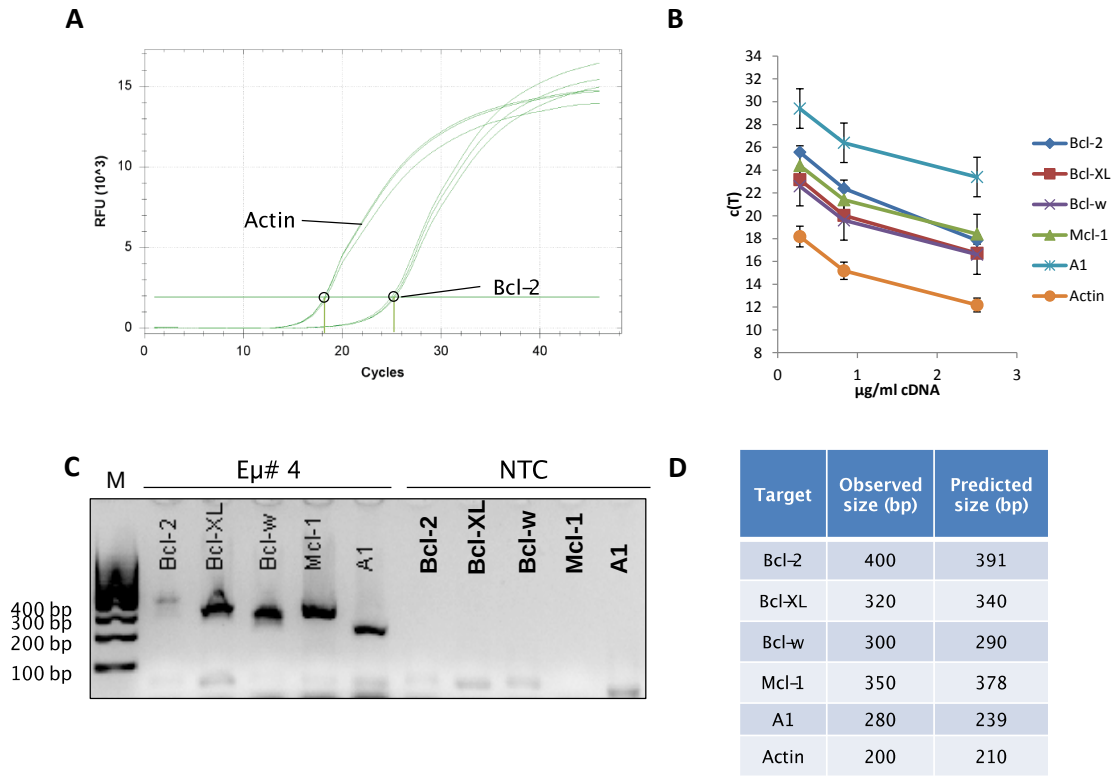

Target	Observed size (bp)	Predicted size (bp)
Bcl-2	400	391
Bcl-XL	320	340
Bcl-w	300	290
Mcl-1	350	378
A1	280	239
Actin	200	210

Figure 4.3 Sybr Green qPCR primer validation

500 ng of non-degraded RNA was converted to cDNA and the indicated concentration was incorporated into Sybr green qPCR reactions in a final reaction volume of 20 µl. **A)** Example traces obtained for Actin and Bcl-2 reactions using goTaq qPCR master mix (Promega, UK). Reactions were analysed over 45 cycles using a C1000 thermal cycler fitted with the CFX96 fluorescence detector (Bio-Rad, UK) using CFX-manager software (Bio-Rad, UK). Arrows indicate calculated c(T) values, curves are representative of all targets. **B)** cDNA was added to reactions at the indicated concentration and the impact upon c(T) was observed. Points represent the average values from Eμ# 16, 15, 8, and 4, bars represent standard deviation **C)** The products of qPCR reactions were subjected to 2% agarose electrophoresis and the size, and specificity of products analysed by UV imaging. **D)** Table comparing the observed size and predicted size of products, as determined by PrimerBLAST analysis (NCBI, USA).

Finally, comparative analysis of the observed and predicted product size was undertaken by electrophoresis in order to determine the fidelity of target amplification. As demonstrated in figures 4.2C-D and 4.3C-D, all but the Hrk primer set produced a single dominant band of approximately the correct predicted size. Since Hrk expression is often only present at extremely low levels in B-cells, such observation are likely attributable to a lack of expression in Eμ-Myc lymphoma cells. Furthermore, the prosurvival primer panel showed a significant change in fluorescence at a single temperature upon melt curve analysis, indicating the presence of a single product as outlined in figure 4.4. Melt curve analysis of Mcl-1 products, however, appeared to demonstrate the presence of a small shoulder, indicative of either a diminutive splice

variant or non-specific amplification. However, only a single product was evident upon analysis by electrophoresis, demonstrated in figure 4.3C, and therefore was deemed acceptable for further use.

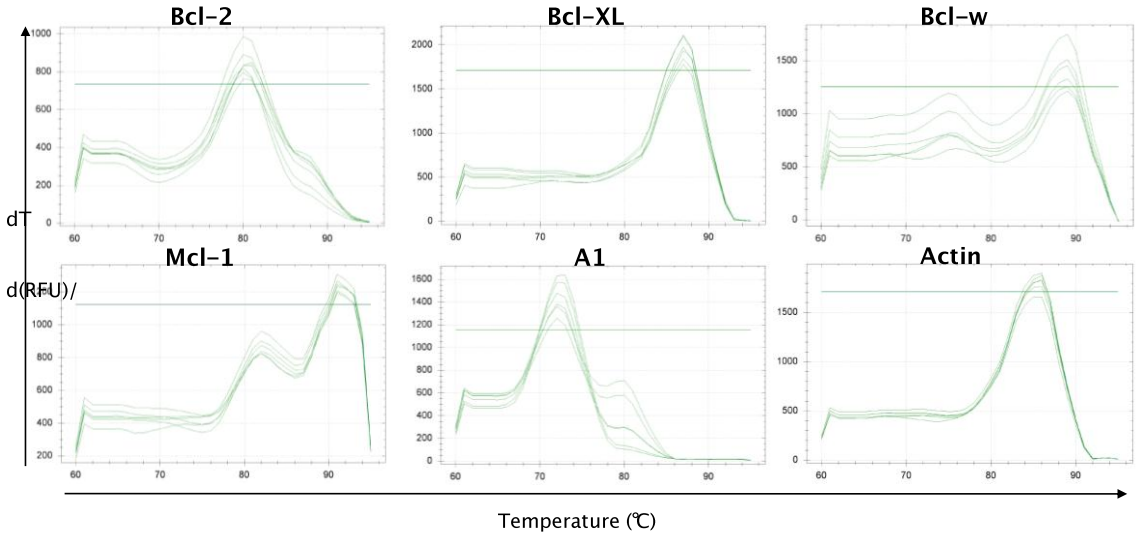

Figure 4.4 Melt curve analysis of Sybr green qPCR products

Reaction products from the pro-survival molecule PCR using cDNA of Eμ# 16 were subjected to melt curve analysis, using the CFX-manager thermal cycling melt curve function (Bio-Rad, UK). The change in relative fluorescence intensity (d(RFU)) was plotted against the change in temperature (dT). In general single peaks were observed for all products except Mcl-1.

Taken together, the above results demonstrate that the primer panel gave c(T) values proportional to target abundance, were efficiently amplified, and gave specific products of the predicted size, with the exception of Hrk. Consequently, BH3-only and prosurvival primer panels were taken forward to assess the levels of gene expression in Eμ-Myc lymphoma cells.

4.2.3 Analysis of basal expression levels of BH3-only and prosurvival Bcl-2 family members

In order to give potential BCR-driven alterations in BH3-only or prosurvival transcript levels context, it was deemed prudent to gain an insight into the relative expression levels of each gene. Whilst the $\Delta\Delta$c(T) method is not the method of choice for such an approach, it can yield accurate results within the limitations of its assumptions. Therefore, for relative gene expression analysis it is assumed that all primer sets bind and amplify with equal efficiency, and the extent of fluorescence produced by each product is equal amongst diverse targets. The latter assumption seems reasonable

since all Sybr green products are of similar length and likely exhibit similar levels of Sybr green interchelation. Such an assumption is irrelevant for Taqman probes, since a single product strand yields a single active fluorophore.

As demonstrated in figure 4.5A-B, Puma and Mcl-1 appear the most highly expressed members of their respective subgroups in Eμ-Myc lymphomas, as evident by possession of the lowest average c(T) value. Therefore, the remaining BH3-only protein and prosurvival subgroup members were normalised against these and expressed as a percentage of Puma and Mcl-1 expression levels, respectively. Bad and Bid represent the next most-abundant BH3-only proteins at 62 and 48% Puma expression respectively, followed by significantly lower expression of Bim, Bik, Noxa, and Bmf. In agreement with the prediction that multiple Hrk products may be attributable to low expression levels, Hrk expression was quantified as approximately 6,200 fold lower than that of Puma. Therefore, all BH3-only proteins except Hrk may have biological relevance in Eμ-Myc lymphoma cells, since expression levels are reasonably comparable.

As previously discussed, Mcl-1 represents the most-abundant prosurvival species in Eμ-Myc lymphoma cells followed by Bcl-2 and Bcl-xL at 56 and 49% expression, respectively. Significantly lower levels of A1 and Bcl-w expression were detected across the Eμ-Myc lymphoma panel, both demonstrating expression levels approximately 20% of Mcl-1. However, unlike the BH3-only subgroup, all prosurvival transcripts were expressed at comparable levels and therefore, all could be Eμ-Myc lymphoma biology.

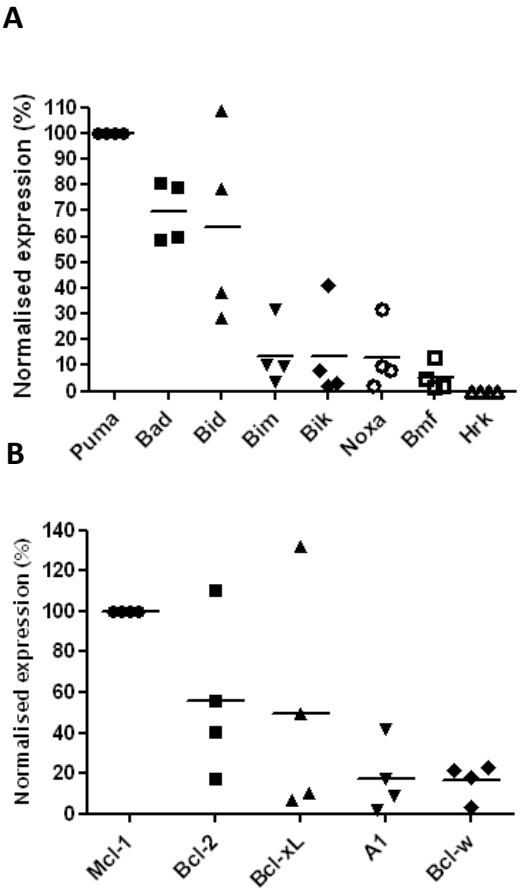

Gene	Average c(T)	Fold lower expression than Puma
GAPDH	18.73	N/A
Puma	26.12	1
Bad	26.50	1.6125
Bid	27.71	2.026
Bim	28.56	7.26
Bik	29.24	7.4168
Noxa	29.63	7.734
Bmf	30.34	19.19
Hrk	39.30	6209.7

Gene	Average c(T)	Fold lower expression than Mcl-1
Actin	15.93	N/A
Mcl-1	21.01	1
Bcl-2	21.43	1.78
Bcl-XL	22.88	2.01
A1	24.24	4.7
Bcl-w	24.24	5.75

Figure 4.5 Analysis of the relative expression levels of BH3-only protein and prosurvival transcripts in Eμ-Myc lymphomas

qPCR was performed as described previously, using 0.83 μg/ ml cDNA from PBS treated samples from four Eμ-Myc lymphoma cell lines (Eμ# 16 ,15, 8, AF47). c(T) values were corrected for housekeeping gene expression (GAPDH in **A** and Actin in **B**) and normalised against the BH3-only (**A**) or prosurvival (**B**) transcript with the lowest c(T) (Puma and Mcl-1, respectively). Statistical analysis was performed utilising a paired Student's T-test ($p < 0.05$). The Fold difference in expression levels are compared in tables in **A** and **B**.

4.2.4 Housekeeping gene validation

In order to provide accurate correction of cDNA content, housekeeping reference genes were required that were not influenced by BCR engagement. GAPDH Taqman probes and conventional Actin primers were initially assessed for suitability as reference genes for BH3-only and prosurvival transcripts, respectively. As evident in figure 4.6, both GAPDH and Actin c(T) values were not influenced by BCR-stimulation and were therefore, deemed appropriate for use as housekeeping controls.

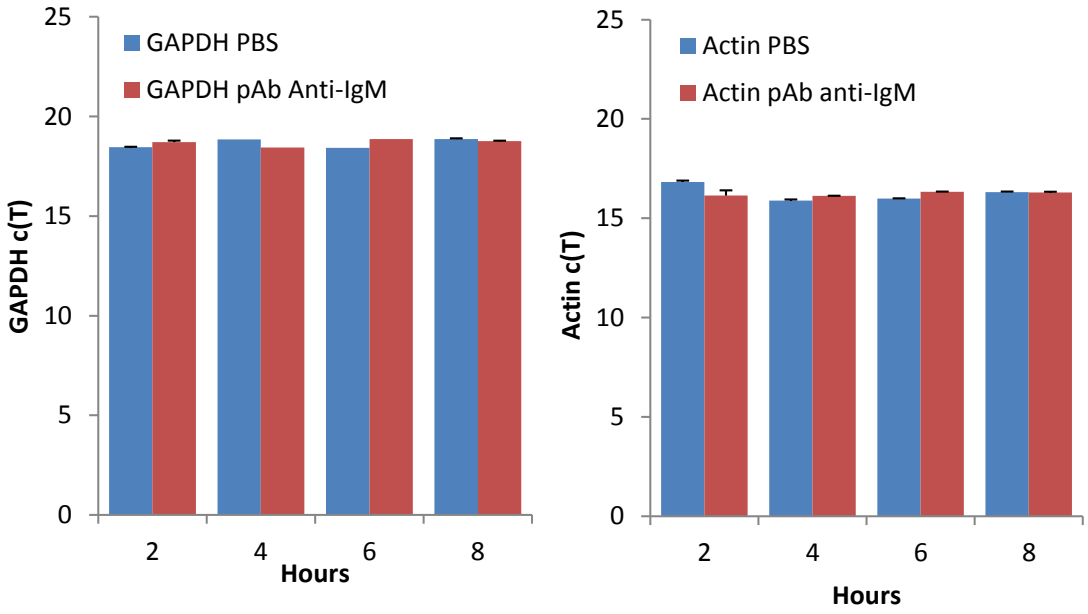

Figure 4.6 Assessment of the suitability of GAPDH and Actin as housekeeping genes

qPCR was performed as previously described. c(T) values for GAPDH and Actin were compared between PBS and 2 µg/ ml pAb ā IgM treated lymphomas at the indicated time-points. Columns represent the c(T) values obtained from a single experiment with each sample assessed in triplicate, bars represent standard error.

4.2.5 Analysis of the effect of BCR engagement upon BH3-only transcript levels in Eµ-Myc lymphomas

In order to assess the impact of BCR engagement upon the transcriptional regulation of BH3-only proteins, comparative qPCR analysis of pAb ā IgM and PBS treated Eµ-Myc lymphomas was performed throughout an 8-hour time course.

As demonstrated in figure 4.7, significant induction of Bim, Bik, Noxa, and Hrk transcripts was evident downstream of BCR signalling, reaching a maximum of 3.72, 3.63, 2.81 and 31.74 fold, respectively. Bik and Noxa transcripts were observed to accumulate rapidly post pAb ā IgM-treatment, reaching near maximal levels only 2 hours post-stimulation, and were maintained throughout the treatment period. In contrast, BCR-induced accumulation of Bim appeared more gradual, reaching maximal levels 8 hours post-treatment.

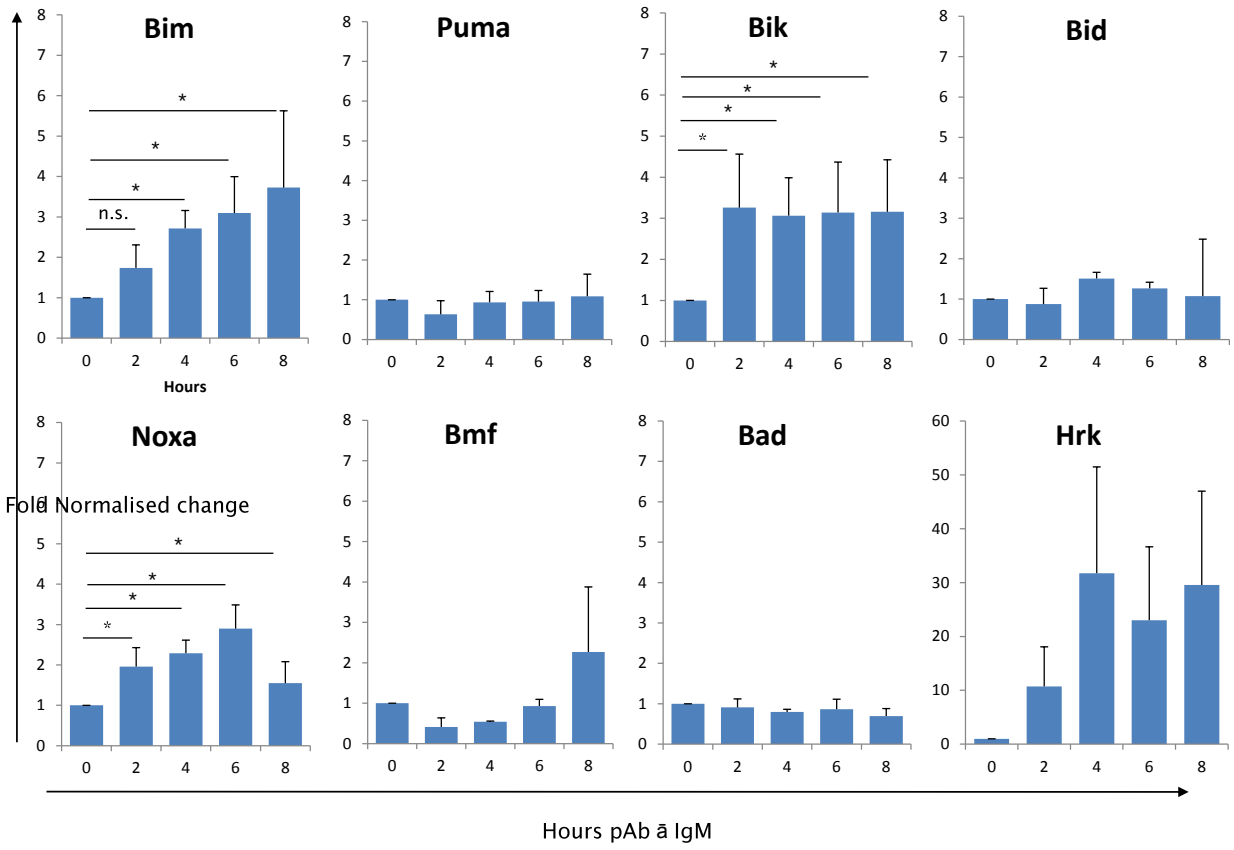

Figure 4.7 Analysis of Eμ-Myc lymphoma BH3-only protein transcript levels upon BCR stimulation
qPCR was performed for all 8 BH3-only protein transcripts and corrected for GAPDH gene expression. Normalisation was then applied, utilizing the ΔΔc(T) method, via subtraction of PBS treated Δc(T) values from those of pAb ā IgM treated cells at each time-point. Columns represent average values from 4 Eμ-Myc lymphomas, each of which was performed in triplicate, bars represent standard deviation. Asterisks denote a statistically significant difference ($p < 0.05$) as assessed by a paired Student's T-test.

Upregulation of Bim, Bik, and Noxa was deemed statistically significant ($p < 0.05$) across the Eμ-Myc lymphoma cell-line panel. However, due to the significant variation in the kinetics of induction and barely detectable baseline expression of Hrk, such values were not statistically significant. However, substantial increases were evident throughout the time course upon BCR-stimulation. The remaining BH3-only protein transcripts (Puma, Bid, Bmf, and Bad) appeared unaffected by BCR signalling, thus ruling out their transcriptional regulation as a mechanism of BCR-induced cell death.

As demonstrated in figure 4.8, the apparent induction of Bim, Bik and Noxa transcripts appeared not to be attributable to deviation in baseline expression levels throughout the time course. A small reduction in basal Bik expression was recorded. However, BCR-stimulation induced accumulation of Bik transcripts to levels far higher than the 0 hour time point, were observed indicating that the relative upregulation in figure 4.7 is not attributable to baseline variation. Therefore, it was concluded that pAb ā IgM-

treatment induced accumulation of Bim, Bik, Noxa, and Hrk transcripts, identifying a link between the BCR and regulation of multiple BH3-only proteins.

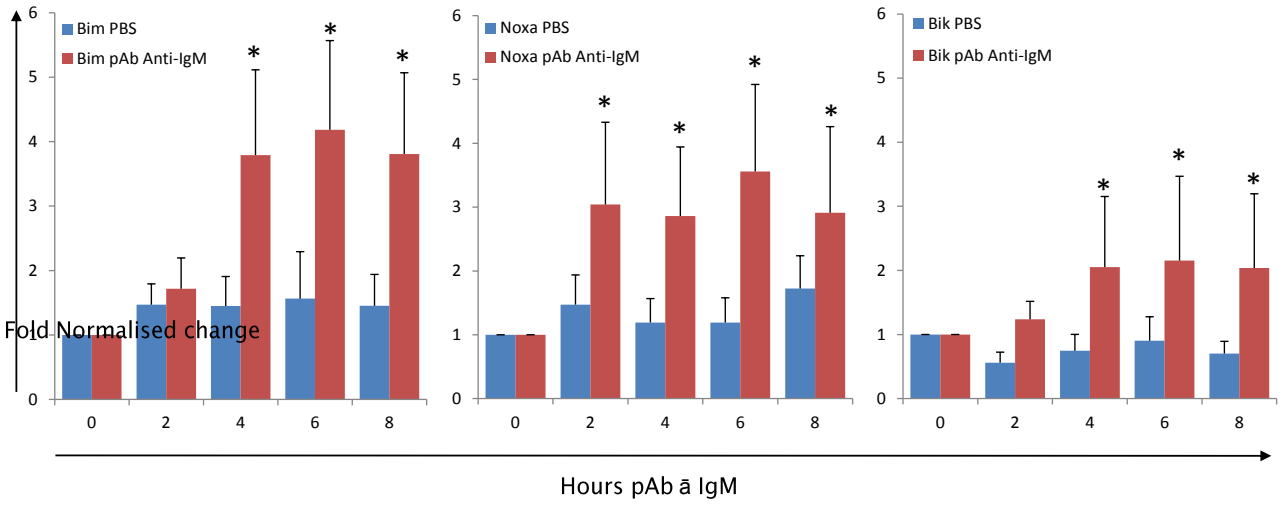

Figure 4.8 Direct comparisons of BCR-induced and baseline BH3-only transcript levels
Data from figure 4.7, c(T) values from BCR-induced BH3-only transcripts Bim, Bik and Noxa were normalised against a 0 hour time-point and their relative expression level was assessed throughout the time-course. Columns represent the average value of 4 Eμ-Myc lymphomas, bars represent standard deviation.

4.2.6 Analysis of the effect of BCR engagement upon prosurvival transcript levels in Eμ-Myc lymphomas

Since Eμ-Myc lymphomas exhibit significant transcriptional upregulation of multiple BH3-only proteins downstream of BCR signalling, we reasoned that reciprocal decreases in prosurvival expression might also be apparent. Therefore, the previously validated prosurvival primer panel was utilised to observe the impact of BCR-engagement upon prosurvival transcripts.

As evident in figure 4.9, prosurvival transcript levels appeared largely unaffected by BCR engagement, with only minimal fluctuation from baseline levels. A notable exception however is found in the form of A1, which demonstrates a gradual accumulation throughout the time-course. Although statistically non-significant, a general trend is evident towards a maximum 1.93-fold increase in A1 expression 8 hours post-treatment. Later time points were not analysed since caspase activity was detectable 8-9 hours post-anti-IgM application. Therefore, it was deemed that any subsequent changes in BH3-only or prosurvival family member transcripts would likely be a consequence of caspase activity.

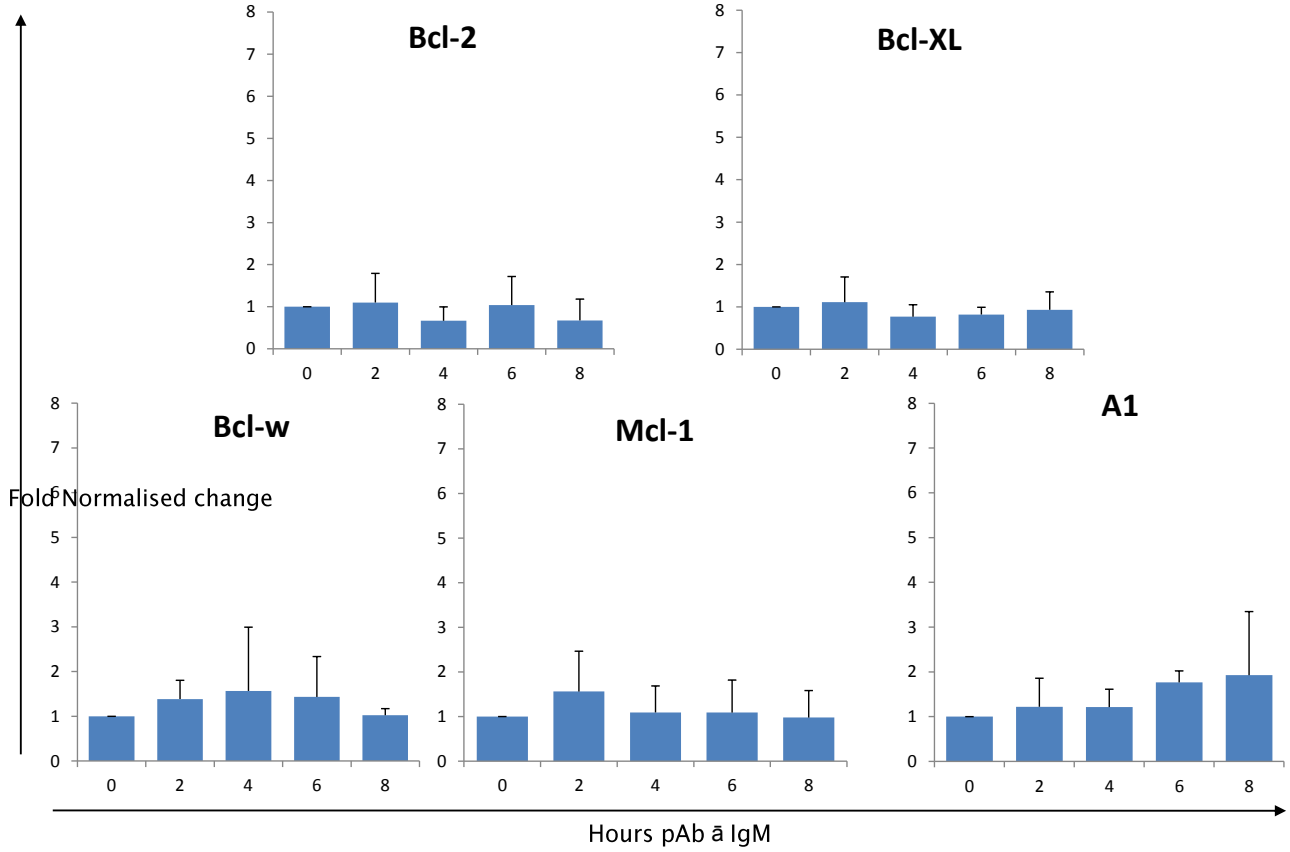

Figure 4.9 Analysis of prosurvival Bcl-2 family member transcript levels upon BCR-stimulation
Sybr green qPCR was performed utilizing primers specific for each prosurvival Bcl-2 family member, as previously described. c(T) values were recorded for each gene at the indicated time point from cells treated with 2 µg/ ml pAb ā IgM or an equivalent volume of PBS. Gene expression levels were normalised to Actin and corrected for baseline variation using the ΔΔc(T) method. Columns represent the average value from 4 different Eµ-Myc lymphoma cells, each of which was performed in triplicate, bars represent standard deviation. No statistically significant variation in prosurvival transcripts was observed following BCR stimulation.

4.2.7 Observing the context of BH3-only and prosurvival transcript levels following BCR engagement in Eµ-Myc lymphomas

In order to examine BCR-induced upregulation of Bim, Bik, Noxa, Hrk, and A1 transcripts in the context of relative Bcl-2 family expression levels, values generated in samples treated for 8 hours were corrected for basal expression levels.

Despite a 31.74-fold upregulation of Hrk downstream of BCR-stimulation, a biologically relevant role is unlikely since basal expression appears 6,200 fold lower than that of Puma. Such minute basal expression dictates that, even after BCR-mediated upregulation, Hrk transcripts are

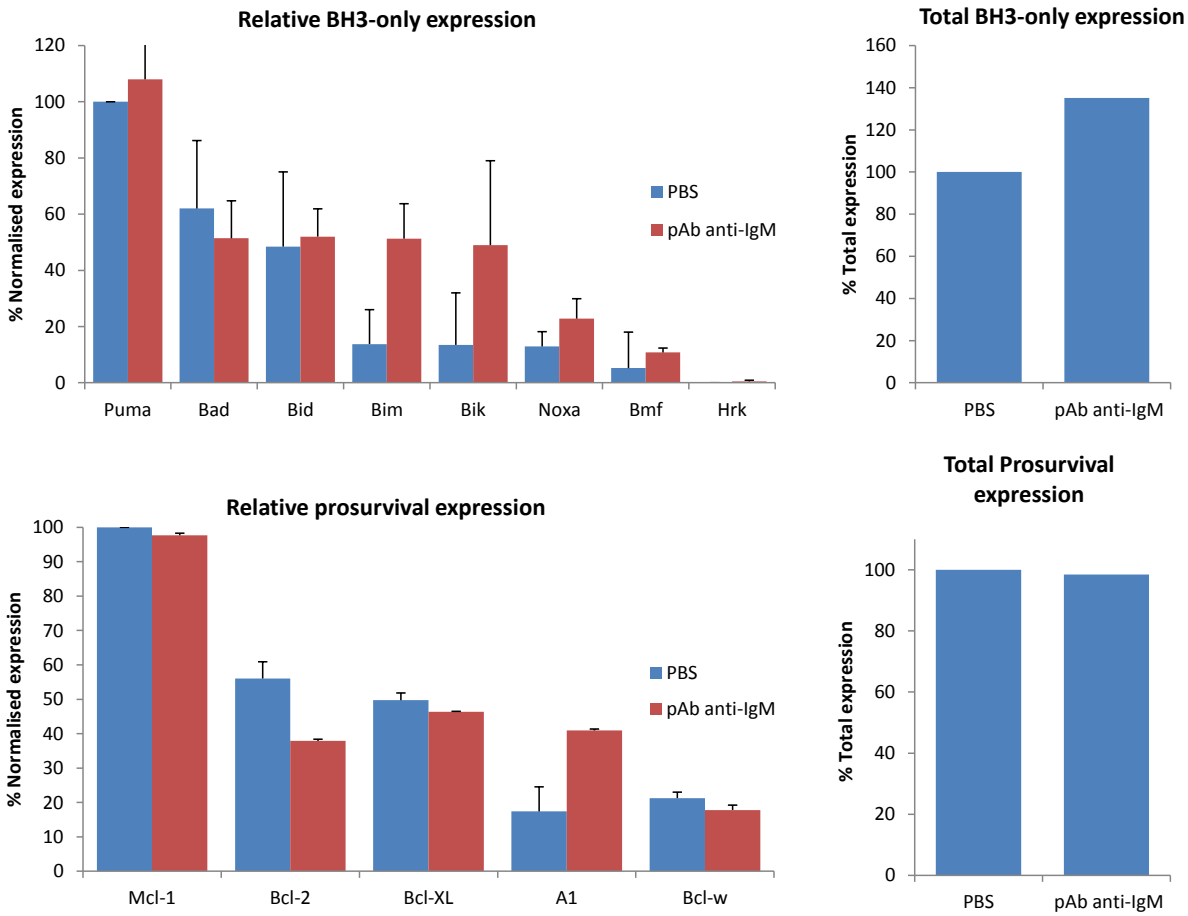

Figure 4.10 Analysis of BCR-induced BH3-only transcript levels in the context of relative expression
Data obtained 8 hours post-anti-IgM treatment from figure 4.7 and 4.9 were corrected for baseline expression levels by multiplication of the relative expression ratios calculated in figure 4.5. Total levels of BH3-only and prosurvival transcripts were calculated by expressing the sum of relative anti-IgM treated gene expression as a percentage of the sum of PBS-treated gene expression.

present at only 0.5% of Puma expression levels, as evident in figure 4.10. Interestingly, the 1.93-fold accumulation of A1 coincides with reciprocal reductions in Bcl-2, Bcl-xL and Bcl-w expression, giving rise to overall unaltered levels of total prosurvival transcripts (as evident in figure 4.10. However, it is possible that at later time-points Eμ-Myc lymphoma cells exhibit a greater dependency upon A1 and, therefore, may be particularly sensitive to Noxa upregulation. However, substantial increases in Bim, Bik, and Noxa transcripts are evident post-BCR stimulation, since they account for a 35%

increase in total BH3-only transcript levels, as evident in figure 4.10B. Therefore, it is likely that the overall 35% increase in BH3-only transcript levels, driven by Bim, Bik, and Noxa accumulation, in the presence of constant prosurvival levels predispose the cell to apoptotic demise. However, the relative apoptotic potency of Bim likely plays a greater role than that of either Bik or Noxa.

4.3 Analysis of the effect of BCR signalling upon Bcl-2 family member protein levels in Eμ-Myc lymphomas

4.3.1 Western blot analysis of whole-cell extracts from Eμ-Myc lymphomas

Whilst robust transcriptional increases in Bim, Bik and Noxa were evident following BCR engagement, such enhancements may not necessarily translate to enhanced protein levels. Therefore, the levels of BH3-only proteins, for which antibodies are available, were assessed in the presence and absence of BCR stimulation over a 24-hour time course by western blotting. Unfortunately, none of the currently available anti-murine Bik and Noxa antibodies appeared specific for the intended target when screened against a panel of the relevant Bik or Noxa KO lymphoma cells. Therefore, this investigation was unable to assess the impact of BCR-stimulation upon their protein levels, as the available antibodies were deemed unsuitable for use. High-quality commercial antibodies directed against Bad, Bid, Bim, Puma and Bmf and all prosurvivals are available, however, and were utilised for further analysis.

As evident in figure 4.11A-B, statistically significant increases in both Bim_{EL} and Bim_{L} protein levels were observed 24 hours post-pAb ā IgM treatment, reaching a maximum of 2.14 and 3.3 fold, respectively. Furthermore, in agreement with transcriptional studies levels of Bad, Bid, and Puma remained unaffected by BCR-stimulation. Interestingly, protein levels of both Bcl-2 and Mcl-1 appeared reduced upon BCR-stimulation, reaching a maximum of 3.73 and 2.28 fold reductions, respectively. Such reductions appeared in a rapid, caspase-independent manner since diminished Bcl-2 and Mcl-1 protein levels were evident only 5 and 8 hours post-BCR stimulation in the presence of qVD.

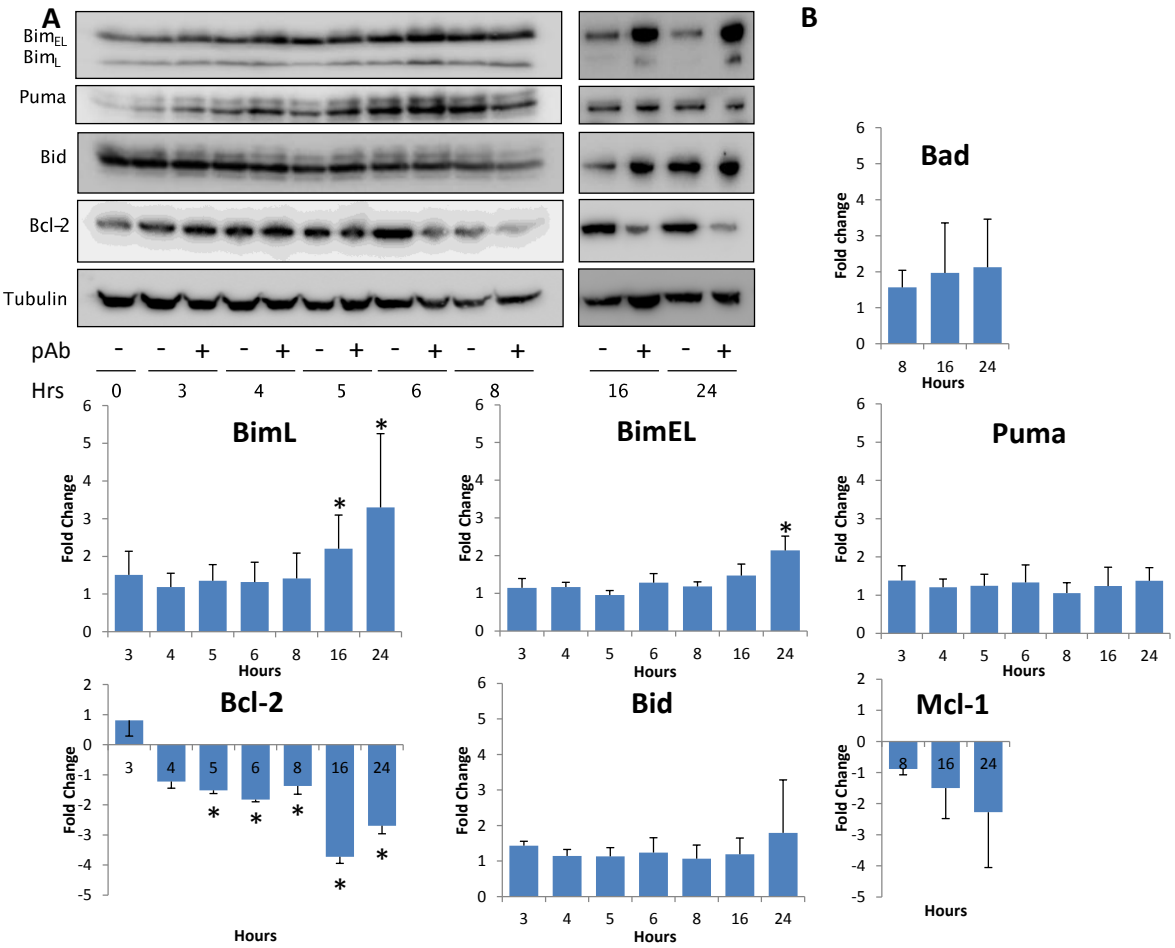

Figure 4.11 Analysis of BH3-only and prosurvival Bcl-2 family member protein levels downstream of BCR-stimulation

Eμ-Myc lymphoma cells were plated at 1.6x106/ ml and pre-treated with the pan-caspase inhibitor qVD-OPH (25 μM) or an equivalent amount of DMSO for 30 minutes at 37°C. Cells were subsequently treated with 2 μg/ ml pAb ā IgM or an equivalent volume of PBS for the indicated time-period and lysates made. Western blotting analysis of BH3-only and prosurvival Bcl-2 family member protein levels was then undertaken. A) Example Western blot from Eμ# 8. B) The intensity of Western blot bands was quantified by densitometry, utilizing the UVP vision works software package (UVP, UK), and corrected for Tubulin levels. pAb ā IgM-treated samples were then normalised against those treated with PBS alone. Columns represent average values of 6 independent experiments using different Eμ-Myc lymphoma cell lines. Bars represent standard deviation. Asterisks denote a statistically significant difference ($p < 0.05$) as assessed by Student's paired T-test.

However, only BCR-mediated reductions in Bcl-2 were adjudged statistically significant, owing to enhanced variation in the extent of Mcl-1 reduction across the lymphoma panel, as demonstrated in appendix A12. The impact of BCR engagement upon Bmf, Bcl-xL, Bcl-w, and A1 levels could not be assessed, however, as their respective expression levels were undetectable by western blotting. The antibodies, however, are known to specifically detect targets from parallel studies utilising cell lines positive for expression. Therefore, in Eμ-Myc lymphomas BCR engagement appears to drive the

accumulation of Bim_{EL} and Bim_L alongside concomitant reduction in both Mcl-1 and Bcl-2 protein levels.

4.3.2 Analysis of the impact of BCR engagement upon Bim: prosurvival complex formation

In order to demonstrate that BCR-induced upregulation of Bim correlated with an enhanced function, co-immunoprecipitation studies analysing the formation of Bim: prosurvival complexes were undertaken. Non-ionic detergents, such as Triton x-100, have been demonstrated to influence the conformational state and heterodimerisation partners of Bcl-2 family members, in particular Bax, and are largely unsuitable for IP analysis (106, 166). Such an observation is apparent in figure 4.12, where Mcl-1 appeared to Co-IP alongside Bax upon use of the non-ionic detergent Trition-x 100 but not the zwitterionic detergent CHAPS. Since Bax is a largely cytosolic protein, subsequent extracts were produced utilising CHAPS lysis buffers in order to minimise detergent-induced interactions between Bcl-2 family members.

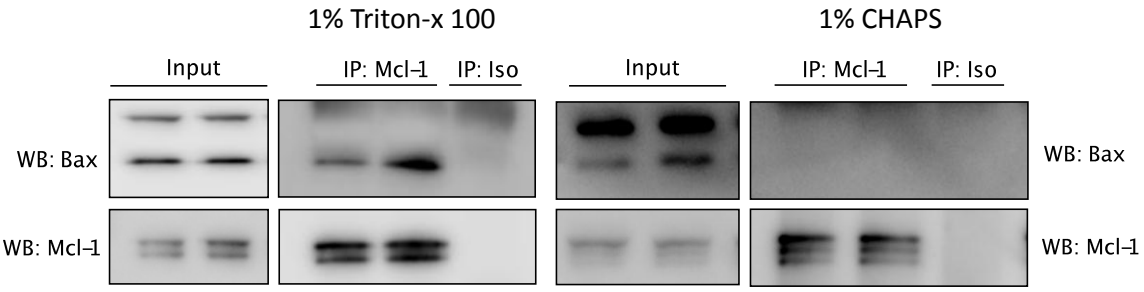

Figure 4.12 Analysis of the impact of IP detergents upon the interaction between Bax and prosurvival Bcl-2 family members

$1x10^8$ Eμ-Myc lymphoma cells per sample were plated at $1x10^6$/ ml and rested for 3 hours. Cells were then washed in PBS and lysed in either CHAPS lysis buffer (20 mM tris pH 7.4, 142.5 mM KCl, 2 mM $CaCl_2$, 1% CHAPS) or IP lysis buffer (50 mM hepes, 150 mM NaCl, 10 mM EGTA, 10% glycerol, 1% Triton x-100) on ice. $5x10^6$ Eμ-Myc lymphomas were also lysed in RIPA buffer and used as a whole cell lysate input control. 500 μg cell lysate was then immunoprecipitated with Rabbit pAb anti-Mcl-1 as outlined in materials and methods, followed by Western blot analysis for Bax: Mcl-1 interaction.

In order to assess the impact of BCR-ligation upon the interaction between BH3-only proteins and prosurvival family members, CHAPS IP extracts were produced from PBS or anti-IgM-treated Eμ-Myc lymphoma cells.

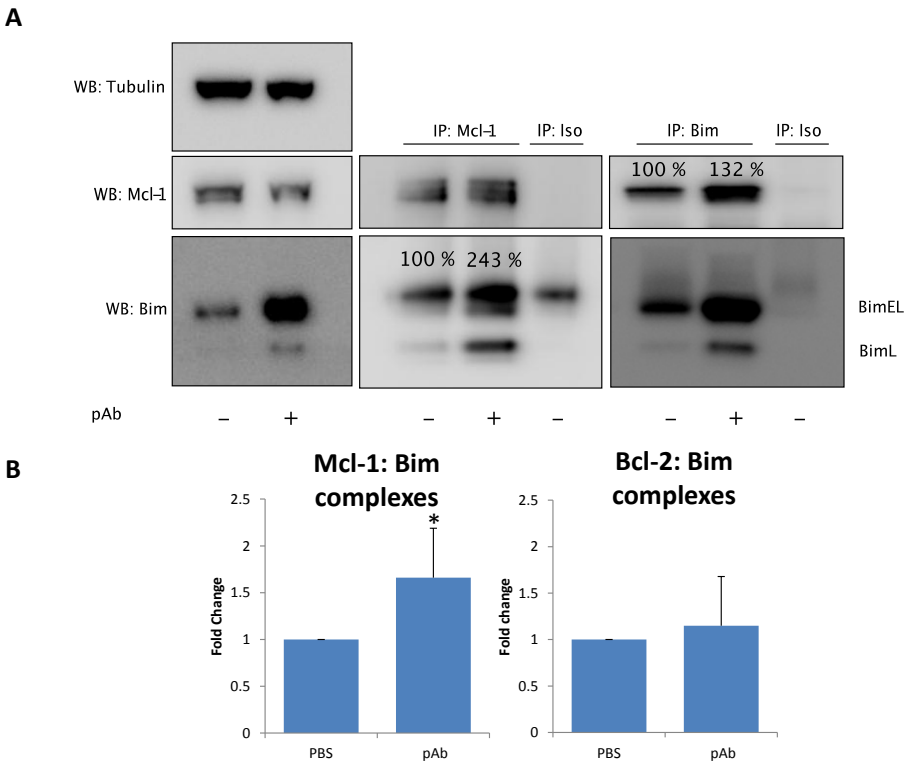

Figure 4.13 Assessing the impact of pAb ā IgM upon interactions between Bim and prosurvivals

1x10^8 Eμ-Myc lymphoma cells per sample were plated at 1x10^6/ ml and rested for 1 hour. Cells were then pre-treated with 10 μM qVD-OPH for 30 minutes at 37^{o}C. Subsequently, cells were treated with 2 μg/ ml pAb ā IgM or an equivalent volume of PBS for 24 hours. Samples were harvested, lysed and immunoprecipitated with anti-Mcl-1/Bim antibodies or an appropriate isotype control, as outlined in materials and methods. **A)** Example western blot of Eμ# 16 lysates immunoprecipitated with anti-Mcl-1/ Bim antibodies and analysed for co-immunoprecipitating proteins. **B)** Quantification of co-immunoprecipitating levels of Mcl-1: Bim or Bcl-2: Bim complexes following BCR engagement. Quantification was undertaken utilizing the UVP vision works software package (UVP, UK) densitometry function. Columns represent average values of five independent experiments, utilising different Eμ-Myc lymphomas (Eμ# 16, 15, 8, 4, and AF47), bars represent standard deviation. Asterisks denote statistically significant differences ($p < 0.05$) assessed by Student's paired T-test.

As evident in figure 4.13, Bim and Mcl-1 co-immunoprecipitated from resting cells. However, such co-immunoprecipitation was enhanced 1.66-fold upon BCR engagement for 24 hours. Such an occurrence was most evident when anti-Mcl-1 was utilised as the immunoprecipitating antibody. The reverse IP was also undertaken however, results were difficult to interpret since the Bim IP was unequal, owing to enhanced Bim protein levels in the input following BCR engagement. However, complex formation was conserved and a greater proportion of Mcl-1 Co-IPd alongside the enhanced Bim levels. Interestingly, significant increases in the formation of Bim: Bcl-2 complexes were less apparent following BCR engagement. Although greater association was evident in some lymphoma cell lines, as evident in Figure 4.13B,

enhanced formation of Bim: Bcl-2 complexes following BCR engagement was not conserved across the cell-line panel. In addition, in the absence of Bim (Bim KO lymphomas) no pro-survival BH3-only complexes were detectable, see appendix A13.

Therefore, the above results demonstrate that chronic BCR-engagement culminates in the upregulation of Bim, Bik, and Noxa at the transcript level leading to enhanced Bim protein levels and prosurvival binding.

4.4 Determining the impact of genetic loss of individual BH3-only proteins upon the extent of BCR-signalling induced cell death

Whilst we have demonstrated significant upregulation of three BH3-only proteins in response to BCR engagement, it remains unclear as to their relative contribution to BCR-induced cell death. Whilst upregulation of BH3-only proteins is likely to drive MOMP, it is conceivable that such a pro-death stimulus may not directly drive cellular death. For example, simultaneous upregulation of IAPs may block the BH3-only protein driven caspase activation and instigate an alternate form of cell death. Therefore, in order to confirm a direct involvement in BCR-induced cell death, the sensitivity of primary Eμ-Myc lymphomas derived from Bim, Bik, and Noxa deficient animals toward BCR-stimulation was observed. BH3-only protein deficient Eμ-Myc lymphoma cells were the generous gift of Prof. C. Scott (Walter and Eliza Hall institute, Melbourne, Aus) and were cultured in vitro utilising the same passage number usage criteria as defined previously for WT Eμ-Myc lymphomas. As demonstrated in table 4.1, the immunophenotype and relative levels of IgM expression was comparable to the WT Eμ-Myc lymphomas derived at this institution.

Genotype	Lymphoma Cell line	CD19	IgM	IgD	CD21	CD23	Relative IgM
WT	Eμ# 16	+	+	-	low	-	40.825
	Eμ# 15	+	+	n.d	low	-	31.57
	Eμ# 8	+	+	-	low	-	29.87
	Eμ# 6	+	Mixed	-	low	-	6.652
	Eμ# 4	+	+	-	low	-	55.730
	AF47	+	+	low	+	-	59.40
Puma $^{-/-}$	MP 291	+	n.d	n.d	n.d		n.d.
	MP 264	+	+	low	-	-	14.11
	MP 219	+	n.d	n.d	n.d	n.d	36.51
	MP 215	+	+	low	-	-	7.54
	MP 211	+	+	low	-	-	50.48
Bik $^{-/-}$	MBik# 42	+	+	-	-	-	17.068
	MBik# 37	+	+	low	low	-	58.40
	MBik# 13	+	+	low	+	low	5.04
Bmf $^{-/-}$	Eμ Bmf# 31	+	+	low	+	-	59.6
	Eμ Bmf# 26	+	+	low	-	-	12.91
	Eμ Bmf# 2	+	+	low	-	-	15.71
Noxa $^{-/-}$	MN 159	+	+	low	low	-	87.14
	MN 156	+	+	-	low	-	12.69
	MN 127	+	+	-	+	-	5.00
	MN 99	+	+	low	low	-	6.96
	MN 97	+	n.d	n.d	n.d	n.d	n.d.
	MN75	+	n.d	n.d	n.d	n.d	n.d.
Bim $^{-/-}$	MB# 63	+	+	-	-	-	3.38
	MB# D3	+	+	low	+	-	68.1
	MB #16	+	n.d	n.d	n.d	n.d	17.89
Bid $^{-/-}$	EμBid# 179	+	+	low	-	-	64.32
Bad $^{-/-}$	Eμ Bad# 184	+	+	-	-	-	12.22
	Eμ Bad# 134	+	+	-	-	-	10.89
	Eμ Bad# 331	+	+	n.d	n.d	n.d	n.d.

Table 4.1 Summary of the immunophenotypes of primary WT and BH3-only deficient Eμ-Myc lymphomas

Cells from the spleen of Eμ-Myc lymphomas derived at this institution, and BH3-only deficient Eμ-Myc lymphomas from the Walter and Eliza Hall Institute Melbourne (Aus) were stained as in figure 3.4 and analysed by flow cytometry. A geometric mean of less than 100 was determined as low expression of surface antigen and over 100 as high. Relative IgM was calculated as described previously. N.D. not determined, - negative for antigen expression, + positive for antigen expression, Mixed presence of both positive and negative populations. N.B BH3-only deficient Eμ-Myc lymphomas were only utilised up to passage 22, as for WT Eμ-Myc lymphomas.

Furthermore, the levels of ā-IgM induced cell death did not correlate with relative IgM expression levels across the panel, see appendix A14. Therefore, it was deemed that any subsequent alteration in the response to BCR engagement was attributable to

genetic loss of a BH3-only protein, and not due to differential developmental status of IgM expression.

As can be seen in figure 4.14A-B, genetic loss of either Noxa or Bik led to a slight reduction in the extent of BCR-induced cell death recorded after 24-hours. Such reductions are statistically significant only at the 10 μg/ml dose, however, a distinct reduction in overall sensitivity is apparent at all doses. Therefore, it appears as though both Noxa and Bik may play minimal, yet biologically relevant, roles in BCR-induced cell death. In addition, Bim deficient lymphomas exhibited statistically significant protection from BCR-induced cell death at all but the 0.08 μg/ml dose, as observed in figure 4.14C. Such protection, however, was not equivalent to that produced by over-expression of a Bcl-2 tg, as seen in figure 4.14D. Therefore, all of the previously identified BH3-only proteins upregulated by BCR-signalling appear to play distinct roles in BCR-induced cell death.

However, it is possible that the subtle protection offered toward BCR-induced cell death upon loss of Noxa or Bik may be due to a general loss of sensitivity to apoptotic stimuli. It is conceivable that loss of a single BH3-only protein may raise the threshold for apoptosis, giving the appearance of stimulus-specific resistance. Evidence against this was provided by experiments where comparable levels of cell death in response to Etoposide between WT, Bim, Bik and Noxa deficient lymphomas was seen, as shown in appendix A15. Furthermore, as evident in figure 4.15, loss of Puma, Bid, Bad, or Bmf had no statistically significant effect upon the extent of BCR-induced cell death. Therefore, it appears as though the protection offered by loss of Bim, Bik, and Noxa is a specific to BCR-induced cell death and not a general phenomenon. Consequently, it appears as though both Noxa and Bik play supplementary roles during BCR-induced cell death, in addition to that played by Bim.

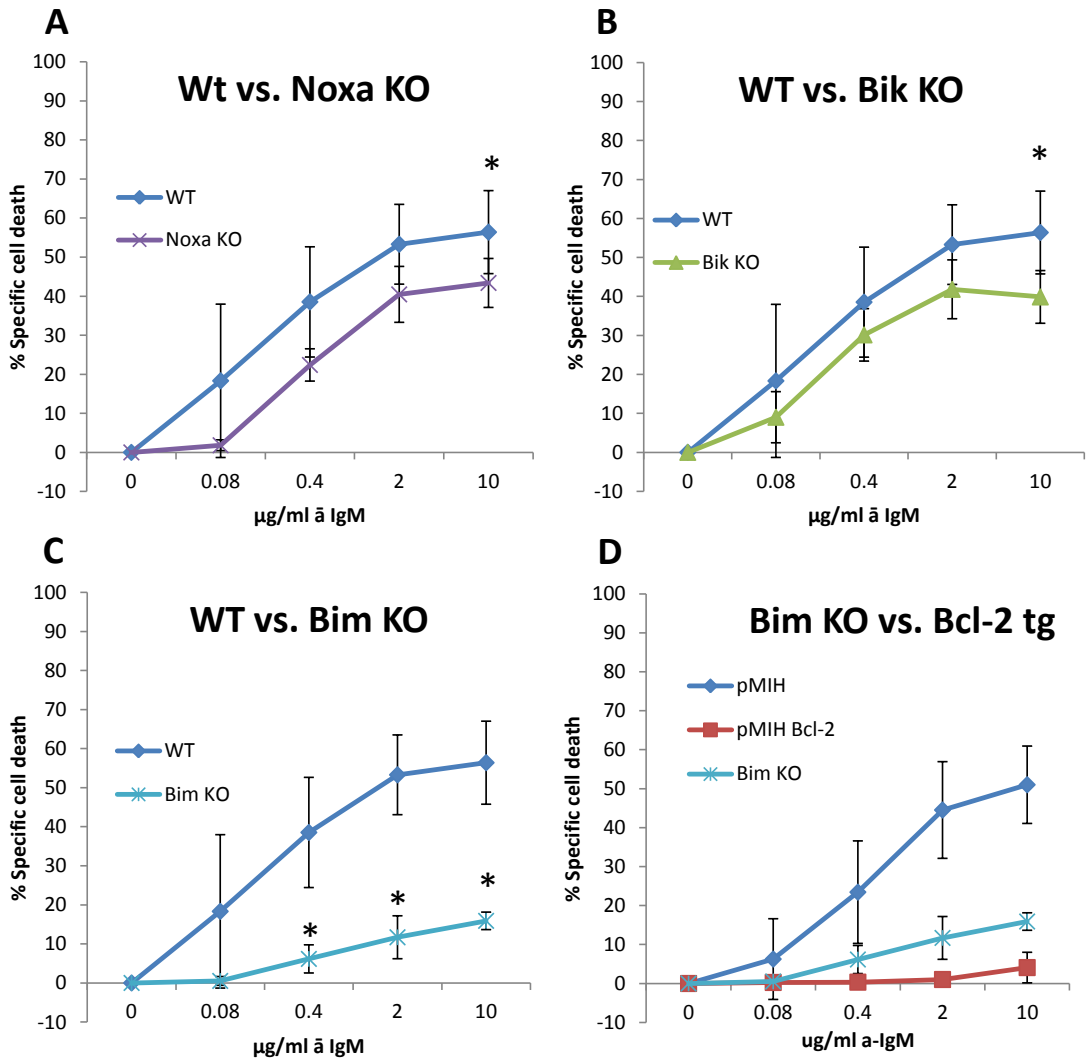

Figure 4.14 Assessment of the sensitivity of Bim, Noxa or Bik deficient Eμ-Myc lymphomas toward BCR-engagement

Eμ-Myc lymphomas were plated at $1.6x10^6$/ ml and treated with pAb ā IgM, at the indicated final concentration, or an equivalent volume of PBS for 24 hours. Subsequently, cells were harvested by pipetting and subjected to Annexin V^{FITC}/ PI staining and analysed by flow cytometry. Levels of pAb ā IgM-induced cell death were compared between **A)** WT (n=5) and Noxa KO (n=5), **B)** WT and Bik KO (n=3), **C)** WT and Bim KO (n=3), and **D)** Bim KO and Bcl-2 transgenic (n=4) Eμ-Myc lymphoma cells. Points represent average values obtained from at least 3 different lymphomas, bars represent standard deviation. Asterisks denote statistically significant differences ($p< 0.05$) assessed by Student's un-paired T-test statistical analysis.

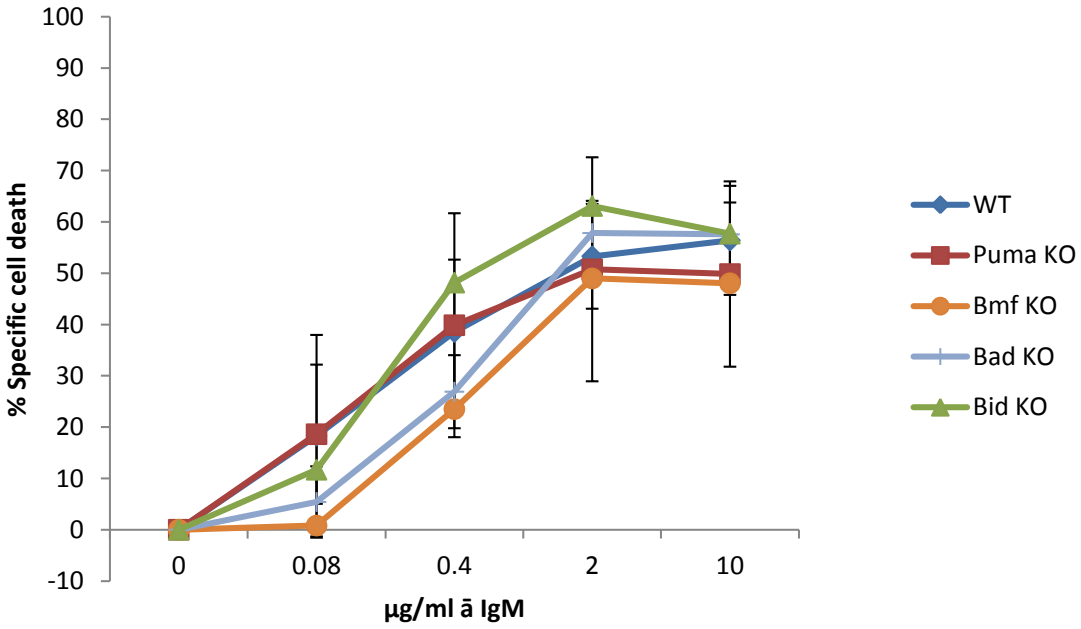

Figure 4.15 Assessment of the sensitivity of Bad, Bid, Bmf, and Puma deficient Eμ-Myc lymphomas toward BCR-engagement

Cells were treated as in figure 4.14 except the response of WT (n=5) Eμ-Myc lymphomas towards pAb ā IgM was compared to Bad (n=3), Bid (n=1), Bmf (n=4), and Puma (n=5) deficient lymphomas. No statistically significant differences ($p > 0.05$) were observed upon Mann-Whitney statistical testing.

4.5 Observing the impact of dual loss of Noxa/ Bik and Bim upon the extent of BCR-signalling induced cell death in Eμ-Myc lymphomas

As observed in figure 4.14D, genetic loss of Bim imparts significant resistance toward BCR-induced cell death. However, such resistance was not equivalent to that produced upon over-expression of a Bcl-2 tg. We reasoned that such residual sensitivity could possibly be attributable to the upregulation of the pro-death functions of Bik and Noxa downstream of the BCR. Therefore, RNAi of Bim expression in Bik and Noxa deficient lymphomas was undertaken to assess their relative contribution to the response in the absence of Bim.

4.5.1 Retroviral transduction of Noxa/ Bik deficient Eμ-Myc lymphomas with a Bim-targeting ShRNA construct

In order to effectively knockdown Bim expression in Eμ-Myc lymphoma cells a retroviral shRNA approach was taken. Phoenix cells were transfected with the mPIG

vector system (outlined in appendix A16) encoding a Bim-targeting shRNA and GFP reporter or vector control. Such an approach allowed high titre recombinant retrovirus-containing supernatant production, for use as a vector delivery mechanism, to deliver shRNA constructs and a means to assess transduction efficiency in the form of the GFP reporter. Phoenix cells were transiently transfected by Calcium: Phosphate-mediated precipitation with mPIG or mPIG shBim vectors, alongside the pCL.Eco helper vector. As demonstrated in figure 4.16, DNA precipitates were evident coating cells immediately post-application, demonstrating an effective precipitation step. 24 hours post-transfection phoenix cells were assessed for GFP positivity by flow cytometry and fluorescence microscopy, as demonstrated in figure 4.16. Recombinant retrovirus-containing supernatants were subsequently removed (from GFP expressing cells) and utilised to transduce Eμ-Myc lymphomas. After 24 hours, Eμ-Myc lymphomas were assessed for GFP positivity, as shown in figure 4.17, and negative clones removed by puromycin selection.

Subsequently, the relative impact of mPIG ShBim transduction upon Bim expression was assessed in comparison to empty vector (GFP) transduced cells. As observed in figure 4.18A-B, transduction of Eμ-Myc lymphomas with mPIG shBim constructs effectively knocked-down Bim expression approximately five-fold in all lymphomas. No observable differences in knock-down efficiency were evident between WT, and Bik or Noxa deficient Eμ-Myc lymphoma cells, as evident in figure 4.18B. Therefore, it was concluded that WT, Bik KO, and Noxa KO Eμ-Myc lymphomas transduced with mPIG ShBim constructs demonstrated comparable levels of Bim knockdown and were suitable for further use.

In order to observe the effect of dual loss of Bim and Bik or Bim and Noxa upon the extent of BCR-induced cell death, GFP and ShBim transduced clones were assessed for their relative sensitivity toward BCR-signalling.

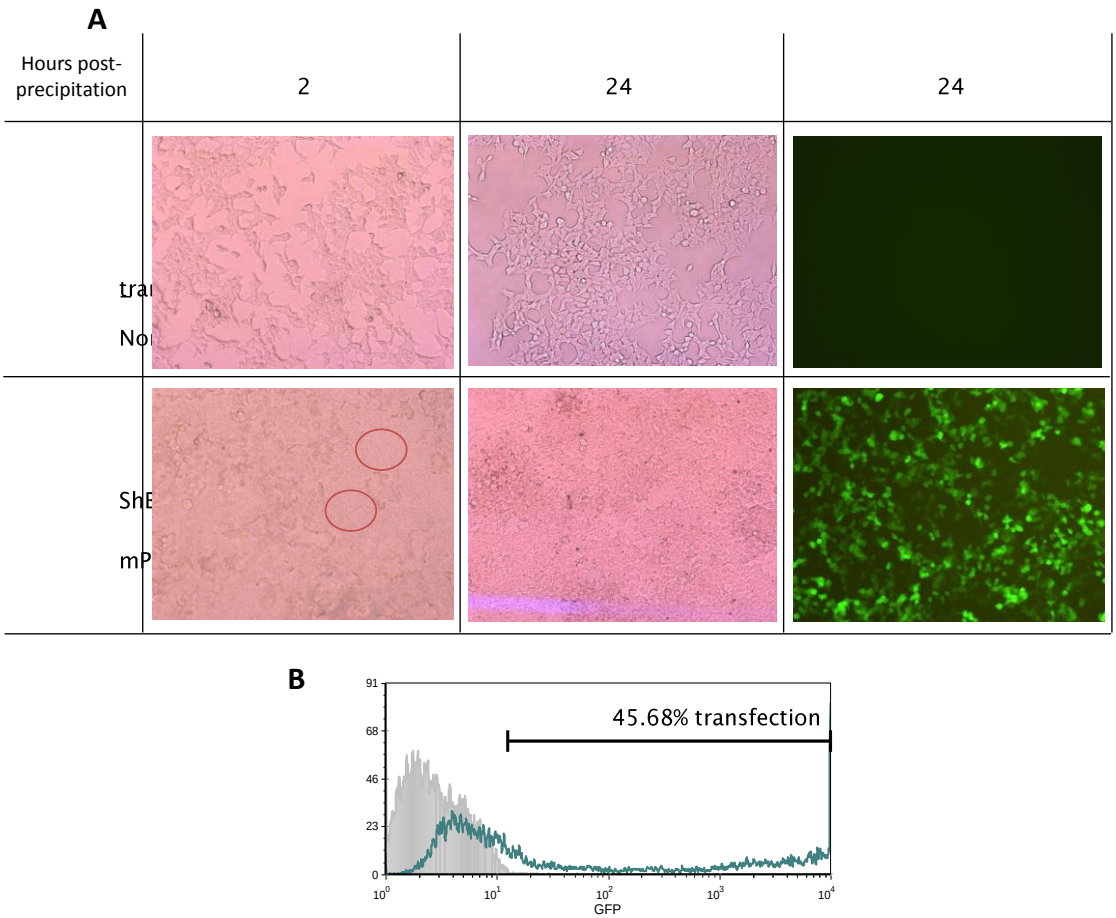

Figure 4.16 Calcium: Phosphate precipitation of mPIG vectors and transient transfection of Phoenix cells

Phoenix cells were transfected with 10 μg of mPIG and 4 μg of the helper vector pCL.eco via Calcium: Phosphate precipitation. **A** After 2 hours visible DNA precipitates were evident coating the base of the culture dish (circled). Furthermore, transfection efficiency was assessed via detection of GFP fluorescence by **A)** fluorescence microscopy, and **B)** flow cytometry after 24 hours.

As demonstrated in figure 4.18 C-D, knockdown of Bim expression in both WT and Bik KO Eμ-Myc lymphomas resulted in a statistically significant increase in resistance toward BCR-induced cell death, in comparison to transduction with empty vector alone (GFP). Such resistance appeared restricted to clones expressing ShBim RNA, since GFP-transduced clones appeared to exhibit comparable sensitivity to WT and Bik KO lymphomas, respectively. Interestingly however, resistance toward BCR-induced cell death by Bim knockdown appeared greater in magnitude than that produced by genetic loss of Bim, as seen in figure 4.14C-D.

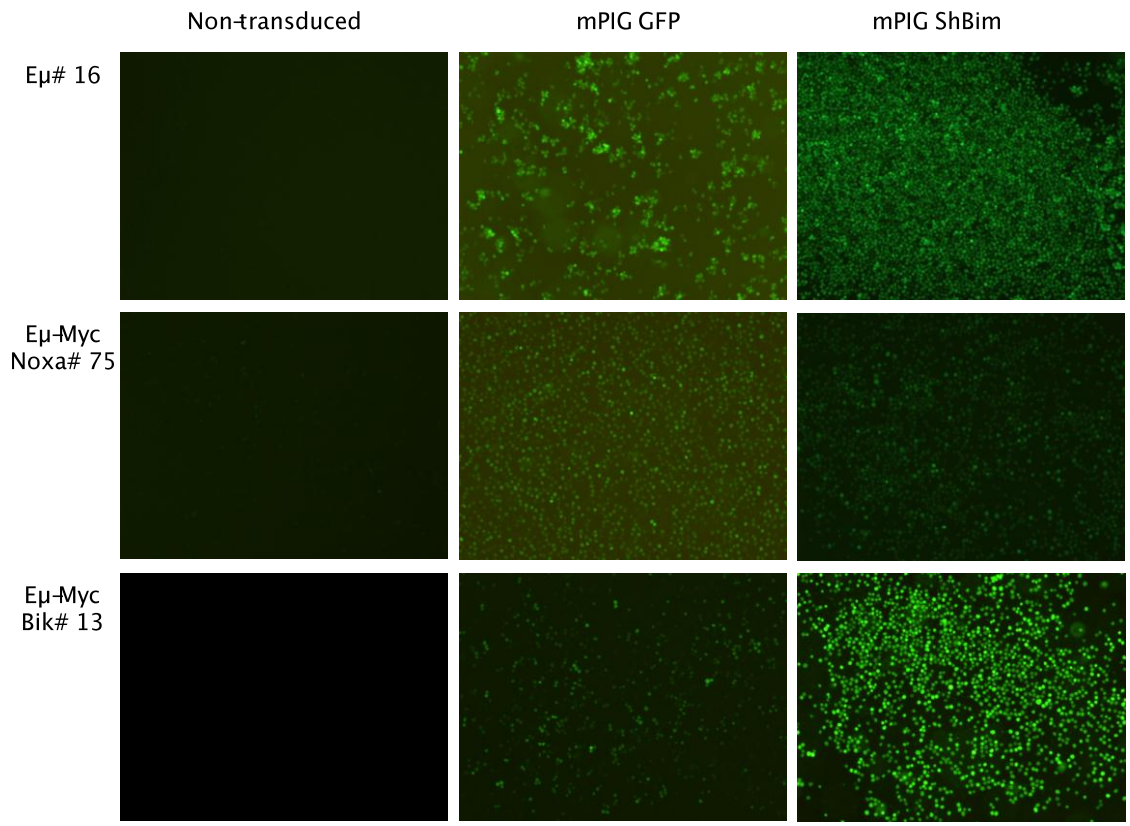

Figure 4.17 Retroviral transduction of Eμ-Myc lymphomas

Retroviral supernatants, incorporating empty vector (mPIG GFP) or mPIG ShBim, from figure 4.16 were applied to 4 WT (Eμ# 16, 15, 8, 4), 3 Noxa KO (Eμ-Myc Noxa# 99, 97, 75) and 3 Bik KO (Eμ-Myc Bik# 42, 37, 13) Eμ-Myc lymphoma cells, as previously described. 48 hours post-transduction, Eμ-Myc lymphoma cells were assessed for GFP positivity by fluorescence microscopy in non-transduced (left panel), empty vector transduced (mPIG GFP) (middle panel), or mPIG ShBim transduced (right panel) cells.

Despite this, Bim knockdown Eμ-Myc lymphomas continued to display greater, albeit non-statistically significant, sensitivity to BCR engagement than cell lines over-expressing a Bcl-2 tg, as observed in figure 4.18D. Interestingly, Bik KO shBim-transduced lymphomas appeared to exhibit a greater resistance towards BCR engagement than WT shBim-transduced lymphomas, as shown in figure 4.18C. In fact, the response made by Bik KO shBim-transduced lymphomas appeared comparable to that produced upon over-expression of a Bcl-2 transgene, as evident in figure 4.18D.

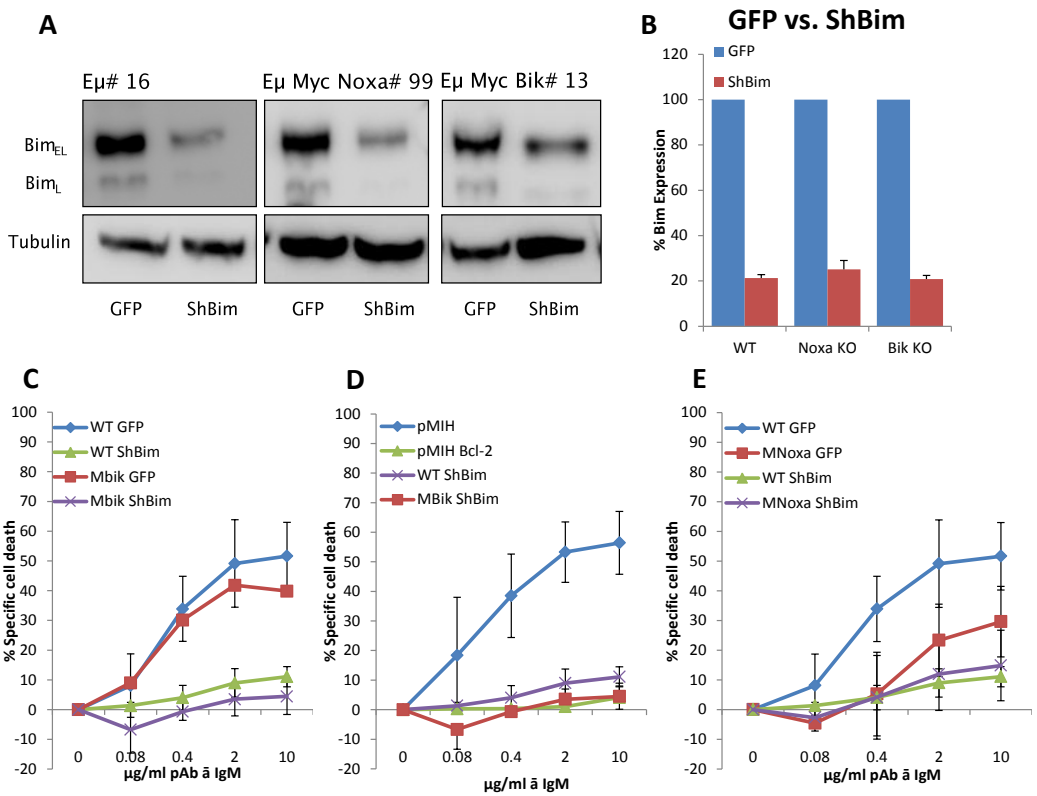

Figure 4.18 Examining the effect of and mPIG ShBim constructs upon Bim expression levels

GFP positive clones, produced in figure 4.18, were sorted and maintained in vitro and assessed for Bim knockdown. A) Lysates were prepared from empty vector (GFP) or mPIG shBim-transduced Eμ-Myc lymphoma cells and samples assessed for Bim or Tubulin expression levels by western blot B) quantification of data in A) by densitometry. Bands were quantified as before and corrected for Tubulin expression. ShBim-transduced Eμ-Myc lymphoma Bim protein levels were expressed as a percentage of empty vector (GFP) transduced. Columns represent the average of 4 WT (Eμ# 16, 15, 8, 4), 3 Noxa KO (Eμ-Myc Noxa# 99, 97, 75) and 3 Bik KO (Eμ-Myc Bik# 42, 37, 13) Eμ-Myc lymphomas, bars represent standard deviation. C) Annexin V/PI death assays were performed as before, utilizing the indicated concentration pAb ā IgM for 24 hours in WT (n=4) and Bik KO (n=3) Eμ-Myc lymphomas transduced with empty vector (GFP) or mPIG ShBim. Bars represent standard deviation D) As in C) except WT (n=4) and Bik KO (n=3) Eμ-Myc lymphoma cells transduced with empty vector (GFP) or mPIG ShBim were compared to Bcl-2 over-expressing clones (n=4). E) As in C) except WT (n=4) and Noxa KO (n=3) Eμ-Myc lymphomas transduced with empty vector (GFP) or mPIG ShBim are compared. Bars represent standard deviation.

Although observed differences in sensitivity toward BCR engagement between WT shBim and Bik KO shBim lymphomas was not statistically significant (p=0.2286), a clear trend is apparent. Such observations indicate that Bik may indeed play a key pro-apoptotic role downstream of the BCR in addition to that played by Bim.

In contrast however, the effect of Bim knockdown upon the extent of cell death exhibited by Noxa KO lymphomas was negligible. As observed in figure 4.18E, transduction of both Noxa and WT Eμ-Myc lymphomas generated a statistically significant increase in resistance toward BCR stimulation. However, upon comparison

of levels of cell death evident in WT shBim ad Noxa KO shBim lymphomas, no discernable difference could be detected.

Therefore, it appears as though dual loss of Bim and Bik expression is capable of generating resistance toward BCR-induced cell death equivalent to that of Bcl-2 over-expression. Such an observation implicates Bik as a major driver of BCR-induced cell death whereas; Noxa appears to play a less important sensitisation-based role.

4.6 Chapter Discussion

Here the effect of BCR engagement upon BH3-only protein levels and their relative contribution to BCR-induced cell death have been assessed.

Our studies identify a hierarchical pattern of BH3-only protein expression in Eμ-Myc lymphomas (Puma > Bad > Bid > Bim > Bik > Noxa > Bmf > Hrk), with Puma and Hrk exhibiting the highest and lowest expression, respectively. Such high levels of Puma expression are likely attributable to both p53 and Myc-dependent transactivation, as a consequence of Myc-driven proliferation (233, 282, 307, 329, 330). However, Puma also appears to play key roles, in co-operation with Bim, in the regulation of normal B-cell homeostasis and memory B-cell survival (229, 233, 320, 324-326, 373, 374). Therefore, its substantial expression levels may occur as a result of both Myc-oncogene-driven and normal B-lineage driven expression. Detectable expression of the majority of BH3-only proteins in Eμ-Myc lymphoma cell lines was largely expected, since Puma, Noxa, Bmf, Bad, and Bim all appear to play key tumour suppressive roles in the model (233, 329, 330). In contrast, Hrk expression levels appear barely detectable in Eμ-Myc lymphomas, being ≈ 6,200-fold lower than those for Puma. Indeed, whilst Hrk plays vital roles in neuronal cell survival, $Hrk^{-/-}$ mice demonstrate normal haemeatopoiesis, secondary lymphoid organ structure and normal rates of spontaneous lymphomagenesis (375). In fact, Hrk has been identified as being entirely absent from cells of the haematopoietic compartment and therefore, largely irrelevant to B-cell biology (375).

An analogous, albeit less pronounced, hierarchical expression pattern of prosurvival Bcl-2 family members was also observed in Eμ-Myc lymphomas (Mcl-1 > Bcl-2 > Bcl-xL > Bcl-w > A1). Although in our hands only Mcl-1 and Bcl-2 were detectable at the

protein level in Eμ-Myc lymphoma cells, Bcl-xL has been successfully detected by our collaborators in these tumours. Since Mcl-1-dependent lymphomas demonstrate enhanced sensitivity toward cytotoxic agents (relative to Bcl-2 dependent counterparts), Mcl-1 dependency may help explain *in vitro* sensitivity of Eμ-Myc lymphoma cells to myriad cytotoxic agents in comparison to long-term cell lines, i.e. WEHI-231 (376).

In our hands BCR engagement appeared linked to apoptosis via upregulation of Bim, Bik, and Noxa transcripts in Eμ-Myc lymphoma cells. Indeed loss any one of these genes resulted in statistically significant attenuation of BCR-induced cell death. In a finding that we recapitulate, Bim has previously been identified as the major driver of BCR-induced cell death (229-231). Such a prominent role appears to be driven by a combination of transcriptional upregulation, JNK-dependent splicing of Bim_{EL} mRNA to Bim_L, and ERK-mediated degradation of Bim_{EL} protein resulting in skewing to Bim_L expression (229-231, 233). In fact, Bim appears inextricably linked to homeostatic control of B-cell populations as a whole, playing key roles in ensuring self-tolerance, production of high affinity antibody responses, protection from lymphomagenesis, and in the resolution of immune responses (229-231, 233, 374, 377). Furthermore, tonic BCR signal-mediated suppression of Bim has been demonstrated to allow maintenance of peripheral B-lymphocyte populations (27). Collectively, such results point toward a central, conserved, outcome-diverse link between the BCR and Bim that plays a central role in B-cell homeostasis. Interestingly, we detect enhanced resistance toward BCR engagement upon Bim knockdown compared to lymphoma cells derived from genetically deficient animals. Such an observation implies that additional BCR-induced cell death mechanisms appear to compensate for the loss of Bim in mice where Bim is absent.

However, we also demonstrate key roles of both Bik and Noxa downstream of BCR engagement. Whilst BCR-induced transcriptional upregulation of Bik and Noxa has been identified previously, attenuation of BCR-induced cell death upon genetic deficiency of either gene represents a novel finding (18, 223, 378).

Whilst regulation of Bim appears fundamentally linked to BCR signals, such a relationship between the BCR and Noxa appears more tenuous. However, recent tantalising evidence suggests the presence of a co-operative relationship between Noxa and Bim downstream of BCR-signalling in multiple cellular contexts (378, 379). For instance, both Noxa and Bim appear to contribute toward low affinity GC centroblast negative selection and the apoptotic response to disruption of tonic BCR-mediated PI3K activity (379, 380). Independently of Bim, Noxa has also been identified to limit the differentiation of activated B-cells to plasma cells, possibly due to its role in BCR-induced cell death (378). Collectively, such studies point to a subtle link between Noxa and the BCR in homeostatic control, which appears to require the presence of Bim. Such a notion is reflected in the findings of this investigation. We identify that Bim is the major player downstream of the BCR with a minor role played by Noxa. However, Noxa appears only to drive BCR-induced cell death in co-operation with Bim, since Noxa KO lymphoma cells retrovirally induced to knock-down Bim fail to show enhanced resistance toward BCR-induced cell death than Bim knockdown cells from WT Eμ-Myc lymphoma cells. It is likely that such co-operation is dictated biologically according to the sensitiser role of Noxa predicted by the direct activation model (172, 197, 198, 201). It is conceivable that, in order for its effect to be observed, Noxa must displace activator BH3-only proteins from prosurvivals, permitting subsequent direct activation of Bax/ Bak (168, 172, 192, 197, 198, 200, 201, 381). Such a role for Noxa during BCR-induced cell death of Eμ-Myc lymphoma cells agrees with our observations that at rest Mcl-1 appears primed by Bim. However, we also observe that in resting Bim KO lymphomas no other BH3-only proteins co-precipitate with Mcl-1, indicating that Mcl-1 priming may be a key role played by Bim in BCR-induced cell death.

Additionally, it is also conceivable that the inability of Noxa to directly drive BCR-induced cell death may be explained by its low affinity for Bcl-xL (192). The prosurvival binding profile of Noxa predicts an inability to prevent Bcl-xL-mediated retrotranslocation of Bax to the cytosol (192, 203). Therefore, Noxa would only be capable of a sensitisation role by displacing BH3-only proteins capable of binding Bcl-xL from other prosurvival molecules (192, 203).

Although Noxa appears to act as a sensitiser BH3-only protein following BCR engagement, Bik appears capable of directly driving BCR-induced cell death. We observe significant transcriptional upregulation of Bik in response to BCR engagement in an analogous finding to previous studies (18, 223, 382). However, our investigation demonstrates for the first time, attenuation of BCR-induced cell death upon genetic loss of Bik. Furthermore, we also demonstrate that combined loss of Bim and Bik yields resistance to BCR-engagement comparable to that provided by Bcl-2 overexpression. Such studies implicate Bik as a key BH3-only protein downstream of the BCR, capable of directly driving cell death.

Such results are in stark contrast to the findings of Coultas et al who demonstrate that normal B-cells of both $Bik^{-/-}$ and $Bim^{-/-}$ $Bik^{-/-}$ mice exhibit equal sensitivity toward BCR engagement as WT and $Bim^{-/-}$ B-cells, respectively (221, 222). In conjunction with observations that $Bik^{-/-}$ mice demonstrate normal haematopoiesis and B-lymphocyte homeostasis, such results suggest that Bik plays a biologically redundant role in normal B-lymphocytes (222). However, although Coultas et al demonstrate that loss of $Bik^{-/-}$ has no impact upon BCR-induced cell death, they failed to assess the effect of BCR ligation upon Bik at either protein or transcriptional levels. It is, therefore, possible that malignant and non-malignant B-lymphocytes recruit members of the apoptotic machinery differently upon BCR-signalling. Interestingly, it has been demonstrated that malignant and non-malignant B-lymphocytes exhibit significantly different kinetics in BCR-induced signalling responses, potentially resulting in activation of different effector mechanisms (234). Indeed, studies in which BCR-induced Bik accumulation is evident exclusively utilise malignant B-cell models (i.e. Ramos and B104) (223, 382). Whereas in contrast, studies assessing the impact of Bik deficiency upon the extent of BCR-induced cell death have exclusively utilised non-malignant B-lymphocytes (18, 221-223). Therefore, further analysis of the relative contribution made by Bik to BCR-induced cell death in both a malignant and non-malignant context is required.

According to the direct activation model both Noxa and Bik represent sensitiser BH3-only proteins (168, 172, 192, 197, 198, 200, 201). However, we observe differences in the effect of dual loss of either Bim and Bik or Bim and Noxa upon the extent of BCR-induced cell death. Whilst Noxa appears to function as a standard sensitiser BH3-only

protein in this context, Bik appears able to directly drive BCR-induced cell death. This observation raises the question: why can the sensitiser BH3-only protein Bik directly drive BCR-induced cell death whereas Noxa is unable to? One explanation may lie in the ability of Bik to bind Bcl-xL, possibly inhibiting Bcl-xL-mediated retrotranslocation of Bax to the cytosol (192, 203). However, since both Bik and Bcl-2 have been implicated in the induction of autophagy, it is possible that such differences may reflect the induction of Bik-mediated autophagy following BCR-engagement (383, 384). Indeed BCR engagement has been linked with the onset of autophagy in the murine lymphoma cell line WEHI-231 (275). Such a notion may also explain the total resistance toward BCR-stimulation produced upon Bcl-2 over-expression, since Bcl-2 also represents a negative regulator of autophagy (267, 268, 383). To further address this question, further characterisation of BCR-induced cell death in Bim KO lymphomas is required, reported in later chapters.

In addition to considerable upregulation of BH3-only proteins, we also observe BCR-induced reductions in the level of Bcl-2 and Mcl-1. Such reductions occur independently of transcriptional regulation and therefore, most likely reflect post-translational modifications.

It is likely that BCR-induced reduction in Mcl-1 expression is mediated by polyubiquitination and proteasomal degradation, since Mcl-1 half-life is tightly regulated by Mcl-1 ubiquitin ligase E3 (MULE) (385). In the context of IL-3 withdrawal, proteasomal Mcl-1 degradation was associated with enhanced GSK3 activity as a result of loss of Akt activity (386, 387). Following BCR engagement, Eμ-Myc lymphoma cells demonstrate extensive Akt phosphorylation up to 3 hours post-treatment. However, the effect upon long-term Akt phosphorylation levels is unknown. If parallels are drawn with ERK signalling, it is possible that Akt activation is also accompanied by a complete block of normal cyclical activity 4 hours post-BCR stimulation (388). Such an occurrence may result in enhanced GSK3 activity and subsequent Mcl-1 degradation.

The observed BCR-induced reduction in Bcl-2 expression has also been described previously in normal B-cells (229). However, as yet the exact molecular mechanisms linking the BCR to prosurvival degradation remain unknown. A similar mechanism is

evident downstream of TNFα and staurosporine-induced cell death in endothelial cells, whereby loss of MAPK-mediated Bcl-2 phosphorylation results in its targeted ubiquitination and proteasomal degradation (389, 390). It is possible that the enhanced protection offered by Bcl-2 over-expression, in comparison to loss of Bim, is due to saturating levels of Bcl-2 reducing the effect of Bcl-2 degradation. Further characterisation of Bcl-2 degradation and its possible relationship with ERK activity will be addressed in a later chapter.

In summary, in this chapter Bim, Noxa, and Bik were identified to play key roles in BCR-induced cell death. It was demonstrated that Noxa likely acts as a sensitiser BH3-only protein, whilst Bim and Bik directly drive BCR-induced cell death. In the next chapter we shall assess the relative contribution of BCR-induced signalling pathways to BCR-induced cell death. Furthermore, extensive characterisation of BCR-induced cell death in $Bim^{-/-}$ lymphomas shall be undertaken in order to further observe the cell death mechanisms driven by Bik and possibly Bcl-2 degradation.

Chapter 5 BCR-induced kinases, the Bcl-2 family, and pharmacological dissection of BCR-induced cell death

5.1 Chapter introduction

In chapter 3, it was demonstrated that rapid and sustained activation of MAPK and Ca^{2+} signalling pathways was evident in response to BCR-engagement in Eμ-Myc lymphoma cells. Such Ca^{2+} signalling responses bore characteristic transient and plateau phases necessary to activate both NF-κB and NFAT pathways, respectively (108, 109). Whilst such engagement of MAPK and Ca^{2+} signalling appears conserved between both activatory and cellular deletion signalling modes, the manner in which they are engaged may differ and contribute towards disparate cellular outcomes (247, 250-254, 256, 257). Continuing with such a theme, BCR-driven cell death appears, at least partially, dependent upon altered NF-κB, PI3K, JNK, ERK, and CN-signalling (223, 230, 231, 250-254, 256, 257). Such pathways are typically considered as predominantly prosurvival; however they have also been implicated as pro-death in the context of the negative signalling mode of the BCR.

Since many BCR-induced signalling pathways appear to exert regulatory forces upon Bcl-2 family members in alternate contexts, the involvement of Bcl-2 family members in BCR-induced apoptosis is perhaps somewhat unsurprising. Both ERK and PI3K/Akt pathways appear primarily to negatively regulate BH3-only proteins, culminating in degradation, sequestration, and transcriptional repression of both Bim and Bad (96, 151, 204-206, 213). However, ERK-driven degradation of Bim_{EL} has also been implicated as a key participant in Bim skewing to Bim_L expression downstream of the BCR (230, 231). Therefore, it appears as though an overtly inhibitory signal can also be involved in cell death responses to BCR engagement if integrated with other pro-death signals.

In contrast however, JNK signalling appears largely associated with upregulation and/ or activation of BH3-only proteins. Such a function appears to manifest in the reversion of PI3K/Akt pathway-mediated sequestration of Bim, and augmentation of BH3-only function by direct phosphorylation (152, 153, 209, 210). Furthermore, JNK has also

been implicated in triggering CHOP and AP-1 dependent Bim transactivation downstream of ER-stress (211, 212). Since both JNK-mediated transactivation of Bim, and ER stress have been observed downstream of BCR engagement, it seems likely that the two phenomena may be linked (193, 230, 231, 242).

In addition, we also observe BCR-induced degradation of Bcl-2 and Mcl-1 in Eμ-Myc lymphomas. Whilst Bcl-2 degradation has been observed upon BCR engagement previously, the molecular mechanisms triggering such an event remain unknown (229). In the context of TNF-αR signalling, Bcl-2 degradation has been attributed to a loss of ERK signalling, an occurrence which may also be reflected during BCR-induced cell death (389, 390).

Therefore, whilst the identities of BCR-induced signalling pathways appear conserved between alternate cellular outcomes, the manner in which activation occurs differs (234). It is, therefore, conceivable that pathways responsible for substantial prosurvival roles during activatory signalling may also undertake a significant role in death signalling. Therefore, in this chapter we aim to identify the key molecular signalling pathways responsible for BCR-induced cell death in both WT and $Bim^{-/-}$ Eμ-Myc lymphomas. Furthermore, we aim to identify the specific molecular repercussions such signals impart upon the Bcl-2 family and identify their relative contribution toward BCR-induced cell death.

5.2 Investigating the kinase dependency of BCR-induced cell death in WT Eμ-Myc lymphomas

In chapter 3, rapid, sustained pERK accumulation up to 8 hours post-BCR stimulation in Eμ-Myc lymphoma cells was observed. Since both BCR-induced pERK accumulation and upregulation of Bim mRNA appeared concomitantly, we hypothesised that ERK may play a key role in generating the cell death response via an effect on Bim.

In order to dissect the relative contribution of ERK signalling toward BCR-induced cell death, we utilised the small molecule MEK inhibitor PD0325901 (PD) in an attempt to block the Ras/Raf/MEK/ERK signalling pathway. As demonstrated in figure 5.1A, pre-incubation of Eμ-Myc lymphomas with PD completely ablated BCR-induced pERK

accumulation at all concentrations tested (160 – 10 nM), reducing pERK below baseline to non-detectable levels. Interestingly, ablation of ERK phosphorylation coincided with a downward shift in bands corresponding to Bim_{EL}, consistent with reduced phosphorylation, clearest in figure 5.1B (200). As a consequence, it appears that Bim is subjected to continual ERK-dependent phosphorylation in resting cells, which likely contributes toward the strict regulation of basal Bim activity and expression. Since all concentrations of PD yielded comparable inhibition of ERK phosphorylation, 10 nM was selected for further use in dissecting the BCR-induced cell death response. As demonstrated in figure 5.1 C-F, PD-mediated disruption of Ras/Raf/MEK/ERK signalling (red bars/ lines) imparted statistically significant protection (approximately 1.6-fold) from BCR-induced cell death after 24 hours, in comparison to vehicle controls (blue bars/ lines). Such observations imply that ERK not only appears to directly influence Bim phosphorylation levels but also that it plays a vital role in regulating BCR-induced cell death.

Since ERK is classically associated with prosurvival signalling, and proteasomal degradation of Bim_{EL}, we wished to determine whether the protective effect of Ras/Raf/MEK/ERK disruption extended to WT B-lymphocytes. However, in contrast to Eμ-Myc lymphomas PD-mediated disruption of Ras/Raf/MEK/ERK signalling (red lines) significantly enhanced the extent of BCR-induced cell death in WT B-lymphocytes (from 31.78 to 54.57%), as evident in figure 5.2. Furthermore, the protective effect of ERK pathway neutralisation was not associated with the presence of elevated Myc signalling per se (due to the Myc tg), since Myc transgenic pre-neoplastic B-cells also demonstrated significantly enhanced levels of BCR-induced cell death upon PD treatment (from 43.2 to 63.7%). Furthermore, such observations were not due to significant variation in toxicity, since Eμ-Myc lymphomas, Myc Tg B-cells, and normal C57BL/6 B-cells all exhibited only moderate toxicity in response to PD. Such observations imply that specific biological differences between non-malignant and malignant B-lymphocytes, and more specifically Eμ-Myc lymphomas, alter the activity and/or targets of the ERK pathway downstream of BCR engagement.

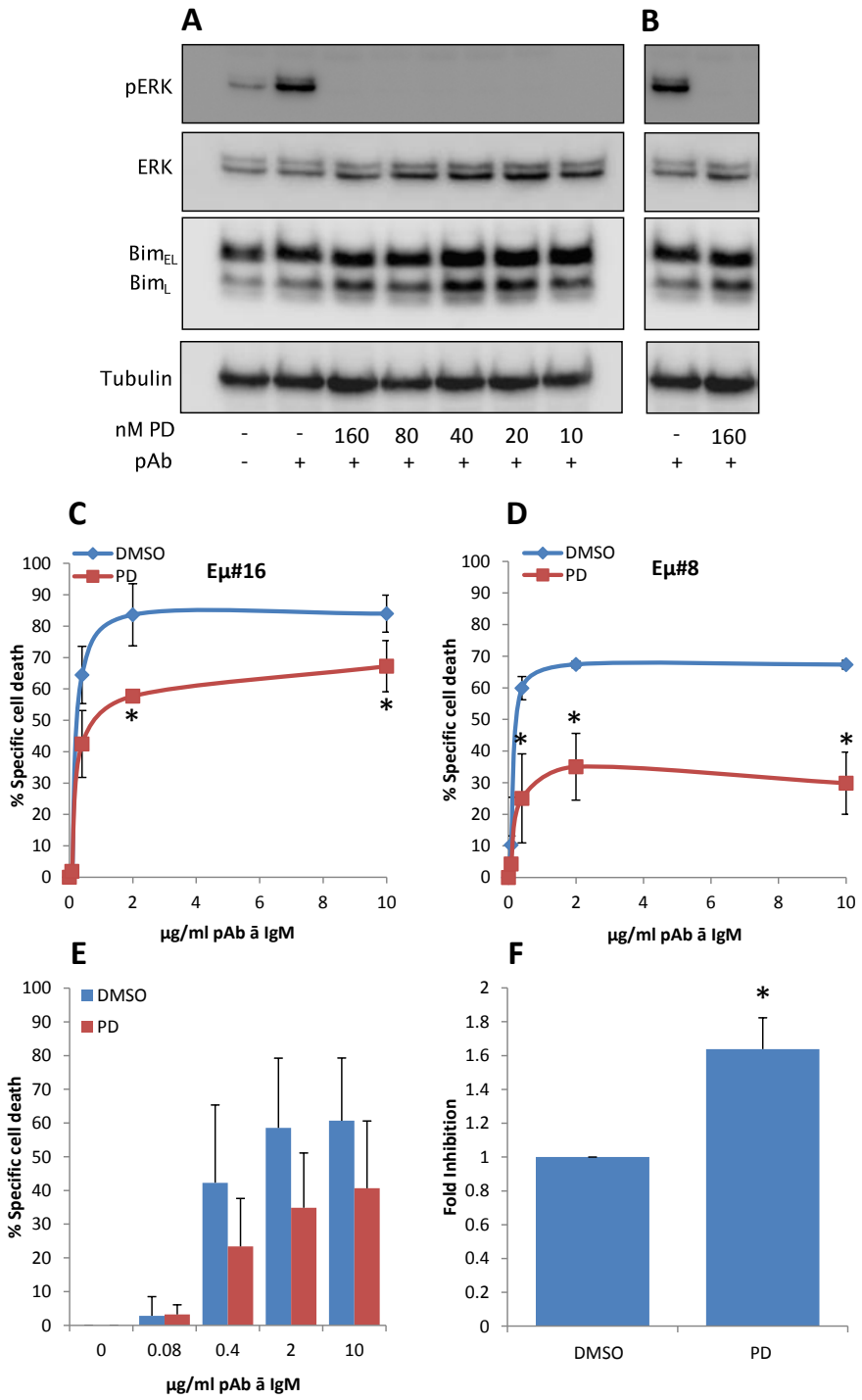

Figure 5.1 Impact of MEK-inhibition upon the extent of BCR-induced cell death in Eμ-Myc lymphomas

A 5x10^6 Eμ# 16 Eμ-Myc lymphoma cells per sample were re-suspended at 1x10^6/ ml in pre-equilibrated medium and rested overnight at 37°C, 10% CO_2. Cells were subsequently pre-incubated with PD0325901 (PD), at the indicated dose, or the equivalent volume of DMSO for 30 minutes. Subsequently, cells were treated with 2 μg/ml pAb ã IgM or an equivalent volume of PBS for 1 hour, lysed and subjected to western blotting analysis. **B** Cropped version of A better demonstrating the PD-induced Bim$_{EL}$ band shift. **C-F** Eμ-Myc lymphomas (n=4) were pre-incubated with 10 nM PD, or the equivalent volume of DMSO, for 30 minutes prior to pAb a IgM treatment (10 - 0.08 μg/ml). 24 hours later cells were harvested by pipetting and subjected to Annexin V/PI flow cytometry, as previously described. Values represent the average of three independent experiments from the indicated Eμ-Myc lymphoma cells **(C-D)** or an average of 4 different Eμ-Myc lymphoma cells **(E-F)**, each performed in triplicate. Bars represent

standard deviation. Asterisks denote statistically significant differences as adjudged by paired Student's T-test statistical analysis ($p<0.05$).

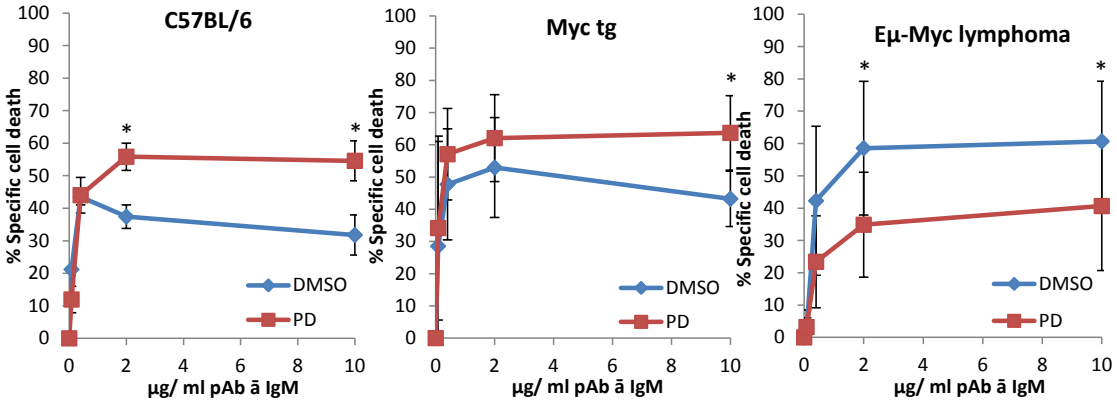

Figure 5.2 Impact of MEK-inhibition upon the extent of BCR-induced cell death in normal and Myc-tg B-cells

Purification of total splenic B-lymphocytes from **A** WT C57BL/6 (n=3) or **B** pre-neoplastic Eμ-Myc mice (n=3) was undertaken via MACS-purification, as outlined in materials and methods. Cells were rested for 1 hour at 37°C, 10% CO_2 and subjected to pre-incubation with 10 nM PD or an equivalent volume of DMSO for 30 minutes. Subsequently cells were subjected to pAb ã IgM treatment and Annexin V/ PI flow cytometry after 24 hours, as described in figure 5.1B. Values represent the average of 3 independent experiments of cell populations derived from different mice, each performed in triplicate. Bars represent standard deviation. Asterisks denote statistically significant differences as adjudged by paired Student's T-test statistical analysis ($p<0.05$). For comparison results with Eμ-Myc lymphoma cells are shown (right panel).

Moreover, since the Bim KO Eμ-Myc lymphoma cell line MB63 demonstrated identical levels of BCR-induced cell death in the presence and absence of PD (see appendix A17), it is possible that the pro-death function of ERK centres upon Bim downstream of the BCR.

In addition to sustained activation of ERK, BCR engagement significantly enhanced levels of pJNK throughout the treatment period, reaching a maximum after 180 minutes, as determined in chapter 3. Therefore, the relative contribution of JNK activity toward BCR-induced cell death was assessed via use of the small molecule JNK inhibitor SP600125 (SP6).

As evident in figure 5.3A, only a small increase in the level of phosphorylated c-Jun (p c-Jun) was evident following BCR-engagement of Eμ-Myc lymphoma cells. However, SP6 did appear to effectively block BCR-induced accumulation of p c-Jun at all concentrations tested (40 – 2.5 μM).

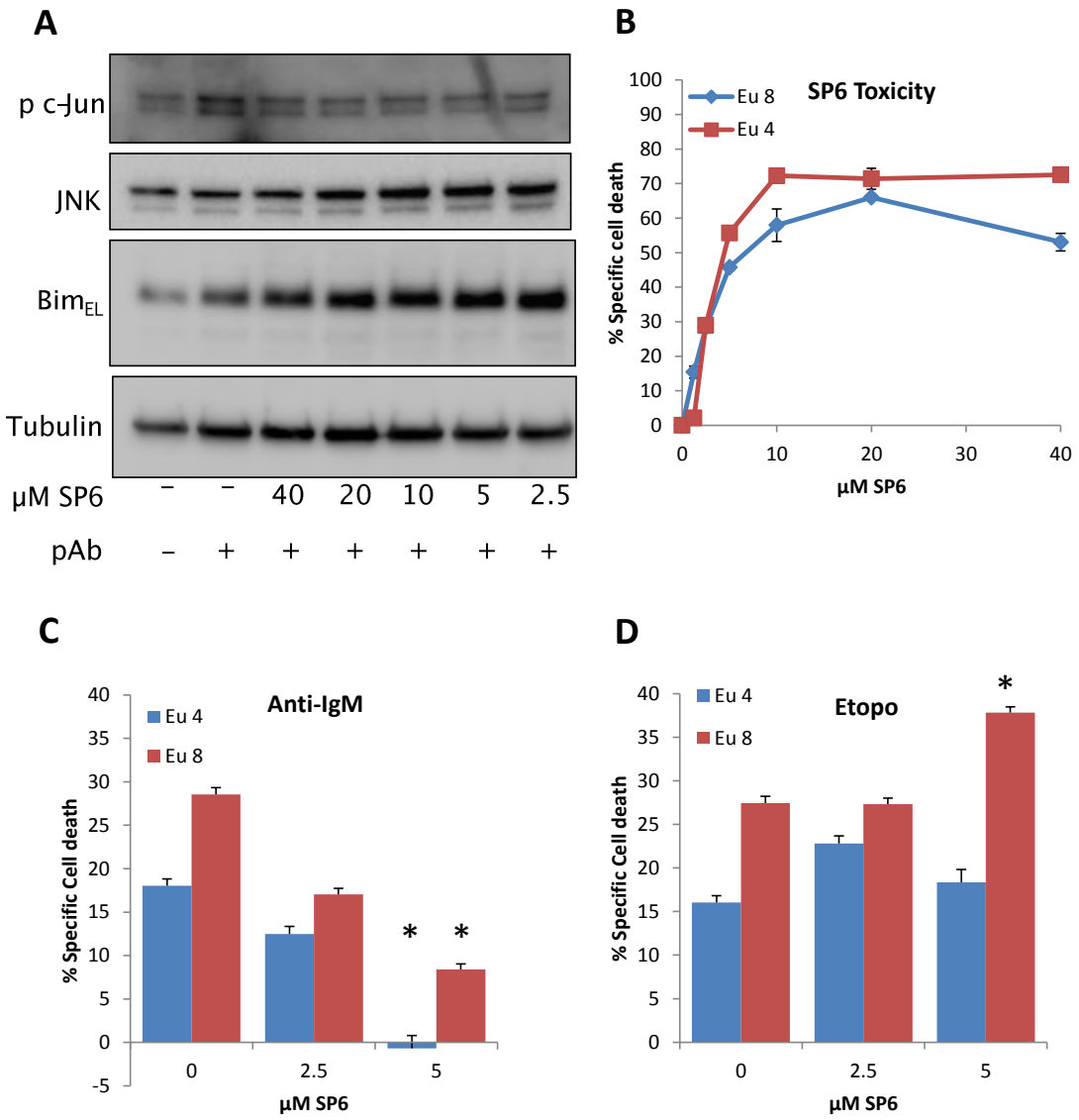

Figure 5.3 Effect of JNK inhibition upon BCR-induced cell death in Eμ-Myc lymphoma cells

A Eμ# 16 was treated as in figure 5.1A, with the exception that cells were first pre-incubated with the indicated dose of SP600125 (SP6). **B** Eμ# 4 and Eμ# 8 Eμ-Myc lymphoma cells were subjected to Annexin V/ PI flow cytometry, as previously described, 6 hours post-treatment with the indicated dose of SP6 to assess toxicity of the drug. **C-D** Eμ# 4 and Eμ #8 Eμ-Myc lymphoma cells were pre-treated with 2.5 or 5 μM SP6 for 30 minutes prior to pAb ã IgM (10 μg/ ml) or Etoposide (5 μg/ ml) treatment for 6 hours to assess the impact upon the early stages of BCR-induced cell death. Levels of cell death were subsequently assessed by Annexin V/ PI flow cytometry, as previously described. Values represent the average of three independent experiments, each performed in triplicate. Bars represent standard deviation. Asterisks denote statistically significant differences as adjudged by paired Student's T-test statistical analysis ($p<0.05$).

However, it is apparent that SP6 treatment was insufficient to reduce p c-Jun to below baseline levels. Therefore, it is implied that either additional kinases also contribute toward c-Jun phosphorylation in Eμ-Myc lymphoma cells or SP6 does not fully inhibit JNK activity. Despite such observations, SP6 did appear to effectively block BCR-

induced accumulation of p c-Jun, and therefore, was deemed a useful tool for further dissection of the BCR-induced cell death pathway.

Since B-lymphocytes appear to exhibit particular sensitivity toward disruption of JNK signalling, a toxicity screen was also performed to assess the suitability of SP6 for further use (391). As evident in figure 5.3B, Eμ-Myc lymphomas appear to demonstrate high levels of toxicity toward SP6 at doses above 5 μM after 6-hours (over 50% above background). Since SP6 appeared to generate upregulation of Bim protein levels, it is likely that such toxicity is due to an effect upon Bim, as evident in figure 5.3A. Therefore, further use of SP6 was restricted to 6-hour incubation periods with sub-5 μM doses. As demonstrated in figure 5.3C-D, pharmacological inhibition of JNK activity resulted in a dose-dependent, statistically significant reduction in BCR, but not Etoposide, induced cell death after 6 hours. In fact, pre-treatment with SP6 significantly enhanced Etoposide-induced cell death in Eμ# 8. Therefore, SP6-mediated protection from BCR-induced cell death appears stimulus-specific and not due to a general effect on cell death. Consequently, it appears that JNK signalling contributes toward the early phase of BCR-induced cell death. However, the profound toxicity of SP6 prevented observation of its impact after 24 hours therefore, its relative contribution to the death pathway as a whole remains un-assessed.

Furthermore, in chapter 3 we also observed rapid accumulation of pAkt in response to BCR engagement, reaching a maximum of approximately 12-fold enhancement after only 30 minutes. Therefore, in order to dissect the relative contribution of PI3K-mediated PIP_3 production and Akt activation toward BCR-induced cell death, the PI3K inhibitor LY294002 (LY) was utilised.

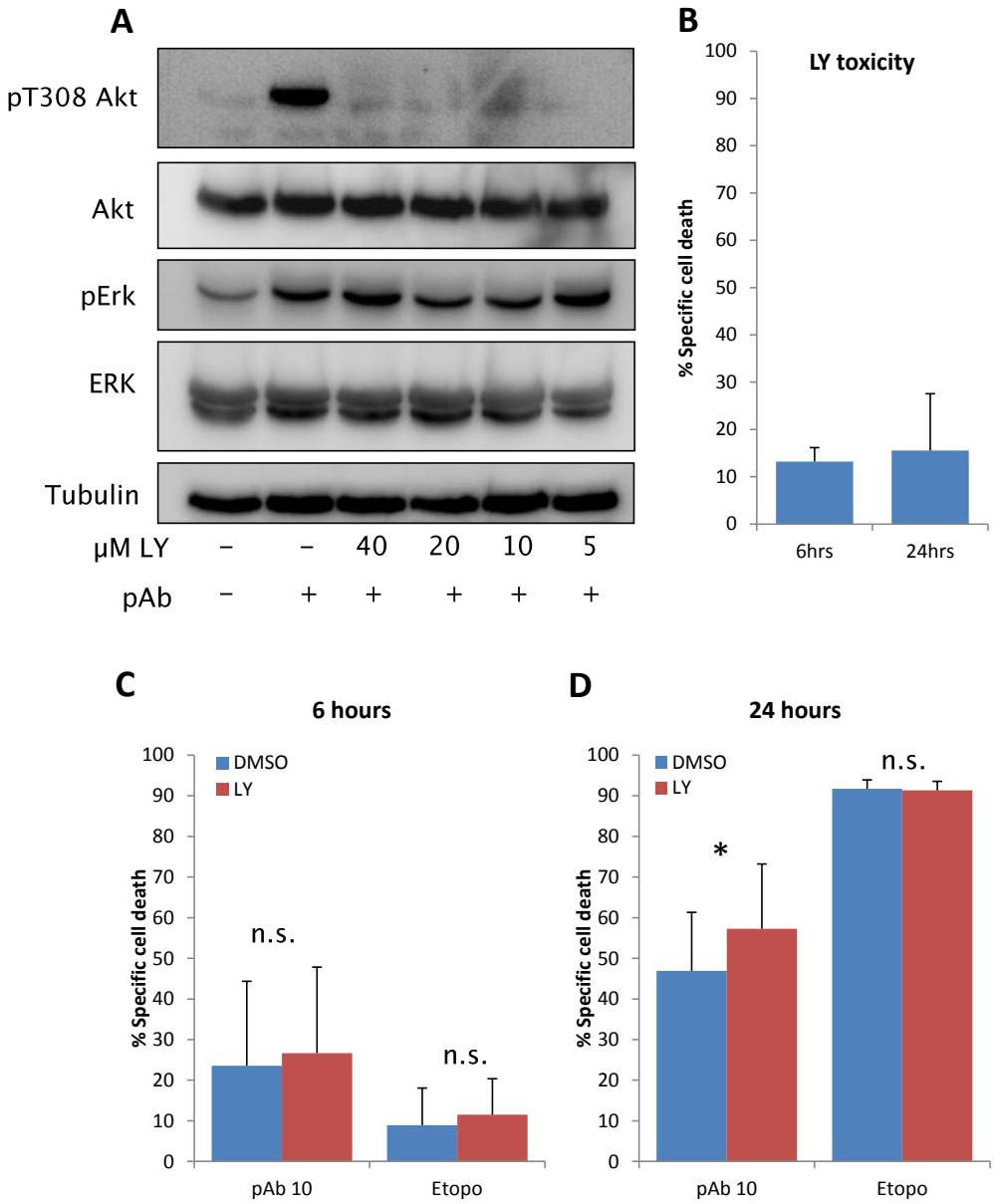

Figure 5.4 Effect of PI3K inhibition upon BCR-induced cell death in Eμ-Myc lymphoma cells

A Eμ# 16 was treated as in figure 5.1A, except cells were pre-incubated with the indicated dose of LY294002 (LY). **B** Eμ-Myc lymphoma cells (n=3) were subjected to Annexin V/ PI flow cytometry, as previously described, 6 and 24 hours post-treatment with 5 μM LY, or an equivalent volume of DMSO, to assess levels of cytotoxicity. **C-D** Eμ-Myc lymphoma cells were pre-treated with 5 μM LY, or an equivalent volume of DMSO, for 30 minutes prior to pAb ã IgM (10 μg/ ml) or Etoposide (5 μg/ ml) treatment for 6 (C) or 24 (D) hours followed by Annexin V/ PI flow cytometry, as previously described. Values represent averages obtained from three different Eμ-Myc lymphomas, each the average of three independent experiments performed in triplicate. Bars represent standard deviation. Asterisks denote statistically significant differences as adjudged by paired Student's T-test statistical analysis ($p<0.05$).

As evident in figure 5.4A, LY completely ablated Akt Thr 308 phosphorylation (PDK-1-dependent site) at all concentrations utilised (40 – 5 μM) downstream of BCR engagement in Eμ-Myc lymphomas.

Furthermore, the lowest effective dose, 5 μM, appeared to demonstrate minimal toxicity after both 6 and 24-hour incubations (invoking only 13.2 and 15.5% cell death above background, respectively), as evident in figure 5.4B, and was therefore selected for further use. As observed in figures 5.4C-D, inhibition of PI3K had no impact upon the extent of Etoposide-induced cell death at either 6 or 24 hours. However, LY did appear to slightly enhance the levels of BCR-induced cell death recorded at both time-points. Although such differences were non-statistically significant at 6 hours, a clear trend is apparent linking PI3K inhibition to enhanced BCR-induced cell death. Such observations imply that the PI3K/Akt does not play a significant role in transducing signals for BCR-induced cell death in Eμ-Myc lymphoma cells.

Finally, since both ERK and JNK activation appear reliant upon the activity of Syk in multiple models, the impact of the Syk inhibitor R406 upon the extent of BCR-induced cell death was assessed. Unfortunately, antibodies directed against the autophosphorylation site of murine Syk (Y519/520) are not widely available. However, standard doses of 1 and 2 μM R406 have been used in previous studies and demonstrated to specifically target Syk. As R406, and its pro-drug form R788, represent targeted therapies for disruption of tonic BCR signals and deletion of B-lymphocyte populations, it was deemed prudent to assess its relative toxicity in Eμ-Myc lymphomas prior to further use.

As evident in figure 5.5A, R406 induced significant levels of cell death at all doses analysed (1-10 μM). However, acceptable levels of cell death above background (around 30%) appeared to be imparted upon doses of 1 μM. Therefore, such a dose was further utilised to assess the role of Syk in BCR-induced cell death.

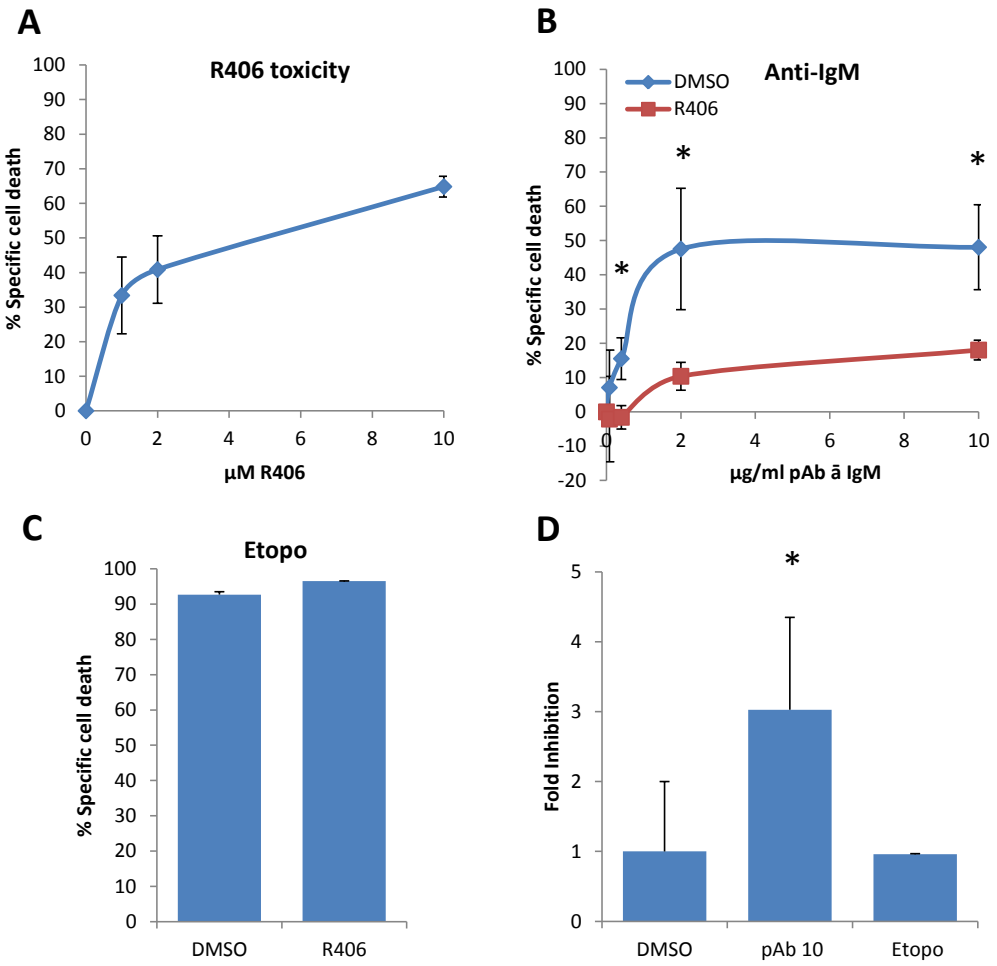

Figure 5.5 Effect of Syk inhibition upon BCR-induced cell death in Eμ-Myc lymphomas

A Eμ# 16 was treated as in figure 5.3B except cells were incubated with the indicated dose of R406, or the equivalent amount of DMSO, for 24 hours. Subsequently, Annexin V/ PI flow cytometry was undertaken to assess levels of cell death. Values represent a single experiment performed in triplicate. Bars denote standard error. **B-C** Cells were treated as in figure 5.1 B-D except were pre-incubated with 1 μM R406 30 minutes prior to **B** pAb ã IgM (10 – 0.08 μg/ml) or **C** Etoposide (5 μg/ml) treatment for 24 hours. Levels of subsequent cell death were assessed by Annexin V/ PI flow cytometry. Values represent an average of results from four different Eμ-Myc lymphomas, each the average of three independent experiments performed in triplicate. Bars represent standard deviation. Asterisks denote statistically significant differences as adjudged by paired Student's T-test analysis ($p<0.05$). **D** Fold inhibition was calculated by dividing levels of cell death, recorded in 5.5B, in the absence of R406 by that in its presence.

As demonstrated in figures 5.5B-D, R406-mediated disruption of Syk activity offered significant protection from BCR, but not Etoposide, induced cell death after 24 hours. In the presence of R406 (red lines), levels of BCR-induced cell death were approximately 3-fold lower than that of vehicle treated cells (blue lines). Such reductions were roughly double that produced upon pre-treatment with PD. It is likely that R406 inhibits multiple BCR-induced signalling pathways, which may be responsible for the enhanced protection. However, factors such as drug half-life, efflux rates, and

affinity for target may also influence the magnitude of response. Therefore, the relative magnitude of protection offered by PD and R406 cannot be directly compared. However, such studies highlight the fact that Syk also plays a key pro-death role downstream of BCR engagement in Eμ-Myc lymphomas.

Taken together, the above studies highlight that Syk, ERK, and JNK, but not PI3K/Akt play key roles in transduction of BCR-induced cell death signals. In the next section, we attempt to identify how BCR-induced ERK and Syk activity might regulate the apoptotic machinery, with a particular focus upon the Bcl-2 family.

5.3 Examining the impact of BCR-induced ERK and Syk activity upon the Bcl-2 family

In order to ascertain whether ERK and/or Syk facilitate the observed changes in Bcl-2 family member expression seen after BCR engagement, outlined in chapter 4, the impact of PD and R406 upon such processes was assessed.

5.3.1 BCR-induced ERK activity and BH3-only proteins

Initially the impact of PD-mediated disruption of Ras/Raf/MEK/ERK signalling upon baseline expression of Bim, Noxa, and Bik transcripts was assessed by qPCR, as demonstrated in figure 5.6. It is clear that loss of ERK signalling capacity (red lines) does not significantly influence baseline Bim, Noxa and Bik transcript levels in comparison to vehicle-treated cells (blue lines) over the 6-hour time-course. Therefore, PD was deemed appropriate for further use in dissecting the link between the BCR and BH3-only protein transcripts. As evident in figure 5.7, PD-mediated inhibition of MEK signalling (red bars) was associated with a statistically significant reduction in BCR-induced upregulation of Bim mRNA.

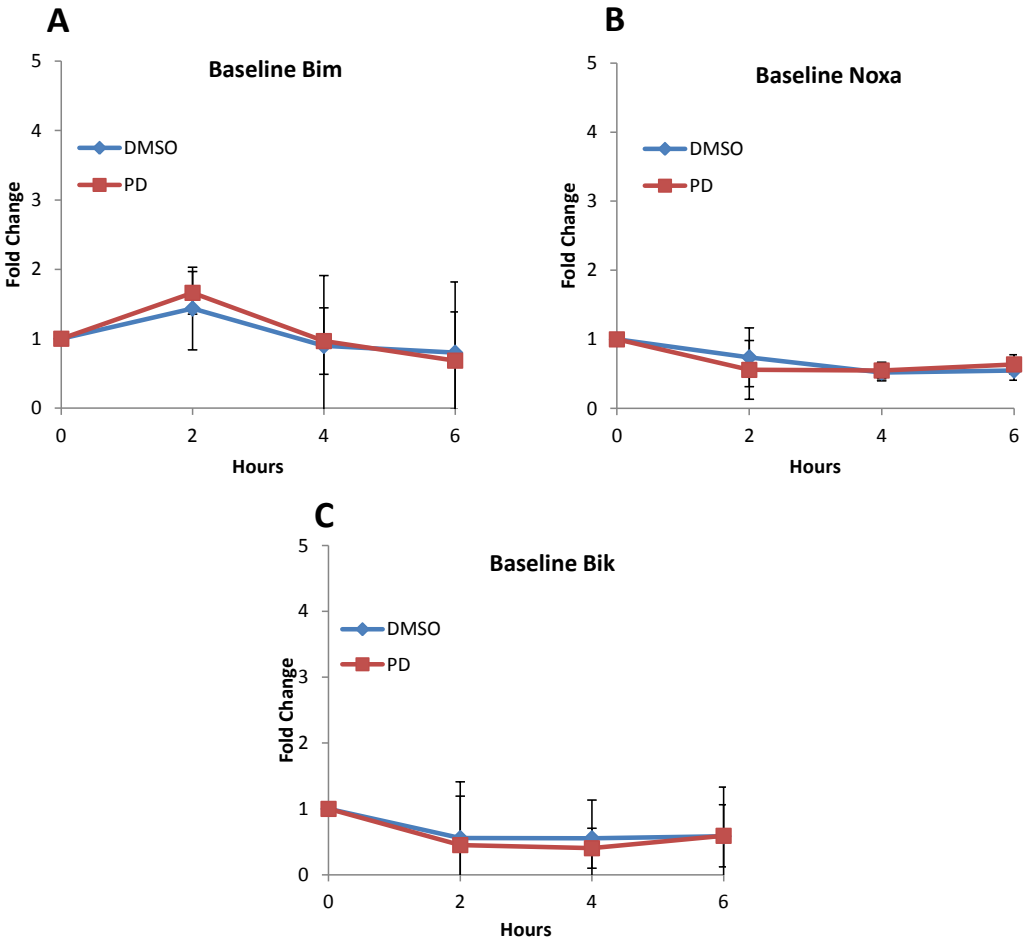

Figure 5.6 Effect of MEK inhibition upon Bim, Noxa, and Bik expression levels

RNA was purified from 1x10^6 Eμ-Myc lymphoma cells per sample (n=4 Eμ# 16, 15, 8, and 4) treated with 10 nM PD or an equivalent volume of DMSO at the indicated time points and converted to cDNA, as outlined in materials and methods. qPCR analysis of **A** Bim, **B** Noxa and, **C** Bik transcript levels was then performed, corrected for GAPDH expression and normalised against a 0 hour time-point, as outlined previously, to observe fluctuations in baseline gene expression after PD treatment. Values represent an average of results from four different Eμ-Myc lymphomas, each using 1 cDNA performed in triplicate. Bars represent standard deviation.

However, PD pre-treatment had no discernable effect upon Noxa and Bik upregulation. Such observations demonstrate that BCR-induced upregulation of Bim appears dependent upon ERK signalling. However, a separate ERK-independent pathway also appears to link the BCR to Bik and Noxa transcripts.

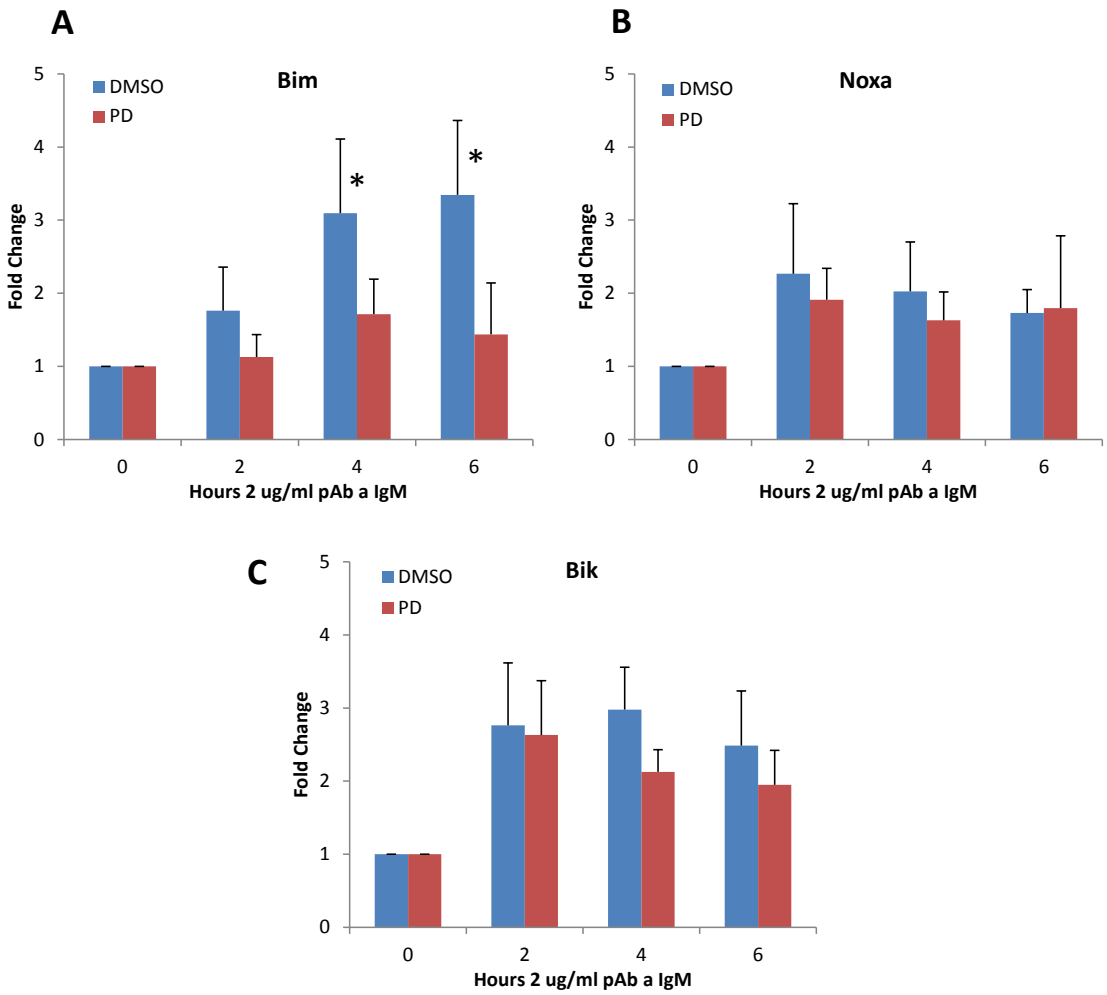

Figure 5.7 Effect of MEK inhibition upon BCR-induced transcriptional up-regulation of Bim, Noxa, and Bik expression

$1x10^6$ Eμ-Myc lymphoma cells were pre-incubated with 10 nM PD or an equivalent volume of DMSO for 30 minutes prior to addition of 2 μg/ml pAb ã IgM or an equivalent volume of PBS. RNA was isolated at the indicated time points, converted to cDNA and utilised for qPCR analysis of **A** Bim, **B** Noxa, and **C** Bik transcript levels, as before. c(T) values were corrected for GAPDH expression and pAb ã IgM treated samples normalised to their respective PBS-treated controls. Values represent the average of four different Eμ-Myc lymphomas, each utilising 1 cDNA performed in triplicate. Bars represent standard deviation. Asterisks denote statistically significant differences as adjudged by paired Student's T-test statistical analysis ($p<0.05$).

In order to determine whether PD also influenced BCR-induced upregulation of Bim at the protein level, western blotting studies were undertaken. As evident in figure 5.8, BCR-engagement induced small increases in Bim_{EL} protein levels after 24 hours, accompanied by a much larger increase in Bim_L expression.

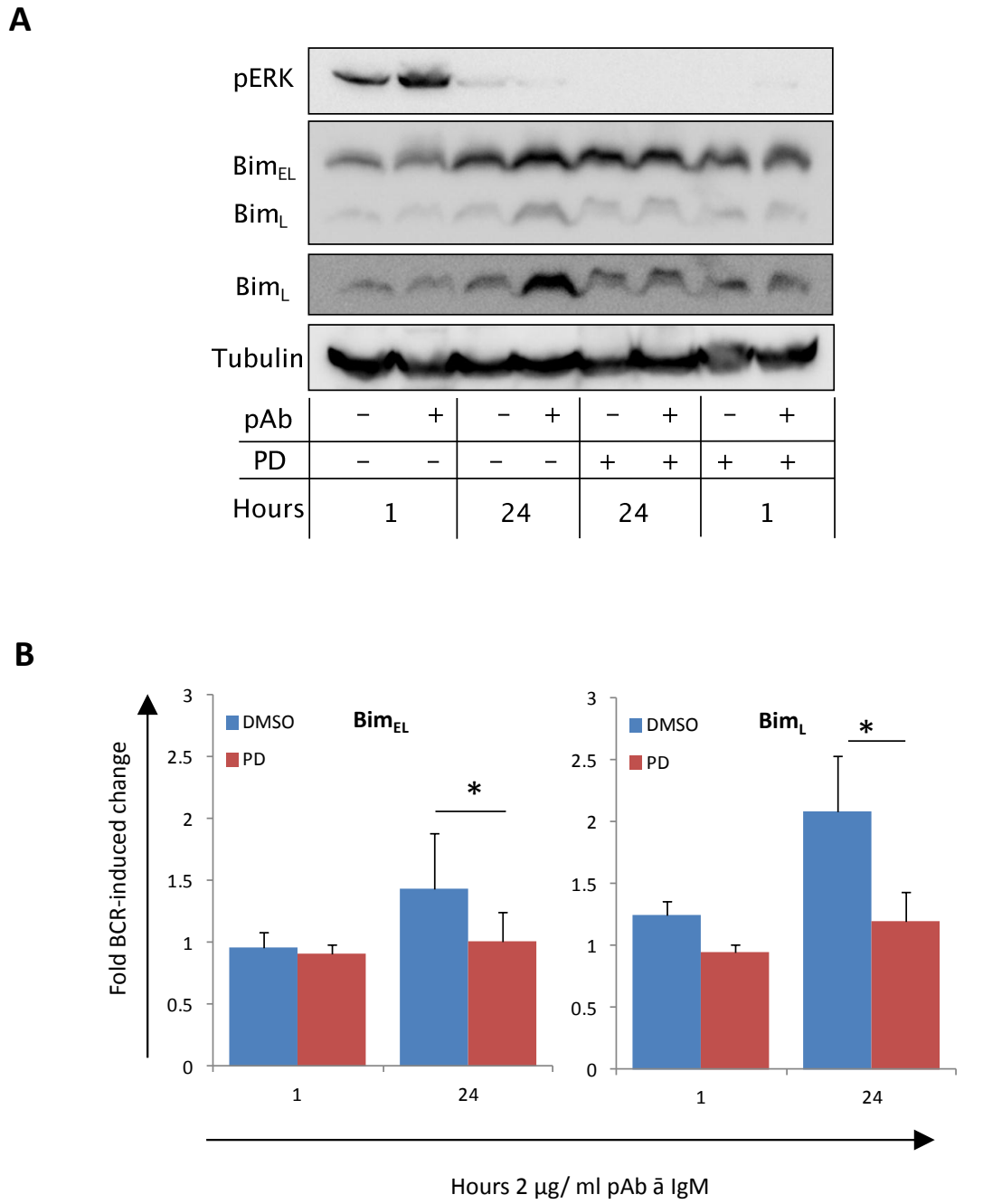

Figure 5.8 Effect of MEK inhibition upon BCR-induced up-regulation of Bim protein levels

A 5x10^{6} Eμ# 4 Eμ-Myc lymphoma cells were pre-treated with 10 nM PD, or an equivalent volume of DMSO, and 25 μM qVD-OPH for 30 minutes prior to addition of 2 μg/ ml pAb ã IgM, or an equivalent volume of PBS, for 1 or 24 hours. Cells were subsequently lysed, and assessed for Bim expression levels by western blotting analysis. Data is representative of three independent experiments utilising three different Eμ-Myc lymphomas. **B** Data collected in **A** was subjected to densitometry using UVP vision works software (UVP, UK). Levels of Bim were corrected for Tubulin expression and normalised against the relevant PBS-treated control. Values represent the average of two different Eμ-Myc lymphoma cell lines (Eμ# 16, and 4), both of which are the average of three independent experiments. Bars represent standard deviation. Asterisks denote statistically significant differences as adjudged by paired Student's T-test analysis ($p<0.05$).

Such increases were, however, blocked by pre-treatment of Eμ-Myc lymphomas with PD. Interestingly, PD-mediated disruption of ERK signalling appeared to block BCR-induced enhancement of both Bim_{EL} and Bim_{L}. Consequently, it appears as though BCR-mediated activation of the ERK pathway directly induces upregulation of Bim at the transcript and protein levels and is responsible for Bim_{EL} to Bim_{L} isoform skewing in Eμ-Myc lymphoma cells.

Since inhibition of ERK-activity appeared to influence basal levels of Bim phosphorylation, as evident in figure 5.1A, we wished to identify whether BCR-induced Ras/Raf/MEK/ERK signalling influenced formation of Bim: prosurvival complexes downstream of BCR engagement, prior to upregulation of Bim protein levels.

As evident in figure 5.9, prior to upregulation of Bim at the protein level, small increases in Bim: Mcl-1 (1.1-1.6 fold average 1.52-fold), but not Bim: Bcl-2, complexes were evident following BCR stimulation. However, PD-mediated disruption of ERK signalling prevented such increases and reduced complex formation to below baseline levels. Whilst the increases in Bim: prosurvival complexes were only small and statistically non-significant, it does appear as though BCR-driven ERK signals may also drive both enhancement of Bim: prosurvival complex formation and upregulation at the protein level.

Since BCR-mediated ERK activity appeared to be associated with Bim transactivation, we rationalised that ERK may drive the response by altering the subcellular localisation of key transcription factors. Utilising the Alggen promo 3.0 bioinformatic transcription factor binding site prediction tool (www.alggen.lsi.upc.es/cgi-bin/promo_v3), we identified putative binding sites for CHOP, SP-1, Elk-1, Foxo3a, and Myb transcription factors in the murine Bim promoter. Subsequently, we analysed the impact of BCR engagement upon the subcellular localisation of candidate transcription factors, and the dependency upon ERK signalling, by nuclear extraction and western blotting.

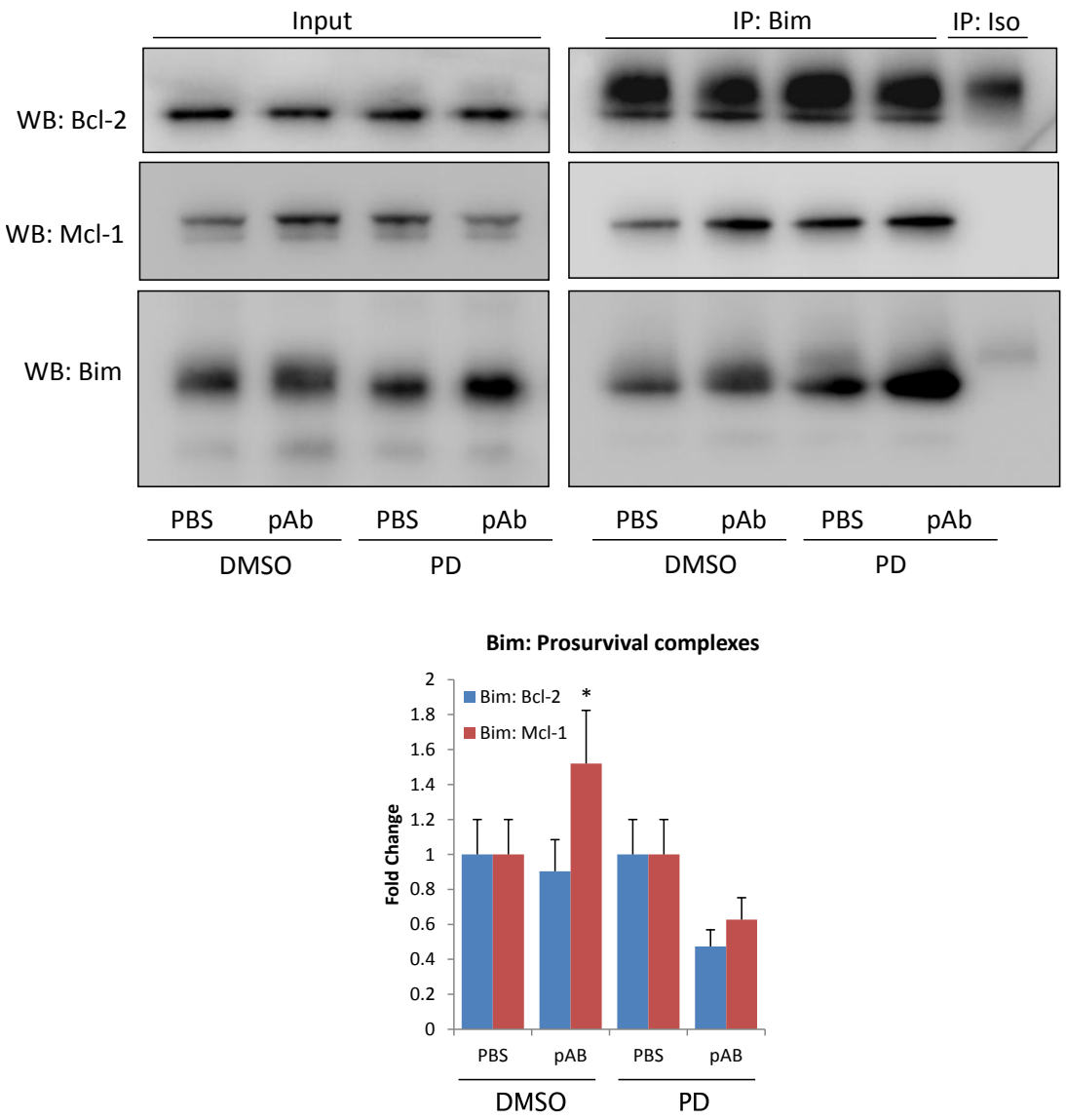

Figure 5.9 Effect of MEK inhibition upon BCR-induced formation of Bim: prosurvival complexes

A 1x10^9 Eμ# 16 Eμ-Myc lymphoma cells per sample were treated with 25 μM qVD-OPH and 10 nM PD, or an equivalent amount of DMSO, for 30 minutes prior to addition of 2 μg/ml pAb ã IgM, or an equivalent volume of PBS, for 8 hours. Cells were subsequently harvested, lysed and subjected to immunoprecipitation, using either anti-Bim or anti-Mcl-1 antibodies, eluted and the immunoprecipitated material assessed by western blotting. 10% of the input material was also removed to serve as a whole-cell lysate input control, corresponding to 50 μg total protein. Data is representative of four independent experiments utilising two different Eμ-Myc lymphomas. **B** Levels of Bim: prosurvival complexes were assessed by densitometry, as previously described. Values represent the average of four independent experiments utilising two different Eμ-Myc lymphomas. Bars represent standard deviation.

As evident in figure 5.10, BCR engagement failed to significantly alter nuclear levels of Foxo3a, Elk-1, or SP-1. However, 2.16 and 1.71-fold increases in the levels of nuclear CHOP and Myb were evident downstream of BCR engagement. Interestingly, PD-mediated disruption of Ras/Raf/MEK/ERK signalling appeared to reverse BCR-induced translocation of CHOP to the nucleus, returning levels to those seen in PBS treated

cells. Therefore, it is possible that BCR-mediated transactivation of Bim proceeds through an ERK and CHOP-dependent mechanism. However, further study is required to assess the relative contribution of CHOP to BCR-induced Bim transactivation. In order to address such a notion, CHOP knockout Eμ-Myc lymphoma cell lines could be developed and the relative effect of BCR engagement compared to WT Eμ-Myc lymphoma cell lines. The role of Myb also remains ambiguous. Whilst it's BCR-induced nuclear localisation was independent of ERK activity, and therefore not responsible for Bim transactivation, the possibility remains that Myb contributes to transactivation of Bik and Noxa downstream of the BCR. Furthermore, whilst a significant reduction in Myc nuclear localisation was evident upon BCR stimulation in Eμ# 16, such an occurrence was not reflected in the remaining Eμ-Myc lymphoma cell lines. Therefore, it is unlikely that loss of Myc nuclear localisation plays a key role in BCR-driven cell death.

5.3.2 Dissecting the role of Syk in linking BCR engagement to BH3-only proteins

Since inhibition of Syk activity appeared to impart greater resistance toward BCR-induced cell death than loss of Ras/Raf/MEK/ERK signalling, we reasoned that Syk may influence the regulation of multiple BH3-only proteins downstream of BCR engagement. In order to address this, we analysed the impact of R406 treatment upon BCR-mediated upregulation of BH3-only transcripts.

As evident in figure 5.11, R406 (red lines) appeared to have minimal influence upon baseline expression levels of Bim, Noxa, and Bik transcripts, in comparison to vehicle treated controls (blue lines). However, as outlined in figure 5.12, R406 (red bars) appeared to impart statistically significant reductions in the magnitude of BCR-induced upregulation of both Bim and Bik transcripts. Such R406-induced blockade of Bim and Bik upregulation reached maxima of 2.4 and 2.91-fold reductions, respectively.

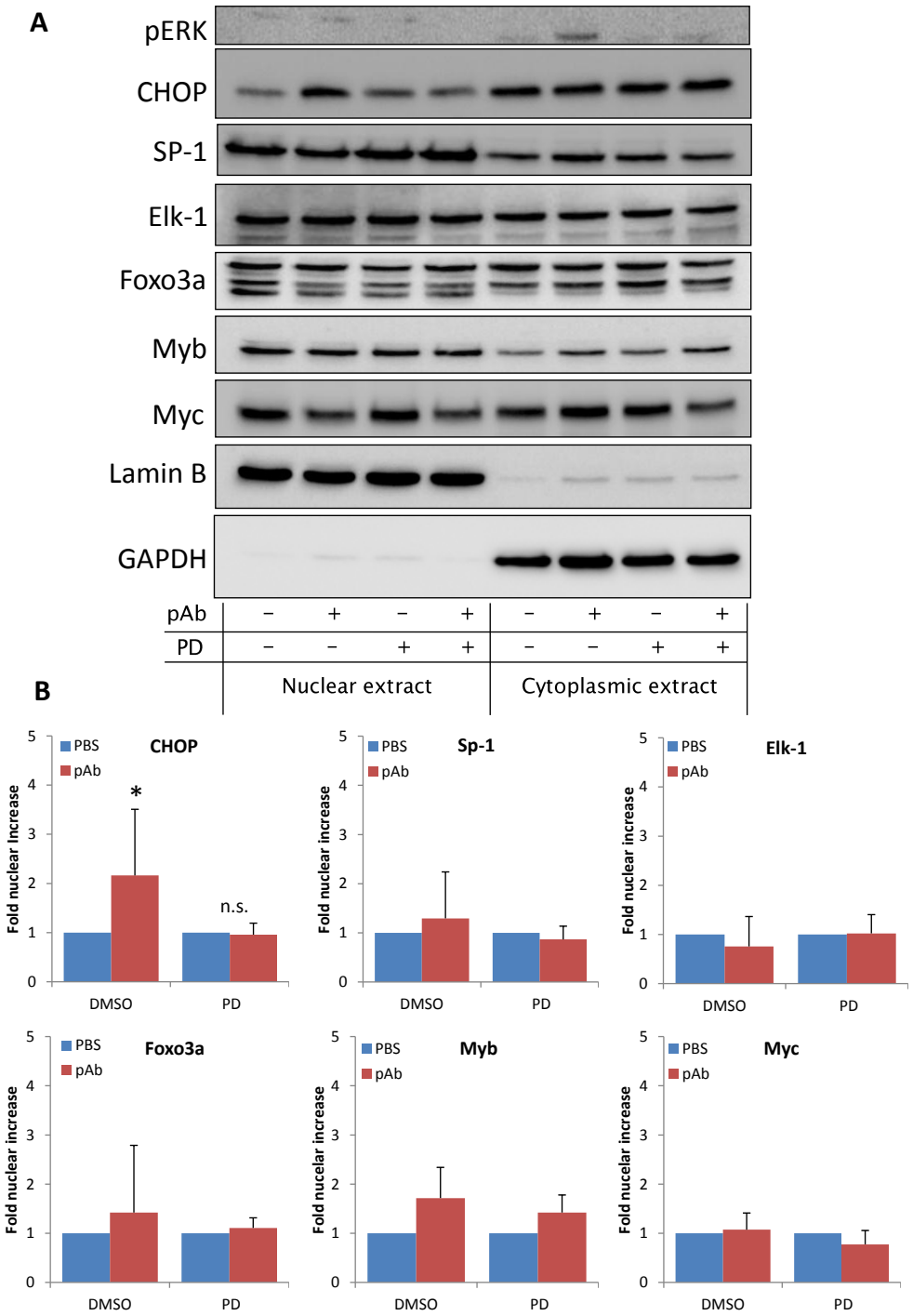

Figure 5.10 Effect of BCR stimulation and MEK inhibition upon the subcellular localisation of potential Bim promoter-interacting transcription factors

A 5x10^7 Eμ# 16 Eμ-Myc lymphoma cells per sample, were pre-incubated with 10 nM PD or an equivalent volume of DMSO for 30 minutes at 37°C, 10% CO_2. Cells were subsequently treated with 2 μg/ ml pAb ã IgM or an equivalent volume of PBS for 8 hours. Samples were harvested and nuclear and cytoplasmic extracts obtained, as outlined in materials and methods section 2.14.2, and subjected to western blotting analysis. Data is representative of values obtained from 2 independent experiments utilising four different Eμ-Myc lymphomas. **B** Data obtained in A was subjected to analysis by densitometry, as before. Transcription factor levels were corrected for Lamin B and GAPDH content for nuclear and cytoplasmic fractions, respectively. pAb ã IgM treated samples were normalised against their respective PBS-treated controls. Data represents averages of 2 independent experiments each utilising four different Eμ-Myc lymphomas. Bars represent standard deviation.

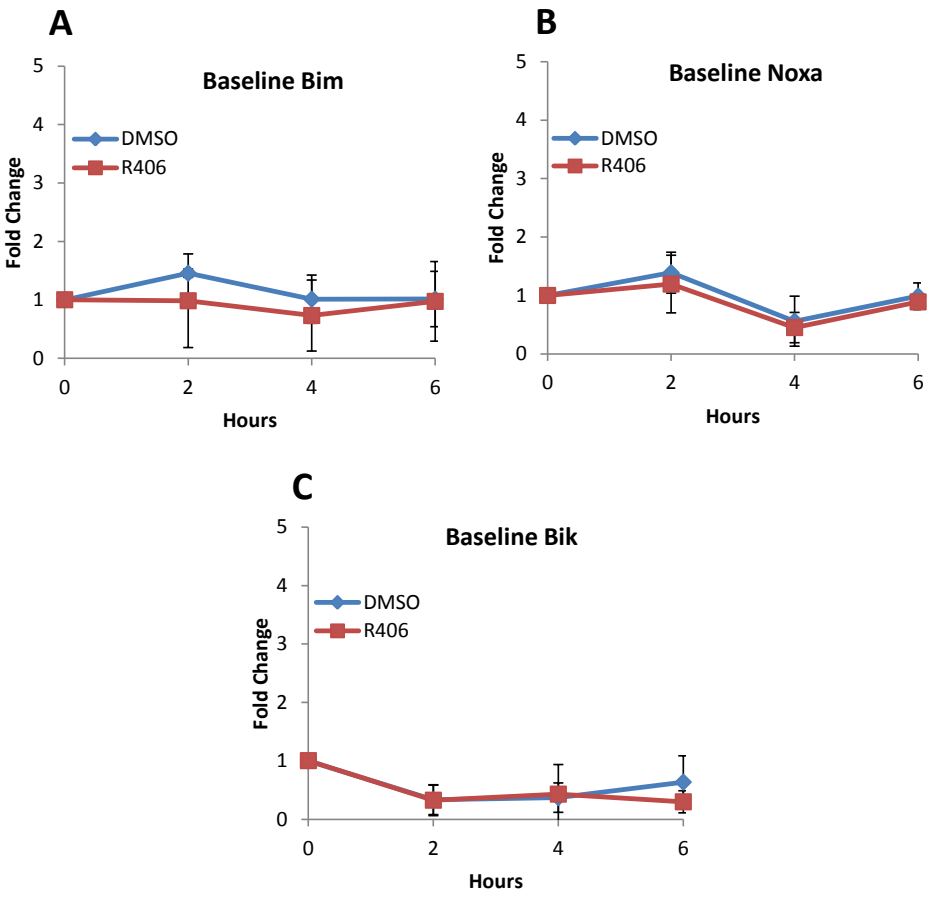

Figure 5.11 Effect of Syk inhibition upon Bim, Noxa, and Bik transcript levels
RNA was purified from $1x10^6$ Eμ-Myc lymphoma cells per sample (n=4) treated with 1 μM R406 or an equivalent volume of DMSO at the indicated time points and converted to cDNA, as outlined in materials and methods. qPCR analysis of **A** Bim, **B** Noxa and, **C** Bik transcript levels was then performed, corrected for GAPDH expression and normalised against a 0 hour time-point, as outlined previously, to observe fluctuations in baseline expression. Values represent an average of results from three different Eμ-Myc lymphomas, each using 1 cDNA performed in triplicate. Bars represent standard deviation.

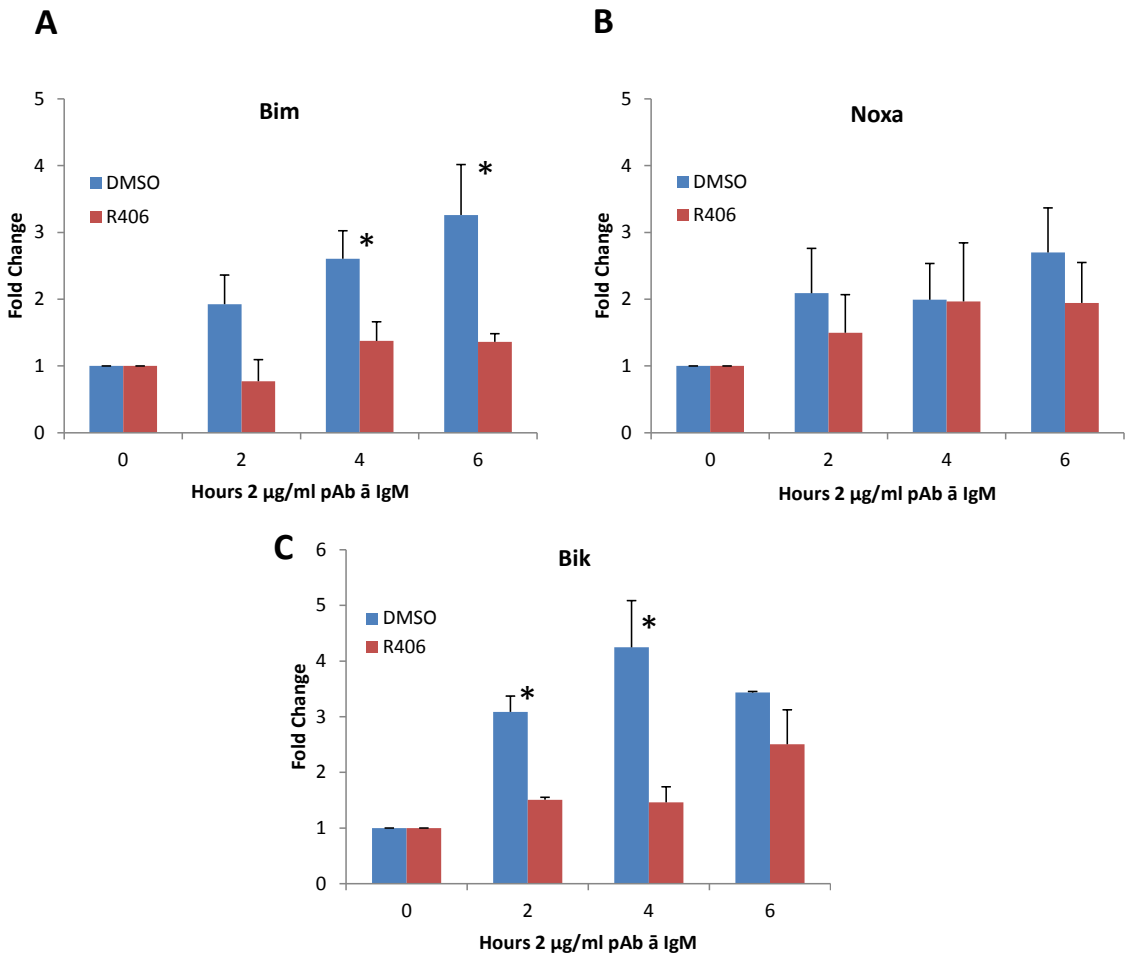

Figure 5.12 Effect of Syk inhibition upon BCR-induced transcriptional up-regulation of Bim, Noxa, and Bik expression

$1x10^6$ Eμ-Myc lymphoma cells were pre-incubated with 1 μM R406 or an equivalent volume of DMSO for 30 minutes prior to addition of 2 μg/ml pAb ã IgM or an equivalent volume of PBS. RNA was isolated at the indicated time points, converted to cDNA and utilised for qPCR analysis of **A** Bim, **B** Noxa, and **C** Bik transcript levels, as before. c(T) values were corrected for GAPDH expression and pAb a IgM treated samples normalised to their respective PBS-treated controls. Values represent the average of three different Eμ-Myc lymphomas, each performed in triplicate. Bars represent standard deviation. Asterisks denote statistically significant differences as adjudged by paired Student's T-test statistical analysis ($p<0.05$).

In contrast however, upregulation of Noxa was unaffected. Such inhibition of Bim upregulation appeared equal in magnitude to that imparted by PD, possibly implicating ERK as a potential downstream regulation of BCR signalling. Interestingly however, after 6 hours levels of BCR-induced Bik transcripts were comparable between R406 and vehicle treated cells. This observation may hint at an additional, delayed, Syk-independent mechanism linking the BCR to Bik. Taken together, these results indicate that BCR-mediated upregulation of both Bim and Bik occurs in a Syk-dependent fashion, with Bim upregulation mediated primarily via the ERK pathway.

5.4 Identifying the mechanism of BCR-induced Bcl-2 degradation

In chapter 4, we identified that BCR engagement appeared to be associated with a dramatic reduction in Bcl-2, and to a lesser-extent Mcl-1, protein levels 8 – 24 hours post-treatment. Chapter 4 demonstrated that such processing was independent of Caspase-activity, since qVD failed to prevent its degradation. Therefore, we aimed to identify whether Bcl-2 degradation was associated with Ubiquitin-dependent proteasomal targeting, and further delineate the molecular mechanism responsible for its degradation.

In order to address this, we observed the effect of the proteasome inhibitor MG132 (MG) upon the extent of BCR-mediated Bcl-2 degradation. As evident in figure 5.13A-B, pre-treatment of Eμ-Myc lymphoma cells with MG appeared to stabilise Mcl-1 levels, indicative of effective proteasomal inhibition (376). Interestingly, MG also appeared to significantly reduce the extent of Bcl-2 degradation evident downstream of BCR engagement, from 2-fold to a 1.3-fold reduction in protein level, thereby, implicating the proteasome in BCR-mediated Bcl-2 degradation. However, since only two experiments were performed, additional repeats are required to validate such observations and to allow the use of statistical testing.

Furthermore, since a loss of ERK signalling has been linked to Bcl-2 degradation downstream of TNFα-R signalling (380, 381), we wished to examine the impact of PD upon the process. It was anticipated that complete loss of ERK signalling, via PD pre-treatment, could accelerate the degradation of Bcl-2 triggered by BCR-engagement. However as evident in figure 5.13C-D, PD-mediated Ras/Raf/MEK/ERK disruption appeared to reduce the extent of Bcl-2 degradation from a 2-fold to a 1.5-fold reduction downstream of BCR signalling. Therefore, it appears that disruption of ERK signalling prevented Bcl-2 degradation to a similar extent to that of proteasome inhibition. However, it is also possible that the observed reduction in Bcl-2 protein levels, following BCR stimulation, is a consequence of reduced protein synthesis rather than specific degradation.

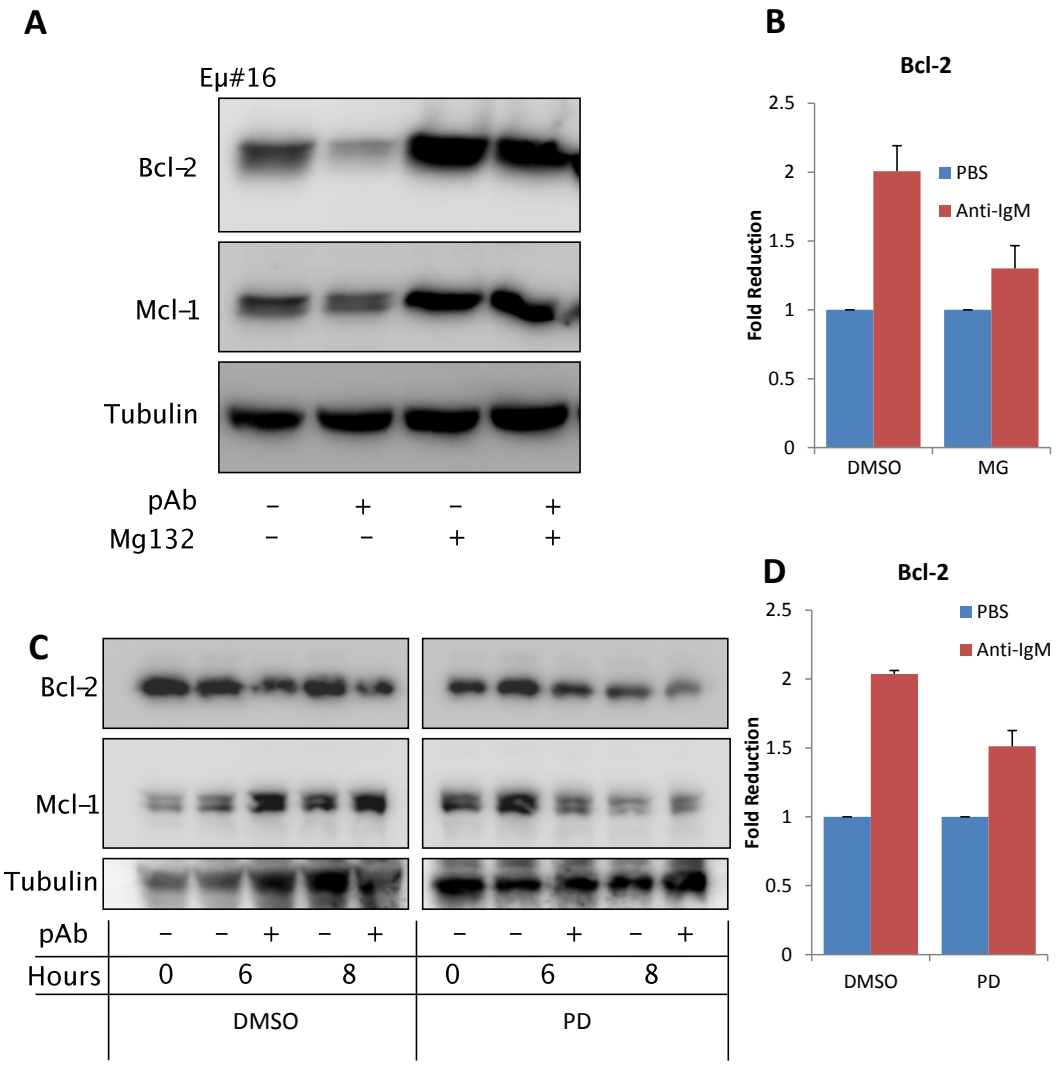

Figure 5.13 Effect of Proteasome and MEK inhibition upon BCR-induced degradation of Bcl-2

A 5x10^6 Eμ# 16 Eμ-Myc lymphoma cells per sample were incubated with 25 μM qVD-OPH and 10 μM MG, or an equivalent volume of DMSO, for 30 minutes at 37°C, 10% CO_2. Cells were subsequently treated with 2 μg/ ml pAb ā IgM or an equivalent volume of PBS for 8 hours, lysed and subjected to analysis by western blotting. Data is representative of two independent experiments utilising two different Eμ-Myc lymphomas. **B** Data obtained in **A** was subjected to analysis by densitometry, as outlined previously. Values represent an average of two independent experiments utilising two different Eμ-Myc lymphomas. Bars represent standard deviation. **C** As in **A** except cells were pre-incubated with 10 nM PD or an equivalent volume of DMSO for 30 minutes prior to addition of 2 μg/ ml pAb ā IgM for 6 or 8 hours. Data is representative of two independent experiments utilising two different Eμ-Myc lymphomas. **D** Data from **C** was subjected to analysis by densitometry as outlined in B, values represent the average of two independent experiments using two different Eμ-Myc lymphomas. Bars represent standard deviation.

Therefore,further experimentation is required to fully assess the mechanism of Bcl-2 degredation. However, it appears likely that ERK signalling not only imparts upregulation of Bim, but may also play a role in reciprocal Bcl-2 degradation downstream of BCR engagement

5.5 Further characterisation of the mode of death downstream of BCR-engagement in Bim KO Eμ-Myc lymphomas

In chapter 4, we identified that dual loss of Bim and Bik produced a level of resistance toward BCR-induced cell death comparable to over expression of a Bcl-2 transgene. However, dual loss of Bim and Noxa had no additive effect in comparison to loss of Bim alone. Since both Bik and Noxa are proposed to function equivalently, as sensitiser BH3-only proteins, we could not justify why Bik but not Noxa could directly drive BCR-induced cell death. Therefore, in an attempt to rationalise such experimental observations, we undertook further characterisation of the cell death mode invoked downstream of BCR-engagement in Bim KO Eμ-Myc lymphomas.

Initially, we wished to identify whether in the absence of Bim, BCR-induced cell death proceeded via a Caspase-dependent mechanism analogous to WT Eμ-Myc lymphomas. In order to address such a question the pan-caspase-inhibitor qVD was utilised and the relative levels of cell death assessed by flow cytometry 8 and 24 hours post anti-IgM treatment.

Interestingly, Bim KO Eμ-Myc lymphomas exhibit high levels of cell death 8 hours post-BCR engagement (30.50%) that appears to resolve and become significantly reduced after 24 hours (7.39%), as evident in figure 5.14. Such an occurrence was not reflected in WT lymphomas, which demonstrate time-dependent enhancement of the levels of cell death, as demonstrated in figure 5.14. Intriguingly, in the absence of Bim, BCR-induced cell death appeared unaffected by qVD pre-treatment at both 8 and 24-hour time points.

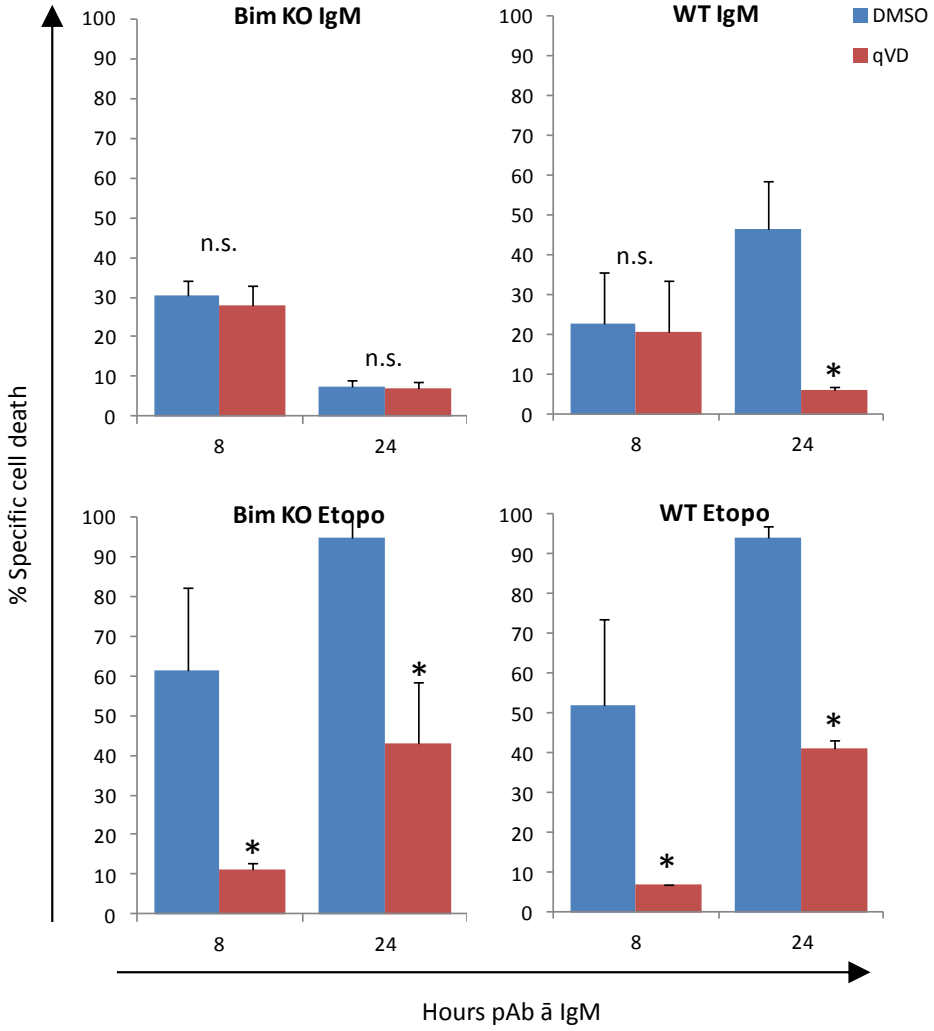

Figure 5.14 Comparative analysis of the caspase-dependent nature of BCR-induced cell death in WT and Bim KO Eμ-Myc lymphoma cells

Cells from Four WT and three Bim KO Eμ-Myc lymphomas were pre-incubated with 25 μM qVD-OPH, or an equivalent volume of DMSO, for 30 minutes at 37°C, 10% CO_2 prior to treatment with 10 μg/ml pAb ā IgM (upper panel) or 5 μg/ml Etoposide (lower panel) or an equivalent vehicle control for 8 and 24 hours. The subsequent level of cell death was then assessed by Annexin V/ PI flow cytometry. Data represents an average of three independent experiments using 4 WT and 3 Bim KO Eμ-Myc lymphomas. Bars represent standard deviation. Asterisks denote statistically significant differences as adjudged by paired Student's T-test statistical analysis ($p<0.05$). n.s. denotes non-statistically significant differences ($p>0.05$).

However, processes linking apoptotic stimuli to caspase activation remained intact in Bim KO lymphoma cells, since qVD reduced Etoposide-induced cell death 2.21-fold, as evident in figure 5.14. In contrast, qVD pre-treatment of WT Eμ-Myc lymphomas only imparted significant reductions in BCR-induced cell death after 24 hours, and not at the 8 hour time point.

These observations indicate that multiple modes of cell death may co-operate downstream of BCR engagement. It appears as though an early caspase-independent cell death occurs in the first 8 hours, followed by a Bim-dependent caspase-driven demise after 24 hours. Consequently, it appears as though BCR-induced cell death in Bim KO Eμ-Myc lymphoma cells results largely from a form of caspase-independent cell death (not blocked by qVD).

We next wished to assess whether the caspase-independent phase of BCR-induced cell death was associated with detectable MOMP. As demonstrated in figure 5.15, BCR-induced cell death is associated with extensive MOMP in WT Eμ-Myc lymphomas after 24 hours, as previously described. However, appreciable MOMP is absent entirely from Bim KO lymphoma cells and the 8-hour time point of WT Eμ-Myc lymphomas. As demonstrated in figure 5.15C-D however, both Bim KO and WT Eμ-Myc lymphomas display comparable levels of MOMP in response to Etoposide treatment after 8 hours. Therefore, it appears as though a caspase-independent cell death, not associated with any discernable MOMP, is invoked early during the response to BCR-engagement, which reverts to intrinsic apoptosis after 24 hours.

In order to further characterise the caspase-independent cell death evident in Bim KO Eμ-Myc lymphomas we screened a panel of various inhibitors for an effect upon the extent of cell death. As demonstrated in figure 5.16, inhibitors of actin polymerisation (Latrunculin B and Cytochalasin D), endosomal acidification (Concanamycin A and Bafilomycin A1), Calpains/ Cathepsins (E64d), Syk (R406), MEK (PD), and RIP appeared to have no impact upon the extent of BCR-induced cell death. Interestingly however, inhibition of both PI3K (via 3-Methyladenine (3MA)) and JNK both yielded statistically significant 2.2-fold reductions in early BCR-induced cell death in Bim KO Eμ-Myc lymphomas. In addition, as evident in figure 5.3, such a phenomenon was also evident in WT Eμ-Myc lymphomas. As 3MA-mediated blockade of Vps34 activity has been utilised as a marker of autophagy in previous studies, it was decided to observe the relative abundance of lipidated LC3 (also known as LC3 ii) in the presence of BCR engagement in Bim KO Eμ-Myc lymphomas. As evident in figure 5.17, enhancement in the abundance of LC3 ii can be observed following BCR engagement for 8 hours.

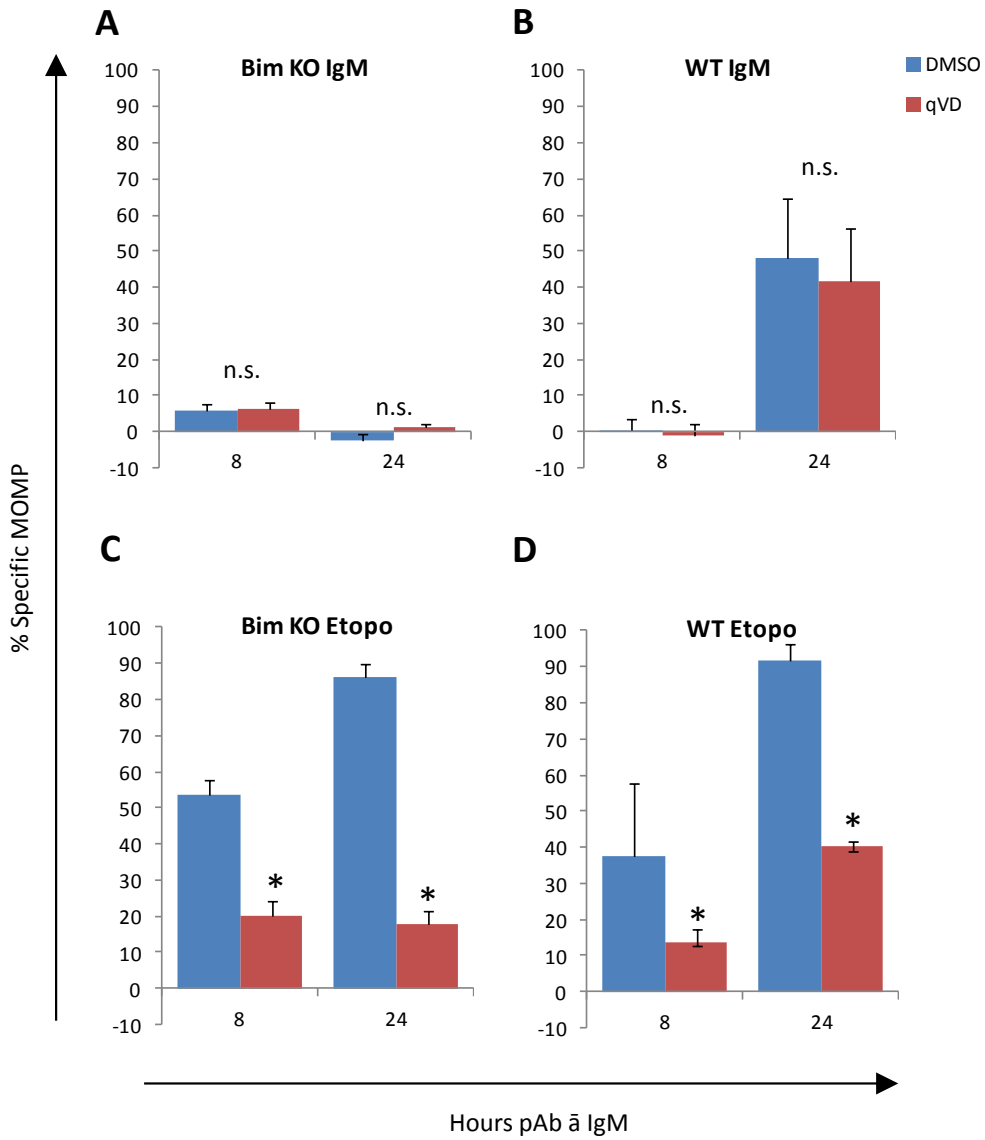

Figure 5.15 Comparative analysis of BCR-induced MOMP in WT and Bim KO Eμ-Myc lymphoma cells
Cells from Three WT and three Bim KO Eμ-Myc lymphomas were pre-incubated with 25 μM qVD-OPH, or an equivalent volume of DMSO, for 30 minutes at 37°C, 10% CO2 prior to treatment with 10 μg/ml pAb ā IgM (upper panel) or 5 μg/ml Etoposide (lower panel) or an equivalent vehicle control for 8 and 24 hours. Levels of MOMP were detected at each time point by incubation with 10 nM DiOC6 for 30 minutes at 37°C, 10% CO2 and analysis by flow cytometry. Data represents an average of three independent experiments using 4 WT and 3 Bim KO Eμ-Myc lymphomas. Bars represent standard deviation. Asterisks denote statistically significant differences as adjudged by paired Student's T-test statistical analysis ($p<0.05$). n.s. denotes non-statistically significant differences ($p>0.05$).

However, LC3 ii accumulation was only evident in 2 out of the 3 Bim KO Eμ-Myc lymphomas assessed. Therefore, further analysis of LC3 ii levels in both WT and Bim KO Eμ-Myc lymphoma cells is required.

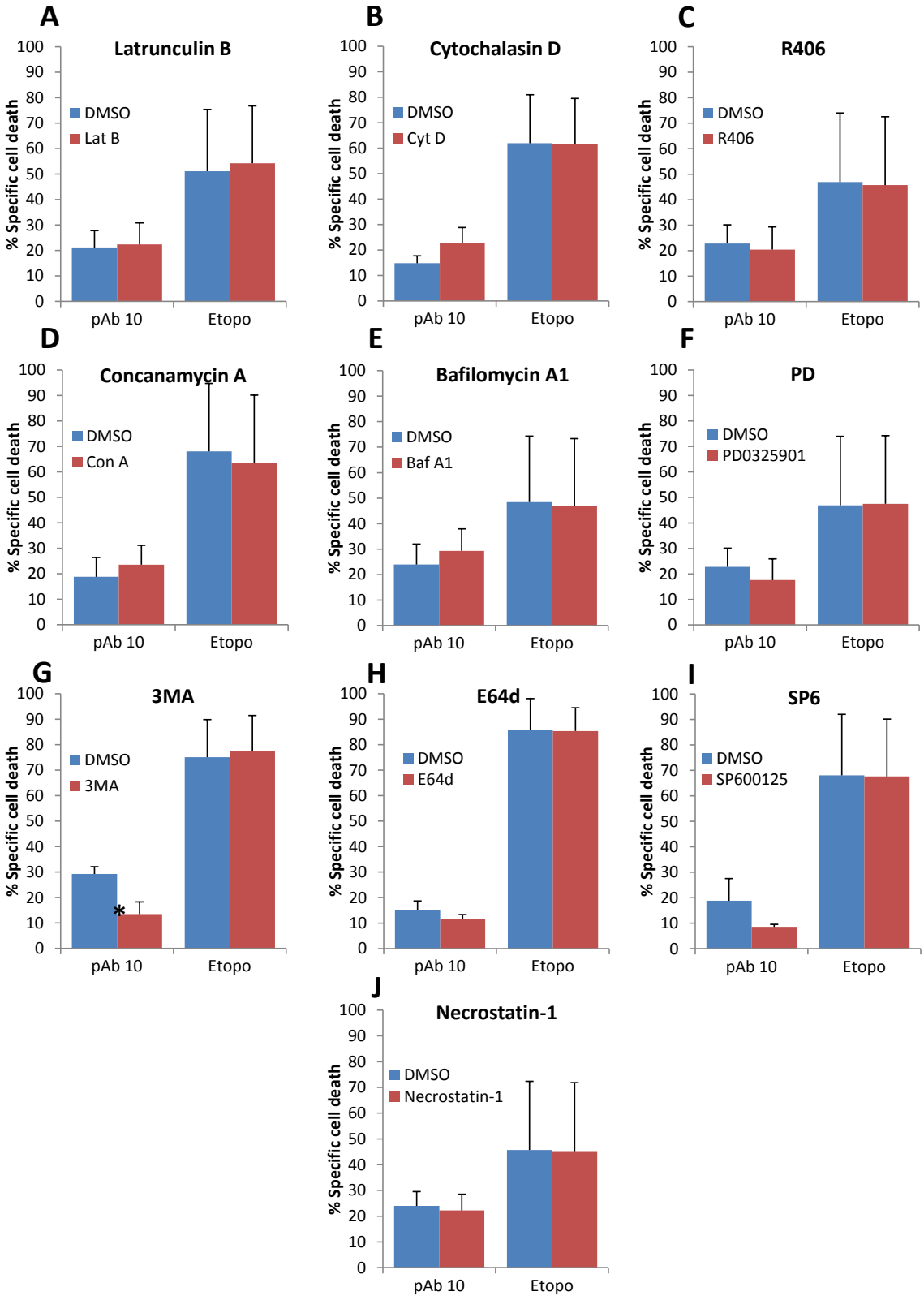

Figure 5.16 Pharmacological dissection of the BCR-induced cell death pathway in Bim KO Eμ-Myc lymphomas

Cells from three Bim KO Eμ-Myc lymphomas were pre-incubated with 10 μM Latrunculin B (Lat B), 5 μM

Cytochalasin D (Cyt D), 1 μM R406, 10 nM Concanamycin A (Con A), 50 nM Bafilomycin A1 (BAF A1), 10 nM PD, 1mM 3-methyladenine (3MA) and 100 μM E64d, 5 μM SP6, 100 μM Necrostatin-1 or vehicle control for 30 minutes at 37°C, 10% CO_2 prior to treatment with 10 μg/ml pAb ã IgM or 5μg/ml Etoposide for 8 hours. Annexin V/ PI flow cytometry was subsequently utilised to assess relative levels of cell death. Values represent an average of three independent experiments each using three different Eμ-Myc lymphomas performed in triplicate. Bars represent standard deviation. Asterisks denote a statistically significant difference as adjudged by paired Student's T-test statistical analysis ($p<0.05$).

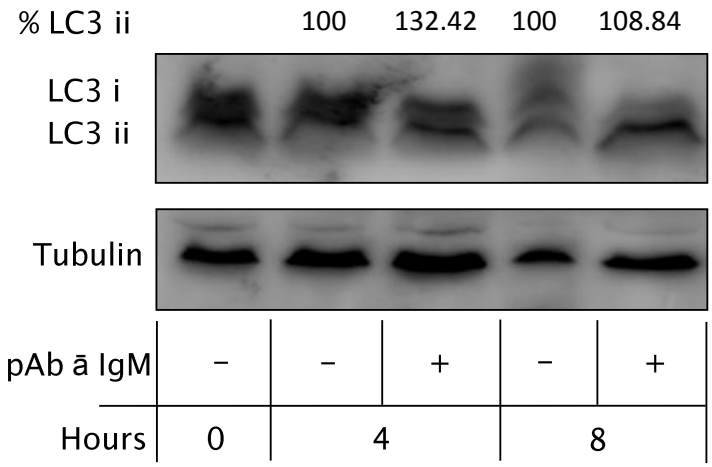

Figure 5.17 Changes in LC3 lipidation downstream of BCR engagement in Bim KO Eμ-Myc lymphoma cells

A 5x10^6 Eμ Myc Bim# 16 cells per sample were plated out a 1x10^6/ ml, in pre-equilibrated medium, and allowed to rest for 30 minutes. Cells were subsequently treated with 2 μg/ ml pAb ā IgM, or an equivalent volume of PBS, for the indicated time period, harvested by pipetting, lysed and subjected to analysis by western blotting. Western blot is representative of 2 Bim KO Eμ-Myc lymphomas (Eμ-Myc Bim# 63 and 16), Eμ-Myc Bim# D3 failed to demonstrate any LC3 ii yet still exhibited non-apoptotic cell death.

5.5.1 Investigating the role of cellular adhesion in BCR-induced cell death

Since R406-mediated Syk inhibition appeared to have little impact upon the extent of BCR-induced cell death in Bim KO Eμ-Myc lymphomas, we reasoned that the resultant caspase-independent cell death might be attributable to increased cellular adhesion downstream of BCR signalling. This idea was derived from previous studies in the group, which demonstrated that type II anti-CD20 mAbs induced a form of non-apoptotic cell death known as homotypic adhesion (392, 393).

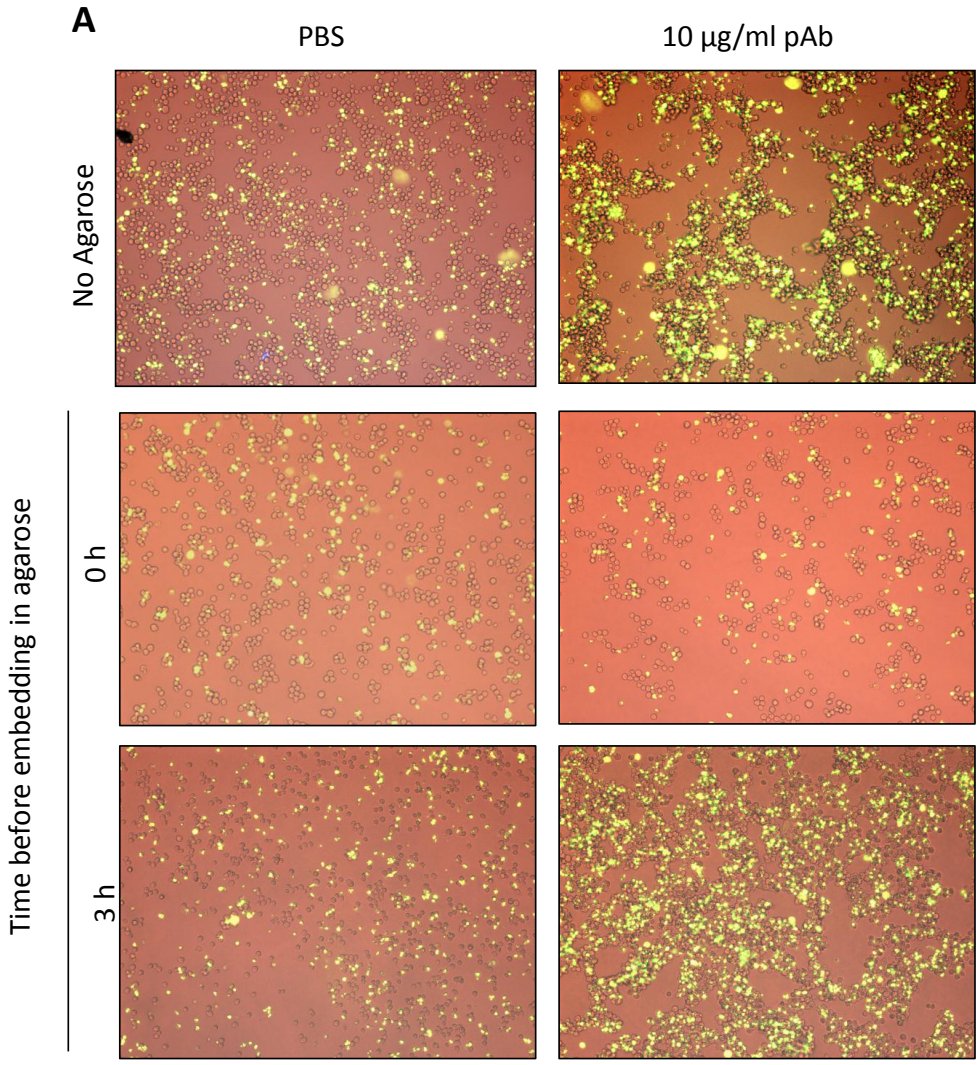
A
PBS
10 µg/ml pAb
No Agarose
Time before embedding in agarose
0 h
3 h

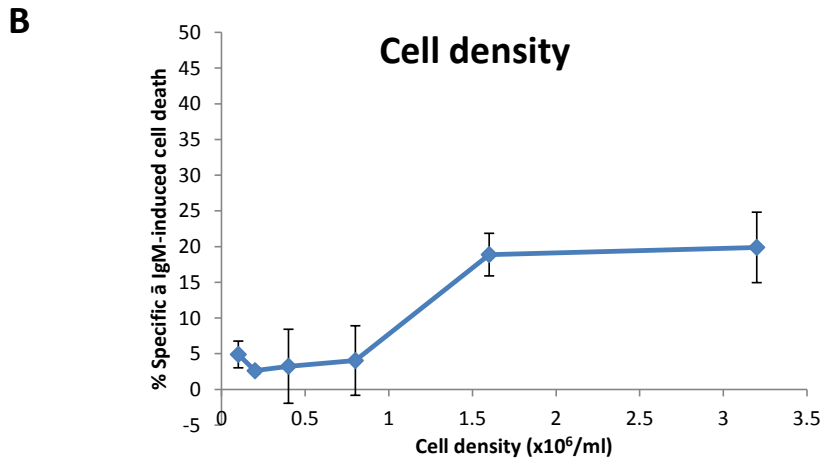
B
Cell density
% Specific ā IgM-induced cell death
Cell density (x10⁶/ml)
50
45
40
35
30
25
20
15
10
5
0
-5
0
0.5
1
1.5
2
2.5
3
3.5

Figure 5.18 Investigating the dependence of BCR-induced cell death in Bim KO Eμ-Myc lymphoma cells upon adhesion

A Eμ-Myc $Bim^{-/-}$ #63 cells were resuspended at $1.6x10^6$/ ml and rested for 30 minutes at 37°C, 10% CO_2. Cells were then treated with 10 μg/ ml pAb ã IgM or an equivalent volume of PBS and mixed 1:1 immediately, or after 3 hours, with 1% agarose-containing medium supplemented with 10 μg/ ml pAb ã IgM, or the equivalent volume of PBS, and 1 μM Sytox green dye and allowed to set on ice for 30s. Fluorescence microscopy was subsequently utilised to determine the relative levels of cell death 8 hours post-treatment. Data is representative of three independent experiments using three different Bim KO Eμ-Myc lymphomas. **B** Bim KO Eμ-Myc lymphomas were plated out at the indicated density and treated with 10 μg/ ml pAb a IgM for 8 hours. Annexin V/ PI flow cytometry was subsequently utilised to assess relative levels of cell death, as previously described. Values represent an average of three independent experiments using three different Bim KO Eμ-Myc lymphomas. Bars represent standard deviation.

To investigate this hypothesis we performed low melting point agarose embedding assays to prevent antibody-induced cellular adhesion and observed the effect upon anti-IgM induced cell death. As evident in figure 5.18, prevention of cellular adhesion by addition of Agarose immediately post-antibody application substantially reduced the extent of anti-IgM induced cell death detected by Sytox green positivity. However, addition of Agarose after cellular contacts had become established yielded comparable levels of anti-IgM-induced cell death to that in the absence of Agarose. Therefore, it appears that, at least in Bim KO Eμ-Myc lymphomas, the formation of cellular aggregates, and possible cell: cell contacts, plays a key role in generating the observed Caspase-independent cell death.

We reasoned that the extent of cellular aggregates might correlate with the extent of anti-IgM-induced cell death. To further assess this, we performed anti-IgM cell death assays utilising Bim KO Eμ-Myc lymphoma cells at varying cell densities in order to observe a correlation between cell number and the extent of cell death. As evident in figure 5.18B, the extent of anti-IgM-induced cell death does indeed correlate with cell number in Bim KO Eμ-Myc lymphomas. Such observations underline the importance of inter-cell cross-linking and the formation of cellular aggregates in caspase-independent anti-IgM-induced cellular death.

5.6 Chapter Discussion

Here it has been identified that BCR-induced cell death can be separated into two distinct phases, driven co-operatively by two mutually exclusive, temporally distinct forms of cell death.

The early BCR-driven cell death observed lacked features characteristic of apoptosis and appeared to be associated with cellular adhesion, JNK, and Vps34 activation, and possibly LC3 lipidation. Furthermore, whilst early BCR-induced cell death appears to co-operate with apoptosis in deletion of WT Eμ-Myc lymphomas, it appears to represent the sole-mediator of BCR-induced cell death in the absence of Bim expression. In addition, since Bcl-2 tg and Bik KO shBim Eμ-Myc lymphomas appear to lack early BCR-mediated cell death, it appears that both Bik and Bcl-2 have key roles in this early non-apoptotic cell death response.

Reports of the involvement of Bcl-2 family members in non-apoptotic cell death have become more widespread in recent years, with specific roles identified for Bmf in necroptosis and Bcl-2, Mcl-1, Bik, and Noxa in autophagy (262, 265, 274, 383, 384, 394). However, since inhibition of RIP failed to influence the extent of early BCR-induced cell death, a role for necroptosis downstream of BCR engagement appears unlikely (263, 264).

It is likely that these molecular signatures are, however, indicative of the occurrence of an autophagic cell death downstream of BCR engagement (particularly Vps34-dependency and LC3 lipidation) (259, 261, 267, 268, 273, 395, 396). Indeed, BCR-mediated induction of PI3K-dependent autophagic features have been observed previously, in WEHI-231 cells (275). However in contrast to previous studies, we provide evidence correlating the onset of BCR-mediated autophagy with the induction of cell death. Although a role for Vps34 and LC3 lipidation was evident following BCR engagement, inhibitors of lysosome: autophagosome fusion (Bafilomycin A1 and Concanamycin A) failed to block early BCR-induced cell death. Therefore, such results implicate Vps34-mediated redistribution of LC3 to autophagosomes as the major contributor toward early BCR-induced cell death. However, further characterisation of early BCR-induced cell death is required in order to confidently attribute such death to autophagy.

Direct induction of autophagy during early BCR-mediated cell death does; however, appear to support the proposed roles played by Bcl-2 over-expression and Bik, detailed above. Since ER-localised Bcl-2 appears to inhibit autophagy via NAF-1-dependent

interactions with Beclin-1, the observed total blockade of early and late BCR-induced cell death upon Bcl-2 over-expression may be attributable to its inhibitory roles in both autophagy and intrinsic apoptosis (267, 268, 274, 383). Furthermore, since Bik appears capable of direct antagonism of Bcl-2: Beclin-1 interactions, it is conceivable that Bik may function as a key driver of autophagy downstream of BCR engagement (383, 384). Such an occurrence would explain the apparent blockade of both apoptotic and non-apoptotic BCR-induced cell death observed upon dual loss of Bik and Bim.

Noxa is also reported to drive Beclin-1 dissociation from Mcl-1 (394). Therefore, it is unclear why Noxa does not also exert an effect on BCR-induced cell death in the absence of Bim. In fact, since BCR-induced proteasomal degradation of Bcl-2 appears far greater than that of Mcl-1, Noxa would be predicted to play a more prominent role in liberating Beclin-1 following BCR-engagement. However, whist direct Noxa-mediated Beclin-1 de-repression has been observed in human model systems, no such role has been identified in the mouse (394). It is possible that the possession of dual BH3-domains exhibited by murine Noxa may compromise its ability to drive autophagy (397). However, further study is required to precisely identify why loss of Noxa appears unable to influence non-apoptotic early BCR-induced cell death. Instead, this investigation demonstrates a key role for Bik in BCR-induced autophagic cell death, but is unable to provide a satisfactory explanation as to why Noxa plays no such role.

Interestingly, BCR-mediated autophagy appeared to occur in a JNK-dependent manner, since SP6 was able to block early BCR-induced cell death in both WT and Bim KO Eμ-Myc lymphomas. It is possible that such JNK-dependency reflects c-jun-mediated upregulation of Atg genes, including Beclin-1, as occurs in response to ceramide and oxidative stress (398, 399). Furthermore, such a role may be associated with direct JNK-mediated phosphorylation of Bcl-2 at Thr 69, Ser 70 and Ser 87, triggering dissociation of Beclin-1 (400). Whilst a clear link between anti-IgM treatment and the induction of autophagy is becoming apparent, further studies into the exact molecular regulators and biological outputs are required. Therefore, this investigation proposes a molecular mechanism linking the BCR to an early autophagic death, summarised in figure 5.19, involving JNK, Vps34, Bik, and Bcl-2.

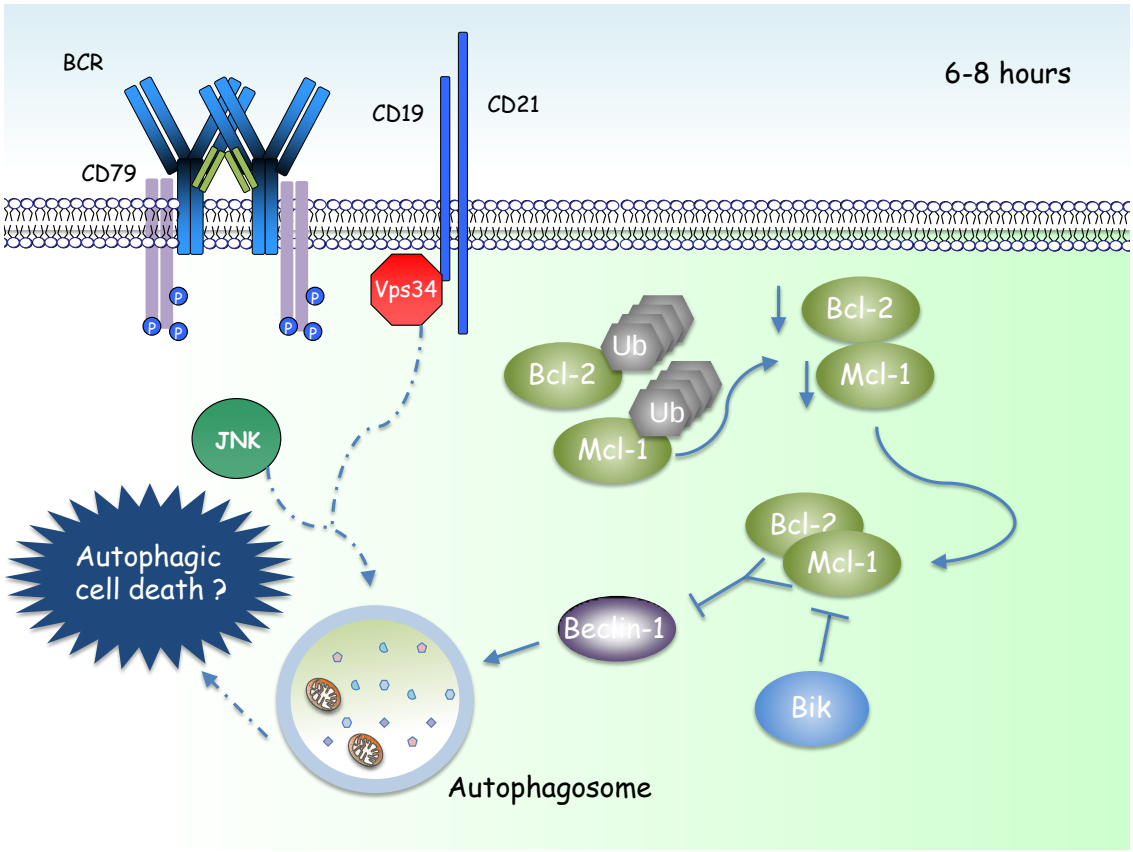

Figure 5.19 Schematic representation of the proposed model for the early phase of BCR-induced cell death.
It is proposed that a non-apoptotic form of cell death is invoked up to 8 hours post anti-IgM application, which demonstrates a dependency upon JNK and pan-PI3K activity. Preliminary data suggests the induction of an autophagic cell death via upregulation of Bik, resulting in a caspase-independent cell death. Green bars represent anti-IgM $F(ab)_2$.

In contrast, late BCR-driven cell death appears to occur with all the molecular hallmarks of intrinsic apoptosis and is largely dependent upon the activities of Bim, Noxa, and Bik, as previously described. In this chapter we have begun to elucidate the key molecular mechanisms linking the BCR to regulation of BH3-only protein transcription.

We determined that BCR-mediated Syk and ERK signalling are responsible for the well-characterised transcriptional upregulation, isoform skewing, and enhanced prosurvival binding of Bim in response to BCR engagement (230, 231). Such dependency upon Syk signals is perhaps unsurprising, since Syk activation is required for activation of virtually all BCR-induced effectors, including ERK (17, 46, 47, 99-102, 154, 155). However, the role of ERK in BCR-driven upregulation of Bim represents a novel finding and is in stark contrast to the previously described JNK dependency (230, 231). This,

however, is completely opposite to the consensus view regarding the effect of ERK-mediated Bim regulation (151, 204, 401, 402). Although ERK appears to directly phosphorylate BimEL at 3-4 distinct sites *in vivo*, all of them are associated with inhibition of Bim and prosurvival functions (151, 204, 401, 402). Perhaps the best-characterised example is ERK-driven proteasomal degradation of Bim_{EL} via Ser 69 phosphorylation (151, 204, 401, 402). However, we also demonstrate that MEK inhibition potentiates BCR-driven cell death in both WT and Myc tg lymphocytes, as is consistent with a role for MEK in the inhibition of Bim (151, 204, 401, 402). Therefore, it appears as though fundamental changes in ERK biology, either through ERK target selection, activity, or downstream effectors coincide with malignant transformation in Eμ-Myc lymphomas.

In addition, we identify that BCR-induced upregulation of Bim transcripts occurs concomitantly with ERK-dependent nuclear translocation of CHOP in Eμ-Myc cells. As CHOP represents a well-documented transcriptional regulator of Bim, it is tempting to speculate that increased nuclear CHOP may be responsible for BCR-driven Bim transactivation (211). Indeed, a putative CHOP binding site is evident within the murine Bim promoter, and ERK-dependent enhancement of CHOP activity has been reported previously in several contexts (403, 404). However, in order to confirm such a link chromatin immunoprecipitation studies and further analysis upon the CHOP-dependency of BCR-induced cell death are required.

Since CHOP-mediated Bim transactivation is most-commonly associated with ER stress, it is possible that BCR-induced activation of the UPR may be sufficient to drive Bim transactivation (211, 242, 405). Indeed, activation of an ER-stress response has been associated with BCR engagement previously (236, 373). However, since substantial ERK activity is not typically associated with ER stress, a role in BCR-induced alteration of CHOP subcellular localisation appears unlikely (406, 407).

In addition to ERK-dependent upregulation of Bim, we also observed simultaneous BCR-driven upregulation of Bik in a Syk-dependent, ERK-independent manner. Previously, BCR-mediated Bik upregulation has been identified to demonstrate dependency upon both PI3K and CN activity (223). However, whilst the role of Syk in

BCR-mediated PI3K activation is unclear, such a role requires further study (83). A role for CN, however, is distinctly possible since BCR-induced CN activation is dependent upon the activity of Syk (47, 80, 92, 110, 133, 136, 137). However, further studies are required to fully elucidate the connection between BCR signalling and Bik.

Whilst this investigation also observes substantial BCR-induced upregulation of Noxa, neither the Ras/Raf/MEK/ERK pathway nor Syk appear to contribute towards its regulation. However, remarkably little is known about Noxa transcriptional regulation. Regulation appears to occur predominantly via p53, owing to the presence of a p53 response element with the Noxa promoter, whilst additional p53-independent roles have been proposed for E2-F, HIF1α, and PKC (397). Interestingly, PKC-mediated upregulation of Noxa has been reported as a consequence of T-cell activation via anti-CD3 and anti-CD28-mediated cross linking (397, 408). However, since Syk demonstrates a key role in PLCγ2 activation downstream of BCR engagement, an analogous role for PKC in BCR-mediated Noxa upregulation appears unlikely (47, 80, 113, 118). However, it is possible that in the absence of Syk activity Btk-mediated activation of PLCγ2 may be sufficient to drive DAG production and PKC activation (47, 80, 113, 118). Therefore, combined inhibition of both Syk and Btk activity should be undertaken in the future to resolve this question.

Finally, we also demonstrate that BCR-induced degradation of Bcl-2 is associated with Ras/Raf/MEK/ERK-independent proteasomal targeting. Since inhibition of MEK signalling is responsible for Bcl-2 degradation downstream of TNF-α signalling but PD failed to enhance Bcl-2 degradation, BCR and TNFα-R-driven degradation of Bcl-2 appears to occur by different mechanisms (389, 390). Interestingly, however, Noxa has been demonstrated to directly regulate Mcl-1 protein levels by proteasomal targeting upon BH3-domain-mediated binding, in response to UV irradiation (397, 409). Therefore, it is possible that BCR-induced upregulation of Noxa facilitates the observed degradation of Mcl-1. In order to assess the relative contribution of Noxa in this process, BCR-induced Mcl-1 degradation should be studied in Noxa KO Eμ-Myc cells. It is, therefore, possible that such activities are reflected across the sensitiser BH3-only protein sub-family. If such an occurrence were true, it may further explain the function of Bik downstream of the BCR. However, further studies are required to

assess this. It is also possible that BCR-induced Bcl-2 degradation is attributable to a reduction in the rate of Bcl-2 synthesis. In order to address such a notion pulse-chase experiments should be carried out in the future. Taken together such observations allow this investigation to propose a mechanism by which BCR signalling is linked to upregulation of multiple BH3-only proteins, as evident in figure 5.20.

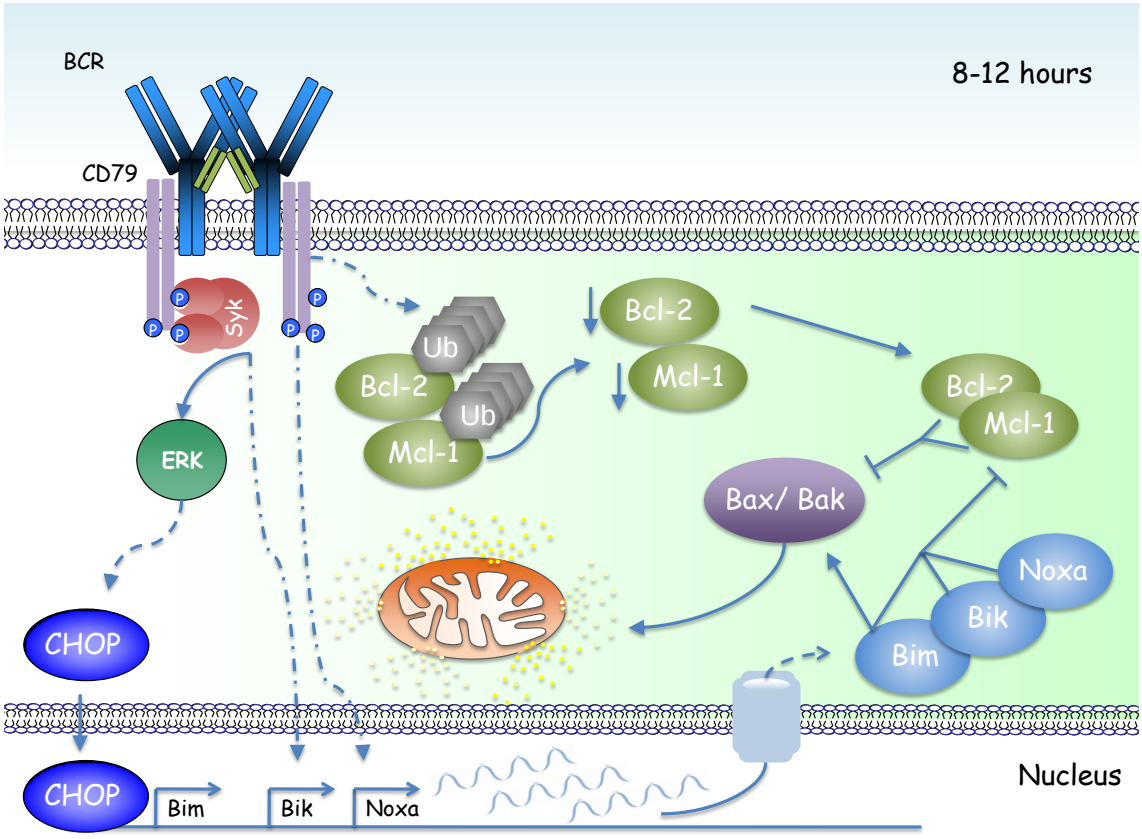

Figure 5.20 Schematic representation of the molecular mechanism of BCR-induced apoptosis
BCR-induced cell death appears associated with upregulation of the BH3-only proteins Bim, Bik, and Noxa and instigates an intrinsic apoptotic cell death 8-12 hours post-stimulation. Bim represents the major driver of BCR-induced apoptosis, with a minor role played by Bik. In contrast, the role of Noxa appears restricted to a sensitisation function, possibly via Mcl-1 binding, therefore reducing the apoptotic threshold. Green bars represent anti-IgM $F(ab)_2$.

Subsequently, it is proposed that BCR-driven MOMP engages caspase-9 and invokes the effector caspase activation profile summarised in figure 5.21. Although caspase-2 auto-processing was evident following BCR engagement, such events appeared to occur after caspase-9 activation. Therefore, such data implies that caspase-9 plays the major initiating role downstream of BCR engagement.

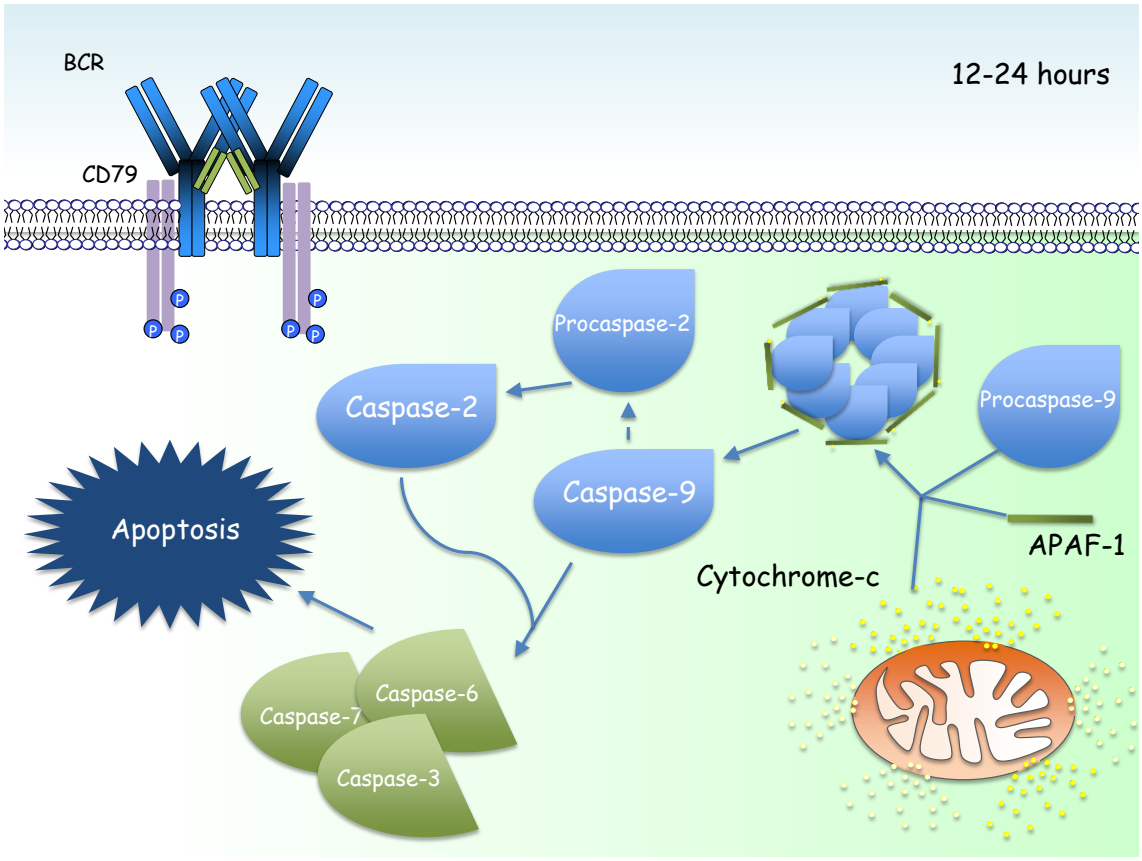

Figure 5.21 Schematic representation of BCR-induced caspase activation

Intrinsic apoptosis-driven MOMP appears to initially drive the processing, and therefore activation, of procaspases-9 which links BCR-driven MOMP to activation of effector caspases 3, 6, and 7. The activation of caspase-2 appears to occur via an auto-processing mechanism which resides downstream of caspase-9 activation. However, the exact temporal spacing and molecular dependency of the response requires further study to confirm such details. Green bars represent anti-IgM $F(ab)_2$.

In summary, in this chapter we demonstrate that BCR-engagement of Eμ-Myc lymphomas drives a bi-phasic cell death response culminating in the early induction of autophagy which later succumbs to intrinsic apoptosis. We also demonstrate that BCR-mediated Bim upregulation is dependent upon ERK activity and may be associated with regulation of CHOP function. Finally, we demonstrate that Bik upregulation is dependent upon Syk activity, possibly due to a link with CN-dependent NFAT activity.

Chapter 6 *A*nalysis of the effect of TGF-β upon BH3-only proteins in Eμ-Myc lymphomas

6.1 Chapter Introduction

Upon its discovery TGF-β was identified as a prolific transforming cytokine capable of enhancing mesenchymal cell proliferation. Subsequently, however, significant pleiotropism in biological activity has become apparent since epithelial, endothelial, and haematopoietic cell lineages often exhibit growth arrest or apoptotic responses toward TGF-β (278, 279). Consequently, TGF-β appears to play a key role in B-lymphocyte biology. For instance, TGF-β-mediated SMAD activation appears to play a central role in deletion of low affinity post-SHM centroblasts in co-operation with a loss of antigen mediated-BCR signals (277, 281, 378, 379). In addition, macrophage-mediated secretion of TGF-β into neoplastic sites surrounding malignant B-lymphocytes appears to drive p53-dependent cellular senescence therefore, slowing tumour growth (282). Taken together, such results implicate TGF-β mediated apoptosis and growth arrest as key processes fundamental to the biology of both malignant and normal B-lymphocytes.

Mechanistically, TGF-β-driven apoptosis appears associated with SMAD3/4-dependent engagement of intrinsic apoptosis and caspase activation pathways in a vast array of cell types (281, 296-301). Therefore, by definition, Bcl-2 members appear to play central regulatory roles downstream of TGF-β. In particular the BH3-only protein Bim appears important (298-302).

Whilst the exact mechanism of TGF-β-mediated up-regulation of Bim appears largely cell-type-specific, most cells employ Foxc1, JNK, and p38-dependent transcriptional upregulation as a key initiating step (286, 294, 296, 298-301). Additionally, in lymphocytes concomitant upregulation of both Bik and Bmf appear to co-operate with Bim and significantly contribute toward TGF-β-induced cell death (281, 298, 299). However, whilst vital in lymphoid lineages, Bmf appears largely dispensable for TGF-β driven apoptosis in gastric carcinoma cells (298, 299). Such a role downstream of TGF-β in lymphocytes may, to some-extent, account for the observed elevation in plasma

cell levels and hypergammaglobulinaemia in Bmf deficient mice, possibly attributable to impaired TGF-β-facilitated deletion of low-affinity centroblasts (235).

Additional roles have also been proposed for both Bad and Bid during TGF-β-mediated apoptosis, via proteolytic processing to more pro-apoptotic forms (297, 303). Although proteolytic activation of Bid is well documented, activation of Bad via this mechanism remains controversial (224). However, since experiments correlating genetic loss of Bid and Bad to an innate resistance toward TGF-β have yet to be performed, their role remains unconfirmed.

Such differential, cell-type-specific roles for BH3-only proteins underline a common theme in TGF-β signalling research, the concept of cell-type-specific pleiotropism. It is currently believed that such a phenomenon is largely attributable to the DNA binding activity of SMADs, which bind targets in collaboration with additional co-factors. Therefore, target selection is extensively dictated by the expression profiles of additional transcription factors, which differ significantly between cell-types (277).

It was rationalised that different stimuli may induce apoptotic cell death via stimulus-specific recruitment of BH3-only proteins, utilising alternate molecular signalling pathways, and not via activation of a common pathway. Therefore, it was anticipated that TGF-β and BCR-stimulation may demonstrate differential dependency upon individual BH3-only proteins in order to invoke maximal apoptosis. Since macrophage-secreted TGF-β appears to drive senescence in Eμ-Myc lymphomas in a p53-dependent manner, we hypothesised that TGF-β may also evoke p53-dependent apoptosis via upregulation of Puma (282). Therefore, in order to observe specific differences in apoptotic signalling between BCR and TGF-β-driven cell death, we characterised TGF-β-induced cell death and its specific molecular pathway.

6.2 Characterisation of TGF-β-induced cell death in Eμ-Myc lymphoma cells

Initially, Annexin V/ PI death assays were performed in order to observe the effect of TGF-β upon Eμ-Myc lymphoma cell line viability. As evident in figure 6.1A, Eμ-Myc lymphomas exhibited dose-dependent, TGF-β-induced cell death responses that

displayed gradual accumulation of dead cells to a maximum after 24 hours. Interestingly, inter-cell-line variance in the magnitude and kinetics of the response appeared less profound upon TGF-β treatment, in comparison to BCR stimulation. Such an occurrence is, perhaps, indicative of a more highly conserved pathway linking TGF-β to cell death between Eμ-Myc lymphoma cell lines, in comparison to BCR stimulation.

Furthermore, in order to confirm that TGF-β-induced cell death was attributable to TβR-signalling in Eμ-Myc lymphoma cell lines, and not as a consequence of off-target effects, the impact of the ALK5 inhibitor SB431542 was assessed. As evident in figure 6.1B, SB431542 pre-treatment led to the statistically significant attenuation of TGF-β-induced cell death in Eμ-Myc lymphoma cells. However, such attenuation was not attributable to a general effect on cell death, since the extent of Etoposide-induced cell death remained unaffected. Furthermore, TGF-β-mediated TβR dimerisation appeared effectively linked to downstream SMAD signalling pathways in Eμ-Myc lymphoma cell lines, since extensive SMAD2 phosphorylation was evident post TGF-β application, as demonstrated in figure 6.1C. Taken together, such observations demonstrate that TGF-β-mediated cell death appears dependent upon the kinase activity of type I TβRs and is associated with activation of downstream SMAD signalling pathways in Eμ-Myc lymphoma cell lines. Therefore, it was deemed that addition of TGF-β to Eμ-Myc lymphomas invoked signalling responses comparable to those previously described and, therefore, was an appropriate model in which to study TGF-β-induced cell death.

Next it was deemed necessary to confirm that TGF-β induced an apoptotic cellular death in Eμ-Myc lymphoma cell lines, as has been widely described in cells of the lymphoid lineage. Therefore, the occurrence of molecular characteristics of apoptosis, namely caspase activity and Bcl-2-mediated inhibition, was assessed in Eμ-Myc lymphoma cell lines following TGF-β treatment. As evident in figure 6.2, a statistically significant accumulation of cPARP was evident following TGF-β treatment, alongside reciprocal decreases in the levels of uPARP.

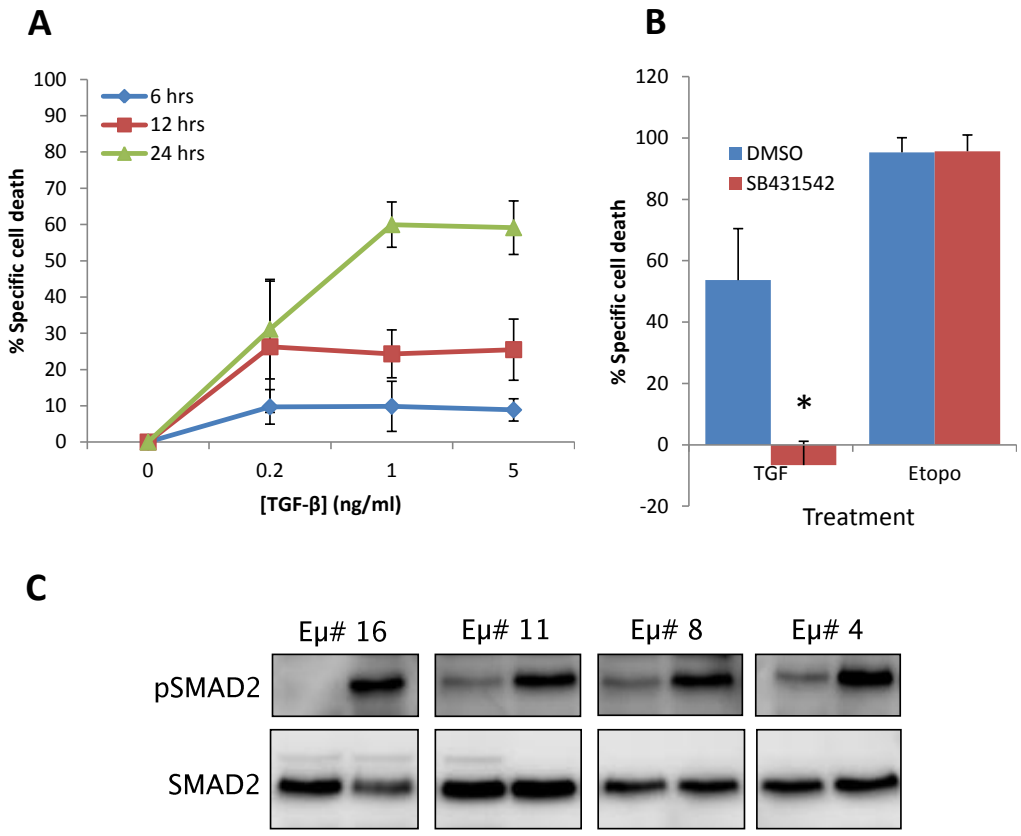

Figure 6.1 Assessing the impact of TGF-β upon Eμ-Myc lymphoma viability

A Eμ-Myc lymphoma cells were plated at 1.6x10^6/ ml and treated with TGF-β, at the indicated final concentration, or an equivalent volume of PBS for 6, 12 and 24 hours. Subsequently, cells were harvested by pipetting and subjected to Annexin V^{FITC}/ PI flow cytometry, as outlined previously. Levels of specific cell death above background were calculated as in materials and methods section 2.13.1.Values represent averages from 4 WT Eμ-lymphoma cell lines (Eμ# 16, 11, 8, and 4) each of which reflects the average of three independent experiments, each performed in triplicate. Bars represent standard deviation. **B** Eμ-Myc lymphomas were treated as in A, except cells were pre-incubated with 10 μM SB431542 (red columns), or an equivalent volume of DMSO (blue columns), for 30 minutes prior to treatment with 5 ng/ ml TGF-β or 5 μg/ ml Etoposide. Columns represent average values obtained from 3 WT Eμ-Myc lymphoma cell lines (Eμ# 16, 8, and 4) each of which was an average of three independent experiments, each performed in triplicate. Bars represent standard deviation. Asterisks denote a statistically significant difference as adjudged by paired Student's T-test statistical analysis ($p<0.05$). **C** 5x10^6 Eμ# 16, 11, 8, or 4 lymphoma cells were plated at 1x10^6/ ml and incubated with 5 ng/ ml TGF-β, or an equivalent volume of PBS, for 6 hours and lysates prepared. Western blotting analysis was then undertaken to examine the effect of TGF-β upon SMAD2 phosphorylation.

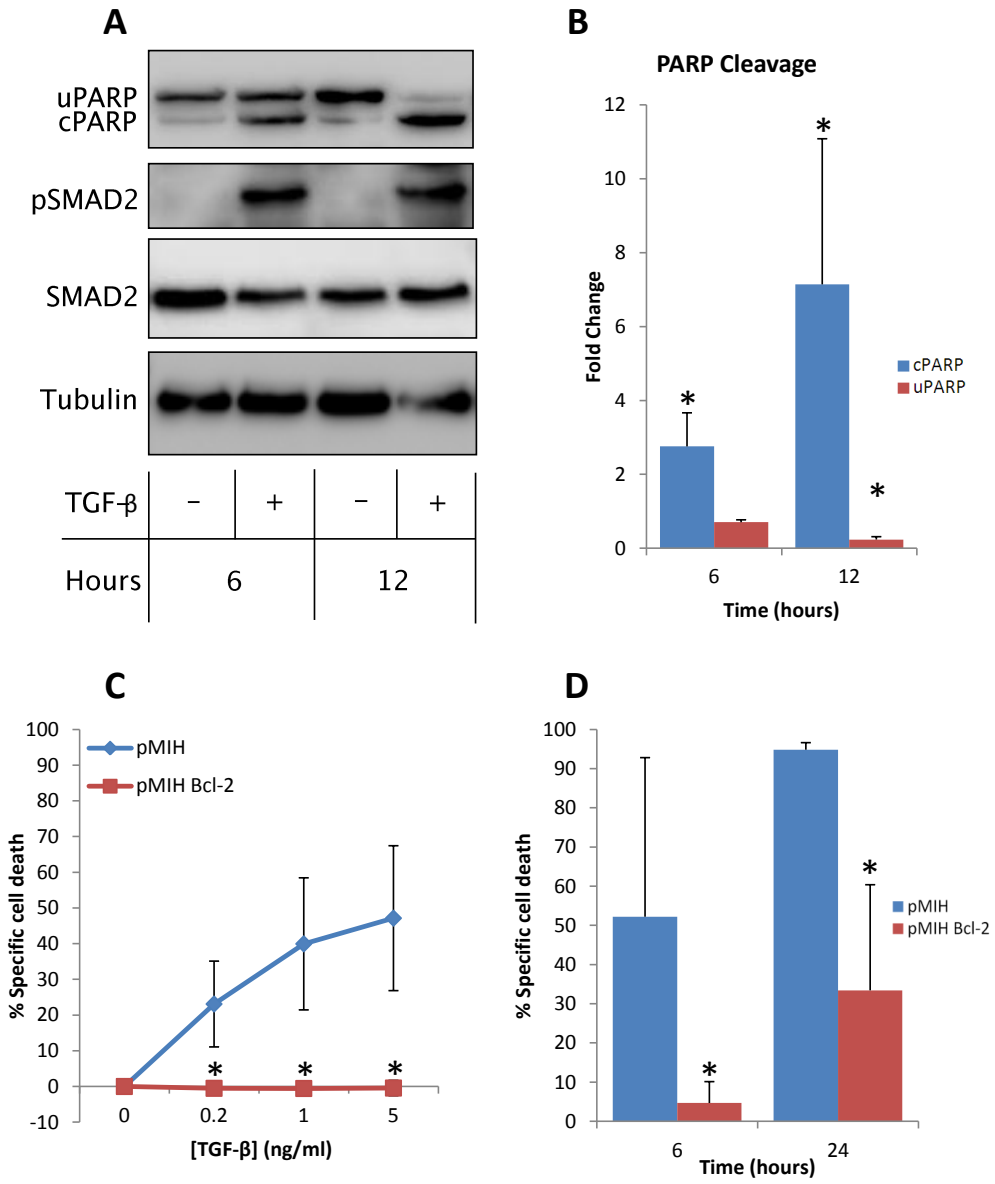

Figure 6.2 Characterising the nature of TGF-β-induced cell death in Eμ-Myc lymphoma cells

A 5x10^6 Eμ# 4 lymphoma cells were plated at 1x10^6/ ml and incubated with 5 ng/ ml TGF-β, or an equivalent volume of PBS, for 6 or 12 hours and lysates prepared. Western blotting analysis was then undertaken to examine the extent of PARP cleavage downstream of TGF-β-mediated SMAD signalling. The Western blots shown are representative of three independent experiments using three different Eμ-Myc lymphomas. **B** Western blots of TGF-β-induced PARP cleavage, exemplified in A, were subjected to densitometry and the relative proportion of cPARP and uPARP calculated, corrected for Tubulin expression and normalised against respective PBS-treated controls. Values represent the average of three independent experiments using Eμ# 16, 8, and 4 lymphomas; bars represent standard deviation. **C** pMIH (blue lines) or pMIH Bcl-2 (red lines) transduced Eμ-Myc lymphoma cells were plated at 1.6x10^6/ ml and treated with the indicated concentration of TGF-β or an equivalent volume of PBS for 24 hours. Subsequently, cells were harvested by pipetting and subjected to Annexin V^{FITC}/ PI flow cytometry, as outlined previously. Levels of specific cell death above background were calculated as in materials and methods section 2.13.1.Values represent averages from Eμ# 16, 15, 8, and 4 each of which reflects the average of three independent experiments, each performed in triplicate. **D** As in **C** except cells were treated with 5 μg/ ml Etoposide for 6 or 24 hours. Bars represent standard deviation. Asterisks denote a statistically significant difference as adjudged by paired student's T-test statistical analysis ($p<0.05$).

Since PARP cleavage represents a classical marker of effector caspase activity, such observations indicate that TGF-β-induced cell death invokes significant levels of caspase activity in Eμ-Myc lymphoma cell lines.

In order to examine whether TGF-β induced cell death via the intrinsic apoptotic pathway, the previously described Bcl-2 tg Eμ-Myc lymphoma cell lines were utilised. Bcl-2 tg Eμ-Myc lymphoma cells appeared deficient in TGF-β-mediated cell death in comparison to empty vector transduced cell-lines. Since a statistically significant attenuation of TGF-β-induced cell death was evident at all concentrations, it appears as though Bcl-2 is capable of completely blocking TGF-β-induced cell death. Such observations are indicative of a complete block of the intrinsic apoptotic pathway, since significant attenuation of cell death was also evident following Etoposide treatment. Taken together, such results indicate that TGF-β signalling invokes cell death in Eμ-Myc lymphoma cells via activation of the intrinsic apoptotic pathway resulting in caspase activation.

6.3 Analysing the impact of TGF-β-induced cell death upon Bcl-2 family expression levels

Since Bcl-2 family members play central regulatory roles in intrinsic apoptosis, their expression levels were subsequently assessed downstream of TGF-β signalling. As evident in figure 6.3, significant enhancement of Bim, Bmf, Noxa and Puma transcript levels were evident downstream of TGF-β signalling in Eμ-Myc lymphoma cell lines. However, whilst sustained upregulation of Bmf and Puma was evident throughout the treatment period, to a maximum of 3.3 and 1.5-fold respectively, induction of Bim and Noxa appeared transient (present only 2 hours post-TGF-β application) and therefore, unlikely to play a key role.

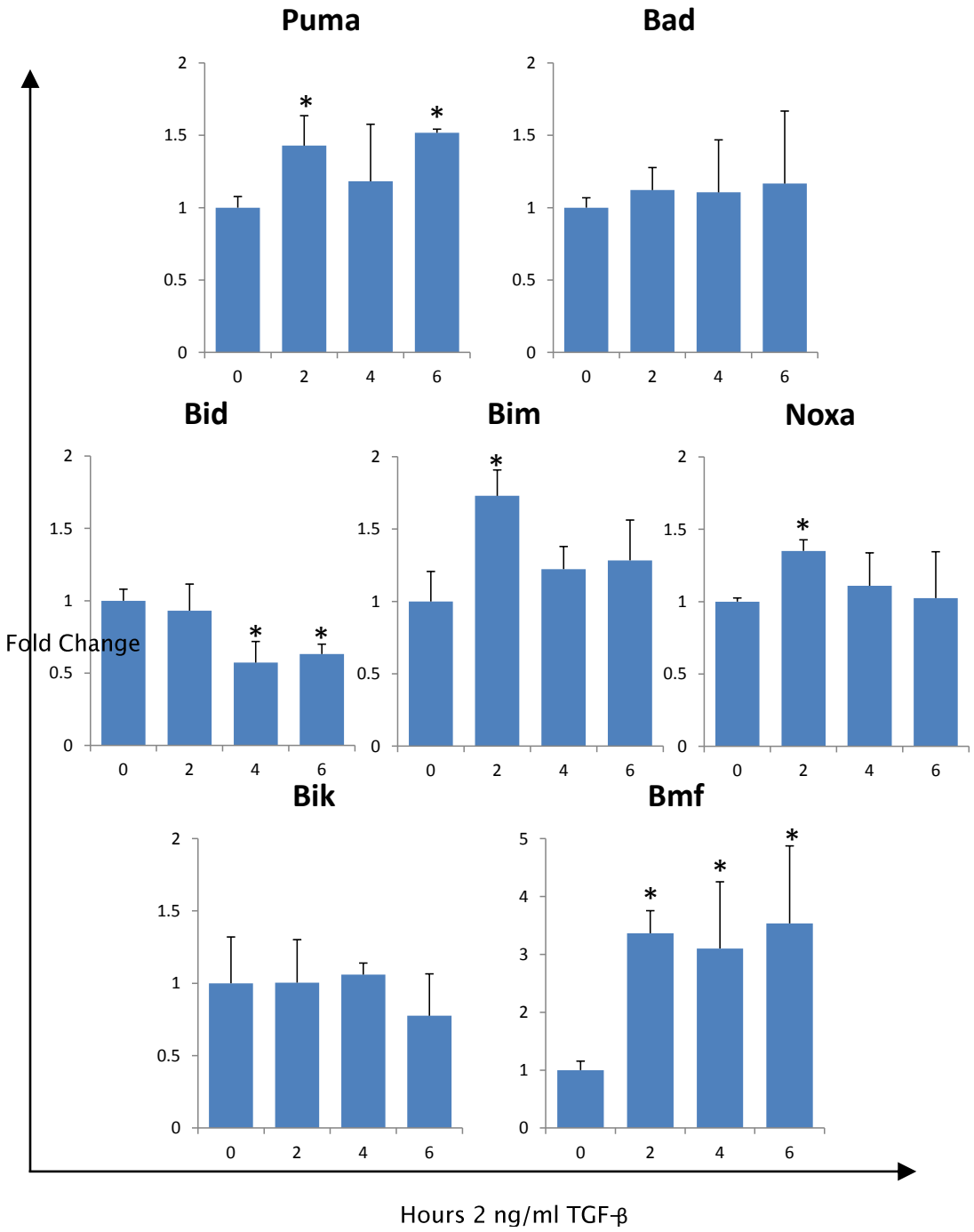

Figure 6.3 Examining the impact of TGF-β-mediated SMAD signalling upon transcript levels of BH3-only proteins in Eμ-Myc lymphoma cells

Three Eμ-Myc lymphoma cell lines (Eμ# 4, 8, and 16) were treated with either 2 ng/ml TGF-β or an equivalent volume of PBS, for the indicated time period, cDNA obtained, and subjected to qPCR analysis of BH3-only protein transcript levels, as outlined in chapter 4. Columns represent the average of values obtained from Eμ# 16, 8, and 4, each of which reflects a single experiment performed in triplicate. Bars represent standard deviation. Asterisks denote statistically significant differences as adjudged by paired Student's T-test statistical analysis ($p<0.05$).

Such small but consistent increases in Puma transcript levels were also observed in a panel of human BL cell-lines treated with TGF-β, as outlined in appendix A18, yielding between 1.8 and 3-fold induction (data kindly provided by Dr L. Spender).

Contrastingly, the expression of Bid seemed repressed downstream of TGF-β signalling, possibly via some form of negative regulation. In summary, TGF-β treatment appears to drive upregulation of 4 BH3-only protein transcripts (Bim, Noxa, Bmf, and Puma) however, only Bmf and Puma upregulation was evident at time points greater than 1 hour. Therefore, both Bmf and Puma may substantially contribute toward TGF-β-induced apoptosis in Eμ-Myc lymphoma cells.

In contrast, TGF-β signalling appeared to have relatively little impact upon the extent of prosurvival Bcl-2 family member expression. As evident in figure 6.4, TGF-β appeared to invoke only transient, non-statistically significant increases in both Bcl-w and A1 4 hours post-TGF-β treatment. However, a statistically significant upregulation of Bcl-2 was evident 6 hours post-TGF-β treatment. It is possible that sustained Bcl-2 upregulation may be evident at later time-points however, such studies were not performed since the induction of TGF-β-induced cell death was recorded after only 6 hours. Therefore, it was assumed that the major changes responsible for the induction of cell death would have taken place prior to the 6 hour time-point. In contrast, relatively consistent levels of the remaining family members were recorded throughout the treatment period.

Therefore, TGF-β signalling appears primarily linked to upregulation of Bim, Bmf, and Puma transcripts in Eμ-Myc lymphoma cell lines. However, in order to further assess their relative contribution, western blotting analysis of BH3-only protein levels following TGF-β-treatment was undertaken. As evident in figure 6.5, TGF-β appeared to invoke statistically significant upregulation of both Puma and Bmf expression 1.8 and 2.7-fold, respectively. Furthermore, TGF-β-driven upregulation of Puma appeared to coincide with SMAD2 phosphorylation, as evident in figure 6.5C. However, little change could be detected in the remaining BH3-only protein levels, including Bim.

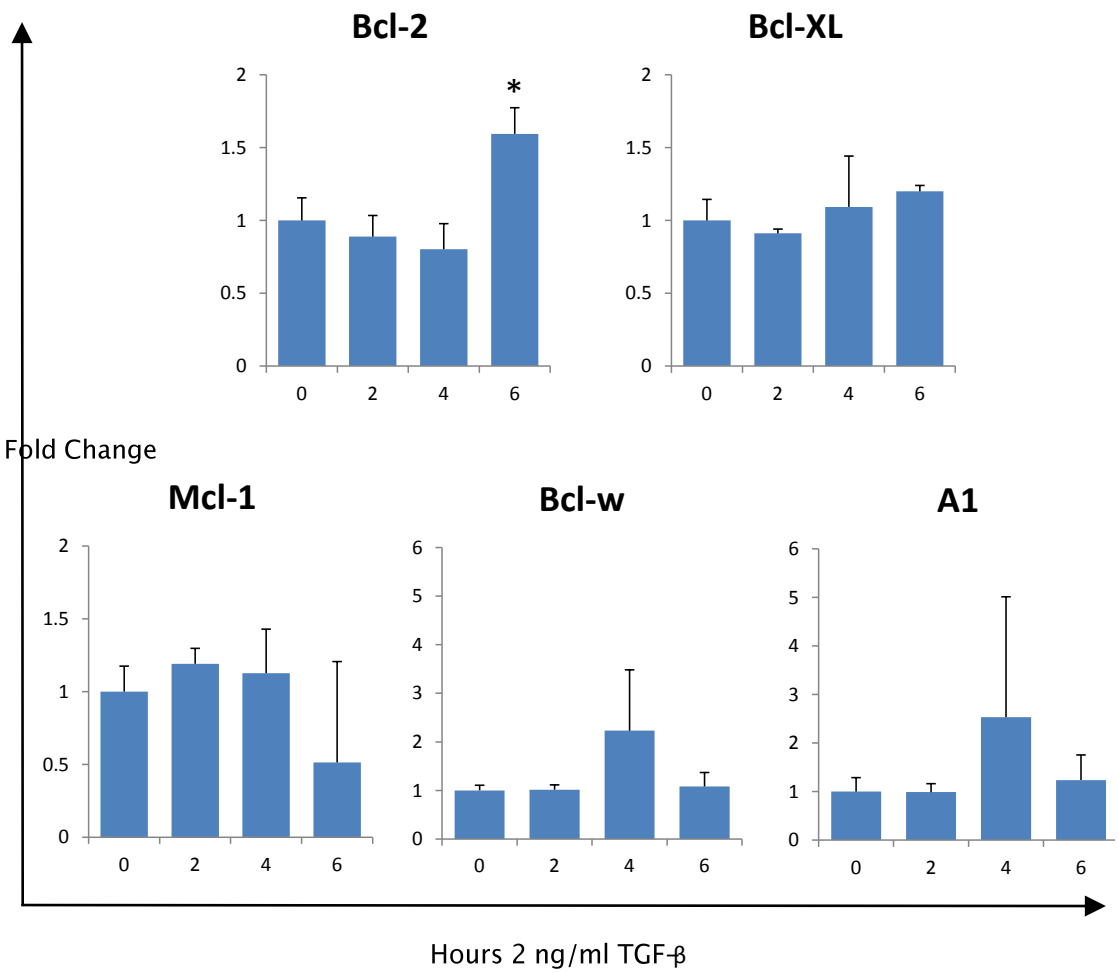

Figure 6.4 Examining the impact of TGF-β-mediated SMAD signalling upon transcript levels of prosurvival Bcl-2 family members in Eμ-Myc lymphoma cells

Three Eμ-Myc lymphoma cell lines (Eμ# 4, 8, and 16) were treated with either 2 ng/ml TGF-β, or an equivalent volume of PBS, for the indicated time period, cDNA obtained, and subjected to qPCR analysis of prosurvival Bcl-2 family member transcript levels, as outlined in chapter 4. Columns represent the average of values obtained from Eμ# 16, 8, and 4 lymphomas each of which reflects a single experiment performed in triplicate. Bars represent standard deviation. Asterisks denote statistically significant differences as adjudged by paired Student's T-test statistical analysis ($p<0.05$).

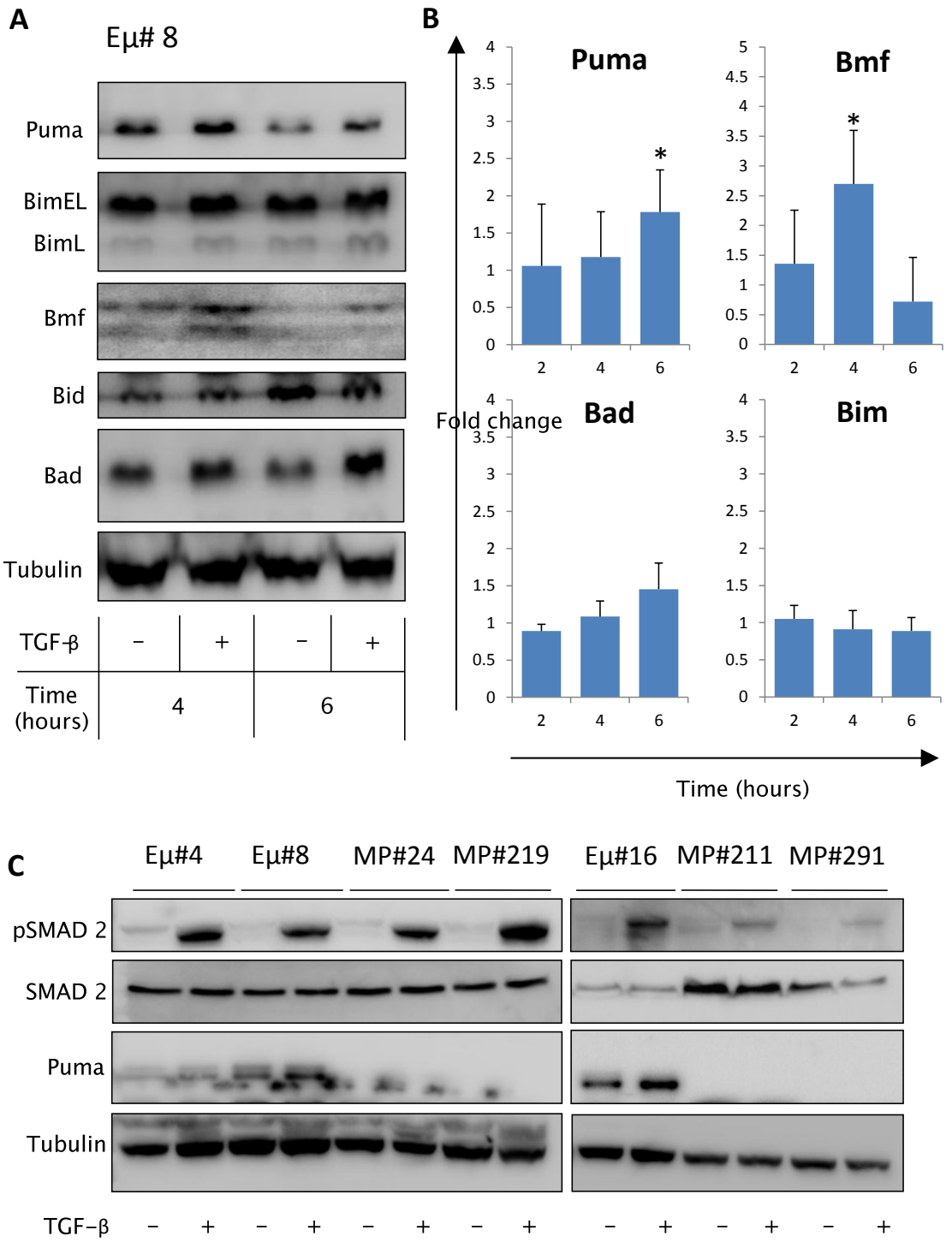

Figure 6.5 Assessing the impact of TGF-β-mediated SMAD signalling upon BH3-only protein levels in Eμ-Myc lymphoma cells

A 5x10^6 Eμ# 8 Eμ-Myc lymphoma cells were plated at 1x10^6/ ml and incubated with 5 ng/ ml TGF-β, or an equivalent volume of PBS, for 4 or 6 hours and lysates prepared. Western blotting analysis was then undertaken to assess expression levels of BH3-only proteins downstream of TGF-β-mediated SMAD signalling. The western blot shown is representative of three independent experiments using Eμ# 16, 8, and 4 cells. **B** Western blots, exemplified in **A**, were subjected to densitometry and the relative levels of

BH3-only proteins calculated, corrected for Tubulin expression and normalised against respective PBS-treated controls. Values represent the average of three independent experiments using Eμ# 16, 8, and 4, bars represent standard deviation. Asterisks denote statistically significant differences as adjudged by paired Students T-test statistical analysis ($p<0.05$). **C** Lysates from 3 WT (Eμ# 16, 8, 4) and 4 Puma KO Eμ-Myc lymphoma cell lines (MP# 24, 219, 211, and 219) were prepared, as in A, following 6 hours treatment with either 5 ng/ml TGF-β or an equivalent volume of PBS. Subsequent western blotting analysis was undertaken in order to observe the occurrence of SMAD2 phosphorylation and absence of Puma expression in Puma KO Eμ-Myc lymphoma cell lines.

Taken together, such results implicate both Bmf and Puma as key promoters of TGF-β-mediated apoptosis in Eμ-Myc lymphomas. Consequently, the relative sensitivity of Eμ-Myc lymphoma cell lines deficient in either Bmf or Puma was assessed, in comparison to WT and Bim KO lymphomas, to assess their relative contribution.

6.4 Examining the extent of TGF-β-induced cell death in BH3-only deficient Eμ-Myc lymphomas

In order to assess the relative contribution of Puma and Bmf toward TGF-β-mediated cell death, Eμ-Myc lymphomas deficient in each gene were assessed for their relative sensitivity toward TGF-β. In addition, Bim KO Eμ-Myc lymphomas were also analysed in an attempt to observe whether loss of any BH3-only protein, up-regulated by TGF-β or otherwise, influenced the extent of TGF-β-induced cell death.

As evident in figure 6.6, little difference in the extent of TGF-β-induced cell death could be observed between WT and BH3-only deficient lymphoma cells 24 hours post-TGF-β treatment. In fact, all Eμ-Myc lymphoma cell lines analysed exhibited comparable sensitivity toward TGF-β at all doses, with the possible exception of Puma KO cells. As evident in figure 6.6, Puma KO Eμ-Myc lymphoma cells consistently exhibited slightly reduced levels of TGF-β-induced cell death in comparison to WT and Bmf KO Eμ-Myc lymphomas at all doses. Therefore, in order to observe whether loss of Puma influenced the kinetics of the response an additional 6 hour time point was included.

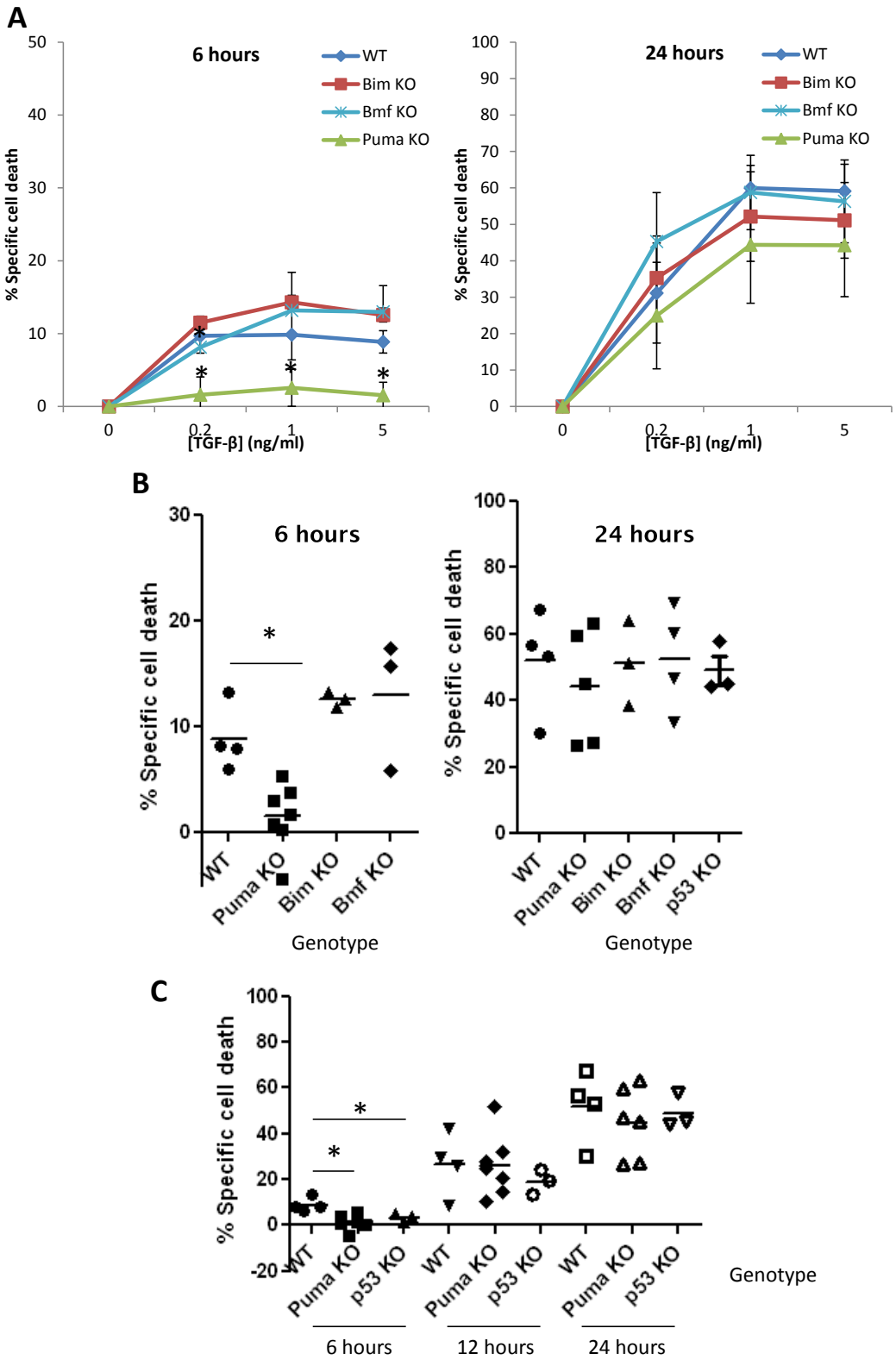

Figure 6.6 Assessing the impact genetic loss of Bim, Bmf, or Puma upon the extent of TGF-β-induced cell death in Eμ-Myc lymphoma cell lines

A WT, Bim KO, Bmf KO, or Puma KO Eμ-Myc lymphoma cells were plated at $1.6x10^6$/ ml and treated with TGF-β, at the indicated final concentration, or an equivalent volume of PBS for 6, or 24 hours. Subsequently, cells were harvested by pipetting and subjected to Annexin V^{FITC}/ PI flow cytometry, as

outlined previously. Levels of specific cell death above background were calculated as in materials and methods section 2.13.1. Values represent averages from 4 WT, 3 Bim KO, 3 Bmf KO and 5 Puma KO Eμ-Myc lymphoma cell lines, each of which reflects the average of three independent experiments, each performed in triplicate. Bars represent standard deviation. Asterisks denote a statistically significant difference as adjudged by unpaired Student's T-test statistical analysis ($p<0.05$). **B** Data from **A** of 5 ng/ml TGF-β or PBS-treated Eμ-Myc lymphoma cell lines depicted as dot plots to show responses of individual tumour cell-lines. **C** WT, Puma KO, or p53 KO Eμ-Myc lymphoma cells were subjected to TGF-β treatment, as before, for 6, 12, or 24 hours and the viability assessed by Annexin V/ PI flow cytometry, as previously described. Data is depicted as a dot plot to show the relative spread of data between the genotypes. Asterisks denote a statistically significant difference as adjudged by unpaired Student's T-test statistical analysis ($p<0.05$).

Interestingly, Puma KO Eμ-Myc lymphomas appeared to exhibit a statistically significant attenuation ($p=0.004$) of early TGF-β-induced cell death, visible after 6 hours. Such attenuation was evident in neither Bim nor Bmf KO Eμ-Myc lymphomas, indicating that such reduction was specific to a loss of Puma expression. Furthermore, loss of Puma was not associated with reduced SMAD2 phosphorylation, as evident in figure 6.5C. Therefore, although an attenuated cellular outcome was observed, the specific molecular signalling mechanisms linking TGF-β to SMADs appeared intact. Such observations imply that Puma plays a key role in the early phase of TGF-β-induced cell death, however, likely co-operates with alternate BH3-only proteins at later time-points.

Since Puma represents the major pro-apoptotic target of p53 (213-215), the impact of loss of p53 expression upon the extent of TGF-β-induced cell death in Eμ-Myc lymphoma cells was also undertaken. Interestingly, p53 deficient Eμ-Myc lymphomas demonstrate an analogous impairment of TGF-β-induced cell death after 6 hours to that produced upon loss of Puma, as evident in figure 6.6C. Furthermore, p53 deficient Eμ-Myc lymphoma cells exhibit comparable levels of cell death at later time-point (12 hours and 24 hours), in an identical finding to that produced upon loss of Puma.

Therefore, although loss of Puma appears to be sufficient to attenuate early TGF-β-induced apoptosis, loss of a single BH3-only protein appears unable to impart significant resistance after 24-hours. Such an observation implies that multiple BH3-only proteins may facilitate TGF-β-mediated cell death, possibly via up-regulation at later time points than those analysed above (0-6 hours). Such a notion is supported by the observation that Bcl-2 over-expression was sufficient to completely block TGF-β-induced cell death. In conclusion, we propose that Puma appears to play a key role in

the early phase of TGF-β-induced apoptosis, and may co-operate with additional BH3-only proteins at later time-points in Eμ-Myc lymphomas.

6.5 Chapter Discussion

Here it has been demonstrated that TGF-β signalling imparts significant upregulation of both Puma and Bmf in Eμ-Myc lymphoma cell lines. However, whilst Bmf appears important in other lymphocyte models, only Puma appears to directly contribute toward TGF-β-induced cell death (298, 299). Furthermore, it has been demonstrated that over-expression of Bcl-2 is sufficient to completely ablate TGF-β-induced cell death, indicative that the intrinsic apoptotic pathway is solely responsible for death. Such findings appear in stark contrast to studies identifying induction of extrinsic apoptosis following TGF-β treatment (294, 303). Such studies identify DAXX-facilitated caspase-8 activation as the key initiating step downstream of TGF-β signalling (294, 303). Such studies predict that MOMP would be dispensable during the induction of the apoptotic programme. However, our finding that Bcl-2 over-expression totally blocks TGF-β-induced cell death disputes this. Although, since induction of an intrinsic apoptotic cell death has been extensively observed in cells of a lymphoid lineage, our finding reflects the consensus view for the cell-type in question (281, 296-301). Furthermore, since TGF-β exhibits cell-type-specific effects, such divergence from observations made in alternate models were not unexpected (277).

In contrast to previous reports, we fail to detect transcriptional upregulation of Bik and repression of Bcl-xL expression levels in response to TGF-β in Eμ-Myc lymphoma cells (281, 298, 299). However, we are unable to detect Bcl-xL at the protein level in these cells, therefore, perhaps TGF-β imparts significant post-translational modification of Bcl-xL which we failed to detect. Furthermore, we also describe the previously documented upregulation of Bmf in response to TGF-β (281, 298, 299). However in contrast to the findings of Bmf knockdown studies, we demonstrated that loss of Bmf alone appears not to influence the extent of TGF-β-induced cell death (298, 299). Such observations were also made regarding the role of Bim. Interestingly, whilst slight upregulation of Bim was evident at the transcript level in response to TGF-β, genetic loss of Bim failed to impart significant resistance at any time point, in contrast to

previous reports (296, 298-301). Whilst Eμ-Myc lymphomas appear to exhibit upregulation of many previously identified TGF-β-responsive BH3-only proteins, it appears as though genetic loss of any one is unable to impart significant resistance (281, 296, 298-301). It is possible that multiple BH3-only proteins contribute toward TGF-β-mediated cell death in Eμ-Myc lymphomas. Consequently loss of any single gene may be unable to influence the extent of cell death, since the remaining TGF-β up-regulated BH3-only proteins are able to compensate. Therefore, studies centred upon Eμ-Myc lymphomas deficient in multiple BH3-only proteins are required to assess the relative roles of Bmf and Bim during TGF-β-induced cell death. Such Eμ-Myc lymphoma cells are available for instance, Puma, Noxa shBim lymphomas.

Furthermore, in contrast to previous studies we failed to identify proteolytic processing of Bid or Bad downstream of TGF-β signalling (297, 303). Whilst it is possible that processing may occur at later time points, as a consequence of caspase-activation, such events are unlikely to play initiating roles in the cell death response since Bcl-2 over-expression appears to completely block the response. Therefore, whilst caspase activity is evident downstream of TGF-β signalling in Eμ-Myc lymphoma cell lines, it appears dependent upon MOMP and therefore caspase-dependent proteolysis of BH3-only proteins is unlikely to play a key role in driving MOMP.

It was demonstrated that p53 KO Eμ-Myc lymphoma cells exhibited a comparable response to that produced by Puma KO Eμ-Myc lymphomas upon TGF-β treatment. Both lymphomas exhibit a statistically significant reduction in TGF-β-induced cell death after 6 hours, in comparison to WT, which appeared to recover to normal levels at later time-points. Therefore, loss of either Puma or p53 appears to impart a significant kinetic delay upon the response. Since Puma represents a major pro-apoptotic target of p53, it is possible that p53 played a direct role in TGF-β-induced Puma transactivation (162, 216-219). Indeed, loss of p53 was demonstrated to significantly reduce the extent of TGF-β-induced senescence of Eμ-Myc lymphoma cells in vivo, upon macrophage-mediated secretion (162). Therefore, p53 appears to play a major role downstream of TGF-β signalling in multiple contexts. Our collaborators show clear evidence that SMAD2 is recruited to a putative SBE in the human Puma promoter

(manuscript in preparation). Therefore, it is possible that SMAD2 acts in collaboration with p53 in the induction of Puma in response to TGF-β in Eμ-Myc lymphomas. In order to further assess such a possibility, the relative levels of p53 and SMAD2 recruited to the murine Puma promoter downstream of TGF-β should be analysed by chromatin immunoprecipitation.

In summary, it is demonstrated that Puma plays a vital role in the early stages of TGF-β-induced cell death and that at later time-points additional death effector mechanims are invoked which contribute to the response. Furthermore, a potential role for p53 is uncovered downstream of TGF-β signalling, in the form of direct Puma transactivation.

Chapter 7 *In vivo* modelling of chronic lymphocytic leukaemia in the Eμ-Tcl1 and IgH.TEμ mouse models

7.1 Chapter Introduction

CLL represents the most-common adult leukaemia in the western world, and is associated with an accumulation of mature, $CD5^+$ B-lymphocytes in the peripheral blood, bone marrow and secondary lymphoid organs of patients (1, 13, 14). Although CLL is a relatively indolent malignancy, there is significant heterogeneity in clinical course (15, 16). Such heterogeneity results from the existence of two distinct subtypes, determined by possession of somatic mutations within the IgVH region of the malignant clone (15, 16). Taken alongside other evidence, these data indicate antigen-driven BCR signalling is important in the selection, proliferation, and survival of B-CLL (13, 14, 336). Since the immunophenotype of B-CLL most closely resembles that of marginal zone B-cells, which commonly exhibit polyreactive, autoreactive BCRs, it is likely that antigenic drive is provided by an auto-antigen (13, 14, 336). It is proposed that such auto-antigen-mediated BCR engagement drives activation of the PI3K/Akt pathway, and subsequent upregulation of Mcl-1 and c-Myc expression levels, resulting in enhanced survival of B-CLL (342-344).

Such dependency upon BCR-mediated upregulation of survival factors represents an attractive and potentially useful target for therapeutic intervention. Therefore, we wished to characterise and develop models of assessing the therapeutic potential of disruption of BCR-driven pro-survival signals in both the Eμ-Tcl1 and IgH.TEμ pre-clinical models of CLL.

Eμ-Tcl1 mice, exhibit a Tcl1 oncogene proximal to the IgH enhancer, and spontaneously develop a CLL like disease exhibiting many of the molecular features of human CLL (352-354). For instance, the malignant clones demonstrate a similar immunophenotype to that of CLL ($B220^+$, IgM^+, $CD5^+$, $CD21^{low}$, and $CD116^+$) and demonstrate highly stereotyped, autoreactive BCRs (353-355). The IgH.TEμ model has also been reported, in which an SV40 large T antigen coding region is placed proximal to the IgH enhancer, driving ectopic B-cell restricted expression (360). Consequently,

aged IgH.TEμ mice spontaneously develop overt leukaemia, lymphadenopathy, and splenomegaly associated with accumulation of $CD19^+$, $B220^+$, $CD5^+$, IgM^+, IgD^{low}, $CD21^-$, $CD23^-$ lymphocytes (360). We aimed to obtain and then further characterise both Eμ-Tcl1 and IgH.TEμ murine models of CLL and subsequently attempt to assess the therapeutic potential of disruption of BCR-mediated survival signals in these models.

7.2 Eμ-Tcl1 Tumour presentation

7.2.1 Eμ-Tcl1 tumour monitoring and Kaplan Meier survival

Cohorts of Eμ-Tcl1 and IgH.TEμ mice were obtained from collaborators, maintained on the C57BL/6 background and monitored monthly for the onset of CLL-like disease. In the case of Eμ-Tcl1 mice, monthly analysis of the percentage of $CD5^+$, $B220^+$ lymphocytes in peripheral blood by flow cytometry and peripheral white blood cell (WBC) counts were utilised as a marker for tumour development, as previously described (356).

Eμ-Tcl1 mice exhibited gradual accumulation of $CD5^+$, $B220^+$ lymphocytes and congruent enhancements in peripheral WBC counts throughout their lifespan, as outlined in figure 7.1. Such increases appeared not to impart overt symptoms upon afflicted mice. However, unexpected mortality was typically associated with an accumulation of $CD5^+$, $B220^+$ cells in excess of 80% of total peripheral lymphocytes (data not shown). Therefore, a humane experimental endpoint of 80% $CD5^+$, $B220^+$ lymphocytes in peripheral blood was established and adhered to throughout the remainder of investigations. As evident in figure 7.1B, the appearance of $CD5^+$, $B220^+$ lymphocytes in the blood of Eμ-Tcl1 mice was not associated with an immediate increase in WBC counts. In fact, overt leukaemia always lagged behind increases in the frequency of $CD5^+$ B-cells in the peripheral blood and appeared only after $CD5^+$, $B220^+$ lymphocytes reached approximately 50% of peripheral blood lymphocytes. Subsequently, WBC counts typically appeared to increase to a maximum 7-fold higher than baseline recordings, in most cases (range 2.5 – 12.1 fold increase).

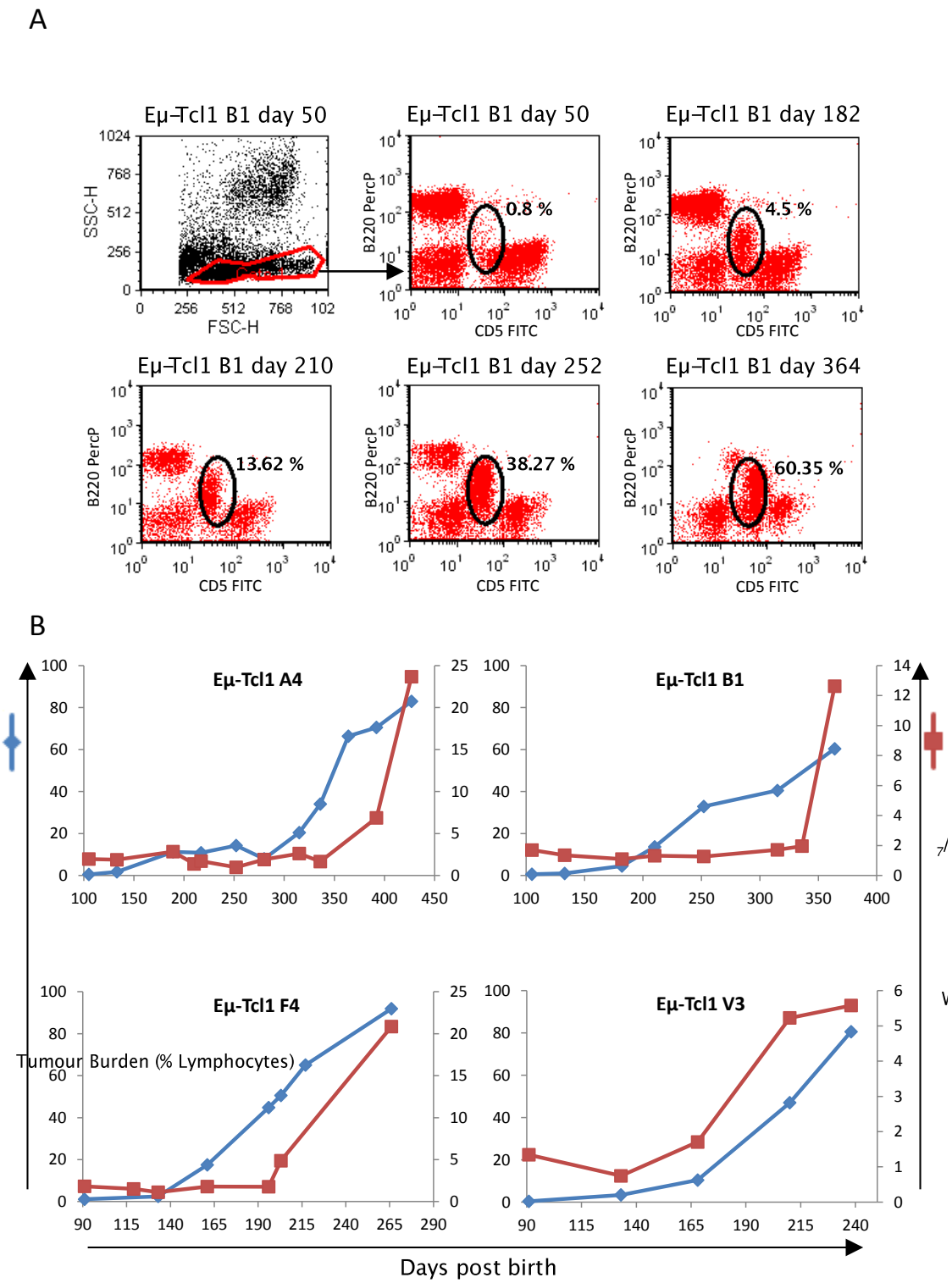

Figure 7.1 Analysis of Eμ-Tcl1 tumour burden and white blood cell count over time

Eμ-Tcl1 mice were monitored for the incidence of CLL like-disease throughout their lifespan from nine weeks of ages via monthly blood sampling, flow cytometry and assessment of WBC counts. **A** Example FACS plots depicting gradual accumulation of cellular populations indicative of CLL-like disease ($CD5^+$, $B220^+$) over the lifespan of the mouse (Eμ-Tcl1 B1). **B** Four example traces demonstrating gradual increases in CLL-like cellular populations (blue lines) and its impact upon WBC counts (red lines) throughout the life span of Eμ-Tcl1 mice. Traces are representative of individual mice, similar results were obtained for all mice analysed (albeit with differing kinetics), see figure 7.2.

Interestingly, the kinetics at which Eμ-Tcl1 tumours arose appeared to divide into two broad subsets, as outlined in figure 7.2, with subset 1 demonstrating an enhanced rate of tumourigenesis in comparison to subset 2.

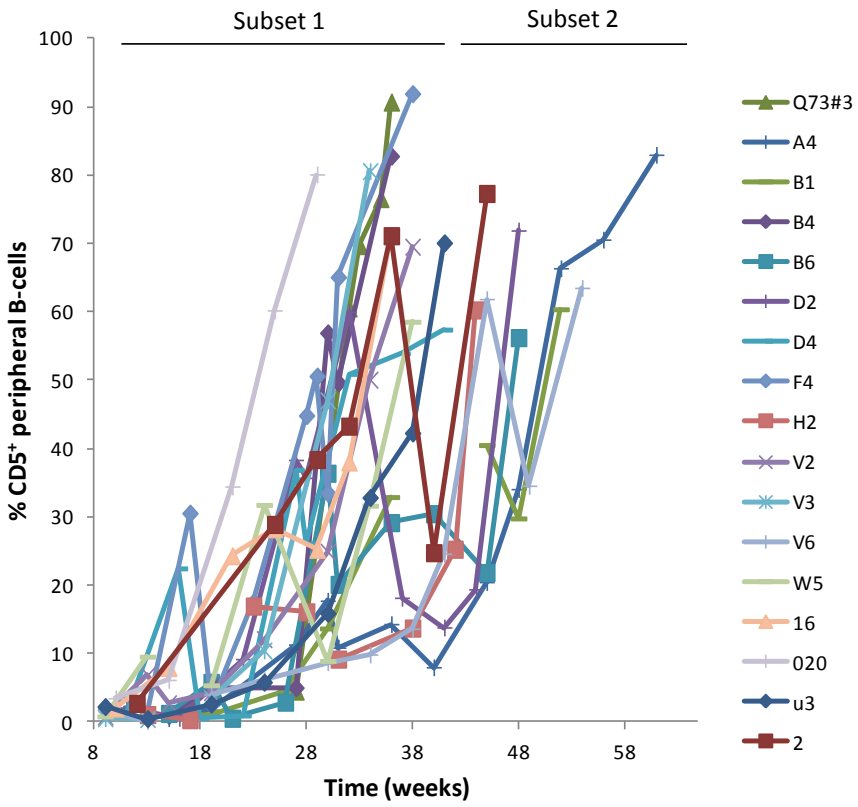

Figure 7.2 Analysis of the onset of $CD5^+$ B-cell leukaemias across the Eμ-Tcl1 cohort
Eμ-Tcl1 mice were monitored for the incidence of CLL like-disease throughout their lifespan, as outlined in figure 7.2. Of the 17 mice that reached the experimental endpoint, all exhibited relatively similar kinetics of leukaemiagenesis. However, two discrete subsets can be identified by the relative rate of leukaemiagenesis. A tight grouping of tumours is evident which became terminal prior to 38 weeks after birth. However, a second (potentially less aggressive) subset is evident which display much slower rates of leukaemiagenesis.

Upon reaching 80% CLL-like B-lymphocytes in peripheral blood, Eμ-Tcl1 mice were culled, as outlined in materials and methods section 2.4, and the presence of tumours assessed by autopsy. As evident in figure 7.3, Eμ-Tcl1 mice exhibit a statistically significant reduction in survival in comparison to congenic C57BL/6 mice, as assessed by Mantel-Cox statistical analysis (p= 0.0033), with a median survival of 353 days from birth.

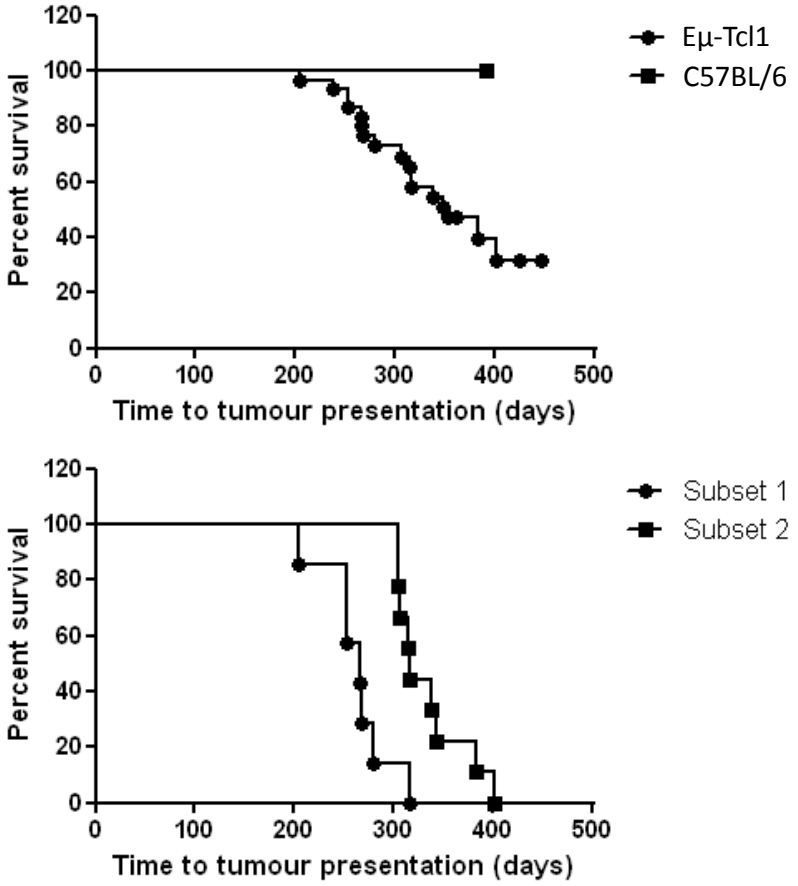

Figure 7.3 Kaplan Meier survival curve of Eμ-Tcl1 and congenic C57BL/6 mice

A Cohorts of Eμ-Tcl1 mice were crossed on to congenic C57BL/6 mice (Black circles n=30) and monitored, from birth, for the incidence of tumours in comparison to C57BL/6 congenic animals (Black squares) (n= 10) held at this institution. Upon the attainment of a tumour burden in excess of 80% of PBMCs, mice were culled as outlined in materials and methods section 2.4. Eμ-Tcl1 mice demonstrate an enhanced incidence of spontaneous tumours and diminished overall survival in comparison to congenic animals ($p < 0.001$) by Mantel-Cox statistical testing. **B** Data from **A** was subdivided into the two subsets identified in figure 7.1 and the relative survival of each cohort assessed. Subset 1 demonstrated a statistically significant reduction in survival in comparison to subset 2 ($p = 0.0019$) as assessed by Mantel-Cox statistical analysis.

Such observations are consistent with previous reports where two individual cohorts were observed to display a median survival of 329 and 420 days, respectively (353, 354). Interestingly, the disease course subsets, identified in figure 7.2, also demonstrate statistically significant differences in survival ($p = 0.0019$ by Mantel-Cox statistical analysis). Subset 1 appeared to succumb to CLL-like leukaemia more rapidly than subset 2, with a median survival of 265 and 316 days, respectively. It is, therefore, possible that additional, spontaneous mutations may alter the disease course in Eμ-Tcl1 tg animals. In an analogy with the Eμ-Myc model, a possible explanation is found in the spontaneous acquisition of p53 mutations throughout leukaemiagenesis (324, 327, 331, 332). However, such results should be viewed with a degree of caution, since

the disease course subsets were defined according to the rate of leukaemiagenesis. Therefore, the occurrence of a statistical significance in median survival is perhaps unsurprising. In order to confirm the existence of two disease course subsets, additional analysis is required in the attempt to find a common genetic abnormality associated with an enhanced rate of leukaemiagenesis, for instance p53 mutational status.

7.2.2 Physical presentation of Eμ-Tcl1 tumours

Having established and characterised the Eμ-Tcl1 model in the laboratory, we subsequently wished to use it as a tool for examining various aspects of tumour biology. As previously described, upon detection of tumours, animals were culled and the sizes of LN, spleen and thymus scored, as outlined in table 7.1, as a sign of tumour development and compared to congenic C57BL/6 animals. As evident in figure 7.4, the physical presentation of Eμ-Tcl1 mice was substantially different to that observed in Eμ-Myc mice. Eμ-Tcl1 tumours presented with only moderate enlargement of LN, but exhibited substantial increases in the size of spleen and thymus, as evident in table 7.2. Such thymic enlargement typically manifested as spreading into the pericardium, where it appeared to impair cardiac function. Quantitation of organ size, either by weight or by score, revealed significant enlargement of all secondary lymphoid organs in Eμ-Tcl1 animals in comparison to congenic C57BL/6 animals, as demonstrated in figure 7.5.

Score	LN Size	Thymus Size	Organ Description
1	<1 mm	<8 mm	Normal
2	1-2 mm	8-10 mm	Small
3	3-5 mm	10-15 mm	Medium
4	8-10 mm	15-20 mm	Large
5	>10 mm	>20 mm	Very large

Table 7.1 Scoring system for LN and Thymus sizes of Eμ-Tcl1 and IgH.TEμ mice
The LN and Thymus of tumour bearing mice were given a score in order to quantitate their relative size. Scores of 1-5 were given, with 1 representing an organ of a normal size that a healthy C57BL/6 mouse would be expected to possess.

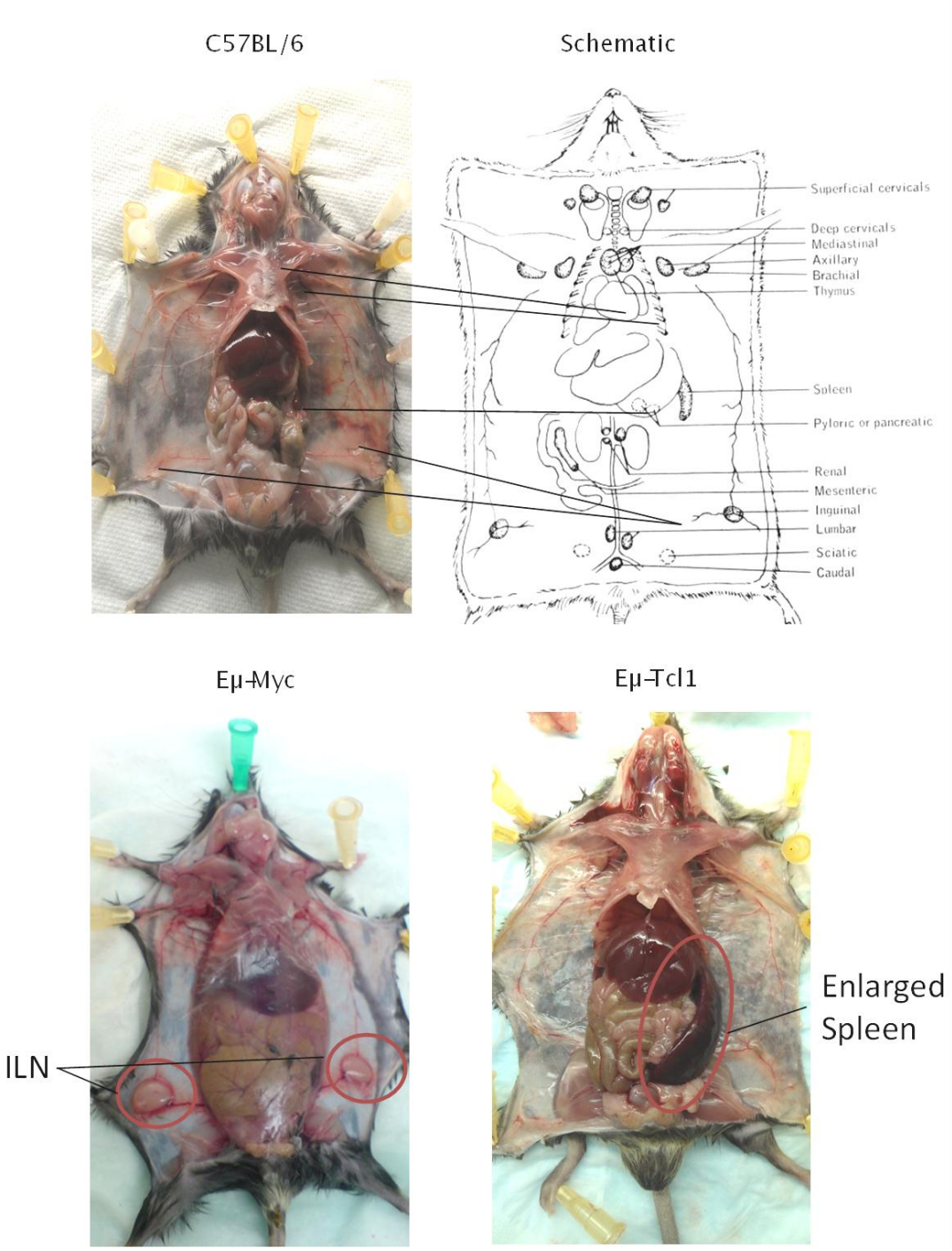

Figure 7.4 Gross anatomy of tumour bearing Eμ-Tcl1, Eμ-Myc mice and congenic C57BL/6 animals

A direct comparison of the gross anatomy of mid-line dissected tumour bearing Eμ-Tcl1 and Eμ-Myc mice in comparison to congenic C57BL/6 animals. Also depicted is a scheme of the layout of the lymphatic system obtained from www.informatics.jax.org/greenbook/images/13-4.jpg. Both Eμ-Tcl1 tumours presented with massive enlargement of the spleen (circled) but only minimal LN enlargement. In contrast, Eμ-Myc tumours typically exhibited massive lymphadenopathy with only minimal splenomegaly. Eμ-Myc image kindly provided by Dr. E.L. Williams.

Eμ-Tcl1	Time to presentation (Days)	Inguinal LN	Brachial LN	Thymus	Spleen weight
Eμ-Tcl1 q70# 2	252	1	2	3	1.22g
Eμ-Tcl1 A4	337	1	1	1	1.46g
Eμ-Tcl1 B1	383	1	1	2	1.2g
Eμ-Tcl1 B4	252	3	1	2	1g
Eμ-Tcl1 D2	353	2	1	1	1.761g
Eμ-Tcl1 D4	252	n.d	n.d	n.d	0.626
Eμ-Tcl1 F4	265	2	2	1	0.615g
Eμ-Tcl1 H2	305	2	2	2	1.219g
Eμ-Tcl1 U3	314	1	1	1	2.129g
Eμ-Tcl1 V2	279	2	1	3	0.792g
Eμ-Tcl1 V3	238	2	2	1	0.734g
Eμ-Tcl1 V6	400	3	3	3	0.596g
Eμ-Tcl1 W3	266	1	1	1	0.29g
Eμ-Tcl1 W5	268	2	2	2	2.9g
Eμ-Tcl1 B6	343	1	2	2	1.4g
Eμ-Tcl1 014	347	2	2	3	1.5
Eμ-Tcl1 016	316	2	1	4	1.2
Eμ-Tcl1 020	204	1	1	2	0.44g
Eμ-Tcl1 002	316	1	1	1	0.8g
Average	299.47	1.667	1.5	1.944	1.19
Std Dev	52.53	0.687	0.618	0.9378	0.444

Table 7.2 Assessment of Spleen, LN and Thymus size of tumour bearing Eμ-Tcl1 mice

The LN and Thymus of tumour bearing Eμ-Tcl1 mice were sized according to the scoring system outlined in table 7.1, whilst the size of spleen was assessed by weight. Time to presentation represents the time, from birth, for spontaneous tumours to arise and reach pre-defined humane end-points.

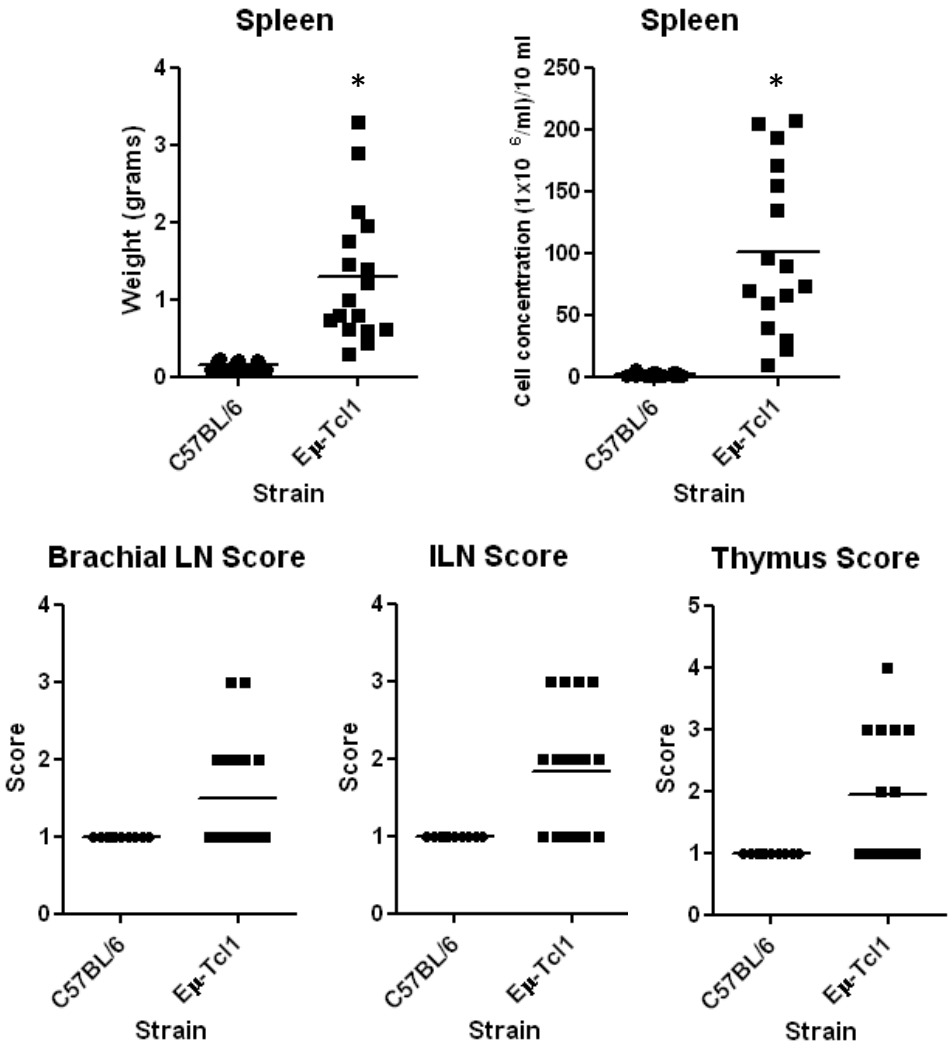

Figure 7.5 Comparative analyses of organ scores/ weights derived from Eμ-Tcl1 mice
Following sacrifice, tumour bearing mice were autopsied and the size, weight, and cellularity of tumour infiltrated organs was assessed and compared to organs derived from congenic C57BL/6 animals. Asterisks denote statistically significant differences ($p < 0.05$), as assessed by Student's unpaired T-test statistical analysis. C57BL/6 data kindly provided by Drs. A. Roghanian and A. White and Mr. H Johnston.

7.2.3 Histological examination of Eμ-Tcl1 tissues

In order to observe the impact of Eμ-Tcl1 tumour development upon the normal architecture of secondary lymphoid organs, H&E staining of formalin fixed organ sections was undertaken and compared to congenic C57BL/6, and Eμ-Myc animals. As evident in figure 7.6, normal splenic architecture of a dense white pulp surrounded by a less dense red pulp was completely absent in Eμ-Tcl1 spleens.

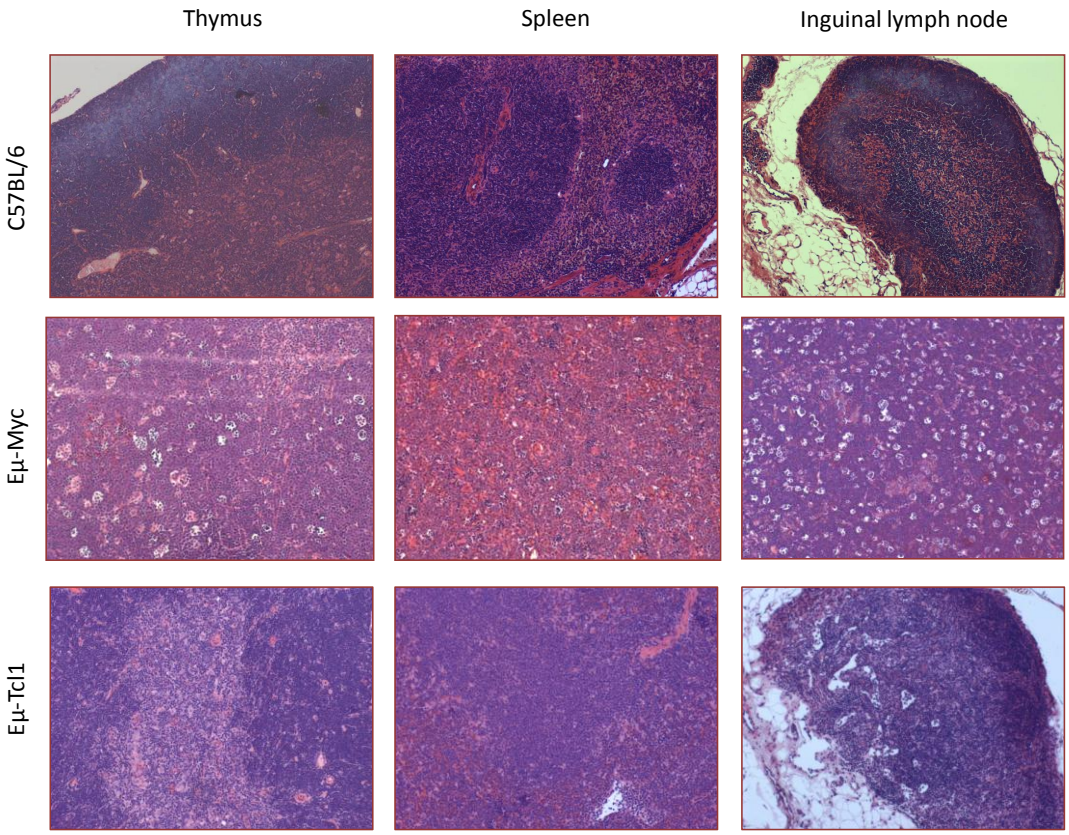

Figure 7.6 Comparative histological examination of secondary lymphoid organ architecture in C57BL/6, Eμ-Tcl1, and Eμ-Myc mice

Upon attainment of the pre-determined experimental endpoints, mice were culled and dissected according to materials and methods section 2.4. Tissue sections were taken, fixed in formalin and paraffin embedded prior to staining with haematoxylin and eosin (H&E). Subsequently, the tissue architecture and the presence of tumour infiltrate was assessed by light microscopy in comparison to congenic C56BL/6 mice. All slides were examined at 10 x magnification. C57BL/6 and Eμ-Myc data kindly provided by Dr. E.L. Williams.

Instead, spleens appeared largely homogeneous, with densely packed nuclei, indicative of tumour proliferation and invasion. In contrast, the remaining secondary lymphoid organs appeared largely normal in appearance with only slight increases in the size of lymphocyte rich areas. In addition, the appearance of secondary lymphoid organs from terminal Eμ-Tcl1 animals was markedly different to that observed in Eμ-Myc mice. As evident in figure 7.6, sections of Eμ-Tcl1 organs were not interspersed with regions of cleared cells and tingible body macrophages, and only minimal tumour infiltration was seen in the thymus of Eμ-Tcl1 mice, in comparison to the extensive invasion and tingible body macrophages seen in Eμ-Myc animals.

In an attempt to observe the extent of tumour infiltration into non-lymphoid compartments further histological analysis of heart, kidney, liver, sternum, and lung sections was undertaken.

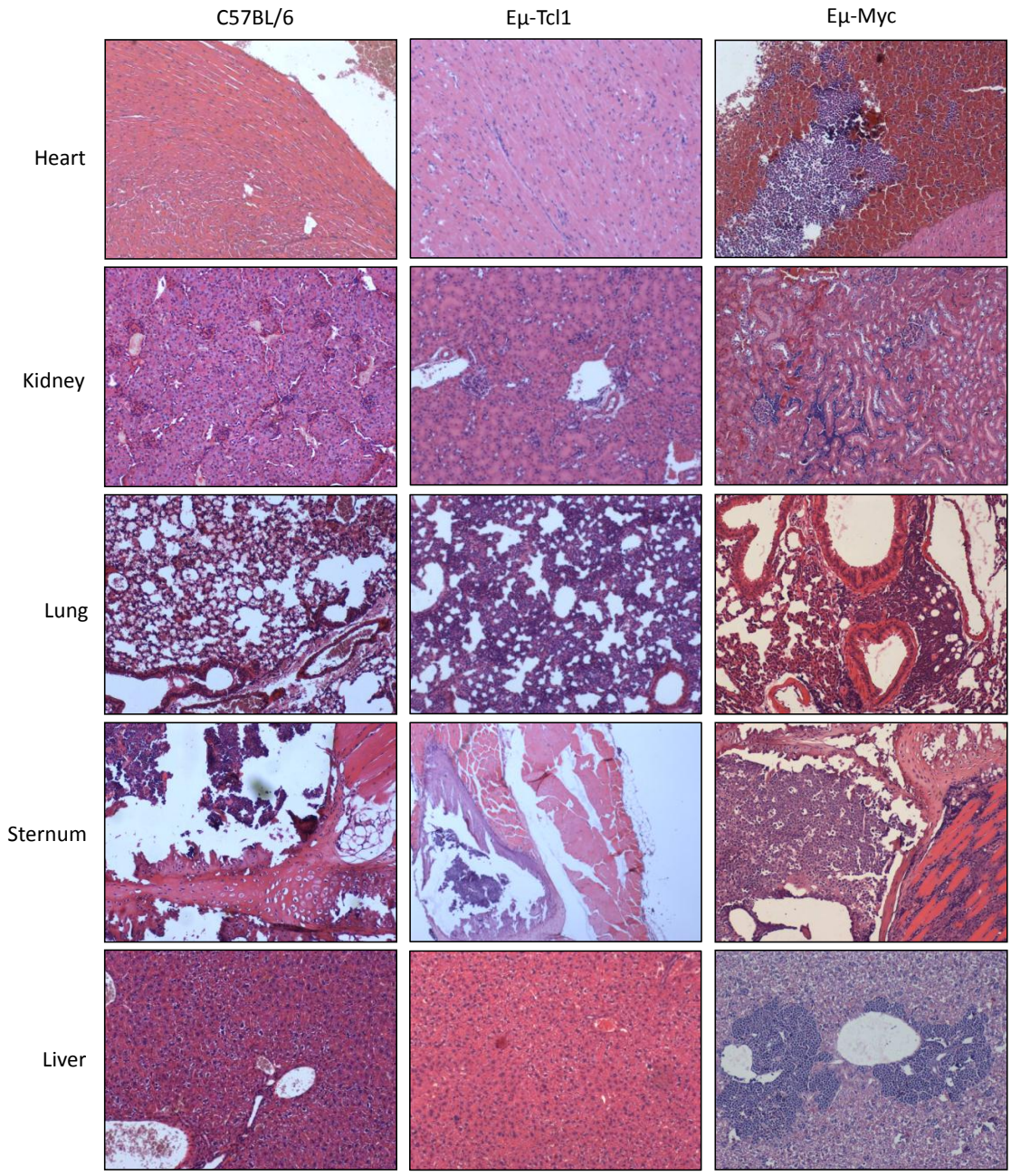

Figure 7.7 Histological examination of tumour infiltration into non-lymphoid tissues in Eμ-Tcl1, Eμ-Myc and congenic C57BL/6 animals

(As in figure 7.6) Upon attainment of the pre-determined experimental endpoints, mice were culled and dissected according to materials and methods section 2.4. Non-lymphoid tissues (heart, kidney, lung, sternum, and liver) were collected and fixed in formalin prior to paraffin embedding and H&E staining. Areas of tumour infiltration were not apparent in any tissues of Eμ-Tcl1 animals, with the possible exception of the lungs, in comparison to C57BL/6 congenic animals (left panel). In contrast, extensive tumour infiltration into the heart, kidney, and liver was evident in Eμ-Myc mice. C57BL/6 and Eμ-Myc data kindly provided by Dr. E.L. Williams.

As evident in figure 7.7, a complete lack of extensive/ obvious tumour infiltration was evident in Eμ-Tcl1 mice in all organs, except the lungs. Lung tissues appeared thickened and exhibited greater density of nuclei in comparison to congenic C57BL/6 animals. Taken together with observations that terminal Eμ-Tcl1 mice commonly exhibited rapid breathing, such data seems to imply that lung invasion is common in the Eμ-Tcl1 model. Such observations are in stark contrast to those made in the Eμ-Myc model, which demonstrated profound tumour infiltration into the kidneys, liver, heart, and sternum of afflicted animals. Therefore, Eμ-Tcl1 leukaemias appear largely restricted to the peripheral blood and spleens of afflicted animals with only minimal expansion in non-lymphoid tissues.

7.2.4 Identification of the immunophenotype of Eμ-Tcl1 leukaemias

In order to assess the fidelity with which Eμ-Tcl1 leukaemias recapitulate human CLL, immunophenotype analysis was undertaken by flow cytometry. At autopsy, the spleen, thymus and lymph nodes of tumour bearing animals were harvested and stored at -80°C. Subsequently, vials of splenocytes were thawed, washed in 10% Eμ-Myc medium, and rested *in vitro* at 37°C, 10% CO_2 for 1 hour prior to analysis. Eμ-Tcl1 leukaemia cells were then incubated with APC conjugated anti-CD19, alongside IgM, IgD, CD21, CD38, CD79a or CD5 specific FITC conjugated antibodies and anti-$CD23^{PE}$. The resulting flow cytometry data is outlined in figure 7.8 and table 7.3. The generated Eμ-Tcl1 leukaemias were found to be 100% of B-cell origin ($CD19^{+}$) and sIgM positive. Such an observation was in stark contrast to the 55% $sIgM^{+}$ frequency of Eμ-Myc lymphomas. Furthermore all Eμ-Tcl1 leukaemias analysed appeared $CD5^{+}$, $CD21^{+}$, $CD79a^{+}$, IgD^{+}, and $CD23^{-}$ whereas, 56% appeared to express low levels of CD38 . Whilst CD38 represents a marker of poor prognosis in CLL, no correlation between CD38 expression and time for tumour presentation has previously been determined in Eμ-Tcl1 leukaemias (16).

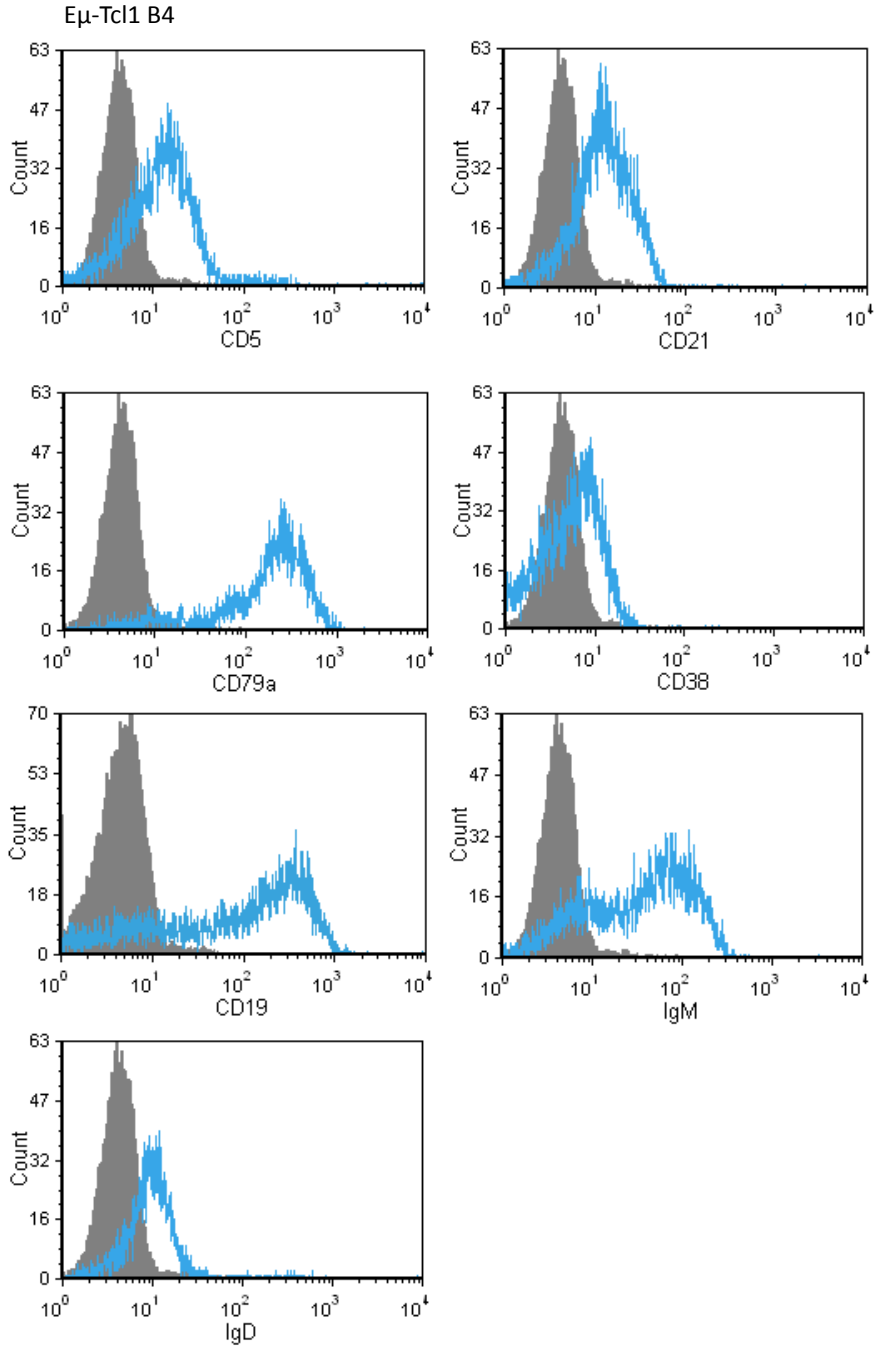

Figure 7.8 Immunophenotype analyses of Eμ-Tcl1 tumours

Single cell suspensions derived from the spleens of Eμ-Tcl1 mice were incubated with 5 μg/ ml PE or APC-conjugated anti-CD19 (Clone 1D3) or 10 μg/ml anti-CD23^{PE} in the presence of 10 μg/ ml anti-IgM^{FITC} (Clone Mc39.12), anti-IgD^{FITC} (Clone 1.19), anti-CD21^{FITC} (Clone 7G6), anti-CD5^{FITC} (Clone 57-7.3), anti-CD38^{FITC} (clone 1A5E8) or an appropriate isotype control for 30 minutes at 4°C, and analysed by flow cytometry. 10,000 viable cells, as determined by the FSC/ SSC profile, were gated and analysed for fluorescence in the FL-1, FL-2, and FL-4 channels, as before. Flow cytometry data was expressed as histograms overlaid upon isotype control values (grey peaks). Geometric means were calculated and normalised, by division, against geometric means calculated for the appropriate isotype control to generate relative surface expression values. Values were subsequently plotted in table 7.3. Plots shown are from Eμ-Tcl1 B4, and are representative of the remaining tumours.

Eμ-Tcl1	CD19	CD5	IgM	IgD	CD79a	CD23	CD21	CD38
Eμ-Tcl1# 020	High	Low	Med	Low	Low	-	Low	Low
Eμ-Tcl1# D4	High	Low	Med	Low	Med	-	Low	Low
Eμ-Tcl1# U3	High	Low	High	Low	Med	-	Low	Low
Eμ-Tcl1# V2	High	Low	Med	Low	Med	-	Low	Low
Eμ-Tcl1# B4	High	Low	Med	Low	Med	-	Low	Low
Eμ-Tcl1# W3	High	Low	Med	Low	Low	-	Low	-
Eμ-Tcl1# W5	High	Low	Med	Low	Med	-	Low	-
Eμ-Tcl1# B6	High	Low	Med	Low	Med	-	Low	-
Eμ-Tcl1# F4	High	Low	Low	Low	Med	-	Low	Low

Table 7.3 Summary of primary Eμ-Tcl1 immunophenotypes

Splenocytes from tumour bearing Eμ-Tcl1 mice derived at this institution were stained as in figure 7.8 and analysed by flow cytometry. Expression levels were determined as Low, Medium (Med) or High, according to their relative normalised geometric means. 1-10 was described as Low, 10-50 Med, and 50+ as High.

Altogether, these data agree with previously published accounts of the incidence and presentation of tumours within Eμ-Tcl1 tg animals and provide a good model of CLL in which therapeutic interventions can be assessed (353, 354).

7.3 IgH.TEμ Tumour presentation

In order to provide an additional model with which to contrast the characteristics of Eμ-Tcl1 tumours and use as a pre-clinical model of CLL, IgH.TEμ mice were obtained and characterised, in a similar manner.

7.3.1 IgH.TEμ tumour monitoring and Kaplan Meier survival

Since IgH.TEμ mice are heterozygotes carrying a single copy of the SV40 large-T antigen oncogene, they exhibit both a targeted, T antigen-encoding, IgH allele derived from 129-mice (IgM^b allotype) and a non-targeted C57BL/6 IgH allele (IgM^a allotype). Therefore, the onset of CLL-like disease was monitored by observing the relative usage of each allele via flow cytometry utilising allotype specific antibodies, as previously described (360). At birth B-cells from IgH.TEμ-mice demonstrate equal usage of both targeted and non-targeted IgH alleles. However, aged mice exhibited gradual accumulation of targeted IgM^b allele expressing clones as the oncogene begins to drive tumour cell accumulation, as evident in figure 7.9.

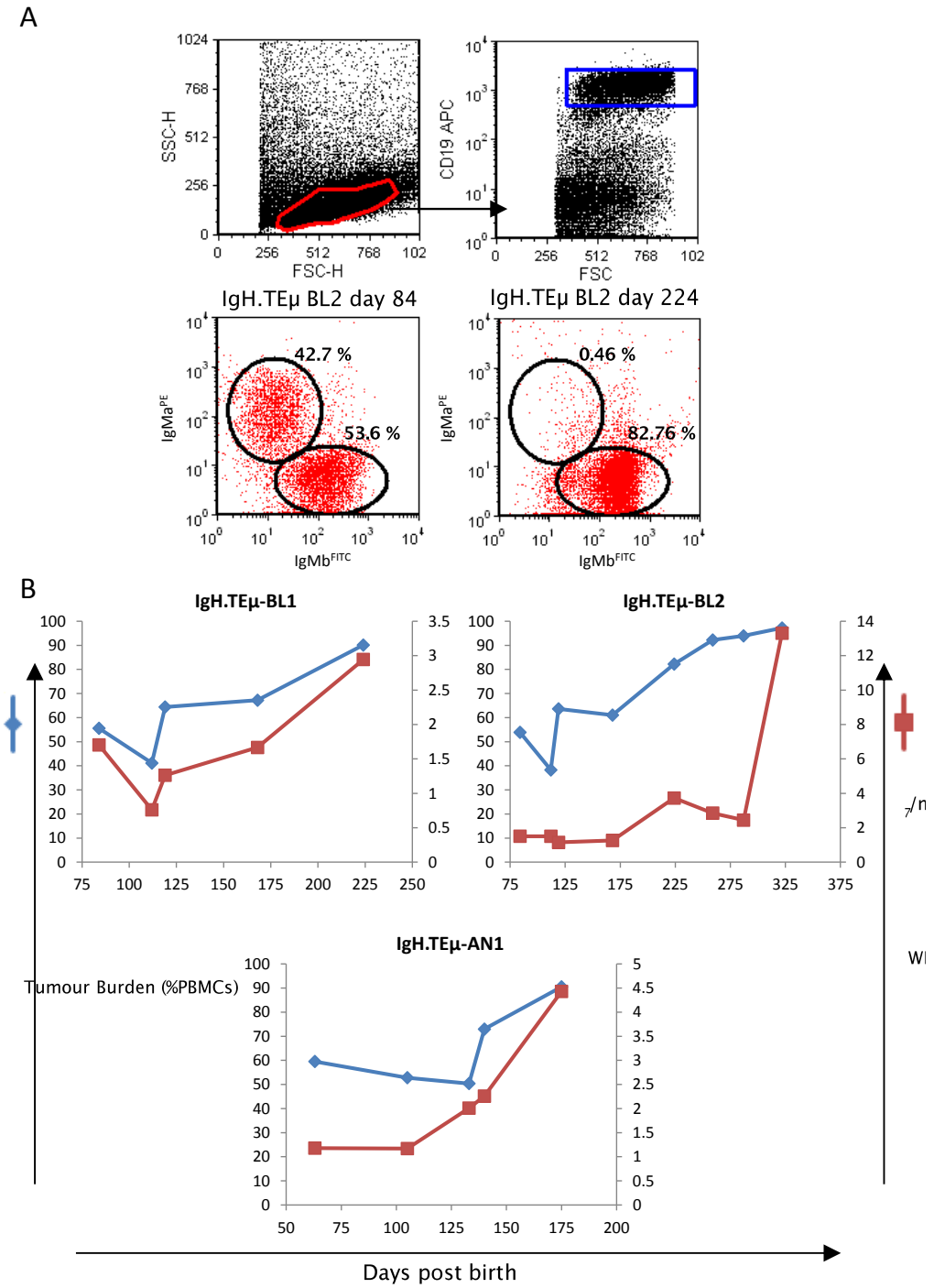

Figure 7.9 Analysis of IgH.TEμ tumour burden and white blood cell count over time

IgH.TEμ mice were monitored for skewing of IgM allotype throughout their lifespan from nine weeks of ages via monthly blood sampling, flow cytometry and assessment of WBC counts. **A** example FACS plots depicting blood exhibiting gradual accumulation of IgM^b positive lymphocytes over the lifespan of IgH.TEμ mouse BL2. **B** Three example traces demonstrating gradual increases in the incidence of IgM^b positive lymphocytes (blue lines) and its impact upon WBC counts (red lines) throughout the life span of IgH.TEμ mice. Traces are representative of individual mice, similar results were obtained for all mice analysed (albeit with differing kinetics).

Such preferential allele usage was associated with enhanced WBC counts, in an analogous fashion to Eμ-Tcl1 mice, to a maximum approximately 10-fold higher than

baseline in most cases. Upon the occurrence of visible symptoms of tumours, animals were culled in accordance with materials and methods section 2.4, and the presence of tumour analysed by autopsy.

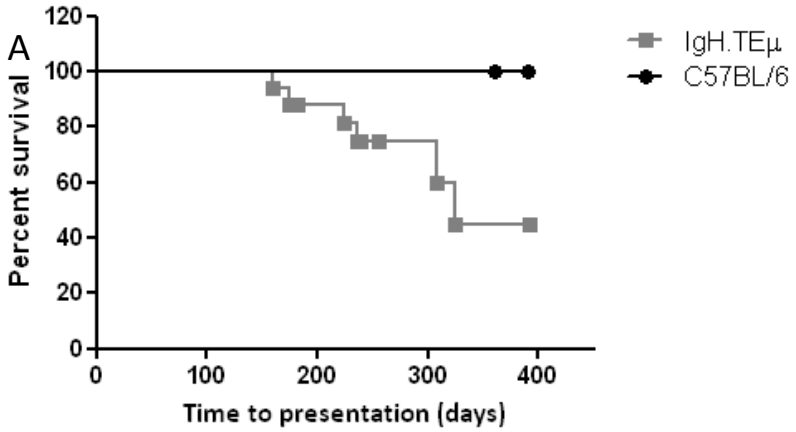

Figure 7.10 Kaplan Meier survival curve analysis of IgH.TEμ and congenic C57BL/6 mice
Cohorts of IgH.TEμ mice were crossed on to congenic C57BL/6 mice (Grey squares n= 11) and monitored, from birth, for the incidence of tumours in comparison to C57BL/6 congenic animals held at this institution (Black circles). Upon detection of symptoms of tumours, mice were culled as outlined in materials and methods section 2.4. IgH.TEμ mice demonstrate an enhanced incidence of spontaneous tumours and diminished overall survival in comparison to congenic animals (p =0.0467) by Mantel-Cox statistical testing.

Similarly to Eμ-Tcl1 animals, IgH.TEμ mice exhibited a statistically significant reduction in survival in comparison to congenic C57BL/6 animals (p= 0.0387) with a median survival of 324 days, as evident in figure 7.10. However, at the time of writing, only 6 out of 16 IgH.TEμ mice had succumbed to CLL-like disease. Therefore, it is anticipated that a more highly statistically significant reduction in survival will be apparent after additional mice succumb to the CLL-like disease.

7.3.2 Physical presentation IgH.TEμ tumours

In an analogous experiment to that performed in section 7.2.2, IgH.TEμ mice were culled upon the detection of tumours, and the sizes of LN, spleen and thymus scored according to the criteria outlined for Eμ-Tcl1 mice in table 7.1. As evident in figure 7.11-12 and table 7.4, IgH.TEμ tumours presented with moderate lymphadenopathy, substantial splenomegaly and thymic hyperplasia, as observed for Eμ-Tcl1 mice. In addition, thymic hyperplasia was often associated with spreading along the sternum and invasion of the pericardium, as was observed in terminal Eμ-Tcl1 animals.

7.3.3 Histological examination of IgH.TEμ tissues

Formalin fixed sections of organs taken from terminal IgH.TEμ animals were subjected to H&E staining, examined by light microscopy, and contrasted with sections taken from congenic C57BL/6, Eμ-Myc and Eμ-Tcl1 animals.

As evident in figure 7.13, H&E staining patterns of secondary lymphoid organ sections appeared highly similar between IgH.TEμ and Eμ-Tcl1 animals. Both IgH.TEμ and Eμ-Tcl1 animals exhibited extensive loss of normal splenic architecture alongside only minimal increases in the size of lymphocyte rich areas in the remaining secondary lymphoid organs. Furthermore, like Eμ-Tcl1 animals, IgH.TEμ tumours demonstrated only minimal infiltration in to non-lymphoid compartments, as evident in figure 7.14. However, again lung tissues appeared invaded, visible as a thickening and greater nuclear density of the tissue. Such observations are again in contrast to the Eμ-Myc model where extensive infiltration is evident in multiple non-lymphoid tissues, as described in chapter 3.

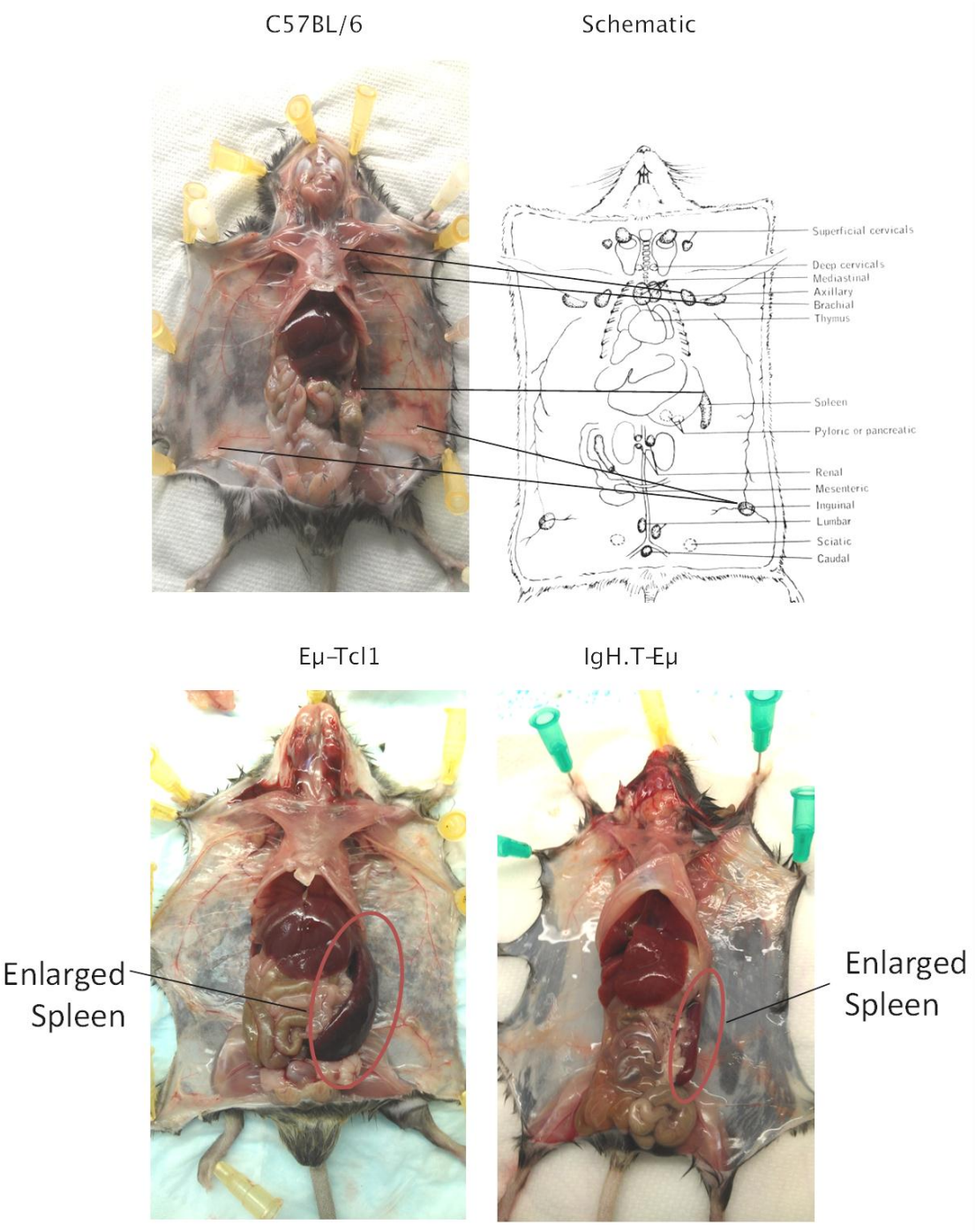

Figure 7.11 Gross anatomy of tumour bearing IgH.TEμ, mice in comparison to Eμ-Tcl1 and congenic C57BL/6 animals

A direct comparison of the gross anatomy of mid-line dissected tumour bearing IgH.TEμ and Eμ-Tcl1 mice in comparison to congenic C57BL/6 animals. Also depicted is a scheme of the layout of the lymphatic system obtained from www.informatics.jax.org/greenbook/images/13-4.jpg. Both IgH.TEμ and Eμ-Tcl1 tumours presented with massive enlargement of the spleen (circled) but only minimal LN enlargement. Eμ-Myc image kindly provided by Dr. E.L. Williams.

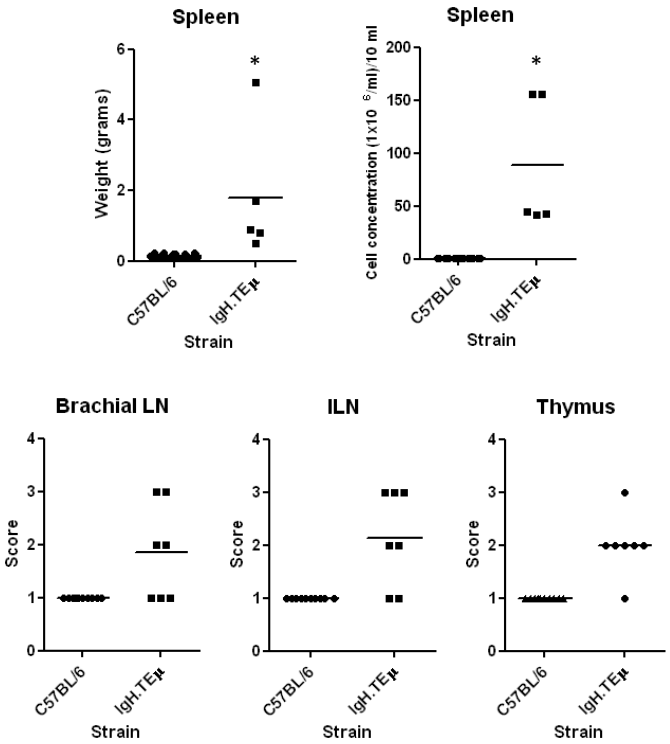

Figure 7.12 Comparative analyses of organ scores/ weights derived from IgH.TEμ mice

Following sacrifice, tumour bearing mice were autopsied and the size, weight, and cellularity of tumour infiltrated organs was assessed and compared to organs derived from congenic C57BL/6 animals. Asterisks denote statistically significant differences ($p < 0.05$), as assessed by Student's unpaired T-test statistical analysis. C57BL/6 data kindly provided by Drs. A. Roghanian and A. White and Mr. H Johnston

IgH.T Eμ	Time to presentation (Days)	Inguinal LN	Brachial LN	Thymus	Spleen weight
001	236	3	3	2	5.05g
AN1	175	1	2	3	0.9g
AN2	159	3	3	4	0.8g
BL1	324	1	1	2	0.504g
BL2	224	2	1	3	1.704
$Bim^{+/-}$ M2	256	2	2	1	1.4g
$Bim^{+/-}$ M4	308	1	1	2	0.44g
$Bim^{+/-}$ N2	302	3	2	3	1.71g
$Bim^{+/-}$ N3	288	2	2	3	4.005g
$Bim^{-/-}$ M3	344	2	2	3	0.65g
$Bim^{-/-}$ N4	329	2	1	4	0.56g
$Bim^{-/-}$ AS4	266	3	3	5	3.46g
$Bim^{-/-}$ AS5	222	3	3	4	1.036g
Average	264.077	2.154	2.000	3.000	1.709
Std Dev	58.696	0.801	0.816	1.080	1.501

Table 7.4 Assessment of Spleen, LN and Thymus size of tumour bearing IgH.TEμ mice
The LN and Thymus of tumour bearing IgH.TEμ mice were sized according to the scoring system outlined in table 7.1, whilst the size of spleen was assessed by weight. Time to presentation represents the time, from birth, for spontaneous tumours to arise and reach pre-defined humane end-points.

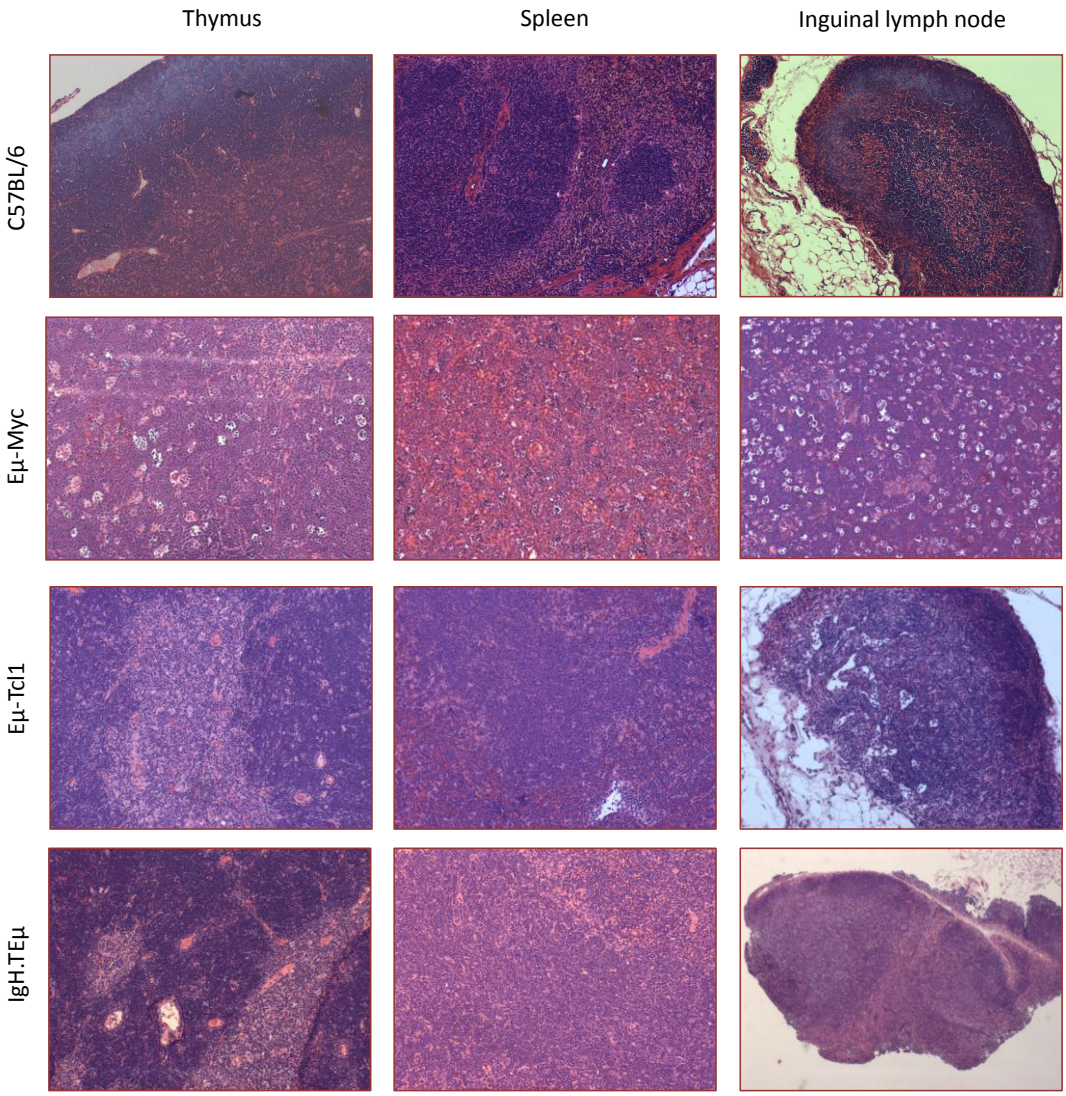

Figure 7.13 Comparative histological examination of secondary lymphoid organ architecture in C57BL/6, IgH.TEμ, Eμ-Tcl1, and Eμ-Myc mice

Upon attainment of the pre-determined experimental endpoints, mice were culled and dissected according to materials and methods section 2.4. Tissue sections were taken, fixed in formalin and paraffin embedded prior to staining with haematoxylin and eosin (H&E). Subsequently, the tissue architecture and the presence of tumour infiltrate were assessed by light microscopy in comparison to congenic C56BL/6 mice. All slides were examined at 10 x magnification. C57BL/6 and Eμ-Myc data kindly provided by Dr. E.L. Williams.

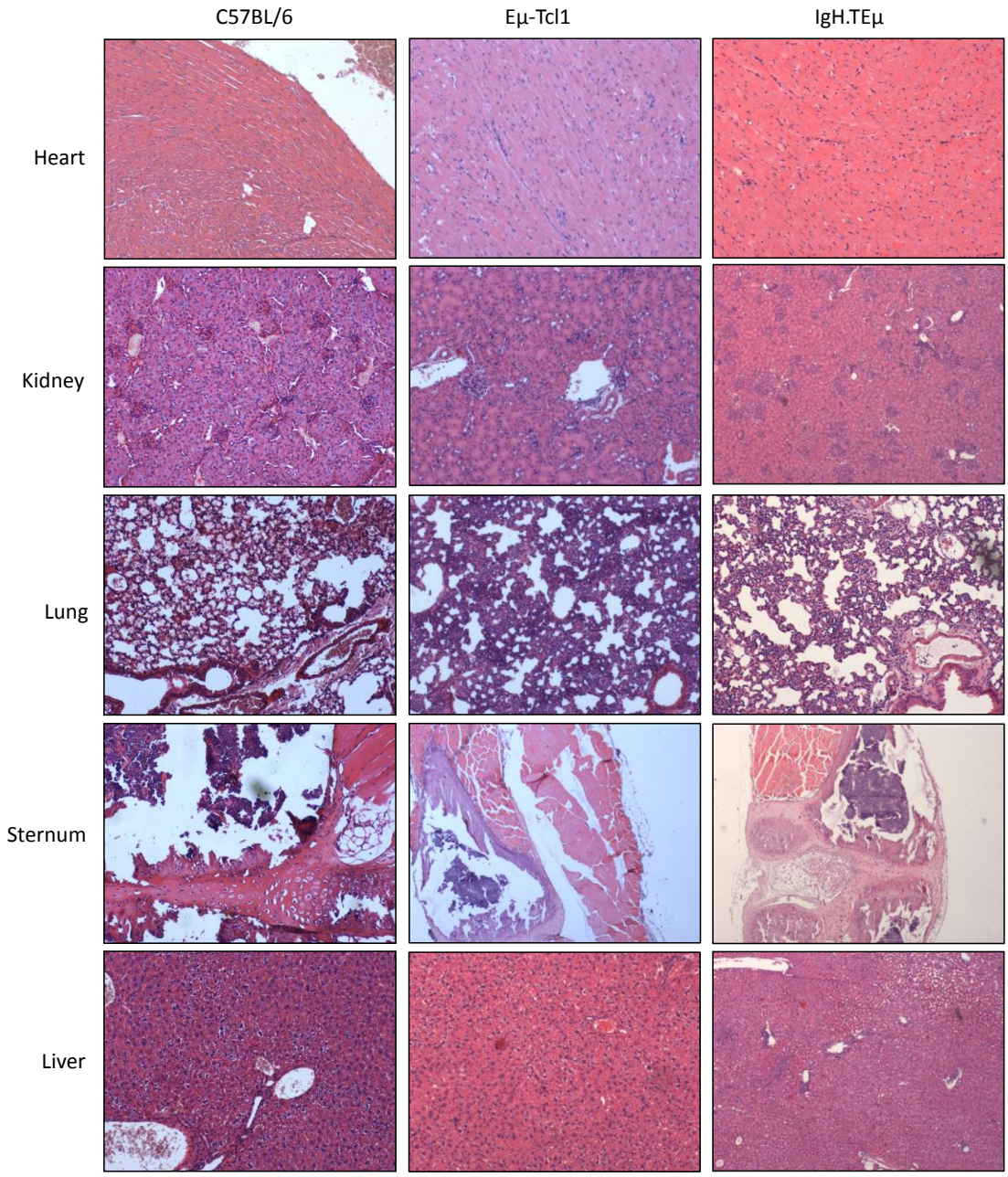

Figure 7.14 Histological examination of tumour infiltration into non-lymphoid tissues in IgH.TEμ animals in comparison to Eμ-Tcl1 and congenic C57BL/6 animals
(As in figure 7.6) Upon attainment of the pre-determined experimental endpoints, mice were culled and dissected according to materials and methods section 2.4. Non-lymphoid tissues (heart, kidney, lung, sternum, and liver) were collected and fixed in formalin prior to paraffin embedding and H&E staining. Areas of tumour infiltration were not apparent in any tissues of both IgH.TEμ and Eμ-Tcl1 animals, with the possible exception of the lungs, in comparison to C57BL/6 congenic animals (left panel). C57BL/6 and Eμ-Myc data kindly provided by Dr. E.L. Williams.

7.3.4 Identification of the immunophenotype of IgH.TEμ leukaemias

In order to characterise the immunophenotype of IgH.TEμ leukaemias, immunostaining of common CLL diagnostic markers was undertaken by flow cytometry. At autopsy, tissues of IgH.TEμ mice were processed as described for Eμ-Tcl1

mice, as demonstrated in figure 7.15 and table 7.5. Like Eμ-Tcl1 leukaemias, all IgH.TEμ tumours generated were $CD19^{+}$, IgM^{+}, $CD5^{+}$, $CD21^{+}$, $CD79a^{+}$, IgD^{+}, and $CD23^{-}$. Interestingly, however, in contrast to Eμ-Tcl1 leukaemias, all IgH.TEμ tumours were negative for surface expression of CD38.

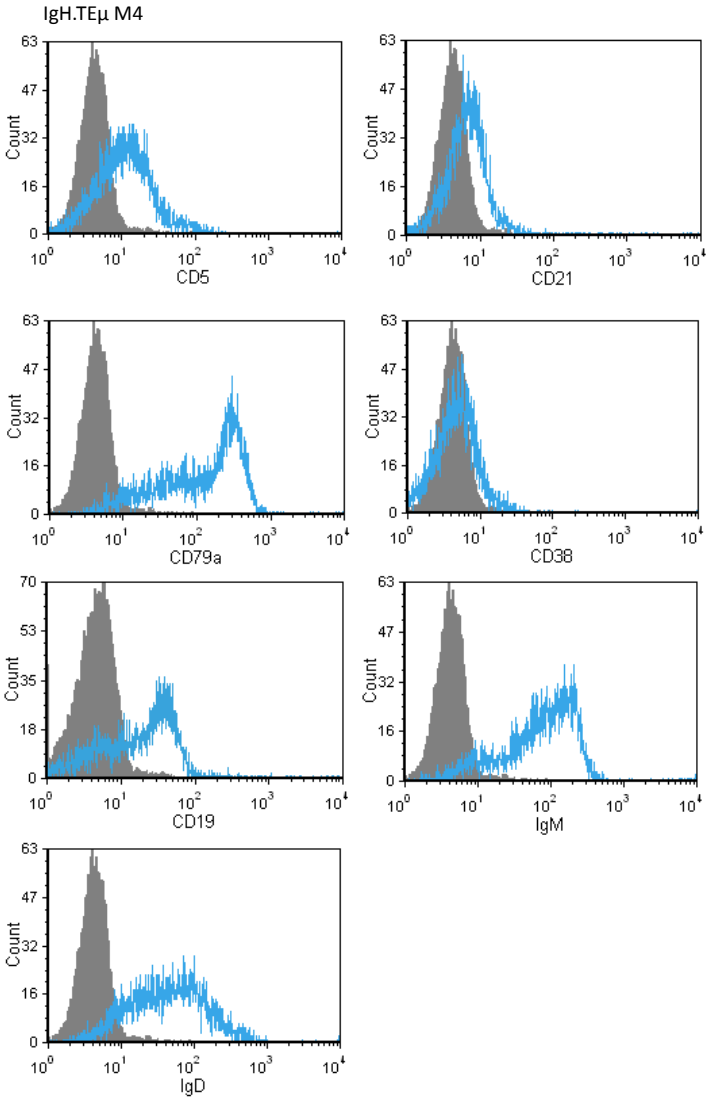

Figure 7.15 Immunophenotype analyses of IgH.TEμ tumours

Single cell suspensions derived from the spleens of IgH.TEμ mice were incubated with 5 μg/ ml PE or APC-conjugated anti-CD19 (Clone 1D3) or 10 μg/ml anti-$CD23^{PE}$ in the presence of 10 μg/ ml anti-IgM^{FITC} (Clone Mc39.12), anti-IgD^{FITC} (Clone 1.19), anti-$CD21^{FITC}$ (Clone 7G6), anti-$CD5^{FITC}$ (Clone 57-7.3), anti-$CD38^{FITC}$ (clone 1A5E8) or an appropriate isotype control for 30 minutes at 4°C, and analysed by flow cytometry. 10,000 viable cells, as determined by the FSC/ SSC profile, were gated and analysed for fluorescence in the FL-1, FL-2, and FL-4 channels, as before. Flow cytometry data was subsequently expressed as histograms overlaid upon isotype control values (grey peaks). Geometric means were subsequently calculated and normalised, by division, against geometric means calculated for the appropriate isotype control to generate relative surface expression values. Such values were subsequently plotted in table 7.5. Plots shown represent data from IgH.TEμ-M4, and are representative of the remaining tumours.

IgH.TEμ#	CD19	CD5	IgM	IgD	CD79a	CD23	CD21	CD38
BL1	High	Low	Med	Low	Med	-	Low	Low
001	High	Low	Med	Low	Med	-	Low	Low
AN1	High	Low	Med	Low	Low	-	Low	Low
AN2	High	Low	Low	Low	Med	-	Low	Low
M4	Med	Low	Med	Med	Med	-	Low	Low
$Bim^{+/-}$ M2	High	Low	Med	Low	Low	-	Low	-
$Bim^{+/-}$ N3	High	Low	Med	Low	Low	-	Low	Low
$Bim^{+/-}$ N2	High	Low	Med	Low	Med	-	Low	-
$Bim^{-/-}$ N4	High	Low	Med	Low	Med	-	Low	Low

Table 7.5 Summary of primary IgH.TEμ-Tcl1 immunophenotypes
Splenocytes from tumour bearing IgH.TEμ mice derived at this institution were stained as in figure 7.15 and analysed by flow cytometry. Expression levels were determined as Low, Medium (Med) or High, according to their relative normalised geometric means. 1-10 was described as Low, 10-50 Med, and 50+ as High.

7.4 Comparison of Eμ-Tcl1 and IgH.TEμ leukaemias

As outlined in figure 7.16, both Eμ-Tcl1 and IgH.TEμ animals appear to demonstrate similar rates of leukaemiagenesis, resulting in comparable median survival of 353 and 324 days, respectively. Whilst the onset of IgH.TEμ leukaemias appeared slightly more rapid, in comparison to Eμ-Tcl1 leukaemias, such differences were not statistically significant ($p > 0.05$ by Mantel-Cox statistical analysis). Furthermore, both leukaemias presented with similar physical characteristics (see tables 7.2 and 7.5) of extensive splenomegaly, alongside moderate lymphadenopathy and thymic hyperplasia. As outlined in figure 7.17, such enlargement in secondary lymphoid organ size and cellularity was comparable between both strains. Furthermore, leukaemias from both models demonstrate extensive infiltration of the spleens and slight enhancement of the size and density of lymphocyte rich areas in the LN and thymus. However, both failed to show any substantial infiltration of non-lymphoid organs, with the exception of the lungs, as outlined in figures 7.6-7 and 7.13-14. Such infiltration of the lungs is perhaps unsurprising for a largely blood-restricted tumour, since the lungs experience high rates of perfusion.

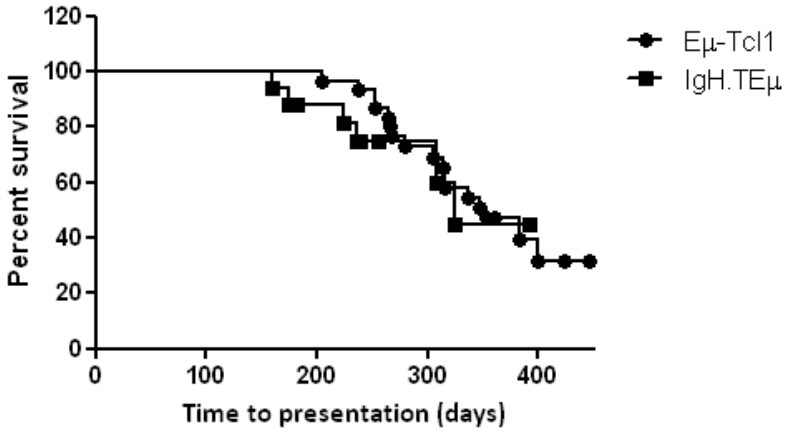

Figure 7.16 Comparative Kaplan-Meier survival curve analysis of Eμ-Tcl1 and IgH.TEμ mice
Cohorts of Eμ-Tcl1 (Black circles n = 30) and IgH.TEμ mice (Black squares n = 11) were crossed on to C57BL/6 background and monitored, from birth. Upon attainment of pre-determined humane experimental end-points, mice were culled as outlined in materials and methods section 2.4. No significant difference could be detected between the median survival of Eμ-Tcl1 and IgH.TEμ animals, as assessed by Mantel-Cox statistical testing.

Furthermore, both models generate leukaemias exhibiting a virtually identical $CD19^{+}$, $CD5^{+}$, IgM^{+}, IgD^{low}, $CD79a^{+}$, $CD21^{low}$, $CD23^{-}$, $CD38^{-/low}$ immunophenotype. As outlined in figure 7.18, the relative expression of such lineage and developmental markers appears largely comparable between both models. However, IgH.TEμ tumours exhibit slightly enhanced levels of cell surface IgD and CD23 expression, albeit non-statistically significant in both cases (p=0.07 by Student's unpaired T-test statistical analysis for both). However, since only 5 IgH.TEμ tumours have been analysed to date, it is predicted that additional samples may provide a statistically significant difference. Furthermore, all IgH.TEμ leukaemias generated appeared negative for surface expression of CD38 whereas, Eμ-Tcl1 leukaemias exhibited significant variation in expression levels. In addition, three Eμ-Tcl1 leukaemias were found to exhibit significantly higher levels of CD5 and CD79a expression than the majority. However, no correlation of CD38, CD5, or CD79a expression could be observed with time to presentation or other characteristics of presentation (spleen size, cellularity etc).

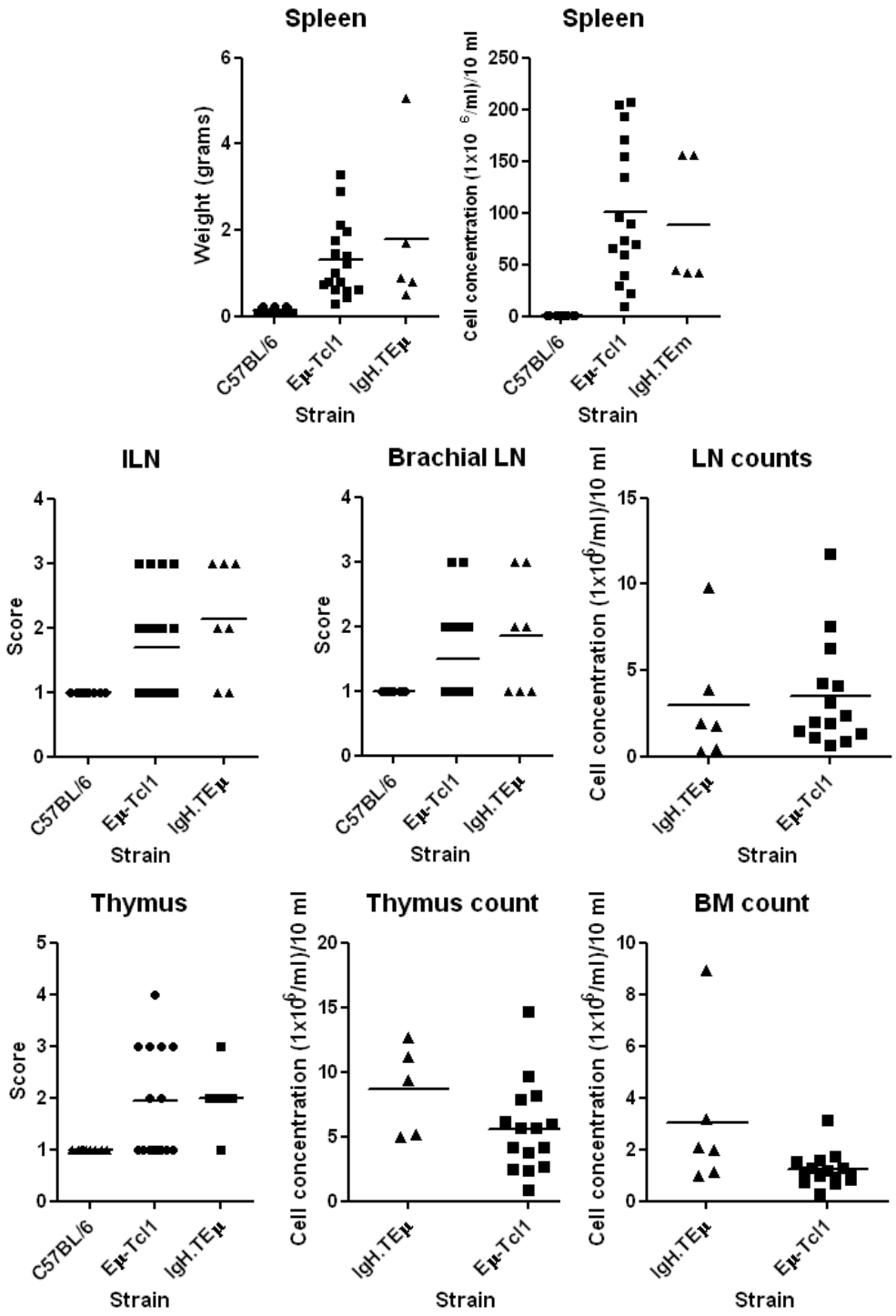

Figure 7.17 Comparative analysis of the cellularity of organs derived from Eμ-Tcl1 and IgH.TEμ mice

Organs harvested from C57BL/6, Eμ-Tcl1 and IgH.TEμ mice were passed through a fine nylon mesh until homogenous cell suspensions were achieved. Subsequently, suspensions were diluted to 10 ml final volume, red blood cells lysed, and the total number of cells assessed by counting using a Coulter Industrial D Cell counter. No significant differences were observed between the cellularities of IgH.TEμ or Eμ-Tcl1 mouse organs. C57BL/6 data kindly provided by Drs. A. Roghanian and A. White and Mr. H Johnston

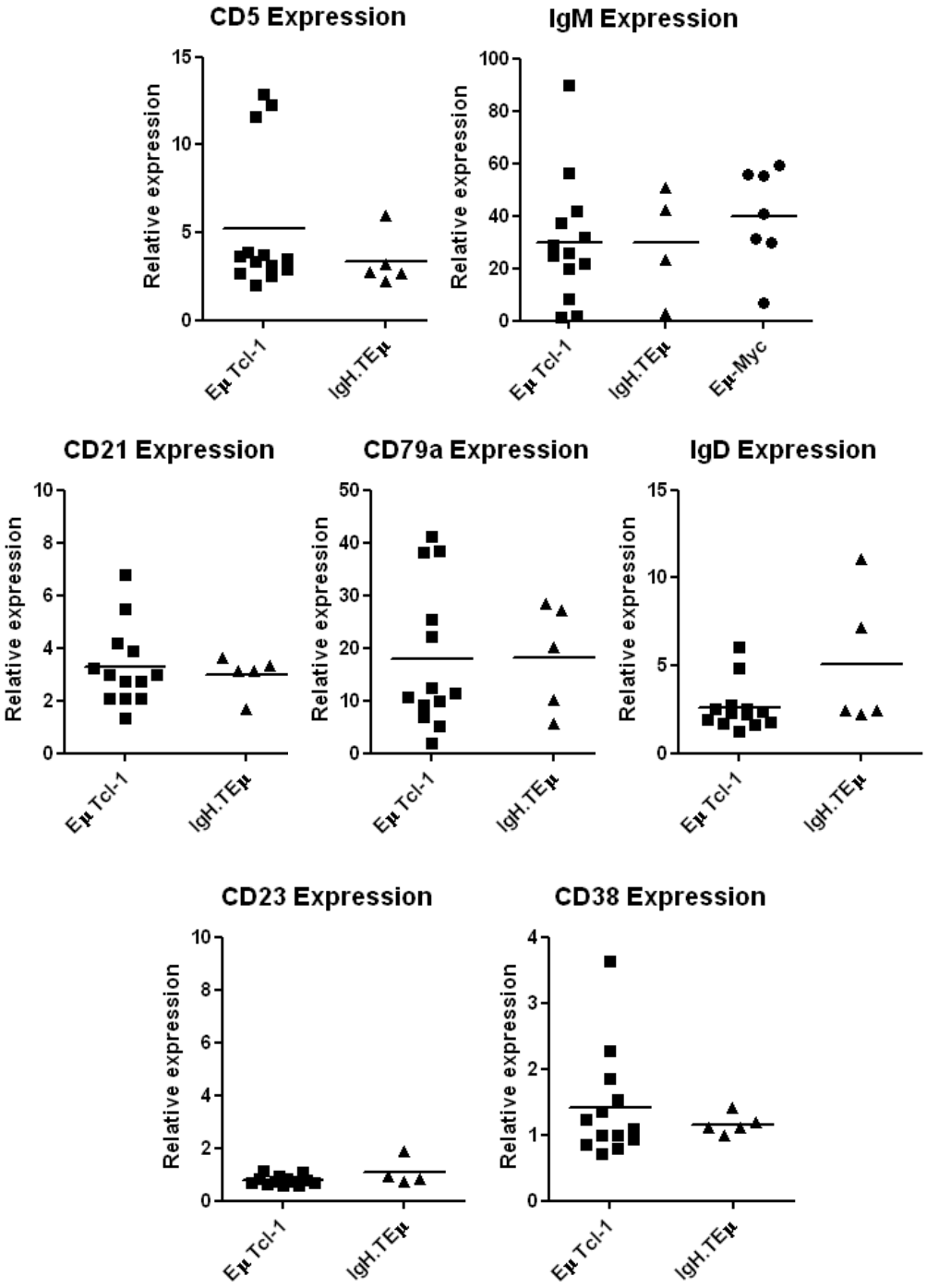

Figure 7.18 Comparative analyses of the immunophenotypes of tumours derived from Eμ-Tcl1 and IgH.TEμ mice
Normalised geometric means for each cell-surface marker analysed in Eμ-Tcl1 and IgH.TEμ tumours were plotted as dot plots to observe the relative levels of surface expression. Each dot represents data obtained from a single experiment utilising an individual spontaneous tumour.

Therefore, although driven by different oncogenes, both Eμ-Tcl1 and IgH.TEμ models of CLL generate largely comparable tumours which may provide an invaluable *in vivo* pre-clinical model for human CLL.

7.5 Examining the tumour microenvironment of Eμ-Tcl1 and IgH.TEμ leukaemias

In order to ascertain whether both tumours of Eμ-Tcl1 and IgH.TEμ mice demonstrated significant interaction with the splenic stroma, cellular co-localisation studies were performed upon snap frozen OCT-embedded splenic sections. Immunofluorescence studies were performed utilising markers of myofibroblasts and tumour fibroblasts, smooth muscle actin (SMA) and fibroblast activation protein (FAP), respectively. As evident in figure 7.19, both IgH.TEμ and Eμ-Tcl1 spleens stained positive for SMA. Whilst the vasculature is brightly positive for SMA, as expected, more diffuse patterned staining (circled) is also evident, indicative of myofibroblasts. Interestingly, areas of SMA positivity appeared to surround regions staining positive for CLL-like disease markers (B220 or CD5), indicative of both vasculature and myofibroblast recruitment to neoplastic sites. Whilst SMA positivity could be attributable to vasculature recruitment in the IgH.TEμ spleen, evident in figure 7.19, a much clearer area of cellular staining is apparent in the Eμ-Tcl1 spleen. Therefore, it appears as though neoplastic sites within the spleens of Eμ-Tcl1 and IgH.TEμ mice exhibit significant overlap with myofibroblast-rich areas. Such observations indicate that significant interactions between Eμ-Tcl1 tumours and the splenic stroma occur and, at least in part, facilitate leukaemiagenesis. However, further study is required to observe how frequent such interactions are in Eμ-Tcl1 and IgH.TEμ mice.

In addition, further analysis of tumour: stromal cell interaction was undertaken by Immunofluorescence utilising the marker of activated fibroblasts FAP.

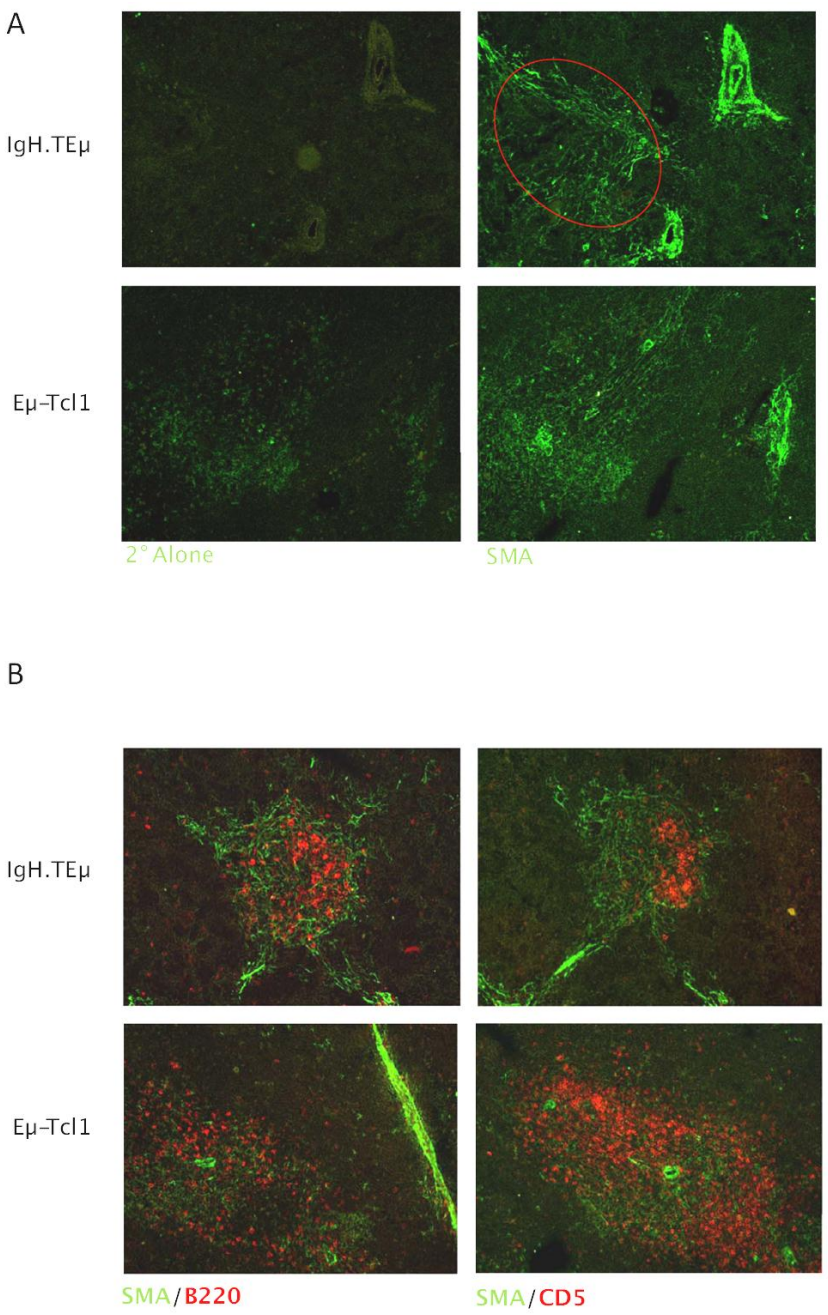

Figure 7.19 Identification of the localisation of CLL-like B-lymphocytes and myofibroblasts in the spleens of tumour bearing Eμ-Tcl1 and IgH.TEμ mice

Upon occurrence of terminal end-points, tumour bearing animals were sacrificed and dissected according to materials and methods section 2.4. During dissection, splenic samples were snap frozen in OCT and later sectioned using a cryostat and subjected to analysis of mouse smooth muscle actin (SMA), B220, and/ or CD5 distribution by immunofluorescence using Alexa-488 and Alexa-647 conjugated secondary anti-Fc antibodies. SMA positivity (green) denotes tumour vasculature and myofibroblasts whereas CD5 or B220 (red) were utilised to highlight CLL-like B-lymphocytes. In the absence of primary antibody (2° alone) vasculature appeared positive, due to auto-fluorescence, however distinct patterned areas, circled in red, were entirely absent in IgH.TEμ mice. However, in contrast Eμ-Tcl1 mice exhibited significantly higher background levels of fluorescence. Images represent a single experiment performed utilising a single IgH.TEμ or Eμ-Tcl1 tumour. Data kindly provided by Dr. S. James.

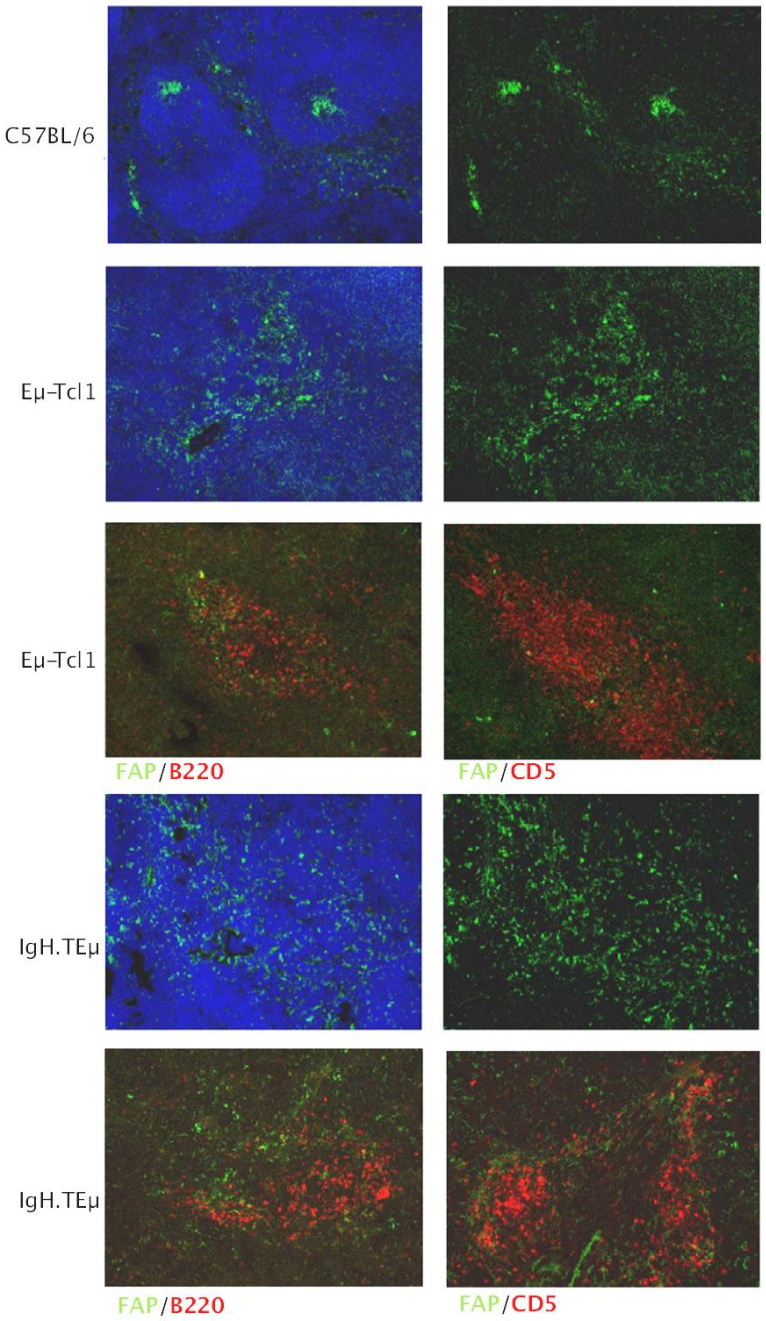

Figure 7.20 Identification of the localisation of CLL-like B-lymphocytes and tumour fibroblasts in the spleens of tumour Eμ-Tcl1 and IgH.TEμ mice

Upon occurrence of terminal end-points, tumour bearing animals were sacrificed and dissected according to materials and methods section 2.4. .During dissection, splenic samples were snap frozen in OCT and later sectioned using a cryostat and subjected to analysis of Fibroblast activation protein (FAP), B220, and CD5 distribution by immunofluorescence using Alexa-488 and Alexa-647 conjugated secondary anti-Fc antibodies. FAP positivity (green) denotes the presence of activated tumour fibroblasts, whereas CD5 and B220 (red) were utilised to highlight CLL-like B-lymphocytes. The FAP staining pattern of Eμ-Tcl1 and IgH.TEμ mice was compared to that of C57BL/6 congenic animals utilising DAPI as a nuclear counter-stain. Data represents a single experiment performed utilising a single Eμ-Tcl1 and IgH.TEμ tumour. Data kindly provided by Dr. S. James.

As evident in figures 7.20, normal C57BL/6 spleens demonstrate extensive positive staining for FAP in germinal centres. However, a much more diffuse pattern of staining

was observed in the spleens of Eμ-Tcl1 and IgH.TEμ mice, which was not restricted to germinal centres. Indeed areas of FAP positivity in Eμ-Tcl1 and IgH.TEμ spleens appeared to correlate with CD5/ B220-rich areas. Therefore, it appears that both Eμ-Tcl1 and IgH.TEμ tumour exhibit significant recruitment of both myofibroblasts and tumour fibroblasts to neoplastic sites. Such observations indicate that both Eμ-Tcl1 and IgH.TEμ tumours significantly alter splenic architecture and recruit cell types associated with the tumour microenvironment. Therefore, it appears as though Eμ-Tcl1 and IgH.TEμ mouse models of human CLL represent an appropriate model in which to study the interaction between tumours and the microenvironment.

7.6 Assessing the Eμ-Tcl1 as a pre-clinical *in vivo* model of CLL

It was demonstrated in Chapter 5 that disruption of ERK or Syk signalling significantly impaired BCR-induced cell death in the Eμ-Myc model. Therefore, it was hypothesised that such pathways may also be responsible for conveying key pro-survival signals in antigen driven tumours, such as CLL. If true, such observations may implicate Syk and ERK signalling as key molecular components linking the BCR to disparate cellular outcomes. As a consequence, it was hypothesised that disruption of antigen-mediated Syk and ERK signalling may represent a therapeutically beneficial strategy in the treatment of CLL.

Since spontaneous Eμ-Tcl1 and IgH.TEμ tumours demonstrate a median time to presentation in excess of 300 days, syngeneic transfer experiments utilising the well-documented Eμ-Tcl1 cell line Eμ-Tcl1-002 cell line, which typically presents in approximately 28 days, were undertaken in preliminary experiments. Since the Eμ-Tcl1-002 cell line was originally generated in C3H x C57BL/6 F1 mice, syngeneic transfer experiments were performed utilising recipient C3H x C57BL/6 F1 hybrid animals.

Cells were obtained as the generous gift from our collaborator Prof D. Efremov (Rome, Italy) and were first utilised in a pilot experiment to assess median survival. Briefly, $1x10^7$ Eμ-Tcl1-002 splenocytes or PBS was introduced into 9 C3H X C57BL/6 F1 (4 male, 5 female) mice of equal age by intraperitoneal injection. Subsequently, the onset of CLL-like disease was assessed by flow cytometry and WBC counts, as previously described. As outlined in figure 7.21, Eμ-Tcl1-002 tumours rapidly presented in

recipient C3H x C57BL/6 F1 mice, resulting in a median survival of 28 days with all animals succumbing to the CLL-like disease by day 35.

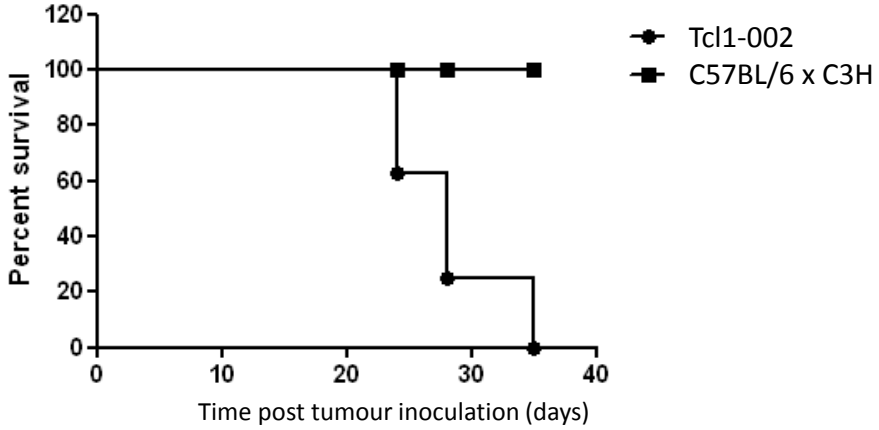

Figure 7.21 Identification the median survival of Eμ-Tcl1-002 recipient mice

$1x10^7$ Eμ-Tcl1-002 cells (Black circles) or PBS (Black squares) were injected intraperitoneally into syngeneic 9 C57BL/6 x C3H F1 recipients and the onset of CLL-like disease was assessed by routine blood flow cytometry and counts, as previously described. Mice were culled when tumours reached 80% peripheral lymphocytes, as previously described. Kaplan-Meier curve analysis of mice receiving Eμ-Tcl1-002 in comparison to congenic C3H x C57BL/6 mice. Eμ-Tcl1-002 recipient mice exhibit statistically significantly reduced survival (p= 0.0014) according to Mantel-Cox statistical analysis in comparison to PBS treated animals and recorded a median survival of 28 days post-tumour inoculation.

Within the same time frame, no C3H x C57BL/6 F1 mice receiving PBS alone displayed any symptoms of tumours and all out lived their Eμ-Tcl1-002 recipient counterparts. As a consequence, Eμ-Tcl1-002 recipient mice demonstrate a significantly reduced survival in comparison to non-recipient counterparts (p=0.0014 by Mantel-Cox statistical analysis). Therefore, Eμ-Tcl1-002 syngeneic transfers provide a rapid, short-term model within which to study the effects of Syk and MEK/ERK inhibition in a CLL-like disease.

To assess this, cohorts were established containing 2 male and 3 female C3H X C57BL/6 mice of equal age and $1x10^7$ Eμ-Tcl1-002 were given by intraperitoneal injection. Subsequently, the onset of CLL-like disease was assessed by flow cytometry and WBC counts, as previously described. Treatment regimes were initiated 14 days post-transfer, when CLL-like lymphocytes became elevated above baseline values in peripheral blood. PD was administered at 3 mg/kg/day daily from days 14-17 and then 20-24 days post tumour by oral gavage. In contrast the pro-drug form of the Syk inhibitor R406, R788, was given orally at a dose of 80 mg/kg/day, split into three doses spaced evenly throughout the day, on days 14-17 post tumour.

As evident in figure 7.22, Eμ-Tcl1-002 tumours typically appeared in the peripheral blood of C3H X C57BL/6 mice approximately 14 days post-administration, with elevation in WBC counts evident 2 days later. Interestingly, the onset of CLL-like disease appeared more rapid in female C3H X C57BL/6 mice than in males, possibly owing to their smaller size. However, no difference in overall median survival could be detected between males and females in the PBS treated group.

Mice were monitored for symptoms of illness and culled when $CD5^+$, $B220^+$ peripheral blood lymphocytes reached 80%, as before, and were examined by autopsy. As demonstrated in figure 7.22, Eμ-Tcl1-002 recipient mice exhibited a statistically significant reduction in survival in comparison to non-recipient C3H X C57BL/6 mice ($p = 0.0027$ as assessed by Mantel-Cox statistical analysis), recording a median survival of 24 days. However neither PD nor R788 administration significantly influenced the extent of $CD5^+$, $B220^+$ lymphocyte accumulation, WBC count or median survival (both PD and R788 gave a median survival of 24 days), as demonstrated in figures 7.23-24. A single PD-treated mouse appeared to exhibit substantial delay in the onset of disease in comparison to other members of its group. However, such an occurrence was attributed to a failure of the tumour to grow or a failed injection rather than any therapeutic effect, as PD treated female 4 (F4) failed to demonstrate any accumulation of Eμ-Tcl1-002 in the peripheral blood up to 68 days post-tumour administration.

Since disruption of BCR signalling appeared not to delay the onset of CLL-like disease or have an impact upon increases in WBC counts, we attempted to utilise a therapeutic strategy currently used in CLL patients, namely anti-CD20 mAb therapy. Anti-CD20 (clone 18B12) mouse IgG2a (mIgG2a) was applied by intravenous injection at a dosage of 250 μg/ mouse on days 14, 20 and 28 post-tumour. As evident in figure 7.25, anti-CD20 treatment significantly extended median survival from 24 days in non-treated mice to 49 days ($p = 0.0027$ by Mantel-Cox statistical analysis).

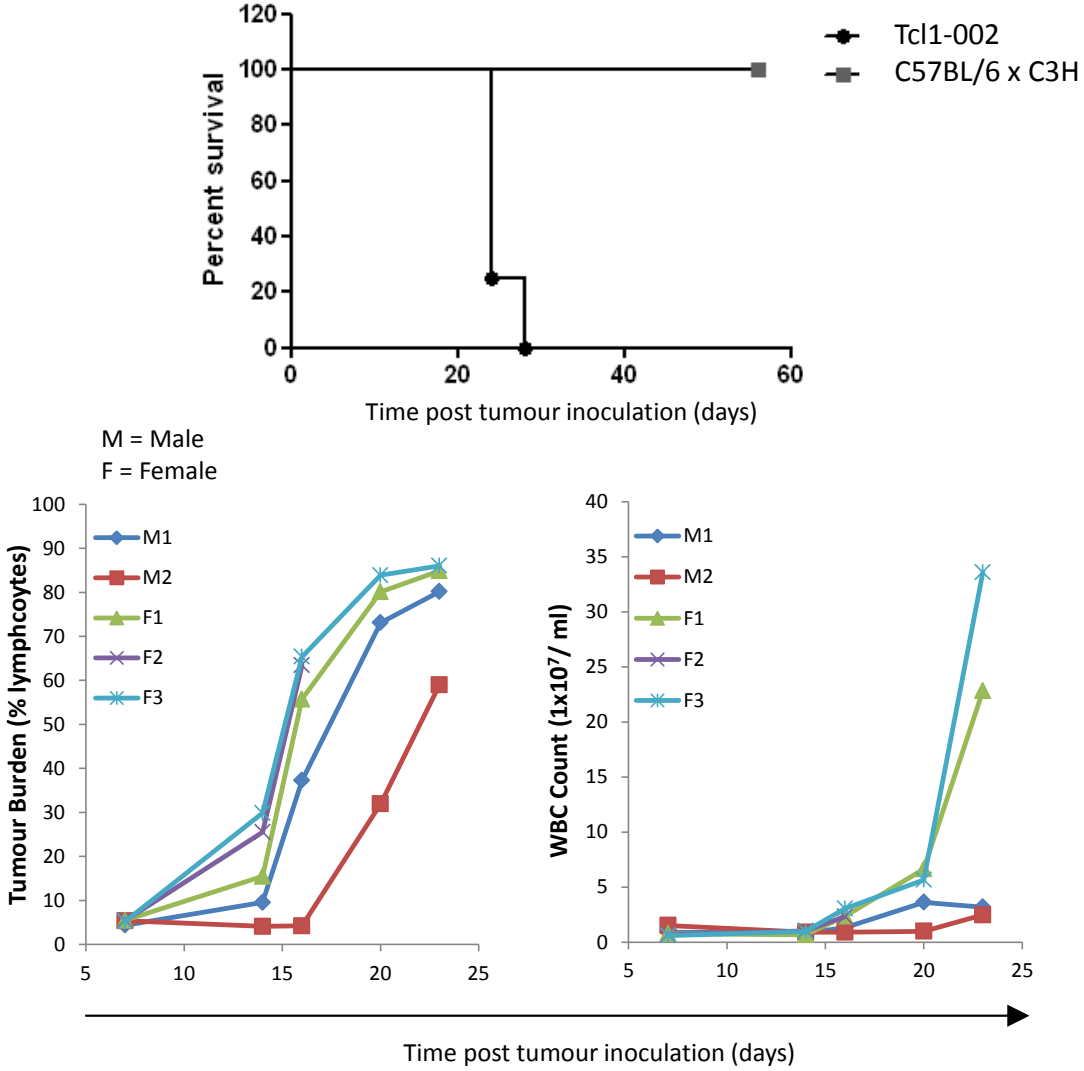

Figure 7.22 Identification of Eμ-Tcl1 xenograft as an effective pre-clinical model for CLL-like disease

$1x10^7$ cells from the Eμ-Tcl1-002 cell line were injected intraperitoneally into syngeneic C57BL/6 x C3H F1 recipients (5 per group) and the onset of CLL-like disease was assessed by routine blood flow cytometry and counts, as previously described, 7, 14, 16, 21, and 24 days post-tumour administration. Mice were culled when tumour burdens reached 80% of peripheral lymphocytes, as previously described. **A** Kaplan Meier curve analysis of mice receiving Eμ-Tcl1-002 in comparison to PBS treated congenic C3H x C57BL/6 mice. Eμ-Tcl1-002 recipient mice exhibit statistically significantly reduced survival (p= 0.0027) according to Mantel-Cox statistical analysis. **B** Traces depicting peripheral tumour burden (left) and WBC counts (right) over time post Eμ-Tcl1-002 transfer in individual mice. Each line represents a single mouse in the group monitored over time.

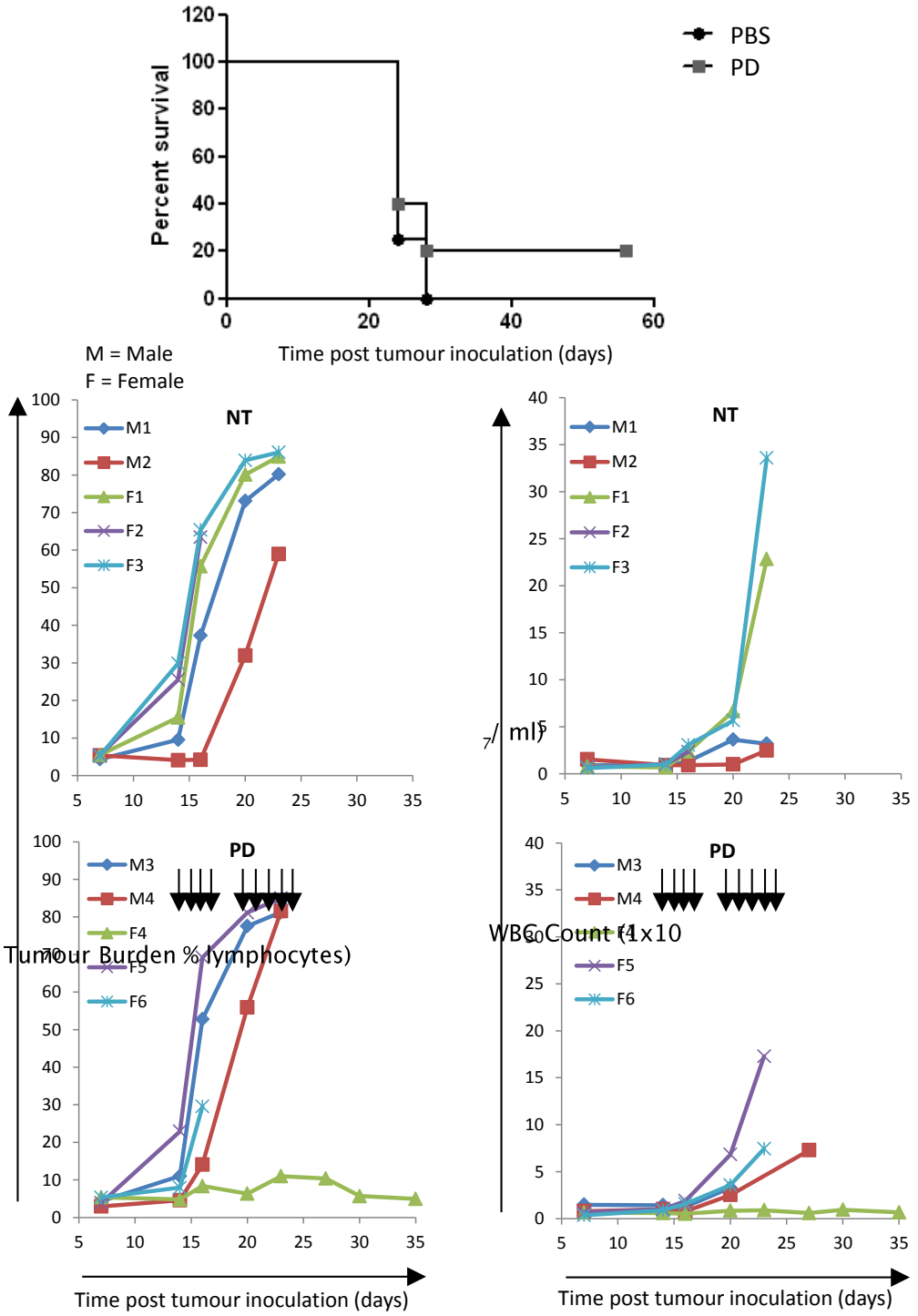

Figure 7.23 Assessing the impact of MEK inhibition upon the growth and survival of Eμ-Tcl1 recipient mice

5 C3H x C57BL/6 per group received 1x10^7 Eμ-Tcl1-002 cells by intraperitoneal injection and were monitored for signs of tumour over time, as outlined in figure 7.15. PD treated mice received 3 mg/kg PD by oral gavage on days 14, 15, 16, 17, 20, 21, 22, 23, and 24 post-tumour (depicted by arrows). **A** Subsequently, the survival of PD-treated mice was compared to that of untreated animals. No statistically significant differences in overall survival were observed by Mantel-Cox statistical analysis. **B** Depiction of the impact of PD treatment upon deposition of CLL-like B-lymphocytes into the peripheral blood and the subsequent impact upon WBC counts.

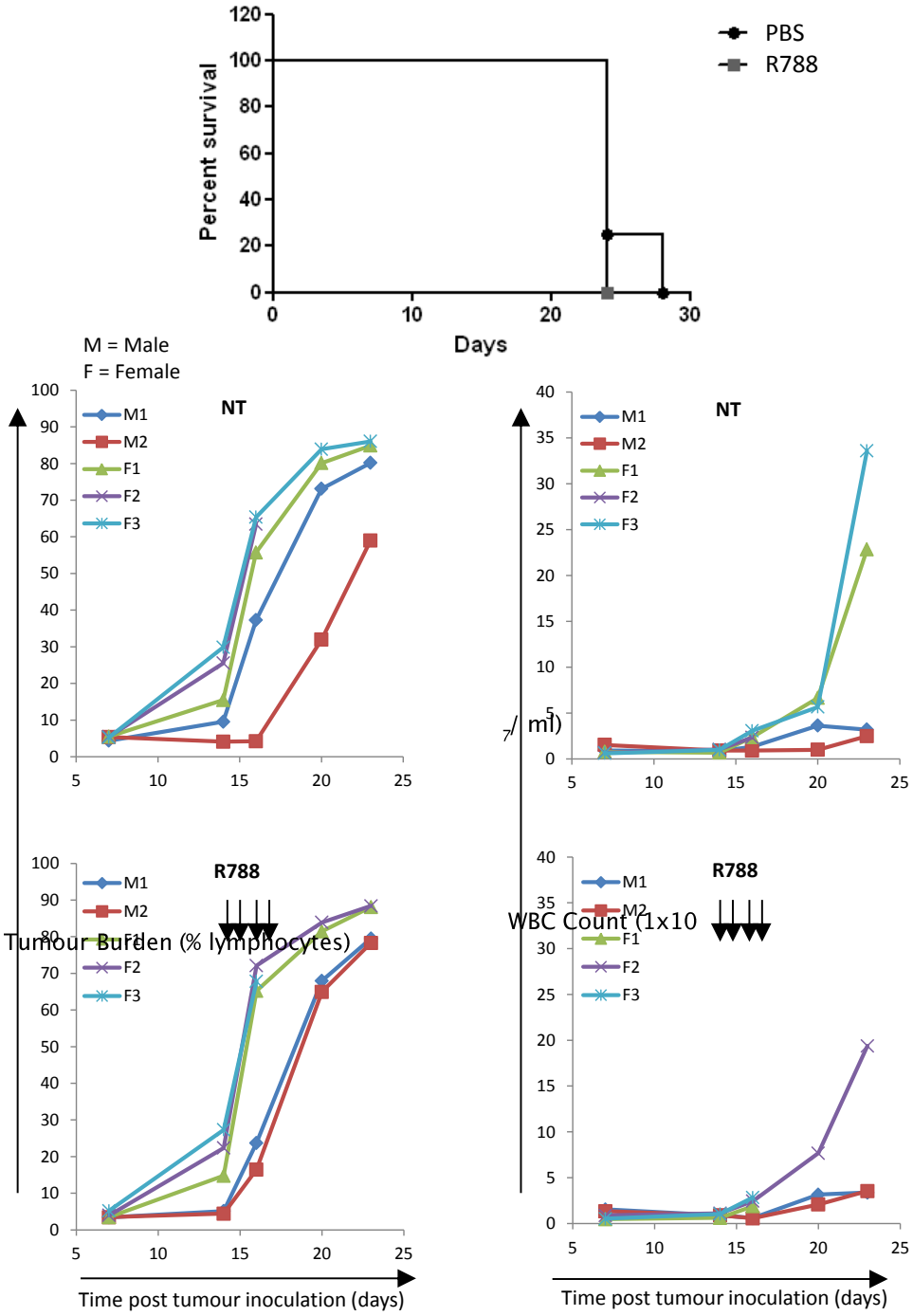

Figure 7.24 Assessing the impact of Syk inhibition upon the growth and survival of mice receiving Eμ-Tcl1 tumours

5 C3H x C57BL/6 per group received 1x10^7 Eμ-Tcl1-002 by intraperitoneal injection and were monitored for signs of tumour over time, as outlined in figure 7.15. R788 treated mice received 80 mg/kg split into three doses equally spaced throughout the day by oral gavage on days 14, 15, 16, and 17 post-tumour (depicted by arrows). **A** Subsequently, the survival of R788-treated mice was compared to that of untreated animals. No statistically significant differences in overall survival were observed by Mantel-Cox statistical analysis. **B** Depiction of the impact of R788 treatment upon deposition of CLL-like B-lymphocytes into the peripheral blood and the subsequent impact upon WBC counts.

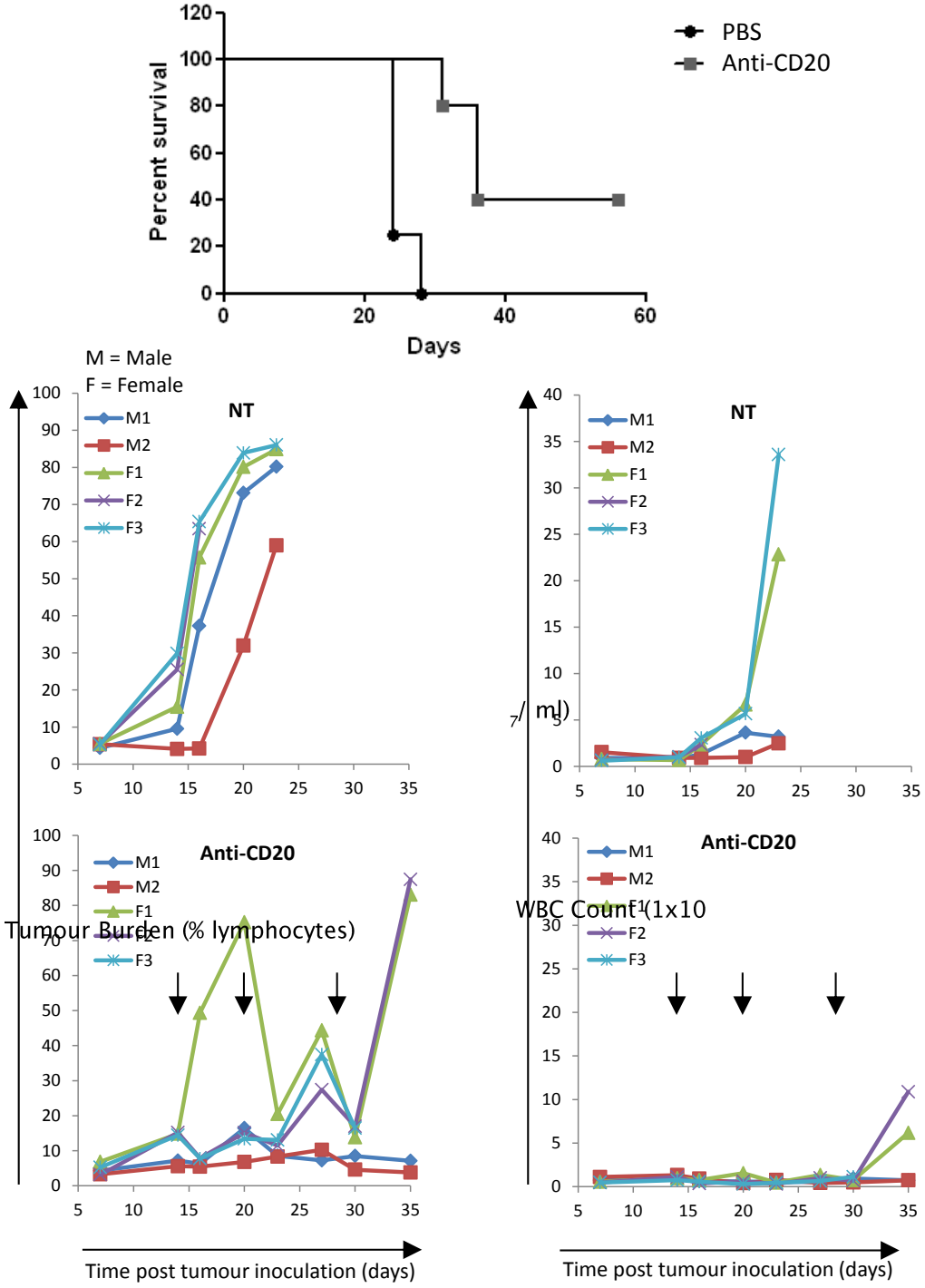

Figure 7.25 Assessing the impact of anti-CD20 treatment upon the growth and survival of Eμ-Tcl1 recipient mice

5 C3H x C57BL/6 per group received 1x10^7 Eμ-Tcl1-002 by intraperitoneal injection and were monitored for signs of tumour over time, as outlined in figure 7.15. Anti-CD20 treated mice received 250 μg 18B12 mouse IgG2a (anti-CD20) by intravenous injection on days 14, 20, and 28 post-tumour (depicted by arrows). **A** Subsequently, the survival of anti-CD20-treated mice was compared to that of untreated animals. A statistically significant improvement in survival was observed in anti-CD20-treated animals as assessed by Mantel-Cox statistical analysis (p=0.0047) **B** Depiction of the impact of anti-CD20 treatment upon deposition of CLL-like B-lymphocytes into the peripheral blood and the subsequent impact upon WBC counts.

Furthermore, anti-CD20 administration resulted in a rapid decrease in circulating $CD5^+$, $B220^+$ levels two days post-treatment, which appeared to persist for approximately four days. As a consequence the previously documented increases in peripheral WBC counts appeared delayed from day 16 to day 35.

Initially, anti-CD20-treated female 1 (F1) appeared not to respond to mAb therapy however, comparable tumour depletion was seen when subsequent doses were given. Therefore, it appears likely that a failed injection was responsible for the initial lack of an effect rather than any intrinsic resistance in this mouse. Since the frequency and number of leukaemic cells returned to comparable levels upon subsequent doses, female 1 was included in subsequent data analysis. Therefore, such data reveal that Eμ-Tcl1 leukaemias respond to therapies already known to be effective in the treatment of CLL.

Previous work in the laboratory has demonstrated that mAb therapy directed against CD40 significantly enhanced the survival of mice inoculated with the aggressive lymphoma cell-lines (410). Therefore, we aimed to identify whether such a therapeutic strategy may also yield therapeutically beneficial results in Eμ-Tcl1-002 recipient mice. Therefore, 1 mg/ mouse anti-CD40 Rat IgG (clone 3.23) was administered on day 14 and a subsequent dose of 250 μg/ mouse given on day 28 post-tumour (dosing based on previous studies (413)). As evident in figure 7.26, anti-CD40 treatment significantly enhanced the median survival of Eμ-Tcl1-002 recipient mice; from 24 days to 36 days, and delayed WBC count increases, albeit to a lesser extent than anti-CD20 treatment. Whilst anti-CD20 offered rapid B-cell depletion, anti-CD40 treatment appeared to slow the deposition rate of CLL-like B-lymphocytes into the periphery. Consequently, both anti-CD20 and anti-CD40 treatment appeared to effectively delay the onset of Eμ-Tcl1 leukaemia but appear mechanistically different in how this effect is achieved. Interestingly though, at the time of writing anti-CD40-treated female 5 (F5) exhibited only 10.8% peripheral $CD5^+$ B-lymphocytes and appeared in good health 78 days post-tumour administration. Since F5 exhibited initial tumour population expansion in a comparable fashion to other group members, it appears as though tumour inoculation was successful. Therefore, anti-CD40 treatment led to stable disease and slowed progression.

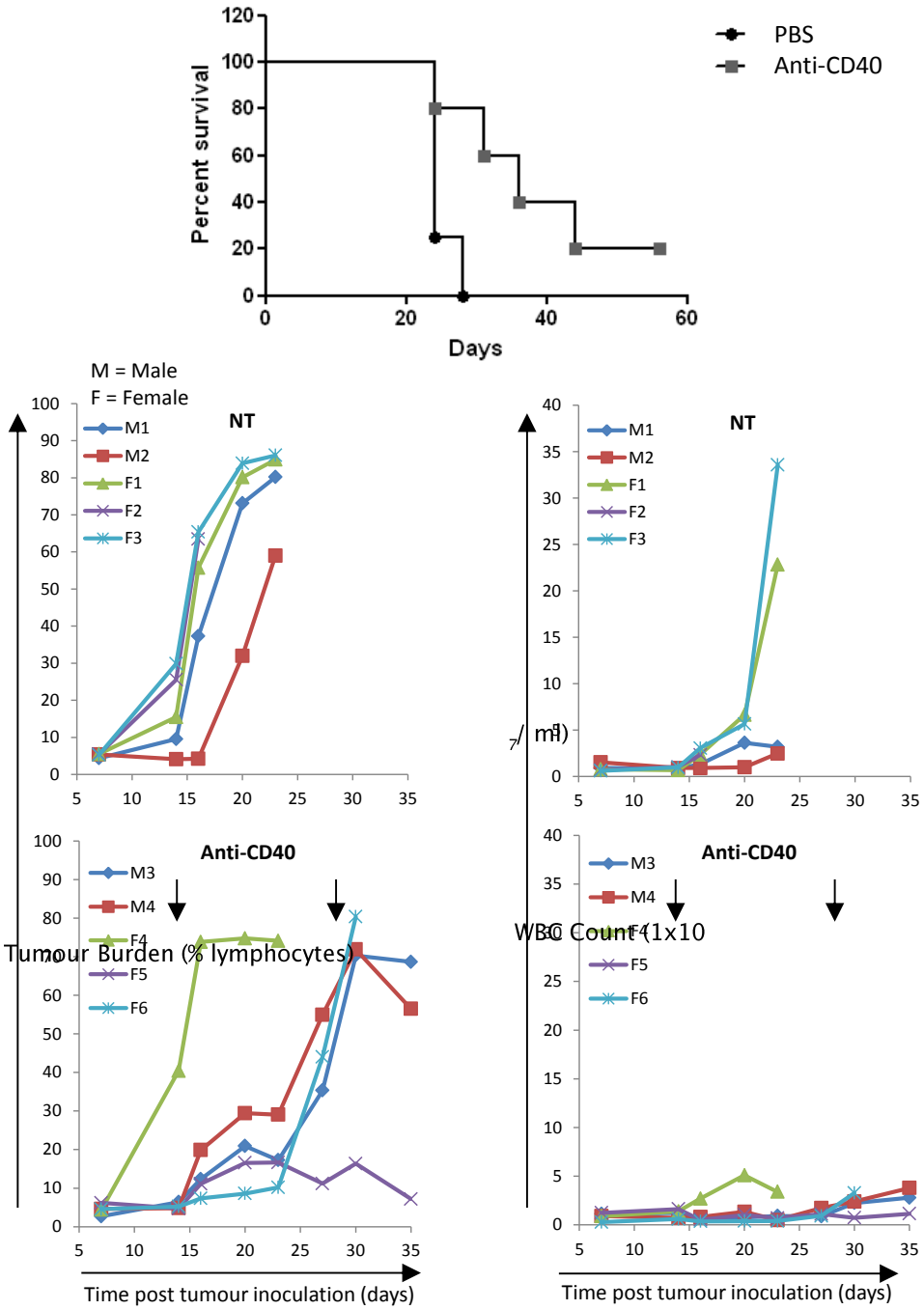

Figure 7.26 Assessing the impact of anti-CD40 treatment upon the growth and survival of mice receiving Eμ-Tcl1 tumours

5 C3H x C57BL/6 per group received 1x10^7 Eμ-Tcl1-002 by intraperitoneal injection and were monitored for signs of tumour over time, as outlined in figure 7.15. Anti-CD40 treated mice received 1mg 3.23 Rat IgG (anti-CD40) by intravenous injection on days 14, and 250 μg on day 28 post-tumour (depicted by arrows). **A** Subsequently, the survival of anti-CD40-treated mice was compared to that of untreated animals. A statistically significant improvement in survival was observed in anti-CD40-treated animals as assessed by Mantel-Cox statistical analysis (p=0.0128) **B** Depiction of the impact of anti-CD40 treatment upon deposition of CLL-like B-lymphocytes into the peripheral blood and the subsequent impact upon WBC counts.

Therefore, it appears that only mAb therapy directed against CD20 and CD40 antigens proved capable of offering enhanced survival. The relative success of anti-CD20/ CD40

mAb therapy and failure of MEK and Syk inhibition is most evident in figure 7.27, whereby significant reductions in WBC count and $CD5^+$, $B220^+$ percentage was evident only in mAb-treated mice.

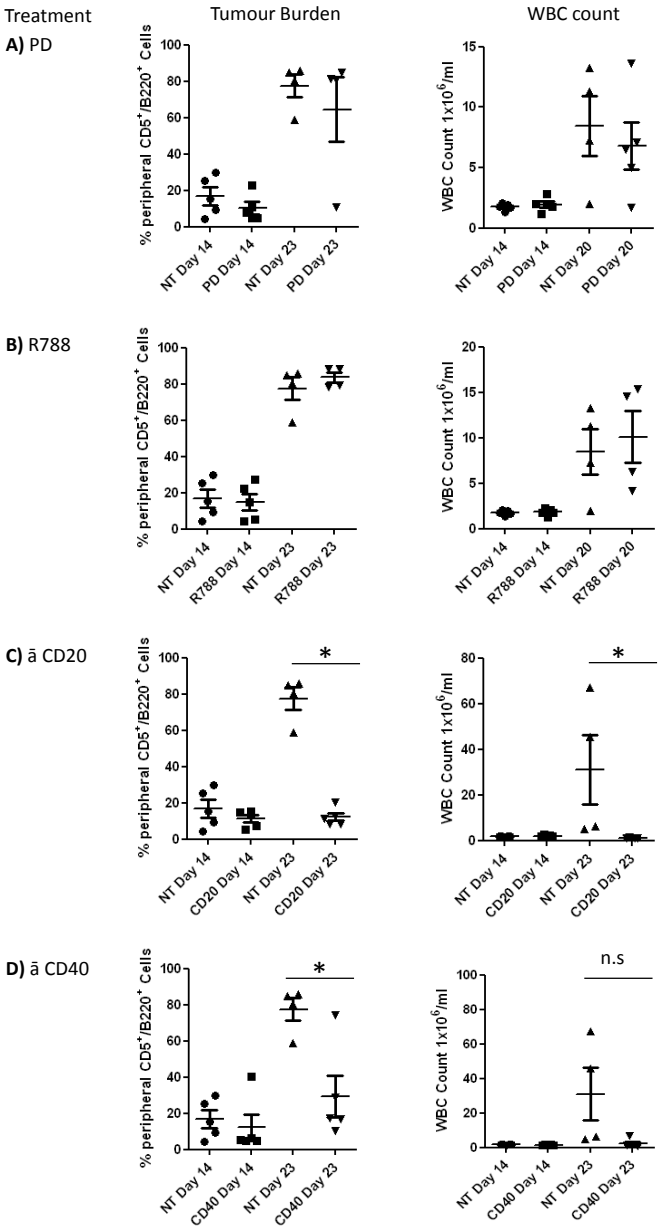

Figure 7.27 Comparative analysis of the effect of therapies upon the extent of CLL-like B-cells in peripheral blood

Dot plot analysis of Tumour burden and WBC counts recorded in Eμ-Tcl1 recipient mice, as outlined in figures 7.22 – 7.26, after 14 and 23 days. Asterisks denote statistically significant differences as adjudged by Student's T-Test statistical analysis ($p<0.05$).

At the pre-defined experimental endpoint, mice from all treatment groups were culled the total cell number and size of spleens analysed. As evident in figure 7.28, no discernable differences in splenic cellularity or size could be detected between

experimental groups (except for the time taken to reach endpoint). As a consequence, it appears as though whilst anti-CD20 and anti-CD40 mAb therapy extend survival, they are unable to prevent the final outcome of splenomegaly and chronic leukaemia. Therefore, whilst anti-CD20/ CD40 appear therapeutically beneficial, additional work is required to optimise treatment regimens (probably via combination therapy) in order to offer a complete cure, rather than just extend survival.

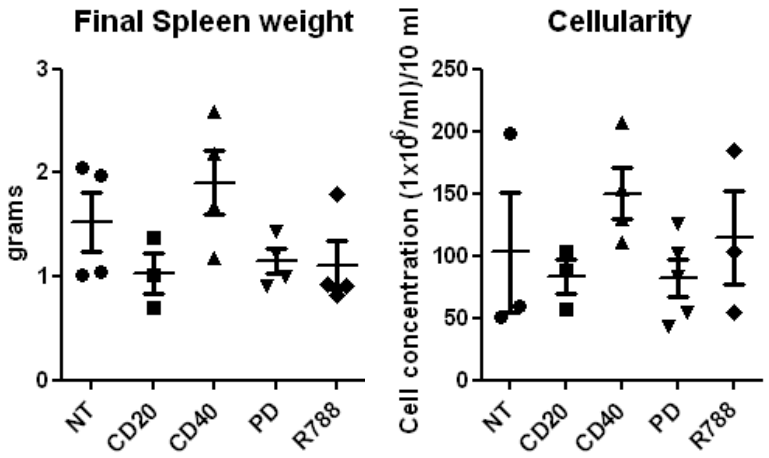

Figure 7.28 Comparative analyses of organ size and cellularity in Eμ-Tcl1-002 recipient mice

Upon attainment of 80% tumour burden in peripheral blood, Eμ-Tcl1-002 recipient mice were culled and organs harvested, as previously described. Spleen weights were taken and harvested organs were passed through a fine nylon mesh until a homogenous cell suspension was achieved. Subsequently, suspensions were diluted to 10 ml final volume, red blood cells lysed, and the total number of cells assessed by using a Coulter Industrial D Cell counter. Subsequently, comparative analysis between the previously defined treatment groups was undertaken using Students T-Test analysis. No significant differences were observed between the cellularities or weight of organs from tumour bearing mice.

7.7 Assessing the potential tumour suppressor role of Bim in both the Eμ-Tcl1 and IgH.TEμ models of leukaemia

In chapter 4, we described Bim as a key molecular regulator of apoptosis downstream of the BCR. Therefore, we hypothesised that the proposed antigen-driven process of CLL-like leukaemiagenesis may be accelerated by genetic loss of Bim, since tumours likely have to attain resistance to the apoptotic outcome of BCR-signalling during leukaemiagenesis.

Therefore, in order to assess the potential role of Bim as a tumour suppressor in the Eμ-Tcl1 and IgH.TEμ models, transgenic mice were crossed on to $Bim^{-/+}$ and $Bim^{-/-}$ C57BL/6 backgrounds and assessed for the onset of CLL-like disease, as previously described. Unfortunately, once crosses had been performed the animal facility housing

$Bim^{-/-}$ and $Bim^{+/-}$ Eμ-Tcl1 and IgH.TEμ cohorts suffered an outbreak of murine hepatitis virus (MHV). Therefore, all animals had to be culled, the facility de-contaminated, and strains double re-derived by caesarean blastocyst implantation. Subsequently, the relevant crosses were initiated once again. However, due to the approximate 18 month delay, and the time taken for tumour presentation (≈ 300 days), at the time of writing insufficient numbers of $Bim^{-/-}$ and $Bim^{-/+}$ Eμ-Tcl1 and IgH.TEμ mice had succumbed to CLL-like disease to allow detection of a difference in median survival in comparison to $Bim^{+/+}$ Eμ-Tcl1 or IgH.TEμ animals, as demonstrated in figure 7.29. Although statistically non-significant, both mono-allelic and bi-allelic loss of Bim did appear to slightly enhance the rate of leukaemiagenesis in the IgH.TEμ model. In order to further assess the effect of loss of Bim, in light of the insufficient number of data points, IgH.TEμ $Bim^{-/-}$ and $Bim^{+/-}$ survival data was pooled and compared to $Bim^{+/+}$ IgH.TEμ animals. However, as can be seen in figure 7.29, the overall trend of Bim deficient IgH.TEμ survival appears not statistically different to comparison to $Bim^{+/+}$ IgH.TEμ animals. However, in order to confirm any findings, survival curve analysis is required after additional mice succumb to CLL-like disease.

Furthermore, Bim deficient IgH.TEμ tumours failed to demonstrate significant increases in size or cellularity of secondary lymphoid organs, as evident in figures 7.30-31. As expected, slight increases in both the size and cellularity of LN and thymus were evident upon bi-allelic loss of Bim (233) However, a trend in the reduction in the cellularity of the BM was also evident in Bim deficient IgH.TEμ animals, albeit to statistically non-significant levels.

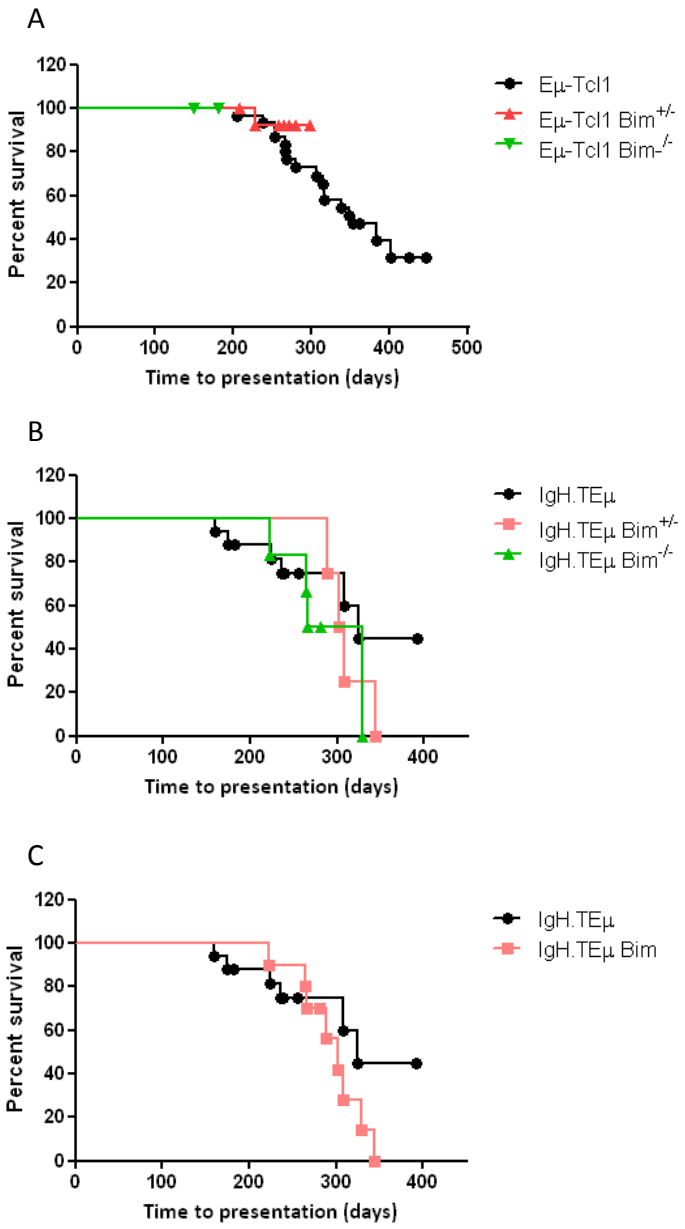

Figure 7.29 Examining the effect of mono or bi-allelic loss of Bim upon the rate of leukaemiagenesis in Eμ-Tcl1 and IgH.TEμ mice

A Cohorts of Eμ-Tcl1 mice were crossed onto $Bim^{-/+}$ (Red triangles n= 24), and $Bim^{-/-}$ (green triangles n= 8) C57BL/6 backgrounds and monitored, from birth, for the incidence of tumours in comparison to $Bim^{+/+}$ Eμ-Tcl1 animals (n= 30) held at this institution. **B** Cohorts of IgH.TEμ mice were crossed onto $Bim^{-/+}$ (Red squares n= 4), and $Bim^{-/-}$ (green triangles n= 6) C57BL/6 backgrounds and monitored, from birth, for the incidence of tumours in comparison to $Bim^{+/+}$ IgH.TEμ animals (n= 11) held at this institution. Upon occurrence of the pre-defined experimental endpoints, mice were culled as outlined in materials and methods section 2.4. Insufficient numbers of Eμ-Tcl1 $Bim^{-/-}$ or $Bim^{-/+}$ mice were generated at the time of writing to confidently observe an effect upon the rate of tumourigenesis. However, genetic loss of Bim does not appear to enhance the rate of leukaemiagenesis in Eμ-Tcl1 mice. In addition, neither mono-allelic nor bi-allelic loss of Bim appeared to have a significant effect upon the incidence of spontaneous tumour development in the IgH.TEμ model (p= 0.2612 and 0.4531 respectively) by mantel-Cox statistical testing. C In order to boost animal numbers, IgH.TEμ $Bim^{-/+}$ and $Bim^{-/-}$ groups were combined in order to better assess the role of Bim in IgH.TEμ leukaemiagenesis. Again loss of Bim failed to enhance the rate of IgH.TEμ leukaemiagenesis (p = 0.262) as assessed by Mantel-Cox statistical analysis

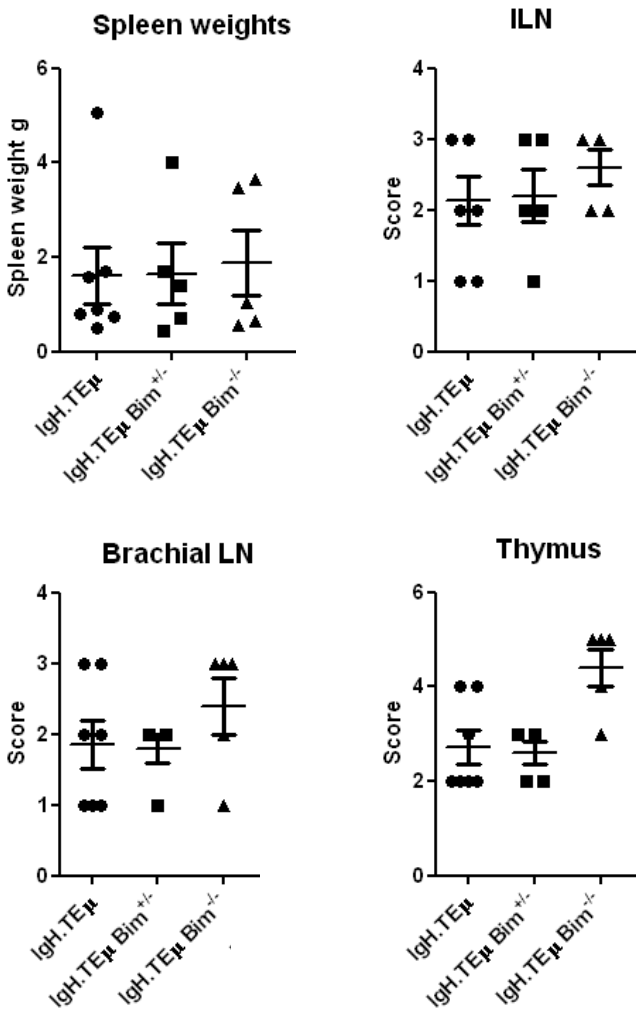

Figure 7.30 Analysing the effect of mono or bi-allelic loss of Bim upon the size of secondary lymphoid organs in tumour bearing IgH.TEμ mice

Upon the onset of tumour symptoms, tumour bearing animals were sacrificed as outlined in materials and methods section 2.4. Subsequently, the size of secondary lymphoid organs was assessed by weight or according to the guidelines identified in table 7.1. Loss of Bim failed to significantly enhance the size of any secondary lymphoid organs taken from terminal IgH.TEμ animals ($p > 0.05$) as assessed by Student's unpaired T-test statistical analysis. However, Bim-/- animals generally exhibited greater enlargement of the ILN, brachial LN and Thymus in comparison to $Bim^{+/+}$ IgH.TEμ animals, albeit to a statistically non-significant extent.

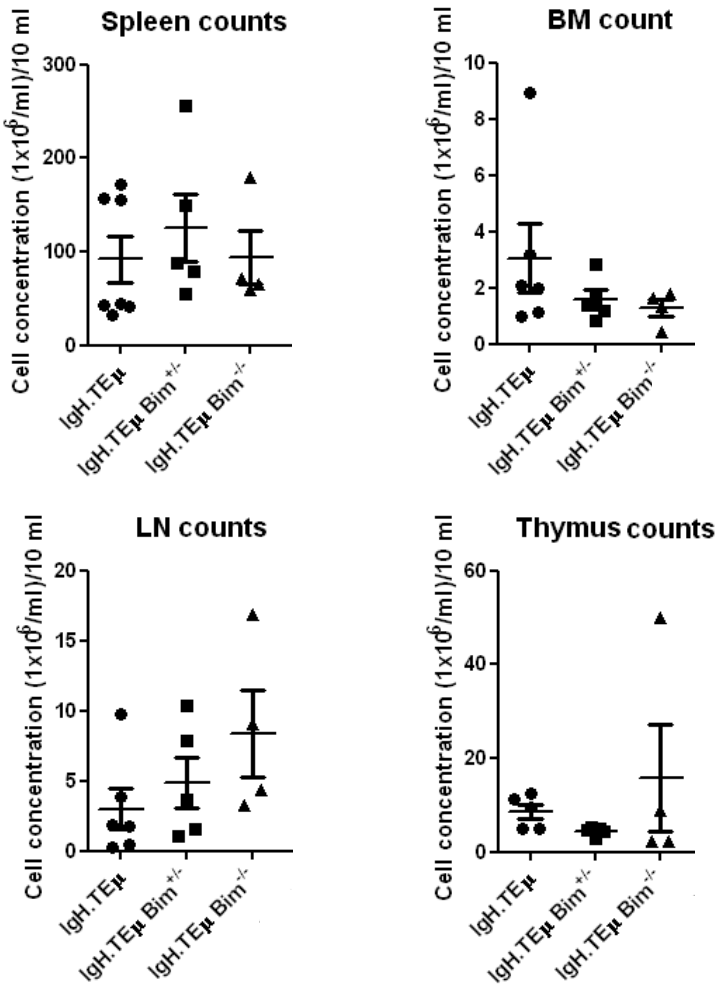

Figure 7.31 Analysing the effect of mono or bi-allelic loss of Bim upon the cellularity of secondary lymphoid organs in tumour bearing IgH.TEμ mice

Upon the onset of tumour symptoms, tumour bearing animals were sacrificed as outlined in materials and methods section 2.4, and secondary lymphoid organs harvested. Harvested organs were subsequently passed through a fine nylon mesh until a homogenous cell suspension was achieved. Subsequently, suspensions were diluted to 10 ml final volume, red blood cells lysed, and the total number of cells assessed using a Coulter Industrial D Cell counter. Subsequently, comparative analysis between the previously defined treatment groups was undertaken using Students T-Test analysis. No significant differences were observed between the cellularities or weight of organs from tumour bearing mice. However, in general loss of Bim appeared to increase the cellularity of LN and decrease that of the BM, albeit to a statistically non-significant extent. Bars represent standard deviation.

Taken together, the above data appears to suggest that genetic loss of Bim does not accelerate the rate of spontaneous leukaemiagenesis and only minimally impacts the extent of secondary lymphoid organ enlargement and cell number. Such observations suggest that Bim does not play a key tumour suppressor role in the IgH.TEμ model of CLL. However, further analysis is required following the development of additional spontaneous $Bim^{+/+}$, $Bim^{+/-}$, and $Bim^{-/-}$ IgH.TEμ tumours to support this conclusion.

7.8 Chapter Discussion

In this chapter, a panel of spontaneous, primary Eμ-Tcl1 and IgH.TEμ leukaemias has been generated and assessed as an *in vivo* pre-clinical model for human CLL. Consistent with previous studies, Eμ-Tcl1 and IgH.TEμ mice exhibited overt $CD5^+$ B-cell leukaemia, splenomegaly, and mild lymphadenopathy, resulting in a significantly reduced median survival (353 and 324 days, respectively) in comparison to congenic C57BL/6 animals (352-354, 360). Whilst splenomegaly and lymphadenopathy are also common amongst CLL patients, such observations are consistent in the majority of lymphoid malignancies, and not necessarily specific to CLL (7).

Whilst the observed median survival of Eμ-Tcl1 mice appears comparable to previous studies (352-354, 360), IgHTEμ mice have been previously documented to demonstrate median survival of 164 days (360). At present the causes of such a disparity remain unclear. However, at the time of writing, only a single study of spontaneous leukaemia formation in IgH.TEμ mice has been documented (360). Therefore, it is possible that significant variation in conditions between institutions may explain the relative disparity in median survival. For instance, upon arrival IgH.TEμ mice were double re-derived by caesarean blastocyst transplantation and backcrossed onto the C57BL/6 background for six generations. Therefore, it is possible that mice held at this institution more accurately reflect effects on the pure C57BL/6 background and may, therefore, not be comparable to the previously documented cohort held at another institution.

In this investigation both Eμ-Tcl1 and IgH.TEμ leukaemias presented with massive disruption of normal splenic architecture, owing to tumour infiltration and a slight alteration in the appearance of LN. However, comparatively normal architecture was observed in the thymus and non-lymphoid tissues (with the exception of the lungs). Such observations are entirely consistent in the Eμ-Tcl1 model however; extensive histological examinations of IgH.TEμ mice have yet to be documented (352-354, 360). Typically, CLL patients demonstrate tumour infiltrates in LN, spleen, liver and BM (7). Such infiltrates, typically appear with a pseudofollicular structure of dark areas of dense nuclei surrounded by a paler background in the spleen and LN (7). Such an

observation is also made in the LN and spleens of afflicted Eμ-Tcl1 and IgH.TEμ mice. However, such regions were significantly less well defined than those observed in CLL patients.

Interestingly, Eμ-Tcl1 CLL-like B-lymphocytes have also been demonstrated to exhibit massive accumulation within the peritoneal cavity (352-354, 360). Whilst this investigation did not directly measure such an occurrence, observations of white ascitic fluid, indicative of WBC expansion, were common in terminal mice at sacrifice. Therefore, it appears as though the Eμ-Tcl1 and IgH.TEμ leukaemias generated at this institution exhibit a comparable physical presentation to that found in previous studies (352-354, 360). Furthermore, the physical presentation of both Eμ-Tcl1 and IgH.TEμ leukaemia appears to be broadly similar to that exhibited by CLL patients (7). However, the similarity in response to conventional treatments (e.g. chemotherapy and rituximab) between these murine CLL-like diseases and CLL remains to be determined and is the subject of ongoing studies.

Preliminary data, documented above, also demonstrates that mono or bi-allelic loss of Bim appeared not to accelerate the rate of spontaneous leukaemiagenesis in either model. Unfortunately, as detailed earlier, during the course of study the animal facility housing the Eμ-Tcl1 and IgH.TEμ mice suffered from an outbreak of murine hepatitis virus (MHV). Therefore, all animals had to be culled and data discounted. Subsequently, strains were re-derived and the survival study was re-commenced. However, due to time constraints insufficient numbers of Eμ-Tcl1/ IgH.TEμ $Bim^{+/-}$ or $Bim^{-/-}$ animals reached experimental endpoints. Therefore, further studies are required to fully assess the role of Bim as a tumour suppressor in CLL-like disease.

In the context of the Eμ-Myc model of lymphoma, loss of only a single Bim allele was sufficient to dramatically enhance the onset of B-cell lymphomas and leukaemia (233). Since evasion of apoptosis represents a key step during Myc-induced tumourigenesis, such an occurrence is perhaps unsurprising (233, 324-327, 329-332). The apparent inability of Bim to act as a key tumour suppressor in mouse models of CLL-like leukaemia is perhaps attributable to the potential role of antigenic drive in CLL aetiology (13, 14, 336). It is possible that antigen-driven enhancement of Mcl-1

expression and Bcl-2 hypomethylation, as is commonly documented in CLL (342-344, 411), may be sufficient to significantly block the tumour suppressive activity of Bim making its loss redundant in terms of tumourigenesis. However, as many treatments induce apoptosis through upregulation of Bim, this may have relevance for treatment studies. Furthermore, it is also possible that loss of Bim may not accelerate leukaemiagenesis but may influence the dependency of tumours upon interactions with the microenvironment. It is known in CLL that specific micro-environmental interactions result in the dysregulation of the apoptotic machinery downstream of Bim, for instance increased expression of IAPs attributable to CD40L and IL-4 receptor signalling in particular (412, 413). However, genetic loss of Bim may allow tumours to exit microenvironment niches and proliferate in the periphery in the absence of such signals. Therefore, in the future we aim to utilise the generated panel of Bim sufficient and deficient Eμ-Tcl-1 and IgH.TEμ tumours to examine the dependency upon Bim for interactions with the microenvironment, utilising techniques outlined in section 7.4.

In addition, it was demonstrated that all primary Eμ-Tcl1 and IgH.TEμ leukaemias generated possessed an immunophenotype similar to that of CLL patients, as has been reported previously in both models (13, 414). However, in both cases significant variation from a typical human CLL immunophenotype is found in the form of CD23 expression. Since CD23 positivity is associated with a more mature, antigen-experienced B-lymphocytes (40, 41), it is possible that accumulation of CLL-like B-lymphocytes occurs at an earlier developmental stage in mice in comparison to CLL patients. Such differences may reflect the relatively sterile conditions in which transgenic animals were maintained. It is possible that the greater frequency of bacterial and viral infections within the human population may be responsible for such disparity. Furthermore, similarly to Eμ-Myc animals, such differences may be attributable to the expression of an oncogene upon BCR-expression, at the immature B-cell stage. In contrast, in CLL patients, oncogenic changes possibly occur at later developmental stages.

Remarkably, IgH Eμ-driven Tcl1 and SV40 large T-antigen both gave rise to 100% IgM^+ B-cell leukaemias. Such observations are in stark contrast to the 55% $sIgM^+$ Eμ-Myc lymphomas outlined in chapter 3. Interestingly, whilst the oncogene differs between

the three models, expression was driven via the same promoter/ enhancer. Therefore, the onset of Eμ-Myc tumours at an earlier developmental stage likely reflects an intrinsic property of Myc as an oncogene. For example, perhaps Myc tumourigenesis is particularly short and rapid in comparison to other oncogenes. However, the exact molecular reasons for such observations remain unknown.In most other respects the immunophenotype of malignant Eμ-Tcl1 and IgH.TEμ B-lymphocytes resemble that of CLL. Therefore, both the Eμ-Tcl1 and IgH.TEμ models represent a reasonably faithful recapitulation of human CLL in mice, albeit with the caveats already described. Despite this observation, both Eμ-Tcl1 and IgH.TEμ mice represent an invaluable *in vivo* model of CLL, which until recently had not been widely available.

In this chapter it was demonstrated that R788 mediated disruption of signals emanating from the BCR was not an effective therapeutic strategy in Eμ-Tcl1 syngeneic transfer experiments. Such observations were in contrast to the findings of Sulgajic et al, who demonstrated that R788 treatment significantly extended overall survival and reduced accumulation of B-CLL-like lymphocytes in Eμ-Tcl1-002 recipient mice (356). Such differences are likely attributable to variance in dosing strategy, since in previous studies a dose of 80/mg/kg was maintained for 18 days (356, 392, 415-418). Since R788 has only around a 2-hour half-life in mice, such differences likely significantly impact the therapeutic outcome. However, such studies reported that a decrease in $CD5^+$ leukaemia populations should have been seen after 2 days of treatment (356). However, in this investigation no such decreases were observed. Therefore the in vivo efficacy of R788-mediated Syk inhibition requires further study in both the Eμ-Tcl1 and alternate models of tumours. Therefore, further experimentation is required utilising a longer dosing strategy in order to draw conclusions with any degree of confidence.

We also demonstrated that blockade of ERK signalling failed to yield a therapeutic effect in Eμ-Tcl1-002 recipient mice. However, as of yet it remains to be determined whether significant inhibition of MEK was evident in Eμ-Tcl1-002 recipient mice. It is likely that the dosing strategy, vehicle, and administration technique were sufficient to effectively block MEK activity, since previous studies in the lab optimised such strategies in B-Raf mutant tumours (419). Therefore, it is possible that ERK does not play a significant maintenance role downstream of antigen-driven survival signals in

CLL-like leukaemias. Since, PI3K activity has been demonstrated to provide key maintenance signals downstream of the BCR, which allow cells to persist in the periphery, the potential therapeutic potential of PI3K inhibitors should be assessed in the future (27). In addition, further *in vitro* and *in vivo* studies of the effect of MEK (and Syk) inhibition upon Eμ-Tcl1-002 and less aggressive Eμ-Tcl1 tumours are required, in order to fully assess the therapeutic potential of MEK inhibitors in CLL.

In contrast, however, mAb therapy appeared therapeutically beneficial in Eμ-Tcl1-002 recipient mice. In the case of anti-CD20 therapy, it was observed that 18B12 mouse IgG2a anti-CD20 treatment significantly depleted peripheral malignant B-cells from tumour bearing mice. In humans anti-CD20 antibodies appear to exhibit multiple mechanisms of action, depending upon the propensity of antibodies to drive re-distribution of CD20 to lipid rafts (416, 417). Type I antibodies appear to re-distribute CD20 to lipid rafts, thus driving its internalisation, and appear to act mainly via complement-dependent cytotoxicity (CDC) and antibody-dependent cell-mediated cytotoxicity (ADCC) (416, 417). In contrast, type II anti-CD20 mAbs appear not to re-distribute CD20 to lipid rafts, are less efficient at complement fixation, yet drive more efficient B-cell depletion via a combination of macrophage-mediated ADCC and direct cell death (392, 415-418). 18B12 mIgG2a anti-CD20 appears to resemble a type II antibody, as defined in human model systems (M.S. Cragg unpublished observation) therefore, such efficient B-cell depletion in the periphery was entirely expected (416, 417).

However, whilst anti-CD20 therapy initially appeared to rapidly deplete peripheral B-CLL-like lymphocytes, malignant clones re-appeared in the periphery approximately six days later. Such an observation implies that whilst anti-CD20 therapy is able to rapidly clear peripheral targets, it is unable to effectively penetrate secondary lymphoid organs and delete targets within microenvironment niches (420, 421). However, further analysis of OCT-embedded sections from secondary lymphoid organs of anti-CD20 treated mice by immunohistochemistry is required to confirm this. If true, such a notion may explain the observations that anti-CD20 treatment only delayed the onset of terminal illness, and had little impact upon the size and cellularity of secondary lymphoid organs compared to un-treated mice at terminal tumour burdens. Indeed,

the efficacy of anti-CD20-mediated B-cell depletion within secondary lymphoid organs has been correlated with the extent of vascularisation of the organ (422). Furthermore, the extent of B-cell depletion, mediated via anti-CD20 treatment, appeared enhanced upon mobilisation of B-cells from secondary lymphoid organs via anti-integrin mAb co-treatment (422). Therefore, it appears as though anti-CD20 is capable of effectively depleting peripheral Eμ-Tcl1 leukaemias however, additional therapies may also be required to mobilise tumours from protective niches in order to allow complete deletion.

In contrast, anti-CD40 treatment appeared to dramatically slow the rate at which CLL-like B-lymphocytes appeared in the periphery without the obvious depletion seen in anti-CD20 treated animals. Since anti-CD40 therapy has been demonstrated to evoke DC activation and $CD8^+$ T-cell-dependent tumour cell depletion, such an observation may reflect sustained activation of T-cell responses (410, 423). However, $CD3^+$ cell numbers appeared unchanged upon anti-CD40 treatment in Eμ-Tcl1-002 recipient mice (data not shown), but the relative sizes of $CD4^+$ and $CD8^+$ T-cell populations were not assessed. Furthermore, the observation that anti-CD40 treatment apparently yielded a stable disease in female F5 seems to imply the production of an immunological mechanism of control through T-cell activity. Therefore, in order to further assess the relative contributions of T-cell responses to the observed therapeutic benefit of anti-CD40 treatment, further studies are required. For instance, co-administration of anti-CD3, to deplete T-cells, alongside anti-CD40 could be undertaken to analyse the relative contribution of T-cells toward Eμ-Tcl1-002 depletion. Consequently, in the future, further studies are required to determine the nature of therapy provided by both anti-CD20 and CD40 antibodies in Eμ-Tcl1 recipient mice. Furthermore, further studies utilising anti-CD20 and anti-CD40 treatment as part of a combination therapy including inhibitors of BCR signalling should be performed in order to assess the relative therapeutic potential of such strategies. It is anticipated that a greater understanding of the therapeutic mechanisms may allow an improvement in the relative efficacy of both treatments, with the final aim being an improved therapeutic strategy for CLL patients.

8. Final Discussion and concluding remarks

Prior to this investigation the relative contribution of BH3-only proteins, other than Bim, toward BCR-induced cell death was largely uncertain (223, 229-231, 233, 235, 236). However, this investigation provides evidence of cooperative roles for Bik and Noxa alongside Bim during induction of a caspase-dependent; intrinsic apoptotic cell death downstream of BCR engagement in the Eμ-Myc lymphoma model, similar to that reported previously in alternate models (225-231, 233). These findings were made utilising WT, Noxa$^{-/-}$, or Bik$^{-/-}$ Eμ-Myc lymphomas expressing diminished levels of Bim through virtue of a shRNA approach. However, such observations could be further validated via use of Noxa$^{-/-}$, Bim$^{-/-}$ or Bik$^{-/-}$, Bim$^{-/-}$ double knockout Eμ-Myc lymphoma cell lines in the future.

As detailed previously, the Eμ-Myc lymphoma model was utilised in order to study the process of BCR-mediated clonal deletion in cells that more closely resembled the biology of primary lymphomas than the long-term *in vitro* cell lines previously used. The Eμ-Myc model fulfils these criteria via provision of low passage number cell lines, which can be maintained *in vitro*. Indeed, such an approach appeared to be ratified by the observation that Eμ-Myc lymphoma cells spontaneously developed an intrinsic resistance to BCR-induced cell death after approximately 22 *in vitro* passages. It is possible that such resistance was attributable to continual telomere shortening, resulting in the onset of a replicative crisis, and the emergence of clones exhibiting massive dysregulation of the apoptotic and/ or DNA damage sensing machinery. It is likely that the commonly used long-term *in vitro* cell lines extensively utilised in the study of BCR-induced cell death, i.e. Ramos, B104, WEHI-231 etc (223, 230, 231), may also have passed through similar processes during adaptation to cell culture. Therefore, it is anticipated that the biology exhibited by in vitro Eμ-Myc lymphoma cell lines more closely resembles that of primary lymphomas.

The findings of this investigation are in agreement with previous studies highlighting Bim as the major driver of BCR induced cell death (229). However, significant sensitisation roles were also apparent for both Bik and Noxa. Whilst BCR-induced

upregulation of both Bik and Noxa has been documented previously, significant resistance toward BCR-induced cell death upon Bik/ Noxa knockout represents a novel finding (18, 223, 378).

Recently, co-operative activity of both Noxa and Bim has been reported downstream of BCR-signalling in alternate cellular contexts (378, 379). In fact, genetic loss of Noxa alone has been demonstrated to result in a significant reduction in the relative affinity of antibody responses in comparison to WT mice (378, 379). Furthermore, Noxa upregulation has been observed following BCR-engagement in mature B-cells, and appears to sensitise activated B-cells to negative selection within GCs (378, 379). However, in a situation analogous to the findings of this investigation, Noxa appears to facilitate such processes whereas the major execution role appears to be played by Bim (378, 379). It is, therefore, apparent that both Bim and Noxa co-operatively facilitate apoptotic clonal deletion of B-lymphocytes exhibiting disrupted tonic signals and of low-affinity GC centroblasts during the GC reaction (379, 380). Furthermore, Noxa appears to limit the extent of plasma cell production following BCR-mediated activation, possibly in an analogous role to that during BCR-induced cell death (378). Collectively, the results of this investigation and others, point toward a subtle link between Noxa and the BCR in homeostatic control, which appears to require the presence of Bim. However, this investigation was unable to delineate the key molecular mechanisms responsible for transcriptional up-regulation of Noxa following BCR-engagement. In contrast to Bim and Bik, BCR-mediated Noxa upregulation in the Eμ-Myc lymphoma cells occurred in a Syk- and Ras/Raf/MEK/ERK-independent fashion. In the future, it would be useful to screen a panel of kinase inhibitors for an impact upon Noxa upregulation, with a particular focus upon inhibitors of PI3K, p38 and mTOR. Furthermore, the relative contribution of p53, a major transcriptional regulator of Noxa, toward BCR-induced Noxa upregulation should be assessed via the use of $p53^{-/-}$ Eμ-Myc lymphomas (424).

Interestingly, previous studies utilising $Bik^{-/-}$ or $Bim^{-/-}$ $Bik^{-/-}$ C57BL/6 lymphocytes demonstrated similar levels of BCR-induced cell death of normal B-cells in comparison to WT and $Bim^{-/-}$ mice, respectively (221, 222). Such observations raise the intriguing possibility that BCR engagement triggers cell death via alternate means in malignant

and non-malignant B-lymphocytes. Indeed, it is known that malignant follicular lymphoma and normal tumour-infiltrating B-lymphocytes exhibit significant kinetic differences in signalling downstream of the BCR (234). Therefore, it remains possible that such kinetic differences may lead to the differential recruitment of death effectors downstream of BCR-engagement. Indeed, in chapter 3 we observed a heightened sensitivity of Eμ-Myc lymphomas toward BCR-induced cell death in comparison to normal C57BL/6 B-lymphocytes. Since Bik does not appear to significantly contribute toward BCR-induced cell death in normal B-cells (221, 222), it is tempting to speculate that such sensitisation may be attributable to malignant B-lymphocyte restricted upregulation of Bik in response to BCR engagement. In order to address this possibility, comparative qPCR analysis of BH3-only transcript expression levels following BCR-engagement should be performed in WT C57BL/6 B-lymphocytes. Furthermore, if possible, it would be interesting to isolate malignant and non-malignant Eμ-Myc B-cells from the same mouse and directly compare the extent and mechanisms of cell death. However, such an approach is likely technically challenging, since the Eμ-Myc transgenic cells do not possess an obvious surface marker which distinguishes them from normal B-cells. However, a crude extraction procedure of splenic B-cells (as a source of malignant B-cells) and PBMCs (as a source of non-malignant B-cells) from tumour bearing Eμ-Myc animals could prove sufficient, as performed in (Irish). If malignant and non-malignant B-lymphocytes exhibit differential recruitment of BH3-only proteins downstream of the BCR, it may also be possible that different tumours may also exhibit this. For example, comparative analysis of BH3-only upregulation in response to BCR-stimulation could be performed in CLL, follicular lymphoma, diffuse-large B-cell lymphoma, and mantle-cell lymphoma.

This investigation also identifies that, in the absence of Bim, BCR-induced cell death proceeds in a non-apoptotic fashion and exhibits several hallmarks of an autophagic cell death, as has been described previously (275). This cell death appears driven by Bik and blocked by Bcl-2 over-expression. Indeed both observations are consistent with the onset of an autophagic-cell death downstream of the BCR and possibly implicate Beclin-1 as a major player in the response (267, 273, 274, 383, 384, 394). However, since currently available assays for the detection of autophagy remain largely

subjective, such conclusions should be viewed with a certain degree of caution. In the future it would be useful to produce $Bim^{-/-}$ Eμ-Myc lymphoma cell lines retrovirally transduced with an LC3-GFP, to allow the potential visualisation of autophagosomes downstream of BCR-engagement. This investigation did attempt to utilise the monodansylcadaverine (MDC)-staining technique to assess such structures by flow cytometry and fluorescence microscopy. However, Eμ-Myc lymphoma cell lines constitutively exhibited granular MDC staining patterns indicative of autophagosome formation and, therefore, the assay was deemed unsuitable for further use. It is possible; however, that oncogenic Myc may drive high levels of background autophagy. Indeed, Myc overexpression has been associated with a marked increase in autophagosome formation, and autophagy has been identified as a constitutively active survival mechanism in Myc driven lymphomas responsible for resistance to various treatment regimes (425, 426). In fact recent studies identify that pharmacological inhibition of autophagy appears to slow rates of lymphomagenesis in the Eμ-Myc model (425, 427). As a consequence, it is possible that autophagy may play a key role in Myc-driven tumourigenesis (268, 269). In order to better assess the involvement of autophagy in both BCR-induced cell death and Eμ-Myc lymphomagenesis, Eμ-Myc mice should be crossed with mice deficient in specific Atg-genes such as ATG6 (Beclin-1) and Vps34. Ideally these should be conditional allowing assessment of whether autophagy is important early or late in tumour development. Subsequently, the rate of lymphomagenesis and the relative levels of cell death downstream of BCR-engagement following Bim knockdown could be assessed. However, care should be taken in interpreting such data since the exact pro-survival or pro-death role of autophagy remains controversial (267-269). Furthermore, upon confident identification of an autophagic cell death downstream of BCR engagement in the absence of Bim, the potential impact of both Bik and Bcl-2 upon Beclin-1 subcellular localisation could be also assessed (383, 384).

This investigation also identified that both Syk and ERK play key roles during BCR-induced cell death. We observed that BCR-mediated upregulation of the Ras/Raf/MEK/ERK pathway is responsible for driving transcriptional upregulation of

Bim, potentially via an effect upon CHOP. Such observations are completely opposed to the consensus view that ERK-mediated regulation of Bim has an inhibitory effect and, therefore, pro-survival outcome (151, 204, 401, 402). However, we also demonstrate that such pro-death signals are only facilitated by the Ras/Raf/MEK/ERK pathway in malignant Eμ-Myc lymphomas but not WT or Myc tg B-lymphocytes. Therefore, it is possible that distinct biological differences exist between non-malignant and malignant B-lymphocytes and appear to centre upon the Ras/Raf/MEK/ERK pathway, akin to that detailed above relating to signalling differences in normal vs. malignant B-lymphocytes. Therefore, the previously described process of isolating malignant and non-malignant B-lymphocytes could also be applied to better study the effect of malignant transformation upon the Ras/Raf/MEK/ERK pathway. Consequently, comparative analysis of the expression level and activity of ERK targets could be assessed throughout Eμ-Myc lymphomagenesis and between malignant and non-malignant B-lymphocytes. Furthermore, additional assessment of the role of CHOP in BCR-driven upregulation of Bim should be performed. CHOP knockout mice are available from our collaborators and could be crossed with Eμ-Myc animals (211). Such an approach would not only allow assessment of the potential tumour suppressive role of CHOP in lymphomagenesis (due to roles in ER stress), but would also allow *in vitro* analysis of the impact of CHOP on BCR-induced Bim transactivation (211). Whilst a link between the Ras/Raf/MEK/ERK pathway and CHOP has been alluded to in the past, such a connection is far from certain (403, 404). Therefore, such studies may further highlight a novel molecular mechanism linking ERK to transcriptional regulation of BH3-only proteins. It is possible that the potential pro-death characteristics imparted upon the Ras/Raf/MEK/ERK pathway during malignant transformation could be harnessed as a cancer therapy as an alternative to anti-Id therapy. For instance, application of a synthetic pharmacological activator of ERK (possibly an inhibitor of phosphatases which target ERK) may drive CHOP-dependent upregulation of Bim in malignant tumours but enhance survival of normal B cells. Consequently, artificial activation of ERK could be incorporated into a combinatorial therapy regime incorporating DNA damage inducing drugs and anti-CD20 antibodies as a potentially more effective intervention against B-lymphocyte malignancies.

In addition to molecular mechanisms of BCR-induced apoptosis we also studied TGF-β, and observed a completely different signature of BH3-only protein upregulation. In chapter 6, upregulation of Puma, at both transcript and protein levels, appeared to significantly contribute toward the early phase of TGF-β induced cell death. Whilst direct-transactivation of Puma following TGF-β signalling represents a novel finding, *in vivo* TGF-β appears to facilitate tumour senescence via a p53-dependent mechanism (282). Indeed, in our hands $p53^{-/-}$ Eμ-Myc lymphomas exhibited a comparable resistance toward TGF-β-induced cell death as $Puma^{-/-}$. Therefore, it is tempting to speculate that p53 directly transactivates Puma downstream of TGF-β signalling, since Puma represents one of the major pro-apoptotic transactivation targets of p53 (424). However, the direct DNA binding activity of SMADs likely facilitates such a process, since our collaborators demonstrated SMAD2 recruitment to an SBE in the human Puma promoter (Spender et al 2012, manuscript submitted). Furthermore, since SMADs often co-operate with additional transcription factors during transactivation of targets (277), it would be interesting to determine whether a co-operative relationship with p53 was apparent downstream of TGF-β. Such a relationship could be assessed fairly easily by chromatin immunoprecipitation and subsequent analysis of p53 and SMAD2 recruitment to the murine Puma promoter.

Taken together, the results of this investigation demonstrate that distinct apoptotic stimuli often invoke a unique pattern of BH3-only protein upregulation, akin to a response fingerprint. Therefore, it is possible that specific drug combinations could be devised that upregulate all three activator BH3-only proteins (Bim, Bid, and Puma) in an attempt to drive maximal apoptosis of targets. It is anticipated that such an approach could provide almost complete deletion of malignant clones therefore, minimising the chances of tumour regression. For example, combinational use of Etoposide alongside inducers of ER stress may be beneficial, since Etoposide has been linked to upregulation of Puma, Bim, and Noxa (428) whilst ER stress is linked to Bim and Bid activation (211, 224). Additionally, combinational use of Etoposide, or other DNA-damage inducing drugs or treatments alongside the proteasome inhibitor Bortezomib may represent an effective therapeutic strategy, since Bortezomib has been linked to Bim, Bik, and Noxa upregulation alongside concomitant Mcl-1

degradation (429, 430). Since analogous molecular events are evident upon BCR engagement in Eμ-Myc lymphomas, it is known that such events are particularly efficient at deleting tumours. Therefore, the additional upregulation of Puma provided by Etoposide treatment may represent a particularly potent combination therapy (428).

Whilst the use of Etoposide treatment may be an effective therapeutic strategy for tumours exhibiting WT p53, such a strategy is likely less effective in mutant p53 tumours, since the upregulation of Noxa and Puma is largely p53-dependent (424, 428). However, alternate cytotoxic drugs that exhibit p53-independent activator BH3-only protein upregulation could be utilised as an alternative. For instance, Dexamethasone and Paclitaxel have been demonstrated to upregulate Puma and Bim independently of p53 activity (218, 431). Therefore, it is anticipated that an enhanced knowledge of the therapeutic mechanisms of cytotoxic drugs may allow therapeutic strategies to be effectively tailored to fit the specific molecular lesions exhibited by patient's tumours.

Recently, a new class of drugs has emerged that may by-pass the need for or augment the activity of conventional chemotherapy, and effectively mimic the effect of upregulating multiple BH3-only proteins, known as the BH3-mimetics (432). The proof-of concept archetypal BH3-mimetic Abbot-737 (ABT-737), and it's orally bio-available pro-form ABT-263, represent an effective Bad-BH3 mimetic and display the characteristic Bcl-2, Bcl-XL, Bcl-w restricted binding profile exhibited by Bad (192, 433, 434).

As a consequence, ABT-737 is unable to bind Mcl-1 and A1 and therefore, requires additional BH3-only protein-mediated neutralisation of Mcl-1 and A1 to be effective (434). Interestingly, such a phenomenon may allow the specific targeting of tumours by ABT-737, since tumours often exhibit "primed" prosurvival Bcl-2 family members (i.e. bound by activator BH3-only proteins) due to the effect of oncogenic stress, a phenomenon not shared by normal somatic cells (381). Subsequently, ABT-737 is proposed to bind Bcl-2, Bcl-Xl, and Bcl-w, displace activator BH3-only proteins, and induce cell death specifically in tumours. Therefore, ABT-737 likely represents an

effective anti-tumour agent as both a single therapeutic agent (in non-Mcl-1 dependent tumours) and as part of a combinational approach (in Mcl-1 dependent tumours). Indeed, the pro-form of ABT-737, ABT-263, is now the subject of ongoing phase II clinical trials, investigating its effectiveness as both a single agent and part of a combinational therapeutic approach in small cell lung cancer (SCLC) and refractory CLL, respectively (435, 436). Provisional results indicate that ABT-263 is safe and exhibits potent anti-tumour activity (435, 436). Therefore, its development should represent an interesting paradigm to which the rest of the BH3-mimetic class of drugs can be compared.

Increasingly, BH3-mimetics that target alternate prosurvival Bcl-2 family members are under development, such as the Bim-like, pan-prosurvival binding BH3-only mimetics GX15-070, gossypol and its enantiomer AT-101 (432). Furthermore, more selective Noxa-like BH3-mimetics have also been recently developed, including the stapled BH3-domain class of drugs known as stabilised alpha helix of Bcl-2 domains (SAHB). Specifically, SAHBs of Mcl-1 and Bim domains (Mcl-1 SAHB, and BimS2a SAHB, respectively) have been identified as highly selective inhibitors of Mcl-1 and A1 (437, 438). Therefore, it is possible that combination therapy of Mcl-1 SAHB-like drugs and ABT-737 may ensure maximal apoptosis of tumours via neutralisation of all prosurvival molecules (192, 433, 434, 438). Indeed, proof of principle has been performed *in vitro*, whereby BH3-domain peptides of Bad and Noxa were able to invoke maximal apoptosis independently of other stimuli (192). However, some BH3-mimetic drugs are also able to invoke cell death in the absence of both Bax and Bak, indicating induction of non-apoptotic cell death (432). Therefore, further research into their specific modes of action is required prior to use as a therapeutic agent.

Intriguingly, the development of highly specific and selective prosurvival binding BH3-mimetics may allow any combination of BH3-only proteins to be mimicked. Therefore, using such drugs, the exact nature of the pro-apoptotic response can be tailored to fit a patient's specific malignancy. For example, CLL is thought to be a mainly Mcl-1 dependent malignancy and, therefore, may respond well to Noxa BH3-mimetics.

We also investigated two further models of B-cell malignancies in the form of the Eμ-Tcl1 and IgH.TEμ models of CLL (353, 360). Neither model permits the development of cell lines for *in vitro* manipulation and analysis. Instead, we sought to develop these for *in vivo* studies on the molecular mechanims of tumourigenesis and treatment resistance. Although CLL patient samples are readily available for *in vitro* analysis, *in vivo* models are required to study the key-role played by the tumour microenvironment in offering support to B-CLL.

We demonstrated that both Eμ-Tcl1 and IgH.TEμ mice develop an overt CLL-like leukaemia at approximately 1 year of age, consistent with previous reports (352-354, 360). However, our very preliminary findings indicate that genetic loss of Bim failed to increase the rate of tumourigenesis, in contrast to observations made in the Eμ-Myc model (233). If borne out such an observation would be surprising, given the well-studied role of Bim downstream of BCR signalling and the apparent dependence upon antigen-driven BCR signalling in CLL aetiology (439). Whilst such studies appear to provide a negative finding, the tumours derived from Bim deficient animals will provide a useful tool for study of the molecular mechanisms of apoptosis inducing therapies in the future. Interestingly, tumourigenesis of both Eμ-Tcl1 and IgH.TEμ leukaemias appear accelerated by genetic loss of p53 (360, 440). Therefore, such observations imply that mechanisms downstream of p53 may play important tumour suppressive functions in murine CLL-like diseases. It is possible that such a function is played by Puma, since it represents a major pro-apoptotic protein downstream of p53 (219). Therefore, in the future the tumour suppressive role of Puma will be analysed in both Eμ-Tcl1 and IgH.TEμ models of CLL.

We also demonstrated that anti-CD20 mAb therapy was capable of significantly depleting peripheral leukaemia cells, in the Eμ-Tcl1 model. Given the rapid return of these cells post-treatment, it appeared that tumour cells in the secondary lymphoid organs are protected resulting in therapeutic resistance, as has been previously documented (420, 421). The studies of Chan et al identified that the extent of anti-CD20 mAb-mediated B-cell depletion in secondary lymphoid organs was proportional to the relative access of each organ to the circulatory system (422). However, the reduced depletion of targets in secondary lymphoid organs was not attributable to the

inability of mAbs to penetrate such sites (422). Rather, such resistance appears reliant upon interactions with the microenvironment, since anti-integrin mAbs were able to mobilise anti-CD20 opsonised B-cells into the periphery where they could be effectively depleted by interaction with effectors (422).

Existing data in the laboratory suggests that anti-CD20 mediated B-cell depletion appears dependent upon interactions with macrophages via Fc receptors (441). It is possible that interaction with the tumour in the secondary lymphoid organs alters the cellular behaviour of macrophages to a more immuno-suppressive tumour-associated macrophage (TAM)-like phenotype (442). Subsequently, TAMs may be unable to drive phagocytosis and destruction of anti-CD20 mAb opsonised targets, giving rise to ineffective depletion in secondary lymphoid organs (442). As a consequence, it is possible that mobilisation of CLL-like B-lymphocytes from the tumour microenvironment may enhance the effectiveness of anti-CD20 mAb therapy, by allowing interaction with classical non-TAM macrophages and subsequent destruction. However, the involvement of macrophages in the depletion of anti-CD20 mAb-treated Eμ-Tcl1 leukaemias requires further study. For instance, Clodronate-mediated deletion of macrophages or syngeneic transfer of Eμ-Tcl1 tumours into γ-chain knockout (Fc-receptor deficient) mice would help confirm macrophage-mediated FcR-dependent destruction as the key effector mechanism involved in the deletion of malignant Eu-Tcl-1 cells from the periphery by anti-CD20 mAbs (415, 416).

In addition, evidence suggests that B-CLL also receive extensive support from the tumour microenvironment in the form of interactions with nurse-like cells and follicular dendritic cells, giving rise to prosurvival signals resulting from CXCL12, BAFF, VCAM1, and CD40L signalling (439). Since antigenic drive has been implicated in disease maintenance and aetiology, it is possible that microenvironment retention may be facilitated by BCR-signalling via upregulation of chemokine receptors and adhesion factors (439). Therefore, in the future the impact of specific inhibitors of BCR signalling components, i.e. Syk, ERK, PI3K, and Btk, upon the retention of B-CLL in secondary lymphoid organs should be undertaken. It is possible that such agents may disrupt BCR-mediated upregulation of adhesion factors, allowing mobilisation of B-CLL and, therefore, enhancing the efficacy of anti-CD20 mAb therapy. Consistent with such

predictions inhibition of Syk, mTOR, PI3K, and Btk have been associated with leucocytosis; resulting in increased numbers of malignant cells in the periphery after treatment in several clinical trials (443-446). Therefore, whilst anti-CD20 mAb therapy already represents an effective strategy for the treatment of some B-cell malignancies, its therapeutic outcome may be improved via implementation of rational combinational therapies such as those leading to egress of the tumour cells into the periphery.

In addition, we observed a sustained reduction in the deposition rates of leukaemic cells into peripheral blood upon anti-CD40 treatment, possibly owing to the induction of cytotoxic T-cell responses (410, 423). In the future, further analysis of the mechanisms of anti-CD40-mediated target cell deletion should be undertaken in order to gain a better insight into its therapeutic mechanism. It is possible that anti-CD40 treatment induces cytotoxic T-cell responses, as previously reported, capable of entering secondary lymphoid organs and clearing B-CLL (French). Therefore, it is possible that co-administration of both anti-CD40 and anti-CD20 mAbs may prove an effective combination therapy. Such a combination may permit anti-CD20-mediated depletion of peripheral tumours, whilst anti-CD40-mediated cytotoxic T-cell responses are capable of clearing tumours within the secondary lymphoid organs. However, further analysis of the therapeutic mechanisms of anti-CD40 therapy with respect to the Eμ-Tcl1 model is required as T cell function is known to be impaired in this model (similar to the reported defect in CLL). Therefore it remains to be seen whether anti-CD40 treatment can overcome this defect. The specific role of T-cells in anti-CD40 therapy could be addressed by syngeneic transfer of Eμ-Tcl1 tumours into T-cell depleted mice via application of mAbs (anti-CD8 to target cytotoxic T-cells, anti-CD4 to target TH cells, and anti-CD3 to deplete all T-cells) and the effect upon anti-CD40 therapy observed, as in (410).

In conclusion, it appears as though combinatorial therapies utilising both mAbs and small molecule apoptosis-inducing agents may be an effective therapeutic strategy. It appears that mAbs are particularly effective at clearing peripheral tumours via non-apoptotic mechanisms therefore, overcoming resistance to apoptosis. However, their therapeutic function appears reliant upon immune effector cells, which can be

influenced by the tumour microenvironment. In contrast, small-molecule apoptosis inducing agents show no such dependency on host effector cells and may be able to effectively target tumours within microenvironment niches. Furthermore, it is possible that such therapies could be targeted to break the interaction with the tumour microenvironment, causing mobilisation of tumours to the periphery where effective targeting by anti-CD20 therapy can be achieved. It is clear that a better understanding of the pathways leading to cell death and survival will aid and assist in this rational combinatorial targeting strategy improving on effective but not curative treatments in order to offer improved survival and quality of life for cancer patients.

Chapter 9 References

1. CRUK (2012) Cancer Research UK, UK Cancer Incidence (2008) and Mortality (2009) Summary, January 2012.

2. CRUK (Cancer research UK, patient information.

3. Lowe SW, Cepero E, & Evan G (2004) Intrinsic tumour suppression. *Nature* 432(7015):307-315.

4. Kindt T, Goldsby R, & Osborne B (2007) *Kuby immunology 6th edition, W.H Freeman and Company.*

5. Hanahan D & Weinberg RA (Hallmarks of Cancer: The Next Generation. *Cell* 144(5):646-674.

6. Hanahan D & Weinberg RA (2000) The hallmarks of cancer. *Cell* 100(1):57-70.

7. SH Swerdlow EC, NL Harris, ES Jaffe, SA Pileri, H Stein, J Thiele, JW Vardiman (2008) *WHO Classification of tumours of Haematopoietic and Lymphoid tissues, Fourth edition* (WHO).

8. Blum KA, Lozanski G, & Byrd JC (2004) Adult Burkitt leukemia and lymphoma. *Blood* 104(10):3009-3020.

9. Burkitt D (1958) A sarcoma involving the jaws in African children. *Brit Jour Surg* 46((197)):218-223.

10. Hoffbrand P, Moss (2001) *Essential Haematology* (Blackwell Science, Oxford, UK).

11. Swerdlow C, Harris, Jaffe, Pileri, Stein, Thiele, Vardiman (2008) *WHO Classification of tumours of Haematopoietic and Lymphoid tissues, Fourth edition* (WHO).

12. Richter-Larrea JA*, et al.* (2010) Reversion of epigenetically mediated BIM silencing overcomes chemoresistance in Burkitt lymphoma. *Blood* 116(14):2531-2542.

13. Caligaris-Cappio F & Hamblin TJ (1999) B-cell chronic lymphocytic leukemia: A bird of a different feather (vol 17, pg 399, 1999). *Journal of Clinical Oncology* 17(3):1092-1092.

14. Ghia P, Ferreri AJM, & Caligaris-Cappio F (2007) Chronic lymphocytic leukemia. *Critical Reviews in Oncology Hematology* 64(3):234-245.

15. Hamblin TJ, Davis Z, Gardiner A, Oscier DG, & Stevenson FK (1999) Unmutated Ig V-H genes are associated with a more aggressive form of chronic lymphocytic leukemia. *Blood* 94(6):1848-1854.

16. Damle RN*, et al.* (1999) Ig V gene mutation status and CD38 expression as novel prognostic indicators in chronic lymphocytic leukemia. *Blood* 94(6):1840-1847.

17. Dal Porto JM*, et al.* (2004) B cell antigen receptor signaling 101. *Molecular Immunology* 41(6-7):599-613.

18. Eldering E & vanLier RAW (2005) B-cell antigen receptor-induced apoptosis: looking for clues. *Immunology Letters* 96(2):187-194.

19. Wang HS & Clarke SH (2003) Evidence for a ligand-mediated positive selection signal in differentiation to a mature B cell. *Journal of Immunology* 171(12):6381-6388.

20. LeBien TW (2000) Fates of human B-cell precursors. *Blood* 96(1):9-23.

21. LeBien TW & Tedder TF (2008) B lymphocytes: how they develop and function. *Blood* 112(5):1570-1580.

22. Delves P, Martin S, Burton D, & Roitt I (2006) *Roitt's essential immunology 11th edition, Blackwell publishing*.

23. Bannish G, Fuentes-Panana EM, Cambier JC, Pear WS, & Monroe JG (2001) Ligand-independent signaling functions for the B lymphocyte antigen receptor and their role in positive selection during B lymphopoiesis. *Journal of Experimental Medicine* 194(11):1583-1596.

24. Kraus M, Alimzhanov MB, Rajewsky N, & Rajewsky K (2004) Survival of resting mature B lymphocytes depends on BCR signaling via the Ig alpha/beta heterodimer. *Cell* 117(6):787-800.

25. Lam KP, Kuhn R, & Rajewsky K (1997) In vivo ablation of surface immunoglobulin on mature B cells by inducible gene targeting results in rapid cell death. *Cell* 90(6):1073-1083.

26. Rowland SL, DePersis CL, Torres RM, & Pelanda R (2010) Ras activation of Erk restores impaired tonic BCR signaling and rescues immature B cell differentiation. *Journal of Experimental Medicine* 207(3):607-621.

27. Srinivasan L*, et al.* (2009) PI3 Kinase Signals BCR-Dependent Mature B Cell Survival. *Cell* 139(3):573-586.

28. Tze LE*, et al.* (2005) Basal immunoglobulin signaling actively maintains developmental stage in immature B cells. *Plos Biology* 3(3):463-475.

29. Peschon JJ*, et al.* (1994) EARLY LYMPHOCYTE EXPANSION IS SEVERELY IMPAIRED IN INTERLEUKIN-7 RECEPTOR-DEFICIENT MICE. *Journal of Experimental Medicine* 180(5):1955-1960.

30. Vonfreedenjeffry U*, et al.* (1995) LYMPHOPENIA IN INTERLEUKIN (IL)-7 GENE-DELETED MICE IDENTIFIES IL-7 AS A NONREDUNDANT CYTOKINE. *Journal of Experimental Medicine* 181(4):1519-1526.

31. Sugiyama T, Kohara H, Noda M, & Nagasawa T (2006) Maintenance of the hematopoietic stem cell pool by CXCL12-CXCR4 chemokine signaling in bone marrow stromal cell niches. *Immunity* 25(6):977-988.

32. Nagasawa T*, et al.* (1996) Defects of B-cell lymphopoiesis and bone-marrow myelopoiesis in mice lacking the CXC chemokine PBSF/SDF-1. *Nature* 382(6592):635-638.

33. Miyake K*, et al.* (1991) A VCAM-LIKE ADHESION MOLECULE ON MURINE BONE-MARROW STROMAL CELLS MEDIATES BINDING OF LYMPHOCYTE PRECURSORS IN CULTURE. *Journal of Cell Biology* 114(3):557-565.

34. Veiby OP, Lyman SD, & Jacobsen SEW (1996) Combined signaling through interleukin-7 receptors and flt3 but not c-kit potently and selectively promotes B-cell commitment and differentiation from uncommitted murine bone marrow progenitor cells. *Blood* 88(4):1256-1265.

35. Blume-Jensen P, Janknecht R, & Hunter T (1998) The Kit receptor promotes cell survival via activation of PI 3-kinase and subsequent Akt-mediated phosphorylation of Bad on Ser136. *Current Biology* 8(13):779-782.

36. Ashman LK (1999) The biology of stem cell factor and its receptor C-kit. *International Journal of Biochemistry & Cell Biology* 31(10):1037-1051.

37. Kondo M, Weissman IL, & Akashi K (1997) Identification of clonogenic common lymphoid progenitors in mouse bone marrow. *Cell* 91(5):661-672.

38. Meffre E, Casellas R, & Nussenzweig MC (2000) Antibody regulation of B cell development. *Nature Immunology* 1(5):379-385.

39. Hardy RR & Hayakawa K (2001) B cell development pathways. *Annual Review of Immunology* 19:595-621.

40. Su TT, Guo B, Wei B, Braun J, & Rawlings DJ (2004) Signaling in transitional type 2B cells is critical for peripheral B-cell development. *Immunological Reviews* 197:161-178.

41. Carsetti R, Rosado MM, & Wardemann H (2004) Peripheral development of B cells in mouse and man. *Immunological Reviews* 197:179-191.

42. Adams JM*, et al.* (1985) The c-Myc oncogene driven by immunoglobulin enhancers induces lymphoid malignancy in transgenic mice. *Nature* 318(6046):533-538.

43. Cancro MP & Kearney AE (2004) B cell positive selection: Road map to the primary repertoire? *Journal of Immunology* 173(1):15-19.

44. Buhl AM, Nemazee D, Cambier JC, Rickert R, & Hertz M (2000) B-cell antigen receptor competence regulates B-lymphocyte selection and survival. *Immunological Reviews* 176:141-153.

45. Wang XD (2001) The expanding role of mitochondria in apoptosis. *Genes & Development* 15(22):2922-2933.

46. Cornall RJ, Cheng AM, Pawson T, & Goodnow CC (2000) Role of Syk in B-cell development and antigen-receptor signaling. *Proceedings of the National Academy of Sciences of the United States of America* 97(4):1713-1718.

47. Takata M*, et al.* (1994) Tyrosine kinases Lyn and Syk regulate B-cell receptor coupled Ca2+ mobilization through distinct pathways. *Embo Journal* 13(6):1341-1349.

48. Hartley SB*, et al.* (1991) Elimination from peripheral lymphoid-tissues of self-reactive B-lymphocytes recognizing membrane-bound antigens. *Nature* 353(6346):765-769.

49. Cyster JG (1999) Chemokines - Chemokines and cell migration in secondary lymphoid organs. *Science* 286(5447):2098-2102.

50. Mills DM & Cambier JC (2003) B lymphocyte activation during cognate interactions with CD4+T lymphocytes: molecular dynamics and immunologic consequences. *Seminars in Immunology* 15(6):325-329.

51. Davis RE*, et al.* (2010) Chronic active B-cell-receptor signalling in diffuse large B-cell lymphoma. *Nature* 463(7277):88-U97.

52. Okada T*, et al.* (2005) Antigen-engaged B cells undergo chemotaxis toward the T zone and form motile conjugates with helper T cells. *Plos Biology* 3:1047-1061.

53. Reif K*, et al.* (2002) Balanced responsiveness to chemoattractants from adjacent zones determines B-cell position. *Nature* 416(6876):94-99.

54. Ansel KM, McHeyzer-Williams LJ, Ngo VN, McHeyzer-Williams MG, & Cyster JG (1999) In vivo-activated CD4 T cells upregulate CXC chemokine receptor 5 and

reprogram their response to lymphoid chemokines. *Journal of Experimental Medicine* 190(8):1123-1134.

55. Chaturvedi A, Martz R, Dorward D, Waisberg M, & Pierce SK (Endocytosed BCRs sequentially regulate MAPK and Akt signaling pathways from intracellular compartments. *Nature Immunology* 12(11):1119-U1130.

56. Siemasko K & Clark MR (2001) The control and facilitation of MHC class II antigen processing by the BCR. *Current Opinion in Immunology* 13(1):32-36.

57. Cozine CL, Wolniak KL, & Waldschmidt TJ (2005) The primary germinal center response in mice. *Current Opinion in Immunology* 17(3):298-302.

58. Thorbecke GJ, Amin AR, & Tsiagbe VK (1994) Biology of germinal-centers in lymphoid-tissue. *Faseb Journal* 8(11):832-840.

59. Wolniak KL, Shinall SM, & Waldschmidt TJ (2004) The germinal center response. *Critical Reviews in Immunology* 24(1):39-65.

60. Victora GD*, et al.* (2010) Germinal Center Dynamics Revealed by Multiphoton Microscopy with a Photoactivatable Fluorescent Reporter. *Cell* 143(4):592-605.

61. Tolar P, Sohn HW, & Pierce SK (2005) The initiation of antigen-induced B cell antigen receptor signaling viewed in living cells by fluorescence resonance energy transfer. *Nature Immunology* 6(11):1168-1176.

62. Treanor B (B-cell receptor: from resting state to activate. *Immunology* 136(1):21-27.

63. Campbell KS & Cambier JC (1990) B-Lymphocyte antigen receptors (MLG) are non-covalently associated with disulfide linked, inducibly phosphorylated glycoprotein complex. *Embo Journal* 9(2):441-448.

64. Flaswinkel H & Reth M (1994) Dual role of the Tyrosine activation motif og the Ig-alpha protein during signal-transduction via the B-cell antigen receptor. *Embo Journal* 13(1):83-89.

65. Tolar P, Hanna J, Krueger PD, & Pierce SK (2009) The Constant Region of the Membrane Immunoglobulin Mediates B Cell-Receptor Clustering and Signaling in Response to Membrane Antigens. *Immunity* 30(1):44-55.

66. Yang JY & Reth M (2010) Oligomeric organization of the B-cell antigen receptor on resting cells. *Nature* 467(7314):465-U117.

67. Sohn HW, Tolar P, Jin T, & Pierce SK (2006) Fluorescence resonance energy transfer in living cells reveals dynamic membrane changes in the initiation of B cell signaling. *Proceedings of the National Academy of Sciences of the United States of America* 103(21):8143-8148.

68. Ohnishi K & Melchers F (2003) The nonimmunoglobulin portion of lambda 5 mediates cell-autonomous pre-B cell receptor signaling. *Nature Immunology* 4(9):849-856.

69. Guo BC, Kato RM, Garcia-Lloret M, Wahl MI, & Rawlings DJ (2000) Engagement of the human pre-B cell receptor generates a lipid raft-dependent calcium signaling complex. *Immunity* 13(2):243-253.

70. Cheng PC, Dykstra ML, Mitchell RN, & Pierce SK (1999) A role for lipid rafts in B cell antigen receptor signaling and antigen targeting. *Journal of Experimental Medicine* 190(11):1549-1560.

71. Pleiman CM*, et al.* (1994) Distinct p53/56 (Lyn) and p59 (Fyn) domains assiciate with non-phosphorylated and phosphorylated Ig-alpha. *Proceedings of the National Academy of Sciences of the United States of America* 91(10):4268-4272.

72. Johnson SA*, et al.* (1995) Phosphorylated immunoreceptor signaling motifs (ITAMs) exhibit nique abilities to bind and activate Lyn and Syk Tyrosine Kinases. *Journal of Immunology* 155(10):4596-4603.

73. Pao LI, Famiglietti SA, & Cambier JC (1998) Asymmetrical phosphorylation and function of immunoreceptor tyrosine-based activation motif tyrosines in B cell antigen receptor signal transduction. *Journal of Immunology* 160(7):3305-3314.

74. Hata A, Sabe H, Kurosaki T, Takata M, & Hanafusa H (1994) Functional analysis of CSK in signal-transduction through the B-cell antigen receptor. *Molecular and Cellular Biology* 14(11):7306-7313.

75. Pao LI, Bedzyk WD, Persin C, & Cambier JC (1997) Molecular targets of CD45 in B cell antigen receptor signal transduction. *Journal of Immunology* 158(3):1116-1124.

76. Rowley RB, Burkhardt AL, Chao HG, Matsueda GR, & Bolen JB (1995) Syk protein Tyrosine kinase is regulated by Tyrosine-phosphorylated Ig alpha: Ig beta immunoreceptor tyrosine activation motif binding and autophosphoyrlation. *Journal of Biological Chemistry* 270(19):11590-11594.

77. Keshvara LM*, et al.* (1998) Syk- and Lyn-dependent phosphorylation of Syk on multiple tyrosines following B cell activation includes a site that negatively regulates signaling. *Journal of Immunology* 161(10):5276-5283.

78. Saouaf SJ*, et al.* (1994) Temporal differences in the activation of 3 classes of nontransmembrane protein-Tyrosine kinases following B-cell antigen receptor surface engagement. *Proceedings of the National Academy of Sciences of the United States of America* 91(20):9524-9528.

79. Khan WN*, et al.* (1995) DEFECTIVE B-CELL DEVELOPMENT AND FUNCTION IN BTK-DEFICIENT MICE. *Immunity* 3(3):283-299.

80. Takata M & Kurosaki T (1996) A role for Bruton's tyrosine kinase in B cell antigen receptor-mediated activation of phospholipase C-gamma 2. *Journal of Experimental Medicine* 184(1):31-40.

81. Jin H*, et al.* (1995) IDENTIFICATION OF BTK MUTATIONS IN 20 UNRELATED PATIENTS WITH X-LINKED AGAMMAGLOBULINEMIA (XLA). *Human Molecular Genetics* 4(4):693-700.

82. Rawlings DJ*, et al.* (1993) Mutation of unique region of Bruton's Tyrosine kinase in immunodeficient XID mice. *Science* 261(5119):358-361.

83. Buhl AM & Cambier JC (1999) Phosphorylation of CD19 Y484 and Y515, and linked activation of phosphatidylinositol 3-kinase, are required for B cell antigen

receptor-mediated activation of Bruton's tyrosine kinase. *Journal of Immunology* 162(8):4438-4446.

84. Nore BF*, et al.* (2000) Redistribution of Bruton's tyrosine kinase by activation of phosphatidylinositol 3-kinase and Rho-family GTPases. *European Journal of Immunology* 30(1):145-154.

85. Scharenberg AM*, et al.* (1998) Phosphatidylinositol-3,4,5-trisphosphate (PtdIns-3,4,5-P-3) Tec kinase-dependent calcium signaling pathway: a target for SHIP-mediated inhibitory signals. *Embo Journal* 17(7):1961-1972.

86. Rawlings DJ*, et al.* (1996) Activation of BTK by a phosphorylation mechanism initiated by SRC family kinases. *Science* 271(5250):822-825.

87. Otero DC, Anzelon AN, & Rickert RC (2003) CD19 function in early and late B cell development: I. Maintenance of follicular and marginal zone B cells requires CD19-dependent survival signals. *Journal of Immunology* 170(1):73-83.

88. Gold MR*, et al.* (1999) The B cell antigen receptor activates the Akt (protein kinase B)/glycogen synthase kinase-3 signaling pathway via phosphatidylinositol 3-kinase. *Journal of Immunology* 163(4):1894-1905.

89. Andjelkovic M*, et al.* (1997) Role of translocation in the activation and function of protein kinase B. *Journal of Biological Chemistry* 272(50):31515-31524.

90. Sarbassov DD, Guertin DA, Ali SM, & Sabatini DM (2005) Phosphorylation and regulation of Akt/PKB by the rictor-mTOR complex. *Science* 307(5712):1098-1101.

91. Alessi DR*, et al.* (1997) Characterization of a 3-phosphoinositide-dependent protein kinase which phosphorylates and activates protein kinase B alpha. *Current Biology* 7(4):261-269.

92. Lodish*, et al.* (2003) *Molecular cell biology, fifth edition* (W.H. Freeman and company, New York).

93. Nave BT, Ouwens DM, Withers DJ, Alessi DR, & Shepherd PR (1999) Mammalian target of rapamycin is a direct target for protein kinase B: identification of a

convergence point for opposing effects of insulin and amino-acid deficiency on protein translation. *Biochemical Journal* 344:427-431.

94. Jacinto E*, et al.* (2004) Mammalian TOR complex 2 controls the actin cytoskeleton and is rapamycin insensitive. *Nature Cell Biology* 6(11):1122-U1130.

95. delPeso L, GonzalezGarcia M, Page C, Herrera R, & Nunez G (1997) Interleukin-3-induced phosphorylation of BAD through the protein kinase Akt. *Science* 278(5338):687-689.

96. Brunet A*, et al.* (1999) Akt promotes cell survival by phosphorylating and inhibiting a forkhead transcription factor. *Cell* 96(6):857-868.

97. Cross DAE, Alessi DR, Cohen P, Andjelkovich M, & Hemmings BA (1995) Inhibition of Glycogen-synthase Kinase-3 by Insulin, mediated by Protein-Kinase-B. *Nature* 378(6559):785-789.

98. Datta SR*, et al.* (1997) Akt phosphorylation of BAD couples survival signals to the cell-intrinsic death machinery. *Cell* 91(2):231-241.

99. Padeh S, Levitzki A, Gazit A, Mills GB, & Roifman CM (1991) Activation of Phospholipase-C in human B-cells is dependent on Tyrosine phosphorylation. *Journal of Clinical Investigation* 87(3):1114-1118.

100. Fu C, Turck CW, Kurosaki T, & Chan AC (1998) BLNK: a central linker protein in B cell activation. *Immunity* 9(1):93-103.

101. Hashimoto S*, et al.* (1999) Identification of the SH2 domain binding protein of Bruton's tyrosine kinase as BLNK - Functional significance of Btk-SH2 domain in B-cell antigen receptor-coupled calcium signaling. *Blood* 94(7):2357-2364.

102. Chiu CW, Dalton M, Ishiai M, Kurosaki T, & Chan AC (2002) BLNK: molecular scaffolding through 'cis'-mediated organization of signaling proteins. *Embo Journal* 21(23):6461-6472.

103. Kabak S*, et al.* (2002) The direct recruitment of BLNK to immunoglobulin alpha couples the B-Cell antigen receptor to distal signaling pathways. *Molecular and Cellular Biology* 22(8):2524-2535.

104. Abudula A*, et al.* (2007) SLP-65 signal transduction requires Src homology 2 domain-mediated membrane anchoring and a kinase-independent adaptor function of Syk. *Journal of Biological Chemistry* 282(39):29059-29066.

105. Miyazaki A, Yogosawa S, Murakami A, & Kitamura D (Identification of CMTM7 as a transmembrane linker of BLNK and the B-cell receptor. *PloS one* 7(2):e31829.

106. Hsu YT & Youle RJ (1998) Bax in murine thymus is a soluble monomeric protein that displays differential detergent-induced conformations. *Journal of Biological Chemistry* 273(17):10777-10783.

107. Mizuno K*, et al.* (2002) Src homology region 2 domain-containing phosphatase 1 positively regulates B cell receptor-induced apoptosis by modulating association of B cell linker protein with nck and activation of c-jun NH2-terminal kinase. *Journal of Immunology* 169(2):778-786.

108. Antony P*, et al.* (2003) B Cell receptor directs the activation of NFAT and NF-kappa B via distinct molecular mechanisms. *Experimental Cell Research* 291(1):11-24.

109. Dolmetsch RE, Lewis RS, Goodnow CC, & Healy JI (1997) Differential activation of transcription factors induced by Ca2+ response amplitude and duration (vol 386, pg 855, 1997). *Nature* 388(6639):308-308.

110. Engelke M, Engels N, Dittmann K, Stork B, & Wienands J (2007) Ca2+ signaling in antigen receptor-activated B lymphocytes. *Immunological Reviews* 218:235-246.

111. Coggeshall KM, McHugh JC, & Altman A (1992) Predominant expression and activation-induced Tyrosine phosphorylation of Phospholipase c-gamma-2 in B-lymphocytes. *Proceedings of the National Academy of Sciences of the United States of America* 89(12):5660-5664.

112. Nishibe S*, et al.* (1990) Increase of the catalytic activity of Phospholipase c-gamma-1 by Tyrosine phosphorylation. *Science* 250(4985):1253-1256.

113. Rodriguez R*, et al.* (2001) Tyrosine residues in phospholipase C gamma 2 essential for the enzyme function in B-cell signaling. *Journal of Biological Chemistry* 276(51):47982-47992.

114. Wilde JI & Watson SP (2001) Regulation of phospholipase C gamma isoforms in haematopoietic cells - Why one, not the other? *Cellular Signalling* 13(10):691-701.

115. Williams RL (1999) Mammalian phosphoinositide-specific phospholipase C. *Biochimica Et Biophysica Acta-Molecular and Cell Biology of Lipids* 1441(2-3):255-267.

116. Fukami K (2002) Structure, regulation, and function of phospholipase C isozymes. *Journal of Biochemistry* 131(3):293-299.

117. Ishiai M*, et al.* (1999) BLNK required for coupling Syk to PLC gamma 2 and Rac1-JNK in B cells. *Immunity* 10(1):117-125.

118. Kim YJ, Sekiya F, Poulin B, Bae YS, & Rhee SG (2004) Mechanism of B-cell receptor-induced phosphorylation and activation of phospholipase C-gamma 2. *Molecular and Cellular Biology* 24(22):9986-9999.

119. Jumaa H*, et al.* (1999) Abnormal development and function of B lymphocytes in mice deficient for the signaling adaptor protein SLP-65. *Immunity* 11(5):547-554.

120. Berg J, Tymoczko J, & Stryer L (2002) *Biochemsity fifth edition* (W.H. Freeman and company., New York).

121. McConnell FM, Shears SB, Lane PJL, Scheibel MS, & Clark EA (1992) Relationships between the degree of cross-linking of surface-immunoglobulin and the associated Inositol 1,4,5-Trisphosphate and Ca2+ signals in human B-cells. *Biochemical Journal* 284:447-455.

122. Sugawara H, Kurosaki M, Takata M, & Kurosaki T (1997) Genetic evidence for involvement of type 1, type 2 and type 3 inositol 1,4,5-trisphosphate receptors in signal transduction through the B-cell antigen receptor. *Embo Journal* 16(11):3078-3088.

123. Yokoyama K*, et al.* (2002) BANK regulates BCR-induced calcium mobilization by promoting tyrosine phosphorylation of IP3 receptor. *Embo Journal* 21(1-2):83-92.

124. Jayaraman T, Ondrias K, Ondriasova E, & Marks AR (1996) Regulation of the inositol 1,4,5-trisphosphate receptor by tyrosine phosphorylation. *Science* 272(5267):1492-1494.

125. Saci A & Carpenter CL (2005) RhoA GTPase regulates B cell receptor signaling. *Molecular Cell* 17(2):205-214.

126. Zhang SL*, et al.* (2006) Genome-wide RNAi screen of Ca2+ influx identifies genes that regulate Ca2+ release-activated Ca2+ channel activity. *Proceedings of the National Academy of Sciences of the United States of America* 103(24):9357-9362.

127. Roos J*, et al.* (2005) STIM1, an essential and conserved component of store-operated Ca2+ channel function. *Journal of Cell Biology* 169(3):435-445.

128. Baba Y*, et al.* (2006) Coupling of STIM1 to store-operated Ca2+ entry through its constitutive and inducible movement in the endoplasmic reticulum. *Proceedings of the National Academy of Sciences of the United States of America* 103(45):16704-16709.

129. Zhang SYL*, et al.* (2005) STIM1 is a Ca2+ sensor that activates CRAC channels and migrates from the Ca2+ store to the plasma membrane. *Nature* 437(7060):902-905.

130. Penna A*, et al.* (2008) The CRAC channel consists of a tetramer formed by Stim-induced dimerization of Orai dimers. *Nature* 456(7218):116-U112.

131. Prakriya M*, et al.* (2006) Orai1 is an essential pore subunit of the CRAC channel. *Nature* 443(7108):230-233.

132. Hao SL, Kurosaki T, & August A (2003) Differential regulation of NFAT and SRF by the B cell receptor via a PLC gamma-Ca2+-dependent pathway. *Embo Journal* 22(16):4166-4177.

133. Hogan PG, Chen L, Nardone J, & Rao A (2003) Transcriptional regulation by calcium, calcineurin, and NFAT. *Genes & Development* 17(18):2205-2232.

134. Beals CR, Clipstone NA, Ho SN, & Crabtree GR (1997) Nuclear localization of NF-ATc by a calcineurin-dependent, cyclosporin-sensitive intramolecular interaction. *Genes & Development* 11(7):824-834.

135. Porter CM, Havens MA, & Clipstone NA (2000) Identification of amino acid residues and protein kinases involved in the regulation of NFATc subcellular localization. *Journal of Biological Chemistry* 275(5):3543-3551.

136. Garcia-Cozar FJ*, et al.* (1998) Two-site interaction of nuclear factor of activated T cells with activated calcineurin. *Journal of Biological Chemistry* 273(37):23877-23883.

137. Chen L, Glover JNM, Hogan PG, Rao A, & Harrison SC (1998) Structure of the DNA binding domains from NFAT, Fos and Jun bound specifically to DNA. *Nature* 392(6671):42-48.

138. Beals CR, Sheridan CM, Turck CW, Gardner P, & Crabtree GR (1997) Nuclear export of NF-ATc enhanced by glycogen synthase kinase-3. *Science* 275(5308):1930-1933.

139. Ferch U*, et al.* (2007) MALT1 directs B cell receptor-induced canonical nuclear factor-kappa B signaling selectively to the c-Rel subunit. *Nature Immunology* 8(9):984-991.

140. Saijo K*, et al.* (2002) Protein kinase C beta controls nuclear factor kappa B activation in B cells through selective regulation of the I kappa B kinase alpha. *Journal of Experimental Medicine* 195(12):1647-1652.

141. Saijo K*, et al.* (2003) Essential role of Src-family protein tyrosine kinases in NF-kappa B activation during B cell development. *Nature Immunology* 4(3):274-279.

142. Shinohara H*, et al.* (2005) PKC beta regulates BCR-mediated IKK activation by facilitating the interaction between TAK1 and CARMA1. *Journal of Experimental Medicine* 202(10):1423-1431.

143. Schulze-Luehrmann J & Ghosh S (2006) Antigen-receptor signaling to nuclear factor kappa B. *Immunity* 25(5):701-715.

144. Hayden MS & Ghosh S (2008) Shared principles in NF-kappa B signaling. *Cell* 132(3):344-362.

145. Stadanlick JE*, et al.* (2008) Tonic B cell antigen receptor signals supply an NF-kappa B substrate for prosurvival BLyS signaling. *Nature Immunology* 9(12):1379-1387.

146. Ghosh S & Karin M (2002) Missing pieces in the NF-kappa B puzzle. *Cell* 109:S81-S96.

147. Egawa T*, et al.* (2003) Requirement for CARMA1 in antigen receptor-induced NF-kappa B activation and lymphocyte proliferation. *Current Biology* 13(14):1252-1258.

148. Schuman J*, et al.* (2009) A critical role of TAK1 in B-cell receptor-mediated nuclear factor kappa B activation. *Blood* 113(19):4566-4574.

149. Cheng J, Montecalvo A, & Kane LP (Regulation of NF-kappa B induction by TCR/CD28. *Immunologic Research* 50(2-3):113-117.

150. Johnson GL & Lapadat R (2002) Mitogen-activated protein kinase pathways mediated by ERK, JNK, and p38 protein kinases. *Science* 298(5600):1911-1912.

151. Luciano F*, et al.* (2003) Phosphorylation of Bim-EL by Erk1/2 on serine 69 promotes its degradation via the proteasome pathway and regulates its proapoptotic function. *Oncogene* 22(43):6785-6793.

152. Donovan N, Becker EBE, Konishi Y, & Bonni A (2002) JNK phosphorylation and activation of BAD couples the stress-activated signaling pathway to the cell death machinery. *Journal of Biological Chemistry* 277(43):40944-40949.

153. Lei K & Davis RJ (2003) JNK phosphorylation of Bim-related members of the Bcl2 family induces Bax-dependent apoptosis. *Proceedings of the National Academy of Sciences of the United States of America* 100(5):2432-2437.

154. Kumar G, Wang S, Gupta S, & Nel A (1995) The membrane immunoglobulin receptor utilizes a Shc/Grb2/hSos complex for activation of the mitogen-activated protein-kinase cascade. *Biochemical Journal* 307:215-223.

155. Nagai K, Takata M, Yamamura H, & Kurosakiso T (1995) Tyrosine phosphorylation of Shc is mediated through Lyn and Syk in B-cell receptor signaling. *Journal of Biological Chemistry* 270(12):6824-6829.

156. Boriack-Sjodin PA, Margarit SM, Bar-Sagi D, & Kuriyan J (1998) The structural basis of the activation of Ras by Sos. *Nature* 394(6691):337-343.

157. Kolch W (2000) Meaningful relationships: the regulation of the Ras/Raf/MEK/ERK pathway by protein interactions. *Biochemical Journal* 351:289-305.

158. Oh-Hora M, Johmura S, Hashimoto A, Hikida M, & Kurosaki T (2003) Requirement for Ras guanine nucleotide releasing protein 3 in coupling phospholipase C-gamma 2 to Ras in B cell receptor signaling. *Journal of Experimental Medicine* 198(12):1841-1851.

159. Jiang A, Craxton A, Kurosaki T, & Clark EA (1998) Different protein tyrosine kinases are required for B cell antigen receptor-mediated activation of extracellular signal-regulated kinase, c-Jun NH2-terminal kinase 1, and p38 mitogen-activated protein kinase. *Journal of Experimental Medicine* 188(7):1297-1306.

160. Walmsley MJ*, et al.* (2003) Critical roles for Rac1 and Rac2 GTPases in B cell development and signaling. *Science* 302(5644):459-462.

161. Kerr JFR, Wyllie AH, & Currie AR (1972) Apoptosis - Basic biological phenomenon with wide-ranging implications in tissue kinetics. *British Journal of Cancer* 26(4):239-&.

162. Adams JM & Cory S (2007) The Bcl-2 apoptotic switch in cancer development and therapy. *Oncogene* 26(9):1324-1337.

163. Chipuk JE, Moldoveanu T, Llambi F, Parsons MJ, & Green DR (2010) The BCL-2 Family Reunion. *Molecular Cell* 37(3):299-310.

164. Strasser A (2005) The role of BH3-only proteins in the immune system. *Nature Reviews Immunology* 5(3):189-200.

165. Huang DCS & Strasser A (2000) BH3-Only proteins - Essential initiators of apoptotic cell death. *Cell* 103(6):839-842.

166. Hsu YT & Youle RJ (1997) Nonionic detergents induce dimerization among members of the Bcl-2 family. *Journal of Biological Chemistry* 272(21):13829-13834.

167. Wolter KG*, et al.* (1997) Movement of Bax from the cytosol to mitochondria during apoptosis. *Journal of Cell Biology* 139(5):1281-1292.

168. Kim H*, et al.* (2009) Stepwise Activation of BAX and BAK by tBID, BIM, and PUMA Initiates Mitochondrial Apoptosis. *Molecular Cell* 36(3):487-499.

169. Cheng E*, et al.* (2001) BCL-2, BCL-X-L sequester BH3 domain-only molecules preventing BAX- and BAK-mediated mitochondrial apoptosis. *Molecular Cell* 8(3):705-711.

170. Zong WX, Lindsten T, Ross AJ, MacGregor GR, & Thompson CB (2001) BH3-only proteins that bind pro-survival Bcl-2 family members fail to induce apoptosis in the absence of Bax and Bak. *Genes & Development* 15(12):1481-1486.

171. Kuwana T*, et al.* (2002) Bid, Bax, and lipids cooperate to form supramolecular openings in the outer mitochondrial membrane. *Cell* 111(3):331-342.

172. Terradillos O, Montessuit S, Huang DCS, & Martinou JC (2002) Direct addition of BimL to mitochondria does not lead to cytochrome c release. *Febs Letters* 522(1-3):29-34.

173. Wei MC*, et al.* (2001) Proapoptotic BAX and BAK: A requisite gateway to mitochondrial dysfunction and death. *Science* 292(5517):727-730.

174. Dejean LM*, et al.* (2005) Oligomeric Bax is a component of the putative cytochrome c release channel MAC, mitochondrial apoptosis-induced channel. *Molecular Biology of the Cell* 16(5):2424-2432.

175. Antonsson B, Montessuit S, Lauper S, Eskes R, & Martinou JC (2000) Bax oligomerization is required for channel-forming activity in liposomes and to trigger cytochrome c release from mitochondria. *Biochemical Journal* 345:271-278.

176. Kinnally KW, Peixoto PM, Ryu S-Y, & Dejean LM (Is mPTP the gatekeeper for necrosis, apoptosis, or both? *Biochimica Et Biophysica Acta-Molecular Cell Research* 1813(4):616-622.

177. Nakagawa T*, et al.* (2005) Cyclophilin D-dependent mitochondrial permeability transition regulates some necrotic but not apoptotic cell death. *Nature* 434(7033):652-658.

178. Baines CP*, et al.* (2005) Loss of cyclophilin D reveals a critical role for mitochondrial permeability transition in cell death. *Nature* 434(7033):658-662.

179. Dejean LM, Martinez-Caballero S, & Kinnally KW (2006) Is MAC the knife that cuts cytochrome c from mitochondria during apoptosis? *Cell Death and Differentiation* 13(8):1387-1395.

180. Basanez G*, et al.* (2002) Bax-type apoptotic proteins porate pure lipid bilayers through a mechanism sensitive to intrinsic monolayer curvature. *Journal of Biological Chemistry* 277(51):49360-49365.

181. Qian S, Wang W, Yang L, & Huang HW (2008) Structure of transmembrane pore induced by Bax-derived peptide: Evidence for lipidic pores. *Proceedings of the National Academy of Sciences of the United States of America* 105(45):17379-17383.

182. Terrones O*, et al.* (2004) Lipidic pore formation by the concerted action of proapoptotic BAX and tBID. *Journal of Biological Chemistry* 279(29):30081-30091.

183. Cande C*, et al.* (2002) Apoptosis-inducing factor (AIF): a novel caspase-independent death effector released from mitochondria. *Biochimie* 84(2-3):215-222.

184. Joza N*, et al.* (2001) Essential role of the mitochondrial apoptosis-inducing factor in programmed cell death. *Nature* 410(6828):549-554.

185. Susin SA*, et al.* (1999) Molecular characterization of mitochondrial apoptosis-inducing factor. *Nature* 397(6718):441-446.

186. Li LY, Luo L, & Wang XD (2001) Endonuclease G is an apoptotic DNase when released from mitochondria. *Nature* 412(6842):95-99.

187. Nicholson DW (1999) Caspase structure, proteolytic substrates, and function during apoptotic cell death. *Cell Death and Differentiation* 6(11):1028-1042.

188. Zou H, Li YC, Liu HS, & Wang XD (1999) An APAF-1 center dot cytochrome c multimeric complex is a functional apoptosome that activates procaspase-9. *Journal of Biological Chemistry* 274(17):11549-11556.

189. Oltvai ZN, Milliman CL, & Korsmeyer SJ (1993) BCL-2 HETERODIMERIZES IN-VIVO WITH A CONSERVED HOMOLOG, BAX, THAT ACCELERATES PROGRAMMED CELL-DEATH. *Cell* 74(4):609-619.

190. Korsmeyer SJ, Shutter JR, Veis DJ, Merry DE, & Oltvai ZN (1993) BCL-2/BAX - A RHEOSTAT THAT REGULATES AN ANTIOXIDANT PATHWAY AND CELL-DEATH. *Seminars in Cancer Biology* 4(6):327-332.

191. Willis SN*, et al.* (2007) Apoptosis initiated when BH3 ligands engage multiple Bcl-2 homologs, not Bax or Bak. *Science* 315(5813):856-859.

192. Chen L*, et al.* (2005) Differential targeting of prosurvival Bcl-2 proteins by their BH3-only ligands allows complementary apoptotic function. *Molecular Cell* 17(3):393-403.

193. Chen WP, Wang HG, Srinivasula SM, Alnemri ES, & Cooper NR (1999) B cell apoptosis triggered by antigen receptor ligation proceeds via a novel caspase-dependent pathway. *Journal of Immunology* 163(5):2483-2491.

194. Liu XQ, Dai SD, Zhu YN, Marrack P, & Kappler JW (2003) The structure of a Bcl-x(L)/Bim fragment complex: implications for bim function. *Immunity* 19(3):341-352.

195. Fletcher JI*, et al.* (2009) Inaugural Article: Apoptosis is triggered when prosurvival Bcl-2 proteins cannot restrain Bax (vol 105, pg 18081, 2008). *Proceedings of the National Academy of Sciences of the United States of America* 106(5):1678-1678.

196. Merino D*, et al.* (2009) The role of BH3-only protein Bim extends beyond inhibiting Bcl-2-like prosurvival proteins. *Journal of Cell Biology* 186(3):355-362.

197. Letai A*, et al.* (2002) Distinct BH3 domains either sensitize or activate mitochondrial apoptosis, serving as prototype cancer therapeutics. *Cancer Cell* 2(3):183-192.

198. Cartron PF*, et al.* (2004) The first alpha helix of Bax plays a necessary role in its ligand-induced activation by the BH3-only proteins bid and PUMA. *Molecular Cell* 16(5):807-818.

199. Gallenne T*, et al.* (2009) Bax activation by the BH3-only protein Puma promotes cell dependence on antiapoptotic Bcl-2 family members. *Journal of Cell Biology* 185(2):279-290.

200. Gavathiotis E*, et al.* (2008) BAX activation is initiated at a novel interaction site. *Nature* 455(7216):1076-U1076.

201. O'Connor L*, et al.* (1998) Bim: a novel member of the Bcl-2 family that promotes apoptosis. *Embo Journal* 17(2):384-395.

202. Llambi F*, et al.* (2011) A Unified Model of Mammalian BCL-2 Protein Family Interactions at the Mitochondria. *Molecular Cell* 44(4):517-531.

203. Edlich F*, et al.* (Bcl-x(L) Retrotranslocates Bax from the Mitochondria into the Cytosol. *Cell* 145(1):104-116.

204. Ley R, Balmanno K, Hadfield K, Weston C, & Cook SJ (2003) Activation of the ERK1/2 signaling pathway promotes phosphorylation and proteasome-dependent degradation of the BH3-only protein, Bim. *Journal of Biological Chemistry* 278(21):18811-18816.

205. Dijkers PF, Medema RH, Lammers JWJ, Koenderman L, & Coffer PJ (2000) Expression of the pro-apoptotic Bcl-2 family member Bim is regulated by the forkhead transcription factor FKHR-L1. *Current Biology* 10(19):1201-1204.

206. Qi XJ, Wildey GM, & Howe PH (2006) Evidence that Ser(87) of Bim(EL) is phosphorylated by Akt and regulates BimEL apoptotic function. *Journal of Biological Chemistry* 281(2):813-823.

207. Puthalakath H*, et al.* (2001) Bmf: A proapoptotic BH3-only protein regulated by interaction with the myosin V actin motor complex, activated by anoikis. *Science* 293(5536):1829-1832.

208. Puthalakath H, Huang DCS, O'Reilly LA, King SM, & Strasser A (1999) The proapoptotic activity of the Bcl-2 family member Bim is regulated by interaction with the dynein motor complex. *Molecular Cell* 3(3):287-296.

209. Bouillet P*, et al.* (2002) BH3-only Bcl-2 family member Bim is required for apoptosis of autoreactive thymocytes. *Nature* 415(6874):922-926.

210. Putcha GV*, et al.* (2001) Induction of BIM, a proapoptotic BH3-only BCL-2 family member, is critical for neuronal apoptosis. *Neuron* 29(3):615-628.

211. Puthalakath H*, et al.* (2007) ER stress triggers apoptosis by activating BH3-only protein Bim. *Cell* 129(7):1337-1349.

212. Whitfield J, Neame SJ, Paquet L, Bernard O, & Ham J (2001) Dominant-negative c-Jun promotes neuronal survival by reducing BIM expression and inhibiting mitochondrial cytochrome c release. *Neuron* 29(3):629-643.

213. Danial NN (2008) BAD: undertaker by night, candyman by day. *Oncogene* 27:S53-S70.

214. Bonni A*, et al.* (1999) Cell survival promoted by the Ras-MAPK signaling pathway by transcription-dependent and -independent mechanisms. *Science* 286(5443):1358-1362.

215. Tan Y, Demeter MR, Ruan H, & Comb MJ (2000) BAD Ser-155 phosphorylation regulates BAD/Bcl-XL interaction and cell survival. *Journal of Biological Chemistry* 275(33):25865-25869.

216. Vogelstein B, Lane D, & Levine AJ (2000) Surfing the p53 network. *Nature* 408(6810):307-310.

217. Zhao RB*, et al.* (2000) Analysis of p53-regulated gene expression patterns using oligonucleotide arrays. *Genes & Development* 14(8):981-993.

218. Jeffers JR*, et al.* (2003) Puma is an essential mediator of p53-dependent and -independent apoptotic pathways. *Cancer Cell* 4(4):321-328.

219. Nakano K & Vousden KH (2001) PUMA, a novel proapoptotic gene, is induced by p53. *Molecular Cell* 7(3):683-694.

220. Pinon JD, Labi V, Egle A, & Villunger A (2008) Bmf and Bmf in tissue homeostasis and malignant disease. *Oncogene* 27:S41-S52.

221. Coultas L*, et al.* (2005) Concomitant loss of proapoptotic BH3-only bcl-2 antagonists Bik and Bim arrests spermatogenesis. *Embo Journal* 24(22):3963-3973.

222. Coultas L*, et al.* (2004) Proapoptotic BH3-only Bcl-2 family member Bik/Blk/Nbk is expressed in hemopoietic and endothelial cells but is redundant for their programmed death. *Molecular and Cellular Biology* 24(4):1570-1581.

223. Jiang AM & Clark EA (2001) Involvement of Bik, a proapoptotic member of the Bcl-2 family, in surface IgM-mediated B cell apoptosis. *Journal of Immunology* 166(10):6025-6033.

224. Upton JP*, et al.* (2008) Caspase-2 cleavage of BID is a critical apoptotic signal downstream of endoplasmic reticulum stress. *Molecular and Cellular Biology* 28(12):3943-3951.

225. Berard R*, et al.* (1999) Mitochondria connects the antigen receptor to effector caspases during B cell receptor-induced apoptosis in normal human B cells. *Journal of Immunology* 163(9):4655-4662.

226. Yoshida T*, et al.* (2000) Rapid B cell apoptosis induced by antigen receptor ligation does not require Fas (CD95/APO-1), the adaptor protein FADD/MORT1 or CrmA-sensitive caspases but is defective in both MRL-+/+ and MRL-lpr/lpr mice. *International Immunology* 12(4):517-526.

227. Nemazee DA & Burki K (1989) Clonal deletion of Lymphocyte-B in a transgenic mouse bearing anti-MHC Class-I antibody genes. *Nature* 337(6207):562-566.

228. Kroesen BJ*, et al.* (2001) Induction of apoptosis through B-cell receptor cross-linking occurs via de novo generated C16-ceramide and involves mitochondria. *Journal of Biological Chemistry* 276(17):13606-13614.

229. Enders A*, et al.* (2003) Loss of the pro-apoptotic BH3-only Bcl-2 family member Bim inhibits BCR stimulation-induced apoptosis and deletion of autoreactive B cells. *Journal of Experimental Medicine* 198(7):1119-1126.

230. Mouhamad S*, et al.* (2004) B cell receptor-mediated apoptosis of human lymphocytes is associated with a new regulatory pathway of Bim isoform expression. *Journal of Immunology* 172(4):2084-2091.

231. Takada E, Hata K, & Mizuguchi J (2006) Requirement for JNK-dependent upregulation of BimL in anti-IgM-induced apoptosis in murine B lymphoma cell lines WEHI-231 and CH31. *Experimental Cell Research* 312(19):3728-3738.

232. Clybouw C*, et al.* (2009) BimL upregulation induced by BCR cross-linking in BL41 Burkitt's lymphoma results from a splicing mechanism of the BimEL mRNA. *Biochemical and Biophysical Research Communications* 383(1):32-36.

233. Egle A, Harris AW, Bouillet P, & Cory S (2004) Bim is a suppressor of Myc-induced mouse B cell leukemia. *Proceedings of the National Academy of Sciences of the United States of America* 101(16):6164-6169.

234. Irish JM, Czerwinski DK, Nolan GP, & Levy R (2006) Altered B-cell receptor signaling kinetics distinguish human follicular lymphoma. B cells from tumor-infiltrating nonmalignant B cells. *Blood* 108(9):3135-3142.

235. Labi V*, et al.* (2008) Loss of the BH3-only protein Bmf impairs B cell homeostasis and accelerates gamma irradiation-induced thymic lymphoma development. *Journal of Experimental Medicine* 205(3):641-655.

236. Malissein E, Verdier M, Ratinaud MH, & Troutaud D (2006) Activation of Bad trafficking is involved in the BCR-mediated apoptosis of immature B cells. *Apoptosis* 11(6):1003-1012.

237. Eldering E*, et al.* (2004) Apoptosis via the B cell antigen receptor requires Bax translocation and involves mitochondrial depolarization, cytochrome C release, and caspase-9 activation. *European Journal of Immunology* 34(7):1950-1960.

238. Eeva J*, et al.* (2009) Feedback Regulation of Mitochondria by Caspase-9 in the B Cell Receptor-Mediated Apoptosis. *Scandinavian Journal of Immunology* 70(6):574-583.

239. Herold MJ, Kuss AW, Kraus C, & Berberich I (2002) Mitochondria-dependent caspase-9 activation is necessary for antigen receptor-mediated effector caspase activation and apoptosis in WEHI 231 lymphoma cells. *Journal of Immunology* 168(8):3902-3909.

240. Degterev A, Boyce M, & Yuan JY (2003) A decade of caspases. *Oncogene* 22(53):8543-8567.

241. Krumschnabel G, Sohm B, Bock F, Manzl C, & Villunger A (2009) The enigma of caspase-2: the laymen's view. *Cell Death and Differentiation* 16(2):195-207.

242. Yan BC, Adachi T, & Tsubata T (2008) ER stress is involved in B cell antigen receptor ligation-induced apoptosis. *Biochemical and Biophysical Research Communications* 365(1):143-148.

243. Ruiz-Vela A, de Buitrago GG, & Martinez-A C (1999) Implication of calpain in caspase activation during B cell clonal deletion. *Embo Journal* 18(18):4988-4998.

244. Cragg MS, Zhang L, French RR, & Glennie MJ (1999) Analysis of the interaction of monoclonal antibodies with surface IgM on neoplastic B-cells. *British Journal of Cancer* 79(5-6):850-857.

245. Besnault L*, et al.* (2001) B cell receptor cross-linking triggers a caspase-8-dependent apoptotic pathway that is independent of the death effector domain of Fas-associated death domain protein. *Journal of Immunology* 167(2):733-740.

246. Goodnow CC*, et al.* (1988) Altered Immunoglobulin expression and functional silencing of self-reactive B-lymphocytes in transgenic mice. *Nature* 334(6184):676-682.

247. Healy JI & Goodnow CC (1998) Positive versus negative signaling by lymphocyte antigen receptors. *Annual Review of Immunology* 16:645-670.

248. Hertz M & Nemazee D (1997) BCR ligation induces receptor editing in IgM(+)IgD(-) bone marrow B cells in vitro. *Immunity* 6(4):429-436.

249. Norvell A, Mandik L, & Monroe JG (1995) Engagement of the antigen-receptor on immature murine B-lymphocytes results in death by apoptosis. *Journal of Immunology* 154(9):4404-4413.

250. Benschop RJ, Melamed D, Nemazee D, & Cambier JC (1999) Distinct signal thresholds for the unique antigen receptor-linked gene expression programs in mature and immature B cells. *Journal of Experimental Medicine* 190(6):749-756.

251. Monroe JG (2004) Ligand-independent tonic in B-cell receptor function. *Current Opinion in Immunology* 16(3):288-295.

252. Monroe JG (2006) ITAM-mediated tonic signalling through pre-BCR and BCR complexes. *Nature Reviews Immunology* 6(4):283-294.

253. Wechsler RJ & Monroe JG (1995) Immature B-lymphocytes are deficient in expression of the Src-family kinases p59(Fyn) and p55(Fggr1). *Journal of Immunology* 154(4):1919-1929.

254. Hoffmann R, Seidl T, Neeb M, Rolink A, & Melchers F (2002) Changes in gene expression profiles in developing B cells of murine bone marrow. *Genome Research* 12(1):98-111.

255. Grumont RJ, Rourke IJ, & Gerondakis S (1999) Rel-dependent induction of A1 transcription is required to protect B cells from antigen receptor ligation-induced apoptosis. *Genes & Development* 13(4):400-411.

256. Andrews SF & Rawlings DJ (2009) Transitional B Cells Exhibit a B Cell Receptor-Specific Nuclear Defect in Gene Transcription. *Journal of Immunology* 182(5):2868-2878.

257. Cheng SH*, et al.* (2009) BCR-mediated apoptosis associated with negative selection of immature B cells is selectively dependent on Pten. *Cell Research* 19(2):196-207.

258. Sproul TW, Malapati S, Kim J, & Pierce SK (2000) Cutting edge: B cell antigen receptor signaling occurs outside lipid rafts in immature B cells. *Journal of Immunology* 165(11):6020-6023.

259. Galluzzi L*, et al.* (Molecular definitions of cell death subroutines: recommendations of the Nomenclature Committee on Cell Death 2012. *Cell Death and Differentiation* 19(1):107-120.

260. Kroemer G*, et al.* (2005) Classification of cell death: recommendations of the Nomenclature Committee on Cell Death. *Cell Death and Differentiation* 12:1463-1467.

261. Kroemer G*, et al.* (2009) Classification of cell death: recommendations of the Nomenclature Committee on Cell Death 2009. *Cell Death and Differentiation* 16(1):3-11.

262. Galluzzi L & Kroemer G (2008) Necroptosis: A Specialized Pathway of Programmed Necrosis. *Cell* 135(7):1161-1163.

263. Degterev A*, et al.* (2008) Identification of RIP1 kinase as a specific cellular target of necrostatins. *Nature Chemical Biology* 4(5):313-321.

264. Degterev A*, et al.* (2005) Chemical inhibitor of nonapoptotic cell death with therapeutic potential for ischemic brain injury. *Nature Chemical Biology* 1(2):112-119.

265. Hitomi J*, et al.* (2008) Identification of a Molecular Signaling Network that Regulates a Cellular Necrotic Cell Death Pathway. *Cell* 135(7):1311-1323.

266. Rodriguez-Enriquez S, Kim I, Currin RT, & Lemasters JJ (2006) Tracker dyes to probe mitochondrial autophagy (mitophagy) in rat hepatocytes. *Autophagy* 2(1):39-46.

267. Levine B, Sinha S, & Kroemer G (2008) Bcl-2 family members - Dual regulators of apoptosis and autophagy. *Autophagy* 4(5):600-606.

268. Levine B & Yuan JY (2005) Autophagy in cell death: an innocent convict? *Journal of Clinical Investigation* 115(10):2679-2688.

269. Lum JJ*, et al.* (2005) Growth factor regulation of autophagy and cell survival in the absence of apoptosis. *Cell* 120(2):237-248.

270. Berry DL & Baehrecke EH (2007) Growth arrest and autophagy are required for salivary gland cell degradation in Drosophila. *Cell* 131(6):1137-1148.

271. Elgendy M, Sheridan C, Brumatti G, & Martin SJ (2011) Oncogenic Ras-Induced Expression of Noxa and Beclin-1 Promotes Autophagic Cell Death and Limits Clonogenic Survival. *Molecular Cell* 42(1):23-35.

272. Shimizu S*, et al.* (2004) Role of Bcl-2 family proteins in a non-apoptotic programmed cell death dependent on autophagy genes. *Nature Cell Biology* 6(12):1221-1228.

273. Liang XH*, et al.* (1999) Induction of autophagy and inhibition of tumorigenesis by beclin 1. *Nature* 402(6762):672-676.

274. Pattingre S*, et al.* (2005) Bcl-2 antiapoptotic proteins inhibit Beclin 1-dependent autophagy. *Cell* 122(6):927-939.

275. Watanabe K, Ichinose S, Hayashizaki K, & Tsubata T (2008) Induction of autophagy by B cell antigen receptor stimulation and its inhibition by costimulation. *Biochemical and Biophysical Research Communications* 374(2):274-281.

276. Elliott RL & Blobe GC (2005) Role of transforming growth factor beta in human cancer. *Journal of Clinical Oncology* 23(9):2078-2093.

277. Massague J, Blain SW, & Lo RS (2000) TGF beta signaling in growth control, cancer, and heritable disorders. *Cell* 103(2):295-309.

278. Kulkarni AB*, et al.* (1993) TRANSFORMING GROWTH FACTOR-BETA-1 NULL MUTATION IN MICE CAUSES EXCESSIVE INFLAMMATORY RESPONSE AND EARLY DEATH. *Proceedings of the National Academy of Sciences of the United States of America* 90(2):770-774.

279. Shull MM*, et al.* (1992) TARGETED DISRUPTION OF THE MOUSE TRANSFORMING GROWTH FACTOR-BETA-1 GENE RESULTS IN MULTIFOCAL INFLAMMATORY DISEASE. *Nature* 359(6397):693-699.

280. Sanderson N*, et al.* (1995) HEPATIC EXPRESSION OF MATURE TRANSFORMING GROWTH-FACTOR-BETA-1 IN TRANSGENIC MICE RESULTS IN MULTIPLE TISSUE LESIONS. *Proceedings of the National Academy of Sciences of the United States of America* 92(7):2572-2576.

281. Spender LC*, et al.* (2009) TGF-beta induces apoptosis in human B cells by transcriptional regulation of BIK and BCL-X-L. *Cell Death and Differentiation* 16(4):593-602.

282. Reimann M*, et al.* (2010) Tumor Stroma-Derived TGF-beta Limits Myc-Driven Lymphomagenesis via Suv39h1-Dependent Senescence. *Cancer Cell* 17(3):262-272.

283. Xu XL*, et al.* (2000) Haploid loss of the tumor suppressor Smad4/Dpc4 initiates gastric polyposis and cancer in mice. *Oncogene* 19(15):1868-1874.

284. Zhu YA, Richardson JA, Parada LF, & Graff JM (1998) Smad3 mutant mice develop metastatic colorectal cancer. *Cell* 94(6):703-714.

285. Xu J, Lamouille S, & Derynck R (2009) TGF-beta-induced epithelial to mesenchymal transition. *Cell Research* 19(2):156-172.

286. Hoshino Y, Katsuno Y, Ehata S, & Miyazono K (Autocrine TGF-beta protects breast cancer cells from apoptosis through reduction of BH3-only protein, Bim. *Journal of Biochemistry* 149(1):55-65.

287. Shi YG & Massague J (2003) Mechanisms of TGF-beta signaling from cell membrane to the nucleus. *Cell* 113(6):685-700.

288. Zhang Y, Feng XH, Wu RY, & Derynck R (1996) Receptor-associated Mad homologues synergize as effectors of the TGF-beta response. *Nature* 383(6596):168-172.

289. Wrana JL, Attisano L, Wieser R, Ventura F, & Massague J (1994) MECHANISM OF ACTIVATION OF THE TGF-BETA RECEPTOR. *Nature* 370(6488):341-347.

290. Huse M*, et al.* (2001) The TGF beta receptor activation process: An inhibitor- to substrate-binding switch. *Molecular Cell* 8(3):671-682.

291. Tsukazaki T, Chiang TA, Davison AF, Attisano L, & Wrana JL (1998) SARA, a FYVE domain protein that recruits Smad2 to the TGF beta receptor. *Cell* 95(6):779-791.

292. Xu L, Chen YG, & Massague J (2000) The nuclear import function of Smad2 is masked by SARA and unmasked by TGF beta-dependent phosphorylation. *Nature Cell Biology* 2(8):559-562.

293. Liu F, Pouponnot C, & Massague J (1997) Dual role of the Smad4/DPC4 tumor suppressor in TGF beta-inducible transcriptional complexes. *Genes & Development* 11(23):3157-3167.

294. Perlman R, Schiemann WP, Brooks MW, Lodish HF, & Weinberg RA (2001) TGF-beta-induced apoptosis is mediated by the adapter protein Daxx that facilitates JNK activation. *Nature Cell Biology* 3(8):708-714.

295. Takekawa M*, et al.* (2002) Smad-dependent GADD45 beta expression mediates delayed activation of p38 MAP kinase by TGF-beta. *Embo Journal* 21(23):6473-6482.

296. Clybouw C*, et al.* (2008) TGF beta-mediated apoptosis of Burkitt's lymphoma BL41 cells is associated with the relocation of mitochondrial BimEL. *Oncogene* 27(24):3446-3456.

297. Kim BC, Mamura M, Choi KS, Calabretta B, & Kim SJ (2002) Transforming growth factor beta 1 induces apoptosis through cleavage of BAD in a Smad3-

dependent mechanism in FaO hepatoma cells. *Molecular and Cellular Biology* 22(5):1369-1378.

298. Ohgushi M*, et al.* (2005) Transforming growth factor beta-dependent sequential activation of Smad, Bim, and caspase-9 mediates physiological apoptosis in gastric epithelial cells. *Molecular and Cellular Biology* 25(22):10017-10028.

299. Ramjaun AR, Tomlinson S, Eddaoudi A, & Downward J (2007) Upregulation of two BH3-only proteins, Bmf and Bim, during TGF beta-induced apoptosis. *Oncogene* 26(7):970-981.

300. Wildey GM, Patil S, & Howe PH (2003) Smad3 potentiates transforming growth factor beta (TGF beta)-induced apoptosis and expression of the BH3-only protein bim in WEHI 231 B lymphocytes. *Journal of Biological Chemistry* 278(20):18069-18077.

301. Yu J*, et al.* (2008) Identification of the gene transcription and apoptosis mediated by TGF-beta-Smad2/3-Smad4 signaling. *Journal of Cellular Physiology* 215(2):422-433.

302. Ramesh S*, et al.* (2008) TGF beta-mediated BIM expression and apoptosis are regulated through SMAD3-dependent expression of the MAPK phosphatase MKP2. *Embo Reports* 9(10):990-997.

303. Kim SG*, et al.* (2004) Transforming growth factor-beta 1 induces apoptosis through Fas ligand-independent activation of the Fas death pathway in human gastric SNU-620 carcinoma cells. *Molecular Biology of the Cell* 15(2):420-434.

304. Landstrom M*, et al.* (2000) Smad7 mediates apoptosis induced by transforming growth factor beta in prostatic carcinoma cells. *Current Biology* 10(9):535-538.

305. Okado T*, et al.* (2002) Smad7 mediates transforming growth factor-beta-induced apoptosis in mesangial cells. *Kidney International* 62(4):1178-1186.

306. Valderrama-Carvajal H*, et al.* (2002) Activin/TGF-beta induce apoptosis through Smad-dependent expression of the lipid phosphatase SHIP. *Nature Cell Biology* 4(12):963-969.

307. Nilsson JA & Cleveland JL (2003) Myc pathways provoking cell suicide and cancer. *Oncogene* 22(56):9007-9021.

308. Zeller KI*, et al.* (2006) Global mapping of c-Myc binding sites and target gene networks in human B cells. *Proceedings of the National Academy of Sciences of the United States of America* 103(47):17834-17839.

309. Wu SQ*, et al.* (2003) Myc represses differentiation-induced p21CIP1 expression via Miz-1-dependent interaction with the p21 core promoter. *Oncogene* 22(3):351-360.

310. Blackwell TK, Kretzner L, Blackwood EM, Eisenman RN, & Weintraub H (1990) SEQUENCE-SPECIFIC DNA-BINDING BY THE C-MYC PROTEIN. *Science* 250(4984):1149-1151.

311. Blackwood EM & Eisenman RN (1991) MAX - A HELIX-LOOP-HELIX ZIPPER PROTEIN THAT FORMS A SEQUENCE-SPECIFIC DNA-BINDING COMPLEX WITH MYC. *Science* 251(4998):1211-1217.

312. Blackwood EM, Luscher B, & Eisenman RN (1992) MYC AND MAX ASSOCIATE INVIVO. *Genes & Development* 6(1):71-80.

313. McMahon SB, Van Buskirk HA, Dugan KA, Copeland TD, & Cole MD (1998) The novel ATM-related protein TRRAP is an essential cofactor for the c-Myc and E2F oncoproteins. *Cell* 94(3):363-374.

314. McMahon SB, Wood MA, & Cole MD (2000) The essential cofactor TRRAP recruits the histone acetyltransferase hGCN5 to c-Myc. *Molecular and Cellular Biology* 20(2):556-562.

315. Park J, Wood MA, & Cole MD (2002) BAF53 forms distinct nuclear complexes and functions as a critical c-Myc-interacting nuclear cofactor for oncogenic transformation. *Molecular and Cellular Biology* 22(5):1307-1316.

316. Wood MA, McMahon SB, & Cole MD (2000) An ATPase/helicase complex is an essential cofactor for oncogenic transformation by c-Myc. *Molecular Cell* 5(2):321-330.

317. Ayer DE, Lawrence QA, & Eisenman RN (1995) MAD-MAX TRANSCRIPTIONAL REPRESSION IS MEDIATED BY TERNARY COMPLEX-FORMATION WITH MAMMALIAN HOMOLOGS OF YEAST REPRESSOR SIN3. *Cell* 80(5):767-776.

318. Hurlin PJ*, et al.* (1995) MAD3 AND MAD4 - NOVEL MAX-INTERACTING TRANSCRIPTIONAL REPRESSORS THAT SUPPRESS C-MYC DEPENDENT TRANSFORMATION AND ARE EXPRESSED DURING NEURAL AND EPIDERMAL DIFFERENTIATION. *Embo Journal* 14(22):5646-5659.

319. Peukert K*, et al.* (1997) An alternative pathway for gene regulation by Myc. *Embo Journal* 16(18):5672-5686.

320. Askew DS, Ashmun RA, Simmons BC, & Cleveland JL (1991) Constitutive c-Myc expression in an IL-3-dependent Myeloid cell-line suppresses cell-cycle arrest and accelerates apoptosis. *Oncogene* 6(10):1915-1922.

321. Harris AW*, et al.* (1988) The E-Mu-Myc transgenic mouse - A model for high-incidence spontaneous lymphoma and leukemia of early B-cells. *Journal of Experimental Medicine* 167(2):353-371.

322. Alexander WS, Schrader JW, & Adams JM (1987) Expression of the c-Myc oncogene under control of an immunoglobulin enhancer in E-Mu-Myc transgenic mice. *Molecular and Cellular Biology* 7(4):1436-1444.

323. Colley SM, Tilbrook PA, & Klinken SP (1997) Increased transcription of the E mu-myc transgene and mRNA stabilisation produce only a modest elevation in Myc protein. *Oncogene* 14(22):2735-2739.

324. Eischen CM, Weber JD, Roussel MF, Sherr CJ, & Cleveland JL (1999) Disruption of the ARF-Mdm2-p53 tumor suppressor pathway in Myc-induced lymphomagenesis. *Genes & Development* 13(20):2658-2669.

325. Jacobsen KA, Prasad VS, Sidman CL, & Osmond DG (1994) Apoptosis and Macrophage-mediated deletion of precursor B-cells in the bone-marrow of E-Mu-Myc transgenic mice. *Blood* 84(8):2784-2794.

326. Sidman CL, Denial TM, Marshall JD, & Roths JB (1993) Multiple mechanisms of tumorigenesis in E-Mu-Myc transgenic mice. *Cancer Research* 53(7):1665-1669.

327. Strasser A, Harris AW, Bath ML, & Cory S (1990) Novel primitive lymphoid tumours induced in trasgenic mice by cooperation between Myc and Bcl-2. *Nature* 348(6299):331-333.

328. Happo L, Phipson B, Smyth GK, Strasser A, & Scott CL (Neither loss of Bik alone, nor combined loss of Bik and Noxa, accelerate murine lymphoma development or render lymphoma cells resistant to DNA damaging drugs. *Cell Death & Disease* 3.

329. Frenzel A*, et al.* (2010) Suppression of B-cell lymphomagenesis by the BH3-only proteins Bmf and Bad. *Blood* 115(5):995-1005.

330. Michalak EM*, et al.* (2009) Puma and to a lesser extent Noxa are suppressors of Myc-induced lymphomagenesis. *Cell Death and Differentiation* 16(5):684-696.

331. Hsu B*, et al.* (1995) Evidence that c-Myc mediated apoptosis does not require wild-type p53 during lymphomagenesis. *Oncogene* 11(1):175-179.

332. Schmitt CA, McCurrach ME, de Stanchina E, Wallace-Brodeur RR, & Lowe SW (1999) INK4a/ARF mutations accelerate lymphomagenesis and promote chemoresistance by disabling p53. *Genes & Development* 13(20):2670-2677.

333. Mori S*, et al.* (2008) Utilization of Pathway Signatures to Reveal Distinct Types of B Lymphoma in the E mu-myc Model and Human Diffuse Large B-Cell Lymphoma. *Cancer Research* 68(20):8525-8534.

334. Nesbit CE, Tersak JM, & Prochownik EV (1999) MYC oncogenes and human neoplastic disease. *Oncogene* 18(19):3004-3016.

335. Refaeli Y*, et al.* (2008) The B cell antigen receptor and overexpression of MYC can cooperate in the genesis of B cell lymphomas. *Plos Biology* 6(6):1208-1225.

336. Krysov S*, et al.* (2010) Surface IgM of CLL cells displays unusual glycans indicative of engagement of antigen in vivo. *Blood* 115(21):4198-4205.

337. Johnson TA, Rassenti LZ, & Kipps TJ (1997) Ig V(H)1 genes expressed in B cell chronic lymphocytic leukemia exhibit distinctive molecular features. *Journal of Immunology* 158(1):235-246.

338. Messmer BT*, et al.* (2004) Multiple distinct sets of stereotyped antigen receptors indicate a role for antigen in promoting chronic lymphocytic leukemia. *Journal of Experimental Medicine* 200(4):519-525.

339. Rosenwald A*, et al.* (2001) Relation of gene expression phenotype to immunoglobulin mutation genotype in B cell chronic lymphocytic leukemia. *Journal of Experimental Medicine* 194(11):1639-1647.

340. Damle RN*, et al.* (2002) B-cell chronic lymphocytic leukemia cells express a surface membrane phenotype of activated, antigen-experienced B lymphocytes. *Blood* 99(11):4087-4093.

341. Mockridge CI*, et al.* (2007) Reversible anergy of sIgM-mediated signaling in the two subsets of CLL defined by V-H-gene mutational status. *Blood* 109(10):4424-4431.

342. Petlickovski A*, et al.* (2005) Sustained signaling through the B-cell receptor induces Mcl-1 and promotes survival of chronic lymphocytic leukemia B cells. *Blood* 105(12):4820-4827.

343. Longo PG*, et al.* (2008) The Akt/Mcl-1 pathway plays a prominent role in mediating antiapoptotic signals downstream of the B-cell receptor in chronic lymphocytic leukemia B cells. *Blood* 111(2):846-855.

344. Krysov S*, et al.* Surface IgM stimulation induces MEK1/2-dependent MYC expression in chronic lymphocytic leukemia cells. *Blood* 119(1):170-179.

345. Gobessi S*, et al.* (2009) Inhibition of constitutive and BCR-induced Syk activation downregulates Mcl-1 and induces apoptosis in chronic lymphocytic leukemia B cells. *Leukemia* 23(4):686-697.

346. Herman SEM*, et al.* (2011) Bruton tyrosine kinase represents a promising therapeutic target for treatment of chronic lymphocytic leukemia and is effectively targeted by PCI-32765. *Blood* 117(23):6287-6296.

347. Friedberg JW*, et al.* (2010) Inhibition of Syk with fostamatinib disodium has significant clinical activity in non-Hodgkin lymphoma and chronic lymphocytic leukemia. *Blood* 115(13):2578-2585.

348. Burger JA*, et al.* (2000) Blood-derived nurse-like cells protect chronic lymphocytic leukemia B cells from spontaneous apoptosis through stromal cell-derived factor-1. *Blood* 96(8):2655-2663.

349. Narducci MG*, et al.* (1997) The murine Tcl1 oncogene: embryonic and lymphoid cell expression. *Oncogene* 15(8):919-926.

350. Herling M*, et al.* (2006) TCL1 shows a regulated expression pattern in chronic lymphocytic leukemia that correlates with molecular subtypes and proliferative state. *Leukemia* 20(2):280-285.

351. Santanam U*, et al.* (2007) Tcl1 expression in chronic lymphocytic leukemia is regulated by microRNA-29 and microRNA-181. *Proceedings of the American Association for Cancer Research Annual Meeting* 48:1259.

352. Virgilio L*, et al.* (1998) Deregulated expression of TCL1 causes T cell leukemia in mice. *Proceedings of the National Academy of Sciences of the United States of America* 95(7):3885-3889.

353. Bichi R*, et al.* (2002) Human chronic lymphocytic leukemia modeled in mouse by targeted TCL1 expression. *Proceedings of the National Academy of Sciences of the United States of America* 99(10):6955-6960.

354. Johnson AJ*, et al.* (2006) Characterization of the TCL-1 transgenic mouse as a preclinical drug development tool for human chronic lymphocytic leukemia. *Blood* 108(4):1334-1338.

355. Yan X-j*, et al.* (2006) B cell receptors in TCL1 transgenic mice resemble those of aggressive, treatment-resistant human chronic lymphocytic leukemia. *Proceedings of the National Academy of Sciences of the United States of America* 103(31):11713-11718.

356. Suljagic M*, et al.* The Syk inhibitor fostamatinib disodium (R788) inhibits tumor growth in the E mu-TCL1 transgenic mouse model of CLL by blocking antigen-dependent B-cell receptor signaling. *Blood* 116(23):4894-4905.

357. Pekarsky Y*, et al.* (2000) Tcl1 enhances Akt kinase activity and mediates its nuclear translocation. *Proceedings of the National Academy of Sciences of the United States of America* 97(7):3028-3033.

358. Palamarchuk A*, et al.* Tcl1 protein functions as an inhibitor of de novo DNA methylation in B-cell chronic lymphocytic leukemia (CLL). *Proceedings of the National Academy of Sciences of the United States of America* 109(7):2555-2560.

359. Pekarsky Y*, et al.* (2008) Tcl1 functions as a transcriptional regulator and is directly involved in the pathogenesis of CLL. *Proceedings of the National Academy of Sciences of the United States of America* 105(50):19643-19648.

360. ter Brugge PJ*, et al.* (2009) A mouse model for chronic lymphocytic leukemia based on expression of the SV40 large T antigen. *Blood* 114(1):119-127.

361. Vuist WMJ, Levy R, & Maloney DG (1994) Lymphoma regression induced by monoclonal antiidiotypic antibodies correlates with their ability to induce signal-transduction and is not prevented by tumor expression of high levels of Bcl-2 protein. *Blood* 83(4):899-906.

362. Tagawa H*, et al.* (2005) Genome-wide array-based CGH for mantle cell lymphoma: identification of homozygous deletions of the proapoptotic gene BIM. *Oncogene* 24(8):1348-1358.

363. Mestre-Escorihuela C*, et al.* (2007) Homozygous deletions localize novel tumor suppressor genes in B-cell lymphomas. *Blood* 109(1):271-280.

364. Gee KR*, et al.* (2000) Chemical and physiological characterization of fluo-4 Ca2+-indicator dyes. *Cell Calcium* 27(2):97-106.

365. Vermes I, Haanen C, Steffensnakken H, & Reutelingsperger C (1995) A NOVEL ASSAY FOR APOPTOSIS - FLOW CYTOMETRIC DETECTION OF PHOSPHATIDYLSERINE

EXPRESSION ON EARLY APOPTOTIC CELLS USING FLUORESCEIN-LABELED ANNEXIN-V. *Journal of Immunological Methods* 184(1):39-51.

366. Rottenberg H & Wu SL (1998) Quantitative assay by flow cytometry of the mitochondrial membrane potential in intact cells. *Biochimica Et Biophysica Acta-Molecular Cell Research* 1404(3):393-404.

367. Nicoletti I, Migliorati G, Pagliacci MC, Grignani F, & Riccardi C (1991) A RAPID AND SIMPLE METHOD FOR MEASURING THYMOCYTE APOPTOSIS BY PROPIDIUM IODIDE STAINING AND FLOW-CYTOMETRY. *Journal of Immunological Methods* 139(2):271-279.

368. Andrews NC & Faller DV (1991) A RAPID MICROPREPARATION TECHNIQUE FOR EXTRACTION OF DNA-BINDING PROTEINS FROM LIMITING NUMBERS OF MAMMALIAN-CELLS. *Nucleic Acids Research* 19(9):2499-2499.

369. Ho LH*, et al.* (2009) A tumor suppressor function for caspase-2. *Proceedings of the National Academy of Sciences of the United States of America* 106(13):5336-5341.

370. Hoek KL*, et al.* (2006) Transitional B cell fate is associated with developmental stage-specific regulation of diacylglycerol and calcium signaling upon B cell receptor engagement. *Journal of Immunology* 177(8):5405-5413.

371. Berger AB, Sexton KB, & Bogyo M (2006) Commonly used caspase inhibitors designed based on substrate specificity profiles lack selectivity. *Cell Research* 16(12):961-963.

372. Pereira NA & Song Z (2008) Some commonly used caspase substrates and inhibitors lack the specificity required to monitor individual caspase activity. *Biochemical and Biophysical Research Communications* 377(3):873-877.

373. Clybouw C*, et al.* (Regulation of memory B-cell survival by the BH3-only protein Puma. *Blood* 118(15):4120-4128.

374. Erlacher M*, et al.* (2006) Puma cooperates with Bim, the rate-limiting BH3-only protein in cell death during lymphocyte development, in apoptosis induction. *Journal of Experimental Medicine* 203(13):2939-2951.

375. Coultas L*, et al.* (2007) Hrk/DP5 contributes to the apoptosis of select neuronal populations but is dispensable for haematopoietic cell apoptosis. *Journal of Cell Science* 120(12):2044-2052.

376. Brunelle JK, Ryan J, Yecies D, Opferman JT, & Letai A (2009) MCL-1-dependent leukemia cells are more sensitive to chemotherapy than BCL-2-dependent counterparts. *Journal of Cell Biology* 187(3):429-442.

377. Fischer SF*, et al.* (2007) Proapoptotic BH3-only protein Bim is essential for developmentally programmed death of germinal center-derived memory B cells and antibody-forming cells. *Blood* 110(12):3978-3984.

378. Bretz J*, et al.* Noxa mediates p18(INK4c) cell-cycle control of homeostasis in B cells and plasma cell precursors. *Blood* 117(7):2179-2188.

379. Wensveen FM*, et al.* BH3-only protein Noxa regulates apoptosis in activated B cells and controls high-affinity antibody formation. *Blood* 119(6):1440-1449.

380. Galan PP*, et al.* (2009) The PI3K Inhibitor ON 01910.Na Inhibits Critical Survival Pathways and Induces Apoptosis in CLL Cells through Induction of NOXA and BIM. *Blood* 114(22):171-172.

381. Certo M*, et al.* (2006) Mitochondria primed by death signals determine cellular addiction to antiapoptotic BCL-2 family members. *Cancer Cell* 9(5):351-365.

382. Hase H*, et al.* (2002) CD27 and CD40 inhibit p53-independent mitochondrial pathways in apoptosis of B cells induced by B cell receptor ligation. *Journal of Biological Chemistry* 277(49):46950-46958.

383. Chang NC, Nguyen M, Germain M, & Shore GC (Antagonism of Beclin 1-dependent autophagy by BCL-2 at the endoplasmic reticulum requires NAF-1. *Embo Journal* 29(3):606-618.

384. Rashmi R, Pillai SG, Vijayalingam S, Ryerse J, & Chinnadurai G (2008) BH3-only protein BIK induces caspase-independent cell death with autophagic features in Bcl-2 null cells. *Oncogene* 27(10):1366-1375.

385. Zhong Q, Gao WH, Du FH, & Wang XD (2005) Mule/ARF-BP1, a BH3-only E3 ubiquitin ligase, catalyzes the polyubiquitination of Mcl-1 and regulates apoptosis. *Cell* 121(7):1085-1095.

386. Maurer U, Charvet C, Wagman AS, Dejardin E, & Green DR (2006) Glycogen synthase kinase-3 regulates mitochondrial outer membrane permeabilization and apoptosis by destabilization of MCL-1. *Molecular Cell* 21(6):749-760.

387. Opferman JT (2006) Unraveling MCL-1 degradation. *Cell Death and Differentiation* 13(8):1260-1262.

388. Gauld SB, Blair D, Moss CA, Reid SD, & Harnett MM (2002) Differential roles for extracellularly regulated kinase-mitogen-activated protein kinase in B cell antigen receptor-induced apoptosis and CD40-mediated rescue of WEHI-231 immature B cells. *Journal of Immunology* 168(8):3855-3864.

389. Breitschopf K, Haendeler J, Malchow P, Zeiher AM, & Dimmeler S (2000) Posttranslational modification of Bcl-2 facilitates its proteasome-dependent degradation: Molecular characterization of the involved signaling pathway. *Molecular and Cellular Biology* 20(5):1886-1896.

390. Dimmeler S, Breitschopf K, Haendeler J, & Zeiher AM (1999) Dephosphorylation targets Bcl-2 for ubiquitin-dependent degradation: A link between the apoptosome and the proteasome pathway. *Journal of Experimental Medicine* 189(11):1815-1822.

391. Bennett BL*, et al.* (2001) SP600125, an anthrapyrazolone inhibitor of Jun N-terminal kinase. *Proceedings of the National Academy of Sciences of the United States of America* 98(24):13681-13686.

392. Illidge T*, et al.* (2008) Novel Mechanisms of Non-Apoptotic Cell Death Evoked by Type II Anti-CD20 (Tositumomab) and HLA-DR Monoclonal Antibodies. *Blood* 112(11):326-326.

393. Ivanov A*, et al.* (2009) Monoclonal antibodies directed to CD20 and HLA-DR can elicit homotypic adhesion followed by lysosome-mediated cell death in human lymphoma and leukemia cells. *Journal of Clinical Investigation* 119(8):2143-2159.

394. Elgendy M, Sheridan C, Brumatti G, & Martin SJ Oncogenic Ras-Induced Expression of Noxa and Beclin-1 Promotes Autophagic Cell Death and Limits Clonogenic Survival. *Molecular Cell* 42(1):23-35.

395. Miller S*, et al.* Shaping Development of Autophagy Inhibitors with the Structure of the Lipid Kinase Vps34. *Science* 327(5973):1638-1642.

396. Jaber N*, et al.* Class III PI3K Vps34 plays an essential role in autophagy and in heart and liver function. *Proceedings of the National Academy of Sciences of the United States of America* 109(6):2003-2008.

397. Ploner C, Kofler R, & Villunger A (2008) Noxa: at the tip of the balance between life and death. *Oncogene* 27:S84-S92.

398. Wu H, Wang MC, & Bohmann D (2009) JNK protects Drosophila from oxidative stress by trancriptionally activating autophagy. *Mechanisms of Development* 126(8-9):624-637.

399. Li DD*, et al.* (2009) The pivotal role of c-Jun NH2-terminal kinase-mediated Beclin 1 expression during anticancer agents-induced autophagy in cancer cells. *Oncogene* 28(6):886-898.

400. Wei Y, Pattingre S, Sinha S, Bassik M, & Levine B (2008) JNK1-mediated phosphorylation of BcI-2 regulates starvation-induced autophagy. *Molecular Cell* 30(6):678-688.

401. Ley R, Ewings KE, Hadfield K, & Cook SJ (2005) Regulatory phosphorylation of Bim: sorting out the ERK from the JNK. *Cell Death and Differentiation* 12(8):1008-1014.

402. Craxton A, Draves KE, Gruppi A, & Clark EA (2005) BAFF regulates B cell survival by downregulating the BH3-only family member Bim via the ERK pathway. *Journal of Experimental Medicine* 202(10):1363-1374.

403. Oh Y-T*, et al.* ERK/Ribosomal S6 Kinase (RSK) Signaling Positively Regulates Death Receptor 5 Expression through Co-activation of CHOP and Elk1. *Journal of Biological Chemistry* 285(53):41310-41319.

404. Sung B, Ravindran J, Prasad S, Pandey MK, & Aggarwal BB Gossypol Induces Death Receptor-5 through Activation of the ROS-ERK-CHOP Pathway and Sensitizes Colon Cancer Cells to TRAIL. *Journal of Biological Chemistry* 285(46):35418-35427.

405. Iwakoshi NN*, et al.* (2003) Plasma cell differentiation and the unfolded protein response intersect at the transcription factor XBP-1. *Nature Immunology* 4(4):321-329.

406. Szegezdi E, Logue SE, Gorman AM, & Samali A (2006) Mediators of endoplasmic reticulum stress-induced apoptosis. *Embo Reports* 7(9):880-885.

407. Breckenridge DG, Germain M, Mathai JP, Nguyen M, & Shore GC (2003) Regulation of apoptosis by endoplasmic reticulum pathways. *Oncogene* 22(53):8608-8618.

408. Alves NL*, et al.* (2006) The Noxa/Mcl-1 axis regulates susceptibility to apoptosis under glucose limitation in dividing T cells. *Immunity* 24(6):703-716.

409. Nijhawan D*, et al.* (2003) Elimination of Mcl-1 is required for the initiation of apoptosis following ultraviolet irradiation. *Genes & Development* 17(12):1475-1486.

410. French RR, Chan HTC, Tutt AL, & Glennie MJ (1999) CD40 antibody evokes a cytotoxic T-cell response that eradicates lymphoma and bypasses T-cell help. *Nature Medicine* 5(5):548-553.

411. Hanada M, Delia D, Aiello A, Stadtmauer E, & Reed JC (1993) BCL-2 GENE HYPOMETHYLATION AND HIGH-LEVEL EXPRESSION IN B-CELL CHRONIC LYMPHOCYTIC-LEUKEMIA. *Blood* 82(6):1820-1828.

412. Granziero L*, et al.* (2001) Survivin is expressed on CD40 stimulation and interfaces proliferation and apoptosis in B-cell chronic lymphocytic leukemia. *Blood* 97(9):2777-2783.

413. Schliep S, Decker T, Schneller F, Wagner H, & Hacker G (2004) Functional evaluation of the role of inhibitor of apoptosis proteins in chronic lymphocytic leukemia. *Experimental Hematology* 32(6):556-562.

414. Stevenson FK & Caligaris-Cappio F (2004) Chronic lymphocytic leukemia: revelations from the B-cell receptor. *Blood* 103(12):4389-4395.

415. Beers SA*, et al.* (2008) Type II (tositumomab) anti-CD20 monoclonal antibody out performs type I (rituximab-like) reagents in B-cell depletion regardless of complement activation. *Blood* 112(10):4170-4177.

416. Beers SA*, et al.* (2008) The mechanism through which type II (tositumomab-like) anti-CD20 monoclonal antibody out performs type I (rituximab-like) reagents in B-cell depletion. *Immunology* 125:52-52.

417. Cragg MS & Glennie MJ (2004) Antibody specificity controls in vivo effector mechanisms of anti-CD20 reagents. *Blood* 103(7):2738-2743.

418. Glennie MJ, French RR, Cragg MS, & Taylor RP (2007) Mechanisms of killing by anti-CD20 monoclonal antibodies. *Molecular Immunology* 44(16):3823-3837.

419. Cragg MS*, et al.* (2008) Treatment of B-RAF mutant human tumor cells with a MEK inhibitor requires Bim and is enhanced by a BH3 mimetic. *Journal of Clinical Investigation* 118(11):3651-3659.

420. Burger JA, Ghia P, Rosenwald A, & Caligaris-Cappio F (2009) The microenvironment in mature B-cell malignancies: a target for new treatment strategies. *Blood* 114(16):3367-3375.

421. Zenz T, Mertens D, Kueppers R, Doehner H, & Stilgenbauer S From pathogenesis to treatment of chronic lymphocytic leukaemia. *Nature Reviews Cancer* 10(1):37-50.

422. Gong Q*, et al.* (2005) Importance of cellular microenvironment and circulatory dynamics in B cell immunotherapy. *Journal of Immunology* 174(2):817-826.

423. Caux C*, et al.* (1994) ACTIVATION OF HUMAN DENDRITIC CELLS THROUGH CD40 CROSS-LINKING. *Journal of Experimental Medicine* 180(4):1263-1272.

424. Villunger A*, et al.* (2003) p53- and drug-induced apoptotic responses mediated by BH3-only proteins Puma and Noxa. *Science* 302(5647):1036-1038.

425. Amaravadi RK*, et al.* (2007) Autophagy inhibition enhances therapy-induced apoptosis in a Myc-induced model of lymphoma. *Journal of Clinical Investigation* 117(2):326-336.

426. Tsuneoka M*, et al.* (2003) c-myc induces autophagy in rat 3Y1 fibroblast cells. *Cell Structure and Function* 28(3):195-204.

427. Maclean KH, Dorsey FC, Cleveland JL, & Kastan MB (2008) Targeting lysosomal degradation induces p53-dependent cell death and prevents cancer in mouse models of lymphomagenesis. *Journal of Clinical Investigation* 118(1):79-88.

428. Happo L*, et al.* Maximal killing of lymphoma cells by DNA damage-inducing therapy requires not only the p53 targets Puma and Noxa, but also Bim. *Blood* 116(24):5256-5267.

429. Gomez-Bougie P*, et al.* (2007) Noxa up-regulation and Mcl-1 cleavage are associated to apoptosis induction by bortezomib in multiple myeloma. *Cancer Research* 67(11):5418-5424.

430. Nikrad M*, et al.* (2005) The proteasome inhibitor bortezomib sensitizes cells to killing by death receptor ligand TRAIL via BH3-only proteins Bik and Bim. *Molecular Cancer Therapeutics* 4(3):443-449.

431. Wang TH, Wang HS, & Soong YK (2000) Paclitaxel-induced cell death - Where the cell cycle and apoptosis come together. *Cancer* 88(11):2619-2628.

432. Vogler M, Dinsdale D, Dyer MJS, & Cohen GM (2009) Bcl-2 inhibitors: small molecules with a big impact on cancer therapy. *Cell Death and Differentiation* 16(3):360-367.

433. Oltersdorf T*, et al.* (2005) An inhibitor of Bcl-2 family proteins induces regression of solid tumours. *Nature* 435(7042):677-681.

434. van Delft MF*, et al.* (2006) The BH3 mimetic ABT-737 targets selective Bcl-2 proteins and efficiently induces apoptosis via Bak/Bax if Mcl-1 is neutralized. *Cancer Cell* 10(5):389-399.

435. Gandhi L*, et al.* Phase I Study of Navitoclax (ABT-263), a Novel Bcl-2 Family Inhibitor, in Patients With Small-Cell Lung Cancer and Other Solid Tumors. *J. Clin. Oncol.* 29(7):909-916.

436. Kipps TJ*, et al.* Navitoclax (ABT-263) Plus Fludarabine/Cyclophosphamide/Rituximab (FCR) or Bendamustine/Rituximab (BR): A Phase 1 Study in Patients with Relapsed/Refractory Chronic Lymphocytic Leukemia (CLL). *Blood* 118(21):1669-1669.

437. LaBelle JL*, et al.* A stapled BIM peptide overcomes apoptotic resistance in hematologic cancers. *Journal of Clinical Investigation* 122(6):2018-2031.

438. Stewart ML, Fire E, Keating AE, & Walensky LD The MCL-1 BH3 helix is an exclusive MCL-1 inhibitor and apoptosis sensitizer. *Nature Chemical Biology* 6(8):595-601.

439. Packham G & Stevenson F The role of the B-cell receptor in the pathogenesis of chronic lymphocytic leukaemia. *Seminars in Cancer Biology* 20(6):391-399.

440. Liu J*, et al.* (2012) Abstract LB-106: A novel TCL1-TG:p53-/- mouse model of human CLL. *Cancer Research* 72(8):Supplement 1.

441. Beers SA*, et al.* (Antigenic modulation limits the efficacy of anti-CD20 antibodies: implications for antibody selection. *Blood* 115(25):5191-5201.

442. Mantovani A, Sozzani S, Locati M, Allavena P, & Sica A (2002) Macrophage polarization: tumor-associated macrophages as a paradigm for polarized M2 mononuclear phagocytes. *Trends in Immunology* 23(11):549-555.

443. Herman SEM. Bruton tyrosine kinase represents a promising therapeutic target for treatment of chronic lymphocytic leukemia and is effectively targeted by PCI-32765. *Blood* 117(23):6287-6296.

444. Friedberg JW. Inhibition of Syk with fostamatinib disodium has significant clinical activity in non-Hodgkin lymphoma and chronic lymphocytic leukemia. *Blood* 115(13):2578-2585.

445. Zent CS. The Treatment of Recurrent/Refractory Chronic Lymphocytic Leukemia/Small Lymphocytic Lymphoma (CLL) With Everolimus Results in Clinical Responses and Mobilization of CLL Cells Into the Circulation. *Cancer* 116(9):2201-2207.

446. Furman RR. CAL-101, An Isoform-Selective Inhibitor of Phosphatidylinositol 3-Kinase P110 delta, Demonstrates Clinical Activity and Pharmacodynamic Effects In patients with Relapsed or Refractory Chronic Lymphocytic Leukemia. *Blood* 116(21):31-31.

447. Wienands J, Larbolette O, & Reth M (1996) Evidence for a preformed transducer complex organized by the B cell antigen receptor. *Proceedings of the National Academy of Sciences of the United States of America* 93(15):7865-7870.

448. Pasparakis M, Schmidt-Supprian M, & Rajewsky K (2002) I kappa B kinase signaling is essential for maintenance of mature B cells. *Journal of Experimental Medicine* 196(6):743-752.

449. Ruland J*, et al.* (2001) Bcl10 is a positive regulator of antigen receptor-induced activation of NF-kappa B and neural tube closure. *Cell* 104(1):33-42.

450. Gass JN, Gifford NM, & Brewer JW (2002) Activation of an unfolded protein response during differentiation of antibody-secreting B cells. *Journal of Biological Chemistry* 277(50):49047-49054.

Appendix

A1 BCR tonic signalling

A1.1 BCR ablation studies identify a role in cellular maintenance

The molecular events associated with BCR signalling, described in section 1.4, result from studies identifying the functional consequences associated with antigen-driven signalling. However, it is clear that the signalling role of the BCR is multi-faceted and dependent upon the nature of receptor engagement. For instance, in the absence of

antigen binding the BCR still plays a vital role in cellular maintenance and development, via the production of antigen-independent tonic signals (19, 23-28).

A1.2 Tonic signals and downstream molecular events

Antigen-mediated BCR engagement is classically associated with an accumulation of protein Tyr phosphorylation, leading to a phospho-Tyr fingerprint. Interestingly, treatment of resting B-cells with the tyrosine-phosphatase inhibitor pervanadate yielded phospho-Tyr fingerprints identical to those produced after antigen engagement (447). Such resting-state phospho-Tyr fingerprints are indicative of basal signals emanating from the BCR, in the absence of receptor engagement, resulting in the Tyr phosphorylation of downstream signalling components (23). Such basal signals are known as tonic signals and are vital for the maintenance of B-cell populations in the periphery, since in their absence peripheral B-cells undergo apoptosis and are deleted (24, 25, 27). It is proposed that such signals are produced in the absence of any receptor engagement, since expression of a plasma membrane-targeted CD79a/b cytoplasmic domain construct was sufficient to fully recapitulate tonic BCR signalling and overcome B-cell developmental arrest in $IgH^{-/-}$ cells (23).

It is proposed that tonic B-cell signals are translated into downstream signalling through the same components as employed during antigen-driven signalling, albeit at much lower levels (46). Therefore, it is unsurprising that many of the key regulators of antigenic BCR signalling are also implicated in tonic signalling. The NF-κB pathway represents one such pathway since B-cell-restricted ablation of NF-κB signalling, through genetic deletion of IKK2, has been identified to result in a deficiency of mature B-cells (448). Furthermore, it is proposed that tonic BCR signals and B-cell activating factor-receptor (BAFF-R) signalling integrate at the level of the NF-κB pathway in provision of key maintenance signals vital for B-cell survival. It is proposed that tonic BCR signal-mediated activation of the canonical NF-κB pathway results in elevated expression of the non-canonical pathway substrate p100 (145). P100 is subsequently processed by the non-canonical NF-κB pathway following BAFF-R signalling, resulting in activation of both pathways (145). Therefore, the collective outputs of both BCR and BAFF-R signalling are proposed to enhance cellular survival by activation of both the classical and non-canonical NF-κB pathways (145).

However, tonic NF-κB signalling appears to be dispensable since Bcl-10$^{-/-}$ mice, which demonstrate an inability to activate NF-κB upon BCR signalling, do not demonstrate B-cell developmental arrest (449). Furthermore, it has been demonstrated that co-induction of constitutively active IKK2 upon IgH ablation fails to rescue mature B-cells from apoptotic deletion (27). Therefore, evidence largely points to a diminished role of NF-κB in tonic signalling, at least in producing protection against apoptotic deletion during development and maintenance.

A role for ERK in tonic signalling has also been suggested as constitutive activation, via active-Ras mutant transduction, enables tonic-signalling impaired cells to overcome the associated developmental blockade (26). However, in those studies Rowland et al utilised a model in which severely reduced Igα expression is presented as being analogous to impaired tonic signalling. In this model developmental arrest occurs at the immature B-cell stage and not at the pro-pre B-cell stage typically demonstrated (26). Such cellular differentiation past the pro-pre B cell stage transitional arrest observed in other models implies that the proposed disruption of tonic signalling is not complete. Therefore, this perhaps does not represent a suitable model of tonic signalling disruption. This viewpoint is perhaps justified by the fact that co-induction of constitutively active MEK1 upon IgH ablation fails to rescue mature B cells from apoptotic deletion (27). Therefore, the suggestion of ERK involvement in tonic signalling remains currently unproven.

In contrast, PI3K signalling may be the key to tonic signalling, since inducible IgH ablation-induced cellular deletion can be offset via co-induction of a constitutively active p110 (p110*) PI3K subunit (27). In this model IgH ablation results in increased FOXO transcription factor activity and a 3.5 fold induction of Bim, both of which are reversed upon p110* induction (27). Presumably, p110* expression results in Akt-mediated phosphorylation of Foxo3a, resulting in its nuclear exclusion, therefore, resulting in repression of Bim expression (96, 205). This data is the most robust produced to date however, may yet prove inaccurate. It is possible that expression of oncogenic PI3K merely ensures cellular survival in a fashion that does not reflect the key physiological survival signals generated during tonic signalling. Therefore, the key

survival signals downstream of tonic signalling remain largely ambiguous yet PI3K represents the most likely contributor to date.

A2 The Unfolded protein response

BCR engagement has been associated with the induction of large-scale ER remodelling and ER stress, via activation of the unfolded protein response (UPR). Although primarily pro-survival, the UPR is capable of initiating a pro-apoptotic arm, which has been suggested to contribute toward BCR-induced apoptosis (211, 242, 450).

ER stress results as a consequence of the accumulation of mis-folded proteins in the ER lumen, typically driven via imbalances in ER [Ca^{2+}], ATP availability and redox levels (406). Such an accumulation triggers activation of an initial repair and protection response, which has the potential to induce apoptosis should the repair fail (406, 407).

UPR regulation is undertaken by three ER-resident transmembrane proteins: double-stranded RNA-activated protein Kinase-like ER Kinase (PERK), Inositol-requiring enzyme-1 (IRE1) and Activating transcription factor 6 (ATF6) (406, 407). Accumulation of misfolded protein triggers Binding immunoglobulin protein (Bip) dissociation from UPR effectors, allowing homo-oligomerisation and activatory transphosphorylation of Ser/Thr Kinase domains (406, 407). Activated PERK halts Cap-dependent translation via Eukaryotic initiation factor ii α (Eif2α) phosphorylation, lessening ER load (406, 407). Consequently translation of the Cap-independent Activating transcription factor 4 (ATF4) is enhanced, which engages a pro-survival response whilst simultaneously transactivating the pro-apoptotic transcription factor CHOP (406, 407). CHOP sensitises the cell to BH3-only induced apoptosis via induction of Tibbles homologue 3 (TRB3) (a negative regulator of Akt and NF-κB), repression of Bcl-2 and transactivation of Bim (211, 406, 407). Furthermore, engagement of the pro-apoptotic arm of the UPR is also thought to proceed via IRE1-mediated activation of JNK and p38 (406)

A3 Tcl-1 tg detection by PCR

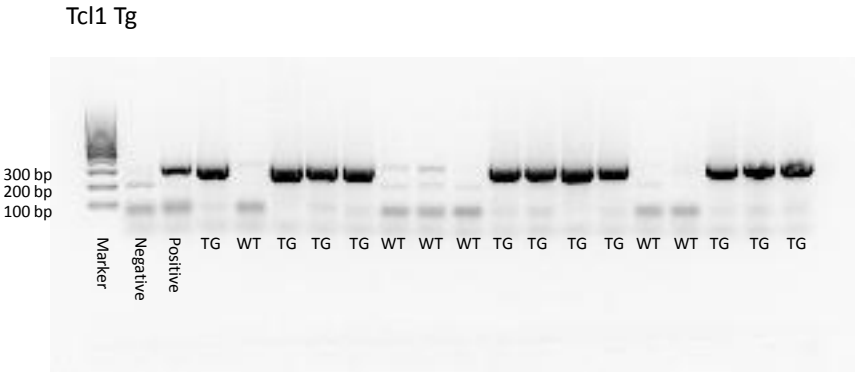

A3 Ear tips were obtained from prospective transgenic animals and digested in 50 mM Tris pH 8.9, 12.5 mM $MgCl_2$, 0.5% Tween-20, and 0.4 mg/ ml proteinase K for 18 hours at 55°C. Digests were diluted 1/5 with sterile H_2O and 1 µl of digested material containing DNA was assessed by genomic PCR. PCR reactions were performed as described in materials and methods section 2.6.1. A strong band at approximately 300 bp was interpreted as possession of the Tcl1 transgene.

A4 Large T antigen tg detection by PCR

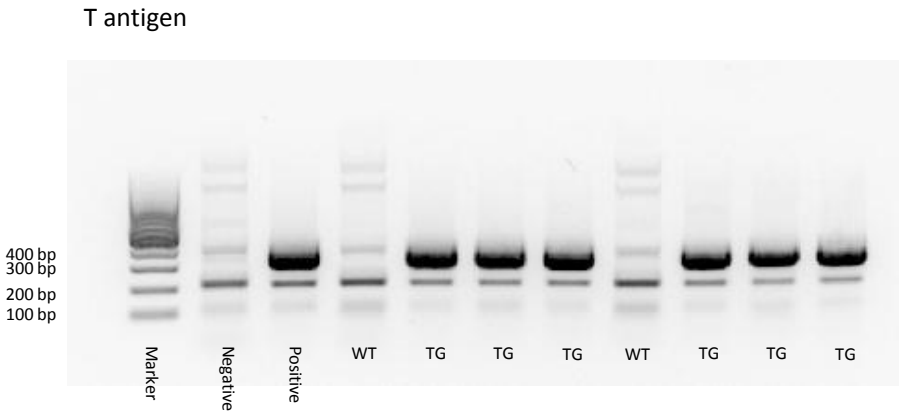

A4 Ear tips were obtained from prospective transgenic animals and processed, as outlined in A3. PCR reactions amplifying Large T antigen encoding sequences were performed as described in materials and methods section 2.6.2. A strong band at approximately 350 bp was interpreted as possession of the Large T antigen transgene.

A5 Myc tg detection by PCR

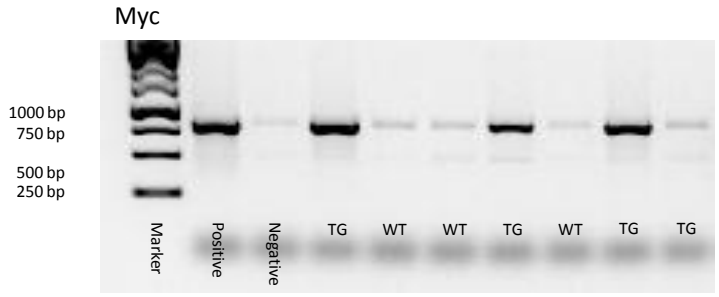

A5 Ear tips were obtained from prospective transgenic animals and processed, as outlined in A3. PCR reactions amplifying Myc tg encoding sequences were performed as described in materials and methods section 2.6.3. A strong band at approximately 900 bp was interpreted as possession of the Myc transgene.

A6 Assessing Bim allele status by PCR

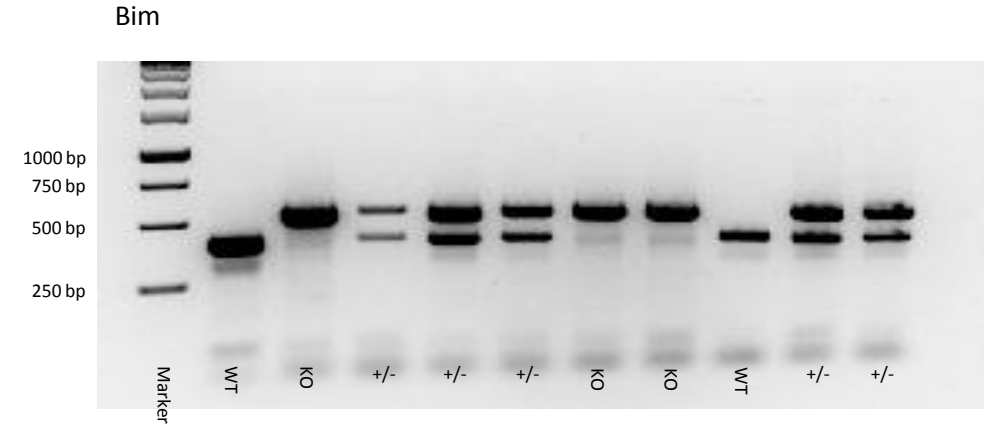

A6 Ear tips were obtained from prospective transgenic animals and processed, as outlined in A3. PCR reactions amplifying Bim alleles were performed as described in materials and methods section 2.6.4. A strong band at approximately 400 bp was indicative of the WT Bim allele whereas a strong band at approximately 500 bp was derived from the targeted Bim allele. Heterozygotes (+/-) possessed both bands.

A7 Observing the accumulation of Annexin V+/PI- cells upon mAb ā IgM treatment

In order to demonstrate that BCR-induced PS externalisation was a consequence of BCR stimulation and not a pAb ā IgM-specific phenomenon, an alternative mAb ā IgM

(whole IgG) was utilised to provide stimulation followed by Annexin V/PI flow cytometry, as previously described. As evident in A7, mAb ā IgM induced modest, dose-dependent increases in the frequency of Annexin V^+/PI^- cells, a hallmark of an apoptotic cell death. Therefore, the occurrence of such observations appears as a consequence of BCR stimulation and not antibody-specific.

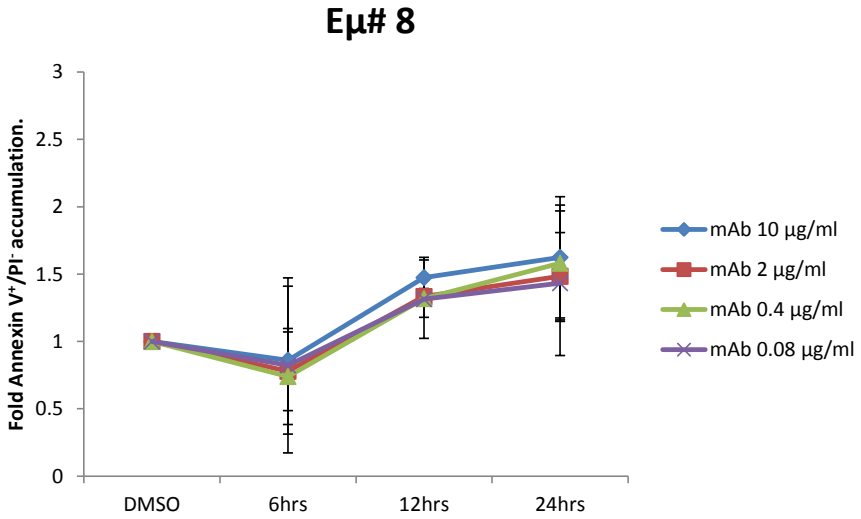

A8 Observing the impact of anti-F_c antibodies upon the extent of BCR-induced cell death elicited by mAb ā IgM

Since mAb ā IgM was demonstrated to impart a reduced level of cell death in comparison to pAb ā IgM, it was deemed necessary to determine whether such differences were attributable to reduced receptor cross-linking by mAb ā IgM. In order to assess the contribution of cross-linking, mAb ā IgM was applied alongside excess (10 μg/ml) Sheep anti-mouse F_c antibodies and the extent of cell death assessed after 24 hours by Annexin V/PI flow cytometry, as previously described. As evident below, the extent of mAb ā IgM-induced cell death was enhanced upon application of Sheep anti-mouse F_c antibodies. Such observations demonstrate that the extent of BCR-induced cell death is directly proportional to the magnitude of receptor cross-linking. However, even when applied alongside anti-Fc antibodies, the level of cell death produced by mAb ā IgM was significantly lower than that provided by pAb ā IgM. Therefore, it is possible that the use of whole IgG (as is the case for mAb ā IgM) modulates BCR signalling via engagement of the inhibitory Fc receptor CD32b, which is known to be expressed by Eμ-Myc lymphoma cell lines (E.L. Williams, verbal communication). Irr denotes application of an irrelevant antibody. Data represents the average of values

from Eμ# 8 and Eμ# 4, each performed in triplicate in a single experiment. Bars represent standard deviation.

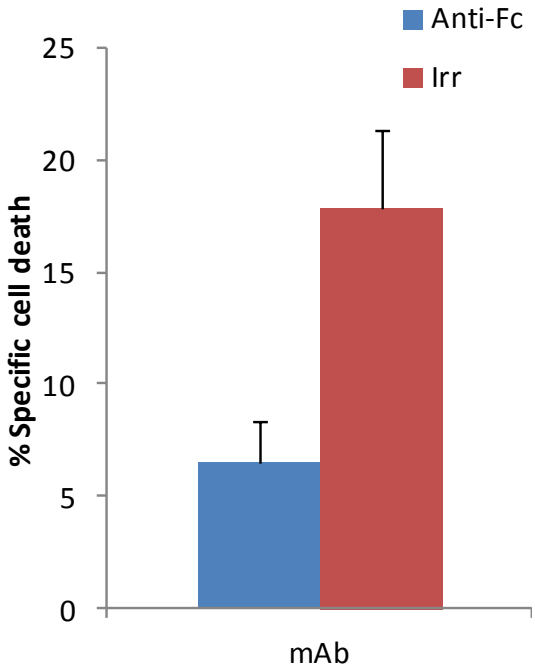

A9 Assessing the relative purity of purified B-cells

In order to confirm successful purification of B-lymphocytes from the spleens of C57BL/6 mice by MACS separation, immunostaining using anti-CD3^{FITC} (clone KT3) and CD19^{PE} (clone 1D3) and subsequent analysis by flow cytometry was performed as previously described.

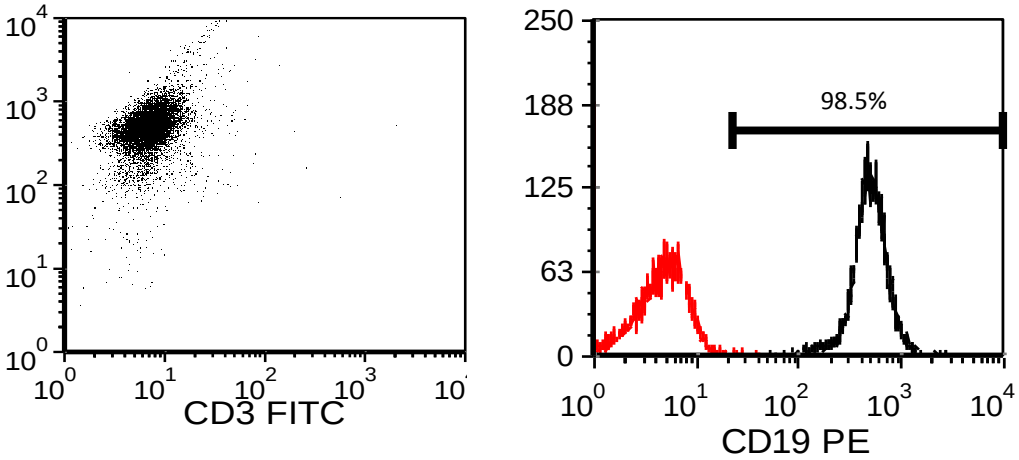

Red traces represent isotype control stained cells, black overlays demonstrate CD19 staining. As can be seen above, purified cell populations exhibited extensive CD19

staining but only minimal CD3 positivity. Overall purified cell population were over 97% CD19 positive. Therefore, cell populations were deemed to be highly pure B-cells.

A10 Assessing the impact of adaptation to cell culture upon BCR-induced cell death

In order to observe whether the relative passage number of Eμ-Lymphoma cell lines influenced the extent of BCR-induced cell death, death assays were performed, as previously described, at various passage numbers. Data demonstrates values obtained from Eμ# 16, 15, 8, and 4.

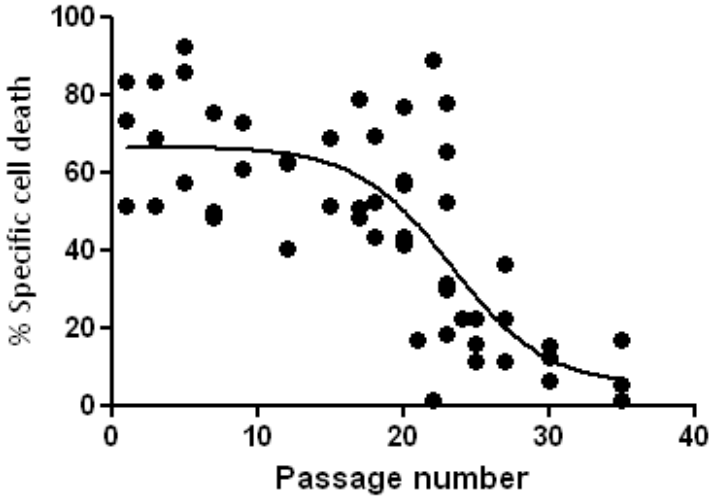

As demonstrated above, Eμ-Myc lymphoma cell lines exhibit a sharp reduction in the extent of BCR-induced cell death recorded after around 22 in vitro passages. Such observations indicate that *in vitro* cell culture selects clones resistant to BCR-induced cell death. It is possible that such clones exhibit defective stress-induced kinase signalling, allowing evasion of telomere-shortening-mediated replicative crises.

A11 Assessing the impact of BCR engagement upon Caspase-1 and -8 processing

In order to determine whether BCR engagement invokes activation of procaspases-1 and -8, western blotting was performed to allow detection of both active and procaspases forms of each caspase, as previously described.

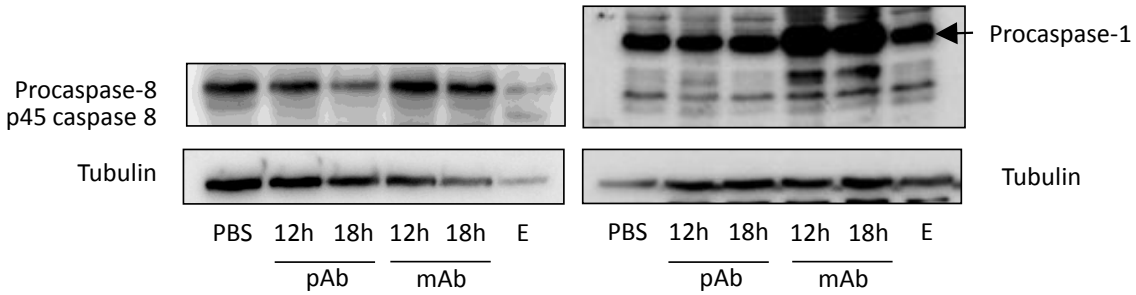

As demonstrated above, BCR engagement did not appear to influence the level of procaspase-1 or the occurrence of its active fragment. However, reductions in the level of procaspase-8 were apparent following 18 hours pAb ā IgM treatment, although unusually no activation was evident after 12 hours. Therefore, procaspase-8 appears to become activated downstream of BCR engagement, however, only well after the induction of effector caspases. Consequently, caspase-8 is unlikely to play a key role in BCR-induced cell death. Data was obtained from Eμ# 16 and is representative of the remaining lymphoma cell lines.

A12 Observing the occurrence of BCR-induced Mcl-1 degradation across the Eμ-Myc lymphoma cell line panel

In order to observe the extent of BCR-induced Mcl-1 degradation across the Eμ-Myc lymphoma cell line panel, western blotting analysis of Mcl-1 protein levels was undertaken utilising Eμ# 16, 15, 8, 4, E20, D3, and AF47. As evident below, only Eμ# 16, 4, and E20 exhibited substantial Mcl-1 degradation downstream of BCR engagement. Such observations are in contrast to the more common Bcl-2 degradation which was evident in nearly all lymphoma cell lines tested.

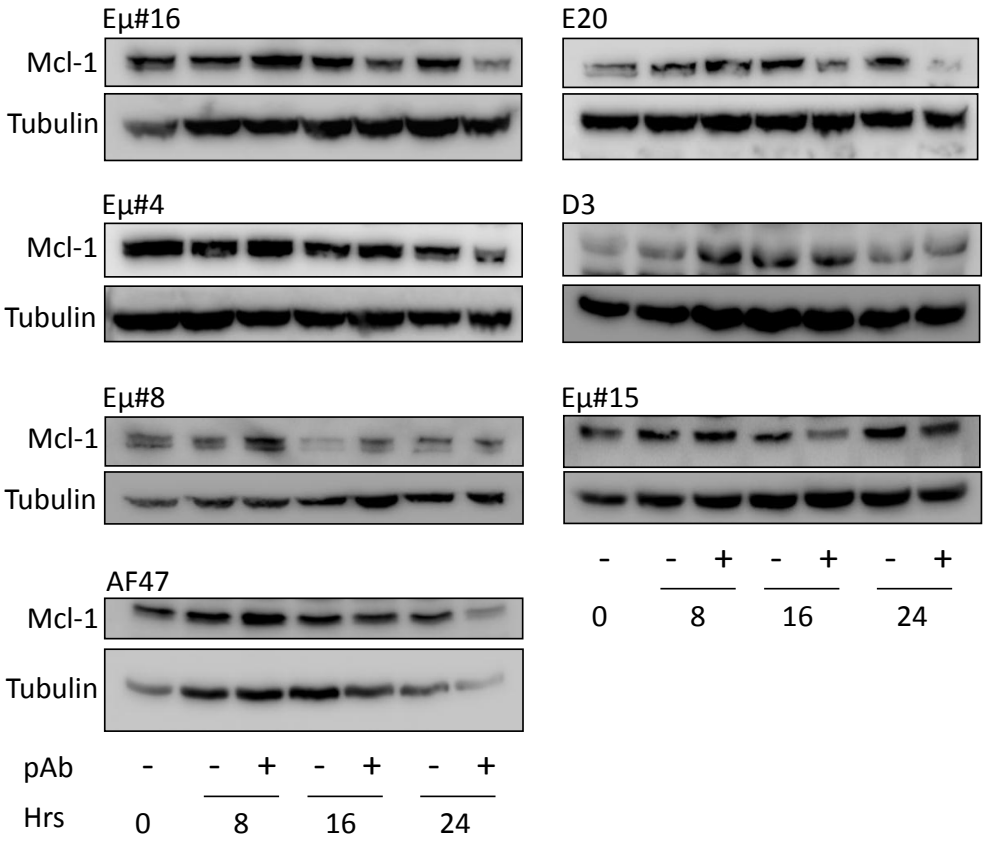

A13 Examining the binding of BH3-only proteins to prosurvivals in the absence of Bim

In order to observe whether BH3-only proteins other than Bim could be co-precipitated alongside prosurvival Bcl-2 family members, immunoprecipitation experiments were performed utilising Bim knockout Eμ-Myc lymphoma cell lines in the presence or absence of BCR stimulation, as previously described.

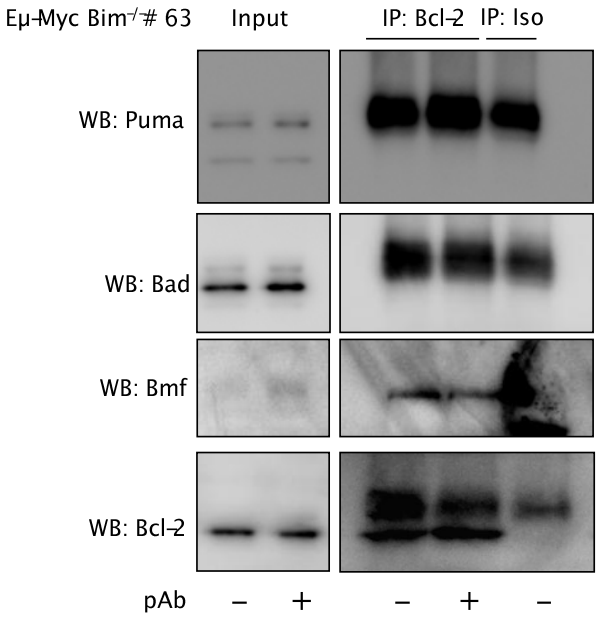

As evident above, in the absence of Bim only Bmf could be co-precipitated alongside Bcl-2. However, the extent of Bcl-2: Bmf complex formation was not influenced by BCR engagement. Such observations highlight the fact that Bim represents the major BH3-only protein responsible for pro-survival priming in resting Eμ-Myc lymphoma cell lines.

A14 Examining the correlation between relative IgM expression and the extent of BCR-induced cell death in Eμ-Myc

In order to determine whether genetic loss of BH3-only proteins influenced the relative surface expression of IgM, and therefore the extent of BCR-induced cell death, relative surface IgM expression levels were plotted against the levels of BCR-induced cell death for each cell line utilised. As evident below, no correlation between surface IgM expression and the extent of BCR-induced cell death was evident. Therefore, it was subsequently assumed that any differences in the extent of BCR-induced cell death were attributable to loss of gene expression, rather than due to differences in BCR expression levels.

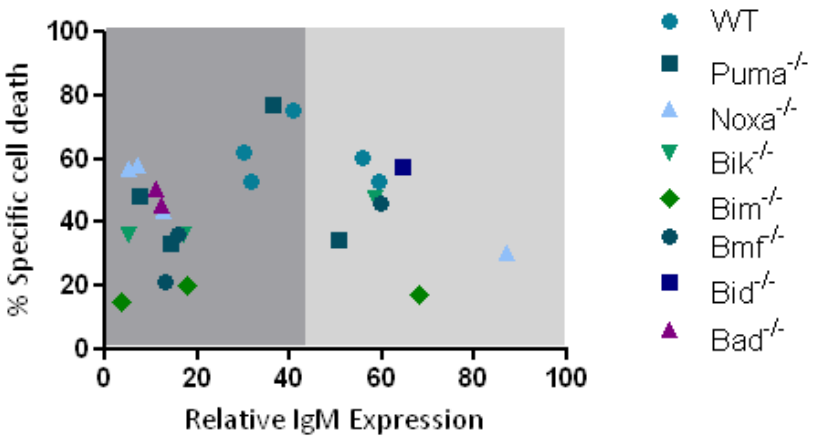

A15 Examining the sensitivity of WT, Bik$^{-/-}$, and Noxa$^{-/-}$ Eμ-Myc lymphoma cells toward Etoposide treatment

Since both Bik and Noxa deficient Eμ-Myc lymphomas exhibit a statistically reduced sensitivity toward BCR-induced cell death in comparison to WT cells, it was deemed necessary to demonstrate that such an effect was not due to a general reduction in sensitivity to apoptotic stimuli. Therefore, the relative sensitivity of Bik and Noxa deficient Eμ-Myc lymphomas toward Etoposide treatment was assessed by Annexin V/PI flow cytometry, as previously described. As demonstrated below, both Bik and Noxa deficient lymphoma cell lines exhibit statistically similar levels of death in response to Etoposide treatment after 6 and 24 hours, in comparison to WT lymphomas. Interestingly, Bik and Noxa deficient lymphomas exhibit an enhanced sensitivity toward Etoposide after 6 hours, albeit to a statistically non-significant level. Data represents the average of Eμ# 16, 15, 8, and 4 (for WT lymphomas), MB13, MB37, and MB42 (for Bik$^{-/-}$ lymphomas), and MN159, MN99, MN97, and MN75 (for Noxa$^{-/-}$ lymphomas), each the average of three independent experiments performed in triplicate. Bars represent standard deviation. **N.s.** non-significant.

A16 Pictorial representation of the MscV vector system utilised for retroviral transduction studies

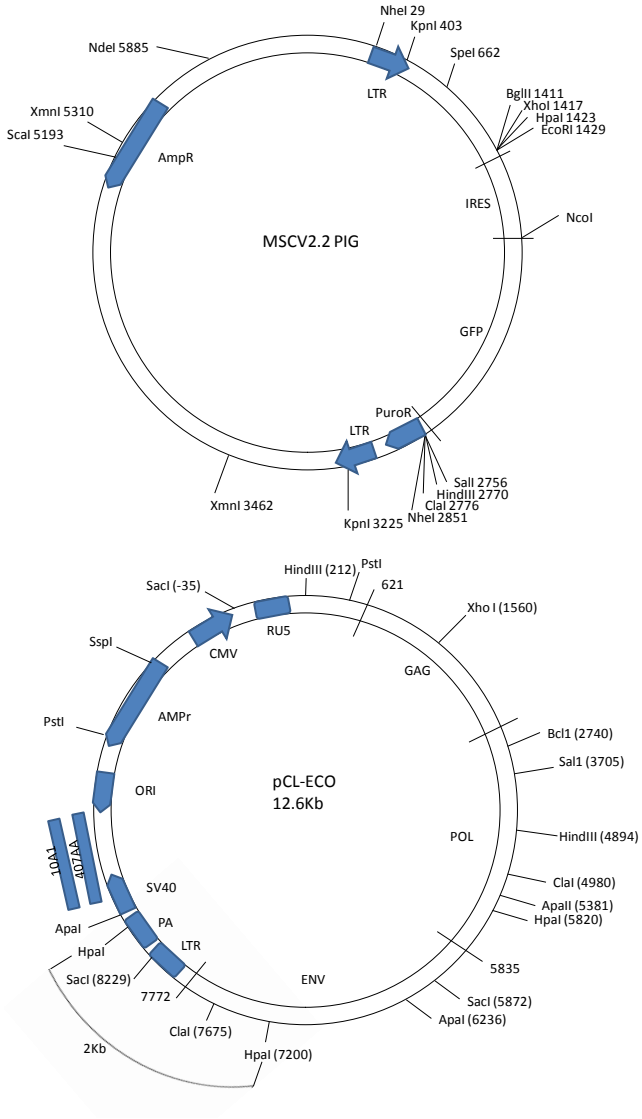

(AmpR) Ampicillin, (CMV) cytomegalovirus promoter, resistance cassette, (ENV) envelope reading frame, (GAG) Gag reading frame, (GFP) Green fluorescence protein, (IRES) internal ribosome entry sequence, (LTR) Long terminal repeat, (ORI) Origin of replication, (PuroR) Puromycin resistance cassette. ShBim constructs were cloned into EcoRI, BglII digested MscV2.2 PIG constructs.

A17 Assessing the impact of MEK inhibition upon BCR-induced cell death in Bim$^{-/-}$ Eμ-Myc lymphoma cells

Since PD treatment appeared to generate a downward shift in Bim_{EL} bands by western blotting, it was hypothesised that ERK may be responsible for regulation of Bim function in Eμ-Myc lymphomas. Therefore, it was also hypothesised that ERK may link apoptotic BCR-engagement to the upregulation of Bim transcripts and protein levels and therefore explain the relative protection PD-treatment offered to BCR-induced cell death. Therefore, PD-treated MB# 63 were subjected to pAb ā IgM-induced death assays by Annexin V/PI flow cytometry after 24 hours, as previously described.

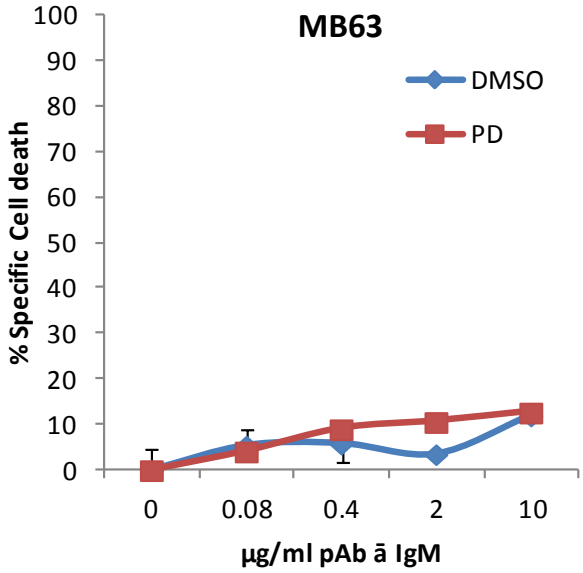

As demonstrated above, MEK inhibition failed to influence the extent of BCR-induced cell death evident in the Bim deficient Eμ-Myc lymphoma cell line MB# 63. Therefore, such studies highlight the possibility that ERK may drive the apoptotic response to BCR engagement by an effect upon Bim transactivation or upregulation at the protein level. Data represents the average of three independent experiments, each performed in triplicate. Bars represent standard deviation.

A18 Observing the effect of TGF-β upon Puma expression levels in human BL cell lines

Since TGF-β induced upregulation of Puma at both the transcript and protein levels in Eμ-Myc lymphomas, it was deemed appropriate to determine whether it was also upregulated in the Human BL cell lines BL40, CA46, Ramos, BL2, and BL30. Therefore,

qPCR and western blotting analysis of Puma expression levels was undertaken, as previously documented. As demonstrated below, TGF-β invoked small but consistent up-regulation of Puma transcripts and protein levels in such cells.

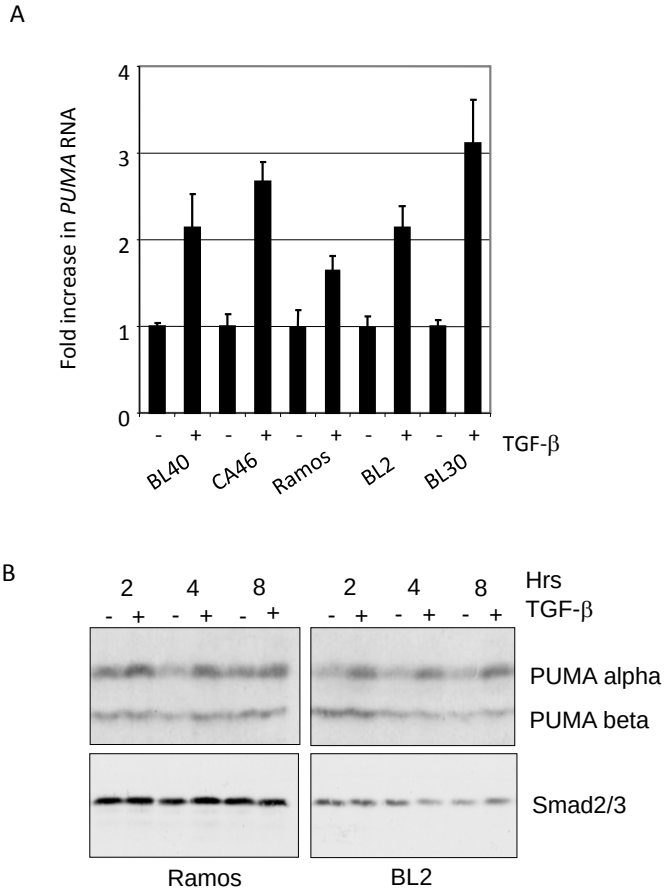

Such studies identify that both human and mouse cell lines demonstrate induction of Puma in response to TGF-β and, therefore, the link between TGF-β signalling and Puma regulation is evolutionarily conserved. qPCR data represents a single cDNA from each cell line performed in triplicate, bars represent standard deviation. Data kindly provided by Drs. L. Spender and G. Inman (University of Dundee).